(14) Bull-46-Pt-2

Bulletin 46

(Part 2 of 5 Parts)

(6) (1)

THE SHOCK AND VIBRATION BULLETIN.

Part 2

Opening Session, Panel Session, Shock Testing and Analysis, Fluid-structure Topics

(11) AUGUST 1976

(12) 304 p.

A Publication of
THE SHOCK AND VIBRATION
INFORMATION CENTER
Naval Research Laboratory, Washington, D.C.

Office of
The Director of Defense
Research and Engineering

389004

SYMPOSIUM MANAGEMENT

THE SHOCK AND VIBRATION INFORMATION CENTER

Henry C. Pusey, Director
Rudolph H. Volin
J. Gordan Showalter
Barbara Szymanski
Carol Healey

Bulletin Production

Graphic Arts Branch, Technical Information Division,
Naval Research Laboratory

Bulletin 46
(Part 2 of 5 Parts)

THE SHOCK AND VIBRATION BULLETIN

AUGUST 1976

A Publication of
THE SHOCK AND VIBRATION
INFORMATION CENTER
Naval Research Laboratory, Washington, D.C.

The 46th Symposium on Shock and Vibration was held at the Royal Inn at the Wharf, San Diego, California on October 20-23, 1975. The Naval Electronics Laboratory Center and the Naval Undersea Center, San Diego, California were the hosts.

Office of
The Director of Defense
Research and Engineering

Partial

CONTENTS:

PAPERS APPEARING IN PART 2

(Contd pr)

PAPERS APPEARING IN PART 5

Dynamic Analysis

KEYNOTE ADDRESS

by
Rear Admiral Samuel L. Gravely, Jr.
Commandant 11th Naval District
San Diego, California

It is indeed my pleasure as Commandant, Eleventh Naval District, to also welcome you to San Diego. We are delighted that you chose this city for your meeting.

When I was first approached concerning the possibility of addressing this group I stated quite frankly that I knew nothing about shock and vibration. Of course, there have been times in my Naval career when I have been both shocked and vibrated and, on reflection, I think that the vibrations were the best. However, the chairman assured me that this was not exactly what you had in mind. At the same time, your chairman also assured me that I was far from alone in lacking specific knowledge on shock and vibration. After that I felt a bit better, and here I am.

My shipboard experience includes duty on anti-submarine patrol craft, battleships, cruisers, amphibibous ships and several destroyers. I have been primarily a communicator, but I have commanded four destroyers. While I may not be a shock and vibration expert, I know well from personal experience the value of highly reliable and survivable combat ships. I am reminded of several experiences where shock and vibration played a significant part in the completion of my missions. Let me give you an example. In 1960 I was executive officer of the Theodore E. Chandler (DD-717) in the Western Pacific. We had just completed a firing exercise and were enroute to join the carrier. The sea was relatively calm with a few swells. We were making 15 knots, suddenly a large wave hit and with a loud crash I heard something snap. Believe it or not, mount 51 had just caved into the chiefs' quarters. We limped back to port.

The average combat life of a destroyer during World War II was approximately 22 minutes. When I first heard that figure I was ready to argue, but I remembered that I had ridden the Lofberg DD-759 in 1959 and witnessed a shock and vibration test. The test consisted of Lofberg simulating a submarine attack and the actual firing of her MK-9 depth charges. I remembered four things about this test. The first one was that as the patterns were being fired; Lofberg, at 25 knots, appeared to be running for her life. The second was that I felt that when those tests were completed that Lofberg would need a new hull and superstructure as well. The third was that the depth charge and depth charge racks were all removed soon after the test. Fourth, there were no more tests. I also wondered how many of our destroyers lived a shorter life as a result of our own depth charge firings during World War II.

Perhaps one of our most serious peace time threats is our tendency to forget the hard learned lessons of war time. The pressures brought about by cost and schedule constraints as they affect both the weapons system acquisition process, and the operational exercise of such systems, are quite real.

As most of you are well aware, the first question frequently asked is how much will it cost? An innovative proposal during peace time is likely to be dismissed based upon cost alone without any particular regard as to merit. On the other side of the coin during a national emergency a likely response to proposals with even a hint of merit is, "Lets do it." Somewhere between these two extremes is a reasonable balance. Maintaining this balance and getting the necessary job done, while accommodating various imposed constraints is a difficult task that faces the entire defense complex. You are a part of that complex, as I am, and our challenges will surely increase rather than decrease.

Many of the requirements imposed on the design of our ships, aircraft and other weapons systems are necessary to meet normal operating conditions, and are fully maintained throughout the design. Other requirements are related to the adverse environments of combat which may never actually be realized during the life of a system. Yet it is for this later purpose that the ship, aircraft or tank or other system actually exists.

Addressing the adverse combat environments in the design of our weapons is almost always difficult and usually the most expensive. Because of our peace time amnesia, these requirements are frequently candidates for trade-off during negotiations. While shock and vibration and similar considerations should not be exempt from competing in the design trade-off ring, these factors are sometimes not capable of surviving the competition for several reasons. First, the real need for these requirements may not be fully appreciated by people who may be principally operations oriented. The customer or user must in some way be sensitized to the value and importance of these requirements. It is not unreasonable to exepct that many military

customers at the Pentagon level will have less than a firm grasp on complex specialties such as shock and vibration. Yet as the decision maker they still must be presented with those factors so that the pros and cons are described in terms meaningful to them as users. It is critical that you as technical experts in the field be able to communicate effectively so that the less knowledgeable customer will avoid making decisions which are not necessarily correct or in his best interest. It is important also that you not become discouraged by the frustrations you are likely to encounter when trying to effect such communications.

Another reason that shock and vibration and similar considerations tend to come out poorly in the trade-off ring is simply that the price of doing business in terms of dollars, time, weight and space limitations, is high. As you are all well aware, the competition between performance features during a design development is keen and force solutions to shock and vibration problems.

I am not convinced that the technical community, has given enough emphasis to the matter of efficiency of design when you add unnecessary weight any item of shipboard equipment, the excess weight must be carried around by the ship for most of its life, and at serious operational penalty. Unfortunately, desing requirements tend to set the ceiling below incentive, except for aircraft missiles which are designed close to the limit. If the design requirement is 10g, it is not uncommon to find that the item has been designed with a 20g or hundred g capability for shock and vibration. I am told that the more common practice is to check the design for shock and vibration characteristics rather than specifically designing for certain performance. If it checks out all right, meaning that the stresses could be in an order of magnitude lower than allowable, the designer is usually satisfied and stops. It is becoming increasingly important, that if adequate shock and vibration considerations are to find their way into design, the efficiency of such designs must improve.

The consequences of ignoring potential shock and vibration effects were unfortunately well demonstrated recently when one of our newer ships conducted its first gun firing tests. The guns worked fine everytime they were fired. However, the ships fire control radar was put off the line rendering the weapons to near zero effectiveness. The problem was corrected, but it could and should have been avoided in the first place by adequate awareness.

The ship shock hardening effect is illustrated by a recent experience in Vietnam. Two ships under-went essentially identical mine explosions. One, an older ship with no shock design requirements, was incapacitated, towed back to port and eventually scrapped, because it was unsalvageable. Fortunately there were no injuries to the crew and the hull was intact. The other ship, designed to current practice, stayed on station and returned to port only for routine maintenance. This is a good test of the capabilities of our technology.

My message today is simple. We know that it is absolutely essential that our weapons systems perform as intended when we are exposed to likely adverse environments. But there is a real tendency during peace time periods and imposed tight budgets to give less attention than what may be desirable. It is vitally important that the technical community keep the customers aware and sensitized to these needs.

Keeping these things in mind, I trust that you will gear yourselves for even better competition in the design area.

Again, it is a pleasure to have you here in San Diego. I sincerely hope you have a good meeting and I wish you the best of luck.

INVITED PAPERS

S and V in T and E

CAPT LOUIS COLBUS, USN
Ship Evaluation Division, COMOPTEVFOR
Norfolk, Virginia

My current assignment is Assistant Chief of Staff for Ship Evaluation at Commander Operational Test and Evaluation Force which is located in Norfolk, Va. In my division, we presently are working with 15 ships, ranging from the 65' Patrol Boat to USS NIMITZ. We also have projects on CGN 38, DD 963, FFG 7, LHA, PHM, SES, SSN 688 and TRIDENT. In order not to slight any of our other ship programs, here is a listing of the entire 15 ships.

SHIP EVALUATION DIVISION
15 SHIPS/ 8 OFFICERS

AALC
AO 177
ASR 21
CGN 38
CPIC
CSGN
CVN 68
DD 963
FFG 7
LHA
PB (65')
PHM
SES
SSN 688
TRIDENT

Let me assert myself as a shock and vibration mavin. Twenty years ago as a Gun Boss on a destroyer, I was responsible for firing a full pattern of depth charges, set at 50 feet while the ship steamed at 5 kts. The primary damage it caused was the total destruction of the piping and commodes in the after J. O. Bunk Room (where I lived). My interest in restoring this area had me out at night in Key West, procuring replacement parts via the old midnight requisition route. As you can imagine, that was a tough introduction into the world of S and V.

A more recent encounter with shock and vibration was in the late '60's when I worked in the OPNAV arena, associated with the New Construction Destroyer Program. One of my areas was to explore the feasibility of placing the compact aircraft comm gear in a ship's radio shack. One of the hang-ups was that we were told the gear would have to be shock-tested at a cost in time, money and growth in order to "marinize" such equipment. Having just completed 2½ years on a carrier group staff and having ridden all the Atlantic carriers, I now look back and wonder what shock tests could have been performed that weren't accomplished during launch and recovery of the aircraft carrying the subject comm gear.

In August of this year, the TRIDENT multi-function mast antenna underwent vibration testing at NELC. It failed. Subsequently, re-testing was accomplished after modifications were made. We looked over the shoulder of the developing agency, NAVELEX PME 117, who coordinated the tests.

Now that I hope I have established myself as a shock and vibration mavin, let me tell you about COMOPTEVFOR and how our test and evaluation function fits into the overall acquisition program. (Define the word "mavin".)

COMOPTEVFOR is in a unique position in heading the Navy's sole independent OT&E agency. He works <u>directly</u> for the CNO.

Four years ago, a minor revolution took place in the defense material acquisition process. Part of that revolution could be termed the Test and Evaluation Explosion. The impact on the way we acquire new Navy hardware was so far-reaching that almost all our directives, Defense and Navy, were rewritten.

At the working level, unfamiliarity with the new policies, procedures, and

definitions was -- and is -- almost the rule rather than the exception. The result is a waste of time, money, and a great deal of effort. And Navy programs are suffering at all levels. And fleet readiness is hurt because new equipment doesn't work as well as it should or could.

In general terms, almost all Test and Evaluation can be divided into two separate and distinct categories: Development Test and Evaluation by the Developing Agency and Operational Test and Evaluation by COMOPTEVFOR. There is a third category, PAT&E (Production Acceptance Test and Evaluation) which is done primarily by the INSURV/BIS organization; however, that is so clearly defined in scope and so definite in time that I will not address this category due to our time limitations.

As a way of identifying OT&E, let me give a somewhat exaggerated example of the difference between DT&E and OT&E in the case of HARPOON and the NATO hydrofoil, the PHM.

For DT&E, the developing agency would properly optimize all conditions. He would pre-select a missile for firing and Peak and Tweak it, with field engineers and contractor reps doing most of the work. The PHM, also with technical people aboard, would sortie specifically for this test in good weather. The PHM would probably steam a steady course and speed at a predetermined range and would launch a missile at an anchored target hulk. If a member of the contractor's launch team made a personnel error, the shot would be a no-test. For OT&E by COMOPTEVFOR, the PHM and the HARPOON missile will be handled only by the ship's regular crew -- no engineers or contractor reps will be allowed aboard. Several HARPOON missiles, selected at random, have been loaded in the PHM's launcher and subjected to the normal shipboard environment of high seas, vibration, sun and spray, gun firing, and even paint chipping in port! The HARPOON firing will take place at the end of a typical five-day mission profile at sea, hopefully in poor weather. The PHM will close the target at maximum speed, using zig-zag courses to avoid simulated return fire. The ship will have other tasks to perform such as gun firing, contact reporting and navigation during the run-in. The target will be a high-speed SEPTAR, equipped with remote-control chaff launchers and expendable DECM equipment to counter the HARPOON. The hydrofoil would have to detect the target, identify it, make tactical decisions on engagement, fire the missile, assess the effect of the shot, and make decisions on subsequent action -- all of which would be part of the evaluation. If the shot missed because of a personnel error among the crew, in some aspects the firing would be evaluated a failure -- even though the HARPOON itself performed well.

Although this example is somewhat overdrawn, it emphasizes that DT&E attempts to optimize all conditions and evaluates hardware only, whereas OT&E attempts to create combat conditions and evaluates the entire system, including the men in the loop and the interfaces with other systems.

Another way of describing Operational Test and Evaluation, here is the "official" definition from the most basic source document, DOD Directive 5000.3.

DEFINITION OF OT&E

"OT&E is that test and evaluation conducted to estimate the prospective system's military utility, operational effectiveness, and operational suitability (including compatibility, interoperability, reliability, maintainability, and logistic and training requirements), and need for any modifications."

This slide defines OT&E by its characteristics. These are taken from the DOD Directive 5000.3 -- The T&E Bible -- and are repeated in Navy Directives. In order to class as OT&E, the testing must be:

- Planned by COMOPTEVFOR.
- Conducted by fleet-type personnel, both for operation and maintenance of equipment.
- Carried out at sea under typical fleet conditions against a simulated enemy who fights back.
- Supervised by COMOPTEVFOR in terms of making on-the-spot decisions.
- Reported to the CNO by COMOPTEVFOR.

Now, with this understanding of OT&E, I'll quickly review the recent changes that have had such an impact upon the material acquisition system.

I'll use OPTEVFOR's history as the backdrop for these changes.

OPTEVFOR was established in 1945, principally to develop hardware and tactics to defeat the Kamikaze threat. VADM W. A. LEE was the first commander. Throughout the next 25 years the size of OPTEVFOR increased and its functions expanded -- but oriented toward fleet introduction of new equipment and development of tactics. It's important to realize that in those years our work generally started after the production decision and we used production hardware.

In 1971, OPTEVFOR was changed into a completely different organization by the major changes that were made in the acquisition system.

DOD Directive 5000.3 guides all test and evaluation in the Department of Defense. Although it is relatively brief -- only 8 pages -- it is quite explicit in its policy, and remarkably powerful in overall impact.

One of the major changes that was instituted by DOD Directive 5000.3 is the requirement that only one organization in each service can carry out operational test and evaluation.

The impact of these changes upon OT&E in terms of its impact upon COMOPTEVFOR is as follows:

- First, and of greatest significance, our involvement has been moved earlier in the acquisition cycle. Instead of becoming involved after the production decision, we are now deeply tied into the entire development process.

- Among the principle new outputs are COMOPTEVFOR's estimates of expected operational effectiveness and operational suitability at key program milestones. These are particularly critical at DSARC II and III for major programs and at the approval-for-service-use decision point for less than major programs.

- Finally, more and more we are drawn into the business of making independent assessments of the progress of test and evaluation during developmental phases.

These new functions are all in addition to the original ones of fleet introduction of new weapons and tactical development.

The really sweeping change for OPTEVFOR is, of course, the matter of early involvement. This takes the form of IOT&E -- Initial Operational Test and Evaluation -- which was the principal buzz-word at the heart of the explosion. All OT&E can be divided into these two categories: Initial Operational Test and Evaluation, which occurs before the first major production decision, and Follow-on Operational Test and Evaluation, which occurs after the first major production decision. Both are done exclusively by OPTEVFOR.

I'd like to make three additional points. First, our entire effort at COMOPTEVFOR is to save time and money: to save time by planning rather than being forced into rescheduling, and to save money by fixing one model before production rather than retrofitting hundreds once they are in the fleet. It's not test and evaluation that causes inordinate delay or expense -- it's equipment that doesn't work when tested. We are not purists about Test and Evaluation. In every program COMOPTEVFOR attempts to minimize T&E!

Second, the organizations outside the Navy which have control over us are dead serious about OT&E.

And third, what we're talking about here is fleet readiness. If the new equipment arriving in the fleet will do its job and is reliable, then we have a fighting chance of digging our way out of the readiness hole. But if new equipment has as many problems as the old, the fight will never be won. OT&E gives you the only measure you have as to how the equipment will perform in the fleet, and it gives you this in time to decide whether to produce or fix.

I hope you now have an understanding of our job at COMOPTEVFOR and a realization how our goals go hand-in-glove. We are scheduled to participate in the shock tests for SPRUANCE (DD 963) and TARAWA (LHA 1) in the near future. One of the quick reference books at my desk is NAVSEA's test plan for routine shock testing of ships. I hope you are interested in T&E directives published at all levels within the Navy Department. With that commercial, I will relinquish this speakers platform and join you in your symposium and look forward to our close associations in the T and E/Shock and Vibration world. Thank you for this opportunity.

REVIEW OF NUCLEAR BLAST AND SHOCK ENVIRONMENT SIMULATION

E. Sevin
Defense Nuclear Agency
Washington, D.C.

An overview is presented of nuclear airblast, cratering, and ground shock environment simulation techniques utilizing conventional high explosives and suitable for large-scale field testing. State-of-the-art capabilities for both full space and limited space simulation are discussed, including the so-called MINE THROW and HEST techniques. Representative data are shown to indicate the degree of the simulation possible in airblast, crater shapes, and ground motions for both the kiloton and megaton range of near surface nuclear explosions.

INTRODUCTION

Since 1963 when the United States agreed to refrain from testing nuclear devices in the atmosphere, the Defense Nuclear Agency (DNA) and its associated DOD laboratories have relied largely on high-explosive sources for generating relevant airblast and ground shock and, of course, target response environments. The aims of such simulations have been, and continue to be, replication of weapons effect free-field environments for the purposes of (1) better understanding and quantifying basic phenomenologies, (2) extending our knowledge of structural and target response, and (3) evaluating the survivability of military equipment and facilities. To these ends, field use of high-explosives to simulate a nuclear source has been supplemented by laboratory and fully contained small yield nuclear detonations.

This paper provides an overview of current approaches to the simulation of nuclear airblast and ground shock environments and is suggestive of the scope of DNA-supported field test activities.

BACKGROUND

The appearance and qualitative nature of a near surface nuclear detonation is quite familiar. The instantaneous release of energy gives rise to prompt nuclear, electromagnetic, and thermal radiation. The fireball forms and expands, causing a high-strength blast wave to propagate outward. The advancing airblast induces stress waves in the ground which, depending on local geologic properties, may eventually outrun the air shock front.

A portion of the source energy acts to vaporize surface material and the resulting blow-off drives extremely intense stress waves into the ground. Close-in, the ground material behaves hydrodynamically, forming a crater and giving rise to so-called crater-induced ground shock. Again, depending on geologic stratifications and earth properties, this shock may overtake the air-induced ground shock and be seismically reflected back toward the surface. Finally, the crater-produced ejecta and surface debris lofted by the rising fireball may constitute another significant aspect of the weapons effects environment.

Airblast is the best understood of the near surface nuclear effects, both phenomenologically and in terms of an empirical data base. Still, there are thermal-related surface effects and reflection phenomena at high pressures which remain important research areas. The ground shock environment arises

from more complicated and less well understood physical processes than does the airblast, with geologic influences making this environment very much site dependent. It is well to emphasize the role of site geology in creating the ground shock environment, as well as the significance of crater-related effects. (Of course, cratering is height of burst dependent; for sufficiently high heights of burst, no crater will be formed and we do not speak of "crater-induced ground shock.")

A simulation technique is expected to replicate in a reasonably accurate manner the following mechanical effects of a nuclear explosion.

- Airblast overpressure/dynamic pressure/impulse
- Crater volume/radius/depth
- Ejecta fields
- Airblast-induced ground motions
- Crater-induced ground motions

How practical (and necessary) it may be to simulate all of these effects simultaneously, or over what region of space and to what measure of accuracy, tends to be application-dependent. With respect to ground motion simulation, it is instructive to note that the physical processes involved span a time and intensity (pressure) range of nearly a decade in orders of magnitude; from fractions of a microsecond to seconds in time, and from thousands of megabars to a few psi in pressure (Fig. 1). There is no practical large-scale way of simulating the energy densities or source intensities associated with a nuclear detonator. In many applications, this limitation is of no great consequence. In others, particularly applications associated with cratering or crater-induced ground motions, special simulation techniques are required.

APPROACHES TO SIMULATION

We may distinguish between what has been termed Full Space (or 4π) simulation and Limited Space (or Directed) simulation. The first refers to simulations intended to replicate desired effects equally well over 360 degrees of azimuth, above and below the earth's surface (hence, 4π). This is appropriate to large-scale field tests requiring axial symmetry, when considering the effects of ground shock involving complex refracted seismic paths, or when considering the influence of airblast on the crater ejecta and/or dust plume. Limited space simulation, as the name implies, is appropriate when targets occupy restricted areas and, particularly, where the source region itself need not be simulated directly. This approach constitutes more efficient energy utilization. Laboratory devices such as shock tubes and blast generators belong to this category of simulation.

4π SIMULATION

Development of high explosive sources for 4π simulation has followed two different approaches. The earliest, and still the more common, approach is rather a pragmatic one employing massive amounts of high explosive configured in simple geometric shapes. The other approach is of more recent development and considerably more sophisticated in the basis of its simulation. We discuss the pragmatic approach first.

Numerous tests have been conducted with source shapes such as spheres (tangent and partially buried), hemispheres, and cylinders; explosive charges have included TNT, ammonium nitrate/fuel oil mixtures (ANFO), nitromethane, and detonable gases; charge weights have varied in size up to 500 tons TNT equivalent. The principal field tests have been SNOWBALL (1964), DISTANT PLAIN (1966-7), PRAIRIE FLAT (1968), MINE SHAFT (1968-9), DIAL PACK (1970), MIDDLE GUST (1971-2), MIXED COMPANY (1972), PRE-MINE THROW IV (1974) and, currently, DICE THROW (1975-6).

The basis of similitude is direct comparison of such measured quantities as airblast waveforms, cratering efficiency (i.e., crater volume/ton nuclear airblast equivalent), and crater shape with corresponding nuclear measurements or estimates. Fig. 2 shows a comparison of HE airblast waveforms with their nuclear counterparts in both the kiloton and megaton ranges. Agreement between these data requires a 2-to-1 equivalency in terms of the nuclear and HE energy sources as indicated in the figure. The high explosive-to-nuclear yield equivalence established in this manner is not really a constant over the entire range of effects (as is well-known for air overpressure) and, indeed, may be different for different effects. However, if one is careful not to extrapolate too far, such

equivalents have meaning and can establish in a semi-quantitative way the degree of simulation provided by high explosive sources utilized in this manner. Since the DISTANT PLAIN event in 1967, which showed good correlation with then best estimates of nuclear crater dimensions, the surface tangent sphere has been most used for large-scale field tests.

With respect to ground motions produced by simple high explosive sources, it has been tacitly assumed that, if the airblast pulse and crater dimensions replicate their nuclear counterparts, then the resulting ground motions will "scale." There are ample nuclear data available for comparison with airblast-induced ground motions to support the practicality of the approach. However, the case for cratering-induced ground motions is not so easily established due to the scarcity of nuclear data and our lesser degree of understanding of cratering processes, especially for modern large-yield weapons. Since much of our knowledge of "nuclear" cratering comes from simulations, we must be careful not to draw erroneous conclusions as to the nature of the crater-induced ground motions and the adequacy of the simulations.

The tangent sphere geometry is known to produce undesirable airblast effects; notably the "squish" effect resulting from the trapping of the airblast between the ground plane and the high explosive combustion products. In addition, blast anomalies (jetting) occur which are believed to be caused by instabilities due to the large gradients of density in the "squish" region and perhaps augmented by the polystyrene foam base support. The hypothesis of blast anomalies being associated with block-built TNT charges has been eliminated by the observance of anomalies on the PRE-MINE THROW IV nitromethane tangent sphere detonations.

The tangent sphere geometry also produces weak secondary shocks which appear in the negative phase of the overpressure pulse. These secondary shocks are not important from an overpressure viewpoint, but they appear to influence the character of the ground shock in a significant, and unscalable, manner. Striking evidence of this was obtained in the PRE-MINE THROW IV event over a range of charge weights (W) from 1,000 pounds to 100 tons. At a fixed overpressure ($W^{1/3}$ scaled range), the ground motion time base scales approximately as $W^{1/6}$, whereas arrival times of the secondary pulse scale as $W^{1/3}$. Moreover, the magnitude and timing of the secondary pulse varies with charge geometry; e.g., it is not apparent in the ground motion for a half-buried charge, and its timing is different for the nuclear counterpart.

The current DICE THROW test series involves development of cylindrically configured ANFO charges and direct comparison with tangent TNT spheres. The charge development effort is directed toward reducing blast anomalies, improving the ground shock simulation, and reducing total costs.

A more fundamental approach to 4π simulation aimed at better replicating of cratering-induced ground motions is known as the MINE THROW technique, after the first field event in which it was tested. The method depends on an ability to predict, in quantitative detail, the energy coupling process and the resulting pressure and particle velocity distributions within the forming crater region to times when the earth material is behaving hydrodynamically. High explosives are used to create these (initial) conditions within a pre-established volume of earth. Then, according to principles of Newtonian mechanics, the ensuing crater formation and ground motions should be identical to those that would have been caused by a nuclear source producing the same initial conditions.

The specific technique used in MINE THROW was to calculate a contour of constant peak pressure corresponding to the detonation pressure of an available explosive; this latter pressure being sufficiently great so that the earth material could be considered to act hydrodynamically. At each point along the detonation pressure contour, the specific impulse is defined by the nuclear source calculation. The high explosive source is then designed to replicate this specific impulse and the timing over which it is delivered. ANFO was selected for the MINE THROW charge in a simulation of the nuclear test, JOHNIE BOY (surface, 0.5 kt). The charge design matched the calculated pressure and impulse from about 50 to 75 kbar, and involved only a few percent of the JOHNIE BOY nuclear energy release. A schematic cross-section of the MINE THROW design is shown in Fig. 3. Representative test results are shown in Fig. 4. 5 and 6. The crater and crater-induced motions of the JOHNIE BOY nuclear event were adequately well reproduced, but surface overpressures simulation was poor. Thus, while this tends to confirm our

theoretical understanding of the energy coupling and early time hydrodynamic behavior within the crater region, in its present form, the MINE THROW technique is not suitable for field testing where airblast is a primary weapons effect. Modifications of this technique applicable to above-ground bursts where the coupled energies are a substantially less fraction of yield than JOHNIE BOY have been proposed.

A related, but less sophisticated, simulation technique for shallow buried nuclear munitions is currently being explored in the ESSEX test series. ESSEX (Effects of Subsurface Explosion) deals with simulation of subkiloton yields at shallow depths of burial (3 to 12 meters) by means of cylindrical charges of nitromethane. The choice of the explosive and proportions of the charge are based on achieving the same final kinetic energy within the crater region as predicted theoretically for a nuclear explosion at the same depth of burial and conditioning of stemming (Fig. 7). The choice of kinetic energy, a global scalar quantity, as a criterion for similitude of the cratering process is a less fundamental approach than the distribution of pressure and specific impulse in MINE THROW. Hence, the ESSEX concept lacks the same rigorous theoretical basis. Still, test results to date seem very plausible and the approach is considered promising.

LIMITED SPACE SIMULATIONS

This class of approaches to simulation is based on replicating certain mechanical effects of the nuclear explosion only over a limited region of the ground surface, usually in the immediate vicinity of a target or test item. The shock tube, a conventional example of this approach, seeks only to reproduce the airblast flow field over a very limited distance. Extensions to the shock tube concept to include airblast-induced ground motions also are under development. In contrast, the HEST (High Explosive Simulation Technique) technique developed by the Air Force Weapons Laboratory reproduces only the static overpressure conditions at the ground surface and, consequently, the resulting air-induced ground motions at shallow depths. The basic technique has been extended to incorporate certain aspects of crater-induced motions (DIHEST) and cumulative effects of the upstream airblast impulse (BLEST).

The HEST-BLEST technique has as its basis the substitution of detonation waves for the air shock. Early studies (1964) showed that detonable gas mixtures could be tailored to duplicate the overpressure and velocity of an airblast wave, but that both the Mach number and dynamic pressures of the flow field would be too low. Similar results were obtained from a matrix of detonating fuse such as Primacord, which offered considerable advantages from the point of view of handling and expense.

The HEST test bed consists of an earth-bermed chamber within which Primacord is wrapped over wooden forms to create an interwoven pattern. The "wrap angle" is chosen to achieve the desired "wave front" speed as indicated in Fig. 8. The earth overburden confines the detonation for sufficient time to effectively couple the impulse to the ground (Fig. 9). There is considerable test experience with this method and the simulation of air overpressure is quite satisfactory for times of interest (Fig. 10). Peak overpressures in excess of 1,000 psi have been obtained on HEST test beds measuring up to 300 by 300 ft.

HEST ground motion simulation is limited to air-induced effects, and then only to those associated with the wave front created within the test bed. At best, this situation corresponds to the so-called superseismic airblast condition wherein no upstream effects (due to prior passage of the airblast) are included within the test zone. In principal, the HEST bed could be extended back to ground zero, so there is no essential limitation to simulation of air-induced upstream effects. As a practical matter, however, this would not be done. The BLEST technique attempts to simulate such effects by means of explosives buried upstream of the HEST bed. The upstream loaded area is substantially larger than the HEST bed itself. The quantity and arrangement of the buried charges are selected to reproduce the total impulse of the associated airblast; the charges are detonated sequentially in accordance with the desired wave front speed. This technique currently is being utilized in a major field test.

CLOSURE

As is to be expected, this brief overview of nuclear simulation techniques has not been exhaustive. DNA is actively engaged in development of underwater blast simulation techniques, blast generators of various types, and specialized uses of explosives in conjunction with structural models. We are also conducting weapons effects and target response tests in underground nuclear tests.

Most of our simulations remain imperfect and, with the prospect of complete cessation of nuclear testing, the demands for improved and more comprehensive simulation capabilities surely will increase. The imaginative blend of test and computer-aided analysis leading to improved phenomenological understanding, model building, and facility-equipment qualification remains a challenge to us all.

The mass of test data accumulated over the years has had limited circulation and, it is suspected, constitutes a potentially useful source of information for broad sections of the shock and vibration community, especially in regard to structure-medium interaction, in-structure motion environments, and equipment response. Relatively little such data remain of a classified nature, but finding out what is available and obtaining it in usable form probably is a non-trivial task. Toward this end, the capabilities and general resources of DNA's own information center, DASIAC, and the DNA Blast Shock Master Data File are worth noting.

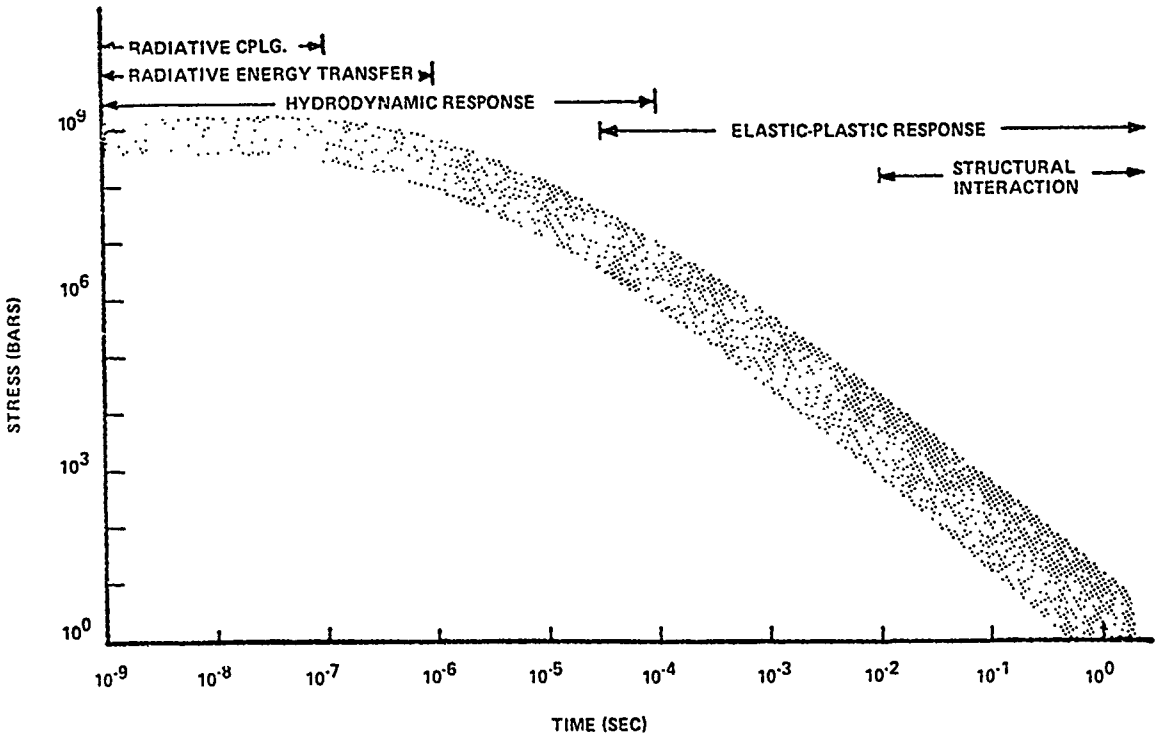

Fig. 1—Scale Range of Processes Associated with Cratering and Related Ground Motion

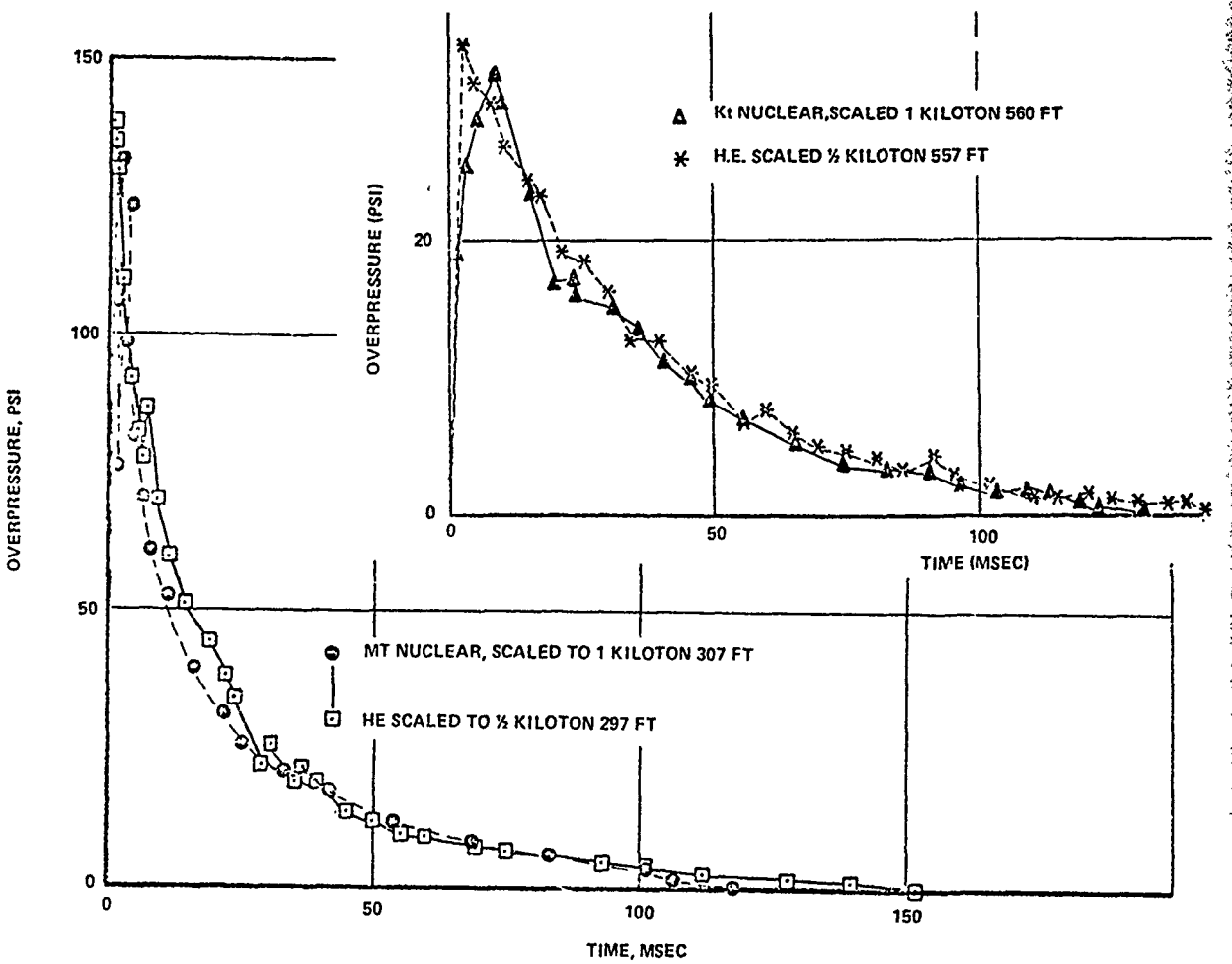

Fig. 2—Comparison of Nuclear and HE Pressure-Time Data

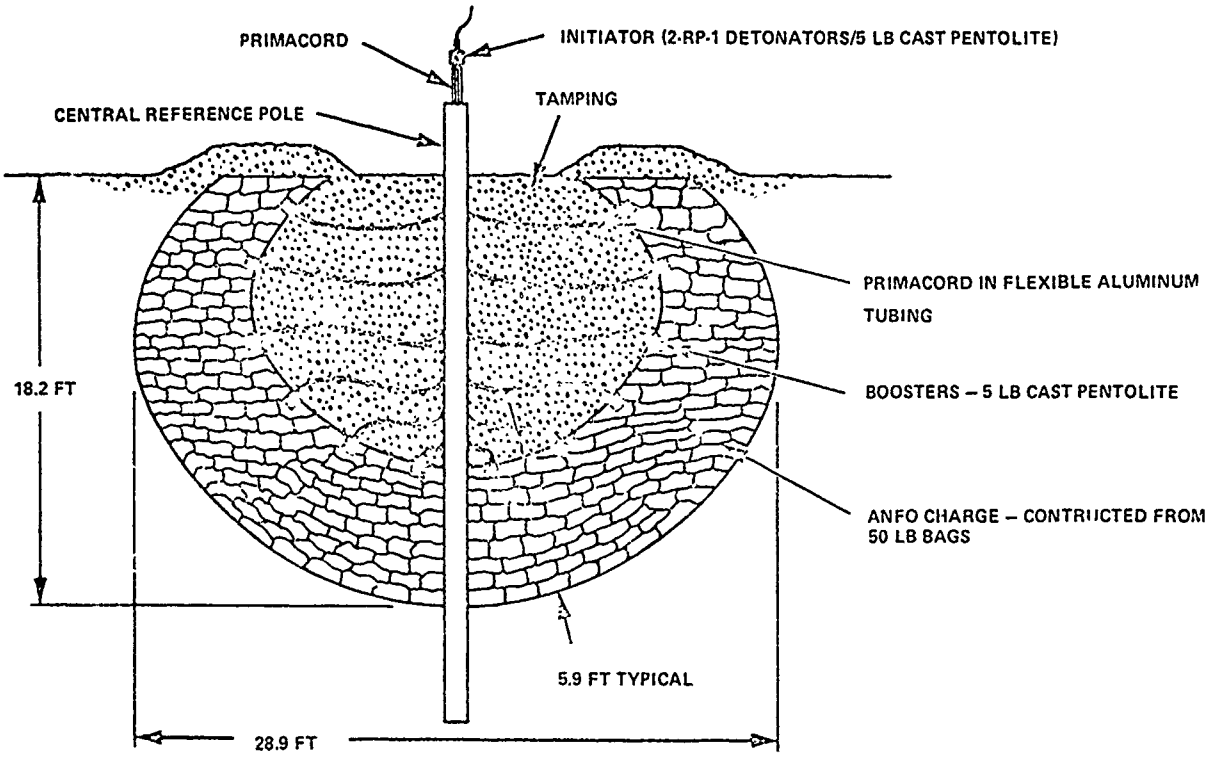

Fig. 3—MINE THROW Event - Conceptual Design

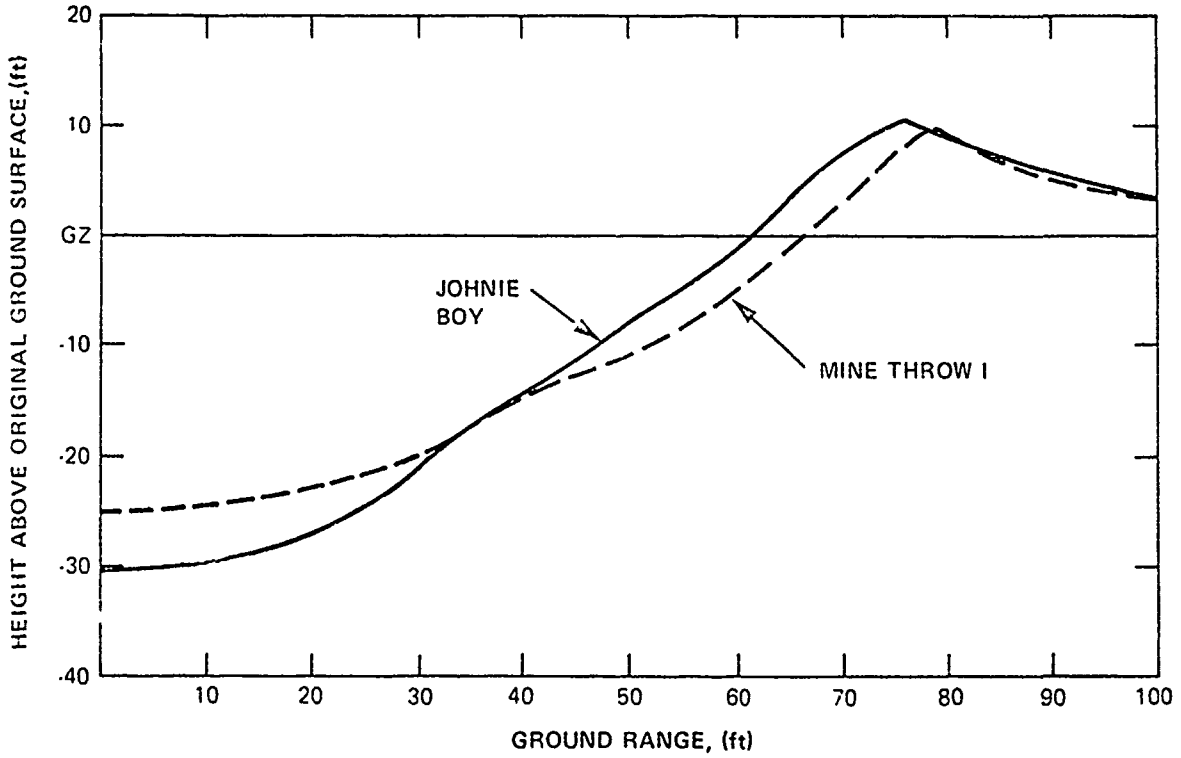

Fig. 4—Comparison of Average Crater Profiles for JOHNIE BOY and MINE THROW I

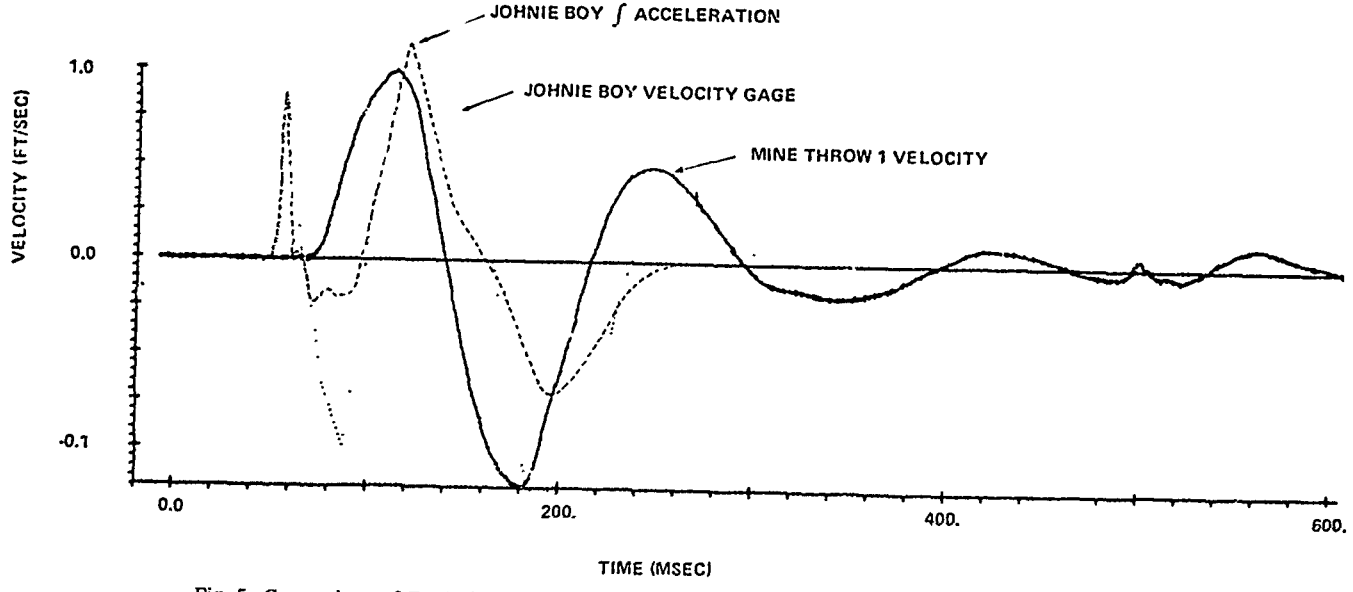

Fig. 5—Comparison of Typical Horizontal Velocity Wave Forms for JOHNIE BOY and MINE THROW I

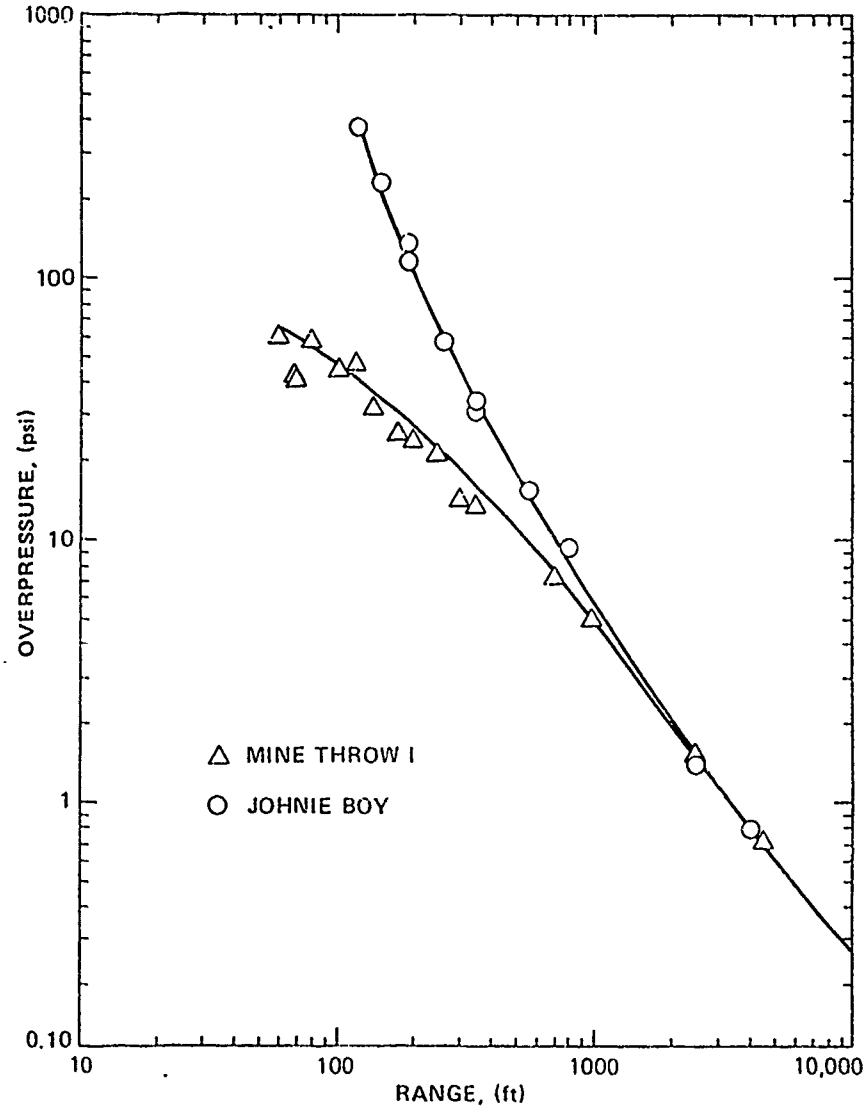

Fig. 6—Comparison of Peak Surface Overpressures for JOHNIE BOY and MINE THROW I

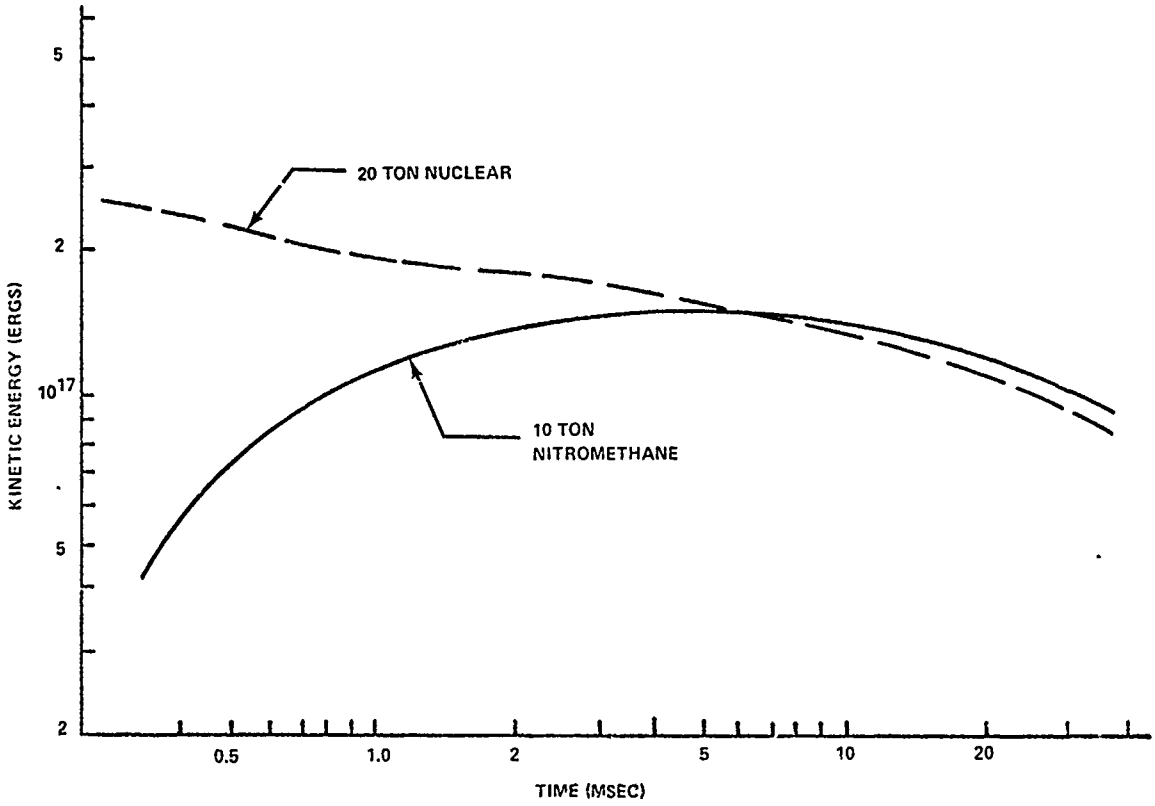

Fig. 7—Basis for ESSEX Charge Selection

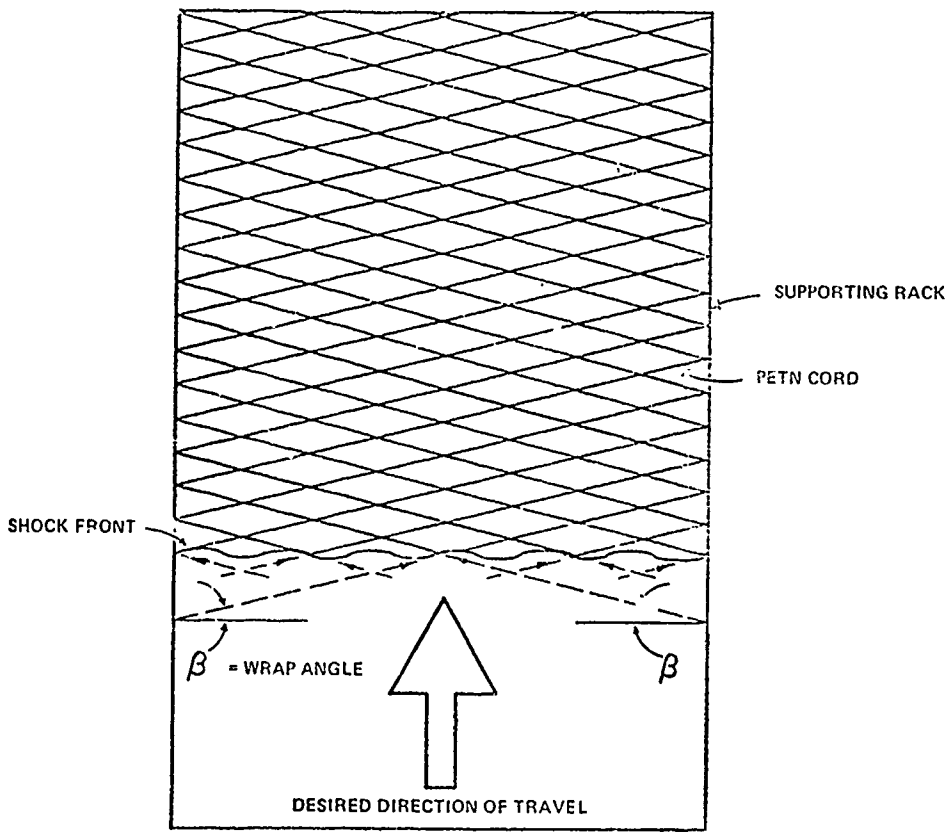

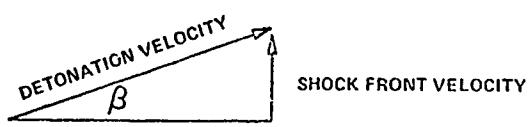

$$\sin \beta = \frac{\text{SHOCK FRONT VELOCITY}}{\text{DETONATION VELOCITY}}$$

Fig. 8—HEST Arrangement of Explosives

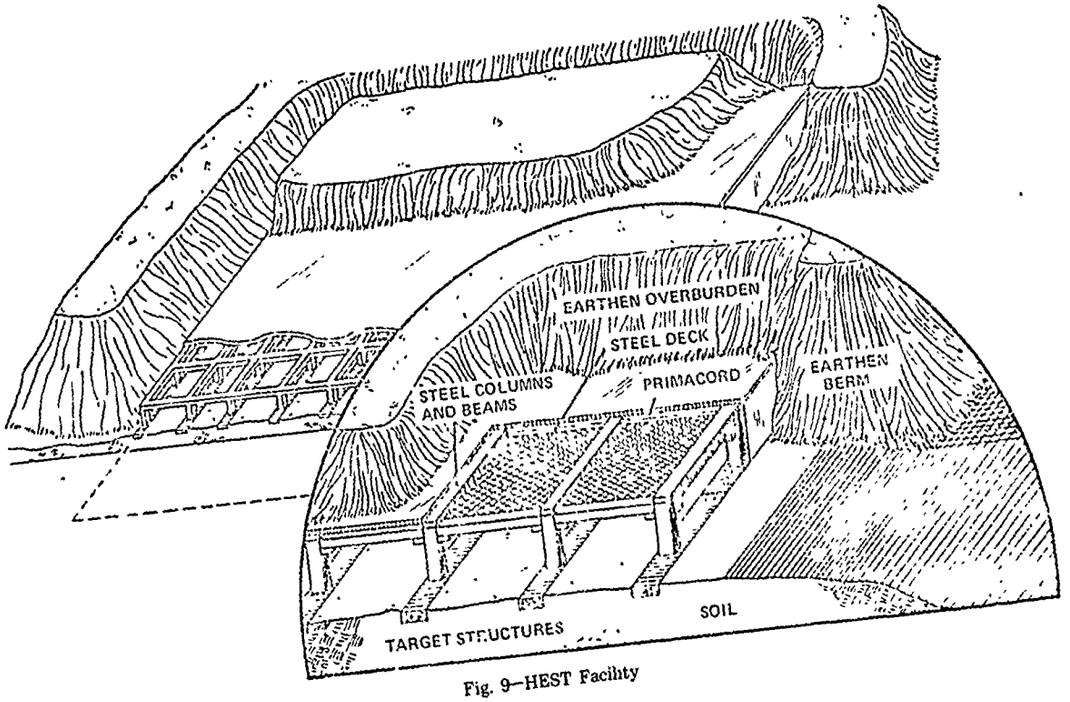

Fig. 9—HEST Facility

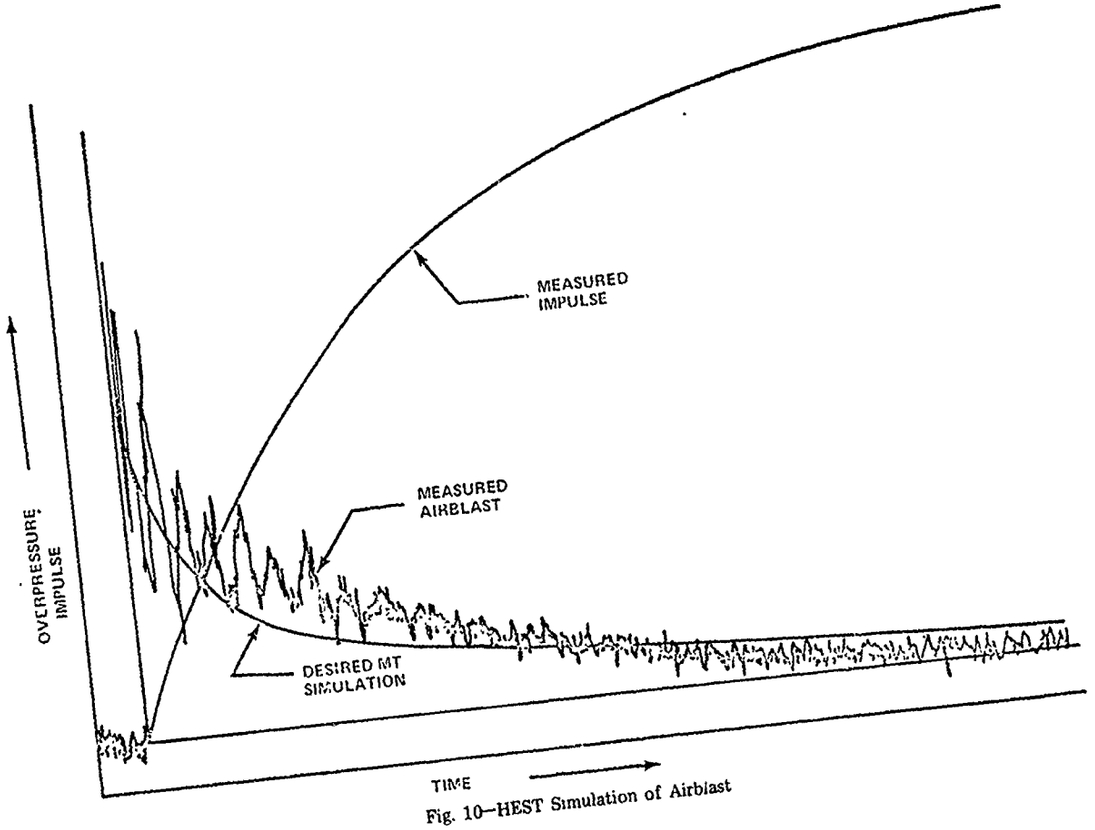

Fig. 10—HEST Simulation of Airblast

METRICATION IN THE NAVY

John Haas
Chairman, Navy Metrication Group
Naval Ship Engineering Center
Hyattsville, MD

I had an automobile with a speedometer in kilometers and at first I thought the gas prices were pretty good and it turned out to be about 40 cents for what they were pumping, until I found out it was a liter. We realize that sooner or later we are all going on the metric system and at present the Navy has a program which is being implemented in this direction. We thought you ought to know about it, because like the beginning of this year we are going to try to put in the bulletin publication at least the metric equivalent of the inch-pound Unit, that the authors are to provide. So we asked John Haas, who is chairman of the Navy Metrication Group to come in and tell us a little bit about what the Navy plans are in this area. John,

Mr. Haas: Thank you Henry. Let's take a look first at what the metric system is not. And I have to emphasize this because some of the last Figures had some terms in there that are going to have to be changed. When I first learned about the Metric System in elementary school we talked about the CGS System:—the centimetre, the gram, and the second. That's great if you're wearing a white smock. A little bitty centimetre, a gram is the mass of water that would be in that cubic centimetre, and the second. Some of the other terms, like ergs and so on are part of the CGS System.

Somewhere about when I was in high school I heard of something called the MKS System. This was more in tune for engineers. It has a metre about so big; a kilogram instead of a gram and if you fill a cubic decimetre with water, it will be about one kilogram in mass; and the second.

Even that is not what we're talking about when we use the word Metric System today. What we are talking about is the SI System, from the French "Le Systéme International" and you'll notice that the date is 1960. That was the date of the official promulgation of the ultimate measuring system, promulgated by the General Conference of Weights and Measures in Geneva and is the basis for all metric measurements today throughout the world. All of the acts before Congress say, that when we use the word metric, we mean SI as interpreted in the United Stated by the Secretary of Commerce, who of course is the boss of the Bureau of Standards. That's why the Secretary of Commerce gets in there.

There are seven basic units Fig. 2 and I want to call your attention to a couple of things on these figures. On the right hand side of all the figures I have something called the symbol. That's exactly what it is, a symbol; its not an abbreviation and there are no periods. If I have a small letter, then it has to be a small letter. If I have a capital letter, it has to be a capital letter. This is standard whether you're speaking English, French, or German; I understand even Russian, but I don't know whether they put it in Cyrillic or whether they teach it in a Latin alphabet. But at any rate, internationally, if you use symbols everybody knows what you're saying.

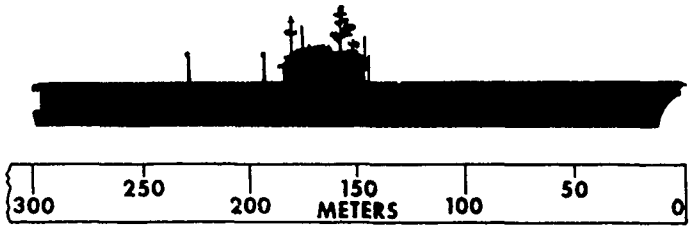

Fig. 1—Metrication and Naval Shipbuilding

QUANTITY	NAME	SYMBOL
LENGTH	metre	m
MASS	kilogram	kg
TIME	second	s
ELECTRIC CURRENT	ampere	A
TEMPERATURE	kelvin	K
LUMINOUS INTENSITY	candela	cd
AMOUNT OF SUBSTANCE	mole	mol

Fig. 2—SI Base Units

Now for the seven basis units. (1) The unit of length is the metre symbol small 'm'. Originally the meter was one ten-millionth of the distance from the North Pole to the Equator; I believe now it is defined in terms of a ceasium atom, the rays that are put out. (2) The unit of mass is the kilogram small kg, and as I said, if you fill a cubic decimetre with water it weighs approximately one kilogram. The kilogram cannot be replicated. The other six units can be replicated in any high class laboratory; the kilogram cannot. The only real kilogram is the one that's over in the air conditioned vault in Paris. If you want to know if your kilogram is as good as that one you have to take it over there and compare it with that. I might mention there is also a standard metre bar, and the United States has two that are made from that. The Bureau of Standards keeps them in an air conditioned space up in Germantown. (3) The third unit is the second, small 's'. (4) The fourth unit, electric current, is the ampere and here it gets a capital 'A'. By convention all units named after people get capital letters. (5) The unit of temperature is the kelvin, not degree kelvin but kelvin with a capital 'K'. (6) The unit of luminous intensity is the candela, little cd. (7) The amount of substance, the mole; I don't know why they bother with a symbol for this one because there is only one letter less than the actual name of it. Now, I used to say that normally engineers don't have to worry about mole; if you're a chemist yes, or chemical engineer maybe. However, there have been some suggestions made recently that gas be sold in terms joule per mole. So maybe we'll have to learn about mole anyway.

There are two supplementary units Fig. 3 in plane angle, its the radian. That's the angle subtended by an arc equal to the radius of a circle. In a plane there are two π radians around a point. The equivalent in the solid world is the steradian, and its the solid angle subtended by a unit area on a unit sphere. If I remember my math correctly, there would be in space four π steradians around the point and that is the same four π that Dr. Sevin used in his presentation before. Notice the units, rad and sr.

QUANTITY	NAME	SYMBOL
PLANE ANGLE	radian	rad
SOLID ANGLE	steradian	sr

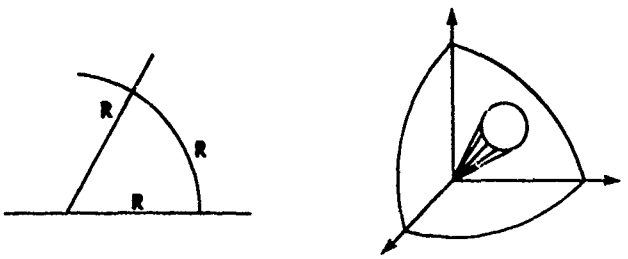

Fig. 3—SI Supplementary Units

Now for some of the derived units Fig. 4 and these are some of the easy ones. The area, square meters written m^2, or m to the two power, not sqm or something like that; it has to be written this way in SI. Volume is cubic metres, m^2. The cubic metre is going to be kind of a big unit. The equivalency is about 35 cubic feet. That's almost a barrel of oil. So therefore for ordinary use what will be used for volume is the litre and by a convenient stroke of fate, a cubic decimetre is the litre; you have a litre of water and it weighs a kilogram; it works out very nicely. That's the nice thing about SI, the constant relating the various units is always equal to one; in other words, it is a coherent system. Density is measured in kilograms per cubic metre it can be written, kg/m^3 or $kg \cdot \bar{m}^3$. Speed is in metres per second, m/s or ms^{-1}. Now I have a mistake; I have written acceleration as metre per second per second; that is wrong, the Figure should read metre per second square, and the symbol m/s^2 or ms^{-2}.

Now for some of the more complicated ones Fig. 5. The first two units here are some of those that are causing a little confusion as people start using the metric language for their calculation. We have to go back to 'f = ma.' Now in the customary system, strictly speaking, if the mass is in pounds the forces is in poundals, or if you want to use the force in pounds then the mass is in slugs. Other than scientists and physicists, I've never heard anybody use either a poundal or a slug. The result is that we use the word pound when we mean mass and we use the word pound when we mean force. If you are working in statics, it doesn't make any difference; the acceleration cancels out. But if you're designing an elevator or use some of the high power calculations for blast and so on you have to be careful. In SI there are two distinctly different units. On the previous Figure, I said the mass is always measured in kilogram. Force is measured in newtons, and a newton is that force which will give a mass of one kilogram an acceleration of metre per second squared. It is named after good old Sir Isaac, so it gets a capital N. And the unit there you will notice is $kg \cdot m/s^2$. Pressure is a unit force; in other words, the force per unit area. The pressure of one newton on one square metre is one pascal; again that's named after someone, so its Pa. The unit is newton per square metre. Now if you will think a second you know the metre is about that big (illustrating), you square it that's a pretty big area; the result is that the pascal is a pretty small unit so that in the ordinary realm the word we use is the kilopascal. As a matter of fact, pressure gages will read kilopascals; tire pressure will be in kilopascals. In round numbers, 29 pounds per square inch is just about equal to 200 kilopascals. Here is something

QUANTITY	NAME	SYMBOL
AREA	square metre	m^2
VOLUME	cubic metre	m^3
DENSITY	kilogram/cubic metre	kg/m^3
VELOCITY,SPEED	metre/second	m/s
ACCELERATION	metre/second/second	m/s^2

Fig. 4—SI Derived Units

QUANTITY	NAME	SYMBOL	UNITS
FORCE	newton	N	$kg{\cdot}m/s^2$
PRESSURE	pascal	Pa	N/m^2
ENERGY, WORK, QUANTITY OF HEAT	joule	J	N·n.
POWER (RATE OF DOING WORK)	watt	W	J/s

Fig. 5—SI Derived Units

else in SI, when you have a term for a certain quantity you use it for all variations of that quantity. In the customary system we use ft. lbs, BTU, and goodness knows what else. In SI there is only one term used and that is the joule and a joule is the amount of work done by a force of one newton acting through a distance of one meter. The symbol is 'J', and the unit is just newtons times metres. Power is the rate of doing work, the joule per second. Lo and behold it comes out are old friend, the watt. The same watt we've always used; gets just a 'W' for the symbol and the unit is 'J' over 's'.

Now for those of you who work in electricity Fig. 6, current was a basic unit, the ampere. Power we just developed in the last Figure. You divide one by the other, you get volts. Resistance, you divide the volts by the current you get ohms of resistance, the symbol the Greek omega. And here we come to a problem, the first of a couple of problems; most typewriters can't print omegas so the various metric bodies have asked the typewriter manufacturers to start putting more keys on their typewriter key board. However, it isn't so bad because its only three letters "ohm", so if you have to spell it out rather than using a symbol, its not too bad. Frequency, this one caught on like wild fire. A hertz (Hz) is a cycle per second. Cycle has no unit, hence, its just s^{-1} or one over s as the unit for frequency.

Let's take a look at temperature for a moment Figure 7. On the left we have the old Fahrenheit scale. Good old Mr. Fahrenheit back when he invented this scale got the coldest thing he could get which was a salt solution and he said you can't get anything colder than that so he said that's zero. On that scale he came out with 32° for the melting point and for the boiling 212°. I've got a line through the middle which is normal body temperature in case you haven't recognized it. On the right hand side is the SI System. The kelvin starts

QUANTITY	NAME	SYMBOL	UNITS
CURRENT	ampere	A	(basic)
POWER	watt	W	J/s
VOLTAGE (POTENTIAL DIFFERANCE)	volt	V	W/A
RESISTANCE	ohm	Ω	V/A
FREQUENCY	hertz	Hz	s^{-1}

Fig. 6—SI Electrical Units

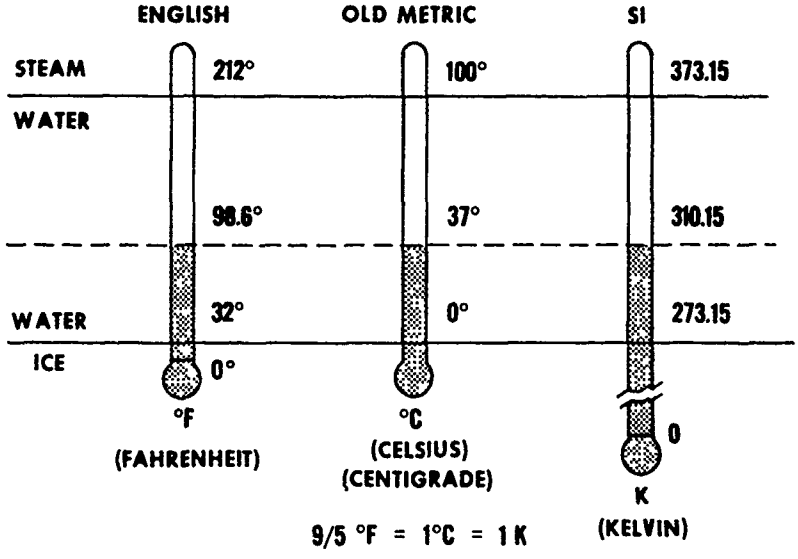

Fig. 7—Temperature Measurement

down at absolute zero; hence the melting point is 273.15 K and the boiling point 373.15 K. However, the thermometer that we'll be using in ordinary engineering practice is degree Celsius, not centigrade; that went out in 1948 but the word just won't go away; it just hangs on. At any rate, in SI its degree Celsius. It goes from zero to hundred and you'll notice that the temperature interval of one degree Celsius is exactly equal to the temperature interval of one Kelvin but of course the actual temperature of any particular body is a different number depending upon that 273.15.

Now quite obviously with a set of basic, supplementary, and derived units we are rather limited unless we can go up and down the scale without bringing in a lot of big numbers. So we have a whole series of prefixes. Now this is the "up" scale Figure 8. To the linguist, why I believe these are Greek letters; the "down" scales are in terms of Latin Prefixes. You'll notice at the bottom I say that deha and hecto are not recommended. That's because SI recommends you jump by cubes, or by a thousand in other words. So you jump from meter to ki·'Lo·me·tre (not ki'Lo·me·tre; that's a

MULTIPLYING FACTOR	PREFIX	SYMBOL
1 000 000 000 000 (10^{12})	tera	T
1 000 000 000 (10^{9})	giga	G
1 000 000 (10^{6})	mega	M
1 000 (10^{3})	kilo	k
100 (10^{2})	hecto	h
10 (10^{1})	deka	da

(hecto AND deka NOT RECOMMENDED)

Fig. 8—SI Multiple Units

British affectation). The words are kilometre, megametre, gigametre, terrametre. To show you how fast things change, in June of this year there was a meeting in Geneva and they added two more: peta and exa; I don't remember which is which, but one is ten to the fifteenth and the other one is ten to the eighteenth. Maybe for some of those blast problems you need a ten to the eighteenth. Notice the symbols they have, you have some capital letters here; they are not named after people but they didn't want to use the small letters like small 'm' is already used for a couple of things so therefore it is a capital 'M' for mega and capital 'G' for giga (jig-a). If you go to England, incidentally, they will call that 'giger' (hard "g").

Down the other direction (Figure 9). Deci and centi are not recommended; I said this was a decimetre on the side of this cube. The only known use so far for the decimetre will be for draft marks on a ship. Centimetre will be used for body measurement, hat, clothing sizes, glove sizes, and shoes. As far as we as engineers are concerned, the milimetre is going to be the important dimension. By international agreement the millimetre is always used on engineering drawings. Now for large ship we will probably use metre with decimals of a metre, but say the size of a large compartment. General Motors has carried this so far that they are even expressing the entire length of an automobile in terms of millimeter and it comes out about these new short cars are about 6000 millimetre long. Next, below that, we have the micrometre. Here's a little interesting thing, that symbol 'μ' is another one you don't have on the typewriter, but you can use a small 'u' and put a little tail on it if you have to. The 'μ' used to be used for the micron; well it just happens that the micron is exactly equal to a micrometer so the word micron has been out for about eight or nine years and the word is micrometre, or a meter times 10^{-6}. Nanometer, the pico (I remember years ago hearing about that one; electronics people talke about the capacitors measured in picofarads). Femto and atto, all the way down to the little bitty things.

I shouldn't use this next figure (Figure 10) because you should think metric, you shouldn't need equivalents. However, it is still nice to know just how they match up. Well one inch is equal to exactly 0.0254 metre and there is a mistake on that line too; there should be a zero in front of the decimal point that's another standard SI rule. Another rule is that numbers should always be broken into groups of three. Notice down the bottom that I say a pound of mass is 0.453 then space 592 space 37; I say that's an exact number also. The rest of the world uses a comma where we use a decimal

MULTIPLYING FACTOR	PREFIX	SYMBOL
0.1 (10^{-1})	deci	d
0.01 (10^{-2})	centi	c
0.001 (10^{-3})	milli	m
0.000 001 (10^{-6})	micro	μ (mu)
0.000 000 001 (10^{-9})	nano	n
0.000 000 000 001 (10^{-12})	pico	p
0.000 000 000 000 001 (10^{-15})	femto	f
0.000 000 000 000 000 001 (10^{-18})	atto	a

(deci AND centi NOT RECOMMENDED)

Fig. 9—SI Decimal Units

1 inch = .0254 metres (EXACT)

1 meter = 39.37 --- inches

= 3.281 --- feet

= 1.09 ---yards

1 km = 3 281.--- feet (APPROX $\frac{5}{8}$ MILE)

100 m = 328.1 --- feet

1 pound (MASS) = 0. 453 592 37 kg (EXACT)

1 kg = 2. 2046 --- pounds

Fig. 10—Common Equivalents

point. So SI says you may use a comma or decimal point for the decimal marker; as a result of that, however, you are not supposed to use commas in the rest of the places to avoid any possibility of confusion. So the idea is to leave spaces. I say this chart will just give you a kind of a quick feeling because everybody knows that a kilometre is about 5/8 of a mile, and the kilogram of water is about 2.2 pounds.

Now for some of the more complicated ones (Figure 11). A pound of force is equal to exactly 4. etc., newtons in other words about 4-1/2 newtons for a pound of force. And getting down there to the pascal, you can see why I mentioned before that 29 pounds per square inch is just about 200 kilopascals. In the last presentation the word bar was used. Well the bar is almost equal to an atmosphere and it is defined as exactly 100 kilopascals. That's about 14.5 pounds per square inch, roughly.

Now for Marine use (Figure 12), of course we use the long ton (not the short ton) and that's 2240 pounds and it's very interesting that it is only 1.6 percent different from the metric ton. Strictly speaking an SI purist would use the word megagram, but that sounds kind of funny so we will probably use the word metric ton for that purpose; that's a thousand

1 pound (FORCE) = 4. 448 221 615 260 5 newtons (EXACT)

1 kip (FORCE) = 4448. 221----newtons

1 newton = 0. 225 ----- pounds (FORCE)

1 kN = 225. ----- pounds (FORCE)

1 pound/sq. in = 6 894. ---pascals

1 pound/sq.ft = 47.88 ----pascals

1 kPa = 0. 144 ---- pounds/sq.in

Fig. 11—Equivalents for New Units

1 Long ton = 2, 240 lbs
= 2, 240 × 0. 454 --
= 1 016. --- kg
= 1.016 --- metric tons (tonnes)
(DIFFERENCE = 16 kg or 36 lbs or 1.6%)

1 nautical mile (INT./U.S.) = 6,076. ---- ft
= 1 852 metres (EXACT)
1 knot = 1 nautical mile/hr
= 0. 514 444 --- m/s

Fig. 12—Special Marine Equivalents

kilograms. Another special marine term is the nautical mile. That was redefined about five years ago to be exactly 1852 metre. Now some people remember that the foot equivalent was about 6080, well it was but its now 6076 something; but the definition is 1852 meters, exact, the knot, of course, is the nautical mile per hour and it comes out pretty nearly a half a metre per second. There has been a lot of agrument just very recently about what to use for wind speed; I find out that internally within the cult of weather people, they transmit wind speeds in metre per seconds then change it over to what they think the populace wants to hear. Of course the Department of Defense, the aviators, and ship navigators, and so on, they all want to hear knots. Now up in Canada they are beginning to broadcast ordinary wind information in kilometres per hour. I don't know what is going to happen in this country. DOD is opting to keep the knot (it's permitted by SI for a "while"). I don't know how long a while is but it is permissible to use it with SI units.

Well, there we are (Figure 13); that was 1972 and you'll notice those powerful allies that the United States had. They've since been reduced; as of today, other than the United Kingdom, Canada, South Africa, Australia, New Zealand, India, are all going metric. As a matter of fact, I guess the two gung ho countries right now are South Africa and Australia.

BURMA
GAMBIA
GHANA
LIBERIA
MUSCAT AND OMAN
SIERRA LEONE
SOUTHERN YEMEN
TONGA
TRINIDAD
UNITED STATES

(ALL EXCEPT LIBERIA ARE FORMER BRITISH COLONIES)

Fig. 13—Non-metric Countries (1972)

Historically, France, of course, was the first to adopt the Metric System, the United States legalized it all the way back 1866. As a matter of fact no body can find any legelization of the present system. So you might say that the Metric System is the only legal system in the United States. An then, really earth-shaking was in 1875 when the United States was a signatory to the International Metric Convention; that's a piece of paper not a meeting. And in 1893 the United States adopted the Metric System or standards. Practically nobody knows this, and that's why on the previous chart I defined the inch and the pound because that is the legal definition. In other words, if somebody says what is an inch? It is defined legally as 2.54 centimetre. And then in 1971 the Secretary of Commerce completed a three-year study and sent it to the Congres and recommended that we go metric according to a certain time. In addition to the basic report, there are ten or twelve volumes that go with it. The DOD report was so lengthy that we have a volume all our own, I think Volume 8. I might mention that DOD estimated that the cost of metrication would be about $18 billion over a twenty-to thirty-year period. Nobody, including the Bureau of Standards, believes that figure, however. The cost of metrication is extremely difficult to get at, even in england, Australia, with all of their progress and companies that have gone metric. General Motors right now is probably most gung ho of all the companies in the United States, they can't tell you what metrication cost. As a matter of fact they will probably tell you that they have saved money; in other words, it's cheaper because it is so much easier to use the system; no fractions, you just take an ordinary millimetre scales and read it off.

Now what the Secretary of Commerce said is that one course is to just sort of drizzle along. The other course is to have some sort of a planned coordinated activity. The constitutional lawyers will tell you that there is no way for the Congress to pass an act saying that everyone is to start using metric tomorrow. The states can do it because they control speed limits; localities can do it because they control the scale the butcher uses to measure your meat; but there is no way for Congress to do anything. Other citations taken from the study give an indication of what companies thought; now I used the manufacturing industry because I figure that's close to shipbuilding. The big companies tend to like it. Also, metric users tend to like it and even the non-users kind of like it. One finding was really surprising; in spite of the fact that it cannot be mandatory, 43% recommended that there be a mandatory program, 50% a voluntary program, and only 7% no program. Also, 3/4 of the people said you could do it in five years. And you know

this isn't a pipe dream; England started in 1965 and expected to be completed in 1975, but they're not going to make it. I was over there last year and I think it will be 1980 before you can get engines, pumps, compressors, and so on in metric units. Australia started about 1971 or 1972 and they are probably going to do it in about five years; they said that in ten years you lose your impetus. They say to stop fooling around and get going and start metricating; that is all there is to it. When the study was concluded, the Secretary of Commerce recommended that there be increased use of the system, that we change by a coordinated national program, and that we base everything on a ten-year period.

In Congress last year, there was a metrication bill in both the House and Senate; unfortunately, due to a parliamentary maneuver when it came up at the House it lost. It was put in under a special rule that wouldn't permit any amendment and more people voted against it than for it, so it died in that Congress. However, in the new Congress, bills went in again but were some what modified. The so-called administration bill sets up a metric conversion board just as this did. It does not give a time period, there does not have to be a plan submitted to either the President or Congress, and it omits all those sticky issues (should you pay the mechanic something to go to school and retrain?, pay him for his tools? and things of that sort). The new bill says merely as these obertians come up, the board may recommend appropriate legislation to the Congress. It came up and went through the Committee in the House and 5 September, then passed in the House by a vote to 300 to 65. Hearings were held in the Senate on 8 and 10 October just a week or two ago. It is expected that there will be a vote very shortly in the Senate and its expected that it will pass; the President has said he will sign it when it comes to him. So we expect that there will be metric legislation before the end of this year.

Meanwhile we've got a big void. General Motors announced, on the 13th of April of last year, a corporate decision to go metric. And, as you know, "as General Motors goes, so goes the entire mid-west". They've got 35,000 suppliers and shops and so on and when they start using metric and see how easy it is, they are going to start using it for their ordinary purposes also.

Meanwhile the American National Standard Institute stepped in to the void and established the American Metric National Council, made up of various companies, the various industry standardization bodies, and other. We have a DOD man on the Board of Directors who is the Chairman of the DOD Metric Panel. There is a special group the Metric Practice Committee that worries about what kind of units to use; I happen to be the DOD member of that committee. Then we get down to the five big coordinating committee areas. I don't think there are any DOD people on the five coordinating committees themselves but when we get down to the separate committees we are all over the place. Under the industrial area, there is a Marine Committee and I'm a member of that. In the primary materials area, we have people in the steel, metals committees and so on. There are a lot of DOD people in this area working with the sectors.

In DOD under Mr. Bennett, the Assistant Secretary of Defense for I&L, there is the Defense Materiel Specification and Standards Board chaired by Mr. Gansler, Now there are several panels under that, and one them is the Metrication Panel. The OSD man from I&L, is the chairman of that panel; there is also a member of R&E, and a single man from Army, Navy, Air Force, and DOD (Iam the Navy member of that panel). One of the things we did was to write the policy memorandum which Deputy Secretary Clemments signed on 10 June 1975. And in that we said that in designing new systems we must give consideration to using metric units, and then to make it stick, after 1 January 1976 all will have to use metric units or justify why not. Also, all R&E reports, position papers, studies after 1 January 1976 have to use metric units in lieu of or in addition to conventional units.

In the Navy we have an Instruction put out by the Secretary of the Navy which directs the Chief of Naval Material to establish a Navy metrication group and get working on seeing how the Navy should metricate. NAVMAT issued an Instruction in February 1974 and, by name, I am designated as chairman of the Navy Metrication Group and I also wear another hat as the Navy Metrication Project Officer. Basically we are a catalytic group; we find out what is happening all over the world, in the Nation, and so on, and feed it to each other to get the word down into the Systems Commands and the other levels within the Navy Department. One of the things we've come up with is a ten-year implementation plan, and we have sent that up the line. I have to report to the Assistant Secretary of the Navy (I&L) every month on what we are doing. And in the latest of those reports we included the implementation plan; it was concurred in by CNM and by CNO, and is now under study by the Secretary. One of the most intriging things in there is that at least tentatively, we've picked New Year's Eve 1980 as "M" day for the Navy. Now I mean, actually for naval operations, because by that time we should have all the general purpose manuals converted. We are not going to convert any existing equipment and we are not going to convert the manuals for any existing equipment ment; they will stay the way they are. We are not going to change any existing designs, we have a standard hatch measuring 24" X 24" and it is going to stay that way. Maybe in 10 or 15 years somebody will start to convert it. But any new hatches will be in metric units. We are starting this off with some of our new specs. Just recently we had a spec for a chronometer, one of these new crystal control gadgets. It is a brand new item, it is going to be with us for the next 25 or 50 years, so we put it out in metric dimensions.

Finally, some of the problems, Lets start with the easy one, the consumer-oriented problem. Just take a look at the grocery shelves; practically every can you see nowadays has both for the mass and you know it is always a fu y number like 1 lb. 13 oz. or something. You will aso see a funny number for grams because they are soft converted. Eventually they will get around. Liquor bottles are all going metric and others who will have to follow suit. But you don't buy things by weight or mass; you buy a big can or little can, or a little box or a big box. Even for gasoline, you say "fill it up" or you say "$5 worth". But nobody measures how many gallons or litres you want.

At the intermediate area I think is the engineers. NASA, since 1964, has been writing all of its reports in metric and the PHM which the captain mentioned before is a metric ship. Now not because metric is so good, but because it is a NATO Ship and the other countries said if you don't make it metric we don't want it. Now what do I mean when I say the PHM is metric. The basic ship is in metric modules, basic range, area, and so on are metric; everything designed for the ship is metric. Now are the pumps and compressors metric? No, they're not. However, you can use an ordinary type of compressor that speaks of customary standards. You can get the pressure gage on it to report pascals; there's no problem in that.

A little bit more difficult and I think a serious problem—manufacturing—the various tools that are used, I mean the big machine tools. But even these—companies like Vickers have jumped in—they've got little gadgets—you unscrew a little plate and take a new one and put it in and it's got metric cutting, and so on. Six months ago I would have told you one of the major problems was screen threads. Today it's not even a problem. In May and June of this year, ANSI and DIN (West Germany) had a little coffe klatsch over in Germany and they decided that screw threads would use the ISO modified the way the U.S. would like to have it modified. Once Germany agreed, ISO agreed, and in June at an official meeting the ISO adopted the U.S. Modified ISO Thread. It's now being written in the form of standards and in a very short time we should have metric screws all over the place.

These are slides of posters that were used in Great Britain. One of the things they believe in very thoroughly is saturation. NASA did the same thing. They put posters all over, down in Huntsville. I think Huntsville, Alabama, is the first place in the U.S. that has speed limits in kilometres per hour. "This is not a foot, it's 300 milimeters; think Metric." And hidden behind the shadow of the viewgraph machine is the symbol of her Majesties Metrication Board. Incidentally, in England, shipbuilding is so important that there is a member of the shipbuilding industry on the Metrification Board. I think we'll be lucky if we get a third deputy clerk in there. "Stamp one hundred milimetres on your mind" and notice how consistent that that milimetre is written 'little m, little m'. "Down a liter, think metric." England has just changed and they are going to drop that "me" at the end of gramme and they're going to spell it the same as we do—just gram.

I've already told you what this is (exhibiting a cardboard decimetre); its a kilogram of water, it's a cubic decimetre of space, and so on. This publication is the official English translation of the international rules; it's known as NBS publication 330, and if you ever want to know the history of why a certain unit is called what it is, why centigrade was changed to Celsius (and there is a valid reason why it was), you'll find all that explained in here. Within DOD, ASTM E380 is the bible; we did not write our own new standard because this was a very good one. Its the 1972 edition and inside on the front cover you'll see a DOD acceptance notice which makes this just like any other Mil-Spec or standard. There is also a 1974 edition, but you don't have to worry; there are about 20 insignificant changes between the two editions. Either by the end of this year or next year, there will be a new American National Standard out; I'm also on the committee for that and it will be a combination of ASTM E380, of the similar IEEE publication, and they will also pick up some of the goodies from NBS 330, all in one place. For the typists in the office or writers, AMNC has put out an editorial guide, very nice, small, and it fits in your pocket or your desk drawer. It's not for engineers, you have to use the other books. A company up in New Jersey puts out a nifty little slide rule. Practically every company has something. I think that Sears Roebuck is putting one out within the next few months. Sears is quite gung ho and they have all their text written for the catalogues, the yellow pages describing all about how to buy your clothing in metric. I think they're just waiting for the national legislation and then the catalogue will be all ready to go.

PANEL SESSION

VIBRATION REQUIREMENTS FOR RELIABILITY DEMONSTRATION TESTS

Moderator: Dr. A.C. Curtis, Hughes Aircraft Co.
Co-Moderator: Robert N. Hancock, LTV, Vought Systems Division

Panelists: David L. Earls, Air Force Flight Dynamics Laboratory
Terry W. Elliott, Pacific Missile Test Center
Joseph Popolo, Grumman Aerospace Corporation
Dick Baker, Hughes Aircraft Company

Dr. Allen Curtis: It was stated in Colonel Swetts report a year ago that field reliability can be as small as one tenth of that demonstrated in the laboratory (1). The report suggests that the major reason for this is that the environment which we used during reliability demonstrations testing is not sufficiently like the field environment and therefore we don't create enough of the right kinds of failures in the laboratory His solution was to suggest that the requirements of 810C or something like that should be used during rel-demo testing instead of those that are typically used now as called out in what is called MIL STD 781B. Colonel Swetts report has had a lot of impact and initiated a lot of efforts. I might mention just a few. A revision to MIL STD 781 which would be the C version is in coordination. I understand that from the vibration point of view what it calls for is as far as I can interpret it anyway, it calls for two tenths of a g squared per hertz from 20 to 2000 Hz which I think comes out to 20 g's rms and this would be instead of the present single frequency non resonant 2.2 g amplitude vibration that we have used so far in rel-demo testing. On the Navy side they have come out with several new AR's or Aeronautical Requirements and 104 A which likewise is in coordination, indirectly calls for random vibration, I guess, or it says that the vibration shall be the same or similar to that in the field. I know in our own company over the last six months we have received a number of requests to substitute random vibration for the typical MS 781 sinusoidal vibration on projects that we either have currently going or expect to have in the future. Colonel Swetts report also started a program at Wright Field called a Combined Environment Reliability Test Program (2) which was to see if we could replicate field failures in the laboratory and we will hear a little report on this in a few minutes. We at Hughes have had a study from Rome Air Development Center (RADC) called "Operational Influences On Reliability" (3) which is a study to see if one can sort out the parameters which effect field reliability to find out what the causes are or how the failures are proportioned amongst different causes. We will have a little report on that. At Grumman again under contract from RADC they have been working for I guess about two years now on the study program called "Evaluation Of Environmental Profiles For Reliability Demonstration" (4). Lastly an effort I would like to mention is that the IES under the leadership of Bob Hancock has been paying attention to this problem and if we have a few minutes at the end of this session I promised Bob that I would let him get close to a microphone. I think if I may express my own view for a minute I think that we have a two things. I think there is a problem in how we should improve reliability demonstration tests but also I am concerned as a taxpayer because we want to

make sure that we spend money wisely and do not fall into the trap of overkill and expect that for instance if we upgrade the environment in rel-demo tests that this is going to solve all the problems in the world. Well I think it perhaps time to introduce the gentlemen sitting up here with me. To my immediate left I would like to introduce David Earls from the Flight Dynamics Laboratory, Wright Field, who I am sure you all know has been very active in the requirements of 810C and vibration requirements for Air Force equipment and he has been heading up the program I mentioned a few minutes ago on "Combined Environment Reliability Tests." To my far right I would like to introduce Terry Elliott, who is head of the Environmental Test Branch at the Pacific Missile Test Center at Point Mugu. Terry has been in the environmental test and reliability testing of Navy Missiles. He and I are well acquainted as he has been Washington's watch dog on the Phoenix Program down in Culver City for several years and kept has me on the straight and narrow. To my immediate right Joe Popolo of Grumman Aerospace. Likewise he and I worked together on the Phoenix program and he has been working on the Grumman study from RADC that I mentioned a few minutes ago. The program also lists Hunter Comstock from General Electric Company, but unfortunately at the last moment he had to cancel out on us. So the gentlemen to my extreme left is Dick Baker from Hughes Aircraft Company who manages the product valuation department which for one thing runs our environmental lab and another thing contains our reliability analysis activity which conducted this study for RADC. For the format of this panel session I am going to try something a little bit new; first of all, requirements for rel-demo testing is a pretty broad field. What I hope we can do is try and keep the discussion on the vibration requirements for those kinds of tests. We are going to have two very short presentations by Dick Baker and David Earls and after that I made up a collection of questions which I am going to direct at the panelists. They haven't seen the questions yet and I thought that might help to keep it spontaneous but I have arranged the questions hopefully to deal with a certain aspect of this whole thing. So I thought if we asked a question and had a couple of answers from the panelists and some from the audience then we will move on to the next question and in that way perhaps we can cover a number of aspects of this whole thing. So first I would like to give the microphone to Dick Baker who will briefly review the results of our study called the Operational Influences on Reliability."

Dick Baker: If you read your Bulletin you will notice that Allen Curtis was really on the docket to give this presentation but you will also notice that it said it allotted five minutes for it and I think after we went over the data earlier this week he decided it was impossible to hold it to five minutes so he conned me into doing it. It isn't right for the Chairman to run over. Before we start the slides there are a couple of things I would like to say about this study. The first thing is that the data that you will be seeing here is prepublication data. The study is still going on but the major effort is to wind up this month. It kind of looks like it will probably get published by RADC sometime after the first of the year. The second item I would like to cover is that this study was unique for two reasons. First of all it attempted to cover a really broad statistical sample from which you could draw valid statistical conclusions and I think we have come close to that if not reached it. The second thing I think that makes it unique is that the data was based completely upon the official Air Force data. In other words there should be no bias imparted by the study people since the source data is all official Air Force data. OK, if we can have the first slide. The basic objective of the study was to identify the reasons for the differences between the predicted reliability, demonstrated reliability and the field reliability for Air Force Avionics type equipment. The key elements of this study are the inclusion of all five of the Air Force operating commands. This wound up including ten weapons systems or air craft and sixteen avionic equipments with thirty applications. Some of the equipments were used on more than one aircraft and that

adds a real element of interest as you will see later. Finally, it does represent over a million hours of equipment flight hours as the data base. The data base was one year ending July 30th of 1975. Regarding the equipment that were studied, the oldest went into the Air Force inventory approximately eight years ago and newest about a year and a half ago. The study sponsor is Rome Air Development Center. Could I have the next slide? This next chart is kind of a busy one and I apologize if those of you in the back can't quite see it but these are the sixteen equipments that make up this study sample in this column. We had immediate problems since these equipments are of different complexities, and types and how do we relate them in some way to normalize the data. We decided that one possible way to do something like this is to normalize it about its contractually required reliability, therefore making the assumption that somehow the required reliability reflected the complexity of the equipment. From that standpoint then we have made the first three headings here. I will read them off if you can't see it. Predicted Reliability, over the Required Reliability. Demonstrated Reliability over the Required Reliability, and the Field Reliability over the Required Reliability, and for those of you who can read down the columns you see that the variation under each of these columns are considerable and with apologies to any statisticians that are here we have just for convenience actually here we have just for convenience made a gross average of those columns and you can see that the predicted reliability compared to the required for these sixteen equipments turns out to be better than two; 2.24 as a matter of fact which says something like the contractor is kind of optimistic in his predictions. The second column dealing with the demonstrated reliability the average for all these come out to be slightly over one, 1.18 and this ties in with Colonel Swetts report saying that the demonstrated reliability tests tended to come out a pass because of the vested interest of both the contractor and Air Force in passing these reliability tests at the late time in the development cycle when they are done. This would tend to corroborate that. The third column there is field reliability, now this is based upon the 66-1 data collection system for the Air Force which is their basic field data collection system. It calculates an MTBF by taking basic maintenance data and removing those maintenance actions not attributed to a true failure, and then divides that by the total flight hours. They come up with an MTBF then which is .29 so it is a little worse than 3 to 1 but that is quite a bit better than the 6½ to 1 or 10 to 1 that we have been hearing about. There is a basic problem with the MTBF number that comes out of the flight field data, the 66-1 data, and that is that both the predicted and the demonstrated are based upon equipment operating hours and that third one is based upon flight hours. As it turns out there can be quite a difference in this time base because some equipments, because of their nature and whatnot, are on much longer than the actual flight hours and so during the study we were able to come out with a means of approximating what that difference was between the actual equipment on hours and the flight hours and that's what is meant by this K factor. So it is flight hours over operating hours or equipment hours over flight hours and you see it varies from slightly over 1 to 2.65 and again the gross average is 1.6. It's quite significant that its an elastic yardstick we are using. If we take this into account and calculate field reliability over required reliability but use the K factor to adjust for this difference in time base we come up with an adjusted field reliability over required reliability that comes to about four tenths, a factor of 2½ to 1. Now we also had access to a number of special kind of reliability studies that have been done, some of them by independent agencies like Arinc specialized programs like a category 2 test, where there is a lot of attention focused for a specific and usually fairly short period of time looking at a particular piece of equipment. The failures tend to get pretty well identified whether they are a true failure or not as opposed to some of the soft definitions of failure. For those equipments that had reports like this in the files we got this kind of information and again a gross average indicates that its getting up to .7. Very interesting! The next area over there we take the theta R which

is the adjusted field failure rate, adjusted for this equipment operating hours, compare that with demonstrated and we tend to come out with about .38. On our sample we would say that on the average the difference between the demonstrated value and the field value if we adjust for the same equipment operating hours, and use the same base, it comes out close to .38. Next we partition the data according to application. We are trying here to get some idea of what the differences are. What the influences are. We divided up the sixteen equipments into these two broad classifications, the high performance type of aircraft versus the low performance type of aircraft and you see that the predicted versus field reliability and the demonstrated versus field reliability are essentially no different, but when you look out at the adjusted field reliability over required you get over a two to one difference. This would strongly infer that there is a significant difference between high performance aircraft and low performance aircraft. Next slide please. Next we looked into the category where we had the same equipments on different kinds of aircraft. We look into things like the aircraft types, the operating command, duration of the mission and the utility rate which is how many flight hours per month. This particular piece of equipment is on six different aircraft and the required reliability for this particular equipment is 450 hours MTBF. It was predicted better than twice that by the contractor. It was demonstrated to be slightly better than what was required, and look at what happened in the field. For the field reliability figure a difference of about 4 to 1. It would be nice to draw some real hard and firm conclusions from this and be able to say its aircraft or its the operating command or its the mission duration but unfortuantely I don't think there is a simple answer to that. There is a number of variables involved here. So let's look at similar equipment or the same equipment on different aircraft and different operating commands and also look at a different piece of equipment which was on three versions of the same aircraft. This shows a required reliability of 193 hours, a predicted again much better than that, 286. It demonstrated slightly better than the required but look what we have in the field 29, 49 and 126 Hours. None of them meet the required reliability but never the less there is a significant difference between them. Again on the utility rate there doesn't seem to be much of a factor here. There is not that much difference. The mission duration certainly doesn't seem to vary either. We do see however, that the operating command kind of stands out as possibly being a factor. And of course this ties in with maintenance procedures because each operating command tends to develop their own kind of maintenance practices and policies and there does appear to be quite a difference in the effectiveness of the maintenance. So let's look now at one other piece of equipment that is on virtually identical aircraft, which has the same operating command, whose mission duration is almost identical, and whose utility rate is almost identical. The equipment has a required MBTF of 140, a predicted MBTF slightly better, a demonstrated MBTF quite a bit better than that. In the field, low and behold, it is meeting its required reliability but you can see there is about a 20-25% difference between the field and demonstrated reliabilities. Again, the maintenance policies *should* be the same because it is the same operating command. There are slight differences between the H and G version. As a matter of fact from an environmental standpoint you would think the G version might be a little more severe. But there is one difference here and that is that the two models of this aircraft are never mixed on a base. In other words all the H's fly out of XYZ bases and the G versions out of different bases. You might say maybe that this is the kind of variation you can get just from base to base variation in maintenance factors. So what does all this tell us? Well, some of the preliminary conclusions are the operational aspects do profoundly influence the field service reliability of avionics. The environmental factors appear to be significant but it looks like its almost impossible, at least on the data base that we have, to quantify this as to exactly how significant. The reliability demonstrated in the lab, via a 781B type of test program, does not correlate

with that achieved in service use. I think all of us recognize that but this just puts a figure on it. A good part of the actual study goes into statistical correlations and a real mathematical treatment of this. When we did that there is a lot of primary, secondary and tertiary correlations but there were two factors that came out very strongly as influencing both the ratio of predicted reliability to achieved reliability and demonstrated reliability to achieved reliability. These two factors were the percent relevant failures that occurred during the rel-demo testing and the sample size that was in the rel-demo these two factors did correlate very strongly with what was achieved in service use. In interpreting this a little bit one would say that maybe a real key factor in the rel-demo testing is how you describe the failures, and that perhaps, as Allen Curtis mentioned, no matter how well we can simulate an actual field environment that we are addressing but one facet of a problem that is a much larger one.

Dr. Allen Curtis: Thank you very much Dick and I hope you all got the picture that while it didn't say too much about vibration requirements it does indicate how complex a problem we are trying to solve here. Now I would like to turn the floor over to Dave Earls who will describe a test program he has been conducting at Wright Field in connection with this particular problem.

Dave Earls: I want to tell you the results of a program that we are conducting or just finishing up at Wright-Patterson which addresses this very problem of reliability in the field, and correlation between field and laboratory results. We call our program 'Combined Environment Reliability Testing' and for this program we took a field radar sub-system in an operational fighter aircraft and subjected it to combined environment reliability testing in the laboratory. This is equipment right out of the aircraft and we are attempting to provide the flight environmental mission profiles. Another name for this could be mission profile testing. To match the testing environments with the way they are in the airplane as it flies. We are putting in temperature, we're putting the bay temperatures in and cycling it the way the bay temperature changes during the flight. We have also put cooling air flow in there which flows at the proper rate. We are also putting humidity into the cooling air because environmental control systems do allow humidity to get through into the equipment. We have altitude in there and we have random vibration. We call this the flying equivalent to the laboratory because this is set up to provide the environments as they would occur in flight. We attempt to identify the engineering failure mechanisms that occur in this test and correlate those with the engineering failure mechanisms that are taking place in service, because there is plenty of 66-1 data which has been mentioned here and field maintenance data on this system and it is a low MTBF system so we can provoke failures fairly rapidly. We are comparing the field failure data to the failures we have in the lab and we are comparing the MTBF, the reliability type of data, too. We call this an initial step and a major reassessment of reliability testing. Putting the better environments into the test set up. Next slide. This is the flight mission, altitude profile to which we flew this airplane equipment in the laboratory. Time here on the bottom is about a four hour mission. We leave we turn the radar on when it is on the airplane and we leave it off on the ground before it starts for thirty minutes or so and then it is turned on again twenty minutes before the airplane takes off. Then the airplane takes off and goes to twenty thousand feet at ten thousand feet per minute, cruises there for a portion of time and comes down ten thousand feet cruises for a portion, has a terrain following mode here at about four thousand feet and then it has simulated combat up here of going up and down in altitude between twenty five thousand and ten thousand feet and three low passes. Next slide please. While this altitude profile is in effect we have cooling air going into the rack the way it does in the airplane. It starts out at this temperature at the low end before the flight starts and then when the airplane goes to altitude the cooling air of course

gets cooler. We use the warm air when it is on the ground and this supplies the air the way the environmental control system supplies the air through the airplane during flight and it is fluctuating the same way that it did during flight. This is the flow rate in pounds per minute, about four and a half pounds was the maximum we used, which is what the environmental control system puts into this rack into the airplane. All this data is pretty much based on measured data except the air flow which had to be calculated, but we know what that is from some other places where we know what the air flow is and the knowledge of the environmental control system, but it fluctuates the same way through the profile. This is the vibration that is put in for the test. The dark line here is the measured data which we took off of pick ups in the avionics bay in the F-111.

We used twelve pickups. The ones that were right on the equipment at the input to our equipment are included in this. We found that using the other pickups did not raise the level or change the level very much from just using say three right at the base of the pickup but we did put them all in there and the enveloping of this is done at a Q of twelve hundred for the airplane. We had data all the way up to twenty four hundred Q or so and the vibration does go up, of course, it does follow the Q squared law pretty well. In that airplane we gave it a twelve hundred. We had planned to give it lower vibration during the cruising portion but this turned out to be sufficiently low level. The maximum vibration there is .002 g squared per hertz measured data right at the location and this is .001 down at the low end of the spectrum and even lower here in the middle, and that is overall RMSG about 1.76 so to us environmental people that was pretty low level vibration. Next slide. This is our test set up in the chamber. There is the equipment we have under test. This is a dual system. It operates one channel in standby and the other in operational mode. We are concerned about the electronics in there. We really want to develop tests for avionics electronic equipment and we used that because it fit the chamber and because it was the major part of electronics. The rest of the electronics is outside, the antenna receiver, the external instrumentation and the indicators. We were concerned with what was going on inside the chamber, with the equipment we had in there. This is the crux of the engineering failure data that we got. We ran this thing for six hundred hours; we ran that flight profile over and over for six hundred hours just like you would fly the airplane for four hour missions for six hundred hours. You will notice an interesting thing in the middle column here; there are the LRU's the replaceable units in that rack and the ones that failed by serial number. When we had what is called a hard failure here we just took that LRU out and shipped it back to the depot and got another one just like they did in the airplane. We had a radar technician on site who maintained the radar and it was not fixed in our site it was turned into the depot for fixing. The initial thing that happened in here was an intermittent failure caused by humidity in the rack. That is an environmental problem, and you will notice intermittence in here. This airplane has a high in flight intermittent rate so we are reproducing failures in the laboratory that they cannot do in maintenance activities because they bring it down on the ground and the maintenance people say it checks ok. I will show you some more of this a little bit later but they have a high intermittent failure rate. The pilot writes it up and it is off for ten minutes or twenty minutes and then on the ground it is ok. So you will see these showed up quite a bit. Then there are other ones in there also such as fuses blowing. Those fuses up there were blown because of an oil leak in the transmitter. This oil leak shows up in field data and a humidity problem in a rack shows up in field data. It is written up in 66-1. Here we have the humidity problem again with the rack. One of the magnetrons are failing. Of course magnetrons do fail in service quite a bit, but these were intermittent and then they finally went bad. We had some more vibration failures down here. This oil leak problem was one of our more significant problems in one of the units. Next slide. This shows the rack opened

up different in a position here where it is viewed from the back of the rack. When you saw the equipment in the chamber it was all plugged into a rack and there was some electronics in the back of the rack. The cooling air that goes into this with the humidity in it goes right in here and it impinges right on the wiring in here and that cooling air goes through ports up in here, one to each one of those LRU's or black boxes in the chamber. So, this was shorting out in here causing the humidity problem we have. This is the unit that had the oil leak problem and this occurred in a 781 test. This was called a random failure in 781 and it has been showing up in service ever since and it showed up in our test and there is a gasket around here and this oil leaks out and the transformer over heats and causes failure. Next slide. This is the initial vibration problem that we had with the first unit. We ran coax cable in here and intermittent breaks happened and that was the major vibration problem. We did have a temperature problem also that was intermittent. It would cut out at below fifteen degrees in our test and they have not been able to reproduce that yet back at the depot. We are going to get that one back and see if we can reproduce it because they haven't been able to correct it. They have taken those boards out and put them in dry ice and done a lot of things with it. We still have something to find out about that one. We also had an altitude failure. When you took a unit above thirty five thousand feet it would cut out due to loss of pressure. That is a typical failure; they know about that problem in the field and in the depot. So we call our test the CERT, Combined Environment Reliability Test. For our test we had a total of seventeen failures and that would give us an MTBF during the six hundred hours or thirty five hours MTBF. We went to the radar technician we had there and he said in some cases we wouldn't report all those failures like the blown fuses and such, he wouldn't report every fuse blown. He is the guy who fills out the cards for repairs in the flight line and so we reported it that way and discounted a few of them. We have reported reliability people are always discounting them and we hesitate to discount them. We tend to call everything a failure. We got thirty five hours if we discount some that have not shown up in service. 80% showed up in service 20% didn't. If we discount some of those that didn't also we would give a maximum of 60 MTBF so we ball parked it and said we were somewhere between thirty five and sixty. MIL STD 781 type test demonstrated a 196 MTBF on this where it was a reliability acceptance test that was done on it. They took fresh systems and ran one of them for fifty nine hours and took it out and ran a whole other system for fifty nine hours. They did that for twenty systems to where they got eleven hundred seventy six hours total. That was how they got their data. The predicted MTBF for it was two hundred and fifty two hours. So the field AFM 66-1 that has been referred to here already with Dick in August of 74 had a fifty seven hours MTBF for the equipment we have in the chamber. but that's all we are talking about is what we have in that chamber and today a year later, we have an MTBF of 42 hours. So we can compare field data versus our data versus the other lab data. Here also is the intermittent rate which is very significant. This is called the field *C and D retock rate* (*C*annot *D*uplicate). This is when the failures Cannot be Duplicated in a retest back at the depot or cannot be duplicated on the flight line. 47% of these equipments fall into this category. We have found out what causes some of those failures by our intermittents where it is the environment at fault. We have an intermittent rate of 35% if you count all of them. If we discount some of them because they did not correlate with the field exactly we could get 60% so we are falling right in the ballpark there with what the field C & D did. We decided to ballpark it rather than give you exact figures cause it would have been so exact you wouldn't believe it. We conclude that we did correlate laboratory and field reliability; we did get failure rates similar to what is in service. We did get failure modes that occur in operational aircraft. We reproduced intermittent flight failures we know what's causing a lot of them and they are correctable, and we correlate

that with the field pretty well also. That is the conclusion of our study at the present time. This is an initial evaluation of field hardware that nas been in service six to eight years. The purpose of this program was just to correlate laboratory and field data.

Allen Curtis: Thank you very much Dave. With those two presentations, which I hope have set the stage and given you a little background of this whole problem, I would like to move on into the question period. I would like to ask you in the audience when you ask a question if you would keep your question, as far as possible, on the aspect we are currently talking about. We will get to the other topics as time goes by.

The first question I would like to address to Dave Earls. The emphasis of all the efforts that we hear about seems to be on tailoring the reliability test environment to the field environment in a very detailed manner, in other words, to do mission profile testing. So I would ask if, in your opinion and with the results of the program you have just been finishing up whether you think the results of the demonstration test would be very sensitive to the degree to which the mission profiles are simulated where by degree I mean both type and magnitude and particularly with this for vibration whether we should cycle the level with time?

Dave Earls: I am following the thesis right now at this point in time that we duplicate the environment as close as we can and that way you are much more assured of getting results. If you can define what that environment is and you put it in there the way it is put in the airplane you are going to get results (correlations). So from the technical standpoint of developing the technology the way to do it is to tailor the test to the application and you get proper results. That's a common sense approach really. On the other hand if you try to generalize and make something for a lot of different applications this will cause some problems. But, I can't really generalize yet because we haven't done that in the laboratory. I would like to see good hard laboratory data on exactly what is happening to equipments. With our technique of putting all those in there the way they are in the airplane and operating the way they are we get good results. I can't tell you if you get good results if you don't put them in that way but in tests done in the past there has not been good correlation either. There has been much testing done like that in the past with similar results so you are going to get it if you tailor it. I am sure there are parts you could take out and accelerate the test by just eliminating certain parts of the profile and not making it more severe but just eliminating certain parts of it; provoking the failures faster. As an environmental qualification type person I would like to see them provoke faster and not correlate exactly and get them and fix them and then you will be ahead in the reliability game.

Allen Curtis: Would anybody else on the panel care to answer that question?

Terry Elliott: Yes I would like to comment on it. Several years ago we ran some tests on the missile where we were trying to accelerate the test and we ran it at varying vibration levels and compared the distributions of failures we got with data we had from fleet. We found that you could accelerate the test only within a very narrow region. We found that at the very high levels we got different kinds of failures than typically was reported at the fleet whereas at the lower levels it correlated a little bit better with what we got. When we looked into that we found that the greatest percentage of the missiles time was spent at lower flight levels and thus the lower vibration levels and very little time was spent at the high levels. We know that the missile does see some high level stuff and does get these different kinds of failures. So what we concluded was that you can get certain kinds of failures at certain vibration levels and different kinds of failures at different levels. Based on that information, in later test plans that we have designed we tried to put in a time varying vibration profile to simulate what we expect the thing to see in flight. I think on a reliability demonstration

test if you really want to duplicate what you are going to expect or hope to see in service you have to take this into account. Our approach right now is to use time varying vibration levels.

Allen Curtis: Do you think the demonstrated reliability measured in whatever terms would be very sensitive to this?

Terry Elliott: Yes, it would be. If you get outside of narrow regions, for instance the .2g per squared hertz that you said they are thinking about using in 781. I think, at least in my opinion, that this is probably misappropriate as the single frequency nonresonant sine. You may get a lot of failures out of this that you don't get out of the sine wave test but you will get, I am sure, very different kinds of failures than you will see in actual service. Regardless of what the reliability prediction is from that kind of a test it won't be appropriate. So it is sensitive, probably insensitive within narrow regions, but over the total flight regime or the service regime that you are going to see, it is sensitive.

Voice: I would just like to say, in personal opinion, I think that when a test profile and a test program is very carefully and competently done, like the program David Earls has described, you definitely are going to get the type of failures and the equivalent amount of failures that you would expect in the field. But I do want to point out that based upon the variations that we see in this study that there are other variables that can swamp out these things and one example is that in Earls profile he took into account very carefully a lot of things in very much detail and did an excellent job I think. We are finding in the course of this study we found some instances where the real key environmental stresses for example were not in captive flight and they were not really spelled out anywhere as a design constraint or anything. The real key stresses occurred during checkout on the apron when you are running—up on the cooling cart type of thing. How do you account for that? How can a contractor account for that? So anyhow beware of that there are a lot of pitfalls here.

Joe Popolo: If you don't know Grumman is primarily a Naval Aircraft contractor. In Dave's work with the Air Force aircraft the environments in my opinion, in some cases are not as severe as what we see Dick had found during run up. Maintenance work on the ground is severe where sometimes we see an airplane sitting on a launch pad ready to catapult off with jet blast deflectors sitting up in the air and rebounding all that nice acoustic noise right back into the tail section, stabilizer and aft fuselage! Some of the work in this investigation that we just completed has tried to set levels based on the not only the flight conditions but also ground conditions and there is a very big problem which we of course have attempted to resolve in trying to associate time with these conditions. Maintenance work is a very very key point in coming up with these environments.

Harold Nevius: General Dynamics, Fort Worth. In Dave's work you profiled everything but the vibration. You only used one level of vibration, isn't that correct? Do you consider that the vibration part of it wasn't as important as the temperature?

Dave Earls: The reason we didn't do that was because the vibration level was so low (.002 g^2/Hz). If we went down to that level in the middle part of that profile it was so low we couldn't even control the shaker. It gets down to a tenth of a g or something. You are in bad shape because it is such a quiet airplane. If it had been a different type of airplane we would have changed it with Q; we would have changed it at high altitude and run it at lower levels, but if we start lowering that level we are down to mud.

Mr. Nevius: What is the equivalent Q you are talking about on that vibration? Is that up near the 2400?

Mr. Earls: 1200 was about average. It would be four times as bad on the PSD levels up at 2400 which it was.

Harry Klein: Aberdeen Proving Ground. The thing I don't understand here is that you are talking about reliability! If so, for how many of the failures do we know the failure mechanism? Are they vibration associated and are they a combined environment? You were talking about accelerating the rate of testing, this means increasing the level. I trust you wouldn't have done that?

Mr. Dave Earls: I don't really believe in increasing the levels. When I said accelerate I mean I like to provoke the failures fast to be economical about it rather than make them come exactly the way they did in the airplane. I would like to get them faster instead of the way it is now where sometimes they don't provoke them at all. I would like to get them more quickly by a follow on to this. If I can keep this project going for another six months I would take the benign portion out of the profile, I just wouldn't even run it. I would just run the others and see if I could get it squeezed down and get a correlation. The K factor in the way they are doing it now is on the wrong side of the table, it should be the other way around.

Mr. Klein: But my question was how many of those failures were truly associated with vibration?

Mr. Earls: 80% of the failures occur in service.

Mr. Klein: But how many of them could you associate with vibration?

Mr. Earls: Of the ones that we had the coax problem that I showed you up there was the only vibration correlated one. That was the only vibration one that correlated with field results.

Mr. Klein: That was the point. It was mentioned here a minute ago that you have failures on the run up pad where we really don't have the type of flight environments you were talking about.

Mr. Earls: Well you have 80% of them there that occurred the way they did in service. There were altitude failures, humidity failures, there were a lot of environmental failures in there.

Bob Hancock, LTV: I thought I might reference one of Dave's published reports with respect to field failures. This one was done by Grumman it was a 71-32 report I think it was. It shows of 31 equipments they studied I believe 52% were environmentally induced. This again is a wheels up to wheels down type 66-1 reporting. But of that 52% I believe they showed 60% roughly thermally induced and 40% containing all the other environments including vibrations. I presume that would correlate if Dave runs enough tests long enough.

Dave Earls: Temperature and moisture were the worst I believe. Temperature vibration moisture were the worst problems shown in that report and they were the ones we concentrated on.

Allen Curtis: Some of these comments are related to the next question I had dreamed up. For years we used and damned the single frequency vibration of the 781 type requirement which, to refresh your memory, calls for a single nonresonant fixed frequency somewhere between 20 and 60 hertz at 2 g's for ten to fifteen minutes per hour. I would like to ask Dick how positive are we that if we go to the time and expense of changing that kind of vibration to random vibration is that really going to be worthwhile or another way of putting it is how much of the problem might that solve?

Dick Baker: I wasn't expecting this one. There is a lot of personal opinion in this. I think the Agree type of vibration test where you have a single nonresonant frequency point is in my view almost completely worthless. I

think the amount of actual pertinent defects which that type of vibration uncovers in a reliability test is essentially nil so anything that you do to make a more realistic vibration environment more realistic with what it is going to see in service use is going to be a plus factor. So, in my view, you have no way to go but up. As to what percentage or how significant the vibration portion would be I would think it would definitely not be the major driver. I would also like to add some comments on temperature effects. The way you define temperature stabilization and where you define turnon of electronic equipment particularly cold start type of turn on can have a rather drastic effect on what how damaging it is or how effective it is at inducing failures

Joe Popolo: I should point out, if people don't realize it, I am a vibrations engineer not a thermal man. I have chased a lot of problems in the electronics and hydraulic actuators and any other piece of equipment that we can find in our airplanes and tried hard to convince people that their problem was not vibration, it was something else. I know that the original report that was put out by Grumman indicated, as Bob has just said, somewhere around 50 or 60% of the failures that they found were definitely associated with temperature. But we know what the environment is in the airplane because nowadays we have the necessary dollars to fly aircraft and get these measurements. I think we should dam well use those measurements to come up with a realistic environment, and not to do a test because it is the least expensive way to go, which has been the problem with MIL STD 781. So the point to be made is that we can do it today with what we know. I know we can come up with a realistic environment. We have a lot of experience now, not only at Grumman of course but in all the aircraft corporations. The Air Force has to do a lot more work than the Navy does as far as allocating an aircraft to take flight measurements compared to the Navy which relies on the contractors to supply them with the vibration environment until they are not satisfied then they go out on their own. But, basically we supply them all the information. I think we are making a big step here. I think the idea is if it is combined environment let's do combined environment, if it is random vibration let's do random vibration and if it is another aircraft type which might be like a turbo prop aircraft where we know the predominant frequencies are sinusoidal in nature not random then we should look at doing sinusoidal testing not a fixed frequency that was decided on only because someone designed a piece of shaker equipment forty years ago and they are still using it. That's where I am.

Voice: Dave I am confused about something and I would like to ask a question. In MIL STD 781 there is statement to the effect that the environmental levels are suggested levels and another statement that says if you have better data to use the better data. Unless I am misreading that there doesn't seem to be any inclination to considering ever using random vibration in 781. Everybody continues to use the mechanical shaker single frequency sine. Does that statement really mean that you can use better data but not use random? Has anybody ever done a 781 and used random and used that statement for a justification? I am kind of limited I never had to do a 781 before.

Allen Curtis: That escape clause as it is sometimes called is in 810 B and C but I don't recall seeing it in 781. Do you remember Dave?

Dave: I don't recognize it as being in 781 but if it is I think the answer is obvious that anybody would be out of their mind to suggest that rather than a nonresonant single spike of frequency, because the one isn't benign.

Voice: I seem to recall seeing it someplace in section six. I hope I am not confusing that with another spec. It seems like someplace in section six those statements do exist.

Voice: I have a copy of the C version but I don't of the B.

Chas Smith, Bell Aerospace: It seems to me everybody is underlinging what we already

know. The closer you get to really simulating the environment whether it is just vibration or combined the better correlation you are going to get with service failures. The more you simplify the test the poorer the correlation you are going to get with service failures. What's new? It seems to me that where we should be improving our skills is in first of all predicting the particular environment in which we are intending to use a piece of equipment and then in predicting what specialized aspects of those environments are most likely to cause failures and then having gone through those two steps into designing an environmental test that will simulate those particular aspects and only those. I would like to hear this session and the panel address those two problems. How do we best predict the environment how do we then best reduce the total environment to those facets only which are most likely to cause failure and enable us to design cheaper tests that are most relevant to the failure problem?

Allen Curtis: Would any panelist care to respond to that one.

Howard Sheafer, Naval Weapons Center, China Lake: The Naval Air Systems Command has just put on the street an environmental MIL STD that addresses the first part of what the last man from the audience was addressing. It is a way of identifying the best environments for a given program or weapon or piece of material. The identifier is MIL STD 1670 and it can be now obtained from the regular MIL STD sources or from Air Systems Command code 52021E. It is environmental criteria guidelines for air launched weapons. In this it does exactly what the community here has been asking for for at least the last twenty years and hopefully it will aid people like Wright Field in tailoring the environments to the reliability needs. MIL STD 1670-AS.

Allen Curtis: Thank you, I think that perhaps one of the things that bothers us is that we are used to qualification testing and a lot of effort has gone in over the years for tailoring our qualification test requirements as closely as we can to our prediction or knowledge of the environments and we have some feel for what is damaging. The thing that is worrying us is that in the reliability demonstration testing you are going to get into testing under these environments for many many hours before you reach an accept or reject point in the test. We are looking into tests that may be hundreds of hours of vibration and that is something new to us and we don't know quite what is going to happen. We get worried about cumulative effects and I would like to bring to mind that up until now we have had a dichotomy or contradiction between qual test and reliability demonstration tests. In qualification vibration test for example we all knew we had an accelerated test. In testing for two or three hours per axis we were trying to simulate a whole operational lifetime and if you really wanted to get an A+ grade on that test you had to have zero failures. These were at extremes. On the other hand with rel-demo testing for years we have a very benign environment dynamically speaking and yet we were allowed to have a certain failure rate and you got a A+ on that one providing the failure rate was not too great and that to me seems a little contradictory. Now with new proposals we are seeing vibration requirements essentially equal to the qualifications levels but several times the duration of the qualification level and yet those several hundred hours of the test only represents two or three percent of the operational lifetime of the equipment. So something looks a little out of balance there. So the question I would like to ask is about this trend we have going. Are we trying to set up an accelerated reliability demonstration analogous to the way in which we have set up qualification test and if we are doing that should we not also adjust the MTBF that is to be demonstrated in a like manner? You know simple mindedly if we wanted to demonstrate a hundred hours out in the field are we setting up levels such that if you demonstrate ten hours in the lab that should be the same as emonstrating a hundred hours in the field. Would anybody like to take a crack at that one?

Voice: I think one of the problems with trying something like that is in order to be sure you adequately accelerated your test you need to know that the failures you got are really representative of what you are going to get in service and that is kind of hard to do until it has been in service for a while. I think trying to accelerate the test is something that you can work on and establish after it has been in service for a few years but initial reliability demonstration, unless it's a very minor modification to come up with a new version, is probably kidding ourselves a bit. I think the only approach is to use realistic levels with realistic times.

Dave Earls: I think we have to go through the realistic approach for a certain time here until we get enough data and enough time to evaluate some of this other part of it. That has not been done in the reliability situation yet. Those K factors that they use are six and a half to one, or four to one, or two to one and ours would be the same way if everybody uses a different way of going about it. We don't have any relationship between the MTBF and what we are getting in the lab. If we go faster we want to know how much faster on the equipment. We are going to apply these things to prototype equipments and get some information on it. I think we are just going to have to experiment with some of these programs like we do with aircraft and get some real hard data on it.

Dick Baker: If I could just add one thing. Let me say I would be reluctant to try to accelerate reliability demonstration testing by upping levels arbitrarily. I think we don't know quite how to do that yet. One additional factor that ties in with this is attempts to get a lifetime of vibration fatigue in a three or four percent of the total operating life that the equipment is supposed to have. This ties in with the study that we have done from the standpoint of the number of samples that were used in the rel-demo testing. I think Dave indicated that there were something like ten samples in the equipment that he studied and in the original demonstration, test twenty samples. Maybe I didn't emphasize this enough but this was one of the two real strong correlations with how well the equipment functioned in the field; the percent of failures during rel-demo that were counted as relevant, had a direct correlation to how well the equipment did in the field. In other words, the higher the percentage of relevant failures in the rel-demo testing the more likely that equipment was going to come close to meeting its requirement in the field. The other one was that the more samples that you use to make up your test sample for the statistical agree test the less likely it would fail in the field compared to what its requirement were so if you take twenty samples to get a lifetime of mission cycles you shouldn't necessarily expect to get a correlation with service type failures.

Mr. Earls: The basic statistical assumption versus the engineering assumption is not very well correlated, you know [illegible] of specimens for a short time and a [illegible] long time. A lot of our failures d[illegible] until after fifty nine hours, [illegible] ney couldn't have got them in tha[illegible]. If you run one for fifty nine hours [illegible] place it with a brand new one why you are going to get different results than if you ran the thing like you do in the airplane for long term. I really challenge the idea of trying to provoke those things with lots of samples in a short time and try and get the same results you are going to get with fewer samples for a long time because the few-samples-long time runs last long enough to give you failures that you won't get in a short time.

Voice: I agree with the whole panel here. I think the main thing here is that we are making a giant step here going to random testing and I don't think we want to convince the powers that be that we could now save them a lot of money by increasing our test levels and decreasing our test time and at the same time get better understanding of what these failures are. I think we should go very slow here. Let's get our feet wet easily. Let us get rid of the fixed frequency requirements, go to the random or whatever a realistic environment simulation is and let's stay here for a while.

Allen Curtis: Thank you gentlemen.

Hank Caruso, Westinghouse Electric: I was just wondering if anyone has approached the area of handling and servicing especially as far as might be required for failure analysis of a nonrelated problem? Is there any movement towards incorporating the handling servicing aspect into the reliability test? In other words, does anybody really know to what extent the failures are environmentally induced or to what extent they may be precipitated by other events that have nothing to do with the environment? The environment as we are describing it right now? When we talk about problems of handling or mishandling or improper fault identification or parts replaced in error that are shuffled back in all of this adds up. Have there been any studies as to the contribution this type fault might make in the reliability cycle?

Dave Earls: Were you here earlier when I put some view graphs on? That really kind of addressed that problem from the standpoint that we really couldn't quantify the differences but they are significant as close as we could get it. Looking at base to base differences in what must have been maintenance factors looks like it might introduce a factor of variability of 30%. If you look at the different operational commands and say that they appear to be different because they are configured a little different there might be a factor of two to one difference.

Hank Caruso: Well is there possibly a practical way that could be introduced into the test cycle? It may be a complete tear down and rebuilding every so many cycles or something like that. That might be a little drastic.

Voice: Which operating command do you want to simulate?

Mr. Caruso: Well one of the practical problems in a test laboratory is generally any handling problems or mishandling failures that occur during a reliability or qual test are often ignored as being unrepresentative of the field experience where it should be just the opposite; they are getting a more benign treatment in the lab than they ever would out in the field and possibly some of these problems have been seen in the test Lab long before they ever surface in the field but they are being shuffled under the rug or just not considered.

Voice: According to this study the more failures that are categorized as non-relevant in a rel-demo test the worse the equipment is going to be in the field and you assume that things are not fixed. You know problems are rationalized away.

Mr. Caruso: Is it possible that some of the tests might be ok if they were interpreted a little better?

Voice: The interpretation is a real factor and of course you get into the whole political aspects when you realize at what point in the problem these rel-demo tests take place. You know usually at the time the rel-demo tests take place you are pretty far down the program and there have been a lot of commitments into production. In many cases you know that because of the advance timing you must have and so it would take a very valiant hero in a customer program office to say that the equipment didn't meet the reliability requirement. In addition the contractor always has a natural bias towards making his equipment look as good as possible so the two work together with the circumstances. I think that in many cases field problems are swept under the rug.

Mr. Caruso: So there you have a situation where maybe the customer is responsible for some of the problems that he is forced in live with later.

Voice: We are all in the same boat really. We are all in it together whether we realize it or not.

Allen Curtis: I think Mr. Caruso you have a very valid point and to answer your question I am not aware that anybody has tried to do this that I have seen documented and I really would

like to recommend that some efforts be made to storing and disseminating, on some kind of a scheduled basis, some of these other extraneous factors. We really want to find out what kind of reliability we can expect in the field. You are going to have to pay for this of course. That is why I have posed some of the questions about what percentage of the problems will be solved. The thing I am worried about is over expectations, which we have seen in social problems in the last few years. I hope there is not an analogy here that we will spend a lot of time and money incorporating random vibration and have too great an expectation of what this is going to do for us.

Mr. Smith: Hughes Aircraft Co., I guess one big philosophical difference between space type testing and aircraft type testing is that space people have the feeling that this thing is going to go out and never come back it has to last forever and be super reliable and the aircraft people seem to feel that because it keeps coming back you can settle for less. I know it is worth it because when I was in aircraft the rationalization was weight penalty. Listening to the things that have been said today, number one, it seems we are not taking advantage of the fact that the plane keeps coming back; it can be fixed. It sounds like certain failures keep coming back too and I don't imply any program to update these. I In fact I wonder if the difference between one command and another is some of the commands might have maybe more active maintenance people that do make efforts to get rid of chronic problems and the other thing that strikes me as being, part of this weight business, it sounds like, for a very few pounds on what must be a 20 to 40 thousand pound airplane it sounds like you could have mean time between failures of the space vehicle type experience. I wonder if you gentlemen would like to comment on that?

Mr. Earls: I'd like to make a stab at it. I think the basic reason that at least the Navy is willing to except something less than 20 to 40 thousand hours mean time between failure, on their equipment is a cost tradeoff. What the Navy wants is as much reliability as they can get for as much money as they have to spend. Based on those numbers then the Navy planers can estimate for a fleet maneuver how many missiles, aircraft, weapons and people they have to have. A Navy maneuver, its probably true with Army and Air Force too, takes into account expected reliability. As long as they have enough weapons available to make their strike that is the most important thing and if they were to try to get 20 to 40 thousand hours of MTBF all the money would go into a few weapons and they would have anything left to support a strike force. The point is it is a cost trade-off.

Voice: One part of your question there was about I ogistics command, upgrading the equipment of the using activity after they get these failures. They have to show how much it is going to save them in money by doing it. Sometimes its after they have got it they find its easier to keep fixing the darn thing than it is to go through a redesign and go back to the contractor and get an ECD action at $300,000 thousand dollars a copy or something, so it can be very costly. They do have an AIROS program Increased Reliability Operational Systems and Logistics Command. It works on their hit parade of 10 or 20 worst systems. Those do get attention.

Mr. Woodfin: Naval Weapons Center, I think I heard this discussion over here a moment ago saying that if I were to be letting out a contract that specified MBTF that I shouldn't allow anything to be defined as a non-relevant failure. It is almost going that way and you have just about convinced me that that is the case. Would you like to comment on it from that aspect?

Mr. Earls: I may have over stated it slightly, because obviously there are some legimate cases for non relevant type failures that are clearly not indicitative of what the equipment is going to see in the field for instance, mistakes on the part of the test personnal and secondary type failures where something goes bad and takes out two or three other equipments with it. It really isn't fair to count that all up as three

failures instead of one, but the fact remains statistically that the longer these rel-demo tests go on the higher percent of failures get classified as non-relevant and the poorer the equipment winds up in the field. So I don't know what the right percentage is as to what we should sort of accept and maybe that might be an interesting way to look at this and additional data to see if we could support it. There are legimate non-relevant failures. It is a matter of degree, how much you play the game.

Allen Curtis: There has been one suggestion to try to attack this problem of relevancy or not. For instance in rel-demo testing when you keep score if you design something out then it doesn't count and you can scratch that one off your list. There has been some talk about integrating or combining the qualification testing and the reliability demonstration testing. Then if you have a failure I guess there will still be some that are non relevant when the guy just accidently knocks it off the table or the shaker runs away or that sort of thing, but then discounting those the ones that are left kind of have to be design problems that you have to fix to get through the qual part or they are reliability failures that are going to count against the MTBF that you are demonstrating so I think combining those two test programs maybe is an incentive for better score keeping.

Mr. Caruso: I would like to go back to the question I asked before in light of a couple of comments that I heard two panel members just make about what are relevant failures and what are non relevant failures. This idea of mishandling where the test operator knocks something off the bench or pulls a wire by mistake are things that you are apparently defining as clearly non relelvant and the question arrises should they be clearly non relelvant or should they be relevant? It sounds like again we are throwing out a whole class of information of data that is relevant to the way things happen in the field and we are getting this experience in the laboratory and not paying any attention to it. I guess what I would like to ask as a specific question is are the accounting systems the same in a reliability test as they are for field data? In other words do these field MTBF take into account operatore errors? Do they total in secondary failures and if so shouldn't the reliability test scoring systems be the same and if they are not can they be made compatable some where along the line?

Voice: They attempt to be the same except for the one major difference and that is that the Air Force data accounts only flight hours as opposed to equipment on hours. This can be a major variable for certain types of equipment Computers particularly tend to be on quite a bit, for say two and a half hours, to cover one flight hour.

Mr. Caruso: Apparently there is a lot of disagreement or lack of agreement on what the proper accounting systems are for all of these. Everybody is not speaking the same language when they are talking MTBF.

Voice: Well that is true as a general statement. But years ago there were a lot of people that just didn't believe all the numbers that came out of this 66-1 system. I think in recent years things have gotten better and we looked at all the data on all the equipment that we had to try and determine what errors were in there that shouldn't be that were kind of obvious goofs. We decided that the data on the 66-1 was somewhere between ninety seven and ninety eight percent accurate. In other words there were only two or three percent in there that appeared to be grossly misclassified or something like that.

Mr. Caruso: If I could ask the question again though. Is mishandling in the field counted towards the MTBF? You mentioned that the Air Force based it on flight hours but does mishandling on the ground get figured against that flight hours time?

Voice: It shouldn't, but the data does depend upon the field maintenance people filling in the categories of how the equipment malfunctioned and if it was clearly something you know that was a goof or something it should be thus classified.

Voice: I think we are doing the same thing we did twenty years ago. In sympathy with your question about maintenance and handling of this equipment we have a very expensive sophisticated piece of equipment here. There is definately a training period; logistics problems with young people handling this equipment. To try and sit down and design a test to cover something like that I think is ludicrous. What we must do here is educate these people and again I think Dick made a very good point in one of his original view graphs over there where he had two different maintenance shops servicing some Air Force equipment and one crew was doing a bang up job and the other crew seemed to be maybe not as aware of the problems as the second crew. How you assign or associate a test requirement to cover something like that I don't know. We don't want to get lost again

Mr. Caruso: One final response to that. I wasn't suggesting that we come up with a test requirement to do that but there is information in the laboratory acquired during testing that isn't taken into account where you have people who are just as inexperienced in handling the equipment. This information could be used towards bettering the reliability of the MTBF later on if it were paid attention too.

Voice: If it is going to cost money and weight to accommodate something like that than I don't know if it is a good rule. If you have a good product it will stay together.

Mr. Condouris: Electronics Command. This maybe in line with Mr. Caruso's remarks, I think we are starting to mix design test with reliability test here. The drop he is talking about should have been taken care of in the design of the equipment at the time. Reliability is something else. Reliability, and I believe Joe Popolo has done some work in this area, is a case where we have poor workmanship, poorly assembled items, a component which has not quite met the complete requirements of the environmental test and in line with this I would like to ask both Dave Earls and Mr. Baker a question. In sifting out your reliability failures did you differentiate between a design failure and what we would call a reliability failure or is there no difference?

Mr. Earls: We didn't. We just reported the failures we had correlated and saw them listed in 66-1. As far as defining what caused them we did define the environment that caused them, which is one of the things we really wanted to know about and there will be a study of this equipment probably aimed at fixing this stuff or a design study done on ECP action as a possibility.

Mr. Condouris: For example, the crack failure, was it the wave guide that had a crack in one of your electronic equipments?

Mr. Earls: It was a rack that cracked.

Mr. Condouris: A wave-guide got broken I believe is that correct?

Mr. Earls: A magnetron

Mr. Condouris: A magnetron anyway, would you call that a design failure rather than a reliability failure?

Mr. Earls: A failure is a failure, I don't know! It happened in service and it happened in test. I don't know how to categorize the difference between reliability and design. Can you redesign it so you won't have it I guess is what you are saying well with reliability you wouldn't still be getting it.

Mr. Condouris: Did you go back and redesign this rack?

Mr. Earls: We weren't in the process of doing doing that. We were just correlating field data. We weren't trying to upgrade the equipment or redesign it, although this is going to be done, but that was not our intent. We had a crash program to correlate field and laboratory data and it was used as a demonstration program for a laboratory development experimental program. We were proving that the same type of failures would occur the way they did in service. The equipment itself was not the real study.

Voice: For our study we didn't try to make that distinction either, it was sort of beyond the scope of the study. There is one other prime category of reliability failures that you didn't mention that is the inherent and true sort of random failure of the electronic parts.

Joe Popolo: In answer to your question Mike I think that is the whole point. If we have been doing realistic reliability testing, then we will not get these failures in the lab like Dave has experienced and everybody has experienced in the airplane. But right away someone says gee, even though maybe its a design deficiency it is just too expensive to fix it right now because we have three thousand units in the field. What we want right now is to come up with a better environment to run in the early stages of development of the piece of equipment. We can't have our managers coming back at that time and saying it cost too much money to fix because we can come back to them and say look there is only two or three units here, we are still early in the design phase, lets make that correction now and not wait a year from now

Dr. Curtis: I have a few questions that are more directly related to vibration, perhaps we can shift to these. Most of the documents I have seen are rather vague on the subject but I assume that if we come up with improved vibration requirements for rel-demo that at least on an intentional basis it will be in a single direction. At least to me it looks kind of cumbersome that we could be changing axis every so many hours or cycles. Given that that is true how do we decided on that one direction. Some possibilities would be the most severe environment or the most damaging direction, to the equipment if we know which that is. I have seen one proposal that says something about orienting the vibration normal to the PC boards in the equipment.

Mr. Popolo: I think you are asking a question and answering the question at the same time. Again I think we have to get to the economics here. Ideally all of us would like to test something in all three axes and do a good job in really evaluating what's going on in that box. We just can't do it. I think now we will have to fall back on to getting the dynamics people involved with packaging very very early and try to determine what the critical areas are. I am not saying it is simple but there is a lot of analysis talent around, a lot of computer programs and we can do a lot of work in trying to find what axis should be used to evaluate that box. There will be other times where we may find a weak axis but unfortunately we may have a very very large unit like maybe a computer detector on some sort of a large CRT display which we can't orient conveniently in the fore, aft or lateral direction. The economics is going to be such that we are going to choose the most convenient axis and it will probably be the vertical. For aircraft, I think I know the answer. I agree we should do it in all three axes but I know I can't and will probably choose the vertical and hopefully we will be able to get in early enough to try and verify the vertical is the worse direction.

Mr. Earls: The only application I know of is where you have small boxes that are real compact and test three at once. You put one in each direction on the same fixture. That is the only application I have seen like that, where you really have small items.

Mr. Popolo: We did some work a while back on the space program, related to what Allen said about this resultant axis testing, where we were trying to come up geometrically with an axis of vibration. That could at least exercise a large percentage of the components. That is being looked at.

Mr. Elliott: I would like to comment on that. I am not sure it is true we can't test in three axes at least for some cases. Using an AGREE-type facility you can't, or using a shaker, you can't. We have been doing some reliability testing not AGREE type or reliability demonstration type so much as determination type testing using acoustics on some missiles. On at least three different missles that we have looked at with multiple accelerometers inside and outside; we have gotten extremely good correlation both spatial and directional, in all three axis at many

locations spaced throughout the missile, with what we have measured from captive flight. So we have been using a technique like that. In fact the facility that we have been using was described in an earlier paper by Doug Everett yesterday, I think it was. The results that we have been getting, which in some cases were looked at by people from outside our facility, looked very incouraging for simulating vibration. You may not be able to use acoustics on all kinds of packages but at least on the missile that we have looked at that gets a lot of turbulent boundary layer airflow where the turbulent airflow seems to be the predominate excitation phenomena, at least in the higher frequencies, the acoustic chamber does a pretty good job.

Dr. Curtis: Does anybody in the audience have any feelings on one axis versus three axis? Assuming that we go to random vibration, normally, qual type requirements go up to two KC starting at 5 or 10 or 20 HZ, somewhere around there. I have a feeling that the reason that we stop at 2KC is because that is the capability our shaker systems have. If people had designed the power amplifiers to cut off at 500 that's probably where we would be but if they had been smarter and gone up to 4 KC that's where we would be. Assuming we have no indication that the environment suddenly stops magically at 2 KC it seems to me that the bandwidth that you need is that which will cover the damaging frequency range. Now if we could convince ourselves that for example five hundred or one KC would cover the necessary sensitive frequency range we might save a lot of money in facility costs; the size of the shaker you need; the size of the power amplifier and whatever. So I would like to ask Terry first how he feels about reliability testing. Is it necessary to test all the way to 2 KC or do you feel that is not high enough?

Mr. Elliott: Well in terms of inducing a vibration type failure, intuitively I think probably 500 HZ is enough. It is nice to simulate the vibration as far as you have data though just to verify that you are doing a good simulation of the environment. I don't really have any technical justification to say that 500 HZ is high enough or 200 HZ is high enough because it really is intuitive. In most of the tests that we have done in the acoustic chamber, the frequencies go out to about a 1,000 HZ and tail off. But looking at the accelerometers in the missile they seem to simulate pretty well at least to 2000 HZ which is as far as we check them, primarily because that is where you have the data. I guess I really don't have a good feeling what would be a high enough vibration frequency to simulate for vibration failures.

Mr. Earls: I haven't seen much above 2,000 as far as vibration data causing failures. There have been some of these whisker type of things that failed at 5,000 cycle, I have heard of that. It seems that the only way to really control it is to put it in with sound, if you want to those higher frequencies. It's a better way of doing it than trying to do it with a vibration shaker. It appears about as easy to do it to 2KC. Facilities are around which go as far as 500. I really don't have a feel for the quantity of failures you would be having if we chose 500 versus 2KC really.

Mr. Popolo: I believe 500 HZ is that number. I believe it is a very practical number to accommodate in your test fixturation. I think the levels that we get up to 500 HZ introduce high enough displacements into the box structure as well as the components to produce the failures we want and in my experience I think I can count on my one hand the number of failures that I have seen that I would definitely associate above 500 HZ. The state-of-the-art eventually may give us something where there is a lot of sophisticated equipment; you may have some very very light weight structure like electronic components that may be sensitive to a 1,200 1,5000 2,000 HZ input, but you have to remember that I can't talk for missiles, Terry is the missile man over here but as far as equipment being installed into a aircraft structure that is going to be sitting on shelves where it is going to be pretty well shielded from the outside environment there is going to be a tremendous amount of attentuation that you get from that structure.

When you start looking at the levels in narrow band type analysis, if you look at the levels above 500 HZ you will see that they are quite low. I would say that 500 HZ is a good number.

Voice: Allen, can I ask you a question? Most sine wave tests cut off at 500 HZ, do you know the reason for that? Is that tied in with the question that you just asked?

Dr. Curtis: We inherited that from the days when variable frequency MG sets cut off at 500 HZ. Before the days of power amplifiers.

Mr. Popolo: That is not true about sine spec, sine specs have changed.

Allen: Many still do cut off at 500 HZ.

Dan Van Ert: Aerospace Corporation, I think this question as well as the one on frequency range as well as the one of which axis shall we shake are leading questions. They suppose that in a rather complex situation which is I take it long term test failures that you are going to ask the vibration expert to presuppose what axis is going to be important, also what portion of the frequency spectrum. I don't think you can answer either one and maybe I am just less capable than others but I feel very unqualified to sit and put myself in the position of a radar box and figure out what is going to hurt me; and how long it is going to take and in which direction it is going to hurt me. I think many of the failures are very insidious and happen to very unimportant elements. We may analyze the basic blobs inside of a component but we aren't going to analyze the little wire that has too sharp a bend or the piece of wave guide that may be poorly designed. They are the small items that generally fail. This question as to whether you should stop at 2 kilohertz; I feel that we in a sense have been a little self defeating in our thinking. We don't know with good clarity what goes on above 2 kilohertz because in many instances we've terminated our data acquisitions systems at 2 kilohertz because we couldn't do anything about the stuff beyond 2 kilohertz but I know in the ballistic reentry systems area there are contractors who want to test beyond 2 kilohertz; there are data acquisitions systems being designed to go out to the 80 kilohertz range and try and find out what is going on out there. It is probably just as true of aircraft systems as it is of space systems that things are getting smaller and smaller and stiffer and stiffer and frequencies are heading up inside of boxes. We have some crystal failure problems where the frequency of interest is 1700 hertz. I sure wouldn't want to not exercise those little guys. So I think whether it a arbritary practical limit that shakers now a days go to 2 kilohertz by God we ought to use it. If we think it ought to go further then we ought to grow that way. I don't think we should presuppose anything beyond the normal practical limitation.

Dr. Curtis: Well I think there is some answer. If one has tested a number of electronic boxes and put monitors inside and had a test that goes out to 2KC and then you look at the response inside it tails off way down into the mud. That doesn't necessarily mean that the inside will be insensitive to 2KC excitation or what have you but it does raise the same question which Terry raised a few minutes ago; I have a feeling that if you really think you ought to exercise those higher frequencies then you better skip vibration as your means of excitation and consider the acoustic excitation in order to get that into the guts of the device.

Mr. Baker: I would just like to say one thing. When I have a dynamics question I always go to Allen so it isn't right for me to answer his question. There is one additional factor that Mike mentioned and that is the use of impact type shock loading as a alternate means of getting excitation in and in this case you can get the higher frequencies. They are considered important, I think there was a paper yesterday where Convair was using little pneumatic actuators that just bang-bang and induce this shock loading and then they varied the frequency at 7 cycles or something like that and they wound up with a fairly close approximation of a broadband type spectrum and I

think this is an area that potentially should have a lot of interest towards reliability type testing.

Dr. Morrow: Allen I wanted to agree with you on the potential of the high intensity noise test up to point. There are some problems with it however. In the first place if you need really intense noise you find that it becomes difficult to get as you go up in frequency. The transducers we have available run into difficulties eventually, which is compensated to some degree by harmonic generation in the throat of the horns, but that's not very controllable. Then, if you are going to use noise the effect you get maybe critically dependent on how you mount what you are testing, and in the case of the missile there is a fairly simple solution to that; you can try to suspend the missile in rubber or on Bungee cord so that it is very nearly in the condition it would be in free flight. The noise impinges on the skin of the missile as it would in flight. There are a few detailed differences related to correlation length but at least the mounting problem has a simple solution in principle. If you are talking about aircraft avionics and you want to test it by itself since the plane is too big to test as a whole perhaps then it is a little harder to decide this question. I would like to throw a little broader question out if I may. I think some of the things we have just been debating are illustrative of the fact if we are going to verify reliability with a high degree of confidence there is a strong implication that we are going to try to simulate the field environments accurately. The one thing that's bothered me about reliability testing since enthusiasm for it got underway is that the emphasis has tended to be on verifying reliability which presumably somehow or other we have achieved prior to that point or would like to and I have seen very little discussion of what is the best way to test so that we actually have something close to our reliability objective with shock and vibration in particular before any such verification begins. What exploration I have done of this state of the art indicates that we have many specialists doing their job very well but the overall system is rather cumbersome and loose with respect to specifying the requirements to which the various specialists work and specifications as used now can help a great deal. They also can stand in the way of achievement. We are in a situation where with reliability testing on one hand we are holding out a motivation to the contractor to achieve a higher degree of reliability but if attention is not given to the earlier part of the process he may not be permitted to attain it. I think the attainment of that reliability is rather subtle problem. I think it deserves an equal amount of airing. I am not saying that we need to do it right here but I think that somewhere it needs an equal amount of airing.

Dr. Curtis: Would anybody care to endorse or disagree with Dr. Morrow's comments. I would like to bring up one other vibration aspect of this which I think has to receive a great deal of attention. Normally reliability demonstration testing kind of has to be done on a system basis; whole radar system, whole navigation system or what ever, so you tend to be talking about rather large items. Maybe it is a whole missile or a whole external part nevertheless it is the problem of how to properly vibrate the large test item, how to control that vibration and in this case we have the problem of making sure we excite all parts of that system but don't over excite other parts in the process. One proposal I have seen suggests that one uses some of the aircraft primary structure as your fixture so you can equalize to some desired spectrum down at the base of that aircraft structure and this is a way in which the system would interact with the system you are trying to test and impedances would take care of themselves and then you could bring the level up. Other approaches might be like a response control testing such as 810C calls out for in parts. So I would like to ask Dave Earls, have you given any thought to how we specify reliability tests of large test items? 781C that is in circulation completely avoids this question, which can have a tremendous impact I think on the results you get.

Mr. Earls: I think you are just talking about a step further and another vibration symposium or something. Doing that type of testing the vibration alone there is a big enough thing without putting the reliability into it. From what you are talking about how you test large items

and introduce structure and things they are all approaches that could be evaluated but I look at the reliability aspect as where it is right now, which is not principally in those large items. I think it is in the black box area and where we can do the most good, we should test the electronic, avionic subsystems that are inside rather than test the whole avoinics bay and structure and everything, because the same items are bought on an individual basis; they have to be integrated in there and I really don't think we are far enough along right now to where we would be doing a lot of that type testing.

Dr. Curtis: I think we are right into that because we are answering proposals to do these kinds of tests on the system for whole radar for example, that may weigh 2 or 3 hundred pounds. We are right into that problem and it has to be addressed.

Voice: Anybody else have any comments on that particular aspect of it; about the vibration testing of large items?

Mr. Kovak: Westinghouse. Let us say you are going to test small boxes which are part of a small radar system which weighs a few hundred pounds. If you want to test the small boxes as part of that system you also have to intercouple to those small boxes the air flow systems and make sure that the heat flow between boxes is similar and if you also do the small boxes it says you have to know what the vibration inputs at those mounting pionts are; which means you may have a six or seven different kinds of vibration profiles for several small parts of a small system so there has got to be a break point between a small system and a large system. If it is below some particular point in size that is physically achievable within a reasonable size chamber and with a reasonable size vibration system then the force drive or force control allowing the inpedance to take care of things is probably the better way. Bigger than that I guess you have to break it up into very small devices and profile each one separately.

Harold Nevius: General Dynamics: Dave, when you run your test didn't you take one line replacement unit and vibrate it and then all the others that were required to keep it running were outside the chamber?

Mr. Earls: We had seven of them in the rack. We were just using that unit in your rack with its installed complement of LRU's (Line Replacement Unit). That was our test, the ones on the outside were hooked to part of the radar system but they weren't part of our test other than just to see what is happening; part of it had to be hooked up operationally that way. We weren't getting the environmental data on each LRU in there which we changed when ever we had failures but it was hooked up the way it would be in the airplane with the rack that is in the airplanes sitting on the shaker.

Mr. Nevius: I guess I was thinking about some systems where we will have 7 LRU's in a system and we will just shake one of them at a time and set the other six out here in case it is a three hundred pound package and that way we break it down. Of course it runs into more expensive tests but that way you can find out which LRU is causing the problem at the time.

Dr. Curtis: Dave, did you control the test at the mounting points of the rack?

Mr. Earls: Yes!

Mr. Popolo: Was not your question whether we used aircraft structure rather than using fixturization? That was the question I thought.

Dr. Curtis: No, I said one possibility I had heard of was to do that. I was trying to suggest that for the testing of large objects that a simple definition of the level at the mounting points of that whole system may not be an adequate way of performing that vibration test, we may need more sophisticated methods. The present spec doesn't say anything about where or whatever.

Voice: I would like to say the present spec doesn't say anything about it. It seems to me as I sit back listening to the discussion that there is more than one frame of reference or

context under which the discussion is taking place. Until you bring in 781 it looks to me like its good bull session like I have heard in this type of gathering for the last twenty years of how can we better do our job for the contractor. This is good. Now when we start bringing in the standard military standard 781 we have to realize and recognize what a MIL-STD is supposed to do. Now if we juxtaposition these two discussions one upon the other we come to the erroneous conclusion that the MIL-STD is supposed to be all things to all men or a Santa Claus. There is no Santa Claus. You will find that a MIL-STD has one job and that is to give the guidelines for the job that needs to be done, and only the guidelines. In fact if you take a look at DSM 4120.3M which is the handbook that says what you are supposed to design a standard to, you will find that a military handbook and a military standard both are covered by the same section in this standardization manual. Standard nor a handbook is to be the rule it is only to be the guidelines. From these guidelines you come up with military specification or a specification of some sort that addresses or is supposed to address the particular set of items that you are interested in. Now I throw the question back to you how can we even begin to purport to put in such detailed information such as "do we use this type of fixture?" or "do we use that type of fixture?" when the military standard is to cover the whole gamut of material for even the electronics portion of the use. The answer of course comes back, you can't and you shouldn't. All you should do in a military standard like 781 is to say in the general requirements portion you will address vibration, you will address shock, you will address vibroacoustics, you will do this, this, this. You get into the detailed requirements section and you say in detail you will look for such things as going back to when I heard this first discussion twenty years ago in the GE five star tube days, you will see whether the plate and the cathode and the grid vibrate at separate frequencies and you will do some sort of a vibration synergism that will find this. In the detailed requirements you call out the most general ways that we have gotten in trouble in the past. Now others that come into this circumstances then rightfully have to identify what the problems are and with this identification treat it in the generalizations of that particular piece of unit and it doesn't matter as Terry Elliott is interested in missiles. If I am designing a poor little wave guide someplace that's to go into a large radar it doesn't matter what happens in the missiles. Conversely Terry Elliott isn't too terribly interested either in my problems with this great big wave guide that I could walk through, and he shouldn't be. We should get the context of what we are discussing here in the reliability area down to general guidelines that are universal and somehow allow the contractor or whoever is the developer the latitude to use the very good technology that he possesses and has worked all these twenty or thirty years to possess. I am kind of at a loss to understand what the thrust of the discussion is and where it is going. What is the context and frame of reference under which we are supposed to be understanding.

Dr. Curtis: If I might respond to that I think I'd like to answer it in two parts. I agree with you entirely on how one should use a standard but I think from my experience as a contractor we many times see a specification which will say you will do thus and so in accordance with MIL STD 810B or C you will conduct a reliability demonstration test in accordance with MIL STD 781 B or C period. That's all it says, which is not a very well thought out requirement in specification; however as a contractor you know that is what is in my spec, so there is the problem. The other part of it was that having seen what is being suggested in 781 C to use random vibration it is a very simple statement and I was kind of using that as a vehicle to try and bring out some of the things we are going to have to pay attention to when we start to do this kind of testing with upgraded requirements. It was certainly not my intent to try to rewrite 781 C this afternoon but merely use that as an example or as a vehicle for the discussion. If I can do that one more time 781 C also says that or it infers that burn in testing typically on a 100 percent of the equipment shall be conducted in the same way as one can conduct the reliability

demonstration test and that is a pretty profound requirement because if one does the rel demo test on a system basis then one would have to do a burn in testing. Yet, in my opinion I think in burn in testing first of all the requirements should not necessarily be the same on a philosophical basis and it is important to try to exercise each LRU or smaller piece of that equipment to that environment which is necessary to weed out the weak sisters and that to my mind is not done on a system basis. I would like to ask for any comments on that.

Mr. Earls: I have no experience in that area. It sounds logical to me to do the burn in under the environmental requirements that you are going to have to operate under in the reliability test for a short period of time. I am not sure just where we are and what the difference between why we are running the burn in and the reliability and the qual where all this fits together in that area. In the burn in what you are trying to do is cull out that workmanship thing.

Dr. Curtis: Yes, burn in test is a proof of workmanship test or weed out the weak systems. What I was trying to say was I don't think that bears any relationship to the conditions under which I conduct a rel-demo test. They have different purposes and I should tailor the requirement to achieve those purposes which then leaves them independent. One is to weed out weak sisters, the second test really finds out whether I did a good job in burn in regardless of how I did it.

Mr. Elliott: I would like to support you on your first part of your answer. MIL STD 781 and a lot of other standards and specifications are being out into contracts misappropriately and what have you. I think a lot of the reason for that is and I have seen some signs of it a lot lately is that there are a lot of people getting into contracts from the purchasers side; the Navy side, Air Force and probably the Army that are new in the business and they have a tendency to grab the nearest spec that looks like the right thing and put it in. The word is not getting to them that there are better ways to do these things. I think it was 5272 which was replaced by 810C. I heard there are contracts being left with 5272 still in them. This shouldn't be. It is because somebody saw something that looked like the right thing and just put it in. I don't know how you beat that unless you get back to them and holler the first time you see that come out. There are a lot of these things that are happening. I think there are more of them happening than were happening five or ten years ago.

Voice: In my view the requirements for the burn in test, and the rel demo test are quite different. As you indicated, the burn in test is simply a way of getting out workmanship failures and incipient or weak sister type component parts. It is typically done on every equipment that's manufactured. Rel demo test is done on a limited number of equipments for so many times their expected lifetime or MTBF with the idea of having some demonstration or verification that you have attained something. But it really has little to do with getting out workmanship or weak sister type of things per se. In other words they are different; in the burn in test the levels and the duration should be approached from that angle rather than the other.

Voice: Let's go back to 781C. I talked to Bill Wallace from Naval Electronics Command who is putting the 781 C together and he told me that this draft that is going around is an unofficial draft and an official draft will come out in about 90 days and so that is for your information.

Dr. Curtis: I hope I prefaced my remarks that it was a copy that was going around for comment etc. It is getting a little late but I think there was one other problem I would like to see us generate a little discussion on. For many years I think almost all avionics were installed on vibration isolators and I think perhaps the reason they were was to get through the qual test, rather than they were really needed. Now with improved packaging and the shift to solid state components and so on, and

because we have come up with better requirements for qualification testing I think most avionics now is hard mounted. As I look at some of the things being suggested I am afraid that if we over kill on the vibration requirements for reliability demonstration we may force the going back to using isolators for the avionics merely to get through the rel demo test because the guts presumably will see less vibration that way. This can open up a whole raft of questions like for example is field reliability better for equipment that is on isolators? In other words do the isolators really work in the field? How should we run if equipment is designed with isolators? Should the reliability demonstration test be done with the isolators in place even though we recognize they're probably more effective in the lab than they are in the aircraft? What do we do for burn in testing? It seems to me considering the purpose of the burn in test you wouldn't put the isolators there even if they were going to be on isolators on the airplane. I think this is a topic that has to be addressed. I would like to ask Dave this question. Do we have any information that shows whether isolators are beneficial for reliability in the field and along with that; the equipment that you tested was it on isolators?

Dave Earls: No, what I tested was not. I don't have any information on that. The best technical answer I can give to you would be that it is adjusting the level in the field as close as you can. If you are going to have it way higher you are going to force design considerations like isolators when you really wouldn't need them in the airplane so apparently from what you are saying there is a lot more hard mounted equipment than there used to be so that means the test environment is better tailored to the real environment than in the past. So you are talking about the same sort of thing reliability wise; if you tailor to the environment you will be alright. If you over test by your 2 tenth g or something you are talking about may be worst the condition. I think the real heart of this reliability thing in terms of the test is what is the vibration where that thing is going to be located? It is pretty tough to know and when you do know that you are alright. But the overtest is going to kill you in reliability if you go to too high a level for too long a duration.

Dr. Curtis: Joe, you have put a lot of equipment in airplanes.

Mr. Popolo: We have evidence on our aircraft that says that as far as reliability an isolated piece of equipment is better than a non-isolated piece of equipment. We have that evidence. Point one, Point two, I find it hard to believe that a rel demo requirement is going to require the use of isolators if it had not already been required because of doing a qualification test. That would be more severe than our rel demo test, and if it was due to that reason then I can see the isolators being there but not because of rel demo. The third point as far as burn in test is concerned, again the burn in test is only there to weed out workmanship problems and you cannot get enough level into that unit if it is on isolators. Because of this we should then do our burn in test off the isolators. That's all we are trying to do is get workmanship, because there is going to be times when those isolators may fail due to fatigue or whatever or just because of some locked or broken out spring or cracked isolators and also there is environments that we are going to be subjecting this equipment to on flight lines where the equipment may not necessarily be on its isolators. Generally what happens the isolations systems stays with the rack and not the unit so therefore we have to worry about the unit itself being transported on a flight deck or just being left on a flight deck or whatever, so we should worry about the workmanship and the way we worry about the workmanship is by testing it off the isolators.

Mr. Van Ert: I guess I have a question that I am not clear on. I take it that you mean burn in test is burn in test and not acceptance test is that correct? Is there still the random vibration acceptance test in addition to this burn in test?

Dr. Curtis: I think Dan that in the avionics business, aircraft business we don't really have a test requirement which is quite analogous to that in the space business where each piece of equipment has to pass a flight acceptance test in the same sense that it does for the space business. Now I think a large majority of units go through some sort of a burn in test which includes vibration but to date those vibration requirements they usually combine temperature, cycling and vibration. The vibration has been the low frequency single frequency nonresonant type vibration, so I think there is a very distinct difference between the space business and the aeronautical equipment business in how that testing is looked at. It is almost a voluntary test on the part of the contractor in many cases. It is kind of loose compared to the space business. Along with introducing random vibration into demonstration tests, which are long term tests, there are a lot of moves afoot to make the burn in test broadband tests whether they be random or merely an impact type testing which was mentioned earlier or whatever. There are efforts to try to upgrade those burn in tests, but they are not related to the field in the same way as a FAT test that you mentioned.

Mr. Van Ert: Consider what is being done in the space business. The thing to do nowadays for acceptance is to expose the flight units to the maximum expected vibration/temperature environments. I guess those are the main ones mostly vibration/temperature off-on cycling, that sort of thing. Why wouldn't it make sense to do that in aircraft?

Dr. Curtis: Well, there is one distinct difference in the space business where you do a flight acceptance test for one minute or two or however many; you have more than covered the dynamic duration of the dynamic environment for that equipment till it gets up there but for avionics you may fly the unit for ten thousand hours. You can't do a ten thousand hour test.

Mr. Van Ert: Ok, that is true in vibration, but certainly something like I think specified now is 8 thermo cycles temperature just up and down temperature cycles with hot starts, cold starts, that sort of thing. Certainly eight cycles is nowhere near the lifetime of a spacecraft that is going to be in orbit for five years. It would seem as though the important element is how long does it take to find the bad actors and you may not be able to tie it in into the expected duration. But, it would certainly seem to me that if I were going to build something and commit it to an airplane it might be thoughtful to give it the vibration level I expect the unit to live in to find out whether my soldering job is a good one.

Dr. Curtis: Burn in tests come in all shapes and sizes and especially durations but typical ones are of the order of fifty hours of temperature cycling plus whatever testing you may have done on piece parts before that and so forth. With this sinusoidal vibration, if it was a fifty hour test what we did was fifteen minutes per hour of this sinusoidal vibration for that fifty hours. Now do we want to do fifty hours times some factor? What if we go to random vibration? What are going to be the effects of that?

Mr. Hancock: There might be a point of clarification in the way draft copy of 781 C is presently written in that they do use five different terms to specify the type of test, the burn in, the reliability growth, they do reference environmental testing, environmental qualification testing for 810 C then they have a demo acceptance test which in paragraph two of this draft says will be performed by the government or independent laboratory. I think that is the way the thing presently reads. There is an indistinction in the specification between what environment is applied during each of these five tests. The problem is inherent; it is recognized. It is one that is spelled out in 781 C. It is one that must be addressed sometime in its promulgation stage.

Voice: There is one additional test we get into more and more that's sort of analogous to an acceptance test and that is what is commonly referred to as a manufacturing run in

which is a type of burn in. Some people refer to it as burn in and typically this has a requirement like of failure free period; you have to go through so many cycles or so many hours of failure free environmental cycling. This would be on all equipment and it is usually done at the system or subsystem level. In other words the level that you are delivering.

Dr. Curtis: That's true. Well the time is rapidly passing. I hope that the discussion has brought out that to improve the vibration requirements for rel-demo testing a lot of careful work will be needed on the part of a lot of people to make sure that we really do improve the situation. I wouldn't dare to try to summarize the discussion. At this point I would like to fulfill a promise I made to Bob Hancock. I will give him the floor for a few minutes to tell you something about the activities that the IES (Institute of Environmental Sciences) is undertaking in this area and mention the next IES meeting this spring which I believe is going to have one or two sessions devoted to this topic.

Bob Hancock: I told Allen this morning when he suggested we might have a little time available that I could speak somewhere between five minutes and four hours. I think we will aim more at the five minute direction. I might say in the way of introduction that I am in the throws of drafting an article for the November/December IES Journal in which I was trying to bring some of these problems into prospective and indicate some of the problems that we have been as an organization working with the joint logistics commanders workshop toward solving. This is again in the nature of an introduction here through some of our local chapter meetings and some of the discussions within the organizations. There were several problem areas defined—I might just flip through a few of these very quickly. Say in effect this does represent some of the membership consensus within the organization and that by and large we can agree with the tri services workshop committee. The Air Force headquarters command was well represented with Colonel Swetts presentation last October. But there is a considerable concern within the organization with some of the activities that we find going on within the Department of Defense organization. Under the tri services plans and activities there have been some improvements suggested as to more participation with industry, getting more laboratory people involved to provide some incite as to what is possible in some of these practices that they have been suggesting. Bring in some of the commercial and space expertise that has been developed over the past few years that's currently missing from some of the workshop groups and we would like to see more of their plans and activities publicized to industry, to allow some industry input. One of the points driving this one was that there has been too much assumed. Some of their recommendations about what is possible with testing have been made without the proper development of rational. We view today the piecemeal interim spectra visions that are presently in progress as troublesome. I will leave the word undefined. The NASC Aeronautical requirements that have been published as an interim measure spec use field environments during reliability testing. That is a bit difficult to interpret particularly for cost quotations, but we do find if we do say get up a weapons system costing out all the reliability testing required under these AR documents we are looking at something on the order of $250,000,000 for testing operations. Now that is opposed to around $40,000,000 at the outside for present systems. It is a considerable increase in scope for both testing time and facilities. There have been numbers talked on the order of $.3 to $3 million in testing equipment requirements for each testing laboratory. There were some suggestions made by the IES membership that R & D funds are necessary to develop the technology that the current funding through Flight Dynamics Lab at (Rome Air Development Center) (RADC) are grossly underfunded in comparison to the scope of the problems that are under discussion. Already I think it is probable that we can identify that contract incentive fees are going to be necessary to achieve some of the goals that they

are aiming for. Item four here was to identify some trends. I think we are talking three levels of growth probably in our testing capabilities in order to get to where the services would like to go. If we look at the laboratories current abilities, about 75% of them can probably make some sequential addition of environments to reliability tests at the present time. In five years maybe 95% of them could, but to combine these environments and apply them to reliability testing probably no more than 10% can now. It will be a full ten years before 95% of the laboratories required to support major weapons systems development could apply these techniques. As far as adding computer flight environmental profiling to reliability testing I presume that is what Dave is finally talking here; no more than 5% of the labs can do that now; 50% perhaps in five years, perhaps 95% in ten years. These are very cursory overview type numbers. I flag this bottom one here for our own discussions; I mentioned that on the last question a few minutes ago, the separation of the contractor test and the DoD run demonstration or acceptance test. I suppose present plans do incorporate the retention of the separate environment qualification test. I haven't heard anything to the contrary recently. I thought we might throw this up just to look at momentarily; this came out of the joint logistics commanders electronic equipment workshop organization. That is a bad title up there now. This is what they set out as original targets in their program. You will notice the revision of all of the reliability specifications beginning with 781 which is currently in DoD circulation. It should come out to industry about January. 785 will start shortly, and work your way down through 756, 721 and so forth. Now they do recognize the field data collections systems is a problem. Most of you are familiar with most of these so I won't go ahead and continue through them. There is a similarity between this and what some of the IES membership consensus reported. I guess in recognition of some of these problems, listening to what Colonel Swett said last October at this meeting, look at some of the revisions that are coming out and the activities also about 60% of the membership of the IES is testing oriented, aerospace testing heavily. We thought it timely to set up a project organization within the IES with some defined goals and target dates for completion of some work items to interact with the Joint Logistics Commander Workshop organization and the joint technical coordinating group for the JLC on these problems. The project organization as it was set up is over here on the left and I have shown the interface, the interaction line with the functional support organization that will provide technical support to man these project functions over on the left. You guys know I think practically all these people that are manning the technical committees and the working project groups. I thought I might say there are project goals and goals defined for each one of these four work groups that I have defined here. I don't know that we should work through the goals but in essence it is the support to help provide some of the rational that is needed for development in this JLC reliability workshop growth. For example under the facility resources under Fred Rush up at Rockwell. One of the things that is in progress now is the survey of testing capabilities categorized for those three developmental phases that I showed a moment ago. Who has the facilities, how much is invested, what is their capabilities to do such and such type test within what time period. Costs I guess get involved too, what does it cost to do certain type test work. Test methods under Paul Turkheimer at Wyle Labs will be looked at, well let's say new concepts, for example, the idea of testing larger systems by simulating vibrations in the acoustic chambers. Borrowing from the space idea of putting the entire missile in, sliding in a chunk of fuselage or something. How efficacious is that? This was asked here a minute ago in relation to development of reliability growth. Another question that has been posed and is under investigation now how necessary let's say in terms of our inability to define triaxis vibration is it to perform three axis vibration tests during reliability growth? I wish I had a slide to show the type of environments we are talking about. MIL STD 781C defines five weapons systems platforms. I don't know if they fit these definitions or not, we have added a sixth. They are Fixed ground based

equipment, ground vehicles, ship and sub Aircraft, missiles, rotor craft. Now for those vehicles or for those equipment platforms Colonel Swett has asked for and I believe the workshop is going along with defining thermal, electrical, vibration and humidity requirements as a beginner. Now each one of those has a breakdown under it, for example under vibration we have type whether as to random, sine, transient, the amplitude, the frequency spectrum, the application and the length of exposure. This gets back to my point a while ago; despite the best intentions of some of the committees either whether it is under the IES the organization here or some of the DoD committees, it is probably going to take more funded R&D on the part of a few aerospace companies to provide the fill in of all these blocks. Under test management and plans, I think I don't have the thing right here in front of me right now, but this would interrelate with how well does the testing organization provide feed-back to the designer. For example one of the problems that we see with segregation of the contractor and government perform tests is that the path is cut for feed-back directly to the designer such as now exists within some of the aerospace companies where all the testing is performed in-house. At any rate you get the idea here this thing I say will be published in the November journal. There are some near term and long term actions being defined for this project group within the IES. We have now worked our way down through item eight or are in the process as I say. The conduct of an environmental reliability seminar has been postponed until the second week in February. We are sponsoring a session at Rams. There will be nine hours of discussion at the annual meeting in 1976 in Philadelphia. There will be sessions on the west coast aerospace testing conference which is scheduled I believe for September of 76 rather than May. We do intend to publish at least one information paper on this topic in each of the Journal issues. The point is I suppose is that we do rather than have the annual meeting such as the one we are having here we wanted to get established a continuing project/action group such that the work can be continuous from year to year or day to day and give you a group of people to contact with questions. I am openly soliciting your participation on any one of these working groups or on the project staff.

Dr. Curtis: Let me say I am glad to see the IES trying to take a lead role in what I think is a very large problem facing us. At this point I would like to thank the panelists for their participation, Bob Hancock for assisting me in putting this session together and I would like to thank you the audience for your attention and participation.

REFERENCES

1. Swett, B. "Avionics Reliability Study—Phase II", HQ AFSC/XRX, Andrews AFB, MD, March 1974.

2. Prather, D. K., and D. L. Earls, "Combined Environment Reliability Test (CERT) For Avionics Subsystems" Journal of Environmental Sciences, Mar/Apr 1976.

3. Kern, G. A. and T. M. Drnas, "Operational Influences on Reliability Study" Final Report, April 1976. To be published by RADC.

4. Hirschberger, G. et al, "Evaluation of Environmental Profiles for Reliability Demonstration", Rome Air Development Center, AFSC, Griffiss AFB, Rome, NY, RADC-TR-75-242, September 1975.

SHOCK TESTING AND ANALYSIS

EARTHQUAKE TEST ENVIRONMENT — SIMULATION AND PROCEDURE FOR COMMUNICATIONS EQUIPMENT

N. J. DeCapua, M. G. Hetman, S. C. Liu
Bell Telephone Laboratories
Whippany, New Jersey 07981

A rational procedure for determining a regional earthquake test environment for communications facilities is described. The approach includes examination of a wide range of telephone building responses to arrive at an upper-bound response spectra. An acceleration time history test environment in the form of a synthesized earthquake is generated to match the spectra. The regional test is then established by linearly scaling the time history to the peak acceleration shown on a national earthquake design regionalization map. Further scaling to account for motion amplification for in-building location of equipment was achieved through examination of data gathered from the 1972 San Fernando earthquake.

INTRODUCTION

Telephone communications facilities are located across the entire contiguous United States, and a significant portion of these installations are in seismically active regions. These earthquake areas include the high-risk regions along the San Andreas Fault in California; moderate risk regions in the Rocky Mountains, Puget Sound (Washington), and the Mississippi Valley near New Madrid, Missouri; and relatively low-risk regions in the northeastern and southeastern sections of the country.

In this paper a seismic qualification procedure is described for determining a regional earthquake test environment for communications facilities. The advantages of the regional approach presented herein, as opposed to a single seismic test for the entire country, are that (1) cost savings can be realized by reducing or eliminating earthquake protection in moderate and low-risk areas, and (2) high reliability can be achieved by increasing protection in high-risk areas.

BASIC APPROACH

The basic procedure used to arrive at a regional earthquake test environment is to:

1. Determine the in-building earthquake response of a variety of communications buildings
2. Develop a realistic upper-bound response spectra for equipment in telephone buildings
3. Generate a test environment to match the upper-bound spectra
4. Scale the upper-bound environment by accounting for the variation of earthquake hazard across the country to arrive at a regional test environment.

UPPER-BOUND RESPONSE SPECTRA

Equipment located on upper floors of multistory buildings generally are subjected to stronger shaking than equipment on ground floors, because the earthquake motion is amplified as it travels through the coupled ground-building-equipment system. In an analytical study of earthquake-induced in-building motion [1], the motion-time histories for the upper floors of multistory telephone buildings with different building characteristics (number of floors and building width) and soil conditions were calculated for earthquakes with Richter magnitudes of 6.3 to 8.0. The results were expressed in terms of motion histories and the envelope response spectra for different damping ratios are shown in Fig. 1. The average peak floor acceleration level corresponding to such spectra is approximately 0.8 to 1.0g.

GENERATION OF TEST MOTION ACCELEROGRAM

Ideally, a simulated earthquake motion employed for equipment testing should resemble an actual earthquake motion as closely as possible in response spectra, peak accelerations, peak velocities, peak displacements, durations, and appearance of waveforms. A number of

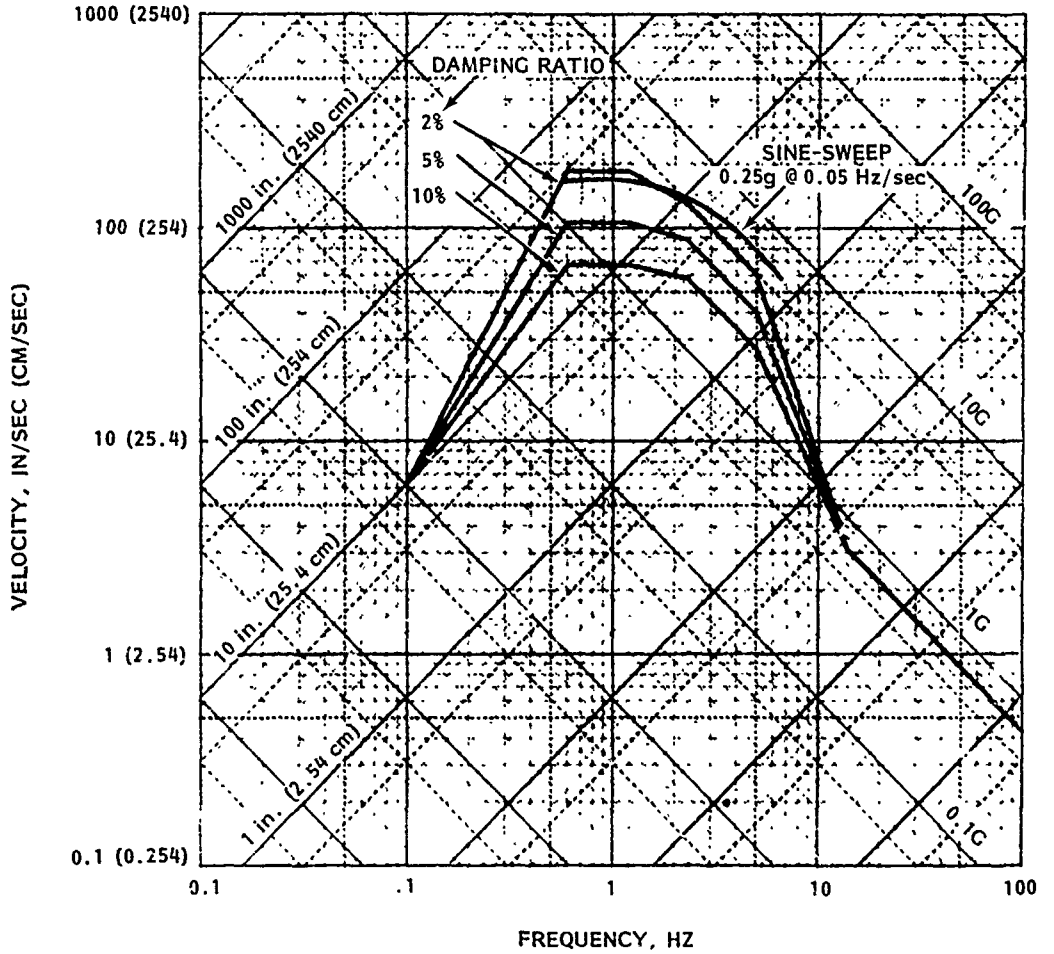

Fig. 1 - Envelope of in-building damped response spectra

different test methods [2] can be employed to simulate an earthquake environment, including sine beat, decaying sine, sine-sweep, and time history. Only the sine-sweep and time history methods are considered in this study.

Sine-Sweep Method

Since the sine-sweep simulation is relatively easy to match to a response spectra, as well as easily generated on a shaker table, it was the first simulation method employed as an earthquake test environment. With the sine sweep method, a 0.25g sweep at 0.05 Hz/sec, starting at approximately 1 Hz, matched the 2 percent upper-bound spectra reasonably well between 2 and 6 Hz, which is the approximate frequency band of cabinet-type communications equipment-framework systems. The 2 percent response spectra of this sine-sweep is shown in Fig. 1.

While the sine-sweep method simulates very well the response spectra characteristics of an actual earthquake, other characteristics such as peak accelerations, velocities, displacements, and durations are not simulated. Therefore, the sine-sweep responses are accurate only for linear systems. The effects of small nonlinearities were examined by testing a typical module of communications equipment (shown in Fig. 2) with a forward (1 to 10 Hz) and a backward (10 to 1 Hz) sine sweep. The spectra for the forward and backward sweeps are of course the same since they represent the response of linear systems. Thus, if the measured equipment responses for the two sine sweeps are compared, the difference, if any, can be attributed to some sort of nonlinearity.

Acceleration at the top of the frame was monitored for both sweeps and it was found that

Fig. 2 - Communications equipment framework test

the backward sweep resulted in peak accelerations that were approximately 25 percent higher than those resulting from the forward sweep. These responses are depicted in Fig. 3. The fact that they were different was not surprising, but the degree of difference was larger than expected. When the measured responses were examined, it was found that as the frame started to respond at its resonant frequency (approximately 3.7 Hz), the anchor bolts tying the frame base to the concrete slab on the test table loosened slightly, resulting in a lowering of the resonant frequency to approximately 3.2 Hz. Therefore, when the forward sweep (1 to 10 Hz) was run, the frame dropped out of resonance very quickly since its fundamental frequency was decreasing as the sweep frequency was increasing. The result was a relatively mild response to the input. On the other hand, when the backward sweep (10 Hz to 1 Hz) was run, the lowering of the fundamental frequency was such that it remained in resonance since the sweep also was decreasing. The result was the significant frame response indicated above.

It was concluded, therefore, that the forward sweep was actually an undertest and the backward sweep possibly an overtest of the specific communications equipment examined. In general, it was concluded that the sine-sweep test, and probably the other tests that employ sine waves to generate a resonance, should be used with extreme caution to avoid misleading results.

Time History Method

The difficulties experienced with the sine-sweep simulation can be eliminated by using a test method that employs an earthquake time history. Such a method is a synthesized waveform, which generates table motion according to digitally generated artificial earthquake accelerograms. This method, which has definite advantages over the other test methods in almost every respect, is analytically developed by employing the techniques described in Ref. [3]. Basically, the technique starts with Gaussian white noise. An envelope function is then used to shape the initial, middle, and final phases of the earthquake motion into a typical earthquake accelerogram. The predominant frequency content is adjusted through parameters which are related to the ground motion transfer function. An upper-bound earthquake environment is generated by matching, as closely as possible, the 2 percent spectra of the synthesized earthquake to the in-building spectra shown in Fig. 1. This typically requires the generation of at least 20 different earthquakes before an acceptable time history is achieved.

The resulting acceleration history of this synthesized earthquake is shown in Fig. 4. This test environment qualifies as the upper-bound criteria since it approximately matches the upper-bound in-building response spectra and has a peak acceleration close to 1g. This peak acceleration value is consistent with the maximum in-building accelerations determined in Ref. [1].

The artificial earthquake acceleration depicted in Fig. 4a must be converted to a displacement history for use on a hydraulic shaker table. This displacement is shown in Fig. 5. As indicated, the peak displacement is approximately +18 in. (45.7 cm.), which, for the facility being employed, is well above the allowable peak-to-peak table displacement of ±6 in. (15.2 cm.). To overcome this difficulty, the low-frequency content, which is appreciable, was filtered out with a high-pass 0.5-Hz filter. This filtered displacement is shown in Fig. 6. As shown, the peak displacement is reduced to approximately 3.5 in. (8.9 cm.), which is acceptable for use on the shaker table. The

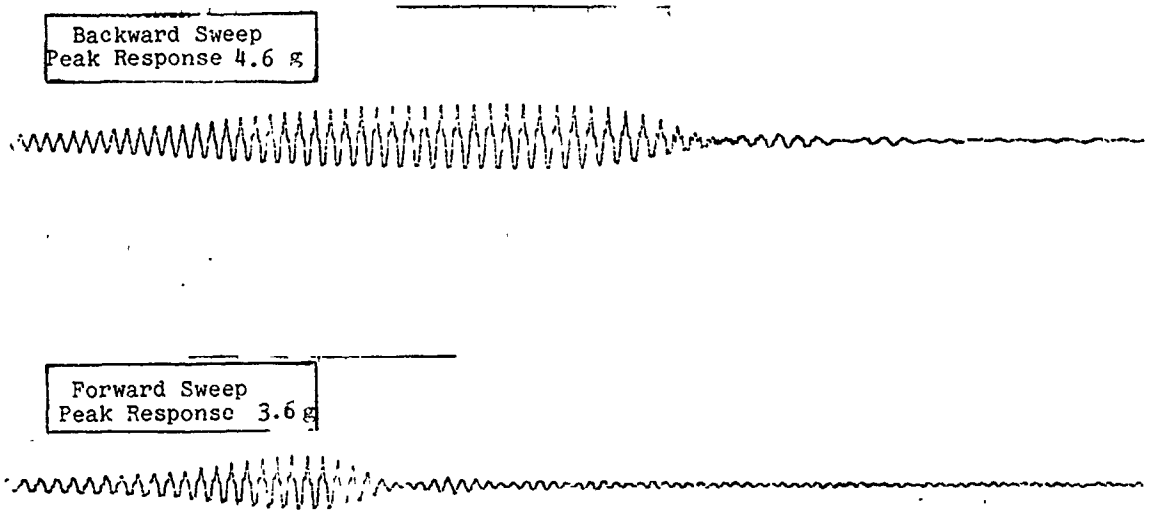

Fig. 3 - Comparison of equipment response using forward and backward sine sweeps (scale: 1 division = 0.5 sec.)

acceleration of the waveform remains approximately 0.9g.

In Fig. 7 the in-building upper-bound spectra (Fig. 1) are compared to the spectra of the analytically generated synthesized earthquake and the spectra of the table motion generated by the displacement history shown in Fig. 4. As indicated, the spectra match reasonably well within the frequency range of interest, i.e., approximately 2.3 Hz to 6 Hz, which bounds the fundamental frequencies of cabinet-type communications equipment. At frequencies below 2 Hz the test environment is lower, and for frequencies above 6 Hz the environment is somewhat higher than specified. It should be emphasized again that the waveform associated with the table spectrum of Fig. 7 is an upper-bound environment.

REGIONAL TEST ENVIRONMENT

The actual test environment that a specific facility must survive is a function of its geographic location and its location within a building, i.e., ground/first floor or upper floors. The expected peak ground acceleration is determined via microzonation studies that depict the regional earthquake environment as a function of geographic location. Peak in-building values are examined for two cases, i.e., ground/first floor locations and upper floor locations. An amplification factor that relates ground values to in-building values is employed. The appropriate test environment is then achieved by linearly scaling the upper-bound waveform down to the expected acceleration level.

Microzonation Analysis

The basis for the development of a regional earthquake test environment is a microzonation map that shows expected peak accelerations as a function of geographic location. In general, a microzonation study [4] results in a characterization of the earthquake environment at a site. It combines historical earthquake data and seismological and geological information with a sound statistical model to determine the expected environment at a site. This information may be presented in such a way that there is a 90 percent probability that the acceleration levels indicated will not be exceeded during the service life of communications equipment.

Building Amplification of Free-Field Motions

The large collection of ground-motion data recorded during the San Fernando earthquake was analyzed [1]. The ratio of upper floor acceleration to ground/first floor acceleration (amplification factor) was found to vary with the amplitude of the ground motion. The mean plus-one standard deviation acceleration amplification factor for moderate to large

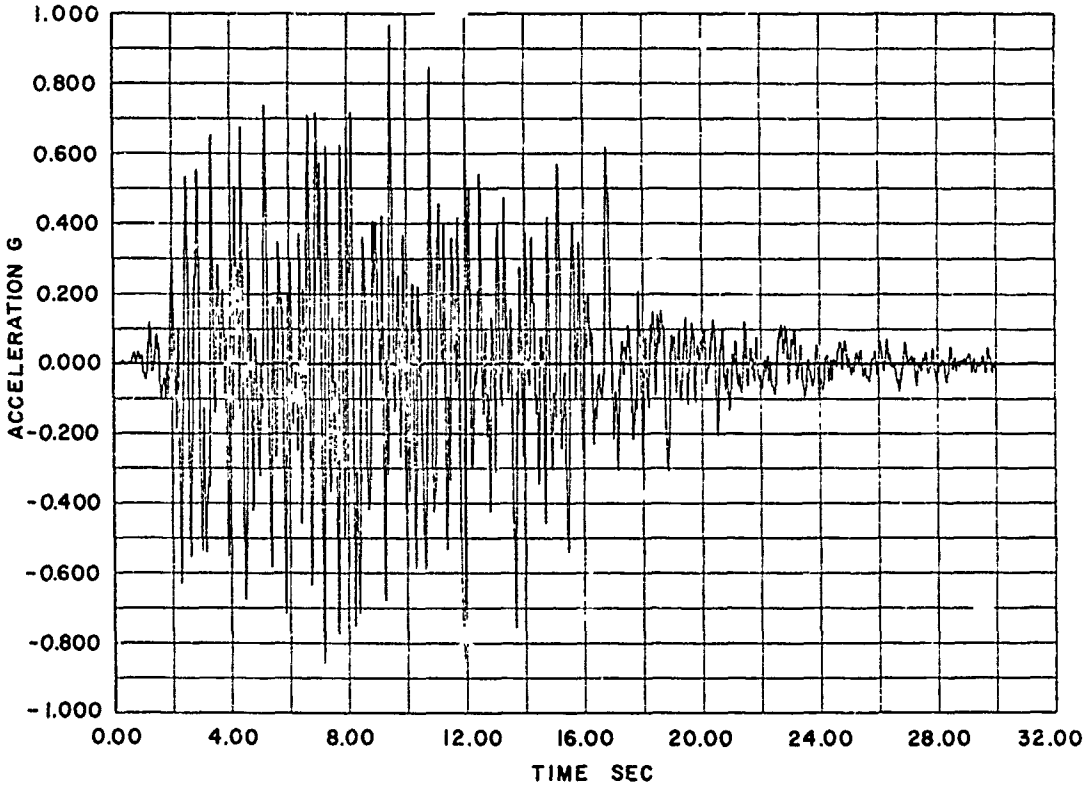

Fig. 4 - Analytically developed artificial earthquake accelerogram

intensities and for conditions common to most telephone building construction is shown in Fig. 8. The one-standard deviation above the mean amplification is judged as being sufficiently, yet not overly conservative for determining equipment protection. As indicated in Fig. 8, the amplification factor varies from 3 at 0.1g ground acceleration down to 1 at 0.5g. For ground acclerations higher then 0.5g, the amplification factor remains unity, i.e., there is no amplification.

Test Environment

An earthquake test environment can now be generated. Consider the situation of a communications facility located geographically where the microzonation map indicates an expected peak acceleration of 0.2g. If the equipment is to be installed on the upper floors of the building, then the amplification factor in Fig. 8 is approximately 2, so that the peak upper floor acceleration is 0.4g.

The test environment can now be determined by linearly scaling the accelerogram of Fig. 4, which has a peak acceleration of approximately 1g down to a peak acceleration of 0.4g. If the equipment to be tested were on the ground/first floor, there would be no building amplification and the test environment would have been scaled to 0.2g instead of 0.4g.

SUMMARY AND CONCLUSIONS

In this paper, a rational procedure is described for determining a regional earthquake test environment for telephone communications equipment. The regional approach has several advantages over a single test for all earthquake areas, i.e., cost savings may be realized by reducing or eliminating earthquake protection in moderate- and low-risk areas, and high reliability is achieved by increasing protection in high-risk areas.

The recommended general test environment is a time history in the form of a synthesized earthquake. It was shown to have a number of advantages over sine-wave tests such as the sine-sweep.

An upper-bound synthesized earthquake test environment was generated by shaping the waveform and adjusting the frequency content of

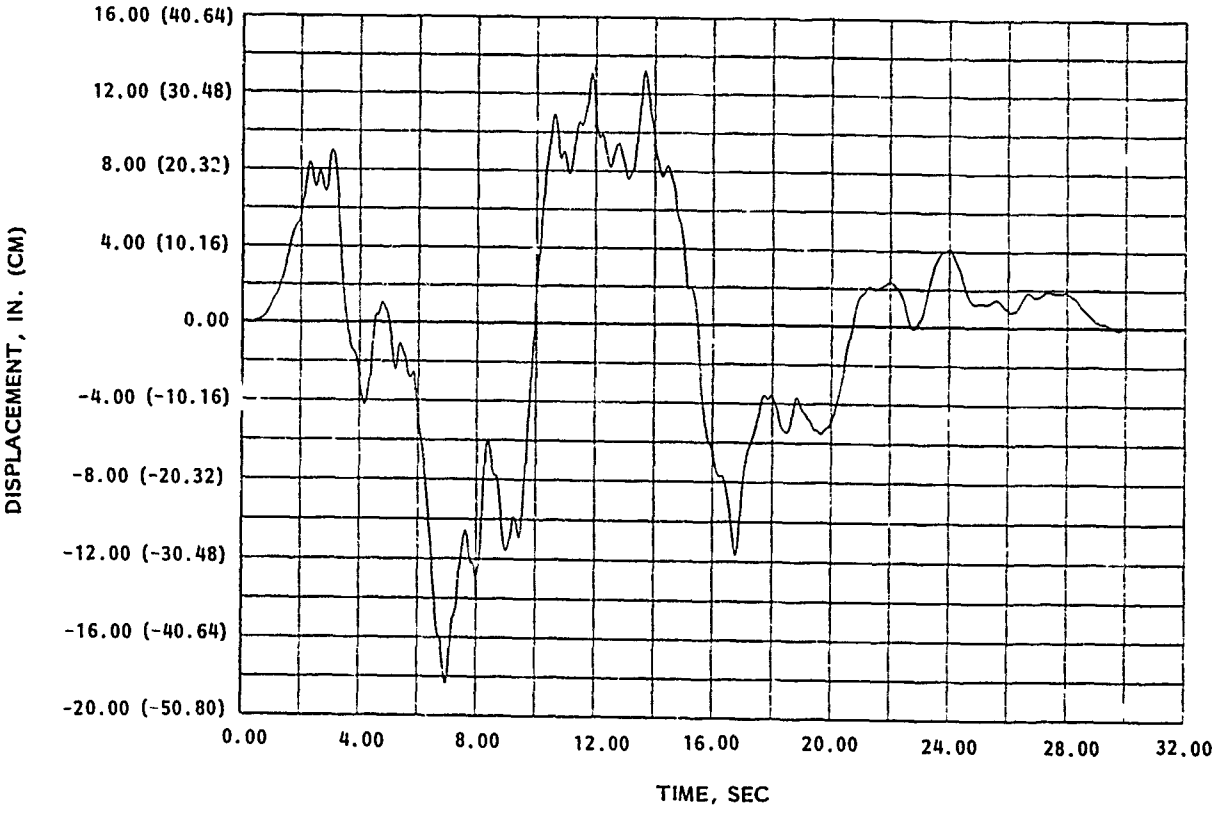

Fig. 5 - Displacement waveform of artificial earthquake

Gaussian white noise and matching its spectra to the envelope response spectra of a range of telephone buildings. The regional test is then determined by linearly scaling the upper-bound environment to the peak acceleration shown on a national earthquake design region-alization map that resulted from a micro-zonation study. Further scaling to account for location of equipment within a building was achieved through examination of data gathered from the 1972 San Fernando earthquake.

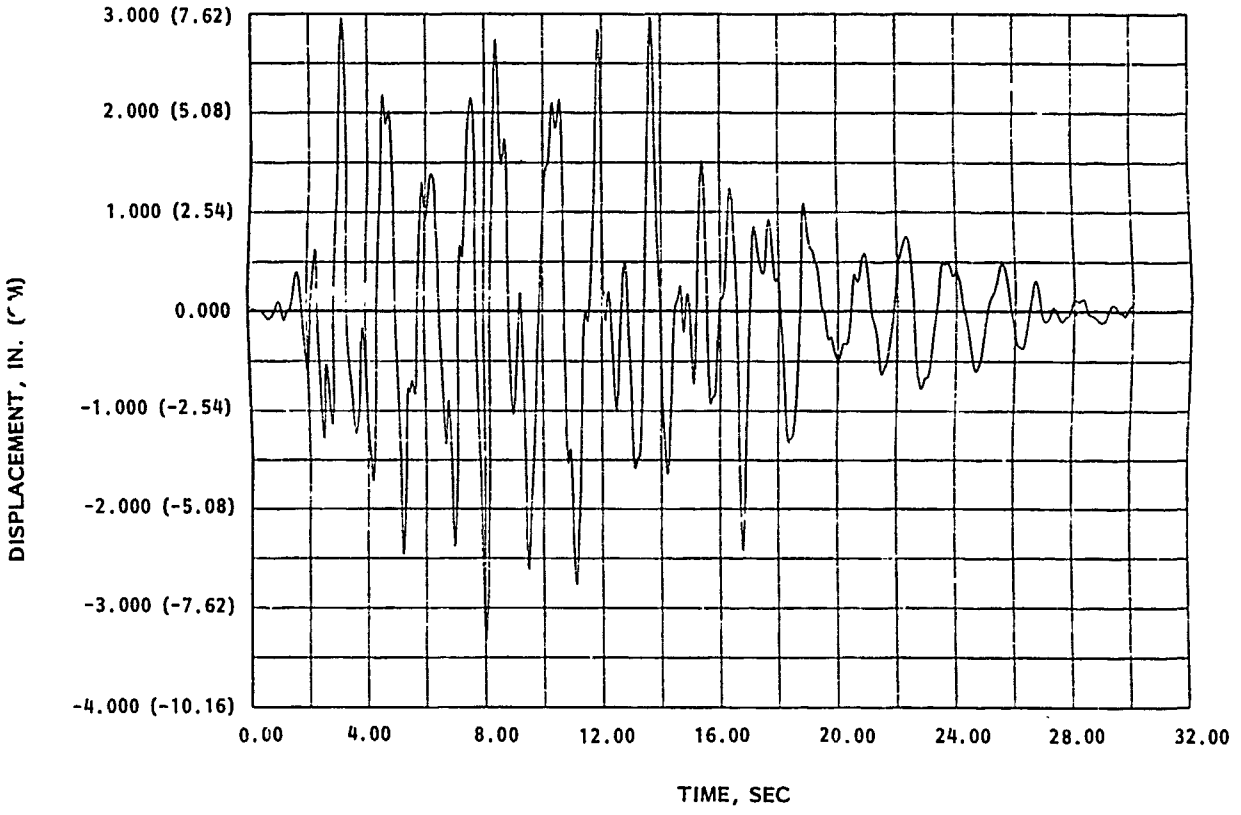

Fig. 6 - Displacem. ɔt waveform of artificial earthquake with 1/2 Hz high-pass filter

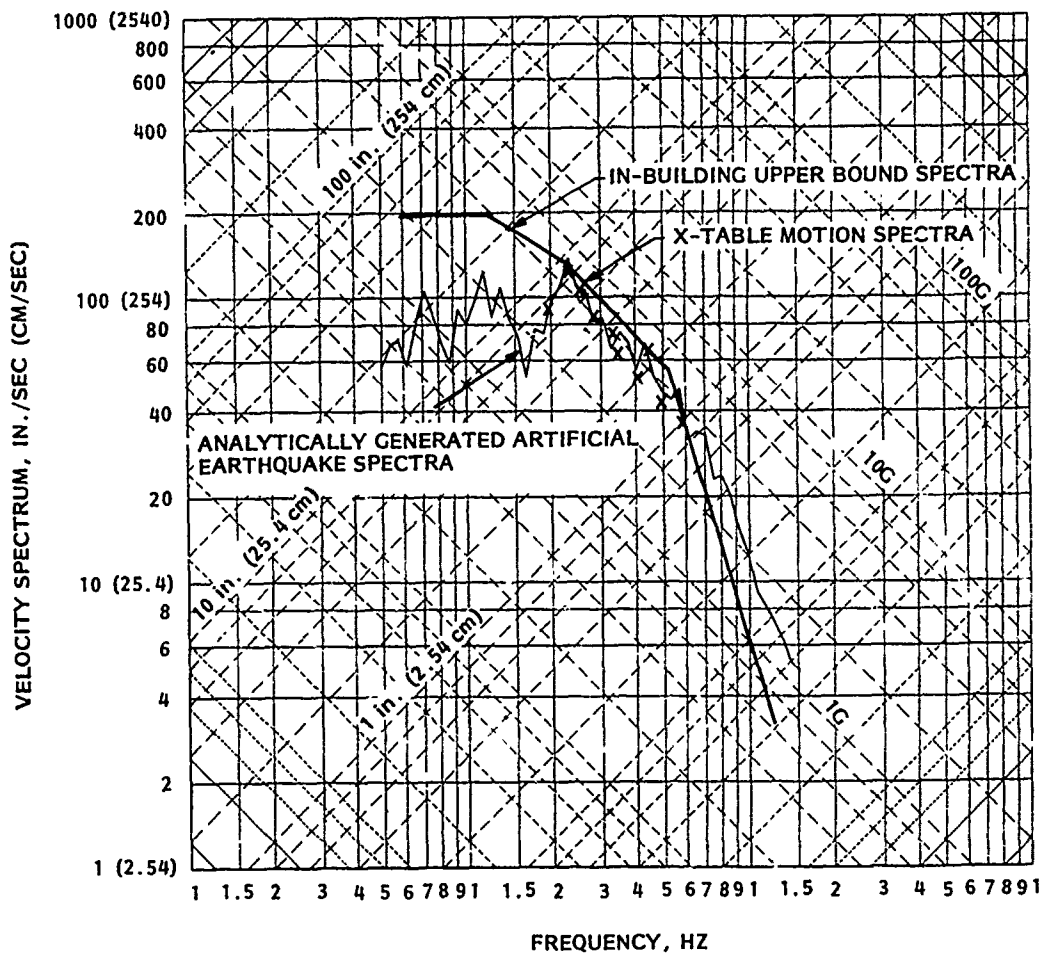

Fig. 7 - Comparison of 2% damped shock spectra

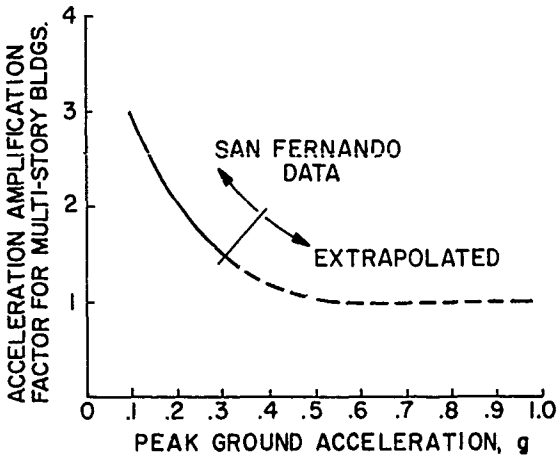

Fig. 8 - Building amplification vs earthquake ground acceleration

REFERENCES

1. L. W. Fagel, S. C. Liu, M. R. Dougherty, "Synthesis of Strong-Motion Earthquake Forcing Environment in Multistory Telephone Buildings," Unpublished work.

2. "IEEE Recommended Practices for Seismic Qualification of Class IE Equipment for Nuclear Power Generating Stations," IEEE Std. 344, 1975.

3. S. C. Liu, L. W. Fagel, "Earthquake Environment for Physical Design: A Statistical Analysis," BSTJ, November 1972.

4. S. C. Liu, N. J. DeCapua, "Microzonation of Rocky Mountain States," Proceedings of U. S. National Conference on Earthquake Engineering, June 1975.

Discussion

Mr. Hutchinson, (Consultant): How did you determine that the damping was 2%?

Mr. DeCapua: The 2% damping is basically a result of all of our testing of our communications equipment on shake tables.

Mr. Hutchinson: Did you determine the damping on the decrement or the width?

Mr. DeCapua: It was log decrement type testing. This has been done over a period of time.

Mr. Hutchinson: How fast was the sine sweep?

Mr. DeCapua: It was at .25 g's and at .05 hzs per second.

Mr. Hutchinson: Did you test in all three principal axles?

Mr. DeCapua: No, our shake table facility is one axis, horizontal.

Mr. Hutchinson: Did you test in the front to back direction?

Mr. DeCapua: Yes, generally that is the weak direction of our equipment configuration.

Mr. Luschei,(Boeing Aerospace Co.): Did you run the acceleration waveform test.

Mr. DeCapua: Yes.

Mr. Luschei: How did you run that test?

Mr. DeCapua: Our shake table has the capability of generating a complex acceleration waveform. We run it through the equipment in the horizontal direction.

Mr. Chalmers,(NELC): Do you plan to revise your test spectrum if buildings get stiffer?

Mr. DeCapua: Actually our buildings are designed for earthquakes; there are different earthquake codes, the California code includes some earthquake requirements, and most of the studies in our building synthesis program are for these types of buildings. I don't forsee any need for a reanalysis in the near future, possibly we may think differently later on.

Mr. Forkois, (NRL): Did you just make one sweep? What was the duration of the testing? Was it just for one earthquake or for several shocks?

Mr. DeCapua: The artificially generated earthquake is supposed to be characteristic of a broad range of earthquake environments and this information is extracted out of our building response study. We do our building response study and we examine the response of buildings to a large number of earthquake accelerograms, actual measured earthquake accelerograms from the El Centro, the Taft, and the San Fernando earthquakes. The resulting time history is one which we think is characteristic of this broad range of earthquake environments.

Mr. Forkois: How long does the test take?

Mr. DeCapua: It is a thirty second test.

Mr. Forkois: In one direction?

Mr. DeCapua: The test is in one direction for our particular facility; you can use the same procedure if you have a more complex facility to generate the other direction inputs as well.

Mr. Mortimer, (Boeing Aerospace Co.): Do you have any equipment sensitivities about 10 hz?

Mr. DeCapua: We have examined a lot of our equipment in this frequency range and we are concerned with the structural aspects of the equipment. For example, we want to avoid catastrophic failures of our frameworks. We will tolerate electronic failures which we can come in and repair, except in very sensitive areas, but generally we will accept some low level electronic problems.

Mr. Fisher,(Lawrence Livermore Laboratory): In your sine sweep testing what determines the use of a linear sweep as opposed to a logarithmic sweep?

Mr. DeCapua: We have been using the linear sweep and we found that we weren't confident of its application. We could have taken it one step further and used the logarithmic sweep, but we felt that we had the capability of going into the time history, so we really haven't examined that particular sweep.

AN ALTERNATE APPROACH TO MODAL DAMPING AS APPLIED TO SEISMIC-SENSITIVE EQUIPMENT

L. A. Bergman, A. J. Hannibal
Lord Kinematics
Erie, Pennsylvania

The influence of damping on the response of dynamic systems subjected to transient excitations such as seismic disturbances cannot be overemphasized. Its mathematical representation and parameter identification, therefore, become extremely important considerations. Unfortunately, the models currently in vogue, such as, viscous, proportional and modal damping are either inadequate representations of the dissipative mechanisms or require a great deal of experience and judgment in their implementation. The authors propose the complex stiffness approach, utilized extensively in other areas of dynamics, as a simple, accurate alternative for many seismic-sensitive systems. The method is presented, its implications discussed, and, finally, it is applied to a scale model of a circuit breaker base-mounted on an elastomeric suspension in order to determine the feasibility of such a system.

INTRODUCTION

It has been pointed out by Housner[9] and Plunkett[14] that damping has a strong influence on the response of dynamic systems subjected to frequency dense transients, such as seismic disturbances. One need only examine a typical response spectrum, as shown on Figure 1, to recognize the impact of damping upon the overall system response. Therefore, its mathematical representation and treatment became critical elements in the analysis of such systems.

In any structural system, there are several dissipative mechanisms at work converting mechanical energy to thermal energy, the preponderance of which is converted via internal and interface hysteresis. Unfortunately, damping models commonly used today for seismic analysis either do not adequately represent these damping mechanisms or are mathematically cumbersome. Some damping models presently in vogue are:

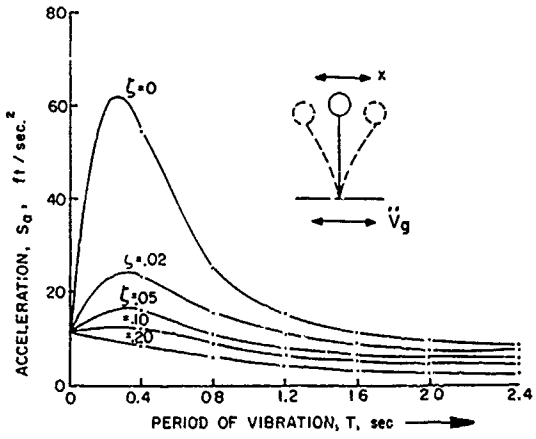

Fig. 1 - Average Response Acceleration Spectrum (intensity of ground motion recorded at El Centro, California, in 1940), After Housner

Viscous Damping: In viscous damping, the dissipative mechanism is defined as a linear function of velocity. When incorporated into a linear system formulation, the damped equations of motion become:

$$M\ddot{\vec{x}} + C\dot{\vec{x}} + K\vec{x} = \vec{F} \qquad (1)$$

where M, C, and K are the mass, damping, and stiffness matrices respectively. For most systems, the elements of C are difficult if not impossible to characterize without relating them to assigned modal damping factors. If perchance the viscous damping coefficients have been defined, Foss[8] has demonstrated that the homogeneous form of equation (1) can be uncoupled by reducing the system to a first order state-space formulation from which system natural frequencies and modal damping factors are readily available.

Proportional Damping (Rayleigh Form): Proportional damping implies that the viscous damping matrix is a linear combination of the mass and stiffness matrices,

$$C = \alpha M + \beta K. \qquad (2)$$

Since M and K diagonalize simultaneously, so also does C. The unfortunate drawback of this form is that it rarely, if ever, realistically models actual damping characteristics.

Modal Damping: In modal damping, the undamped system is uncoupled and viscous damping factors are assigned to each mode through experience and good judgment. Often a great deal of time and expense is spent reconciling the "a priori" analytical model with experimental data[10].

The damping model proposed in this paper is the complex stiffness representation given by the force-displacement equation

$$f_D = k'(1+j\eta)x \qquad (3)$$

where k' is the dynamic stiffness, $j = \sqrt{-1}$ and η is referred to as the loss factor. η is normally defined as a relative measure of the energy dissipated per cycle, D, to the maximum stored energy, E,[6] or

$$\eta = \frac{D}{2\pi E} \qquad (4)$$

and is proportional to the displacement while in phase with the velocity for harmonic motion.

In the literature, the complex stiffness is also referred to as hysteretic damping, structural damping, loss factor damping and solid friction damping. It has been widely utilized, particularly in the aircraft industry, to model flutter problems[15] and in acoustics to characterize the damping of vibrating panel systems[7]. Mathematically, the complex stiffness is no more difficult than viscous damping and offers the advantage of accuracy of representation. One drawback, however, is that hysteretic damping has not been defined for vibrations other than harmonic. This problem will be addressed in the next section.

The objective of this paper is to present hysteretic damping as a viable alternative to viscous forms when modeling seismic-sensitive structural systems. The authors do not suggest that the complex stiffness approach is without limitations; but for many systems in which the loss factors of the spring-like elements have been measured, it should provide fairly accurate results. For more complex systems, the complex modulus approach can at least provide a better "a priori" analytical model.

COMPLEX STIFFNESS APPROACH

Snowdon[16] and others have demonstrated that for cyclic loading the material properties of an isotropic material can be represented by complex moduli, given by:

$$E^* = E'(1+j\eta_E) \text{ and } G^* = G'(1+j\eta_G) \qquad (5)$$

where E^* and G^* are the complex Young's and shear modulus respectively, and η_E and η_G are a measure of the dissipative capacity of the material in the tension-compression and shear modes respectively and are referred to as loss factors. It is generally accepted that for most plastics and rubber-like materials, the loss factors in both modes are nearly equal; that is, $\eta_E = \eta_G$.

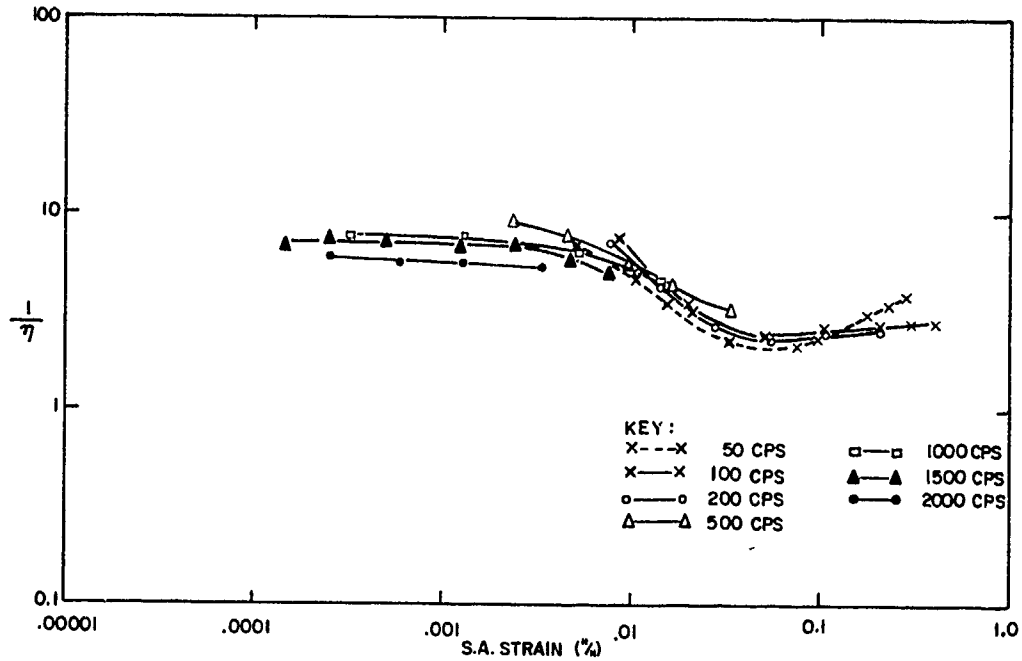

Fig. 2- Effect of Frequency and Dynamic Strain on the Loss Factor (η) for a Typical Silicone-Based Elastomer

For the analysis discussed in this paper, it is assumed that the material properties, E* and G*, are constant over the operating ranges of frequency, temperature and strain. For many materials, particularly highly-damped ones, this assumption is not always valid. For example, Figure 2 depicts the effect of strain and frequency on the loss factor of a typical silicone-based elastomer. As can be noted, the loss factor is maximum near 5% single amplitude strain. As the strain drops below 1%, the loss factor levels off at a value which is only a fraction of that at 5% strain. In the case of seismic disturbances, which normally involve large motions a conservative, minimum-expected value of loss factor should be adopted. With respect to frequency dependence, the majority of seismic energy is propagated in the frequency band of one to ten hertz, over which the properties of many materials may be realistically considered constant. Similarly for temperature dependence, since the duration of most seismic pulses is on the order of 30 to 45 seconds, the material hardly has time to generate sufficient heat internally to raise its temperature very much and, therefore, the material properties related to the ambient temperature will prevail.

The dynamic stiffness of a spring-like element, given by

$$k^* = k'(1+j\eta_k), \qquad (6)$$

is dependent on its geometry, direction of load and material properties. k' may be derived or measured experimentally. However, except for simple geometries, accurate derivation is extremely difficult.

Consider a system comprised of mass elements and spring-like elements whose stiffnesses are modeled by equation (6). In terms of the assigned degrees of freedom and the geometry of the system, a complex stiffness matrix can be derived in the form

$$K^* = [k^*_{i\ell}] = K' + jK'', \qquad (7)$$

yielding n damped equations of motion of the system given by the matrix equation

$$M\ddot{\vec{x}} + K^* \vec{x} = \vec{F}\, e^{j\omega t} \qquad (8)$$

where the excitation is harmonic with frequency ω. In order to determine natural frequencies and modal loss factors, it is natural to reduce equation (8) to its homogeneous form,

$$M\ddot{\vec{X}} + K^* \vec{X} = 0, \qquad (9)$$

and to apply a standard complex eigenvector/eigenvalue extraction routine. Essentially, this is exactly what the authors propose. However, not without justification for free vibration is a decaying sinusoid and, therefore, not harmonic. Equation (9) has been studied by many researchers, Bishop[2, 3], Bishop and Johnson[4], Crandall[6], Mead[11], Myklestad[12], Soroka[17], Tong[18], to name a few. Normally, equations of this form are regarded as having no physical significance[4, 18], and the information derived from them as being meaningless. However, Mead[11] has demonstrated that equation (9) does indeed have meaning by associating it with an external harmonic vibration of the form:

$$j\eta \times [\text{the inertia force of the system}]. \qquad (10)$$

By assuming a solution of the form

$$\vec{x} = \underline{\vec{X}}\, e^{j\omega t} \qquad (11)$$

and defining the excitation as

$$\vec{F} = j\eta\omega^2 M\underline{\vec{X}}\,, \qquad (12)$$

Mead has shown that equation (8) has the form:

$$[-\omega^2(1+j\eta)M + K^*]\underline{\vec{X}}\, e^{j\omega t} = 0. \qquad (13)$$

If a solution of the form

$$\vec{x} = \vec{\phi}\, e^{st} \qquad (14)$$

where $\vec{\phi}$ is a complex vector and s is a complex number is assumed for equation (9), it reduces to:

$$[s^2M + K^*]\vec{\phi}\, e^{st} = 0. \qquad (15)$$

By comparing the determinant of equations (13) and (15), the square of the ith eigenvalue, s_i^2, can be written as:

$$s_i^2 = -\omega_i^2(1+j\eta_i) \qquad (16)$$

and

$$\vec{\phi}_i = \underline{\vec{X}}_i \qquad i = 1, 2, \ldots, n$$

It is apparent that the complex eigenvalue contains both the angular natural frequency, ω_i, and the modal loss factor, η_i, for its respective mode. The natural frequencies and their associated mode shapes are not "natural" in the sense of free vibration but require the presence of a system of complex forces for their existence. Mead has also shown that the complex eigenvectors exhibit the same orthogonality relationships as undamped mode shapes and, furthermore, the response of a harmonically excited system can be written as a linear combination of them.

It may be possible to apply the above theory based on hysteretic dampers to a system excited by a seismic disturbance. Crandall[6] has shown, however, that a damper having constant loss factor does not meet the requirement for causality when a unit impulse is applied; that is, the impulse response function is shown to be dependent on future behavior. The authors have chosen, therefore, to equate the modal loss factors to an equivalent viscous damping factor, given by

$$\zeta_i = \frac{1}{2}\eta_i. \qquad (17)$$

This equality yields equivalent damping at resonance for which a single degree of freedom acts like a filter and is, therefore, reasonably accurate through the region of greatest interest. Furthermore, as both natural frequencies and modal damping factors are directly available, spectral analysis is easily accomplished. Equation (17), unfortunately disregards the coupling due to damping which essentially transfers energy among modes where it is subsequently dissipated. Except for heavily-damped systems, this assumption is normally justified.

Finally, like the modal damping technique, the viscous equivalent, ζ_i, is added to the ith mode, resulting in the uncoupled system equations of motion.

$$\ddot{y}_i + 2\omega_i\zeta_i\dot{y}_i + \omega_i^2 y_i = -\xi_i\ddot{X}_0 \qquad (18)$$

$$i = 1, 2, \ldots n$$

where $\ddot{x}_o$ is the acceleration time history of the seismic disturbance, ξ_i is referred to as the participation factor[5,13] and given by:

$$\xi_i = (\vec{\phi}_i^T M \vec{I}_o)/m_i \qquad (19)$$

where

$\vec{\phi}_i^T$ is the transpose of the ith undamped mode shape,

m_i is the ith generalized mass,

and $\vec{I}_o$ is a vector of ones and zeros.

A question yet to be addressed is, "How do the damped 'natural' frequencies and logarithmic decrements derived from equation (9) differ from those of an equivalently-damped viscous system?" Soroka[17] has investigated this question for a single degree of freedom system. His work can be summarized as follows: The damped natural frequency of a hysteretically-damped system is given by:

$$\omega_D = \omega_n \sqrt{\frac{1 + \sqrt{1+\eta^2}}{2}} \qquad (20)$$

where ω_n is the undamped natural frequency and η is the loss factor. Obviously as η increases, the damped natural frequency becomes greater than the undamped natural frequency. This phenomenon is not consistent with usual understanding of damped, free vibration. However, as Table 1 clearly shows, the deviation, ω_D/ω_n, is within 4% for a loss factor of .40.

The logarithmic decrement for a hysteretically-damped system is given by:

$$\delta_\eta = 2\pi\eta/(1 + \sqrt{1+\eta^2}) \qquad (21)$$

For a comparison of equation (21) with the logarithmic decrement of an equivalent ($\zeta = 1/2\eta$) viscous damped system, given by [19]

$$\delta_\zeta = 2\pi\zeta/\sqrt{1-\zeta^2} \quad , \qquad (22)$$

refer to Table 1. For small damping, the logarithmic decrements are essentially the same. As damping increases, δ_ζ becomes greater than δ_η implying more energy per cycle is dissipated by equivalent viscous damping than by hysteretic damping.

TABLE 1

Comparison of Logarithmic Decrements and Natural Frequencies for Equivalent Viscous and Hysteretic Damping[17]

VISCOUS			HYSTERETIC		
ζ	δ_ζ	ω_D/ω_n	$\eta(=2\zeta)$	δ_η	ω_D/ω_n
0.01	.0628	1.00	0.02	.0628	1.00
0.02	.126	1.00	0.04	.126	1.00
0.05	.315	1.00	0.10	.313	1.00
0.10	.631	.995	0.20	.622	1.00
0.20	1.28	.980	0.40	1.21	1.02
0.30	1.98	.954	0.60	1.74	1.04
0.50	3.63	.866	1.00	2.60	1.10

In general, for loss factors on the order of .4, very little difference (with respect to normal engineering standards) exists between the free vibrations of a hysteretic-damped and an equivalent viscous damped single degree of freedom system. This conclusion can be extrapolated to a multi-degree of freedom system via the associated system of uncoupled equations of motion.

SCALE MODEL OF A HIGH VOLTAGE CIRCUIT BREAKER

- The Model

In order to demonstrate the application of the complex stiffness representation in the analysis of a large piece of electrical switchgear. the General Electric ATB550-3 circuit breaker (Figure 3), model testing and analysis were undertaken. The model utilized was fashioned after but not scaled from the aforementioned equipment, and is shown schematicized in Figure 4. It consists

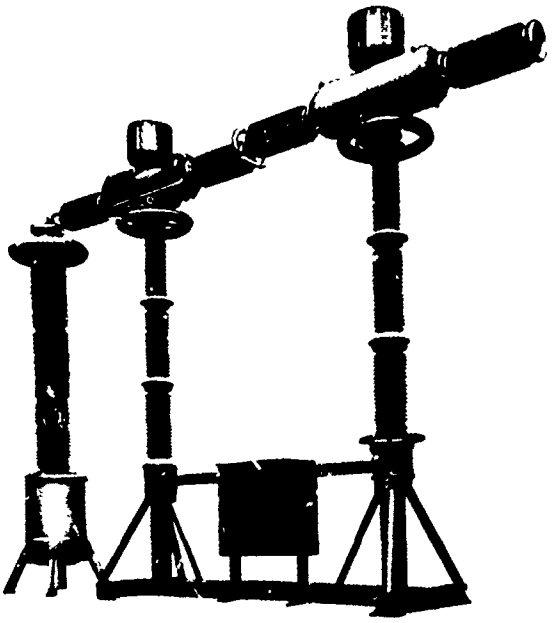

Fig. 3 - The General Electric ATB550-3 High Voltage Circuit Breaker

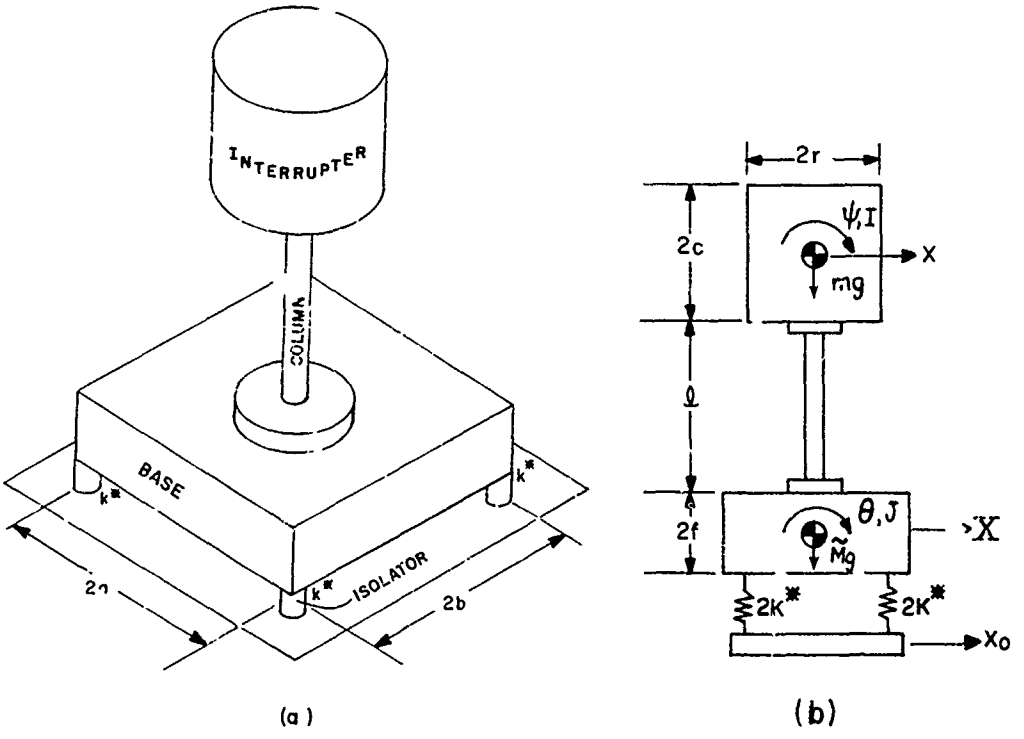

Fig. 4 - A Four D.O.F. Model of a High Voltage Circuit Breaker

of lower and upper masses (base and interrupter) of low carbon steel connected by a thin solid column of alloy steel. The column was coated with approximately .100 inch of structural damping compound, and the entire assembly was mounted on four elastomeric mountings. Two sets of mountings were utilized, each having different stiffness and damping characteristics. The various geometric and physical parameters of the model are defined in Table 2.

The Equations of Motion of the Model

Based upon the four degrees of freedom defined by (b) on Figure 4, and Table 2, the equations of motion may be written in the form

$$M\ddot{\vec{v}} + \mathrm{Re}(K^*)\vec{v} = \vec{Q} \qquad (23)$$

where the mass and stiffness matrices are given by:

$$M = \begin{bmatrix} \tilde{M} & 0 & 0 & 0 \\ 0 & J & 0 & 0 \\ 0 & 0 & m & 0 \\ 0 & 0 & 0 & I \end{bmatrix}, \qquad (24)$$

TABLE 2

Geometric and Physical Parameters of the Four D.O.F. Model

Geometry: $a = .127m$ $b = .127m$ $c = .0838m$ $f = .0288m$ $\ell = .254m$ $r = .127m$	Inertia: $mg = 652.6$ N $Mg = 389.7$ N $J = .3186$ N·m·s $I = .4241$ N·m·s^2
Column: $E^* = E(1 + jn_c)$ $E = 2.068 \times 10^{11}$ Pa $n_c = .0066$ $\tilde{I} = 1.869 \times 10^{-9} m^4$	$\ell_1 = \frac{E^*\tilde{I}}{\ell}$ $\ell_2 = E^*\tilde{I}/\ell^2$ $\ell_3 = E^*\tilde{I}/\ell^3$
Natural Rubber: $k_x = 12522$ N/m $k_y = 58387$ N/m	$n_x = .025$ $n_y = .025$
Silicone: $k_x = 43782$ N/m $k_y = 245178$ N/m	$n_x = .15$ $n_y = .15$

$$K^* = \begin{bmatrix} 4k_x^*+12\ell_3 & -4fk_y^*-6\ell_2 & -12\ell_3 & 6\ell_2+12C\ell_3 \\ & +12(f+\ell)\ell_3 & & \\ & 4a^2k_y^*+4f^2k_x^{*2} & 6\ell_2 & -4\ell_1+6(f+\ell-C)\ell_2 \\ -4fk_y^*-6\ell_2 & +4\ell_1-12(\ell+f)\ell_2 & -12(\ell+f)\ell_3 & +12C(\ell+f)\ell_3 \\ +12(\ell+f)\ell_3 & +12(\ell+f)^2\ell_3 & & \\ -12\ell_3 & 6\ell_2-12(\ell+f)\ell_3 & 12\ell_3 & -6\ell_2 \\ & & & -12C\ell_3 \\ 6\ell_2 & -4\ell_1+6(f+\ell-C)\ell_2 & -6\ell_2 & 4\ell_1+12C\ell_2 \\ +12C\ell_3 & +12C(\ell+f)\ell_3 & -12C\ell_3 & +12C^2\ell_3 \end{bmatrix}, \quad (25)$$

the degrees of freedom by

$$\vec{v}^T = (\underline{X}\ \theta\ x\ \psi) \quad (26)$$

and the excitation by

$$\vec{Q} = \begin{Bmatrix} 4\mathrm{Re}(K_x^*) \\ -4f\mathrm{Re}(K_x^*) \\ 0 \\ 0 \end{Bmatrix} x_o \ . \quad (27)$$

By applying the following definitions, equation (23) can be rewritten in terms of relative translations and absolute rotation.

Let $\underline{X}_r = \underline{X} - x_o$, (28)

$$x_r = x - x_o;$$

$$\vec{x}_g^T = (x_o\ 0\ x_o\ 0) = \vec{I}_o^T x_o; \quad (29)$$

and $\vec{x} = \vec{v} - \vec{x}_g = \vec{v} - \vec{I}_o\, x_o$. (30)

Substitution into equation (23) yields

$$M\ddot{\vec{x}} + \mathrm{Re}(K^*)\vec{x} = -M\vec{I}_o\ddot{x}_o. \quad (31)$$

Let Φ be the matrix of eigenvectors derived from

$$\mathrm{Det}[M^{-1}\mathrm{Re}(K^*)-\lambda I] = 0. \quad (32)$$

Also let

$$\vec{x} = \Phi\vec{y}. \quad (33)$$

Then by substitution of equation (33) in equation (31) and premultiplication by Φ^T, the uncoupled equations of motion can be written as:

$$[m_i]\ddot{\vec{y}} + [k_i]\vec{y} = -\Phi^T M\vec{I}_o\ddot{x}_o \quad (34)$$

where

$[m_i] = \Phi^T M\Phi$ = diagonalized mass matrix

$[k_i] = \Phi^T \mathrm{Re}(K^*)\Phi$ = diagonalized stiffness matrix

and $\omega_i = \sqrt{k_i/m_i}$.

Then, defining the participation factors as in equation (19) by

$$\xi_i = (\Phi^T M\vec{I}_o)_i/m_i,\ i=1,\ 2,\ 3,\ 4 \quad (35)$$

equation (34) can be rewritten as

$$\ddot{y}_i + \omega_i^2 y_i = -\xi_i\ddot{x}_o. \quad i = 1,\ 2,\ 3,\ 4 \quad (36)$$

Since the homogeneous form of equation (31) with Re(K*) replaced by K* is the same as equation (9), its complex eigenvalues are given by equation (16). Therefore, equivalent viscous damping factors for each mode, ζ_i, are derived from the modal loss factors via equation (17), which are then added to equation (36) as modal damping factors resulting in the final form of the equations of motion given by:

$$\ddot{y}_i + 2\zeta_i\omega_i\dot{y}_i + \omega_i^2 y_i = -\xi_i\ddot{x}_o. \quad i = 1, 2, 3, 4 \qquad (37)$$

Referring to a modal displacement response spectra, such as Figure 7, the maximum displacement, $y_{i,max}$, of each mode can be determined based on its natural frequency and damping factor. The influence of $y_{i,max}$ on system response is factored into the analysis through the participation factors; that is, the product $\xi_i y_{i,max}$.

To return to the original coupled degrees of freedom or m linear combinations of them, represented by

$$\vec{u} = A\vec{x}, \qquad (38)$$

where A is an mxn matrix (for the model, n = 4), can be achieved by substituting equation (33) into (38). Then,

$$\vec{u} = A\Phi\vec{y}. \qquad (39)$$

One of the most common means of combining modal responses to obtain a total response is the root-mean-square method; that is, $u_{j,tot}$ is determined as the square root of the sum of squares as in equation (40).

$$u_{j,tot} = \sum_{i=1}^{n}\left[\left((A\Phi)_{ji}\xi_i y_{i,max}\right)^2\right]^{\frac{1}{2}}. \quad j = 1, 2, \ldots, m \qquad (40)$$

Model Tests

Prior to testing of the complete model, the spring and damping characteristics of the column and elastomeric mountings were determined. With the base of the model (Figure 4) secured to ground, the column-interrupter system was "plucked". The free vibration of the interrupter was measured by an accelerometer which was connec through an amplifier to a brush recorder. The logarithmic decrem was calculated from [19]

$$\delta = \frac{1}{n}\ell n\frac{x_n}{x_o}, \qquad (41)$$

and the column loss factor from

$$\eta = \frac{\delta}{\pi}. \qquad (42)$$

Transmissibilities of both elastomeric mounting systems were measured horizontally and vertically, utilizing the base mass only. The frequency response of each system was recorded using an electrodynamic shaker and associated instrumentation. The shaker input was adjusted to reflect the expected strain level in the elastomeric mounting. Mounting spring rates were calculated from the system natural frequency by

$$k = \frac{m}{4}(2\pi f_n)^2. \qquad (43)$$

Similarly, loss factors were calculated from the transmissibilities at resonance by

$$\eta = \frac{1}{T_{res}} \qquad (44)$$

These characteristics are given in Table 2.

The entire model was then assembled, per Figure 4, and frequency response obtained for each system over the range of 1 to 30 hertz. Responses recorded were plots of $\ddot{\underline{X}}/\ddot{x}_o$ and $\ddot{x}/\ddot{x}_o$ versus frequency.

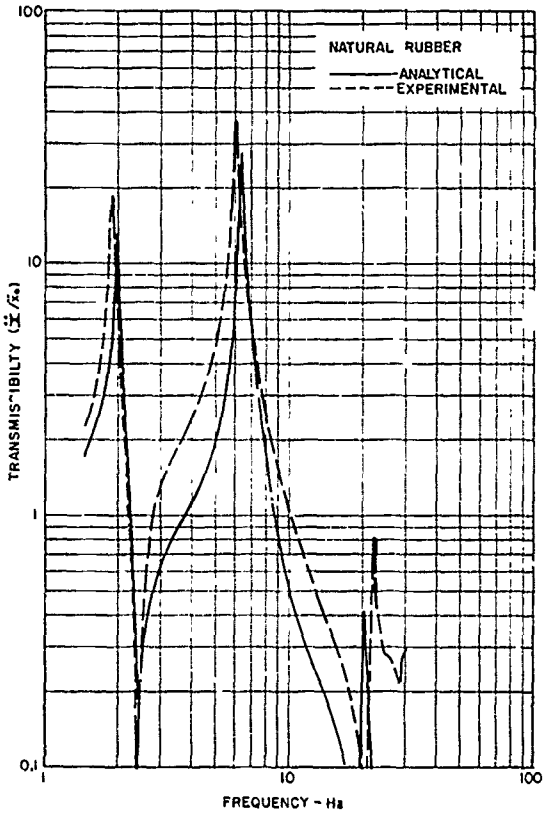

Fig. 5a - Transmissibility of Base

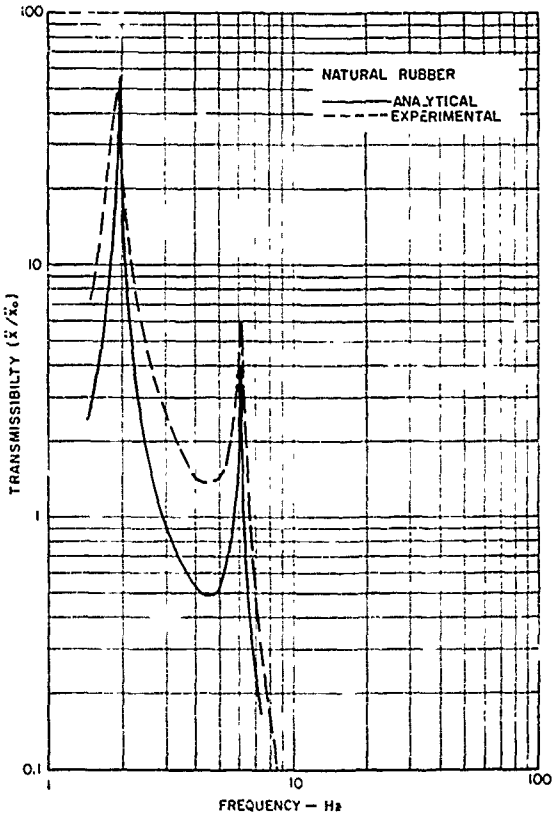

Fig. 5b - Transmissibility of Interrupter

Concurrently, utilizing the component material and physical characteristics obtained earlier, the same responses were developed by subjecting the equations of motion to harmonic analysis. The resulting curves of transmissibility versus frequency are shown in Figures 5 and 6. Correlation between experiment and analysis is seen to be very good for the natural rubber. The silicone mountings, however, display a high degree of strain sensitivity.

- Spectral Analysis

In each case, the complex eigenvalue problem was solved, the systems uncoupled, and natural frequencies and modal loss factors determined. Participation factors were calculated, as was the response in each mode due to a .5g response spectrum per Figure 7. The total response of the base, the interrupter and the motion across the column for each system was calculated using equation (40). These results are shown in Table 3.

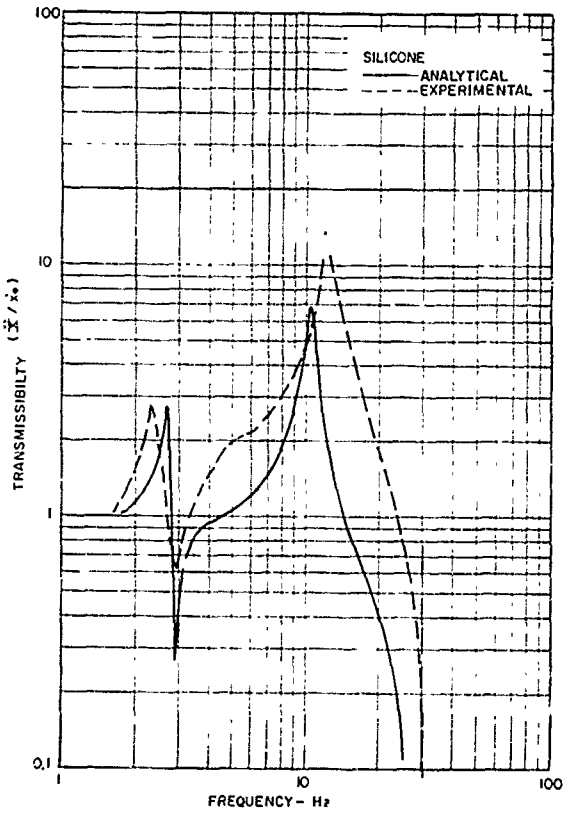

Fig. 6a - Transmissibility of Base

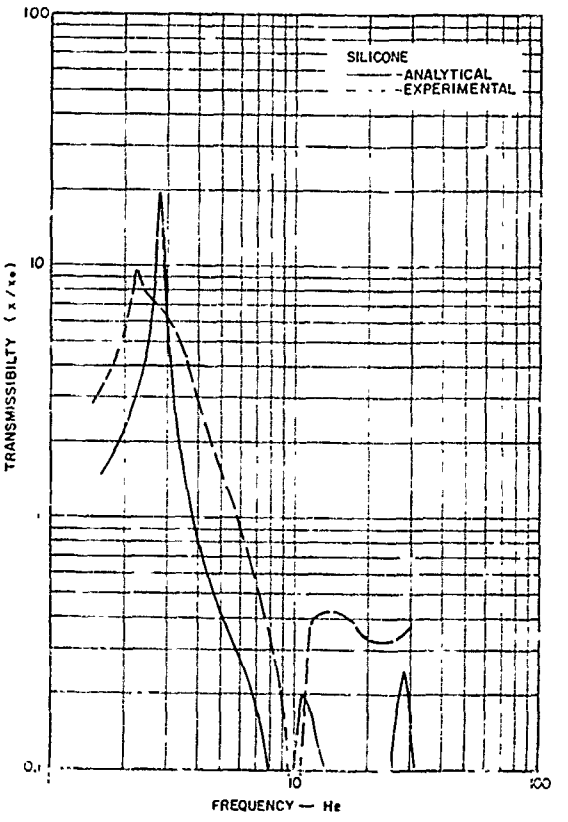

Fig. 6b - Transmissibility of Interrupter

A study of Table 3 illustrates the value of damping in the control of the response of complex dynamic systems. Clearly, the silicone system is more effective in limiting relative displacement than the natural rubber system. Generally, for systems of this basic configuration, additional damping permits the use of greater spring rates for equivalent relative column displacements resulting in more stable, less "jelly-like" suspension systems.

CONCLUSIONS

The complex, or hysteretic, representation of system damping is sufficiently accurate in the regions of greatest interest to be utilized in the development of modal damping factors for seismic-sensitive equipment thus eliminating much of the need for extensive experience. Of course, the complex modulus approach is not without shortcomings. There are frequency, temperature, and strain dependencies to be considered. Particularly strain dependence which for many materials, especially highly-damped ones, is extremely nonlinear. In other cases, the strain may extend into the plastic region.

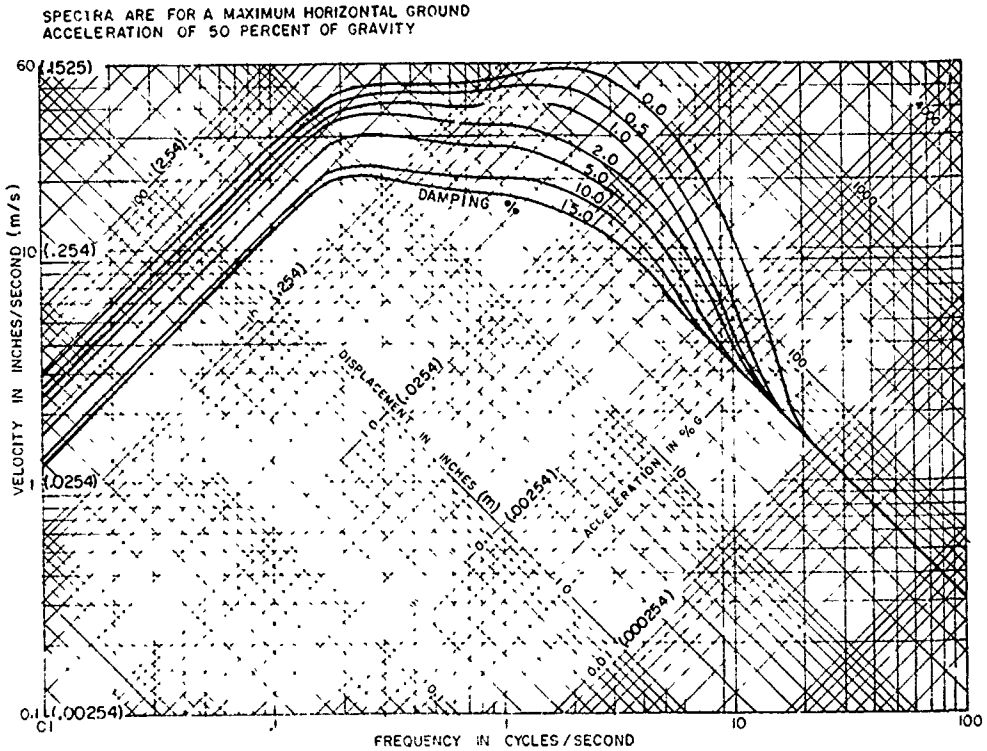

Fig. 7 - Electrical Equipment Seismic Design Response Spectra

Measurement or loss factors of various elements in the system may also present a problem; for example, the loss factor of a rivetted joint or of a wall bolted to a superstructure. In any case, the loss factor is a more accurate representation of the dissipative mechanisms of internal and interface friction as it does not diminish the hysteresis loop at lower frequencies and, therefore, is inherently a more meaningful representation of system damping.

Generally speaking, elastomeric suspension systems offer a viable alternative to structural modification through the introduction of additional damping into modes contributing to failure of the structure.

ACKNOWLEDGMENT

The authors wish to thank the General Electric Company for permission to identify their equipment and for the use of a photograph of the ATB550-3 circuit breaker. This permission does not imply that the General Electric Company, in any way, warrants the performance of the ATB550-3 circuit breaker when mounted on this suspension system or approves this analysis.

TABLE 3

Spectral Response of the Four D.O.F. Model

NATURAL RUBBER:

Modes	fn(hz)	n	ζ	ξ	y^*_{max}(m)	$\xi \cdot y_{max}$(m)
1	2.0	.018	.009	1.87	.0762	.1425
2	6.2	.021	.0105	.068	.00864	.000584
3	20.3	.015	.0075	-.058	.000356	-.00002
4	41.5	.008	.004	.0002	.000076	-

$(\overline{X}-x_o)_{max}$ = .0371 m

$(x-x_o)_{max}$ = .1372 m

$(\text{Column Deflection})_{max}$ = .03226 m

SILICONE:

Modes	fn(hz)	n	ζ	ξ	y^*_{max}(m)	$\xi \cdot y_{max}$(m)
1	2.7	.051	.0255	1.784	.033	.0589
2	10.4	.128	.064	.083	.00127	.0001
3	27.8	.067	.0335	.097	.000165	.0000015
4	47.8	.066	.033	-.0006	.000056	-

$(\overline{X}-x_o)_{max}$ = .00767 m

$(x-x_o)_{max}$ = .0582 m

$(\text{Column Deflection})_{max}$ = .02545 m

*Response calculated using .5g response spectrum per Figure 7.

REFERENCES

1. Adkins, R. L., Modal Analysis of Linear Non-Conservative Systems, Air Force Materials Lab Report TR-75-2, 1975.

2. Bishop, R. E. D., The Treatment of Damping Forces in Vibration Theory, Journal of the Royal Aeronautical Society, Vol. 59, November, 1955.

3. Bishop, R. E. D., The General Theory of "Hysteretic Damping", The Aeronautical Quarterly, February, 1956.

4. Bishop, R. E. D. and Johnson, D.C., The Mechanics of Vibration, Cambridge University Press, 1960.

5. Blume, J. A. and Sharpe, R. L. and Kost, G., Earthquake Engineering For Nuclear Reactor Facilities, John A. Blume and Associates, 1971.

6. Crandall, S. H., The Role of Damping in Vibration Theory, Journal of Sound and Vibration, Vol. 11, 1970.

7. Cremer, L. and Heckl, M. and Ungar, E. E., Structure-Borne Sound, Springer-Verlag, 1973.

8. Foss, K. A., Co-Ordinates Which Uncouple the Equations of Motion of Damped Linear Dynamic Systems, Journal of Applied Mechanics, September, 1958.

9. Housner, G. W., Behavior of Structures during Earthquakes, Proc. ASCE, Vol. 85, No. EM4, 1959.

10. Ibanez, P., Methods for the Identification of Dynamic Parameters of Mathematical Structural Models from Experimental Data, Nuclear Engineering and Design, No. 27, 1974.

11. Mead, D. J., The Existence of Normal Modes of Linear Systems with Arbitrary Damping, Proceedings of Symposium on Structural Dynamics, Paper No. C5, Loughborogh University of Technology, 1970.

12. Myklestad, N. O., The Concept of Complex Damping, Journal of Applied Mechanics, September, 1952.

13. Nelson, F. C., Shock and Seismic Excitation of Mechanical Equipment, ASME paper No. 74-DE-3, 1974.

14. Plunkett, R., Transient Response of Real Dissipative Structures, Shock and Vibration Bulletin, No. 42, Part 4, January, 1972.

15. Scanlan, R. H. and Rosenbaum, R., Introduction to the Study of Aircraft Vibration and Flutter, Macmillan, New York, 1951.

16. Snowdon, J. C., Vibration and Shock in Damped Mechanical Systems, John Wiley and Sons, 1968.

17. Soroka, W. W., Note on the Relations Between Viscous and Structural Damping Coefficients, Journal of the Aeronautical Sciences, July, 1949.

18. Tong, K. N., Theory of Mechanical Vibrations, John Wiley and Sons, 1960.

19. Thomson, W. T., Vibration Theory and Applications, Prentice-Hall, 1965.

20. Yamoda, Y. and Takabatake, N. and Sato, T., Effect of Time-Dependent Material Properties on Dynamic Response, International Journal for Numerical Methods in Engineering, Vol. 8, 1974.

Discussion:

Mr. John Burum (Amber Booth Co.): I get the impression that one would expect that the use of resilient mounts would protect many types of sensitive equipment against earthquakes.

Mr. Hannibal: From what I have seen so far I would say certainly not all equipment. When you look at the different modes of a structure it is important to get damping into those modes which are going to respond most readily to the earthquake. Perhaps a suspension system does not get enough damping into those modes which are critical and in those cases it probably would not be effective.

Mr. Burum: How did you handle problems with resonance in your test? Wouldn't you need restraint systems to avoid a build-up of motion?

Mr. Hannibal: The only testing we did was harmonic testing to obtain the frequency response and there was no difficulty there. If you use an elastomer with sufficient damping in it you won't need the restraints because the damping in the isolator itself will take care of that problem. We have seen silicone mountings with a loss factor of approximately .15 and elastomers exist which contain much more damping than that, up to .3 or.4. Restraints would not necessarily be needed and if damping is properly introduced into the system it would handle the problem.

ACTUATOR DEVELOPMENT FOR SYSTEM-LEVEL SHOCK TESTING

G. Richard Burwell
Boeing Aerospace Company
Seattle, Washington

This paper discusses the design, development and capability of an actuator for system-level shock testing. The actuator was designed to provide input motions to a full-scale test article that simulate the airblast-induced ground motion associated with nuclear attack. The actuator energy source is high-pressure gaseous nitrogen which powers a piston/piston rod connected to a test article. Piston motion is controlled by the flow of hydraulic fluid through piping, accumulators and orifice plates. The design requirements are presented including the wide range of shock levels which the actuator was required to produce. The design approach and the influence of the dynamic response model on the design are discussed. A description of the model, model refinements and improved coefficient values obtained empirically also is presented. Typical test/analysis comparisons of motion histories are provided. A description of the actuator physical operation is provided with an emphasis on configuration elements that control the motion and thus determine the input conditions to the test article.

BACKGROUND

In support of the recent design, development and hardness assessment of sophisticated shock isolation systems for hardened military sites, the complete shock isolation systems were subjected to a wide range of shock test levels. These shock tests were conducted by applying input motions to the isolation system at the ground facility interface that simulated groundshock motions representing those that would be created by nearby nuclear weapon explosions.

The need to provide these high-level input motions to full shock isolation systems was recognized in the early isolation system design stages. Also recognized was the need to design and develop new shock actuators as all existing shock test devices were incapable of producing the required forces, input motions and other performance parameters.

Therefore, in parallel with the shock isolation system design efforts two new shock actuators were designed and developed. The primary actuator, the design and development of which is the subject of this paper, was to provide the high-velocity ground motion associated with the airblast created by nuclear weapon explosions. A secondary actuator was to simulate the much lower velocity ground motion associated with the direct-induced (cratering) effects of nuclear weapon explosions. A discussion of the shock isolation system design procedures, test programs, their interrelationships and the role of the shock test devices is presented by Luschei (Ref. 6).

Associated with the development of the primary actuator was the need to develop an analytic model for use in establishing the geometric parameters to allow the actuator to produce the required test levels. This model would also be used to establish the specific configuration (pressures, orifice size and position, etc.) for each specified test level, waveform type and vector angle. As an added benefit the analytic model then could be used in subsequent test programs to define the detailed actuator configuration that would provide the desired input motion to the test article if that motion did not correspond exactly to one of the specified test levels. Previous shock actuator designs which were much smaller in size were not supported by analytic models and therefore required a combination of simple calculations, engineering judgment and a series of "calibration" tests to establish an acceptable actuator configuration. The confident use of an analytic model, therefore, would eliminate the need to conduct calibration tests which, because of the size of this actuator, would be particularly costly.

The statement of work for the primary actuator design and development referred to it with the descriptive name "prime mover." This name has remained with the actuator to the extent that those closely associated with the test programs involving this actuator refer to it as the prime mover. This paper, however, will refer to it as the primary actuator or test device.

PERFORMANCE REQUIREMENTS

Design performance requirements for the primary actuator were defined in the actuator statement of work in terms of shock levels defined by undamped response shock spectra, synchronization requirements for multiple actuator use, an ability to produce two waveform types and repeatability

requirements. As depicted in Fig. 1, the actuator was required to be capable of providing a wide range of specific response shock spectra levels within a tolerance band of each level. There are five principal levels in the frequency range of 0.1 to 1000 Hz identified in Fig. 1, with level 1 being the lowest and level 5 being the highest. In addition, three sublevels were specified below level 1 (¼, ½ and ¾ level 1) and there were two equally spaced sublevels between each successive principal level from level 1 through level 5 for a total of 16 levels. For clarity, only the principal levels and ¼ level 1 are shown in Fig. 1.

The levels shown in Fig. 1 applied to the vertical component of an actuator motion which could be vertical only or vectored between vertical and horizontal such that the horizontal/vertical motion ratio was 1/3, 2/3 or 1. The equivalent axial requirements, which are a function of both level and vector angle, were the requirements that had to be addressed when designing the actuator. Therefore, each of the 16 specific levels must be multiplied throughout the frequency range by 1.0, 1.054, 1.202 and 1.414 to obtain each of the 64 required axial levels. It is interesting to note that level 5 at a 1/1 vector ratio is more than 20 times the magnitude of vertical ¼ level 1 which demonstrates the shock level range capability for which the primary actuator was designed.

The shock spectra tolerance limits associated with each level also are indicated in Fig. 1. Above 30 Hz, tolerance limits were goals rather than firm requirements. The tolerance limits relative to each shock spectrum were ±10% in the low-frequency (displacement) region, ±50% in the mid-frequency (velocity) region and +100%, −50% in the high-frequency (acceleration) region.

Synchronization requirements were in terms of motion initiation and the relative positions of a number of simultaneously initiated actuators exciting the same test article. Motion initiation of all actuator/isolator attach interface points was to be within a relative time of two milliseconds. For maximum displacements less than 5 inches (12.7 cm), the vertical and horizontal motions were to be maintained so that no attach point would lead or lag the average position of all attach points by more than 10% of the average peak displacement. For maximum displacements greater than 5 inches (12.7 cm), the relative motions were not to lead or lag the average position by more than seven-tenths of an inch (1.8 cm).

Two shock pulse or waveform types were required: positive only and positive followed by partial return. The shape of the velocity histories corresponding to the two pulse types is shown in Fig. 2. Idealized waveforms corresponding to level 3 are used in Fig. 2 as the example. The positive-only pulse type is representative of a fully plastic soil condition, while the positive-with-return pulse type includes the effects of partially elastic soil properties. Notice in Fig. 2 that the return portion of the positive-with-return waveform is lower in velocity and displacement compared to the positive portion, but longer in duration.

The repeatability requirements were in terms of tolerances on a previously generated shock spectrum and as such were similar to the shock level tolerance band. The repeatability tolerance band was ±5% in the low-frequency (displacement) region, ±25% in the mid-frequency (velocity) region and +50% −25% in the high-frequency (acceleration) region. This tolerance band was exactly one-half the shock level tolerance band which was relative to the goal spectrum level.

DESIGN APPROACH

Preliminary design efforts resulted in the selection of a pneumatically powered, hydraulically controlled actuator as the basic design. The expansion of high-pressure gaseous nitrogen (GN_2) would be used as the energy source to power a piston and piston rod inside a cylinder. The piston and rod motion would be controlled by the flow of hydraulic fluid displaced by the piston from the main cylinder through piping to a series of capped cylinders called shaping accumulators. Four fluid ports would be provided in the cylinder end-cap, three for connection to shaping accumulators containing orifice plates and one for connection to an accumulator to be used to provide the partial return motion. A general schematic of the primary actuator is presented in Fig. 3; typical actuator installations in a test facility are shown in Fig. 4.

Concurrent with further design efforts, an analytic model of the actuator concept was developed. This model is described later and was instrumental in sizing the actuator components in terms of establishing the various volumes, diameters, lengths and other fixed hardware geometric parameters that would allow the actuator to produce the required range of test levels. Additionally, many details contained in the final design were selected after the performance effects were determined in the model. The model was developed in parallel with but generally ahead of the detailed actuator design. As the actuator design evolved the modeling representation became more detailed. The model had a positive influence on the actuator design and provided confidence that the final design would perform within specification.

A main piston and cylinder inside diameter of 20 inches and a GN_2 pressure limit of 5000 psi (34.5 MPa) were selected to provide the required acceleration capability. The required shaping accumulator volume was achieved with the use of relatively long (81.75 inch, 208 cm), small diameter (8 inch, 20.3 cm) cylinders to reduce the overall test device width envelope and thus preclude interference problems with adjacent actuators, because some test articles would require the simultaneous use of four primary actuators in close proximity.

One very critical design area in terms of its influence on the actuator performance characteristics is the fluid flow path between the main cylinder and the shaping accumulators. Although the preliminary design concept employed a rather long, 3-inch (7.6 cm) inside diameter flow path, the response model indicated that the resulting large fluid inertia magnitude would limit the acceleration capability to a level below that required for the higher level tests. The analysis indicated that the effective pipe fluid inertia term was directly proportional to the flow path length and inversely proportional to the flow path cross-sectional area. As a result, the design was modified to incorporate the shortest flow length and largest flow area within practical limits to accommodate the higher test levels. A 5-inch (12.7 cm) diameter flow path was thus selected.

The necessity of providing a large flow area and short flow length created other design problems, especially in terms of the device that would initiate fluid flow and thus start the pulse generation. Several basic types of valves and other initiation methods were considered before the concept of an ordnance-initiated, positive-opening valve was selected. This type of valve was selected because of the stringent pulse initiation requirement and the requirement to relieve the

fluid pressure rapidly and thus not degrade the piston response time to peak acceleration. In addition to the 5-inch (12.7 cm) diameter flow path requirement, the valve was required to provide a 90-degree flow elbow as a means of minimizing the flow path length. It should also be noted here that no known ordnance-initiated valve of this flow size had ever been produced before. In addition to the 5-inch (12.7 cm) valve, a similar 2-inch (5.1 cm) valve also was developed for use during lower-level tests and was designed to be completely interchangeable with the larger unit.

For most test conditions, the analytic model indicated that the peak velocity would be too high if the GN_2 pressure was sufficient to provide the required acceleration. The design solution chosen to control the peak velocity was to provide for the placing of an orifice in the flow path between the actuator cylinder and each ordnance valve.

Consideration of the large number of required orifice plate positions led to an accumulator orifice plate design that would provide an infinitely variable orifice plate position adjustment. This was accomplished by providing sleeves, threaded on the inside, that fit inside the shaping accumulators. The threaded orifice plates were made from 1-inch (2.54 cm) steel plate with holes drilled perpendicular to the plane of the plate. Usually, six orifice plates are used per accumulator; however, more or fewer may be specified for any test. To preclude a large leakage of fluid through the first orifice plate prior to filling the volume between the ordnance valve and first plate with oil, that plate contains a number of smaller holes drilled near the outer periphery. The second orifice plate in each accumulator has a single hole in the middle, while the third orifice usually has two to four holes around the periphery. All of the subsequent orifices contain a single hole and are positioned angularly approximately 180 degrees apart.

The design of the return accumulator incorporated the same 8-inch (20.3 cm) diameter cylinder used for the shaping accumulators, but with a return piston separating GN_2 and hydraulic fluid replacing the threaded sleeves and orifice plates. Sleeve segments are used, however, as a means of positioning the return piston to provide both sufficient hydraulic fluid and GN_2 volume. By using the available sleeve segments in combination, the total available sleeve length can be specified anywhere within the range 1.0 to 64.5 inches (2.54 to 164 cm) inclusive, in intervals of ½ inch. Either the small or large ordnance valve may be used to initiate the return flow. For this application the valve is rotated 90 degrees relative to the position when initiating the positive motion to provide for the reversed flow direction. A return pipe orifice may be used to limit the return velocity and in this manner serves a function similar to the pipe orifice leading to the shaping accumulators.

In addition to the return accumulator, a separate return GN_2 accumulator is used. A pipe connects the two accumulators as shown in the figure. This design approach was used as a means of accomplishing three objectives: provide GN_2 capacity in addition to that accommodated in the return accumulator for tests requiring a high return displacement, reduce test device width envelope, and provide GN_2 pressure decay characteristics that will result in a low velocity, long-duration return pulse. The inside diameter of this pipe is 1.50 inches (3.8 cm) which was selected with the help of the analytic model to provide "choked" (sonic) flow conditions during tests requiring a high return displacement. This was done to reduce the return velocity and increase the pulse duration.

A braking and locking unit was designed to arrest and hold the residual piston rod motion following pulse generation. The design incorporates an inner metallic sleeve which forms an interference fit around the outside of the steel actuator piston rod. During pulse generation, the sleeve is highly pressurized with hydraulic fluid so that a high-pressure oil film is provided between the two parts allowing the rod to stroke freely, operating much as a journal bearing. When the unit is activated the sleeve oil is vented, which allows the frictional forces associated with the interference fit to stop and hold the piston rod. Additional holding capacity is achieved by pressurizing the outer housing which provides added sleeve/piston rod interference pressure.

A fire control system separate from the actuator was designed to supply the proper electrical current at the desired time to fire the shaping ordnance valves, return valve and braking unit on each actuator. Likewise, an energy control system was designed to allow the actuators to be charged properly with high pressure GN_2 and hydraulic fluid. These control systems allow the simultaneous use of up to four actuators.

DEVELOPMENT TEST PROGRAM

A development test program was conducted in support of the actuator design. The purpose of this test program was to make possible a comparison between predictions produced by the response model and test results with regard to 1) the contribution to the fluid inertia term of the fluid in the pipe, 2) the difference, if any, in flow loss between single-hole and multihole accumulator orifice plates with the same flow area, 3) the leakage between orifice plates and the air/oil foam generation that could be expected to affect the piston displacement at which the effect of each orifice plate would take place, and 4) the effect of various pipe orifice plate sizes and accumulator orifice sizes on the piston motion.

A schematic of the test setup for the shaping accumulator and orifice tests is presented in Fig. 5. The test setup included a small existing force actuator and an orifice accumulator connected by a single pipe containing an ordnance valve. The flow areas associated with the pipe, ordnance valve, orifice plates and shaping accumulator were chosen to provide a range of local fluid velocities approximately equal to those that would be produced in the primary actuator. Therefore the actuator piston velocity waveforms generated during this development test were not intended to be comparable to the primary actuator waveforms, but were intended to be compared to the predictions of the analytic model modified to represent the development test setup. Parameter variations included: initial GN_2 pressure, pipe length, pipe orifice size, shaping accumulator orifice size and spacing and number of holes in the first orifice plate.

The development test results: 1) confirmed the postulated contribution to the fluid inertia term of the fluid in the pipe as can be seen by comparing the early-time velocity slopes shown in Fig. 6; 2) indicated that the flow area, not the number of accumulator orifice plate holes, determined the flow restriction; 3) indicated that the leakage between orifice plates was much greater than the volume occupied by air trapped in the oil/air foam as can be seen by considering the displacement at the time the effects of the first orifice are seen in Fig. 6; 4) indicated that the pipe orifice flow restriction and to a lesser extent the accumulator orifice restriction was greater than anticipated. Subsequent to the development test, some model coefficient values were modified by increas-

ing the orifice plate flow loss and providing an orifice leakage volume distribution based upon empirical data gathered during the test.

Use of the basic model for both the development test actuator and the primary actuator demonstrates that this model could be adapted to almost any existing or future pneumatic/hydraulic shock actuator.

DESCRIPTION OF OPERATION

Immediately prior to a test, the volume above the main cylinder piston is pressurized (depending on test level) to a limit of 5000 psi (34.5 MPa). At the same time, the volume below the main cylinder piston is pressurized (again depending on test level) to a limit of 6000 psi (41.4 MPa). Because the effective area of the piston on the fluid side is smaller than the GN_2 side, the oil pressure must be greater than the GN_2 pressure to maintain a force balance on the piston. The oil pressure is increased still further to provide the force necessary to support the test article and to ensure that the piston is fully retracted. The shaping accumulators, which at this time are free of oil and contain air at atmospheric pressure, are sealed. If a positive-with-return pulse is desired, the return accumulator and return cylinder above the return piston are charged with GN_2 to a pressure, depending on test level, of up to 5000 psi (34.5 MPa). The volume below the return piston is generally charged with hydraulic fluid to a pressure that exceeds the return GN_2 pressure by 100 psi (0.69 MPa) to ensure that the return piston is fully retracted against the up-stop sleeves.

The separate fire control system supplies the proper electrical current at the desired time to fire the ordnance in the valves leading to the shaping accumulators and thus initiate the test event. The valves generally open fully within two milliseconds after receipt of the fire current, allowing the fluid to accelerate at a very high rate into the valves, and then into the shaping accumulators. The initial acceleration of the fluid into the valves allows the stiff "fluid spring" to expand which in turn drops the pressure and reduces the force on the fluid side of the piston, allowing it to accelerate. The effects of fluid compressibility are further discussed under "The Response Model." Because the initial fluid flow into the valves is associated with fluid expansion, the minimum fluid pressure and peak piston acceleration is reached 2 or 3 milliseconds later. The magnitude of the acceleration is a function of the initial GN_2 pressure, the driven mass and the fluid flow geometry.

As the oil velocity through the valves increases, the oil pressure in the main cylinder starts to increase again. This oil pressure increase in the main cylinder is due to the flow restriction including that provided by the pipe orifice (if used) and the fluid kinetic energy increase associated with accelerating the fluid from the low fluid velocity of the cylinder to the high velocity discharged into the accumulator. While the pressure on the oil side of the piston is increased due to fluid flow, the GN_2 pressure above the piston is decreasing as the GN_2 expands. Peak velocity is reached when the force associated with the oil pressure equals the force associated with the GN_2. The piston and piston rod friction and the test article response forces also contribute to the force balance on the piston. However, the magnitude of these forces is generally quite small compared to those associated with the GN_2 and oil.

The continued expansion of the GN_2 immediately following the peak piston velocity results in a piston (and fluid) velocity decay. This velocity decay continues while the shaping accumulator volume between the accumulator entrance and the first orifice plate is filling with fluid. During this time, some of the extremely turbulent fluid flowing into the accumulator leaks through the holes in the first orifice plate to partially occupy the volume between the first and second plate.

The moment the volume between the accumulator entrance and the first orifice plate becomes filled with fluid, the fluid is forced to accelerate and flow at a very high velocity through holes in the first plate. This produces a very large pressure drop across the orifice plate which correspondingly increases the fluid pressure in the main cylinder and increases the piston velocity decay rate. The fluid, having gone through the holes in the first orifice plate, starts filling the volume between the first and second plate. When this volume becomes filled, the fluid again is forced to accelerate to a very high velocity producing another large fluid pressure increase which again increases the main piston deceleration. This process continues in turn as the fluid reaches each orifice plate.

The orifice hole sizes generally decrease steadily from the first to last plate to provide a steady piston velocity reduction, so that by the time the fluid begins flowing through the hole of the last plate, the piston velocity is very low. The position of the last orifice plate, along with the number of active shaping accumulators, determines the maximum piston displacement while the hole sizes and spacing of all the orifice plates determine the shape of the deceleration portion of the positive piston waveform. If a positive-only waveform is desired, the locking unit is fired by the fire control system at a time after the fluid front has reached the last orifice plate, that is, after the desired piston displacement is reached.

If a positive-with-return pulse is desired, the return valve is fired by the fire control system which allows the return piston to force the oil in the return accumulator to flow into the fluid side of the main cylinder. Because of the large flow restriction associated with the last orifice plate in the shaping accumulators, virtually all of the oil displaced by the return piston produces an equivalent main piston return motion. As the return piston displaces, the GN_2 expands and therefore is reduced in pressure. The pressure reduction allows the gas in the return GN_2 accumulator to flow through the connecting pipe and help maintain the gas pressure in the return accumulator. For low piston return velocities the gas flow rate through the pipe is a function of the pressure differential in the two accumulators. For high test levels, the gas flow velocity approaches the speed of sound at which point the gas flow is "choked" and, regardless of the pressure differential, the flow is sonic. The return velocity profile is a function of the fluid flow resistance including that associated with the return pipe orifice, the residual GN_2 pressure in the main cylinder, the piston rod axial force (if any) applied by the test article, the initial pressure and GN_2 volume in the return accumulator, and the gas dynamics associated with the GN_2 flow through the return GN_2 pipe.

The return motion is terminated by the braking unit which is activated at the desired time by the fire control system. Because orifice plates are not used to control the return pulse oil flow, the main piston return motion cannot be controlled as precisely as the positive motion. Therefore,

the piston velocity at the locking unit activation time is generally between 10 and 20 inches per second (25.4 and 50.8 centimeters per second) rather than the approximate 2 to 4 inches per second (5 to 10 centimeters per second) at the end of the positive pulse. The locking unit timing is more critical for the return pulse than for the positive pulse because the higher velocity at locking unit activation produces, for a given timing misjudgment, a larger deviation from the desired displacement.

THE RESPONSE MODEL

A schematic of the idealized primary actuator showing the degrees of freedom is presented in Fig. 7. The system is idealized by four degrees of freedom that contain second-order time derivatives. In addition, four variables with only first-order derivatives are used to describe the gas flow between the return GN_2 accumulator and the return accumulator.

The motion of the actuator piston, piston rod and isolator attach point is one degree of freedom. This variable (P) and its derivatives are of particular interest because they describe the actuator input motion to the test article. The mass used in calculating the acceleration is the sum of the mass of the piston, piston rod, test article attach structure, and the driven portion of the test article. The forces acting on this mass are the pneumatic force (produced by the main cylinder GN_2 pressure), the axial rod force (produced by the test article and the static weight of the driven mass), the frictional forces (between the piston/cylinder and piston rod/locking unit) and the hydraulic force (produced by the main cylinder oil pressure).

Fluid flexibility is idealized by a spring and a viscous damper in parallel between the piston degree of freedom and the rigid main cylinder fluid degree of freedom (X). The mass associated with the fluid-motion degree of freedom consists of a calculated fluid inertia term. The forces acting on the fluid mass are the force from the fluid spring and the forces associated with the fluid pressure due to flow into and from the accumulators.

A single degree of freedom is used to represent the test article vertical motion. The isolator or connection between the piston rod and test article is idealized as a nonlinear spring, a viscous damper and a coulomb damper in parallel. The forces acting on this mass are the force of gravity and the vertical force provided by the spring and dampers.

The return piston motion is assigned a degree of freedom, XR. The first and second time derivatives of this freedom are set equal to zero until the return fire time is reached. From that time on the return motion is calculated. The forces acting on the return piston mass are the pneumatic force produced by the gas pressure above the piston and the hydraulic force associated with the fluid pressure. Fluid flexibliity in the return accumulator is not modeled because test data have shown that the amplitude of the main piston oscillation, which is associated with return accumulator fluid flexibility, is not significant and because the inclusion of an additional degree of freedom would increase the computation time. The fluid inertia term is calculated in terms that allow direct addition to the return piston mass for use when calculating the return piston acceleration.

Four first-order freedoms are used to describe the gas flow between the GN_2 accumulator and the return accumulator, as this flow is assumed to occur quasistatically. These four freedoms are the pressures and gas densities in the return GN_2 accumulator and return accumulator cylinder.

The fluid flow equations were derived using the modified Bernoulli equation which defines the energy content per unit of fluid mass at any two points along a one-dimensional flow path for a viscous, incompressible fluid in steady flow. This equation was then expanded to include the fluid inertial effects to account for the unsteady flow conditions. The assumption of an incompressible fluid is valid for flow considerations within the piping and accumulators. The effects of fluid compressibility within the main cylinder are significant and are modeled separately.

The modified Bernoulli equation describing a simplified section of the actuator cylinder and one exit pipe is

$$\frac{V_2^2}{2} + \frac{P_2}{\rho} + gZ_2 = \frac{V_3^2}{2} + \frac{P_3}{\rho} + gZ_3 + H_L \qquad (1)$$

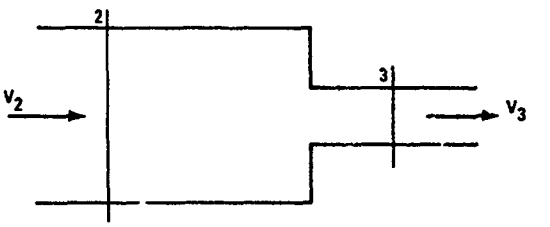

where V_2 and V_3, P_2 and V_3 and Z_2 and Z_3 are the velocity, pressure and height at positions 2 and 3, respectively. ρ is the fluid mass density and g is the gravity acceleration constant. H_L represents the total energy lost per unit mass of fluid when the fluid travels from position 2 to position 3 due to the flow restriction. It can be shown experimentally (as discussed in most fluid mechanics text books; for example, Ref. 1) that H_L is almost always directly proportional to the fluid velocity squared. Therefore

$$H_L = K\frac{V_3^2}{2} \qquad (2)$$

where K is the "minor loss" coefficient and is a measure of the degree of flow restriction between positions 2 and 3. Substituting equation (2) into equation (1), using the continuity equation to describe V_3 as a function of V_2, the area ratio and the number of active accumulators NP, assuming that the change in elevation is negligible, noting that $V_2 = \dot{X}$ in Fig. 7, $P_3 = PA$, and solving for P_2 results in

$$P_2 = \frac{\rho}{2}\left[K + 1.0 - \left(\frac{NP \cdot A_3}{A_2}\right)^2\right]\left(\frac{A_2}{NP \cdot A_3}\right)^2 \dot{X}^2 + PA \qquad (3)$$

P_2 is the pressure on the fluid side of the main piston and PA is the pressure of the gas trapped in the shaping accumulator. K represents the minor loss coefficient for the fluid flow from the main cylinder to the accumulators. This coefficient must be determined empirically from the test data and is a function of the detailed flow geometry. The term $1 - (NP \cdot A_3/A_2)^2$ accounts for the fluid kinetic energy increase which must be produced by the appropriate pressure drop.

To combine the additive terms that account for fluid energy change between positions 3 and 4, C_{34} is defined as follows:

$$C_{34} = K + 1.0 - (NP \cdot A_3/A_2)^2 \quad (4)$$

There is also a substantial flow loss that results if pipe orifices are used in the exit pipes to control the piston velocity. The flow loss increment for the pipe orifice is presented below. It is sufficient here to say that this loss is defined as KPO and is directly additive to C_{34}. K_{34} is defined as $K_{34} = C_{34} + KPO$ and represents the total steady-state fluid energy change plus loss as the fluid flows from the main cylinder to the accumulator entrance. Therefore,

$$P_2 = \frac{\rho}{2} \text{Loss 1} \cdot \dot{X}^2 + PA \quad (5)$$

where

$$\text{Loss 1} = K_{34}\left[\frac{A_2}{A_3 \cdot NP}\right]^2 .$$

The approach discussed above also was used to obtain the fluid flow equations associated with the return accumulator. One important difference, however, is that the "sink" pressure for the fluid on the downstream side of the flow is the pressure below the main piston rather than the gas pressure in the accumulators.

The flow loss algorithm for fluid flow through an orifice originally was developed by assuming the fluid would encounter a sudden contraction in pipe area, down to the orifice area, followed by a sudden expansion back to the original pipe area. This approach was taken because the orifice plates in which the holes are drilled are 1-inch (2.54 cm) thick and therefore, in terms of the flow path, are very short pipe segments.

The flow

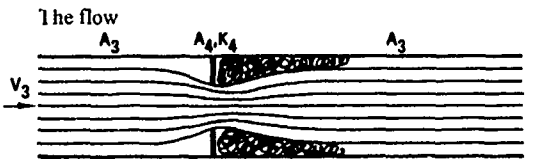

was idealized by

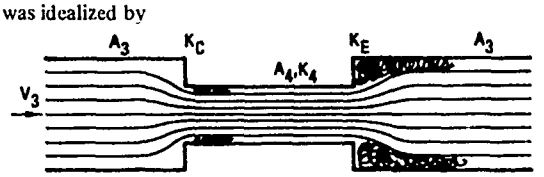

It then became necessary to obtain K_C and K_E and sum them to form the orifice flow loss coefficient K_4. The value for K_E can be derived directly from the momentum considerations and is derived in most fluid mechanics textbooks including Ref. 1. The loss thus derived is

$$H_L = \frac{V_3^2}{2}\left(1 - \frac{A_3}{A_4}\right)^2 \quad \text{or}$$

$$K_E = \left(1 - \frac{A_3}{A_4}\right)^2 \quad (6)$$

The value for K_C is not derived so easily. Various empirical methods have been developed. One such method provides the following

$$H_L = \frac{V_4^2}{2}\left(1 - \frac{A_4}{A_3}\right)^2 \quad (7)$$

or employing the continuity equation and combining equation (7) with (6), the total orifice plate algorithm becomes

$$K_4 = K_C + K_E = \tfrac{1}{2}\left(1 - \frac{A_4}{A_3}\right)^2\left(\frac{A_3}{A_4}\right)^2 + \left(1 - \frac{A_3}{A_4}\right)^2$$

$$= 1.5\left(1 - \frac{A_3}{A_4}\right)^2 \quad (8)$$

Equation (8) provides the form of the loss coefficient algorithm for the accumulator orifice plates and pipe orifice plate. For calculation of KPO to obtain K_{34}, A_3 in equation (8) is the pipe flow area and A_4 is the orifice flow area. When calculating the loss coefficient associated with each accumulator orifice plate, however, A_3 is the accumulator flow area and A_4 is the flow area of the orifice plate under consideration. It should be pointed out here, however, that the coefficient 1.5 in equation (8) has been increased, as discussed later, to provide better test/analysis agreement.

After the fluid has filled the volume upstream of the first shaping accumulator orifice plate, flow develops through the first orifice plate. The computer program logic keeps track of the appropriate displacements, volumes, etc., and when the flow through the first orifice plate develops, it increases the Loss 1 to Loss 2 in equation (5) where

$$\text{Loss 2} = \text{Loss 1} + K_4\left(\frac{A_2}{A_3}\right)^2 /NP^2 \quad (9)$$

and K_4 is the flow loss associated with the second orifice plate. Similarly, the total flow loss is increased appropriately as the flow develops through each successive orifice plate in the shaping accumulator.

Because the fluid flow is not steady, a fluid inertia term was developed for use when calculating the fluid acceleration $\ddot{X}$. Consider the following simplified section:

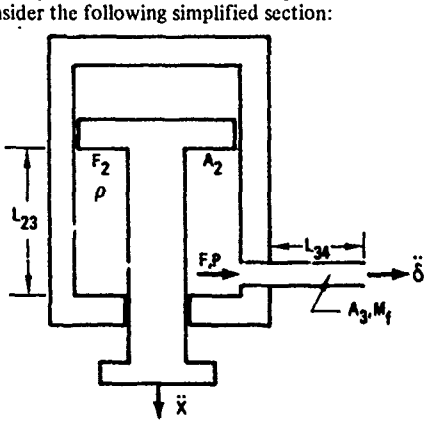

The force at the pipe entrance necessary to accelerate the fluid in the pipe is

$$F = (\rho A_3 L_{34}) \cdot \ddot{\delta} \quad (10)$$

Considering the continuity equation, noting that the pressure at the pipe entrance must also act on the piston, accounting for the number of active accumulators (NP) and solving for the force on the piston in terms of the piston acceleration yields:

$$F_2 = \left[\frac{L_{34} \cdot \rho \cdot A_2^2}{A_3 \cdot NP}\right] \ddot{X} \tag{11}$$

The mass of the fluid directly below the piston must be calculated and added to the bracketed terms in equation (11) to obtain the total fluid inertia. The fluid mass in the cylinder is simply

$$IN_{230} = \rho \cdot A_2 \cdot L_{23} \tag{12}$$

As the fluid fills the accumulator(s) the values of L_{23} and L_{34} in equations (11) and (12) change substantially, thus changing the fluid inertia term. The variable $Z = X + XR(ACR/A_2)$, where ACR is the area of the return cylinder, is calculated to aid the program logic in fully accounting for these changes Using this variable to account for the fluid mass discharged into the accumulators and combining equations (11) and (12) results in the following inertia term

$$INER = IN_{230} + \left\{\left[L_{34} + \frac{A_2 \cdot Z}{A_3 \cdot NP}\right] \cdot \frac{A_2}{A_3 \cdot NP} - Z\right\} \cdot \rho \cdot A_2 \tag{13}$$

The program logic considers the fluid position and the change to A_3 that is associated with Z as the fluid exits the pipes and enters the accumulators and, using equation (13), calculates the fluid inertia for use as the driven weight when calculating $\ddot{X}$.

Fluid compressibility in the main cylinder is modeled as a spring and viscous damper separating the main piston and the "rigid" fluid. The bulk modulus, β, is a measure of the oil "stiffness" when the oil is confined to a given volume. It is defined as

$$\beta \equiv -V\frac{dP_R}{dV} \tag{14}$$

where V = volume and P_R = pressure. The oil "spring rate" can be calculated from the above definition for the following system:

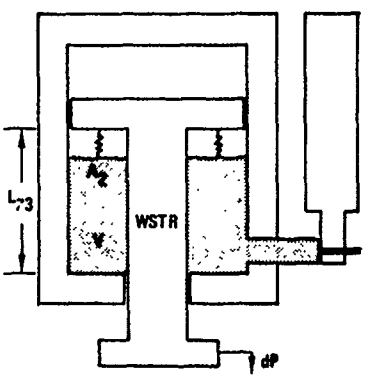

Noting that $dV = -A_2 dP$ and $dP_R = dF/A_2$, substituting these values into equation (14) results in the spring rate dF/dP

$$\frac{dF}{dP} = \frac{\beta A_2^2}{V} \tag{15}$$

The value for β used in the program is discussed later and is less than the nominal handbook values.

It is important also to provide appropriate damping forces to the fluid spring motion. The approach taken was to assume viscous damping for this motion and to input the damping value as a percentage of the critical damping. The critical damping coefficient for the fluid-mode motion is

$$C_c = 2\sqrt{(dF/dP)(WSTR)/g} \tag{16}$$

where WSTR is the driven piston and rod weight. The actual percentage of C_c used in the analysis is that required to provide good amplitude and decay correlation with test results and is discussed later.

There are three areas in the actuator where gas pressure is used for power or control. the air in the sealed accumulators, compressed when the fluid enters the accumulators; the high-pressure GN_2 used as the energy source for the main piston motion; and the high pressure GN_2 in the return accumulator and return GN_2 accumulator, and the gas flow between these accumulators.

The GN_2 above the main piston expands with the piston motion. The expansion process occurs so rapidly (generally within 1/10 second) that no significant heat transfer can take place between the GN_2 and the main cylinder and piston during the piston motion. Therefore the process is assumed to take place adiabatically. The process also is assumed to be frictionless and the GN_2 is assumed to be a perfect gas. For a closed system under such conditions the first law of thermodynamics yields

$$\int \frac{dP_1}{P_1} + \gamma \int \frac{dV}{V} = 0 \tag{17}$$

where P_1 and V are the pressure and volume, respectively, and γ is the ratio of the specific heat at constant pressure divided by the specific heat at constant volume.

Initially, equation (17) was integrated assuming that γ was a constant of 1.4 which results in

$$P_1 = P_I\left(\frac{V_I}{V_I + A_1 P}\right)^{\gamma} \tag{18}$$

where P_I and V_I are the initial GN_2 pressure and volume, respectively, and P_1 and A_1 are the pressure above and area of the main piston. The specific heats and therefore γ are essentially constant if the GN_2 pressure remains relatively low. Published data (for example Ref. 3) indicate, however, that γ increases with increased pressure if the pressure range is substantially above atmospheric.

The best method of accounting for this change would be to obtain γ as a function of volume and use this function in (17) when integrating. The function $\gamma(V)$ is not known, however. A substitute method is employed in the model that allows γ to change and consequently results in better test/analysis correlation of both pressure and piston velocity

In addition to the published data, pressure data from early tests using the primary actuator indicated that the initial pressure decay rate was much greater than predicted when using a constant γ equal to 1.4, when the initial pressure was large (greater than 3000 psi, 20.7 MPa). Consideration of this data led to incorporating a variable γ into the model for use with equation (18) which results in good pres-

sure and velocity correlation. When the pressure is above 3000 psi (20.7 MPa) γ is set equal to 2.0, while a γ equal to 1.5 is used below 3000 psi (20.7 MPa). These values compare with a γ equal to 1.38 which is generally used for GN_2 at pressures near atmospheric and at room temperature.

The pressure increase that occurs in the shaping accumulator when the oil fills the accumulator is calculated using an equation similar to equation (18). In this case a large heat transfer surface area is created by the turbulent fluid in the accumulator. Therefore a γ of 1.2 is used as a compromise between adiabatic and isothermal compression processes.

The gas dynamics equations that describe the density and pressure changes in the return GN_2 accumulator and return accumulator, and the gas flow through the pipe connecting these two volumes, were derived using the following assumptions: 1) the gas expansion and compression takes place adiabatically, 2) the gas flow between these two accumulators is initially assumed to be isentropic and subsequently modified with an empirically obtained discharge coefficient, 3) the gas is a perfect gas with constant specific heats, 4) the thermodynamic properties of the gas in the return GN_2 accumulator are stagnation values in the pipe, 5) the flow through the connecting pipe is quasisteady; that is, steady flow equations may be applied to the flow at any time.

The flow velocity through the pipe must be obtained first and then the change in density and pressure calculated based upon the flow velocity. Consider the two reservoirs connected by a pipe:

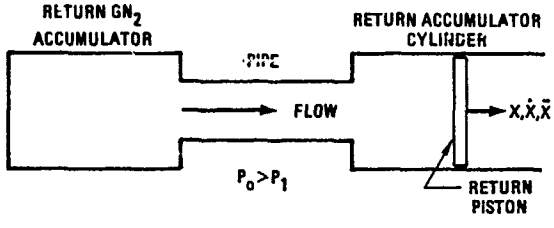

where:

V = volume
v = velocity
P = pressure
T = temperature
h = enthalpy/unit mass
u = internal energy/unit mass
M = Mach number
ρ = gas density
A = cross-sectional area
$\bar{v}$ = specific volume
m = mass

Subscripts:

o = GN_2 accumulator
p = pipe
1 = return accumulator

Also, c_p = GN_2 specific heat at constant pressure
c_v = GN_2 specific heat at constant volume
C_p = speed of sound

The subscript "o" for pressure and temperature also denotes stagnation values in the connecting pipe which are the same as the static values in the upstream GN_2 accumulator.

The first law of thermodynamics for each mass unit of gas entering the pipe is

$$h_p = C_p T_p = U_p + P_p \bar{v}_p \quad \text{and}$$

$$h_o = h_p + \frac{v_p^2}{2} = c_p T_o \tag{19}$$

Noting that the gas constant $R = c_p - c_v$, $\gamma = c_p/c_v$, $C_p = \sqrt{\gamma R T_o}$ and $M_p = v_p/C_p$, equation (19) becomes, after rearranging,

$$\frac{T_p}{T_o} = \frac{1}{1 + \frac{\gamma-1}{2} M_p^2} \tag{20}$$

which defines the ratio of the temperature in the pipe to the stagnation temperature as a function of the gas thermodynamic properties and local Mach number.

Substituting the pressure/temperature relation for the adiabatic expansion of a perfect gas, noting that the static pressure in the pipe is equal to the pressure in the downstream accumulator and solving for the Mach number

$$M_p = \sqrt{\frac{2}{\gamma-1}\left[\left(\frac{P_o}{P_1}\right)^{\frac{\gamma-1}{\gamma}} - 1\right]} \tag{21}$$

Equation (21) provides the Mach number of the gas flow through the connecting pipe in terms of the pressure in each accumulator and the gas constants. This equation is valid if $M_p \leq 1.0$. M_p cannot be greater than 1.0 because "choked" flow will exist.

The maximum pressure ratio necessary for the Mach number to be 1.0 is found by setting equation (21) equal to 1.0. The maximum ratio for $P_1/P_o = 0.528$. The model calculates the Mach number using equation (21) if $P_1/P_o \geq 0.528$. If $P_1/P_o < 0.528$, M_p is set equal to 1.0.

A time-dependent energy balance can be written for a control volume defined as the return GN_2 accumulator

$$\frac{\partial}{\partial t}(m_o u_o) + \frac{\partial m_o}{\partial t}\left[\tfrac{1}{2} v_p^2 + h_p\right] = 0 \tag{22}$$

Differentiating, using the equation of state and rewriting

$$\frac{\partial P_o}{\partial t} = \gamma \frac{P_o}{\rho_o} \frac{\partial \rho_o}{\partial t} \tag{23}$$

Equation (23) defines the time rate of change of pressure in the return GN_2 accumulator and is one of the four first-order equations necessary to obtain the pressure acting on the return piston.

A discharge coefficient, C_{wr}, is introduced here and is defined as the ratio of the actual flow velocity to the isentropic flow rate. The value of C_{wr} affects the flow rate and thus the energy transfer rate through the pipe. The value for C_{wr} used in the analytic model to provide good test/analysis results is 0.95. Therefore

$$v_p = C_{wr} M_p C_p \tag{24}$$

The time-dependent continuity equation can be written for flow between the GN_2 accumulator and the pipe

$$\frac{\partial m_o}{\partial t} = -\rho_p v_p A_p \tag{25}$$

Combining equations (20), (21), (24) and (25), rearranging terms and solving for the rate of change of density in the return GN_2 accumulator results in

(26)

$$\frac{\partial \rho_o}{\partial t} = -\frac{A_p}{V_o} \text{ Cwr} \cdot \frac{M_p}{\left(1 + \frac{\gamma-1}{2} M_p^2\right)^{1/(\gamma-1)}} \sqrt{\frac{\gamma P_o \rho_o}{1 + \frac{\gamma-1}{2} M_p^2}}$$

Equation (26) like (23) is one of the four required first-order equations.

A time-dependent continuity equation can be written for the accumulator volume above the return piston

$$\frac{\partial m_1}{\partial t} = -\frac{\partial \rho_o}{\partial t} V_o - \rho_1 A_1 \frac{dX}{dt} \tag{27}$$

Substituting $\frac{\partial m_1}{\partial t} = V_1 \frac{\partial \rho_1}{\partial t}$ into (27) results in

$$\frac{\partial \rho_1}{\partial t} = -\frac{1}{V_1}\left[V_o \frac{\partial \rho_o}{\partial t} + A_1 \rho_1 \frac{dX}{dt}\right] \tag{28}$$

Equation (28) is also one of the required first-order equations.

The time-dependent energy balance for the gas above the return piston is

$$\frac{\partial}{\partial t}(m_1 u_1) = \frac{\partial m_1}{\partial t}\left[\tfrac{1}{2} v_p^2 + h_p\right] - P_1 A_1 \frac{dX}{dt} \tag{29}$$

Noting that $u_1 = c_v T_1$, $h_o = \tfrac{1}{2} v_p^2 + h_p = c_p T_o$ and writing m_1 as $\rho_1 V_1$ and $\rho_1 T_1$ as P_1/R results in

(30)

$$\frac{\partial}{\partial t}\left(C_v \frac{P_1}{R} \bar{v}_1\right) = \frac{\partial}{\partial t}(\rho_1 \bar{v}_1)(c_p T_o) - P_1 A_1 \frac{dX}{dt}$$

Differentiating and noting that

$$\frac{\partial V_1}{\partial t} = A_1 \frac{dX}{dt}, \gamma = \frac{c_p}{c_v} \text{ and } R = c_p - c_v$$

and solving for $\frac{\partial P_1}{\partial t}$,

$$\frac{\partial P_1}{\partial t} = \frac{\gamma}{\rho_o}\left[P_o \frac{\partial \rho_1}{\partial t} + \frac{A_1}{V_1}(P_o \rho_1 - P_1 \rho_o)\frac{dX}{dt}\right] \tag{31}$$

Equation (31) is the last of the four necessary first-order equations. Equations (23), (26), (28) and (31) calculate the changes in GN_2 properties and, when integrated, provide a history of these properties. The integrated value for P_1 is multiplied by the return piston area A_1 to obtain the return piston driving force which then is used to calculate the return piston motion. Because some of the equations are functions of one of the other equations, the equations are solved in the following order: (26), (23), (28) and finally (31).

TEST/ANALYSIS CORRELATION

The response model has been improved and refined by adding a degree of freedom and selecting model coefficient values such as damping, flow loss, etc., that result in good test/analysis correlation over the entire test range.

The first opportunity to investigate test/analysis correlation occurred during the development test discussed earlier which led to the identified coefficient value changes. The early demonstration tests of the primary actuator indicated that 1) fluid compressibility effects in the main cylinder (but not the return accumulator), which up to that time were not included in the model, were significant and should be included; 2) the flow loss using a small-diameter pipe orifice was greater than predicted by the model; 3) the flow loss without a pipe orifice was less than predicted and varied depending on the number of active accumulators, and 4) the leakage between orifice plates was less than indicated by the model which at that time was based upon the results of the development test. These tests also showed, as dicussed earlier, that, when initial gas pressures were used, the gas pressure decay rate was greater than predicted. As a result, the model was improved by 1) separating the main piston and the fluid into two degrees of freedom, 2) increasing the orifice loss coefficients (particularly that associated with the pipe orifice), 3) decreasing the basic piping and valve loss coefficient and making it a function of the number of active accumulators, 4) decreasing the leakage between orifice plates in the shaping accumulators.

Because the flow loss coefficient values have a major effect on the entire velocity history, it is very important to know these values accurately, and use them in the model. The original values for the basic piping and valve losses were estimated using engineering judgment, while the losses associated with the orifice plates were derived using the assumptions discussed previously. With the use of test data, flow loss coefficients associated with each condition have been established which provide good test/analysis agreement over the entire test range.

The basic loss coefficients associated with flow between the main cylinder and the shaping accumulators vary slightly depending on the number of active accumulators. These nondimensional values are 2.75, 3.00 and 3.25 for one, two and three active accumulators, respectively. The slight increase in loss coefficient with increase in number of active accumulators would be expected because the main cylinder/exit-pipe interface through which the fluid must flow is common to all exit pipes. As a point of reference, the loss coefficient for a standard commercial 90-degree pipe elbow is 0.90 (Ref. 2).

The general form of the orifice loss algorithm discussed earlier is (equation 8)

$$K = C\left(1 - \frac{A_p}{A_o}\right)^2 \tag{32}$$

where

- K = unitless loss coefficient
- C = constant
- AO = area of orifice hole
- AP = aera of pipe or accumulator

The value K is added to the basic loss coefficient to obtain the overall loss. The algorithm derived earlier contained a value of 1.5 for C which proved to be too small to provide good correlation with test results, particularly with respect to the pipe orifice. It was found, however, that very good results could be obtained with respect to each type of orifice by increasing selectively the value of the constant C while maintaining the basic form of the algorithm. A review of piston motion histories from many tests resulted in the selection of the following values for C: 1) accumulator ori-

fice plates, 2.5, 2) return pipe orifice plate, 3.5; 3) shaping pipe orifice, 6.5. Although this range appears quite large, the local flow geometry associated with each of these types of plates is substantially different from the others and the local flow geometry can be expected to affect the loss coefficient substantially.

As indicated in the discussion of the development test, a substantial volume of fluid leaks through the first few orifice plates (which contain large flow areas) prior to filling the volume upstream of the first orifice plate and creating the pressure rise associated with that orifice plate. Before presenting the method used in the model to account for this leakage, it is appropriate to present the following pertinent observations. 1) the leakage volume can be expected to be much greater through the first orifice plate, which generally has the largest flow area, than through subsequent orifice plates; 2) the leakage volume through the first plate can be expected to increase as the distance between the accumulator entrance and the first plate is increased, and 3) because the hole diameter in the last orifice plate is so small, it can be expected that negligible leakage will occur through this plate. Each of these observations has been confirmed by the test data. The method used to account for the leakage is presented below, it is, of necessity, wholly empirical but results in good test/analysis correlation for all test levels.

The leakage volume through the first plate is proportional to the distance from the accumulator entrance to the first plate if this distance is less than 20 inches (50.8 cm). Above 20 inches (50.8 cm), the volume is assumed to be the same as that calculated for a 20-inch (50.8 cm) dimension. The constant of proportionality is 0.40. That is

$$VLEAK = L_{45} \cdot A_4 \cdot 0.40 \qquad (33)$$

where

VLEAK	=	leakage volume past first plate
L_{45}	=	distance, accumulator entrance to first plate
A_4	=	area of accumulator

VLEAK then is added in the program to the physical volume between the accumulator entrance and the first plate for purposes of defining the fluid position and assigning the proper flow loss coefficient. VLEAK is negatively distributed among the volumes between the five subsequent orifice plates in the following manner. $-\delta V \cdot VLEAK/.40$, where δV equals .25, .08, .04, .02, .01, respectively, for the second, third, fourth, fifth and sixth plate. This distribution implies that 1) some leakage occurs through each of the first five orifice plates but not through the last plate, and 2) the leakage volume becomes less as the orifice plate hole sizes become smaller and the distances between the plates decrease.

The handbook value for the fluid bulk modulus defined by equation (14) within the pressure and temperature range of operation is approximately 200,000 psi (1380 MPa). A value of 120,000 psi (828 MPa), however, has been found to provide the most consistent correlation of the "fluid mode" frequency and is therefore used. The change in value is undoubtedly due to a small volume of air trapped in the fluid. This can occur because there is no direct method of completely eliminating the air trapped in the actuator fluid. Likewise, a value of 11% of critical damping provides the most consistent correlation of the fluid-mode amplitude and decay rate. It should be pointed out that these parameters are sensitive to the quantity of air that may be trapped in the fluid and therefore the optimum values can be expected to change slightly from test to test.

Many successful shock test programs have been conducted to date using the primary actuator to provide the simulated air-induced groundshock motion to a variety of test articles. These test programs include the floor segment test addressed by Gustafson (Ref. 5), the missile suspension system testing discussed by Mortimer (Ref. 8), the single isolator performance limit tests discussed by Ashley (Ref. 4), and the shock isolated equipment floor testing presented by Milne (Ref. 7). Each of these tests provided actuator performance data from which test/analysis comparisons were made.

A typical test/analysis velocity history comparison is presented in Fig. 8, which compares the envelope of the velocity histories produced by four primary actuators simultaneously providing inputs to a test article with that indicated by the analysis. The waveform type is positive followed by partial return. The velocity scale is not annotated in this figure so that it will be unclassified. Notice, however, the good correlation during both the positive and return portions of the waveform, and the evidence of the piston oscillating on the main cylinder fluid column.

Fig. 9 presents the envelope of the velocity waveforms produced by two primary actuators, each driving the upper ring during a missile suspension system test, compared to that indicated by the response model. The waveforms are the vertical and horizontal components of the 45-degree vectored motion and are of the positive-only type.

The waveforms shown in Fig. 10 correspond to the actuator axial maximum capability in terms of acceleration and velocity, while the displacement capability is slightly larger than that produced during this test. Because the velocity histories shown are the vertical and horizontal components of a 45-degree vector, the axial motion is 1.414 times that shown. Even at this very high test level the model adequately indicates the measured motion.

The two waveforms shown in Fig. 11 were measured during two sequential tests using the same actuator with the same configuration. Notice the excellent repeatability characteristics demonstrated by these waveforms and the good agreement provided by the model. These waveforms are of moderate velocity with a high displacement and are characterized by a concave velocity decay prior to the effects of the orifice plates as indicated in the figure. This velocity decay shape results from the GN_2 pressure decay and fluid flow/pressure characteristics. The velocity scale on this figure is not annotated so that it will remain unclassified.

The response shock spectra calculated from the motion histories presented in Fig. 11 are shown in Fig. 12 along with the specified shock spectra tolerance for that particular test. Again, the vertical scale is not shown. Notice, however, that the response spectra are well within the specified tolerance up to a frequency of 350 Hz where the local high-frequency response environment is significant. Also notice that the two shock spectra corresponding to the two measured waveforms would be well within the repeatability tolerance which is one-half the bandwidth of the indicated tolerance but drawn about the spectrum corresponding to the first of the two tests.

CAPABILITY AND LIMITATIONS

The capability of the actuator to produce velocity history types is limited to: 1) positive only, 2) positive with

return, 3) return only. Extensive modifications would be required to provide other (such as cyclic) shaping capabilities. Generally, if a required velocity waveform is one of the above three types and the peak values of acceleration, velocity and displacement are within the capability of the actuator, the waveform shape can be controlled so that it is within acceptable limits of the required waveform.

A summary of the maximum and minimum test article and axial input motion parameter values that have been measured during all of the primary actuator tests conducted to date is presented below.

	PARAMETER	MAXIMUM	MINIMUM
TEST ARTICLE	DRIVEN WEIGHT	16,200 LB (7348 KG)	1,900 LB (862 KG)
	STATIC LOAD	60,000 LB (27,200 KG)	0.0 LB (0.0 KG)
MEASURED PEAK VALUES	ACCELERATION (RIGID BODY)	800 G's	17 G's
	VELOCITY		
	POSITIVE	1040 IPS (2642 CM/SEC)	40 IPS (102 CM/SEC)
	RETURN	190 IPS (483 CM/SEC)	13 IPS (33 CM/SEC)
	DISPLACEMENT		
	POSITIVE	36 IN (91.4 CM)	1.5 IN (3.8 CM)
	RETURN	11.5 IN (29.2 CM)	0.8 IN (2.0 CM)

All of the maximum and minimum motion values are associated with an actuator driven weight of 1900 pounds (862 kg)

The maximum positive velocity and acceleration capability are a function of the driven weight and, to a lesser extent, the piston upstop dimension. Because the driven weight associated with the maximum acceleration and velocity in the above table was 1900 pounds (862 kg) which is near the lowest possible driven weight, any increase in this weight will reduce these capabilities accordingly. The displacement capability is 36 inches (91.4 cm) regardless of the driven weight, but this would change with a change in upstop dimension.

The minimum positive capability is much more difficult to define partly because of the lack of test data in this range and partly because of the influence of the forces applied by gravity and the test article to the actuator rod. The minimum controllable displacement is approximately 1.5 inches (3.8 cm) using a 2-inch (5 cm) value. In the very low test range it is difficult to control both the acceleration and the velocity. That is, one probably can produce the goal low level velocity but may deviate significantly from the goal acceleration. Also the fluid mode associated with the driven mass oscillating on the fluid column is excited to a much greater extent at low test levels when the flow restriction is greatest.

The maximum return capability usually is defined in terms of the return displacement capability which is a function of the available fluid volume in the return accumulator. The present configuration uses one return accumulator (and three shaping accumulators) which allows a return displacement of up to 11.5 inches (29.2 cm). The reconfiguration of the actuator to provide two or three return accumulators would involve a modest hardware change but would allow a much larger return displacement potential (at the expense of a corresponding decrease in positive displacement potential). Because the return displacement potential is proportional to the number of accumulators, using two return accumulators would allow approximately a 23-inch (58.4 cm) return displacement. The return velocity capability using the one-return accumulator is approximately 200 IPS (508 cm/sec) at the higher return displacements.

The minimum return velocity and displacement both approach zero although the prediction accuracy, on a percentage basis, can be expected to be lower at the extremely low test levels compared to the higher test levels.

The primary actuators have been successfully used to provide a very wide range of simulated groundshock levels to a number of different test articles. The response shock spectra envelope produced by the actuators to date is shown in Fig. 13 Note the wide range of test levels that have been produced. It is also important to note here that the response shock spectrum associated with each of the almost 200 individual actuator firings during the many test programs at many levels has, without exception, been within shock spectra tolerances except during a very few tests when support equipment malfunctioned.

CONCLUDING REMARKS

The primary actuator has proved to be a very successful design in terms of its ability to reliably and consistently produce a wide range of specific simulated air-induced groundshock motion levels to a wide variety of test articles. During the design phase, the dynamic response model was instrumental in establishing the geometric parameter values that allowed the actuator to confidently produce this wide range of test levels and to confidentiy perform completely within specification. Subsequent to the design support task, the model has been used to provide the detailed actuator configuration so that the actuator will produce a particular motion history and a corresponding response shock spectrum that is within a specified tolerance. The model could easily be adapted to almost any existing or future pneumatic/hydraulic shock actuator.

ACKNOWLEDGEMENT

The author wishes to thank Thomas Martin of the Boeing Aerospace Company, whose efforts in modeling a smaller shock test device formed a basis or starting point from which the actuator response model was developed.

REFERENCES

1. Irving H. Shames, Mechanics of Fluids, McGraw-Hill Book Co., New York, 1962.

2. John K. Vennard, Elementary Fluid Mechanics, 3rd Edition, John Wiley and Sons, Inc., New York, 1954.

3. James B. Jones and George A. Hawkins, Engineering Thermodynamics, John Wiley and Sons, Inc., New York, 1960.

4. J. P. Ashley, "Component Testing of Liquid Shock Isolators in Support of Recent Shock Isolation System Designs," 46th Shock and Vibration Symposium, San Diego, 1975.

5. W. C. Gustafson, "Polyurethane Foam Isolators for Shock Isolated Equipment Floors," 46th Shock and Vibration Symposium. San Diego, 1975.

6. L. L. Luschei, "An Introduction to the Design and Qualification of Large Shock Isolation Systems," 46th Shock and Vibration Symposium, San Diego, 1975 (Classified: SECRET).

7. W. R. Milne, "Analysis and Testing of Full Scale Shock Isolated Equipment Floors," 46th Shock and Vibration Symposium, San Diego, 1975.

8. H. R. Mortimer, "Shock Isolation System Design, Analysis, and Testing for a Silo Based ICBM," 46th Shock and Vibration Symposium, San Diego, 1975 (Classified SECRET).

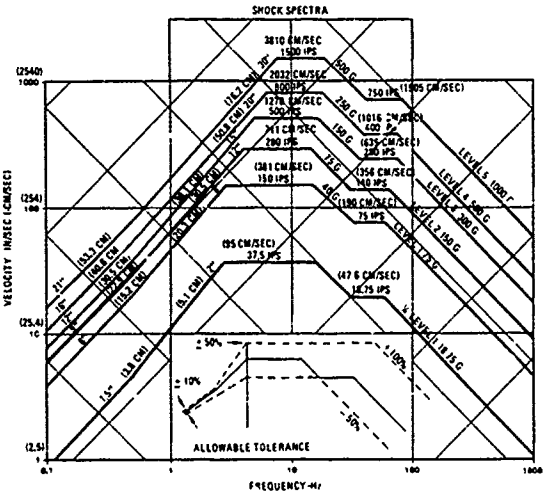

FIGURE 1 PRIMARY ACTUATOR DESIGN SHOCK LEVELS

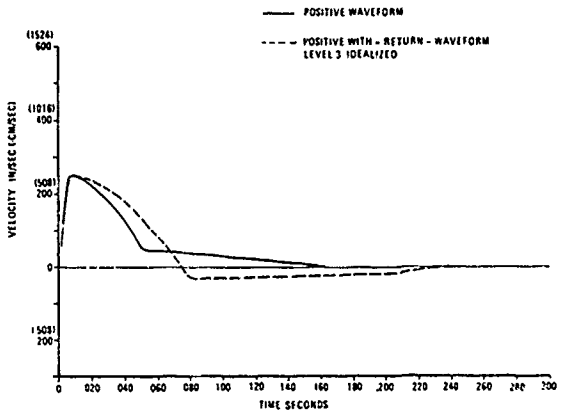

FIGURE 2 ACTUATOR WAVEFORM TYPES

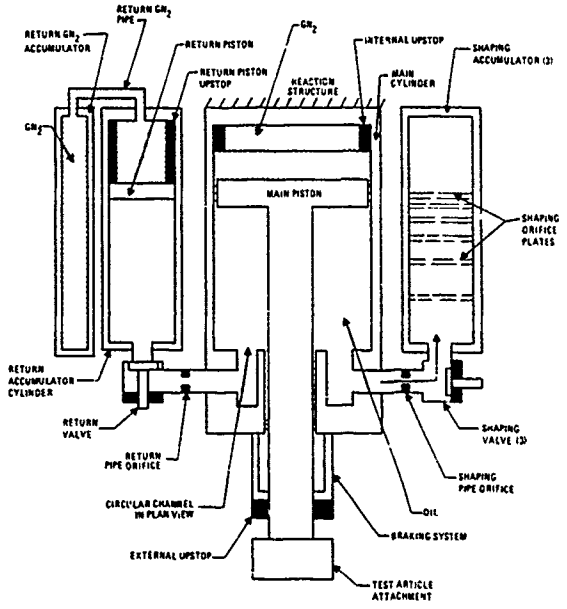

FIGURE 3 SCHEMATIC OF PRIMARY ACTUATOR

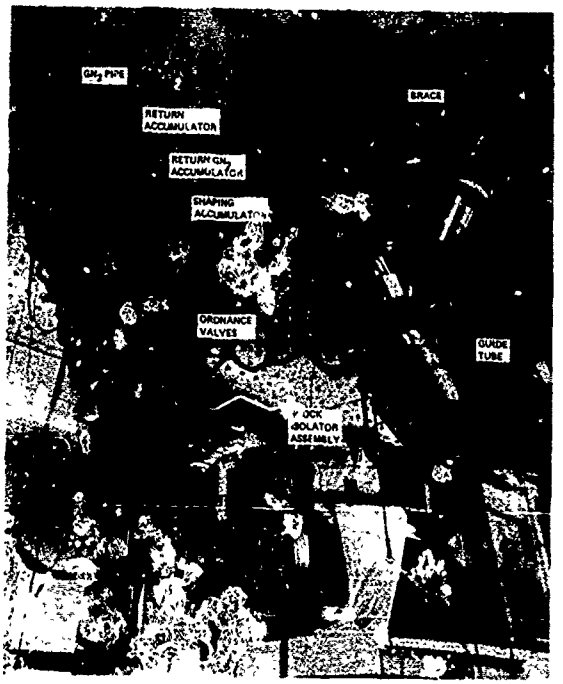

FIGURE 4 PRIMARY ACTUATORS INSTALLED IN TEST FACILITY

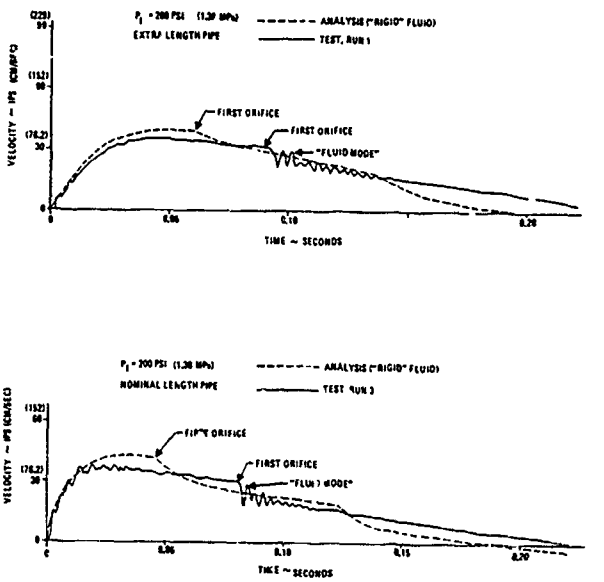

FIGURE 6 TEST/ANALYSIS COMPARISONS, SHAPING ACCUMULATOR AND ORIFICE DEVELOPMENT TEST, NOMINAL AND EXTRA-LENGTH PIPE

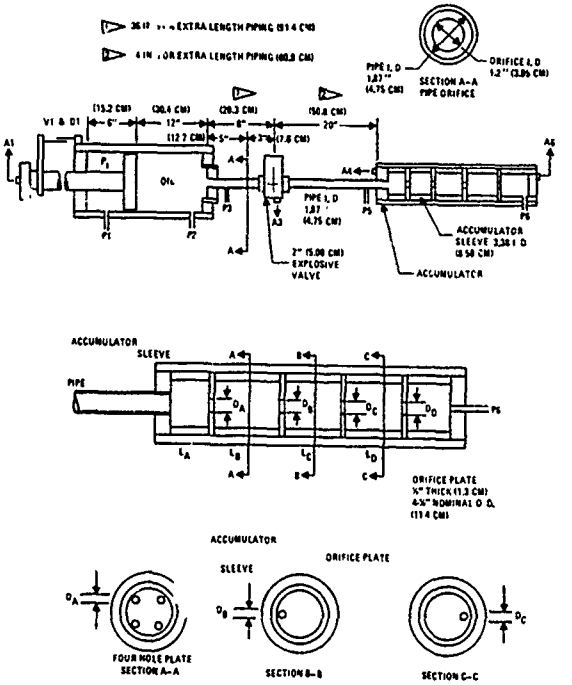

FIGURE 5 SHAPING ACCUMULATOR AND ORIFICE DEVELOPMENT TEST SETUP

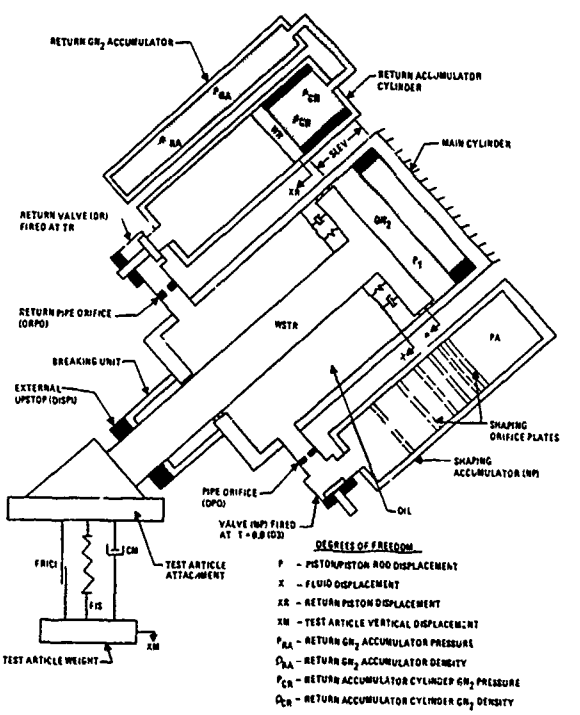

FIGURE 7 ACTUATOR INCLINED FOR VECTORED INPUT SCHEMATIC OF IDEALIZED ACTUATOR

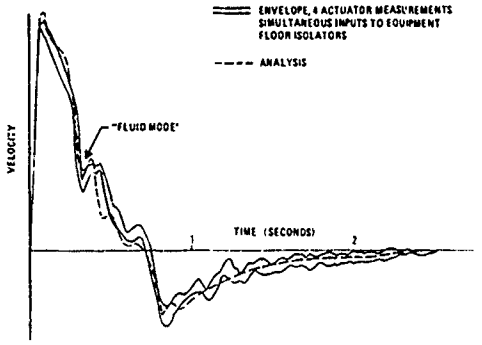

FIGURE 8 TYPICAL TEST/ANALYSIS WAVEFORM COMPARISON POSITIVE WITH RETURN

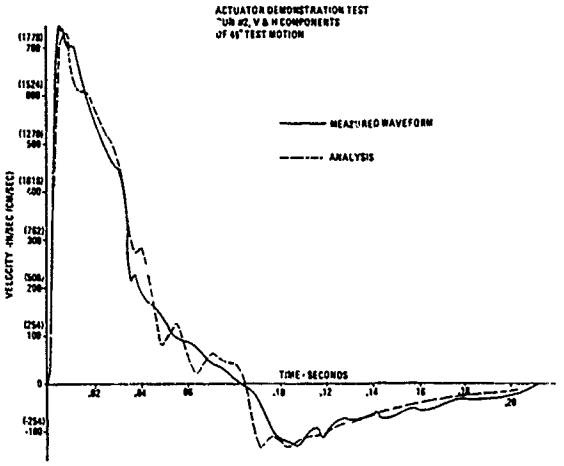

FIGURE 10 TEST/ANALYSIS WAVEFORM COMPARISON, POSITIVE–WITH–RETURN, VERTICAL AND HORIZONTAL COMPONENTS OF MAXIMUM VELOCITY CAPABILITY

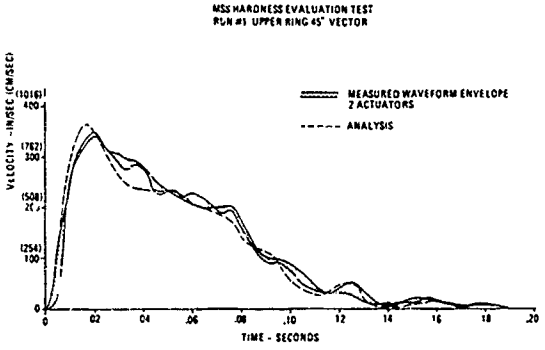

FIGURE 9 TEST/ANALYSIS WAVEFORM COMPARISON POSITIVE ONLY MISSILE SUSPENSION SYSTEM TEST

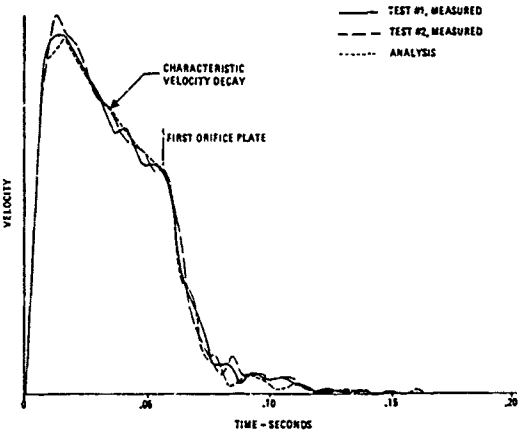

FIGURE 11 TEST/ANALYSIS VELOCITY HISTORY COMPARISONS, TWO TESTS WITH SAME ACTUATOR CONFIGURATION

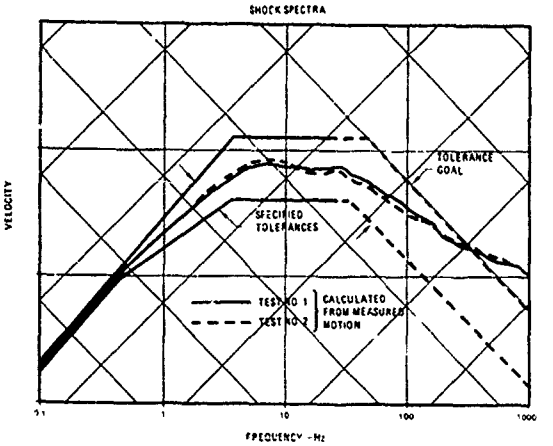

FIGURE 12 RESPONSE SHOCK SPECTRA COMPARISON, TWO TESTS WITH SAME ACTUATOR CONFIGURATION, SPECIFIED TOLERANCES

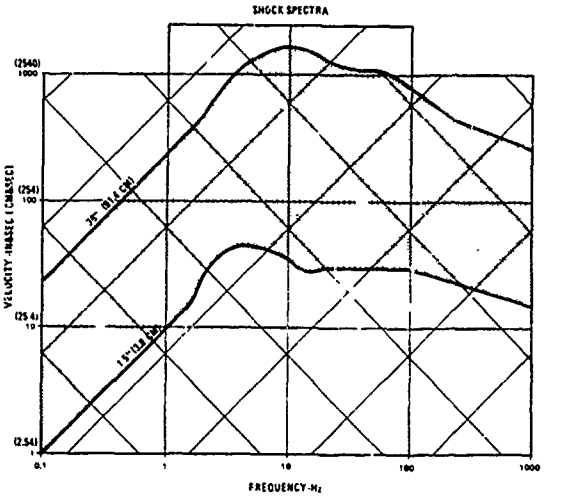

FIGURE 13 APPROXIMATE ENVELOPE OF RESPONSE SHOCK SPECTRA FOR SIMULATED GROUND SHOCK PRODUCED BY ACTUATOR

BOUNDED IMPACT

A REPEATABLE METHOD

FOR PYROTECHNIC SHOCK SIMULATION

Robert T. Fandrich, Jr.
Harris Electronic Systems Division

A method to simulate pyrotechnic shock occurrences is described in this paper. The method fulfils the critical pyrotechnic testing requirements of (1) being capable of simulating shock levels up to 20,000 G spectra, (2) being very repeatable, (3) inducing no residual displacement or velocity, (4) producing time histories similar to field events. A parametric study was performed on a computer model of the technique and a comparison is made of model prediction versus actual results.

INTRODUCTION

This paper describes a test method developed for the performance of pyrotechnic shock simulation. This method, called "Bounded Impact", is capable of performing high-level shock tests with excellent repeatability on a modified drop shock machine. The simulation of pyrotechnic occurrences has long plagued engineers in the testing business because its reproduction is not usually a matter of physically simulating the actual environment. These shocks are usually caused by activation of seperation hardware on a spacecraft or payload in the process of staging or deployment. The shock wave travels along the structure and skin of the missile in all directions, eminating from the explosive device or devices and eventually arriving at some area of interest by several individual paths. This area of interest is the location at which some device is attached and the effect of the pyrotechnic occurrence on the integrity and operation of the device is the point under consideration.

Tests have been performed in which the missile structure is simulated and pyrotechnic devices attached to this structure were exploded to obtain a representation of the environment. Although the authenticity of this technique is enviable, simulating the structure is expensive and handling explosives is dangerous.

For these reasons, many other methods have been developed to describe and simulate this environment. Usually the structure simulation is sacrificed to reduce cost. Several methods use explosives without the expensive structure simulation. Elimination of the use of explosives make the testing totally non-authentic.

For non-authentic testing (testing which attempts to reproduce the environment without reproducing the actual field conditions), some means must be established to define and measure the environment. Several methods of defining pyrotechnic events are currently in use with time history, fourier spectrum, and shock response spectrum being the most popular. This paper will use shock response spectra for defining pyrotechnic events with some consideration of time histories, since a major complaint against shock response spectra is their non-unique time domain solutions.

The method described in this paper is a non-authentic method which can closely reproduce shock response spectra with excellent repeatability and good correlation to actual time histories. The simplicity of setup and the short retest cycle (one pulse every minute) makes this method very attractive to people in the environmental testing industry.

SHOCK RESPONSE SPECTRUM

Shock response spectrum is a method

used to indicate the amount of energy in a pyrotechnic occurrence as a function of the frequency of that energy, in other words, a spectrum. Several excellent papers have been published describing this spectrum in detail and several classic arguments exist on the value of this spectrum. For this paper, the definition above will suffice.

As is true for most spectrum data, different frequency ranges can be considered to be dependent on different sources. The frequency ranges will be defined relative to that frequency at which the highest spectrum value exists so that low frequency is below and high frequency is above this peak. (See Figure I.) Very low frequencies are dependent on displacement. A change in the position of the device after the pyrotechnic event will be represented by a displacement line (12 dB/octave) at very low frequencies. Similarily, a change in velocity is represented by a velocity line (6 dB/octave) at low frequency. At high frequency, the peak acceleration establishes an acceleration line (0 dB/octave slope.) The middle frequency amplitude is a function of the dynamic amplification of the event by the analyzer at these frequencies.

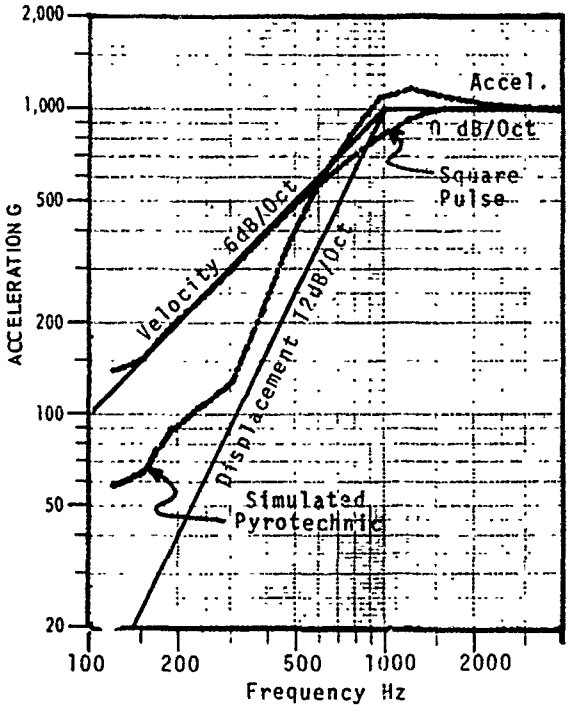

FIGURE I

VELOCITY AND DISPLACEMENT LINES

These dependencies are casual and exceptions can easily be made by varying the event characteristics. For example, if no residual displacement takes place during the event, the very low frequency spectrum becomes dependent on a velocity line.

The reason for these dependancies can be explained through the following example. An acceleration time history is depicted in Figure II, along with its associated velocity and displacement histories.

The end of the event can be defined when all the available energy (both kenetic and potential) has been expended and therefore, no more acceleration can occur. For this reason, the acceleration after this point is zero and is called "residual". Both velocity and displacement may have non-zero residuals since this does not imply energy consumption.

Since the residual acceleration is zero, its integral with respect to time (velocity) cannot change and is therefore a constant. Since velocity must be a constant, displacement can be either a ramp function (case 1) or a constant (case 2) depending on whether the residual velocity is zero or non-zero.

In case 1, the response of a low frequency shock response analyzer is superimposed on the velocity time history. It is obvious that all channels at lower frequencies would respond similarily since the response is effectively a step function response. For zero damping analysis, the peak dynamic response is equal to twice the amplitude of the step. The corresponding peak acceleration is a function of the zero-to-peak velocity response (v) and the analysis frequency. This function is:

$$a = \frac{dv\ (t)}{dt} = \frac{d[v - v\ \cos\ (2\pi f t)]}{dt}$$

$$a = v 2\pi f\ \sin\ (2\pi f t)$$

The peak acceleration is:

$$A\ (\text{peak}) = 2\pi f v$$

This peak acceleration represents a point on the spectrum at some low frequency. The locus of all the points at frequencies which respond similarily to this input is called a velocity line. These lines are depicted in Figure 1.

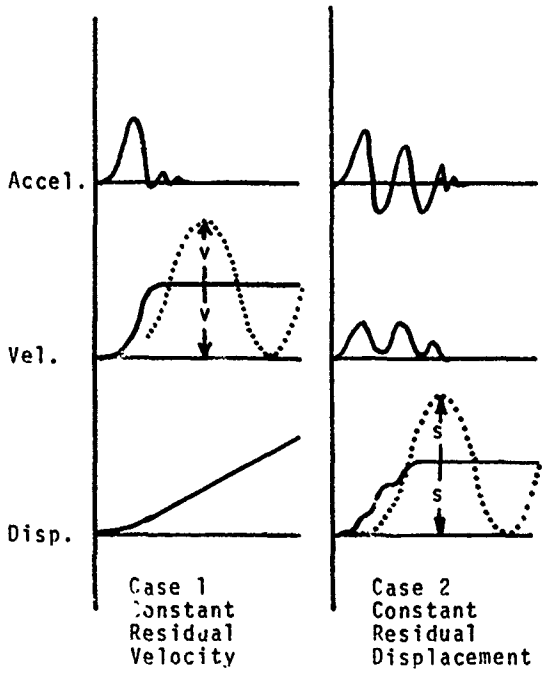

FIGURE II

DERIVATION OF CONSTANT

VELOCITY AND DISPLACEMENT

LINES

Similarily we can show displacement lines are defined by the equation:

$$A = (2\pi f)^2 S$$

In both cases shown, the high frequency analysis is represented by a constant acceleration line at the same level as the maximum acceleration reached in the time history. This occurs because high frequency analysis channels respond to the input by following the acceleration precisely as it occurs and the peak response is the peak input.

The mid range analysis is a function of the dynamic response of the analyzer to the input and cannot be approximated by straight lines.

THE ACTUAL ENVIRONMENT

As stated previously, this environment typically arises from the use of explosive separation devices during missile staging. These devices are intended to separate holding brackets or bolts to allow the stages to move in different directions. They are not generally intended as propulsion devices and; therefore, do not impart significant velocity to the missile body. For this reason, typical pyrotechnic spectra do not have velocity lines at low frequencies, but rather have displacement or even lower order lines.

For this reason, methods used to simulate pyrotechnic occurrences should not allow a velocity change to be imparted to the test item. The most common shock testing machine, that is the drop shock machine, imparts a significant velocity change to the test item by its very nature and is therefore inadequate for pyrotechnic testing.

Typical specifications for pyrotechnic testing require a nominal spectrum constructed from one displacement line and one acceleration line. Figure III shows a typical spectrum requirement along with shock response spectra available from drop machines. Notice these spectra have low frequency velocity lines.

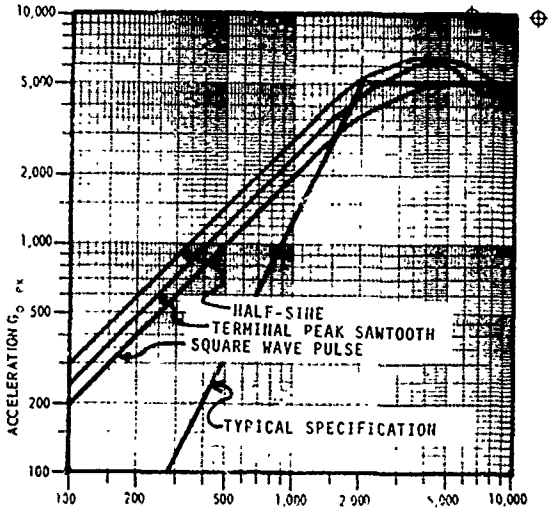

FIGURE III

PULSE SHOCKS DO NOT MATCH SPECTRUM

BOUNDED IMPACT

A test method called "Bounded Impact" has been developed which utilizes the common drop shock machine but produces a pyrotechnic shock.

Instead of attaching the test item to the drop table, which changes both position and velocity during the test, the item is located in a stationary location beneath the table and the test item holding fixture is impacted by the table. Conceptually, this method is somewhat similar to Ikola's method of eliminating low frequency velocity lines described in Reference 11. Shock programmers, usually used to produce half-sine pulses on the table, are used between the fixture and seismic base, and between the fixture and the table so that the falling table is allowed to transfer energy to the fixture through the programmer. See Figure IV.

For this test setup, there are three variables selectable by the test engineer. These are:

1. The height of the table before it is dropped
2. The stiffness of the programmers used (both the same for this case)
3. The effective weight of the table (above a minimum) and the weight of the test fixture.

The two weights have been listed as one variable because the ratio of these weights will establish a particular shock time history and this ratio will be used as a single parameter.

In order to establish the utility of this method, a computer program was written for the solution of the three mass system shown in Figure IV and a parametric study performed. The equations defining the motion of the system are:

$$M_2\ddot{x}_2 + KS_1 = M_2g \qquad \text{I}$$

$$M_1\ddot{x}_1 - KS_1 + KS_2 = M_2g \qquad \text{II}$$

$$M_3\ddot{x}_3 - KS_2 + K_3X_3 = M_3g \qquad \text{III}$$

$$S_1 = (x_2 - x_1) \text{ if } x_2 < x_1 \qquad \text{IV}$$

$$S_1 = 0 \text{ if } x_2 > x_1 \qquad \text{V}$$

$$S_2 = (x_1 - x_3) \text{ if } x_1 < x_3 \qquad \text{VI}$$

$$S_2 = 0 \text{ if } x_1 > x_3 \qquad \text{VII}$$

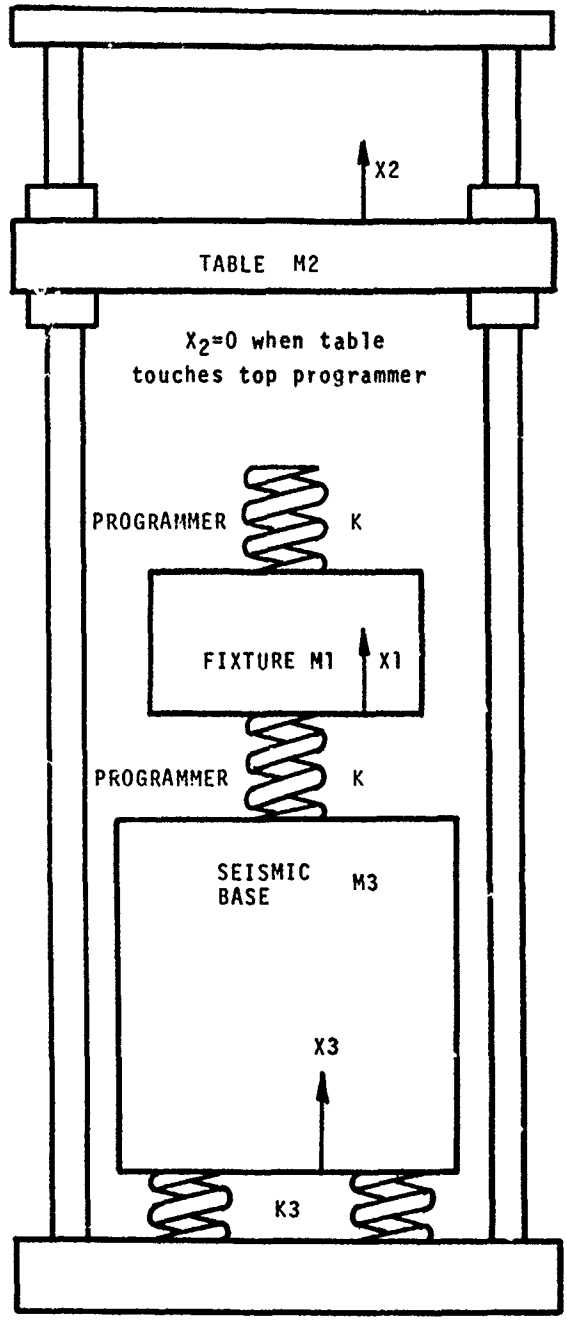

FIGURE IV

STANDARD DROP MACHINE

CONFIGURED FOR

PYROTECHNIC SHOCK ON FIXTURE

Equations V and VII allow separation of the masses from the programmers since the programmers are not capable of operating under tension, and the table must be free to rebound away from the top programmer.

The acceleration time history of Mass-1 is of interest since it represents the imposed test condition. Solutions of this acceleration are approximately sinusoidal. After the table impacts the top programmer, the test fixture oscilates between table and base until the table rebounds. When the table leaves the top programmer, the fixture is free to move upward at some velocity. Since we desire this velocity to equal zero, we only allow solutions which result in zero residual velocity. These solutions occur when the compression of the bottom programmer is zero, allowing no potential energy storage, at the instant the table leaves the top programmer. The acceleration consists of an odd number of half-sine cycles. The downward half-sines are smaller than the upward half-sines and this results in the time history integrating to zero over its duration and thereby having zero residual velocity.

A drop shock machine utilizing a seismic base was used for this program and so a compromise with reality must be explained at this point. The seismic base is modeled as Mass-3 and will have a very small residual velocity due to the energy exchange at impact. If this base is moving downward after impact, and the fixture is not, the base will be returned to its original position by its suspension and the fixture will begin falling due to gravity, resulting in an inevitable collision and its associated shock pulse. For this reason, the residual velocity of the fixture is actually made equal to the residual velocity of the base.

Figure V shows the first possible solution called Mode 3. (Mode 1 is not physically possible.) The parameters have been choosen to exaggerate the residual velocity. Typical tests would have very, very small residual velocities, which would not be present on the spectrum in the frequency range of interest. The fixture acceleration is shown along with the position of the table, fixture, and base. The parameters used were:

Table weight	561 pounds
Fixture weight	346 pounds
Base weight	4838 pounds
Programmers stiffness	5000 pounds/inch
Base suspension	6000 pounds/inch
Drop height	10 inches

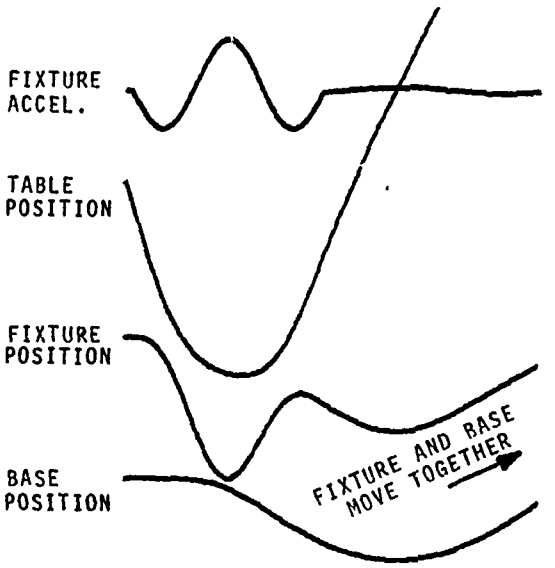

FIGURE V

TIME HISTORY

The parametric study resulted in the following possible fixture weights for modes 3 through 9.

MODE	FIXTURE WEIGHT
3	346
5	109
7	50
9	30

Figure VI is a solution of Mode 9. The residual velocity was set at zero in this case to demonstrate the collision effect. The fixture weight used to obtain zero residual was 32 pounds instead of the recommended 30 pounds. Notice that a residual position exists in this example due to a lowering of the base during the shock.

The parametric study further showed that if the programmers were made stiffer, the fundamental frequency of the time history increased with all other qualities remaining the same. When the drop height was increased, the amplitude of the time history increased with no other changes resulting. These results imply an ease of operation of this method. The amplitude and the frequency can be changed unilaterally by changing

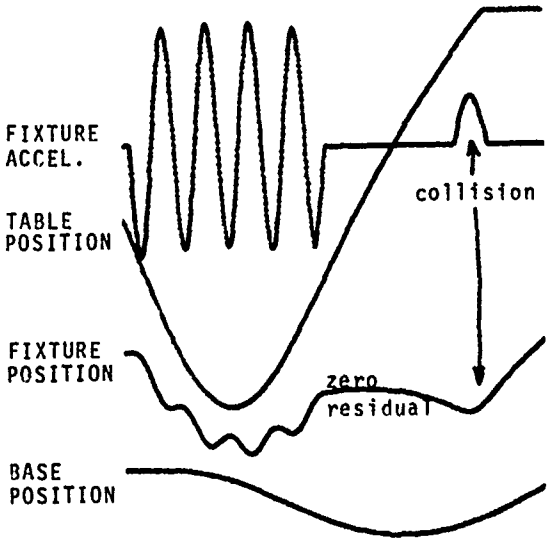

FIGURE VI

TIME HISTORY

MODE 9

one parameter. The mode can be changed by changing the mass ratio.

If we recall that the typical specification is just a displacement and an acceleration line, it is obvious that the best approximation is obtained by the lowest mode. Tests were performed and data collected using the second lowest mode (Mode 5) since the fixture weight of 100 pounds was easy to handle. Mode 3 results is a 346 pound fixture.

EMPIRICAL VERIFICATION

Upon experimenting on an actual test setup, the first conclusion was that the actual programmers posses damping, a variable not included in the computer analysis. This damping made the time histories slightly different from the computer solutions, but did not significantly change the spectra. Figure VII shows a low frequency (140 Hz) solution with some time history deterioration. Figure VIII shows a high frequency (2000 Hz) solution. Considerable time history deterioration occurred due to the high damping of high frequency programmers and considerable distortion has occurred due to the excitation of many fixture resonant modes. The resulting spectrum is still an excellent shape for this type of testing, ano the wave shape degradation and distortion have made the time history appear more representative of actual field events.

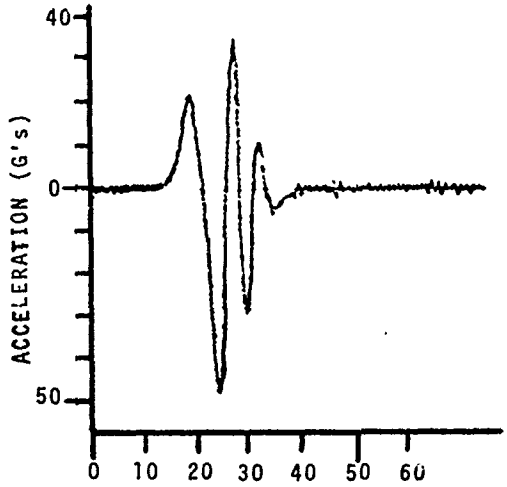

FIGURE VII

SIMULATED LOW FREQUENCY PYROTECHNIC

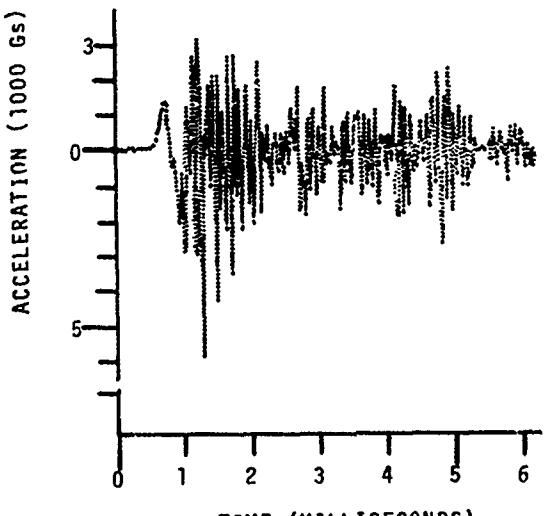

FIGURE VIII

SIMULATED HIGH FREQUENCY PYROTECHNIC

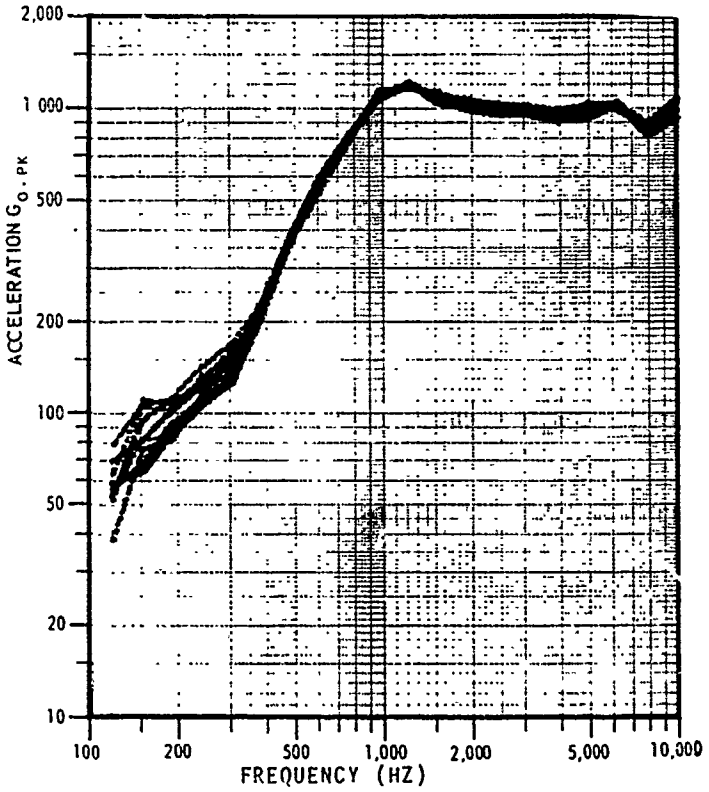

FIGURE IX

REPEATABILITY OF

TEN PYROTECHNIC SHOCKS

IN SIXTEEN MINUTES

A major advantage of this method is that no expendables are used, no damage or fracture is imposed on the test equipment, and all equipment used is commercially designed and manufactured for long life and repeatability. For these reasons, highly repeatable testing can be performed with little time required between consecutive shocks. Figure IX shows 10 consecutive shock tests performed, analyzed, and plotted in 16 minutes.

CONCLUSIONS:

The analysis and tests described in this paper show the method of "Bounded Impact" to be very useful and practical for simulating pyrotechnic occurrences and in particular:

1. This method allows unilateral adjustment of frequency and amplitude parameters.
2. This method is highly repeatable.
3. This method uses comercially available test equipment.
4. This method produces spectra which have pyrotechnic slopes (12 dB/octave) at low frequencies.
5. This method produces time histories similar to field events.
6. "Bounded Impact" has been used to obtain shock spectra to 20,000 Go-pk.

BIBLIOGRAPHY:

1. A.F. Witte and R.J. Wolf
"Comparison of Shock Spectrum Techniques and the Method of Least Favorable Response"

The Shock and Vibration Bulletin 44
(Part 3 of 5 parts) August 1974

2. D.O. Smallwood and A.R. Nord
"Matching Shock Spectra With Sums of Decaying Sinusoids Compensated For Shaker Velocity and Displacement Limitations"

The Shock and Vibration Bulletin 44
(Part 3 of 5 parts) August 1974

3. Dan R. Powers
"Development of a Pyrotechnic Shock Test Facility"

The Shock and Vibration Bulletin 44
(Part 3 of 5 parts) August 1974

4. S.N. Prescott
"Pyrotechnic Shock Reduction"

The Shock and Vibration Bulletin 44
(Part 3 of 5 parts) August 1974

5. Charles L. Thomas
"Pyrotechnic Shock Simulation Using The Response Plate Approach"

The Shock and Vibration Bulletin 43
(Part 1 of 4 parts) June 1973

6. D.O. Smallwood and A.F. Witte
"The Use of Shaker-Optimized Periodic Transients In Matching Field Shock Spectra"

The Shock and Vibration Bulletin 43
(Part 1 of 4 parts) June 1973

7. Phillip Barnett
"Measurement and Analysis of Spacecraft Seperation Transient Response for Mariner-Type Spacecraft"

The Shock and Vibration Bulletin 37
(Part 4 of 7 parts) January 1968

8. M. Gertel and R. Holland
"Simple Strength Concept For Defining Practical High-Frequency Limits of Shock Spectrum Analysis"

The Shock and Vibration Bulletin 37
(Part 4 of 7 parts) January 1968

9. Ralph E. Blake
"Problems of Simulating High-Frequency Mechanical Shocks"

Institute of Environmental Sciences
1964 proceedings

10. E. Aten, T. Jocobi, and D. White
"High Intensity Pyrotechnic Shock Testing of Titan III Airborne Inertial Guidance Equipment"

Institute of Environmental Sciences
1966 proceedings

11. A.L. Ikcla
"Simulation of The Pyrotechnic Shock Environment"

The Shock and Vibration Bulletin 34
December 1964

12. R. T. Fandrich
"Pyrotechnic Shock Testing On A Standard Drop Machine"

Institute of Environmental Sciences
1974 proceedings

13. Russell Lowe and Richard D, Cavanaugh
"Correlation of Shock Spectra and Pulse Shape With Shock Environment"

Environmental Engineering
February 1959

14. Wayne Tustin and George M. Hieber
"Understanding and Measuring The Shock Response Spectrum"

Spectral Dynamics Corp. Tech. Pub.
No. SSA-3 4-73

DYNAMIC RESPONSE OF
ELECTRICAL CABLES TO SHOCK MOTION

R. W. Doll
TRW Defense and Space Systems Group
Redondo Beach, California 90278

The response for flexible cables is derived in terms of the longitudinal, torsional and two-transverse equations of motion. The kinematics of the cable motion are derived in terms of the Frenet-Serret curvature-torsion parameters, and the equations of motion are obtained from Hamilton's Principle. Special attention is given to conditions when the cable's response lies in the plane of excitation or when it is a coupled non-planer response. This investigation shows that only when τ_o is equal to zero and either κ_o or κ_o' is equal to zero, or when all three parameters are equal to zero will the response be planer.

An investigation of the cable response is accomplished using a finite element discretization of the equations of motion. In general the development of the curvilinear finite element is based on the assumption that a set of local intrinsic, curvilinear coordinates are specified a priori and that the local field can be approximated by cubic Hermite interpolation polynomials in these coordinates resulting in an isoparametric cable element.

The resultant algebraic eigenvalue problem is solved by reducing the problem to tri-diagonal form using a Householders reduction and then using the QR algorithm to solve for the cable eigenvalues and eigenvectors. The results are shown for a quarter circular arc which represented a cable section between an isolated floor and a fixed vertical wall. A qualitative comparison with uninstrumented tests is presented.

NOMENCLATURE

A	Area
d	Diameter of cable
ds	Differential segment of rod in unstressed state
D^k	Differential operator $\partial^k()/\partial s^k$
E	Modulus of elasticity
F_{33}	Axial force
G	Shear modulus
I_p	Polar moment of inertia for unit length
I_1	x-axis second moment of area
I_2	y-axis second moment of area
J	Polar moment of area
$\underline{K}$	Stiffness matrix
l	Arc length
m_c	Cable mass per unit length
M_{ii}	Moments
N_e	Total number of elements
R	Radius of centerline curvature
s	Centerline coordinate
η	Curvilinear coordinate of centerline
κ_o	Component of principal initial curvature about x-axis
κ_o'	Component of principal initial curvature about y-axis
τ_o	Initial torsion of rod about centerline

1. INTRODUCTION

An integral part of each missile silo is the launch equipment room which contains monitoring and launch electronic equipment. This equipment is mounted on a suspended shock isolated floor and connected to the missile via electrical cable bundles.

These connections are clamped at each end to the facility and floor, respectively. Slack in the form of shock loops is provided to allow for the relative motion between silo and floor. The integrity of the electrical cable at these clamp points was of interest.

Previously, tests had been conducted at the Naval Weapons Support Center (NWSC), in conjunction with a more extensive battery shock program. The data from these cable tests were qualitative in nature and consisted of high speed movies of each shock event. Post test inspection revealed cable slippage through the clamp and it was decided that an analysis of the clamp reaction loads was needed.

The electrical cable shock loops are not simple geometrical configurations, thus the kinematic relations were derived in terms of the Frenet-Serret curvature-torsion parameters which completely describe a one dimensional curve in Euclidian space. Implementation of these relationships with the Hamiltonian Principle leads to a set of four partial differential equations, two transverse, one torsional and one longitudinal as presented in [1]. Special attention is given to the identification of curvature-torsion conditions under which the response in the plane normal to the excitation may be induced.

The solution to the four partial differential equations involves a finite element discretization prior to spectral analysis. The numerical procedures developed simulate both constant curvature and variable curvature three dimensional cable models. The theoretical results are then tested against known solutions found in current literature.

2. THEORY

The theoretical model consists of a long slender cable whose cross-section displacement is described by the longitudinal coordinate, s, along the cable centerline. The cable centerline displacement may not be small although strains are assumed small. Rotary inertia caused by bending, transverse shear deformation and anticlastic deformation are not included.

The curvatures of the two transverse principal centroidal axes are κ_o and κ_o', with torsion τ_o about the centerline as shown in Figure 1. The resultant curvature at Point "o" is seen to be

$$\kappa_o^* = \left(\kappa_o^2 + \kappa_o'^2 \right)^{1/2} \tag{1}$$

with

$$\kappa_o'/\kappa_o = \tan \nu \tag{2}$$

The curvature-torsion parameters are a function of the position s as shown in Figure 2 and can be described in terms of the four generalized coordinates; w, u, v and θ in the tangent, normal, binormal and rotational directions, respectively. Following extensive manipulations one obtains the three curvature-torsion relationships

$$\begin{aligned} \kappa_1 = {} & \kappa_o - v_{,ss} - (\tau_o u)_{,s} + (\kappa_o w)_{,s} + \kappa_o' \theta \\ & - \tau_o u_{,s} + \tau_o^2 v - \kappa_o' \tau_o w - \kappa_o' u_{,s} v_{,s} \\ & - u_{,s} \theta_{,s} - \tau_o v_{,s} \theta + \kappa_o v_{,s}^2 \end{aligned} \tag{3}$$

$$\begin{aligned} \kappa_1' = {} & \kappa_o' + u_{,ss} - (\tau_o v)_{,s} + (\kappa_o' w)_{,s} - \tau_o v_{,s} \\ & + \tau_o^2 u + \kappa_o \tau_o w - \kappa_o \theta + v_{,ss} \theta + (\tau_o u)_{,s} \theta \\ & + \tau_o u_{,s} \theta + \kappa_o' u_{,s}^2 - \kappa_o u_{,s} v_{,s} \end{aligned} \tag{4}$$

$$\begin{aligned} \tau_1 = {} & \tau_o + \tau_o \kappa_o u + \kappa_o u_{,s} - \kappa_o \tau_o v + \kappa_o' v_{,s} \\ & + \theta_{,s} + \tau_o \theta^2 + \kappa_o' u_{,s} \theta - \kappa_o v_{,s} \theta \\ & + \tau_o u_{,ss} u + u_{,ss} v_{,s} \end{aligned} \tag{5}$$

The development of (3) - (5) reduces to the results found in Love [2] when κ_o and the nonlinear terms are set equal to zero.

Next the equations of motion are obtained from a Hamiltonian formulation. This variational technique has the distinct advantage of being a general approach where the required essential and suppressible boundary conditions are automatically obtained. If the mean cross-sectional dimension of the cable is considerably smaller than the radius of curvature and the overall chord length, the kinematic relations (3) - (5) remain valid and the statement of Hamilton's Principle is simply

$$\delta I = \delta \int_{t_1}^{t_2} L \, dt \tag{6}$$

where the Lagrangian L is the kinetic minus the potential energy of the cable. The kinetic energy of the cable is

$$T = \frac{1}{2} m_c \int_{l_o}^{l_1} \left[u_{,t}^2 + v_{,t}^2 + w_{,t}^2 + \frac{I_\rho}{m_c} \theta_{,t}^2 \right] ds \tag{7}$$

The potential energy of the cable is determined from classical rod theory for bending, torsion and tension

$$\frac{M_{11}}{EI_1} = \kappa_1 - \kappa_o \tag{8}$$

$$\frac{M_{22}}{EI_2} = \kappa_1' - \kappa_o' \tag{9}$$

$$\frac{M_{33}}{GJ} = \tau_1 - \tau_o \tag{10}$$

$$\frac{F_{33}}{AE} = \varepsilon_{33} \tag{11}$$

The curvature-torsion terms are given in (3) - (5) and ε_{33} is the finite strain for small strain and moderate to large rotations;

$$\varepsilon_{33} = e_{33} + \frac{1}{2}(\omega_{23}^2 + \omega_{13}^2) \tag{12}$$

The axial strain becomes upon calculation

$$\varepsilon_{33} = (w_{,s} - \kappa_o' u + \kappa_o v) + \frac{1}{2}\left[(u_{,s} - \tau_o v + \kappa_o' w)^2 + (v_{,s} - \kappa_o w + \tau_o u)^2\right] \tag{13}$$

The centerline deformation is small but not zero. The total potential energy then becomes

$$V = \frac{1}{2}\int_{l_o}^{l_1} \left| M_{11}(\kappa_1 - \kappa_o) + M_{22}(\kappa_1' - \kappa_o') + M_{33}(\tau_1 - \tau_o) + F_{33}\varepsilon_{33} \right| ds \tag{14}$$

The Hamiltonian (1) can now be formulated by substitution. From the linearized (3) - (5), the stationary principle gives

$$\begin{aligned}\delta I_h = \int_{t_1}^{t_2} \Bigg| \delta\Bigg\{ &\frac{1}{2}\int_{l_o}^{l_1} m_c \left[u_{,t}^2 + v_{,t}^2 + w_{,t}^2 + I_\rho \theta_{,t}^2\right] ds \\ &- \frac{1}{2}\int_{l_o}^{l_1} EI_1 \left[-v_{,ss} - 2\tau_o u_{,s} + \kappa_o w_{,s} + \tau_o^2 v - \kappa_o' \tau_o w + \kappa_o' \theta\right]^2 ds - \frac{1}{2}\int_{l_o}^{l_1} EI_2 \left[u_{,ss} - 2\tau_o v_{,s} + \kappa_o' w_{,s} - \tau_o^2 u + \kappa_o \tau_o w - \kappa_o \theta\right]^2 ds \\ &- \frac{1}{2}\int_{l_o}^{l_1} GJ \left[\theta_{,s} + \kappa_o u_{,s} + \kappa_o' v_{,s} + \kappa_o' \tau_o u - \kappa_o \tau_o v\right]^2 ds - \frac{1}{2}\int_{l_o}^{l_1} AE \left[w_{,s} - \kappa_o' u + \kappa_o v\right]^2 ds \Bigg\} \Bigg| dt = 0 \end{aligned} \tag{15}$$

The Euler equations obtained from (15) in a straightforward but lengthy manner are

$$\underset{\sim}{\alpha}\,\ddot{\underset{\sim}{X}} + \underset{\sim}{\beta}\,\underset{\sim}{X} = \underset{\sim}{f} \tag{16}$$

where the coefficients of these 4 x 4 $\underset{\sim}{\alpha}$ and $\underset{\sim}{\beta}$ operator matrices are given in Appendix A, $\underset{\sim}{X}^T = [w,u,v,\theta]$ and the boundary conditions are given in Table I. If κ_o vanishes and the inextensible centerline hypothesis is used, $u = \frac{\partial w}{\partial s}$, this equation reduces to that found in Tso [3] for curved and twisted rods.

The $\underset{\sim}{\alpha}$ matrix is diagonal and associated with the inertial properties of the system, and $\underset{\sim}{\beta}$ is the matrix associated with cable stiffness. Thus a non-vanishing of the off-diagonal β_{ij} components insures coupled motion. In summary, coupled response results for the following cables:

A) If the cable is initially curved and twisted, coupling of all variables occur. Here $\kappa_o \neq o$ and/or $\kappa' \neq o$, $\tau_o \neq o$.

B) If the cable is not twisted and if the principal radius of curvature is not aligned with a cable cross-section principal axis, total coupling of all variables occur. Here $\kappa_o \neq o$, $\kappa_o' \neq o$ and $\tau_o = o$.

C) If the cable is initially straight but twisted, coupled response occurs. Here $\kappa_o = \kappa_o' = o$ and $\tau_o \neq o$. The $\underset{\sim}{\beta}$ coefficients of (16) are

$$\underset{\sim}{\beta} = \begin{bmatrix} \beta_{11} & o & o & o \\ o & \beta_{22} & \beta_{23} & o \\ o & -\beta_{23} & \beta_{33} & o \\ o & o & o & \beta_{44} \end{bmatrix} \tag{17}$$

indicating coupling between the flexual coordinates, (u,v) to produce an out-of-plane response.

An uncoupled response can occur only for the following cable configurations.

A) If the cable is straight and not twisted, then all dependent variables are uncoupled. Here $\kappa_o = \kappa_o' = \tau_o = o$.

B) If the cable is not twisted and its radius of curvature is along a cross-section principal axis, then the in-plane (w,u) and out-of-plane (v,θ) response is uncoupled. Here $\kappa_o = o$ or $\kappa_o' = o$, $\tau_o = o$. Thus coupled motion occurs within each plane so that the $\underset{\sim}{\beta}$ coefficients of (16) are

$$\underline{\beta} = \begin{bmatrix} \beta_{11} & \beta_{12} & 0 & 0 \\ -\beta_{12} & \beta_{22} & 0 & 0 \\ 0 & 0 & \beta_{33} & \beta_{34} \\ 0 & 0 & \beta_{34} & \beta_{44} \end{bmatrix} \tag{18}$$

3. NUMERICAL ANALYSIS

The class of problems analyzed numerically were selected for similarity to typical cable installations or available literature. For the remainder of this paper it will be assumed that the cable cross-section is circular and symmetric with a constant radius of curvature such that

$$\begin{aligned} \kappa_o &= 0 \\ \kappa_o' &= \frac{1}{R} \\ \tau_o &= 0 \\ I_1 &= I_2 = I_o \end{aligned} \tag{19}$$

The conditions imposed by (19) insure an uncoupled in-plane and out-of-plane response.

The finite element discretization of (15) following substitution of (19) divides the cable into N_e elements. The local field variable is

$$\underset{\sim}{u}^{(e)}(\eta,\tau) = \underline{\phi}^{(e)}(\eta)\underset{\sim}{y}^{(e)}(\tau) \tag{20}$$

where the nodal coefficients are

$$\underset{\sim}{y}^{(e)^T} = [w_i', u_i', v_i', \theta_i', w_{i,s}', , , \theta_{i,s}', w_j', , , w_{j,s}', , , \theta_{j,s}'] \tag{21}$$

and the non-zero Hermite interpolation polynomial on $-1 \le \eta \le +1$ is

$$\begin{aligned} \phi_{KK}^{(e)} &= (2 - 3\eta + \eta^3)/4 \\ \phi_{K(K+4)}^{(e)} &= (1 - \eta - \eta^2 + \eta^3)/8 \\ \phi_{K(K+8)}^{(e)} &= (2 + 3\eta - \eta^3)/4 \\ \phi_{K(K+12)}^{(e)} &= (-1 - \eta + \eta^2 + \eta^3)/8 \end{aligned} \tag{22}$$

where $K = 1, \ldots, 4$. The local x, y, z, θ are similarly distributed. The discretization follows directly with a few points worthy of comment. The interpolation (22) uses the curvilinear coordinate η, and the curvature-torsion parameters in (16) are defined in terms of s. The derivatives

$$\frac{\partial \eta}{\partial s} = \left[\left(\frac{\partial x}{\partial \eta}\right)^2 + \left(\frac{\partial y}{\partial \eta}\right)^2 + \left(\frac{\partial z}{\partial \eta}\right)^2 \right]^{-\frac{1}{2}} \tag{23}$$

$$\frac{\partial^2 \eta}{\partial s^2} = \left(\frac{\partial \eta}{\partial s}\right)^4 \left[\frac{\partial x}{\partial \eta}\frac{\partial^2 x}{\partial \eta^2} + \frac{\partial y}{\partial \eta}\frac{\partial^2 y}{\partial \eta^2} + \frac{\partial z}{\partial \eta}\frac{\partial^2 z}{\partial \eta^2} \right] \tag{24}$$

$$\begin{aligned} \frac{\partial^3 \eta}{\partial s^3} = -4 \left(\frac{\partial s}{\partial \eta}\right) \frac{\partial^2 \eta}{\partial s^2} - \left(\frac{\partial \eta}{\partial s}\right)^5 \Bigg[&\left(\frac{\partial^2 x}{\partial \eta^2}\right)^2 + \left(\frac{\partial^2 y}{\partial \eta^2}\right)^2 \\ &+ \left(\frac{\partial^2 z}{\partial \eta^2}\right)^2 + \frac{\partial x}{\partial \eta}\frac{\partial^3 x}{\partial \eta^3} + \frac{\partial y}{\partial \eta}\frac{\partial^3 y}{\partial \eta^3} + \frac{\partial z}{\partial \eta}\frac{\partial^3 z}{\partial \eta^3} \Bigg] \end{aligned} \tag{25}$$

and the curvature-torsion parameters

$$\kappa_o' = -\left[\left(\frac{\partial^2 x}{\partial s^2}\right)^2 + \left(\frac{\partial^2 y}{\partial s^2}\right)^2 + \left(\frac{\partial^2 z}{\partial s^2}\right)^2 \right]^{\frac{1}{2}} \tag{26}$$

$$\tau_o = \frac{1}{\kappa_o'^2} \begin{bmatrix} \frac{\partial x}{\partial s} & \frac{\partial y}{\partial s} & \frac{\partial z}{\partial s} \\ \frac{\partial^2 x}{\partial s^2} & \frac{\partial^2 y}{\partial s^2} & \frac{\partial^2 z}{\partial s^2} \\ \frac{\partial^3 x}{\partial s^3} & \frac{\partial^3 y}{\partial s^3} & \frac{\partial^3 z}{\partial s^3} \end{bmatrix} \tag{27}$$

are required for the necessary coordinate transformation. A second point is that the local coordinates in which the stiffness is formulated must be rotated into the global coordinate system during assemblage of the equations.

The stationarity of the discretized functional (16) leads to N discrete equations of motion

$$\underline{M}\,\ddot{\underline{v}} + \underline{K}\,\underline{v} = \underline{f} \tag{28}$$

where $\underline{M}$ is diagonal and $\underline{K}$ is symmetric. The eigenvalue problem becomes

$$\ddot{\underline{\zeta}} + [\lambda]\,\underline{\zeta} = \underline{P}(t) \tag{29}$$

with $\underline{\zeta}$ defined as the principal coordinate vector

$$\underline{\zeta} = \underline{\Phi}^{-1}\,\underline{v} \tag{30}$$

and

$$[\lambda] = [\omega_n^2] = \underline{M}^{*-1}\,\underline{K}^* \tag{31}$$

The matricies denoted by a superscript asterisk are diagonal with coefficients M^*_{nn} and K^*_{nn} defined by

$$\underline{M}^* = \underline{\Phi}^T \underline{M} \underline{\Phi} \tag{32}$$

$$\underline{K}^* = \underline{\Phi}^1 \underline{K} \underline{\Phi} \tag{33}$$

$$p^{(t)} = \underline{M}^{*-1} \underline{\Phi} \underline{f} \tag{34}$$

and $\underline{\Phi}$ is the matrix array of eigenvectors.

The homogeneous part of (29) is solved numerically by a reduction to tri-diagonal form using a Householder reduction and then utilization of the QR algorithm to solve for the individual eigenvalues.

The complete solution for (29) takes the form

$$\zeta_n(t) = C_n \sin(\omega_n t + \psi_n) + \int_0^t P_n(\tau) h_n(t-\tau) d\tau \tag{35}$$

where

$$h_n^{(t)} = \frac{1}{M^*_{nn}\,\omega_n} \sin \omega_n t \tag{36}$$

The arbitrary constants C_n and ψ_n are determined from the initial conditions.

Lastly, the N solutions to (35) can then be obtained in terms of the generalized coordinates, $\underline{y}$, by applying the proper transformation.

4. RESULTS

Due to the qualitative nature of the experiment, the accuracy of the numerical-algorithm has to be compared with results found in the literature. For straight elements convergence for a wide range of Ritz interpolation functions is guaranteed. Such is not the case for curved elements, but the use of the isoparametric formulation and its ability to introduce rigid body excursions into the displacement field greatly improves the accuracy, especially for the lower modes. Comparisons are made using the incomplete circular ring results of Archer [4].

For a third order interpolation function Fried [5] has shown that in the limit the mean rate of convergence is N_e^{-4}, where N_e is the number of cable elements. In addition the convergence rate decreases as element distortion increases to a lower bound of N_e^{-2}. Furthermore, Sabir [6] shows that the convergence decreases as the relative thickness (R/d) decreases and/or the included angle increases. The convergence of the present analysis is tested against exact solutions for two semi-circular rings [4] in Figure 3. The convergence is satisfactory and consistent with expectations. Figure 4 shows representative mode shapes of the first two fundamental frequencies for increasing curvature.

The electrical cable shock tests were conducted at the Naval Weapons Support Center (NWSC) in conjunction with shock testing of the emergency power battery system. The cable experiment consisted of a single electrical cable attached to the bottom of the shock carriage by means of a cable clamp. The cable hung from the clamp with the opposite end coiled on the floor to form a shock loop as shown in Figure 5. The cable was continuously monitored for electrical continuity. The maximum shock level input to the carriage and cable mount assembly was a 600 G, 4 ms half-sine pulse, shown in Figure 6. The test cable was a rubber jacketed 0.038 m diameter casing containing a bundle of 17 paired copper wires weighing 14.6 N/m with an equivalent EI of 1.38 N/m^2 and a EA of 154,798 N. The cable was tested in two basic configurations, first the bare cable, and secondly, with additional weights attached to provide a uniform inertia loading that could be increased to a maximum of 264.4 N/m. Figure 7 shows the first four mode shapes and natural frequencies for the unweighted cable. For the weighted cable, the corresponding mode shapes are identical. The matching natural frequencies were lowered due to the increase in mass per unit length without a corresponding increase in stiffness. With the eigenvalues and eigenvectors computed the time history response was obtained so that maximum nodal forces along with the resultant cable clamp reactions were established. Table II tabulates the maximum cable reactions for the bare cable, the 52.5 N/m and 264.4 N/m cable loadings.

During these tests and the subsequent cable tear down inspection, no breakage or loss in electrical continuity was observed. The only visible sign of the shock damage was that the 264.4 N/m weighted cable had undergone approximately 10.2 centimeters of slippage through the clamp during shock.

The analytic model developed in this paper has great flexibility in being able to handle a wide variety of cable geometries and providing insight into the type of response one might expect. It is readily adopted to the finite element solution technique for obtaining results with a high degree of accuracy.

BIBLIOGRAPHY

1. Doll, R. W. and C. D. Mote, Jr., "The Dynamic Formulation and the Finite Element Analysis of Curved and Twisted Tubes Transporting Fluids," Report to the National Science Foundation, Department of Mechanical Engineering, University of California, Berkeley, 1974.

2. Love, A. E. H., A Treatise on the Mathematical Theory of Elasticity, Dover Publications, New York, 1966, pp. 444-454.

3. Tso, W. K., "On the Motion of a Curved and Twisted Rod," ACTA Mechanical, Vol. 13, 1972, pp. 163-178.

4. Archer, R. R., "Small Vibrations of Thin Incomplete Circular Rings," Int. S. Mechanical Science, Vol. 1., 1960, pp. 45-56

5. Fried, I., "Accuracy and Condition of Curved (Isoparametric) Finite Elements," J. of Sound and Vibration, Vol. 31, No. 3, 1973, pp. 45-56.

6. Sabir, A. B., and D. G. Ashwell, "A Comparison of Curved Beam Finite Elements When Used in Vibration Problems," J. of Sound and Vibration, Vol. 18, No. 4, 1971, pp. 555-563.

APPENDIX A

The elements of the $\underline{\alpha}$ and $\underline{\beta}$ operators are given here with the notation $D^k = d^k/ds^k$. All elements not included herein are identically zero.

$$\alpha_{11} = \alpha_{22} = \alpha_{33} = -m_c \tag{37}$$

$$\alpha_{44} = -I_\rho \tag{38}$$

$$\beta_{11} = \left[EI_1\kappa_o^2 + EI_2\kappa_o'^2 + EA\right]D^2 - \tau_o^2\left(\kappa_o'^2 EI_1 + \kappa_o^2 EI_2\right) \tag{39}$$

$$\beta_{12} = EI_2\kappa_o'D^3 - \kappa_o\tau_o\left[2EI_1 + EI_2\right]D^2 - \kappa_o'\left[\tau_o(2EI_1 + EI_2) + EA\right]D^1 + EI_2\kappa_o\tau_o^3 \tag{40}$$

$$\beta_{13} = -EI_1\kappa_o D^3 - \kappa_o'\tau_o\left[EI_1 + 2EI_2\right]D^2 + \kappa_o\left[\tau_o^2(EI_1 + 2EI_2) + EA\right]D^1 + EI_1\kappa_o'\tau_o^3 \tag{41}$$

$$\beta_{14} = \kappa_o\kappa_o'\left[EI_1 - EI_2\right]D^1 + \tau_o(EI_1\kappa_o'^2 + EI_2\kappa_o^2) \tag{42}$$

$$\beta_{21} = -EI_2\kappa_o'D^3 - \tau_o\kappa_o\left[2EI_1 + EI_2\right]D^2 + \kappa_o'\left[\tau_o^2(2EI_1 + EI_2) + EA\right]D^1 + EI_2\kappa_o\tau_o^3 \tag{43}$$

$$\beta_{22} = -EI_2D^4 + \left[2\tau_o^2(2EI_1 + EI_2) + GJ\kappa_o^2\right]D^2 - EI_2\tau_o^4 - GJ\kappa_o'^2\tau_o^2 - \kappa_o'^2 EA \tag{44}$$

$$\beta_{23} = 2\tau_o\left[EI_1 + EI_2\right]D^3 + GJ\kappa_o\kappa_o'D^2 - \left[2\tau_o^3(EI_1 + EI_2) + GJ + (\kappa_o'^2\tau_o + \kappa_o^2\tau_o)\right]D^1 + GJ\kappa_o\kappa_o'\tau_o^2 + \kappa_o\kappa_o' EA \tag{45}$$

$$\beta_{24} = \kappa_o\left[EI_2 + GJ\right]D^2 - \kappa_o'\tau_o\left[2EI_1 + GJ\right]D^1 - EI_2\kappa_o\tau_o^2 \tag{46}$$

$$\beta_{31} = EI_1\kappa_o D^3 - \kappa_o'\tau_o\left[EI_1 + 2EI_2\right]D^2 - \kappa_o\left[\tau_o^2(EI_1 + 2EI) + EA\right]D^1 + EI_1\kappa_o'\tau_o^3 \tag{47}$$

$$\beta_{32} = -2\tau_o\left[EI_1 + EI_2\right]D^3 + GJ\kappa_o\kappa_o'D^2 + \tau_o\left[2\tau_o^2(EI_1 + EI_2) + GJ(\kappa_o'^2 + \kappa_o^2)\right]D^1 + GJ\kappa_o\kappa_o'\tau_o^2 + \kappa_o\kappa_o' EA \tag{48}$$

$$\beta_{33} = -EI_1D^4 + \left[2\tau_o^2(EI_1 + 2EI_2) + GJ\kappa_o'^2\right]D^2 - EI_1\tau_o^4 - GJ\kappa_o^2\tau_o^2 - EA\kappa_o^2 \tag{49}$$

$$\beta_{34} = \kappa_o'\left[EI_1 + GJ\right]D^2 + \kappa_o\tau_o\left[2EI_2 + GJ\right]D^1 - EI_1\kappa_o'\tau_o^2 \tag{50}$$

$$\beta_{41} = -\kappa_o\kappa_o'\left[EI_1 - EI_2\right]D^1 + \tau_o(EI_1\kappa_o'^2 + EI_2\kappa_o^2) \tag{51}$$

$$\beta_{42} = \kappa_o\left[EI_2 + GJ\right]D^2 + \kappa_o'\tau_o\left[2EI_1 + GJ\right]D^1 - EI_2\kappa_o\tau_o^2 \tag{52}$$

$$\beta_{43} = \kappa_o'\left[EI_1 + GJ\right]D^2 - \kappa_o\tau_o\left[2EI_2 + GJ\right]D^1 - EI_1\kappa_o'\tau_o^2 \tag{53}$$

$$\beta_{44} = GJD^2 - (EI_1\kappa_o'^2 + EI_2\kappa_o^2) \tag{54}$$

TABLE I
BOUNDARY CONDITIONS

CLAMPED	PINNED	FREE
$\delta w = 0$	$\delta w = 0$	$-(EI_1\kappa_o^2 + EI_2\kappa_o'^2 - EA)w_{,s} + \kappa_o\kappa_o'\tau_o(EI_1 - EI_2)w - EI_2\kappa_o'u_{,ss} + 2EI_2\kappa_o\tau_o u_{,s} + (EI_2\kappa_o'\tau_o^2 + \kappa_o EA)u + EI_1\kappa_o v_{,ss} + 2EI_2\kappa_o'\tau_o v_{,s} - (EI_1\kappa_o\tau_o^2 + EA\kappa_o)v - \kappa_o\kappa_o'(EI_1 - EI_2)\theta = 0$
$\delta u = 0$	$\delta u = 0$	$EI_2\kappa_o'w_{,ss} + \kappa_o\tau_o(2EI_1 + EI_2)w_{,s} + EI_2u_{,sss} - \left[\tau_o^2(4EI_1 + EI_2) + GJ\kappa_o^2\right]u_{,s} - GJ\kappa_o\kappa_o'\tau_o u - 2\tau_o(EI_1 + EI_2)v_{,ss} - GJ\kappa_o\kappa_o'v_{,s} + \left[2EI_1\tau_o^3 + GJ\kappa_o^2\tau_o\right]v - \kappa_o(EI_2 + GJ)\theta_{,s} + 2EI_1\kappa_o'\tau_o\theta = 0$
$\delta u_{,s} = 0$	$-EI_2\left[u_{,ss} - \tau_o^2u - 2\tau_o v_{,s} - 2\tau_o v_{,s} + \kappa_o'w_{,s} + \kappa_o\tau_o w - \kappa_o\theta\right] = 0$	$-EI_2\left[u_{,ss} - \tau_o^2u - 2\tau_o v_{,s} + \kappa_o'w_{,s} + \kappa_o\tau_o w - \kappa_o\theta\right] = 0$
$\delta v = 0$	$\delta v = 0$	$-EI_1\kappa_o w_{,ss} + \kappa_o'\tau_o(EI_1 + 2EI_2)w_{,s} + 2EI_2\kappa_o\tau_o^2w + 2\tau_o(EI_1 + EI_2)u_{,ss} - GJ\kappa_o\kappa_o'u_{,s} - \left[2EI_2\tau_o^3 - GJ\kappa_o'\tau_o\right]u + EI_1v_{,sss} - \left[\tau_o^2(EI_1 + 4EI_2) + GJ\kappa_o'^2\right]v_{,s} + GJ\kappa_o\kappa_o'\tau_o v + \kappa_o'(EI_1 + GJ)\theta_{,s} - 2EI_2\kappa_o\tau_o\theta = 0$
$\delta v_{,s} = 0$	$-EI_2\left[2\tau_o u_{,s} + v_{,ss} - \tau_o^2v - \kappa_o w_{,s} + \kappa_o'\tau_o w - \kappa_o'\theta\right] = 0$	$EI_1\left[2\tau_o u_{,s} + v_{,ss} - \tau_o^2v - \kappa_o w_{,s} + \kappa_o'\tau_o w - \kappa_o'\theta\right] = 0$
$\delta\theta = 0$	$\delta\theta = 0$	$GJ\left[\kappa_o u_{,s} + \kappa_o'\tau_o u + \kappa_o'v_{,s} - \kappa_o\tau_o v + \theta_{,s}\right] = 0$

TABLE II
MAXIMUM CABLE CLAMP REACTIONS

AUXILIARY CABLE LOADING	RADIAL REACTION (N)	TANGENTIAL REACTION (N)
0.0 N/m	28,469	19,127
52.5 N/m	60,940	41,368
264.4 N/m	12,455	84,071

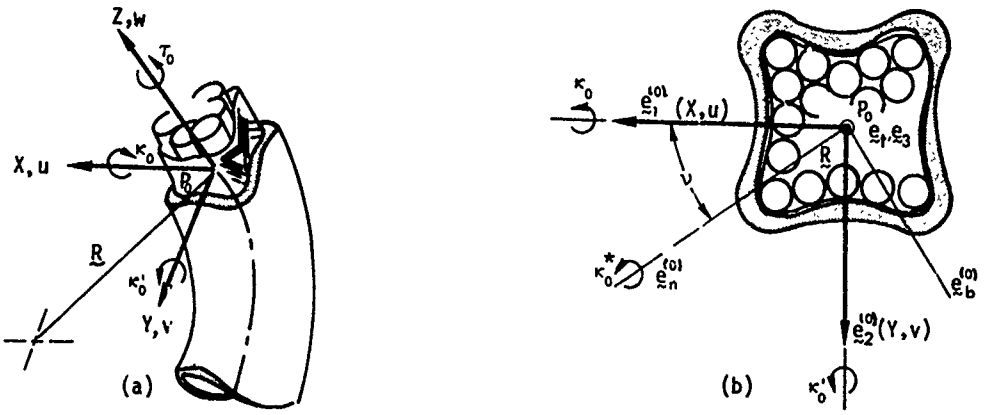

Figure 1 Curvature - torsion parameters and their relationship to cable cross section

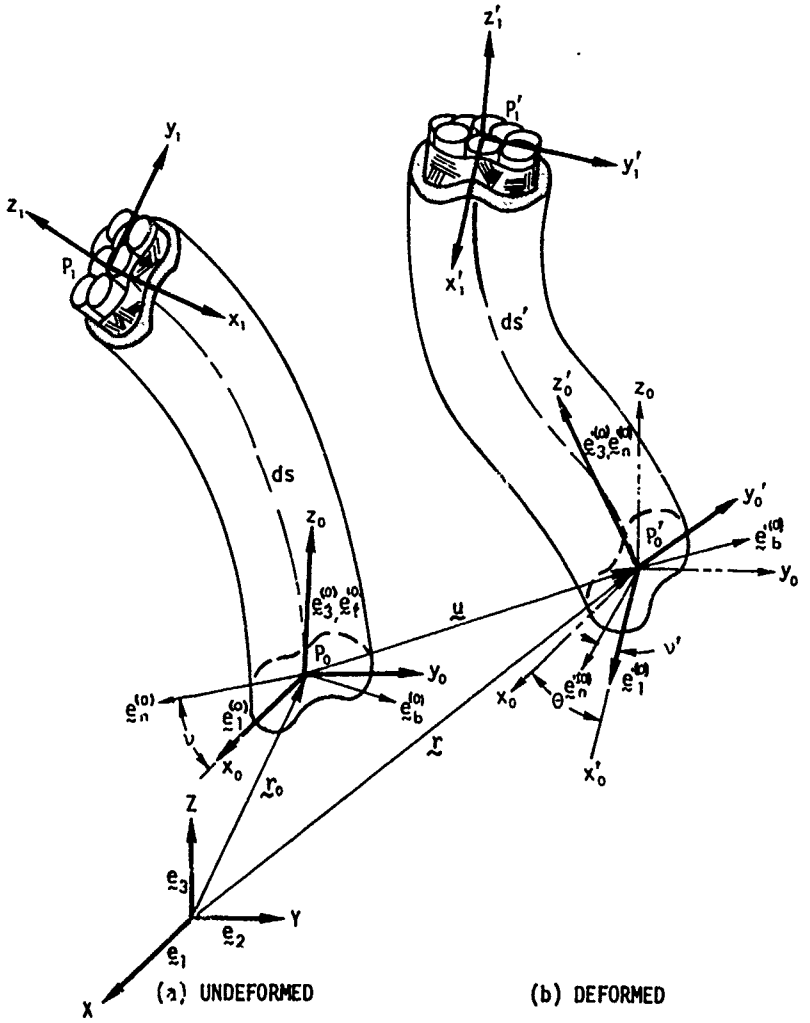

Figure 2 Deflection of a typical curved and twisted cable element

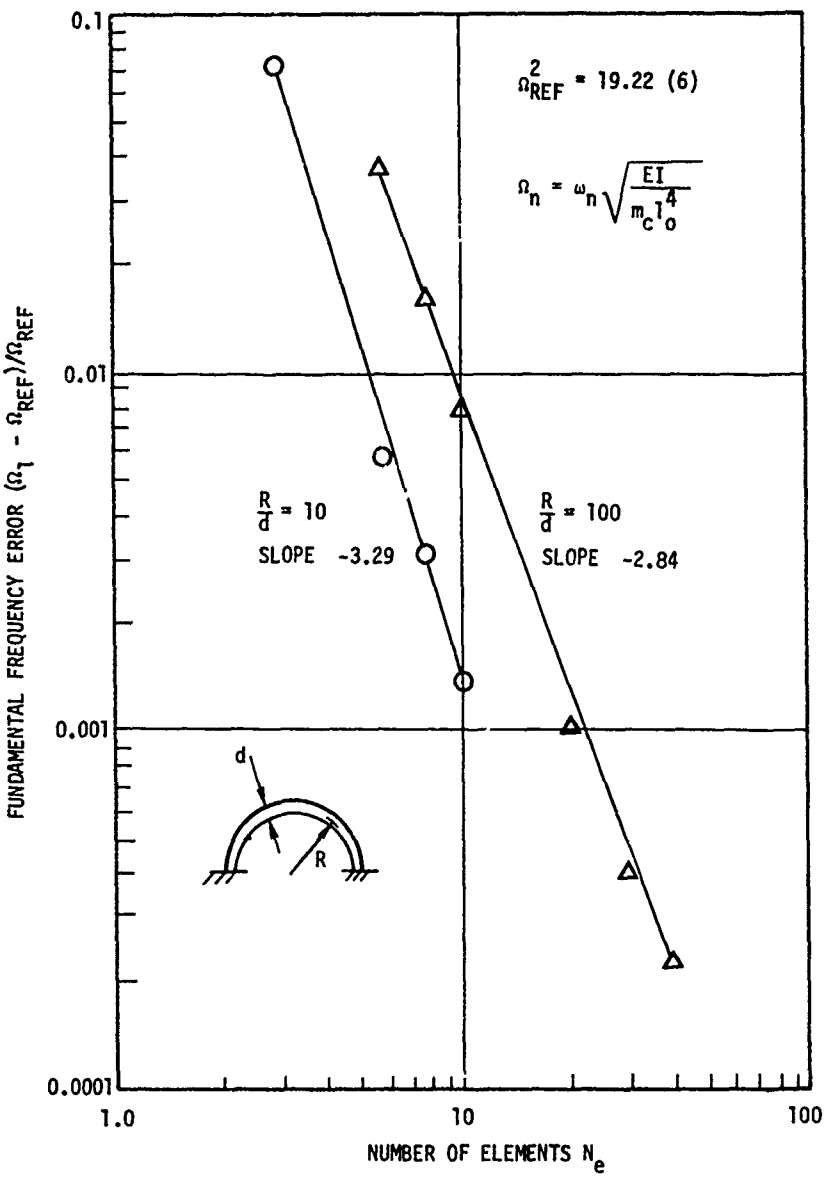

Figure 3 Convergence of finite element for semi-circular ring section

1st MODE
R = 65.8 m
$\alpha = 0.80^{o}$

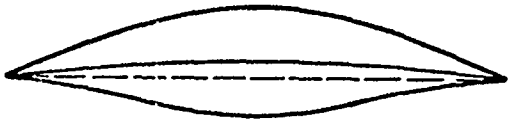

(a)

1st MODE
R = 33.0 m
$\alpha = 3.2^{o}$

(b)

2nd MODE
R = 65.8 m
$\alpha = 0.80^{o}$

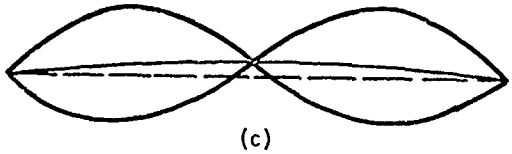

(c)

2nd MODE
R = 33.0 m
$\alpha = 3.2^{o}$

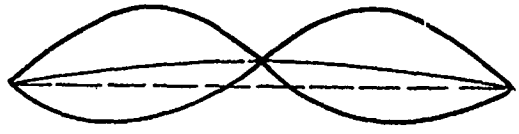

(d)

1st MODE
R = 5.5 m
$\alpha = 83.7^{o}$

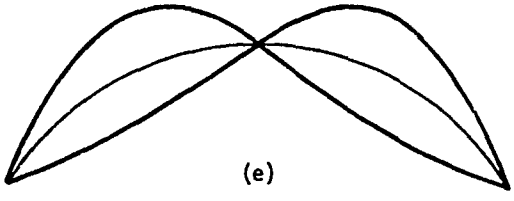

(e)

1st MODE
R = 0.9 m
$\alpha = 180^{o}$

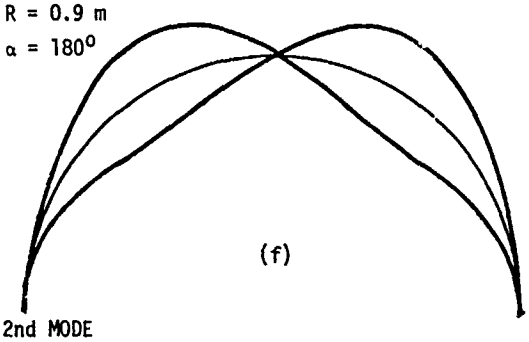

(f)

2nd MODE
R = 5.5 m
$\alpha = 83.7^{o}$

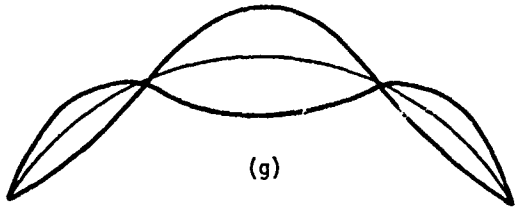

(g)

2nd MODE
R = 0.9 m
$\alpha = 180^{o}$

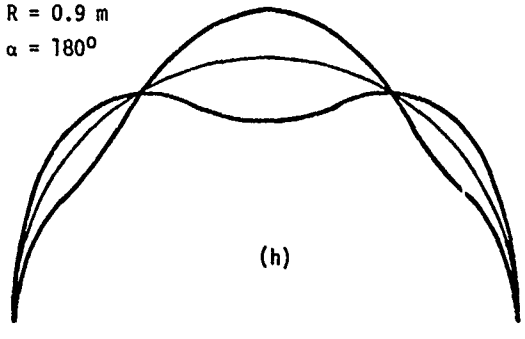

(h)

Figure 4 Mode shapes for first two fundamental natural frequencies for a cable varying curvature

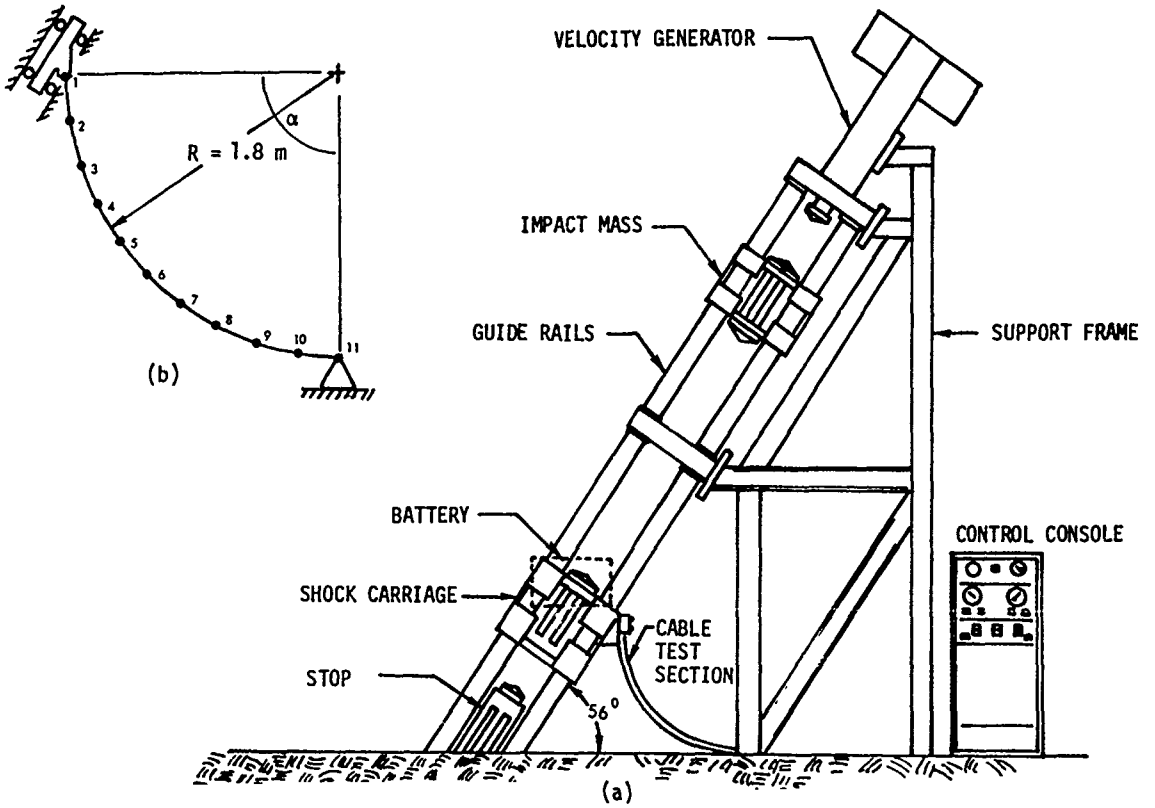

Figure 5 Shock machine schematic and equivalent mathematical model for electrical cable test program

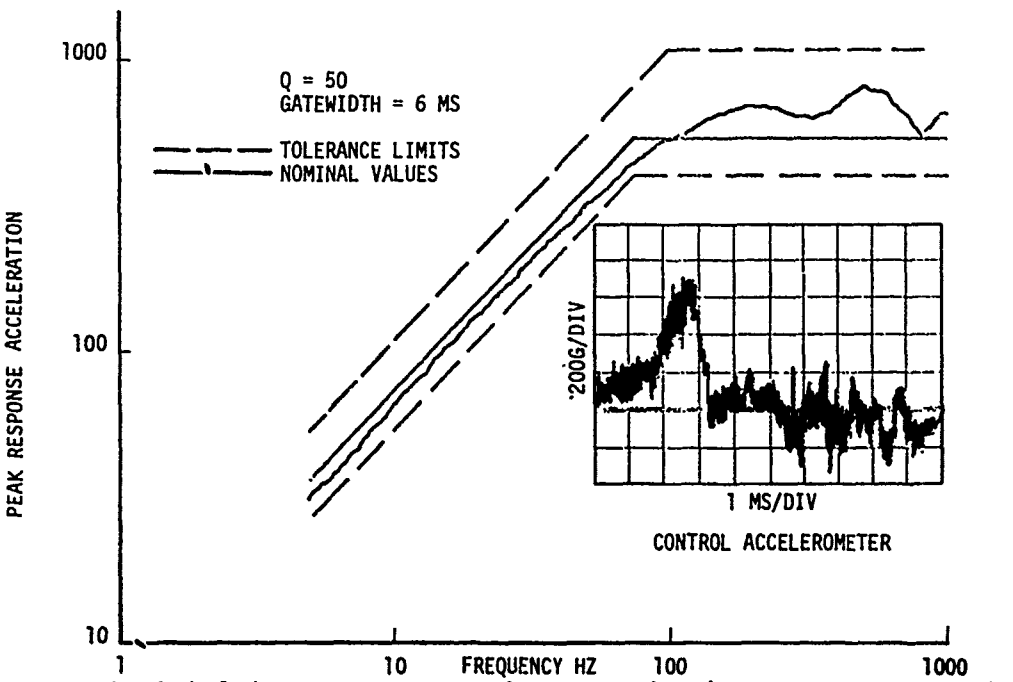

Figure 6 Typical shock spectra response for test carriage (input to cable clamp end)

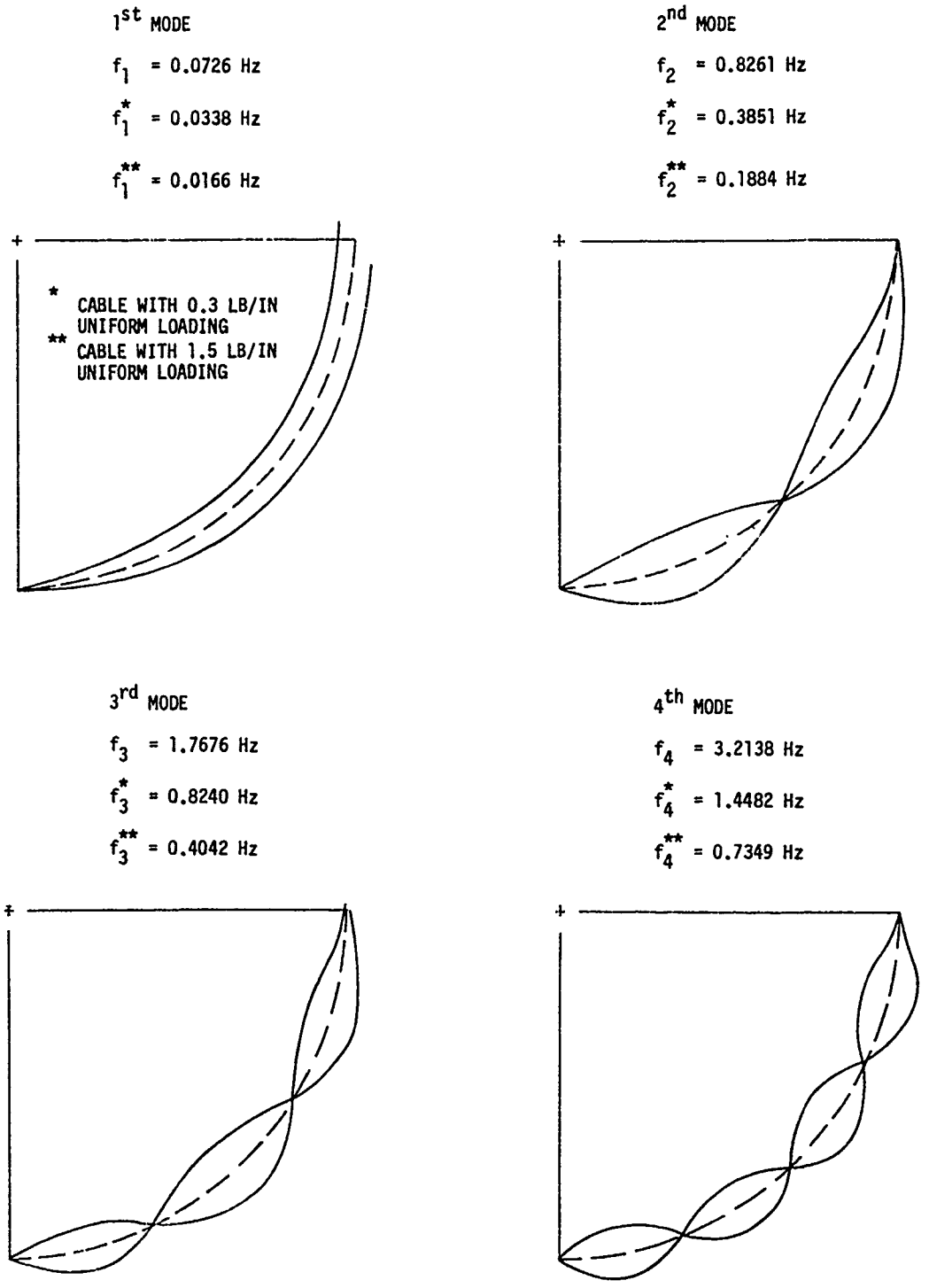

Figure 7 First four mode shapes and natural frequencies for the electrical cable shock loop

AUTOMATED WHEEL-ON-THE-GROUND DETECTION BY DERAILMENT IMPACT SENSING-ANALYSIS AND FULL SCALE TEST RESULTS

William W. Wassmann and John H. Armstrong
Naval Surface Weapons Center
White Oak, Silver Spring, Maryland

Direct, reportable damage costs to railroad property due to equipment-caused freight train derailments in the U.S. amount to $30 million per year; total costs including damage to lading, delays, etc., are estimated to be from $90 to $150 million per year. The largest single contributor to these accident costs is axle failure from overheated journal bearings ("hot boxes") not detected in time. In addition, some derailments caused by wheel, rail or other defects initially involve only a single axle, truck or car, but go undetected for many miles until a general pile-up results when a grade crossing, or turnout is encountered. The severity of such derailments may be reduced by a local derailment detector or "wheel-on-the-ground sensor."

The Naval Surface Weapons Center/White Oak Laboratory, after conducting a feasibility study in 1972/73, has embarked on a two-year program for the Federal Railroad Administration's Office of Research and Development to develop an on-train System for Train-Accident Reduction (STAR). This system includes self-powered hot journal sensors and local derailment detectors which actuate the existing air brake system. It will be installed for test on a 124-car unit ore train of the Duluth, Missabe and Iron Range (DM&IR) Railway Company.

This paper will describe the establishment of design criteria for a seismic local derailment detector based on the measured environment. In November 1974, derailment tests were conducted on an instrumented DM&IR 70-ton ore car. The purpose of the tests was to determine acceleration and velocity thresholds which could be used to identify a derailment condition. A total of 12 tests were conducted to measure the shock effects of a wheel impacting the roadbed, in an empty car vs a loaded car and at the "field-side" wheel location (where the flange side of the wheel drops from the outside of the rail) vs the "gauge-side" location (where the tread of the wheel drops from the inside of the rail). Also investigated were effects of train velocity and of the wheel's impact point with respect to cross ties.

Acceleration measurements were also made during normal, over-the-road operations on both the empty and loaded cars, as well as during loading, unloading and coupling operations. All acceleration measurements were made on the unsprung mass portion of the trucks.

It was determined that a combination of acceleration and velocity-change thresholds exists which can be used to uniquely define a derailment signature. The analysis of data from these tests has led to the development of a seismic detector with an acceleration threshold determined by a preloaded spring and a velocity threshold established by means of the distance of travel prior to actuation.

BACKGROUND

In 1972, the Federal Railroad Administration established a feasibility study at the White Oak Laboratory of the Naval Surface Weapons Center (at that time the Naval Ordnance Laboratory) to investigate the usefulness of various aspects of military technology in relation to the general problem of freight train derailments. This was done in the expectation that certain special materials, fuzing principles and components developed to meet requirements for low false-alarm rate, self-powered actuation, resistance to shock and vibration, and long unattended service life might prove effective in on-train monitoring of the status and performance of critical components, with automatic response in the event of incipient failure; see reference (1).

Figure 1 is a matrix of the various failure modes, detection mechanisms, sensors and action events which were considered in generating and evaluating conceptual complete systems for train-accident reduction.

HOTBOX PROTECTION

The most costly single failure mode against which an on-train, continuous monitor system should be able to provide virtually complete protection is axle failure resulting from overheated journal bearings - the familiar "hotbox". Wrecks from this cause account for from $40 to $60 million in direct and indirect damage annually.

Wayside infra-red bearing-temperature scanners are highly developed and effective in detecting incipient overheating of individual bearings on passing trains. However, the cost of installing, maintaining and monitoring these systems has precluded locating them at close enough intervals to detect all hotboxes prior to catastrophic failure, particularly in the case of roller bearing journals which may progress from an initial abnormal temperature indication to axle failure in a relatively short distance of travel - a matter of a few miles.

The hotbox detection/actuation system devised in the feasibility study and subsequently selected for full-scale development and in-service

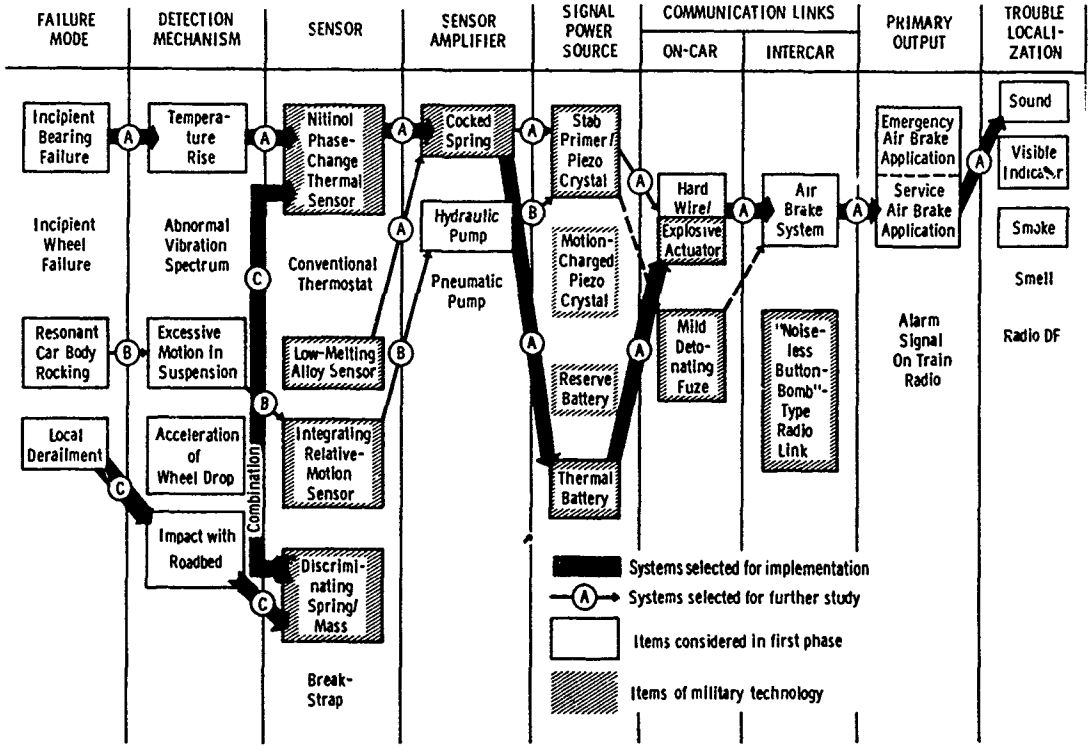

Figure 1 Anti-Derailment Sensor Study Matrix

testing is indicated by sequence A on Figure 1. Temperature rise to a level of about 250°F (120°C) at the location of any sensor (one on each bearing assembly) causes a phase change in a Nitinol (nickel titanium "memory" alloy) element. This causes a rapid, major (up to six percent) dimensional change, releasing a heavily spring-loaded firing pin. This initiates an explosive primer which actuates a thermal (solid electrolyte, pyrotechnically melted upon initiation) battery. Its current then initiates (via hard wiring from each sensor to a single actuator on the brake pipe of the individual freight car) an electro-explosive cartridge actuator. This in turn opens an orifice calibrated to bring about a full service application of the existing air brake system throughout the train and automatically stop it before a hazardous degree of axle heating can occur.

All of the above components have a history of military use which has provided extensive data on their integrity, environmental resistance, shelf life, reliability, and production cost. A target cost for system installation is less than $100 per car, in the quantities required to equip the fleet of 1.8 million cars in service on railroads in the United States. Net savings would result in a significant return on this investment, considering tangible hotbox wreck costs alone, at the current and anticipated rate of undetected bearing failures.

LOCAL DERAILMENT SENSING

In an imprecisely known but significant proportion of the 3000 or more other derailments in road freight service resulting annually from a variety of equipment or track component failures and interactions (e.g. broken wheels, worn flanges, broken rails or joints), an initial derailment affecting a single axle or truck may go undetected. The car may be dragged along for a considerable distance (severely damaging the truck structure) until an obstruction (typically the turnout at a side track) results in a general derailment. The size of this pile-up is related to the speed and make-up of the train; its cost and disruptiveness is also related to its location. Since side tracks are most often located in populated areas, the value of a "wheel-on-the-ground" detector which would act promptly to reduce the train speed is significant.

Under deliberately conservative assumptions as to the frequency of occurrence of such situations, the degree of detectability of local derailment, and the extent to which damage could be mitigated by a brake application, the feasibility study indicated that a self-powered sensor feeding into the hotbox monitoring system could provide a reasonable return on investment if this individual sensing function could be added at low cost - in the range of $1 per sensor or less. Sequence C on Figure 1 shows the relationship of the local derailment detector to the hotbox detector system. Figure 2 gives the estimated return on incremental investment for the local derailment detector.

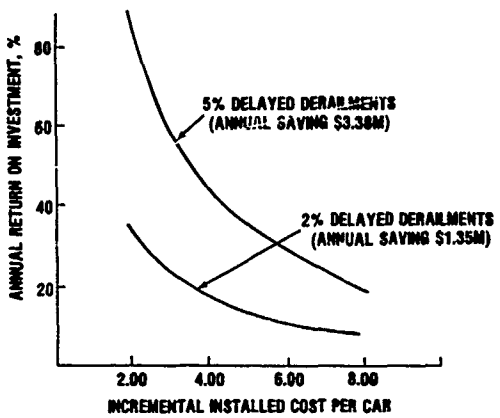

Figure 2 Return on Incremental Investment for Local Derailment Sensor

The operating principle selected is mechanical sensing of the velocity-change (above an acceleration threshold) of the impact of a derailed wheel upon the track structure. A seismic element releases a spring-loaded firing pin, initiating a similar electrical signal to the brake actuating valve. Acceleration sensing permits a completely sealed unit, while the high degree of standardization of freight car suspension characteristics and truck components results in a rather restricted range of impact conditions under a much more diverse set of input parameters, particularly in the case of fully loaded cars.

A preliminary analysis of the derailment process, of the type reported in this paper, indicated that the relative impact conditions under normal running conditions and upon derailment should be sufficiently different to permit derailment sensing, at least in loaded cars, with a sensitivity setting which would have the required near-zero false alarm rate under all other operating conditions.

On the basis of the feasibility study, the Federal Railroad Administration has entered into agreements with the Naval Surface Weapons Center and the Duluth, Missabe, and Iron Range Railway whereby sensor systems developed by NAVSURFWPNCEN will be installed by the DM&IR on a 124-car unit train carrying iron ore (taconite pellets) from the processing plant to the Lake Superior docks and operated in high-mileage service to obtain performance data under a variety of severe operation environments. Derailment tests reported herein were made in November 1974 to provide quantitative inputs for the sensor design.

FREIGHT CAR MATHEMATICAL MODEL

In order to determine the feasibility of establishing an acceleration and velocity threshold to uniquely define a derailment condition, a model was developed to analyze the dynamics of freight car motions during a derailment. For the standard freight car carried on two four-wheel trucks, two modes of unsupported wheel motion were considered. In the first mode, a single wheel drops. In case two, two wheels on the same axle drop simultaneously. Track gauge and wheel tread widths are such that a two-wheel drop is much more typical of an actual derailment. The mechanics of a local derailment are considered to be as follows. At the moment the wheel slips from the rail, it is accelerated downward by gravity and the weight of the car acting through the spring, until the spring is fully extended, after which time the released mass falls due to gravity alone.

In a two-wheel local derailment, the released mass rotates about the second axle which remains on the rail head. In the case of a single-wheel derailment, the wheel is pivoted about the second axle in one plane, and about the far wheel on the same axle in the orthogonal plane. In the two-wheel derailment the force of two springs (half the weight of the car body) accelerates two truck side frames, two wheels and an axle. For a single-wheel derailment, the force of one spring (one quarter of the weight of the car) accelerates one side frame, one wheel and one axle. It can be shown that the single wheel derailment results in a higher impact velocity. In both cases the freight car is assumed to be rotating about the other truck and attempting to compress the freed spring by falling due to gravity. This model is illustrated in Figure 3.

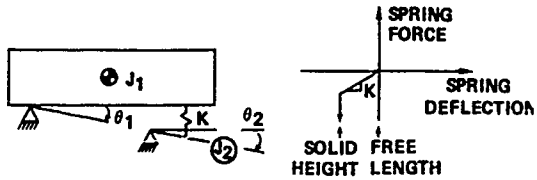

Figure 3 Mathematical Model of Freight Car

It can be shown that the equations of motion for such a system are as follows:

$$\ddot{J_1\theta_1} - \frac{M_c g L_1}{2} + K(L_1\theta_1 - \frac{L_2\theta_2}{2})L_1 = 0 \qquad (1)$$

$$\ddot{J_2\theta_2} - M_{WH} g L_2 - K(L_1\theta_1 - \frac{L_2\theta_2}{2})\frac{L_2}{2} = 0 \qquad (2)$$

where:

$$J_1 = \frac{M_c L_1^2}{3}$$

Two wheel drop:

$$J_2 = L_2^2 \left(\frac{M_{SF}}{2} + 2M_{WH} + M_{ax}\right)$$

One wheel drop:

$$J_2 = L_2^2 \left(\frac{M_{SF}}{4} + M_{WH} + \frac{M_{ax}}{3}\right)$$

L_1 - Truck center distance

L_2 - Truck wheelbase

M_C - Car mass

M_{SF} - Side frame mass

M_{WH} - Wheel mass

Max - Axle mass

Since the single-wheel drop condition yields higher impact velocity than a two-wheel drop, the determining factor in the feasibility of a derailment sensor would be whether a sensor could detect a two-wheel, empty car derailment and yet not yield a false alarm on the most severe one-wheel, loaded car "normal" operating shock, a normal shock being defined as an impact (as at a switch frog, rough joint, etc.) not involving derailment. For the purpose of estimating the severity of normal operating shock, a 0.64 cm drop is assumed. This is the equivalent of a six in.(15.25 cm) flat spot on a 33 in. (83.82 cm) wheel. The Association of American Railroads condemning limit for slid-flat wheels is 2 in. (5.08 cm).

On a field side drop the flange of the wheel rides up over the rail and slips off, dropping about 6 in. (15.24 cm) and landing on the base of the rail. On a gage side drop the tread of the wheel slips off the inside of the rail and the flange of the wheel drops about 5 in. (12.7 cm), landing initially either on a crosstie or on the ballast. Often, in the absence of high ballast, the bottom of the gage-side side frame will impact the top of the rail prior to the impact of the wheel with the crosstie, resulting in a complex impact shock as seen by a sensor mounted on the side frame.

Equations (1) and (2) may be solved simultaneously using a recursive digital integration scheme. The results using the suspension characteristics of a typical, loaded DM&IR ore car are shown in Figure 4. The wheel drop trajectories for the empty car, two-wheel drop are shown in Figure 5. The drop is terminated at 12.7 cm, representing a gage side drop where the tread of the wheel falls toward the inside of the rail. This gives a total drop height equal to the rail height (15.24 cm) less the wheel flange height (2.54 cm). It is important to note that the leverage in the suspension is such that the initial acceleration is quite high - 13g in the case of the loaded car two-wheel derailment. When the spring is completely freed, the wheel then falls at 1g. In the empty car, at the time of impact (88 milliseconds), the wheel velocity is 200 cm/sec, which therefore represents the minimum velocity change, i.e. with zero bounce, on impact. This then is a representation of the least severe derailment condition. A measure of the most severe normal operating shock is obtained with a single wheel, loaded car, 0.64 cm drop. The solution to equations (1) and (2) for this case is illustrated in Figure 6. At the point of impact, 9 milliseconds after the start of the drop, the velocity of the wheel is seen to be 157 cm/sec. Based on these calculations it appears that the kinematics of the drop phase will lead to a unique acceleration and velocity condition during the wheel-roadbed impact phase that may be sensed by a discriminating spring-mass system. The impact phase of the derailment shock is investigated in a measurement

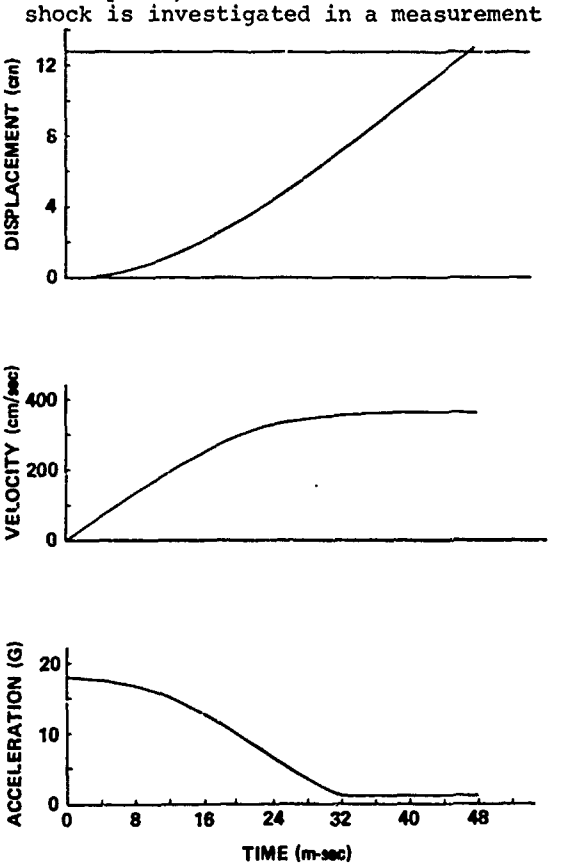

Figure 4 Wheel Drop Trajectory, Loaded Car Derailment

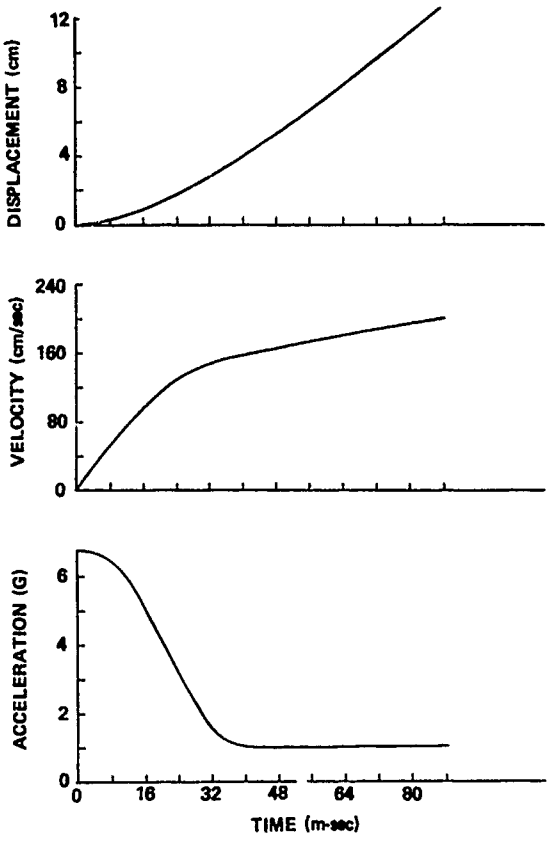

Figure 5 Wheel Drop Trajectory, Empty Car Derailment

DERAILMENT SIGNATURE MEASUREMENT

In order to determine the derailment impact environment as well as the normal operating environment of the unsprung mass (which does not lend itself to a purely analytical approach because the equivalent "height of drop" in such normal situations as switch and crossing frog impacts, is not readily defined), a field test program was undertaken to measure these acceleration signatures. A single truck of an ore car was instrumented with accelerometers located on the unsprung mass (side frames). The accelerometers were of both piezoelectric and piezoresistive type with mounted resonant frequencies ranging from 5000 Hz to 25000 Hz. The data were recorded on an analog magnetic tape recorder in the FM mode. The recording frequency range was DC-5000 Hz. The truck was then repeatedly derailed at speeds ranging from essentially zero to 10 mph (16.1 km/hr) under an empty car (20 long tons tare weight (20,321 kg)) and then

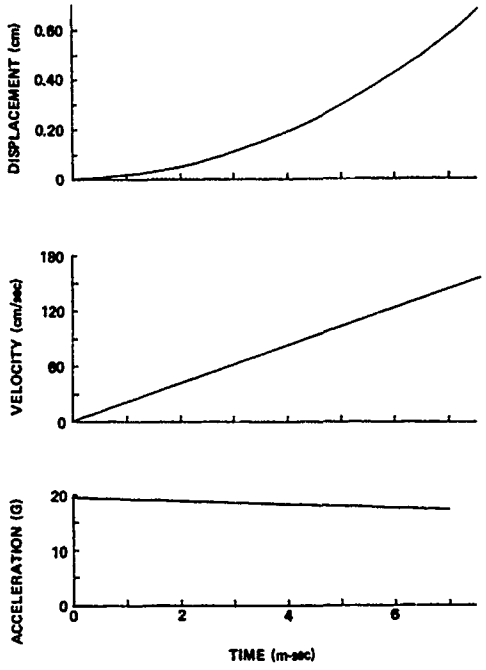

Figure 6 Wheel Drop Trajectory Loaded Car, Normal Operating Shock

while loaded with 70 tons (71,124 kg) of iron ore. The normal operating environment was measured during an over-the-road run from the DM&IR's Proctor yard to the taconite plant at Minntac, a distance of 70 miles (112.7 km). On this route, the northbound run (empty car operation) was over bolted-joint track (39 ft [11.9 m] rail lengths) and the loaded car run was over welded rail track (approximately 450 m sections). Figure 7 shows a photograph of a typical derailment test.

The acceleration signature for the case in which a gage side wheel impacts the ballast is shown in Figure 8. The drop phase, which lasts for about 60 msec, produces a maximum of about 10g acceleration. The impact phase is roughly a 30g, 20 millisecond, half-sine shaped pulse. This data is analogous to the situation shown in Figure 4. The resulting drop phase is seen to produce a smaller amplitude and longer duration than that predicted by the mathematical model. This may be attributed to friction between the wheel and the rail during the early part of the drop. The acceleration signature of a field side drop, in which the wheel impacts the base of the rail, is shown in Figure 9. In this case the impact phase is seen to be a higher amplitude, shorter

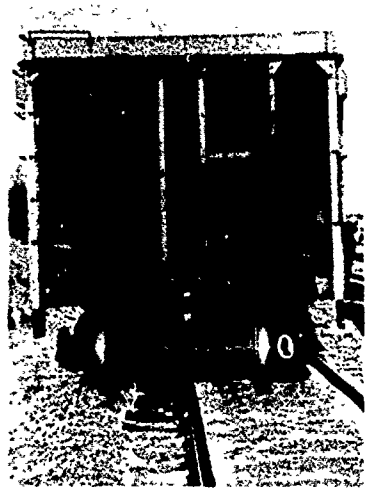

Figure 7 Typical Derailment

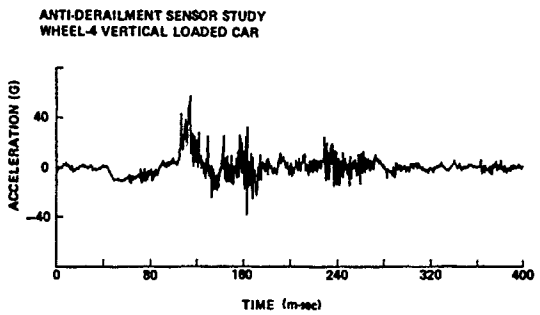

Figure 8 Gage Side Derailment Acceleration Signature

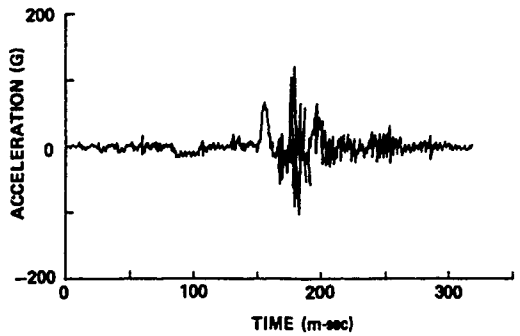

Figure 9 Field Side Derailment Acceleration Signature

duration pulse (70g, 10 msec) than the gage side case with ground impact. The velocity under this pulse is plotted in Figure 10 and is seen to produce about a 300 cm/sec drop velocity with about a 50 cm/sec bounce.

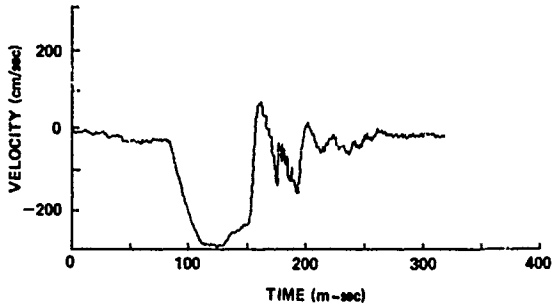

Figure 10 Field Side Derailment Velocity Signature

The most severe normal operating shock observed is shown plotted in Figure 11 and the integral of this pulse in Figure 12. The maximum acceleration is 20g with a velocity change of about 60 cm/sec.

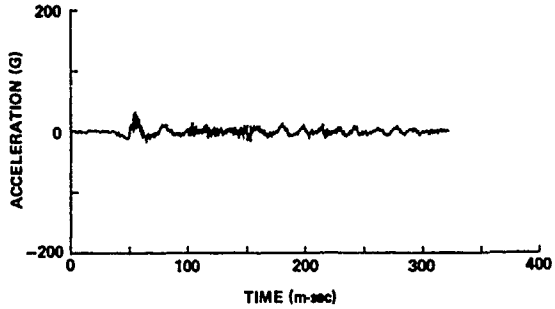

Figure 11 Over the Road Acceleration Signature

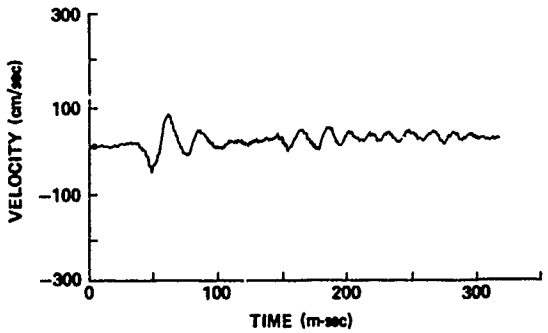

Figure 12 Over the Road Velocity Signature

DERAILMENT SENSOR MODEL

A sensor which could be designed to distinguish between the derailment acceleration signature and a normal operating shock is illustrated in Figure 13. The seismic mass, M, is restrained from motion by a spring, K, with pre-load displacement Xo. The distance of travel required for actuation is denoted by δ. The mass will not leave its preset position until experiencing an upward acceleration level greater than the threshold acceleration

$$a_t = \frac{KXo}{M} .$$

A velocity threshold, Vo, is also imposed on the system. Under the assumption that the input pulse is high in frequency in comparison to the natural frequency, $\omega_n = \sqrt{K/M}$, of the seismic detector, this velocity threshold is given by $Vo = \delta\omega_n$.

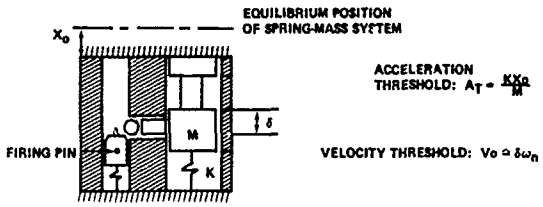

Figure 13 Derailment Sensor

For the purpose of evaluating potential sensor designs, a digital computer model of this sensor was developed. The input acceleration used to evaluate the designs was the actual measured environment of the derailment tests and the over-the-road test. The response of such a sensor model to the loaded car derailment signature of Figure 9 is shown in Figure 14. The pre-load displacement is seen to be about 0.25 cm and the seismic mass is seen to have deflected 0.65 cm. The response of the same sensor to an empty car derailment signature is shown in Figure 15. In this case the seismic mass deflected 0.4 cm from the preset position. The response of the same derailment sensor to the over-the-road normal operating shock of Figure 11 is shown in Figure 16. In this case the seismic mass moved only 0.02 cm from the preset position.

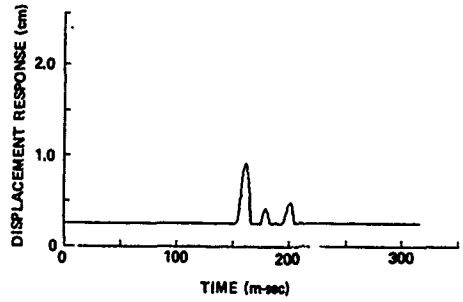

Figure 14 Sensor Response to Loaded Car Derailment Signature

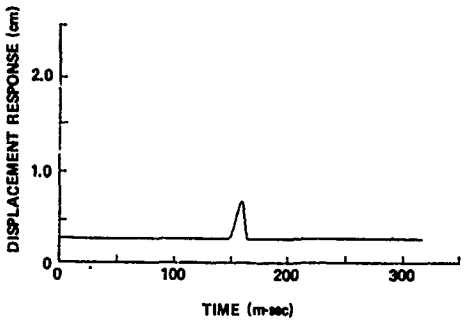

Figure 15 Sensor Response to Empty Car Derailment Signature

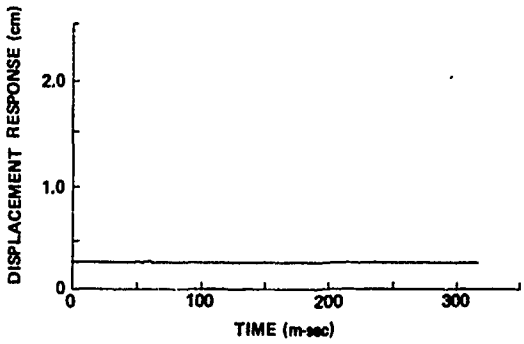

Figure 16 Sensor Response to Normal Operating Shock

SENSOR DESIGN AND EVALUATION

Figure 17 is a photograph of the prototype sensor designed on the basis of the November 1974 data and analyses of the type described above. Five sensor settings, ranging from most sensitive (expected to exhibit relatively low resistance to false alarms) to least sensitive (expected to be marginal in functioning or a full-car

derailment) were selected for full scale test:

Sensitivity	G Threshold (preset)	Velocity Threshold	Spring Constant
1	2.2g	1.25 fps/38.1 cm/sec	0.45(lb/in)/0.79 Nt/cm
2	3.5	1.56/47.5	0.70/1.23
3	6.0	2.04/62.2	1.20/2.10
4	10.9	2.76/84.1	2.20/3.85
5	16.5	3.38/103.0	3.30/5.78

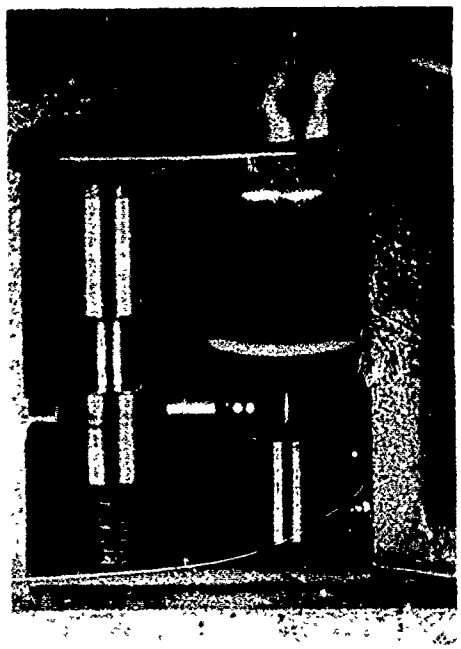

Figure 17 Derailment Sensor

The two-mass system with intermediate cylinder and ball is designed to lock the firing pin mass against a spring force sufficient for reliable firing of the stab primer in the battery while imposing a friction load on the acceleration-sensing mass which is both repeatable and small enough to avoid unduly affecting its actuating characteristics.

Fourteen derailment tests were run in July 1975 to calibrate sensor functioning on gauge-side and field-side drops under empty and loaded conditions. Field-side results were consistent and indicated that sensors through Sensitivity 2+ would trip on empty-car derailments and through 4+ on loaded-car drops. As anticipated, gauge-side results were not consistent.

Eighteen sensors (of sensitivities 1 through 4) on four cars are now in regular service between loading plant and ore docks to obtain false-alarm data.

CONCLUSIONS

The validity of the math model of the derailment event in predicting impact velocity has been demonstrated, as has the use of digital analysis of the response of a preloaded spring-mass system to measured impact signatures.

On the basis of preliminary service test results, it appears definitely practical to detect the derailment of a loaded-car axle with a mechanical sensor capable of generating an output signal of useful power, with sensor sensitivity such that the false alarm rate will be acceptably low in all normal operating modes. It appears likely that the acceptable sensitivity setting ultimately determined by extensive service testing may also detect many empty-car derailments as well.

The difference between field-side and gauge-side impacts is such that sensing at each journal location is required.

ACKNOWLEDGEMENTS

The authors would like to acknowledge the efforts of Mr. Robert S. Reed for instrumentation during the measurements program and Ms. M. Weinberg for her assistance in the design of the prototype sensors.

REFERENCE

1. FRA-ORD&D Report No. 74-17, PB-232-417, Anti-Derailment Sensor System, Phase 1, Feasibility Study, Final Report, April 1973

Discussion

Mr. Volin, (NRL): You mentioned a ¼" (.0063 meters) misalignment between the rails, was it vertical or horizontal?

Mr. Wassman: Vertical.

Mr. Volin: You were quite concerned with over the road shocks. What about the effect of switching shocks?

Mr. Wassman: Did you mean coupling shocks? They were included. The 5000 mile test these sensors have undergone would have obvicusly included some coupling shocks. We haven't specifically done severe coupling tests. We tried to measure some coupling shocks on our first test series in which we had the instrumentation on the truck but we couldn't measure significant vertical velocity changes due to a coupling shock and we didn't want to damage the railroad's cars enough to give them a real severe coupling shock. I think that is something that should be addressed eventually.

Mr. Ataris (Hughes Aircraft Company): In some other tests that I have seen, by the Sandia Corporation, I noticed that during coupling they get quite a bit of vertical shock response. How do you control it?

Mr. Wassman: How do we control the response of the sensor to vertical shock?

Mr. Ataris: When you couple two freight cars you get quite a bit of vertical shock.

Mr. Wassman: Keep in mind that this is on the unsprung portion of the freight car. I don't know where your vertical shock was detected, but I suspect that the worst part of the vertical shock would be on the sprung portion. Do you know if the high vertical shock was detected on the unsprung mass portion of the freight car, the wheels and the trucks? That would have to leave the rail. I think that if you get a high vertical shock on the unsprung mass you might as well let the sensor trip because something is going to go wrong.

Mr. Monroe (Babcock & Wilcox Company): Did you look into the primary causes for derailments? Was it the roadbed condition, the unbalanced load on the car, or the speed going around the curve?

Mr. Wassman: The Federal Railroad Administration keeps very good records on the causes of freight train accidents and publishes them annually. Some of these causes as they relate to the development of this sensor. as an economic justification for its installation, are addressed in our written paper.

Mr. Armstrong: The derailment sensor is intended and can only help in those cases where there is a delayed derailment, that is where one axle or one truck is derailed and the general derailment affecting a good many cars does not occur until some time later; therefore you would reduce the damage by starting to apply the brakes immediately which is what the system does. Therefore, this would apply to accidents due to broken rails, broken flanges, broken wheels, or any sort of an incident in which somehow one wheel is initially derailed and there are about 5000 to 7000 of these cases each year. The other part of the program is related to the most severe and the most frequent single cause of derailments which is the hot box that leads to the burning off of an axle and a derailment at that time. In that case of course the sensor can anticipate and prevent a derailment.

Mr. Nelson (Special Projects): Can you use the instrument to detect a faulty roadbed itself? If you got a fault indication or a false alarm on two of them. Would it be necessary to go back and inspect the roadbed?

Mr. Wassman: I think this sensor as it is designed to actuate would stop the train, so it is not a matter of inspecting the roadbed, it is a matter of getting out and finding out what happened. If the roadbed did indeed cause either a derailment or a shock of sufficient magnitude to actuate this system I would presume that it would be obvious to the observer at that point. The sensor could then be considered as a device for testing roadbeds, but I might add very bad roadbeds.

THE DEVELOPMENT OF A GENERALIZED IMPACT RESPONSE MODEL FOR A BULK CUSHIONING MATERIAL

Don McDaniel
Advanced Systems Concept Office
Research, Development, Engineering and Missile Systems Laboratory
U. S. Army Missile Command
Redstone Arsenal, Alabama 35809

and

Richard M. Wyskida
Industrial and Systems Engineering Department
The University of Alabama in Huntsville
Huntsville, Alabama 35807

This paper presents an automated approach to the design of bulk cushioning systems. The developed procedure can be utilized in package and shipping container design, and other impact absorption applications.

A model of impact response is developed and its validity demonstrated through statistical testing. The model is then used as the objective program for a sequential search procedure that searches out the best cushion design.

INTRODUCTION

In recent years, equipment designers have become increasingly aware of the detrimental effects of extreme temperature upon equipment performance. Consequently, there are now included in the qualification tests of equipment, some tests conducted at temperatures that are representative of the temperature extremes that the equipment is likely to encounter.

This extreme temperature testing has received substantial attention in the military, where the range of temperatures encountered is quite extreme, and the failures can produce catastrophic results. The transportation of military equipment is one area of concern and a study was made of several military containers that used bulk cushioning systems. It was found that temperature had a significant effect on impact response [1] in that the cushioning systems in the containers did not perform properly due to changes in the bulk cushioning materials that were induced by extreme temperatures. Consequently, the items packaged in the containers (guided missile systems and system components) did not receive adequate protection, and the missile system reliability was compromised. This type of failure is a potential problem that can cause damage to very expensive equipment and produce a malfunction in weapon systems that compromises the combat power of a military organization. Also, if proper failsafe provisions are not incorporated into the protection of ordnance items, the safety of any of the personnel that handle the equipment within the logistics system is jeopardized.

Rather than incorporate additional protection into equipment, it is much more cost effective to improve the reliability of cushioning systems. This can be done if a reliable model for predicting cushioning performance can be developed.

DEVELOPMENT OF THE IMPACT RESPONSE MODEL

A valid model of impact response must incorporate all parameters that are expected to have a significant effect on impact response. Temperature has been shown to have a significant effect on impact response [1], and it is postulated that viscoelastic theory can be utilized to formulate a model of impact response that incorporates temperature effects. The current design practice for predicting impact response

is predicated on dynamic cushioning curves, which do not account for temperature effects on impact response. To improve the predictability of cushioning systems, a model of impact response must account for temperature effects, which are expected to be the most dramatic as the temperature tends towards the extremes.

Consequently, a research effort was initiated at the Army Missile Command (MICOM) in 1973 to develop superimposed dynamic cushioning curves that address the effect of temperature on the impact response of cushioning materials. The drop tests were conducted at MICOM and the results analyzed by The University of Alabama in Huntsville (UAH) under a supporting research contract [2]. The initial experimentation was conducted on Minicel material, a cross-linked polyethylene foam material with a 32 kg/m^3 density manufactured by Hercules, Inc.

The drop test program that was conducted on the Minicel material used drop heights of 304.8, 457.2, 609.6, and 762.0 mm; temperatures of 219, 294, and 344 K; cushion thicknesses of 25.4, 50.8, and 76.2 mm; and static stress levels that varied from 275.8 to 34474 Pa. The G-level response and shock pulse duration were recorded for each of 2736 drop tests. An automated data handling system that included outlier tests and other statistical analyses was developed and used to analyze the Minicel data.

This experimental effort resulted in the generation of a data base of 2409 statistically valid data points. A family of second order polynomial equations was found to be the best predictor of impact response of the Minicel cushioning material.

THEORETICAL BASIS OF THE MODEL

The development of an impact response model for cushioning materials at varying temperatures requires the identification of a functional relationship of the variables. The required relationship can be expressed mathematically as follows:

$$G = F(\sigma_s, T, \theta, h) \qquad (1)$$

where

- G = acceleration G-level
- σ_s = static stress in Pa
- T = thickness of cushion in mm
- θ = cushion temperature in K
- h = drop height in mm.

After considerable research, it was determined that the theory of viscoelasticity could be utilized to provide a theoretical basis for the model. Viscoelastic theory recognizes cushioning materials as belonging to a class of materials which have mechanical properties that are common to perfect solids and perfect liquids. Various theories have been developed over the past century for describing the behavior of perfect solids and perfect liquids. Among these, the oldest theories are the classical theory of elasticity and the theory of hydrodynamics. Mathematical models have been formulated for these types of viscoelastic materials; for example, Mustin [3] gives the creep and relaxation functions for a number of simple mathematical models. These are expressed compositely in constitutive equations which, in viscoelastic theory, describe the response of materials to mechanical excitation.

Since temperature effects are required in the constitutive equation that models impact response, one must consider that portion of viscoelastic theory which accounts for the behavior of materials at varying temperatures. A partial basis is found in a paper on the viscoelastic properties of thermorheologically simple cushioning materials by Cost [4]. The general expression developed by Cost is:

$$\ddot{x}_{max} \approx C_0\left(\frac{h}{\sigma_s T}\right)^{\frac{1}{2}} + \sum_{i=1}^{N} \frac{C_i h^{\frac{1}{2}}}{\left(\sigma_s T\right)^{i+\frac{1}{2}}}\left[\sum_{j=1}^{M} K_{ij}\theta^j\right] \qquad (2)$$

where $\ddot{x}_{max}$ is the peak deceleration in g's experienced by a mass impacting a cushion of thickness (T), with a static stress σ_s, from a height of h and at a temperature θ, and $C_i (i=0,1,\ldots,N)$ and K_{ij} $(j=1,2,\ldots,M)$ are constants to be determined by curve fitting procedures.

The required form of the model as given in Equation (1) can be identified in viscoelastic theory as a phenomenological constitutive equation. The model developed by Cost was selected as the most viable candidate and was utilized as the basic underlying structure of the model because it provides a functional relationship of all the variables required in Equation (1) and has a theoretical basis in viscoelastic theory.

Equation (2) shows that $\ddot{x}$ is a progressively decreasing value as σ_s increases, which is not consistent with experimental data. This was anticipated to an extent by Cost during his finite element analysis [4], where a plot of peak acceleration versus static stress was generated in the region where stress is proportional to strain.

This deficiency in a constitutive equation is not at all uncommon as Meinecke [5] suggests that even though the behavior of actual materials is usually different from that predicted by various classical theories, for engineering purposes it may be worthwhile to approximate the actual behavior to the idealized behavior. But for cases where it is not possible to approximate the actual behavior of the material to the idealized behavior without sacrificing the accuracy in prediction, it is very essential to consider the anomalies from the idealized character.

DEVELOPMENT OF THE GENERAL MODEL

The initial model, Equation (2), proved deficient in representing the nonlinear characteristics of cushion response. However an extensive literature search showed it to be the only known model that provides a direct relationship of the required variables. Consequently, a modular technique suggested by Shannon [6] was used to modify this model and construct a valid model of impact response. The relationship of each independent variable (σ_s, T, θ, h) and its effect upon the dependent variable (G-level) was studied and the finalized relationship for each independent variable was then incorporated into the model.

The effect of drop height upon G-level is based upon the relationship

$$V = \sqrt{2gh} \quad . \tag{3}$$

V can be thought of as velocity at impact and it is related as the square root of drop height (h). Mindlin [7], Janssen [8], and others utilized this relationship of G-level versus drop height, and the derivation by Cost in acquiring Equation (2) is on this same basis. Accordingly, it was determined that drop height should be incorporated into the model as $h^{1/2}$.

Several polynomials of various orders of static stress were tested in this research with the conclusion that a second order polynomial was superior, and that the desired U shaped dynamic cushioning curves of G's versus static stress would result. The variables were input with $h^{1/2}$ and a second order polynomial of σ_s. The best fit was obtained using the following functional relationship:

$$G = C_0 + C_1 h^{\frac{1}{2}} + C_2 h^{\frac{1}{2}} \ell n\sigma_s + C_3 h^{\frac{1}{2}} (\ell n\sigma_s)^2 ; \ (h>0). \tag{4}$$

These polynomials generated U shaped curves similar to those in previous research efforts.

Mindlin [7], Janssen [8], and others suggested that G-level was an inverse relationship to thickness. This seems intuitively correct and many attempts were made using this relationship. T was introduced into these as a negative exponential such as $T^{-1/2}$, $T^{-3/2}$, $T^{-5/2}$, $T^{-7/2}$, etc. Computer runs showed good correlation with thickness input as a negative exponential of this type.

Temperature effects were expected to be the most difficult to incorporate and this turned out to be the case. It can be reasoned that the phase shift effect of temperature discussed in viscoelastic theory for thermorheologically simple materials produces the multiplier effect of the exponentials shown by Cost. Models were tried with several orders of temperature, and the polynomial with θ^j, where j=1,2,3,...,n, were the most satisfactory.

Many relationships were tried and rejected. Each time, the basic underlying structure of the variables was rejustified and new formulations were attempted. The process was repeated until a valid General Model of impact response was developed. The General Model is given as follows:

$$G = C_0 + \left(\sum_{\ell=0}^{S} h^{\ell/2} \sum_{k=0}^{R} \frac{1}{T^{(1/2+k)}} \sum_{j=1}^{N} \theta^j \right) \cdot \left(\sum_{i=0}^{M} C_{ijk\ell} (\ell n\sigma_s)^i \right) . \tag{5}$$

This general Model incorporates each of the variables in the manner prescribed in the modular modeling effort. The General Model that resulted from the modeling effort incorporates the following characteristics:

1. The dynamic cushioning curves of G-level versus static stress generated by the model are U shaped. This is consistent with cushioning theory.

2. The predicted G-levels increase with increased drop height. The higher drop heights incorporate more energy into the system which would increase the energy levels experienced by the falling body.

3. The predicted G-levels increase with reduced cushion thickness. The G's experienced by a falling body is dependent on shock pulse duration, and a thinner cushion would allow less shock pulse time and an accompanying increase in G-levels.

4. Temperature effects induce lateral shifts in the dynamic cushioning curves. This is consistent with the phase shift function concept of viscoelastic theory. It is also intuitively consistent in that reduced temperatures would be expected to stiffen the cushioning material and require an increased stress level for comparable shock attenuation.

5. The dynamic cushioning curves generated as output from the General Model form a series of curves that are nested within progressive values of thickness and drop height for all possible temperature conditions and static stress conditions.

A sensitivity analysis was performed using the Minicel data. S is set at 1, R is set at 1, N is set at 3, M is set at 2, and the Minicel Model takes the following special form:

$$G = C_0 + \left(\sum_{\ell=0}^{1} h^{\ell/2} \sum_{k=0}^{1} \frac{1}{T^{(1/2+k)}} \sum_{j=1}^{3} \theta^j \right) \cdot \left(\sum_{i=0}^{2} C_{ijk\ell} (\ell n \sigma_s)^i \right). \quad (6)$$

Successive analysis of variance tables were constructed as each additional variable was entered into solution. These ANOVA tables were used to determine if the incoming variable made a significant contribution to the overall correlation. A Duncan F test [9] is utilized with this format, and it was found that the 25th variable that entered did not make a significant contribution to the G-level response prediction. The test hypothesis can be stated as follows:

H_0: the entering variable has no effect upon the G-level response prediction.

H_1: the entering variable has a significant effect upon the G-level response prediction.

The test is

$$F_{calc} = \frac{MS_{due\ to}}{MS_{about}} \quad (7)$$

and the null hypothesis H_0 can be rejected when $F_{calc} > F_{table}$. Utilizing an α level of 0.05, the final ANOVA's and F tests (Tables 1 and 2) show that the 24th variable makes a significant contribution but the 25th does not. One further test is made to verify that all the regression coefficients in the final Minicel Model are significant. This test is conducted using a "t" statistic as follows:

$$t_n = \frac{C_n}{S_n} \quad (8)$$

where

t_n is the t statistic for the nth term

C_n is the coefficient of the nth term

S_n is the standard error of the nth term.

The test hypothesis is as follows:

H_0: the nth coefficient is the same as zero

H_1: the nth coefficient is significantly different from zero.

In conducting the test, the null hypothesis can be rejected when $t_n > t_{table}$. With an α level of 0.05, the test of all the coefficients in the Minicel Model are found to be significantly different from zero.

The resultant Minicel Model is a 25 term regression polynomial with a 0.983 correlation coefficient. The reliability of the correlation coefficient can be tested statistically using a t statistic defined as follows [10]:

$$t_n = r\sqrt{\frac{n-2}{1-r^2}}$$

where

r = the correlation coefficient

n = the number of samples used to derive the regression equation

t_n = the resulting number of standard errors of r in the interval between the computed r and r=0.

The test hypothesis is as follows:

H_0: $r = 0$

H_1: $r > 0$.

In conducting the test, the null hypothesis can be rejected when $t_n > t_{table}$. This test of the reliability of the correlation coefficient was conducted on the Minicel Model. The null hypothesis can be rejected since $t_n = 291.2 > t_{table}$. The Minicel Model can be written as follows:

$$G = -14.82935 + \frac{0.15023\theta(\ell nS)^2}{T^{1/2}} - \frac{5.84704\theta h^{1/2}\ell nS}{T^{3/2}} + \frac{0.67959\theta h^{1/2}(\ell nS)^2}{T^{3/2}} + \frac{8.82528\theta h^{1/2}}{T^{1/2}} - \frac{1.27913\theta h^{1/2}\ell nS}{T^{1/2}} + \frac{0.03124\theta h^{1/2}(\ell nS)^2}{T^{1/2}} - \frac{0.00912\theta^2\ell nS}{T^{1/2}} - \frac{0.03637\theta^2 h^{1/2}}{T^{1/2}} + \frac{0.00418\theta^2 h^{1/2}\ell nS}{T^{1/2}} - \frac{0.00287\theta^3}{T^{1/2}} + \frac{0.00010\theta^3\ell nS}{T^{1/2}} - \frac{0.00001\theta^3(\ell nS)^2}{T^{1/2}} - \frac{0.00023\theta^3 h^{1/2}}{T^{3/2}} + \frac{0.00010\theta^3 h^{1/2}\ell nS}{T^{3/2}} - \frac{0.00001\theta^3 h^{1/2}(\ell nS)^2}{T^{3/2}} + \frac{0.00005\theta^3 h^{1/2}}{T^{1/2}} - \frac{0.00006\theta^3 h^{1/2}\ell nS}{T^{1/2}} - \frac{1215.11080\theta}{T^{3/2}} + \frac{106.44538\theta\ell nS}{T^{3/2}} +$$

TABLE 1

ANOVA Table and F Tests for Entering the 24th Variable into the Minicel Regression Equation

Source	S.S.	d.f.	M.S.	F_{calc}	$F_{.05}$	Decision
Due to all 24 variables	5,026,531.30	24	209,438.80	1830.76	1.52	Signif
Due to first 23 variables	(5,024,189.80)	(23)	(218,443.00)	1884.90	1.52	Signif
Due to addition of 24th variable to first 23 variables	(2341.50)	(1)	(2341.50)	20.60	3.84	Signif
About regression on all 24 variables (Residual)	172,858.20	1511	114.40			
About regression on the first 23 variables	175,199.70	1512	115.90			
Total	5,199,389.50	1535				

TABLE 2

ANOVA Table and F Tests for Entering the 25th Variable into the Minicel Regression Equation

Source	S.S.	d.f.	M.S.	F_{calc}	$F_{.05}$	Decision
Due to all 25 variables	5,026,771.00	25	201,070.80	1758.90	1.52	Signif
Due to first 24 variables	(5,026,531.30)	(24)	(209,438.80)	1830.80	1.52	Signif
Due to addition of 25th variable	(239.70)	(1)	(239.70)	2.00	3.84	Not Signif
About regression on all 25 variables	172,618.50	1510	114.39			
About regression on the first 24 variables	172,858.20	1511	114.40			
Total	5,199,389.50	1535				

$$\frac{5.73253\theta^2}{T^{3/2}} + \frac{0.47113\theta^2 \ell nS}{T^{3/2}} - \frac{0.10450\theta^2(\ell nS)^2}{T^{3/2}} - \frac{0.00377\theta^3 \ell nS}{T^{3/2}} + \frac{0.000388\theta^3(\ell nS)^2}{T^{3/2}} \quad (9)$$

where S = static stress in Pa x 100.

This model can be used to predict impact response for Minicel cushioning systems. The model specificity is that it is 95% reliable when used within the ranges of the independent variables defined earlier.

The special form of the General Model as given in Equation (6) was used in the validation of the model for the cross-linked polyethylene foam Minicel material. If additional precision had been required the values of S, R, M, and N could have been increased, which may be necessary with other materials but gave only a minimal improvement in precision here. It was apparent, however, that increases in M, which incorporates σ_s with exponentials over 2 is, in general, not worthwhile. Also, increases in N that incorporate θ at exponentials over 3 are of marginal value in improved precision. The changes in R and S that affect the exponentials of thickness and drop height should be explored first if additional precision is required in a model of a particular material.

To fully verify the model as a predictor, a data base independent of that used to generate the model must be utilized. Three such data bases were available: a data base of 25.4, 50.8, and 76.2 mm thickness Minicel material at 219, 294, and 344 K and at a 685.8 mm drop height; and a data base of 101.6 and 127.0 mm thick Minicel material. The 685.8 mm data are contained within the range of the independent variables and were not used in formulating the Minicel Model. However, the 101.6 and 127.0 mm data are beyond the data extremes of the developed model. Also the 101.6 and 127.0 mm samples themselves were not homogeneous. The samples of the 101.6 mm material were two-piece cushions which were 50.8 mm thick. The 127.0 mm material was made using a 50.8 mm piece and a 76.2 mm piece. This stacking is representative of how cushioning is actually used in shock isolation systems requiring thicker sections than the maximum manufactured thickness of 76.2 mm. Whether the Minicel Model can do an adequate job of predicting the impact performance of these stacked samples was questioned. The model's ability to predict adequately under these circumstances would indicate that the stacking did not significantly perturb the cushioning performance from that encountered in 25.4, 50.8, and 76.2 mm continuous samples that form the basis of the model.

To determine statistically how well the model fits a set of independent data, Box and Draper [11] suggest it is appropriate to investigate the bias and variance of the predictor. Two statistical tests can be utilized for this purpose. One test, a test of means, determines whether there is a bias in the predicted values of the model when compared to actual data values. The other test, a test of variances, determines if the variations of the predicted values inherent in the model are comparable with the variations in experimental values.

The test of means and variances were conducted on the Minicel Model using the 685.8 mm drop height data and the 101.6 and 127.0 mm data samples. The results are given in Table 3 and show the following:

1. 685.8 mm drop height data - Analysis indicates that this data is within the range of the independent variables used in the Minicel Model and the null hypothesis cannot be rejected in the test of means or test of variances. This indicates that there is no significant difference between the means and variances of the data and the values predicted by the model. The model appears to be a statistically valid predictor of these data.

2. 101.6 and 127.0 mm data - The test results show that the Minicel Model gives good predictions of the data means at the 101.6 mm thickness. The test of means of the 101.6 mm showed no significant difference but the test on the 127.0 mm showed a significant difference which is not surprising because the model is projecting 50.8 mm beyond its range at the 127.0 mm thickness. The test of variances shows that the model variance at the 101.6 mm thickness is significantly larger, but this is not true at the 127.0 mm level. The model dispersion is comparable to the dispersion of the 127.0 mm data.

There were reservations as to whether the model could predict the 101.6 and 127.0 mm materials since the samples were stacked and not homogeneous and since 101.6 and 127.0 mm are beyond the ranges of the independent variables used in the Minicel Model. The results of the tests of means and variances show that the model was not completely acceptable at either the 101.6 or 127.0 mm thickness. However, the tests indicate that model means were comparable with the data at the 101.6 mm level and the variances were comparable at the 127.0 mm level.

TABLE 3

Tests of Minicel Model As A Predictor of 101.6 and 127.0 mm Thickness

	Minicel Material ($\alpha = 0.05$)		
	685.8 mm Drop Height	101.6 mm Thickness	127.0 mm Thickness
Test of Means			
Number of cells in the data base (N)	99	156	156
Standard deviation of the cells (S)	20.14	8.63	8.56
t_m	1.84	-1.45	-2.61
t_{table}	$\pm$ 1.96	$\pm$ 1.96	$\pm$ 1.96
Decision on H_0: $E(\Delta_j) = 0$	cannot reject	cannot reject	reject
Test of Variances			
Variance of the data, σ_d^2	111.63	26.41	105.35
Variance of the model, σ_m^2	114.39	114.39	114.39
F_{calc}	1.02	4.33	1.08
F_{table}	$F_{1511,193} = 1.17$	$F_{1511,312} = 1.15$	$F_{1511,312} = 1.15$
Decision on H_0: $\sigma_d^2 = \sigma_m^2$	cannot reject	reject	cannot reject

OPTIMIZATION

Once a valid math model of impact response has been developed, it is then possible to formulate an optimization procedure that will provide an automated design of an optimal cushioning system, for a given set of requirements. The procedure which was designed in this research to perform cushion system optimization can best be described as a constrained sequential search technique. The procedure is a direct search technique in that the mathematical model of a material such as the Minicel Model, is used directly as the objective function in the optimization procedure.

The first step in the optimization exercise is to identify the parameters in an optimal cushioning system design; then, the objective or goal of the optimization procedure must be identified. The constraints on the procedure and the objective function are formulated and finally the outputs from the optimization routine itself are identified.

An optimal cushioning system is a system that provides the necessary shock isolation to the protected item at a minimum cost. Because the cost of a cushioning system is dependent upon the amount of cushioning material, the optimal cushioning system will employ the minimum thickness of cushion needed. The optimal point on a dynamic cushioning curve is the minimum G's possible which provides the maximum protection for that particular thickness of cushioning. Therefore, it is the identification of this optimal point that must be determined in selecting the optimal cushion system.

A different dynamic cushioning curve is required to depict cushion performance for each drop height, thickness, and temperature of the cushion; the optimal point is different for each curve. When one considers the many types of cushioning materials and a different curve for each condition, it can be seen that a very large library of curves is required to present even the most likely conditions of drop height, temperature, and thickness of a few candidate cushioning materials.

The model of impact response for a cushioning material, e.g., the Minicel Model, computes the impact response directly from the values of the independent variables. This precludes the need for a library of dynamic cushioning curves in predicting impact response. It is also possible, using the cushioning models for various materials, such as the Minicel Model, to determine an optimal cushioning design for each material, if such a design exists, in a manner as to provide the maximum amount of useful design information.

The development of a valid mathematical model of impact response for a particular cushioning material provides a vehicle for the application of optimization techniques. This model can be reconstituted as an objective function and explored for an optimal cushioning system. This can be done by defining cushioning system design requirements in terms of the external environment and the amount of exposure the protected item can withstand.

The specification of the external environment must contain a definition of those aspects of the environment that have an impact upon cushion system design. This would include a quantitative measure of the magnitude of the maximum shock pulse to which the system will be exposed, which is usually specified in terms of drop height. Also since temperature has a significant effect on impact response, the specification of the external environment should include the range of temperatures to which the system will be exposed $(\theta_{min}, \theta_{max})$.

The specification of the survivability of the protected item is given in terms of its ability to withstand shock. The maximum shock pulse, in G's, that the item can withstand is given as the fragility level of the item (GL_{max}).

These considerations concerning the G-levels and temperatures are incorporated into the model as input values that are utilized to constrain the optimal search to feasible solutions. For the purpose of optimal design, GL is identified as the fragility level of the protected item. The temperature parameter, θ, must consider the range of temperatures of the external environment θ_{min} to θ_{max}. This can be done using the superimposed dynamic cushioning curve format with the curves of extremes of the temperature range superimposed upon the ambient curve.

One parameter in the model, drop height (h), can be determined based on published testing standards. Other parameters, such as the fragility level of the item to be protected (GL_{max}) and the temperature range $(\theta_{min}, \theta_{max})$, are usually specified by overall system requirements. For example, if the cushioning system is to be designed for a military container for a missile, the fragility level of the protected item (GL_{max}) will be specified as part of the hardware specifications in the missile system design criteria. The temperature range $(\theta_{min}, \theta_{max})$ is defined in the missile system requirements and the drop height is specified in various Military Standards depending on total container weight.

There are certain less sophisticated hardware items which require packaging, but the item cost does not warrant a test program to specifically determine the fragility level. In these situations, a combined program can be conducted that will establish package design in conjunction with a G level determination for the packaged item.

The preliminary design fragility can be determined from a knowledge of the dynamics of the missile and the projected design for the package. The theoretical design using this fragility can then be carried out and a preliminary design constructed and tested. If the dynamic interactions were accurately determined, the preliminary design fragility may be acceptable, but more often than not, one or more iterations of the process will be required to determine acceptable fragility.

These parameters, GL_{max}, θ_{min}, θ_{max}, and h, are the exogenous variables in the optimization model. Equation (1) can now be written as follows:

$$GL_{max} = F[\sigma_s, T, (\theta_{min}, \theta_{max}), h] \qquad (10)$$

where GL_{max}, $(\theta_{min}, \theta_{max})$, and h are inputs to the equation which are determined by the cushion system design requirements. The optimization technique will search out the optimal design from this expression, and the optimal design solution will be expressed in terms of σ_s and T.

The optimal design searches upon the functional relationship expressed in Equation (10) and with the inputs introduced, reduces to the selection of the minimum thickness of cushion that will perform satisfactorily at a static stress condition that is determined in the search. It is anticipated that a data base will eventually be available that contains valid impact response models for many of the different types of bulk cushioning materials. The model of each type of material in the data base can be investigated by the direct search routine to determine the feasibility of meeting the design objective function. The optimal design conditions of minimum thickness and acceptable static stress range will be output for each type of cushion in the data base, if an optimal design exists.

The initial step is to select the type of material. Then, a search is initiated on a minimum thickness cushion (25.4 mm) at the drop height and minimum temperature (θ_{min}) stipulated in the design requirements. These values are input into the objective function and the search is conducted across the static stress spectrum at the temperature extreme, θ_{min} and then θ_{max}, to determine the feasibility of meeting the stipulated GL_{max}. It is also necessary that the acceptable static stress range at GL_{max} be greater than 1379 Pa to permit design flexibility and preclude creep problems within the design. (This 1379 Pa value can be changed at the discretion of the designer).

If the search of the acceptable static stress range on the minimum cushion thickness is successful,

the answer is output as a feasible solution. If it is not successful, the thickness is incremented 12.7 mm and the search repeated. A flow chart of the direct search routine is given in Figure 1.

The direct search program output is given in the form of superimposed dynamic cushioning curves such as the typical one given in Figure 2. In Figure 2, the design objective function had the temperature range of 219 to 344 K and a 762.0 mm drop height. The fragility level was 50 G's which is indicated with a dotted horizontal line. The optimal thickness is determined to be 63.5 mm and the feasible static stress range is found to be 4137 to 8274 Pa. One of the inherent advantages of using math models is seen here in the capability of determining G-level response at thicknesses other than those in the data base. In this instance a 63.5 mm thickness of cushion was optimal; tests were not conducted at this thickness in the data base. This advantage can also be seen in Figure 3 which is another output of the optimization program where the temperature range has the non-data base values of 244 and 322 K. The optimal thickness is 50.8 mm and the stress range is 3792 to 5516 Pa to give 50 G protection. Comparison of Figure 2 with Figure 3 demonstrates the effect of temperature on optimal cushion design. When the temperature range was relaxed from the extremes of 219 through 344 K to 244 through 322 K and all other exogenous variables kept the same, the thickness of cushion required for 50 G protection dropped from 63.5 mm to 50.8 mm. Another comparison can be made between Figure 2 and Figure 4, which demonstrates the increase in thickness of cushion required when the fragility level of the protected item is lowered from 50 G's to 40 G's. One other comparison can be made between Figure 2 and Figure 5, which demonstrates how a reduced drop height requirement reduces the thickness of cushion required.

One additional advantage in using the superimposed dynamic cushioning curve format for the output format is that the designer is presented with a convenient tool for minimizing the creep tendency of the materials by maintaining as low a stress condition as possible and yet be able to ascertain the response of the stress level selected.

CONCLUSIONS

There has been limited use made of bulk cushioning in shock isolation systems for commerical and military equipment. One reservation that designers have had regarding bulk cushioning is an inability to predict cushioning performance at temperature extremes. Consequently, many designs incorporate mechanical suspension systems such as elastomeric mounts or springs and dash pots and other types of shock isolation systems that are bulky, very heavy, require substantial structural interfaces, and are very expensive.

One result of this research is the development of a valid model of bulk cushioning response that provides a basis for improving the predictability of temperature performance for bulk cushioning materials. Resultant increases in the use of bulk cushioning for shock mitigation systems will generate dollar savings in the accompanying reduced procurement and development costs.

The developed model is predicted on viscoelastic theory and incorporates the effect of temperature, stress, drop height, and thickness of cushion upon the impact response of a cushioning system. This General Model provides the basic underlying structure of impact response of any one of the many bulk cushioning materials used for shock isolation.

Models that are predicated on the basic underlying structure of the General Model are better predictors of impact response than the dynamic cushioning curves currently being utilized, since the effect of temperature has been incorporated into the model. The Minicel Model is one such model that was constructed for the Hercules, Inc. 32 kg/m^3 Minicel material using the General Model as the basic underlying structure. The Minicel Model showed high correlation with the actual data within the ranges of the variables and also showed promise as a predictor beyond the variable ranges.

The development of a valid model of impact response of bulk cushioning materials defines the relationships and interrelationships of the variables in response to impact. Using this basis, it was possible to employ a search technique to determine optimal cushion design and display the findings in terms of superimposed dynamic cushioning curves. The functional form of the model provides the advantage of determining impact response at non-tested levels of the variables with confidence and precludes the need for a library of dynamic cushioning curves for all the different combinations of conditions.

Once a valid model of a particular cushioning material has been developed, it can be incorporated into the optimization program. This program accepts the design requirements for a shock isolation system and computes and provides, in the form of superimposed dynamic cushioning curves, the optimal design for each cushioning material in the data base, if one exists. The outputted superimposed dynamic cushioning curves give the pertinent information needed in the optimal design of a shock isolation system.

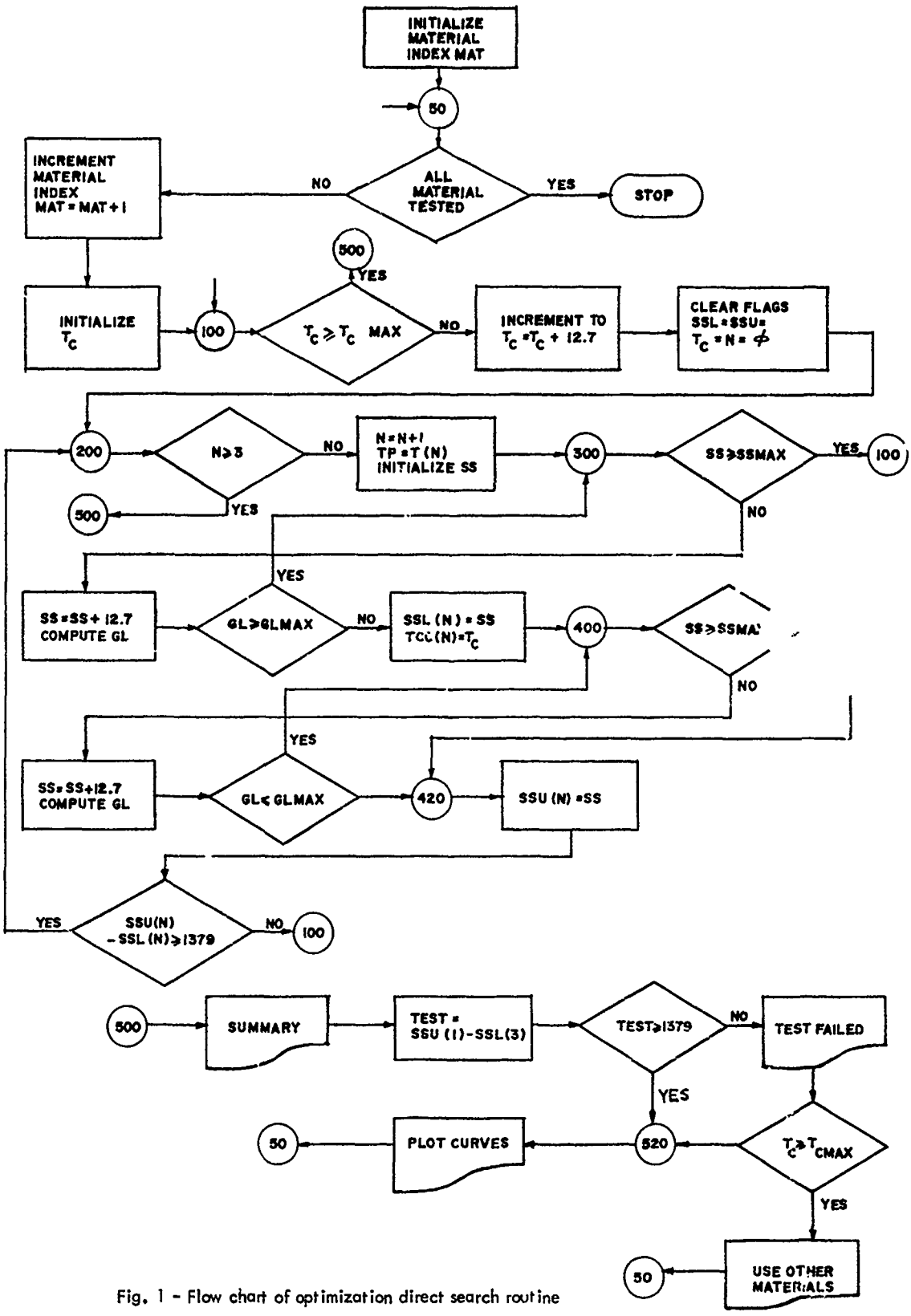

Fig. 1 - Flow chart of optimization direct search routine

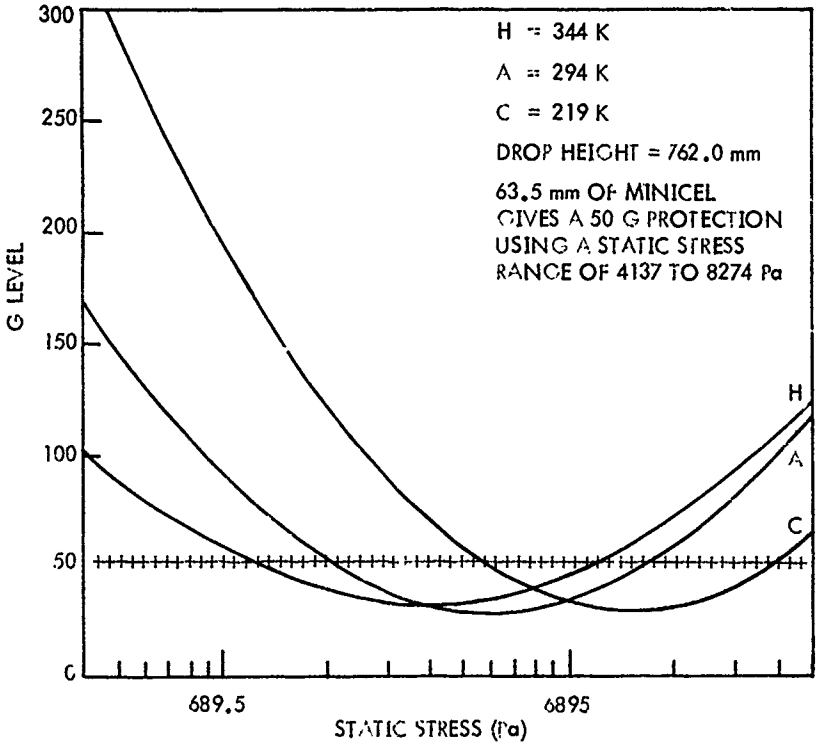

Fig. 2 - Optimal design output, 63.5 mm Minicel

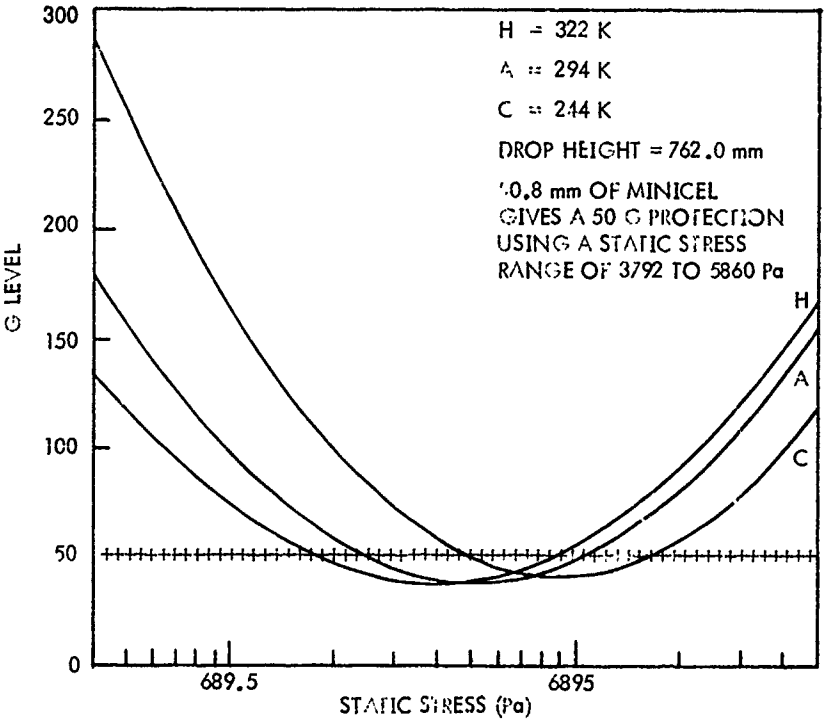

Fig. 3 - Optimal design output, 50.8 mm Minicel

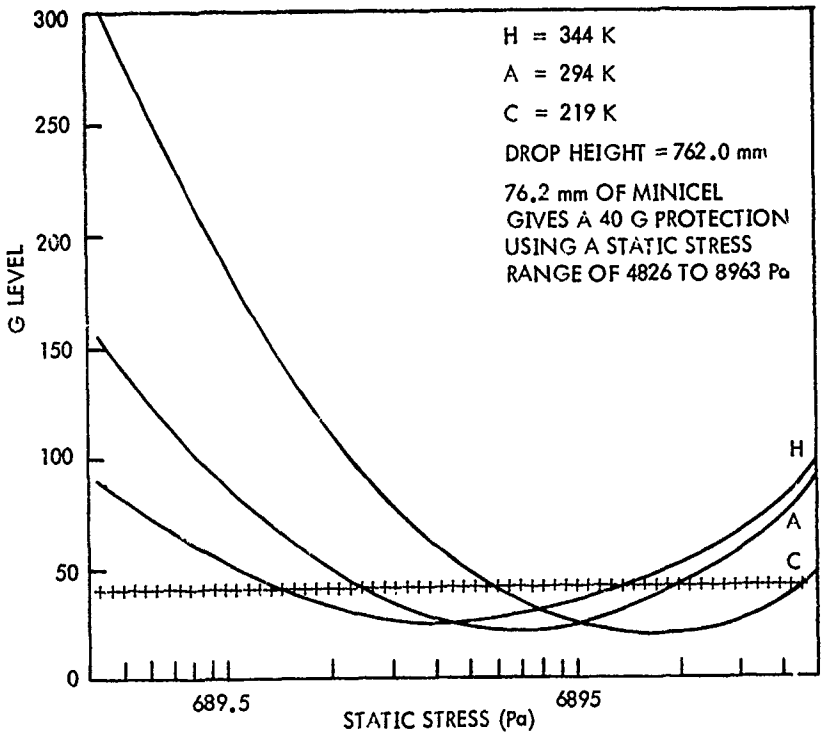

Fig. 4 - Optimal design output, 76.2 mm Minicel

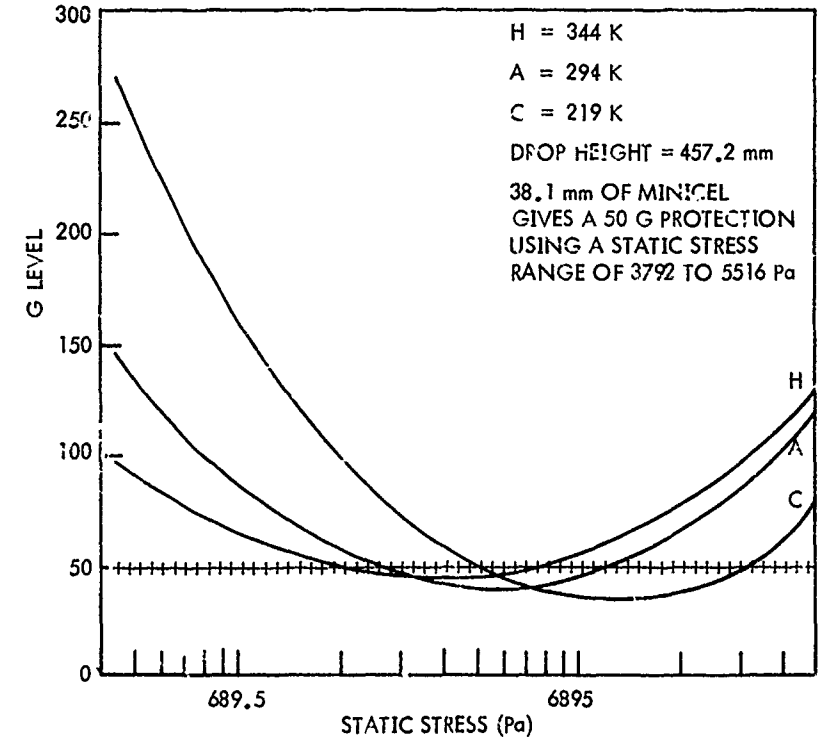

Fig. 5 - Optimal design output, 38.1 mm Minicel

REFERENCES

1. McDaniel, Don, A Study of Impact Test Effects Upon Foamed Plastic Containers, US Army Missile Command, Redstone Arsenal, Alabama, Report No. RL-TR-71-2, 1971.

2. Wyskida, Richard M. and Wilhelm, Mickey R., Temperature Sensitive Dynamic Cushioning Function Development and Validation for Hercules Minicel Thermoplastic Foam, The University of Alabama in Huntsville, Huntsville, Alabama, UAH Research Report No. 159 (MICOM Report No. RL-CR-75-1), September 1974.

3. Mustin, Gordon S., Theory and Practice of Cushion Design, The Shock and Vibration Information Center, United States Department of Defense, 1968.

4. Cost, Thomas L., Dynamic Response of Container and Container Cushion Structures, Athena Engineering Company, Northport, Alabama, Technical Report No. 74-003, October 1974

5. Meinecke, E. A. and Clark, R. C., Mechanical Properties of Polymeric Foams, Technomic Publishing Co., Inc., Westport, Connecticut.

6. Shannon, R. E., Systems Simulation: The Art and Science, Prentice-Hall, Inc., Englewood Cliffs, New Jersey, 1975.

7. Mindlin, R. D., "Dynamics of Package Cushioning," Bell System Technical Journal, 24, and Bell System Monograph B-1369, July-October 1945.

8. Janssen, R. R., A Method for the Proper Selection of a Package Cushion Material and its Dimensions, North American Aviation, Los Angeles, California, Report NA-51-1004, 1952.

9. Duncan, Acheson J., Quality Control and Industrial Statistics, Richard D. Irwin, Inc., Homewood, Illinois, 1965.

10. Daniel, Bailey E., Probability and Statistics - Models for Research, John Wiley & Sons, Inc., New York, 1971.

11. Box, G. E. P. and Draper, N. R., "A Basis for the Selection of a Response Surface Design," Journal of American Statistical Association, Vol. 54, 1959.

Discussion

Mr. Gertel (Kinetic Systems): I question your concept of optimization. You alluded a little bit to it by noting that the cushioning lines, the traditional cushioning lines, are really bands or you intimated that they were bands because they were averages. It is a little worse than that because the material is normally specified by a density or some very simple factor so that if you take nominally the same material, with its present definition for procurement purposes, you get completely different sets of bands; the characteristics are U shaped and that is about the only thing you can say about them. You take nominally the same material and wind up with two different bands each one will be outside of the other's average. This concept of an optimum point or an optimum area is really much broader, you have to be much more conservative about selecting that general area.

Mr. Wyskida: This is not to suggest that you can eliminate judgement from the designer's jurisdiction of course. He still maintains that. We have attempted to take care of some of the things you are addressing through our randomized split design and trying to spread those differences over the sampling. I believe you are aware that we deviated from the Wright Patterson procedure because of the temperature problems. You could not maintain that temperature the way Wright-Patterson says the procedure should be followed, that is an impossibility; so we developed a procedure similar to that.

Mr. Gertel: I want to emphasize that it is bands and not lines and anybody that thinks of them as lines is going to wind up in trouble.

Mr. Wyskida: Well that is why we also don't have a definite point, notice that we said over a static stress region.

Mr. Venetos (Air Force Packaging Evaluation Agency): I just wanted to point out that with polyurethane you are even going to run into more variability, you are talking about "Minicell", but with polyurethane you may even have a size effect. I refer to the 8" x 8" (.2 meter x .2 meter) samples that you used to develop that data; we found that when you go to a larger pad size, 12" x 12" (.3 meter x.3 meter), 15" x 15" (.38 meter x .38 meter) or whatever, the g value will change.

Mr. Wyskida: Yes we are aware of that and we are presently looking into that so we appreciate your comment. It is true that we have problems there.

BARREL-TAMPED, EXPLOSIVELY PROPELLED PLATES FOR OBLIQUE IMPACT EXPERIMENTS

F. H. Mathews and B. W. Duggin
Sandia Laboratories
Albuquerque, New Mexico 87115

ABSTRACT

The use of explosively driven rotating flyer plates for high-velocity impact fuze testing involves the detonation of a solid explosive to accelerate massive, slowly rotating plates to high velocities. The device to be tested is positioned at a distance along the flight path sufficient to allow rotation of the flyer plate before impact. Thus, any angle between the plate's surfaces and the plate velocity vector can be obtained.

In the past an unconfined grazing detonation has been used. Now, an improvement in energy transfer between explosive and plate is achieved by the addition of a massive barrel surrounding the explosive, with detonation normally incident on the plate. Data from small experiments in combination with one-dimensional analysis allow prediction of velocity as a function of plate thickness for geometrically similar barrel-confined systems. Methods are described for fireball suppression, fragment control, and experiment protection which are essential for oblique impact experiments on full-size fuzing hardware. Results are presented from several large experiments, including a 190-kg explosive system which propels a rotating 11-kg aluminum plate at a velocity of 3550 m/s.

INTRODUCTION

Ballistic missile warheads employ impact-actuated fuzes that function at contact velocities up to 4500 m/s. Development tests involve "turn around" impacts where target materials are projected against stationary fuze assemblies. This reciprocal arrangement produces representative impact stresses while avoiding the high cost of flight experiments. Experimental methods suitable for velocities above 1800 m/s present a particular challenge because of the limited velocity capability of such conventional devices as rocket sleds and powder guns.

A previous paper [1] described a technique where solid explosive initiated to produce grazing detonation accelerated a massive, slowly rotating plate to high velocity. Appropriate positioning of the fuze along the plate's

flight path allowed the desired relation between the velocity vector and the surface of the plate. This technique has allowed experiments at oblique angles with both hard and soft target materials (aluminum and nylon) over the velocity range from 1400 to 2700 m/s.

The present paper extends the previous work. Grazing detonation failed when experiments at the highest possible velocity were coupled with requirements for relatively thick (50-mm) plates. These experiments employed thick explosive charges and were dominated by side energy losses which prevented efficient transfer of explosive energy to the rotating plate. Explosive mass tended to increase as a cubic function of plate thickness. The advantages of simplicity and low cost afforded by grazing detonation were more than offset by the need for enormous explosive quantities.

An improved explosive system employing massive side confinement and normally incident detonation is described in this paper. Data from small-size experiments are coupled with one-dimensional analysis to provide a framework for computing plate velocity. Scaled experiments are shown to correspond when weight is increased by 3 orders of magnitude. Finally, the performance of two large explosive systems is discussed.

ONE-DIMENSIONAL ANALYSIS

Two explosive geometries suitable for accelerating metal plates are illustrated in Fig. 1. Grazing detonation produces lower compressive pressures [2] and usually reduces the tendency of the plate to break up as a result of spall. Normal detonation produces highest plate pressures and, with materials relatively resistant to spall, has proved useful at high velocities.

Side losses are small when the explosive is thin in comparison to lateral dimensions. In this case, plate terminal velocities may be predicted from one-dimensional theories. Thus, for the grazing configuration [3] the terminal velocity V_g is

$$V_g = \frac{\sqrt{2E}}{\left(\frac{1}{3} + \frac{5}{3}\frac{M}{C} + \frac{4}{3}\left(\frac{M}{C}\right)^2\right)^{1/2}} , \quad (1)$$

where $\sqrt{2E}$ is a characteristic velocity for the explosive and C/M, the loading factor, is the ratio between explosive mass (C) and plate mass (M).

Final velocity (V_n) for normal detonation [4, 5, 6] is

$$V_n = D\sqrt{\frac{8}{\gamma^2 - 1}\left[\frac{\left(1 + \frac{32}{27}\frac{C}{M}\right)^{1/2} - 1}{\left(1 + \frac{32}{27}\frac{C}{M}\right)^{1/2} + 1}\right]} , \quad (2)$$

where D is the detonation velocity and γ is an explosive constant with a value near 3 for solid explosives.

Terminal velocities predicted for one-dimensional conditions are compared in Fig. 2. The values used to describe composition C-4 explosive [3, 7] are $\sqrt{2E}$ = 2750 m/s, D = 8040 m/s, γ = 2.7.

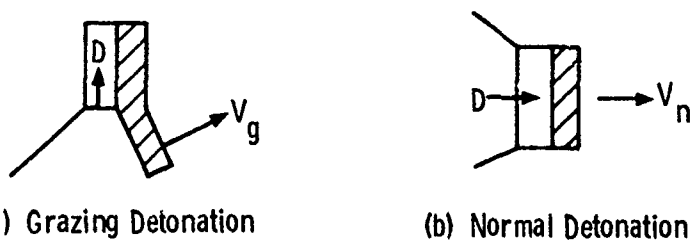

(a) Grazing Detonation (b) Normal Detonation

FIG. 1. EXPLOSIVE GEOMETRY

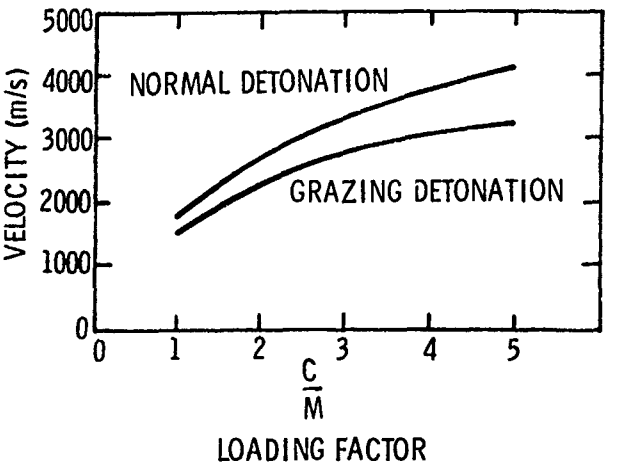

FIG. 2. PLATE VELOCITY AS A FUNCTION OF LOADING FACTOR FOR COMPOSITION C-4 EXPLOSIVE

EXPLOSIVE SYSTEM

The preceding one-dimensional analysis indicates that normally incident detonation yields highest plate velocities for a given explosive weight. A similar situation is anticipated when edge losses are important. The numerous experiments conducted used the small assembly depicted in Fig. 3. Detonation is initiated at the rear surface and moves through the explosive toward the guard plate/flyer plate combination. The shock wave accelerating the plate must be sufficiently planar that the plate is not deformed and broken up during flight. Plane wave initiators are therefore necessary for relatively thin charges when length-to-diameter ratios are less than 0.75. The spherical detonation wave from a centered initiator is satisfactory for longer assemblies.

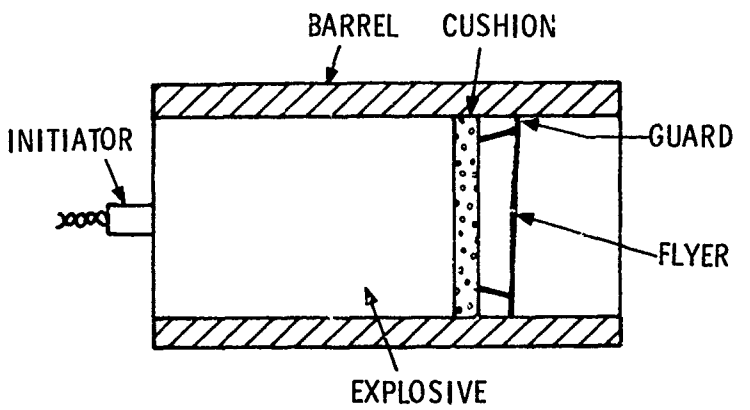

FIG. 3. BARREL-CONFINED EXPLOSIVE ASSEMBLY

Pressures resulting from shock reflection at the plate surface are sufficiently high that shock damage in the form of spallation is an important consideration [2]. Although the rubber cushion affords some protection, thick cushions degrade plate velocity. Aluminum plates launched at high velocity have sufficient strength to resist shock damage when only a thin cushion is used.

The flyer must remain intact and reasonably planar over long flight distances. It is therefore essential that the impulse from the explosive gases vary uniformly over the plate surface. This is accomplished by separating the driven plate into two units. A centered flyer is protected from edge effects by a guard plate. A weak joint is provided by gluing the flyer into the guard plate. Since explosive pressures are relieved most rapidly toward the edges, the guard is free to bend and separate during acceleration without adversely affecting flyer planarity. When the barrel mass exceeded explosive mass during testing, equal flyer and guard areas proved satisfactory. Without side confinement, the flyers were deformed radially and were always torn into fragments.

Flyer rotation is obtained by slightly tapering the flyer and guard plates across their diameters. Rotation rate may be estimated by assuming that plate energy is uniform across the diameter. Plate rotation usually attains about 70 percent of the estimated value.

Accelerating thick plates to high velocity requires relatively long assemblies where side losses are important. The steel barrel surrounding the explosive is intended to reduce lateral expansion and related side losses. The barrel thickness must be selected carefully because its cost is high. Also, barrel fragments must be arrested because they present a significant hazard to experimental apparatus.

EMPIRICAL ANALYSIS

An approximate means of treating systems with side losses is to discount the total explosive (C) to a reduced value, the effective explosive (C_e), which is assumed to act as if one-dimensional flow existed [3]. Thus, $C_e = \alpha C$, where α is the discount factor which takes a value less than 1. Then, along with the effective explosive and the plate mass (M), the one-dimensional analysis yields the terminal velocity of the plate. In this way, charge geometry (i.e., length and confinement) may be considered separately from plate velocity, mass, and explosive properties, which are treated by Eq. (2).

Data for this analysis were obtained by firing two sets of small experiments in which flyer plate velocities were measured and the effective explosive mass was calculated. Confinement and length were fixed in the first experiments and the plate mass was varied, thus yielding the effective explosive mass which, with Eq. (2), was used to compute the curve of Fig. 4. Excellent agreement with data at other velocities confirms that useful velocity predictions are possible once the effective explosive mass has been determined in a single experiment.

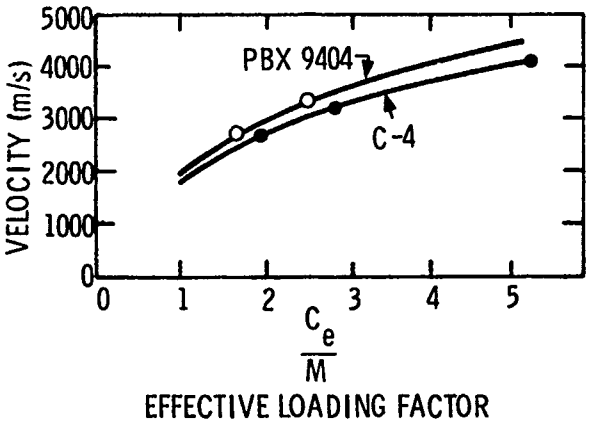

FIG. 4. PLATE VELOCITY AS A FUNCTION OF EFFECTIVE LOADING FACTOR FOR TWO EXPLOSIVES

TABLE I

Data for Figure 4

Shot	Explosive	N/C	L/D	C_e/M	α	V (m/s)
3[a]	C-4[b]	4.4	1.5	1.96	0.43	2670
5	C-4	4.4	1.5	2.83	0.43	3222
6	C-4	4.4	1.5	5.21	0.43	4140
17[a]	PBX-9404[c]	3.9	1.5	1.69	0.35	2660
18	PBX-9404	3.9	1.5	2.51	0.35	3300

[a]Data from this experiment were used to calculate the effective explosive (C_e).

[b]Constants for C-4 explosive are D = 8040 m/s, γ = 2.7.

[c]Constants for PBX-9404 explosive are D = 8800 m/s, γ = 2.7.

In a second set of experiments, barrel length was changed but relative confinement per unit length of charge (N/C) remained constant. Equation (2) was used with measured velocity in each experiment to determine the discount factor (α) as a function of length. Results are given in Table II and Fig. 5.

TABLE II

Discount Factor as a Function of Charge Length for Fixed Confinement (N/C = 4.4)

Shot	L/D	α	C_e/M	V (m/s)
19	0.75	0.57	3.06	3320
1	1	0.52	1.55	2310
3	1.5	0.43	1.96	2670
B	2.5	0.29	2.07	2730
A	3.5	0.22	2.15	2780

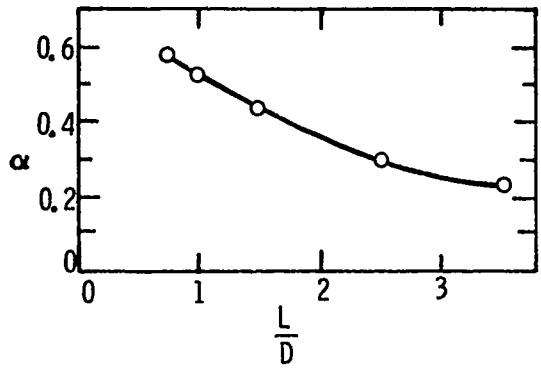

FIG. 5. DISCOUNT FACTOR (α) AS A FUNCTION OF CHARGE LENGTH FOR FIXED CONFINEMENT

The most efficient explosive systems are short. Even with massive confinement (N/C = 4.4), lengthening the explosive charge beyond L/D ≈ 2 results in little gain in effective explosive. The desire to provide a long explosive run to obtain a nearly planar detonation front at the plate favors a long explosive length. Although the amount of confinement was not investigated separately because explosive costs and steel costs are comparable, lack of confinement may be compensated, within limits, by increased explosive quantity.

LARGE EXPLOSIVE SYSTEM

An explosive/barrel combination will yield a particular velocity vs. plate mass performance similar to that depicted in Fig. 4. We elected to construct a single-barrel system and to obtain desired velocity and plate rotation by varying plate thickness, taper, and type of explosive. Figure 6 shows the highest velocity assembly, which employs a machined pressing of PBX-9404 explosive 0.61 m thick and backed by composition C-4 explosive with a total explosive mass of 190 kg. A schedule 160 steel pipe with machined bore provided a confinement value of 2.2. When lower plate velocities were desired, the entire explosive volume was handpacked with 170 kg of less expensive composition C-4 at a confinement value of 2.8. Testing was conducted by using one-eighth scale models of the 170-kg assembly to establish detailed information regarding timing, velocity, effective explosive quantity, and scaled rotation rate. Comparison between the performance of small-scale experiments and full-size experiments is given in Table III, together with the results from a 190-kg system. Scale models of the 190-kg system were not built. Plate velocities are identical, whereas rotation rate for small assemblies is 8 times greater than the large assemblies. The excellent agreement between small and large experiments has reduced requirements for full-size qualifying shots before the committing of expensive fuze hardware to test.

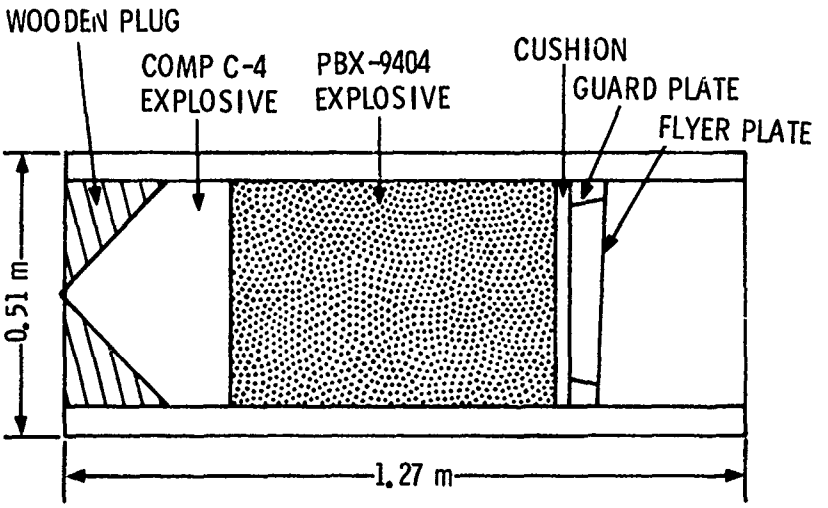

FIG. 6. FULL-SCALE EXPLOSIVE SYSTEM WITH STEEL BARREL AND TAPERED ALUMINUM PLATE

TABLE III

Performance of One-eighth-Scale Systems and Full-Scale Systems

Scale	Launch Velocity (m/s)	Rotation Rate (rad/s)	Plate Thickness[a] (mm)	Explosive Type
Full	2320	0	82.6	Comp C-4
One-eighth	2350	0	10.5	Comp C-4
Full	2350	316	82.6	Comp C-4
One-eighth	2330	2600	10.5	Comp C-4
Full	2960	0	50.8	Comp C-4
One-eighth	3070	0	6.4	Comp C-4
Full	3020	636	50.8	Comp C-4
Full	3010	570	50.8	Comp C-4
One-eighth	3050	4700	6.4	Comp C-4
Full	3570	670	40	PBX 9404

[a]At plate centerline

EXPERIMENTAL CONSIDERATIONS

The arrangement for impact fuze testing with a barrel-confined explosive system is shown in Fig. 7. Two plate configurations were employed at each of three initial velocities, shown in Table III. The first, employing a tapered plate, produced a rotation through 60° after a displacement of about 7 m; the second, employing a uniform plate, did not rotate. With this arrangement, either angled or normal impact experiments could be separated at least 3 m from the explosive, allowing use of sand to control barrel fragments and use of two barriers to prevent explosion gases from striking the fuze assembly before the plate.

Ultrahigh-speed pictures taken at 1×10^6 frames/second with argon flash bomb illumination allow a continuous record of plate motion near the impact location. These pictures clearly depict the air shock carried by the plate as it interacted with the fuze assembly just before plate impact. These pictures are used to relate impact time to electrical events within 1 μs. X-ray film placed in a protective cassette behind the fuze allowed a sequence of three carefully timed shadowgraphs from which plate integrity, impact velocity, angle, and rotation rate may be determined. A pulse X-ray shadowgraph of an 11-kg aluminum plate 49 mm thick moving at a velocity of 3460 m/s and a rotation rate of 670 rad/s after a displacement of 5.7 m is shown in Fig. 8. The slight center bowing is typical. Protection of the X-ray film requires careful attention to cassette design and use of massive protective barriers.

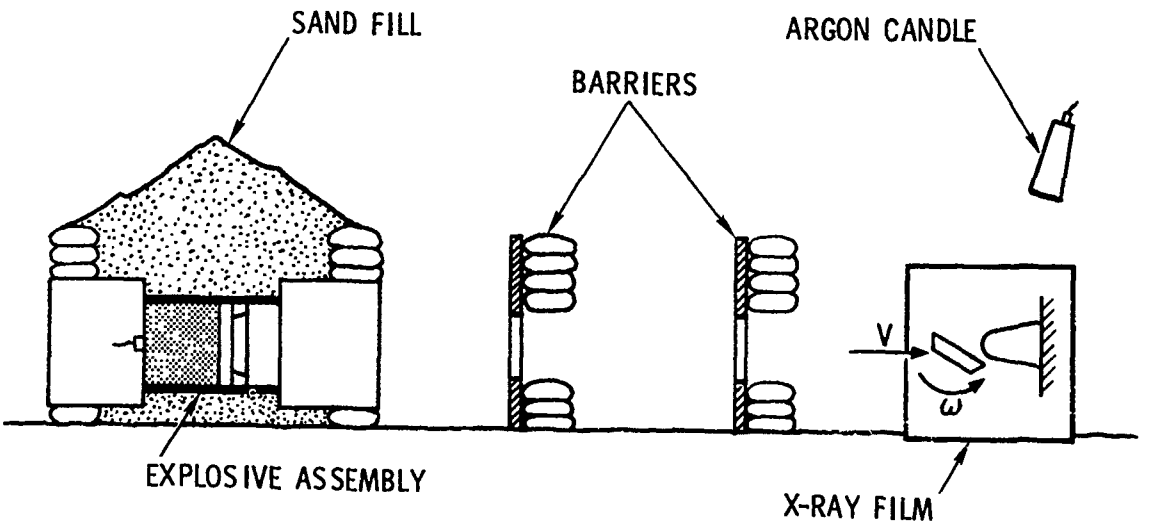

FIG. 7. EXPERIMENTAL ARRANGEMENT

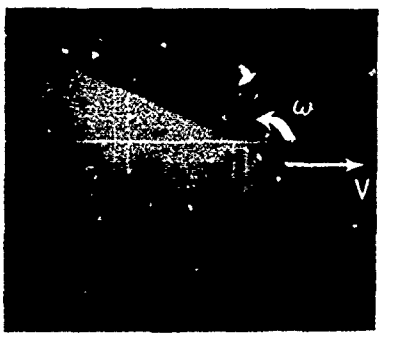

FIG. 8. X-RAY SHADOWGRAPH OF AN 11-kg PLATE PROJECTED BY THE ASSEMBLY OF FIG. 6. VELOCITY 3460 m/s, ROTATION 670 rad/s AND DISPLACEMENT 5.7 m

TRAJECTORY CONSIDERATIONS

The plate trajectory may be considered in three segments: launch, flight, and impact. The launch segment occupies a few tens of microseconds and a few centimeters of motion. The plate is launched on a trajectory coincident with the barrel axis. During launch the velocity of the guard ring is somewhat less than the value attained by the center plate. This effect, coupled with barrel interference and edge relief, results in breakup of the guard plate, which lags behind and is intercepted by apertured barriers placed along the flight path of the plate. The motion and timing during acceleration, as well as the plate stresses, may be estimated by using a one-dimensional hydrodynamic code [8] with appropriate discounting of explosive to achieve an equivalent one-dimensional system for analysis. A more sophisticated, two-dimensional analysis [9] has also been used to study details of barrel and plate motions for a single nonrotating configuration. These computations give an accurate description of timing and plate motion during the launch phase of the plate trajectory.

The flight portion of the trajectory is the interval beginning after the first few centimeters of plate motion and continuing to the impact. Initially, the plate is surrounded by explosion gases. Then, depending upon the presence of barriers and velocity, the plate moves through undisturbed air where appreciable aerodynamic forces retard its motion and displace its trajectory along the pitch axis. These effects and their influence upon timing and target position may be computed [1]

Experiment timing depends upon accurately calculated delays set in relation to explosive initiation. On the first large experiment the discounted one-dimensional model, which depends upon results from small-scale experiments coupled with a calculation of aerodynamic effects, allowed timing within approximately ±60 μs. Timing estimates within ±20 μs, corresponding to a velocity scatter of 1 percent, are possible with repeated application of large explosive assemblies.

CONCLUSIONS

Barrel-confined explosives have been employed to accelerate massive, slowly rotating aluminum plates to high velocity. The aluminum plates remained intact. Velocity performance of the barrel systems which employ normally incident detonation considerably exceeds that attained previously in work with grazing detonation. An approximate analysis forms a basis for interpreting measured velocities in terms of a discounted explosive mass, thus allowing separate consideration of plate velocity, confinement, and charge length.

Experimental results obtained with small assemblies accurately scale to larger systems; therefore, requirements for qualifying experiments are reduced. Because the thick aluminum plates remain intact and reasonably planar over relatively great distances, their application to oblique impact experiments on impact fuzes is feasible. Auxiliary means of trajectory calculation, control of barrel fragments, and control of explosion fireball permit a combination of optical, X-ray, and electrical measurements during impact experiments.

REFERENCES

(1) F. H. Mathews, "Explosively Propelled Rotating Plates for Oblique Impact Experiments," Shock and Vibration Bulletin, 45, Part 4, June 1975.

(2) O. E. Jones, "Metal Response Under Explosive Loading," Behavior and Utilization of Explosives in Engineering Design, 12th Annual Symposium ASME. Published by The New Mexico Section ASME, March 2-3, 1972.

(3) J. E. Kennedy, "Explosive Output for Driving Metal," Behavior and Utilization of Explosives In Engineering Design, 12th Annual Symposium ASME. Published by The New Mexico Section ASME, March 2-3, 1972.

(4) A. K. Aziz, H. Hurwitz, and H. M. Sternberg, "Energy Transfer to a Rigid Piston Under Detonation Loading," Physics of Fluids, 4, 380-384, 196.

(5) Heinz Knoepfel, Pulsed High Magnetic Fields, p. 269-272, North Holland Publishing Co., Amsterdam, 1970.

(6) F. A. Baum, K. P. Stanyvkovich, and B. I. Shekhter, Physics of an Explosion, Moscow, 1959. (English translation from Federal Clearinghouse AD 400151).

(7) B. M. Dobratz, "Properties of Chemical Explosives and Explosive Simulants," UCRL-51319, December 1972.

(8) R. J. Lawrence and D. S. Mason, WONDY IV - A Computer Program for One-Dimensional Wave Propagation With Rezoning, SC-RR-71 0284, Sandia Laboratories, August 1971.

(9) W. T. Brown, Private Communication dtd 1975, Code Development Division, Sandia Laboratories.

This work supported by the Energy Research and Development Administration.

ESTIMATION OF SHIP SHOCK PARAMETERS FOR CONSISTENT DESIGN AND TEST SPECIFICATION

Gary C. Hart and T. K. Hasselman
J. H. Wiggins Company
Redondo Beach, California 90277

and

W. N. Jones
Naval Weapons Center
China Lake, California

The need to characterize recorded ship shock data for use in design and test constitutes one of the reasons for conducting full scale shock tests. The characteristic parameters which one specifies and proceeds to numerically quantify are functions of the underlying approach or philosophy used in design and test practice. Therefore, a fundamental, and most important decision must be made on which characterization procedure is to be used for analyzing the shock data.

This technical paper presents the application of a procedure which analytically represents the shock as a time-modulated nonstationary stochastic process with a time varying mean. The parameters which must be quantified for such a representation are the shock's mean value function, time-modulating function, and power spectral density function. These parameters are defined in the paper. Utilizing actual measured ship shock data the parameters are estimated by statistical methods of analysis. Results from different digital data processing techniques are presented to show their influence on the final parameter estimates. The results from this part of the analysis enable digitally simulated test functions to be generated for use in shock tests.

The paper goes on to demonstrate how the previously defined characterization parameters can be utilized in the development of probabilistic shock spectra. Probabilistic spectra are developed using the parameter values estimated from the ship shock data. These spectra are then compared with standard deterministic shock spectra obtained using the original shock records, and with peak component response data from the same test.

INTRODUCTION

In previous work the authors have described a procedure for the characterization of shipboard shock data for use in design and test [1]. This procedure modeled the ship shock as a time-modulated nonstationary stochastic process. The characterization incorporated time-varying amplitude levels and also the frequency content of the motion.

This paper presents a detailed examination of actual ship shock data from a U.S. Navy test. While the test date, size and location cannot be noted, it is sufficient to state that the data do represent actual shock time-history records. Since the Navy test only involved one shot at a fixed size and location it does present a situation where there only exists one sample function of the process. This experience is typical.

The question is, can such a record be simulated in some way as a basis for deriving consistent design and test criteria? And, if so, how should it be done? A secondary question is, how strongly should one rely on the characteristics of any one particular record, from the standpoint of developing design and test criteria. These questions are not at all easy to answer, particularly the second one, and require that considerable knowledge and judgment be brought to bear. It is beyond the scope of this paper to answer them in depth, but they do help to focus attention on two key issues. This paper addresses primarily the first. To the extent that the second question is left unanswered, the reader should observe caution in making any direct application of the methods outlined here without further qualification.

At the outset, one might first consider trying to use the acceleration wave form directly. Shock spectra can certainly be derived to use in design specification, and the wave form itself could be specified for a test utilizing transient waveform control [2]. The difficulty here is that very little confidence can be placed in the use of a single record which acknowledges no variability whatsoever, ever. if it appears to represent a severe environment.

Another alternative would be to take the single record and derive its average energy distribution with respect to both frequency and time. An average energy distribution with respect to frequency may be obtained by computing an average power spectral density (PSD) function over a specified length of time. This PSD function can be normalized so that its integral over some frequency range is unity. The temporal distribution of energy may then be represented by a time-averaged mean-square value over some time window which is short compared to the total duration of the record. However, this approach raises the question of just how large to choose the window. If the window is too small, the time variation will be very jagged. If it is too large, the intensity of the shock record will be too smooth, i.e., smeared.

Another problem is that by reducing the shock record to a single energy function, all phase information is lost and significant waveform characteristics (if any) will not be preserved.

A third alternative is to separate the low frequency portion of the record from the high frequency portion. The low frequency portion may be treated as "deterministic", preserving any meaningful waveform characteristics, while the high frequency portion is treated as "random". The "random" portion is thus defined to be that which remains from the original record after the "deterministic" portion is subtracted out.

Clearly, there are many ways to "cut the cake", so to speak. It is not the purpose of this paper to indicate how this should be done. It will depend on the nature of each application. It is perhaps worth mentioning, however, that one could remove the particular low frequency portion of a shock transient, leaving only the high frequency "hash", and add to it an artificial low frequency transient derived on the basis of "least favorable response", for example [3]. This approach is justified to some degree by the fact that the high frequency portion of the shock record will usually include more statistical degrees of freedom than the low frequency portion, thus making it possible to derive meaningful statistical parameters to characterize it as a random process. The comparative lack of information regarding the low frequency portion tends to motivate the adoption of more conservative methods for its treatment.

The main point being stressed here, is that regardless of the simulation philosophy appropriate in any particular situation, either a single record or an ensemble of records can be simulated by the nonstationary random process

$$a(t) = m(t) + \psi(t)x(t) = m(t) + y(t)$$

where $m(t)$ is considered to be the mean value function of the process and is deterministic, and $\psi(t)x(t) \equiv y(t)$ is a nonstationary random process with zero mean. In particular, $x(t)$ is chosen to be a stationary random process defined in terms of a PSD function, and $\psi(t)$ represents a deterministic intensity function.

In the remainder of this paper, probabilistic shock spectra are calculated using the characteristic parameters from the above simulation of actual shock records. These are compared with deterministic spectra obtained directly from the recorded time-histories. Finally, comparisons are made with peak accelerations recorded during the same test on deck mounted equipment. The experience gained during the course of this study is summarized in light of requirements for continuing research in this area.

DETERMINISTIC COMPONENT OF DATA

The mean value function of a shock time-history is of considerable importance because it characterizes the fundamental time-history of motion, and helps the engineer determine whether a probabilistic characterization of the shock is warranted for a particular problem.

The mean value function of a shock time-history is defined herein by the symbol $m(t)$. This function possesses a straightforward statistical definition when there exists a large number of shock sample-functions. The definition is

$$\hat{m}(t) = \frac{1}{N} \sum_{k=1}^{N} {}^{(k)}a(t) \qquad (1)$$

where

N = number of sample functions

${}^{(k)}a(t)$ = the kth sample function

$\hat{m}(t)$ = statistical estimate of $m(t)$

Engineering practice indicates that in many cases there is only one sample function of a shock process and, hence, Equation (1) becomes statistically inoperable. Therefore, it is necessary to use alternative techniques which are approximate, but do satisfy the intent of the original definition. The two techniques utilized herein are: (1) Hanning Smoothing of the Acceleration Time-History, and (2) Low-Pass Digital Filtering of the Acceleration Time-History. Both techniques operate on the shock record in such a manner as to eliminate the

high frequency random fluctuations about that part of the process which is defined to be deterministic.

The smoothing of time-history data is standard practice for eliminating random statistical variations which are frequently present. Three point Hanning smoothing is defined as

$$a(t_i) = 0.25a(t_{i-1}) + 0.50a(t_i) + 0.25a(t_{i+1}) \quad (2)$$

where

$a(t_i)$ = value of $a(t)$ at $t = i(\Delta t)$

Δt = time increment

In the above, $^{(k)}a(t) = a(t)$, since N = 1 for the shock data under consideration. The effect of Equation (2) is one of smoothing the time-history while employing a triangular-type local weighting function. After the original shock record is Hanning-smoothed using Equation (2), the resultant time-history may itself be Hanning-smoothed using Equation (2). This process is repeated as many times as desired with visual inspection and the exercise of judgment after every few cycles dictating when the number of smoothings is sufficient.

Figure 1 shows an original ship-shock, acceleration time-history [4]. This record was smoothed utilizing the Hanning scheme and Figures 2 through 4 show several smoothed functions. In this study, one hundred and one Hanning smoothings were used as the basis for defining a "mean value function."

Digital filtering of time histories is performed every time one calculates the response of a single degree-of-freedom oscillator to the support acceleration time-history. The characteristics of the filter are established by taking the Fourier transform of the oscillator's impulse response function. Therefore, the filter characteristics depend upon the type of response calculated (e.g., relative displacement) and the damping and natural frequency of the system.

A low pass filter can be developed using various levels of mathematical sophistication with the "mathematical goodness" of the filter being measured by such items as the time for the transient to attenuate, the sharpness of the filter's upper corner, and the phase lag between original and filtered record. In this study, a simple low-pass filter was used to illustrate a point. The filtered record corresponds to the relative response of a single degree-of-freedom oscillator subjected to a support motion equal to the unfiltered original acceleration time history; i.e.,

$$\ddot{q}(t) + 2\xi\omega_n\dot{q}(t) + \omega_n^2 q(t) = -a(t) \quad (3)$$

where

$a(t)$ = original acceleration time-history

$q(t)$ = low-pass filtered time-history.

The selection of values for damping (ξ) and natural frequency (ω_n) control the form and location of the corner frequency region of the filter.

The acceleration time-history shown in Figure 1 was filtered to obtain an alternate estimate of the mean-value function. Figure 5 shows results for two values of the corner frequency. The results obtained using the low-pass filter are similar to those obtained using the smoothing procedure. However, the filtered records show a significant phase shift which is dependent upon the selected corner frequency.

Since the random portion of the shock process is to be represented by $y(t) = a(t) - m(t)$, phase distortion cannot be tolerated. If it were, $y(t)$ would contain a strong low frequency component, thus defeating its intent. Hanning-smoothing is superior to the use of this simple filter and was therefore used in the present study to evaluate the mean-value function.

RANDOM COMPONENT OF DATA

The previous section discussed the estimation of the mean-value function. This function is visualized as the deterministic component of a stochastic process. When the mean value function is subtracted from the original shock time-history, the stochastic process, denoted by $y(t)$, is obtained; i.e.,

$$y(t) = a(t) - m(t) \quad (4)$$

The stochastic process $y(t)$ is an important characteristic of most shock environments. If the shock time-history $a(t)$ is essentially repeatable, and therefore essentially deterministic, then the amplitude of $y(t)$ will be small compared to the amplitude of $a(t)$. Stated differently, $a(t) \approx m(t)$. Often there is a significant variation among sample records of a "selected process" and hence, the shock process is probabilistic and one must analyze the data accordingly.

The process defined by $y(t)$ can be, and often is, very general in nature. However, as with most practical problems, one seeks to find an idealization which models the process within sufficient engineering accuracy. In this study, $y(t)$ is modeled as a time-modulated nonstationary process. Mathematically, such a process is represented by

$$y(t) = \psi(t)x(t) \quad (5)$$

where

$x(t)$ = stationary random process defined by its power spectral density function

$\psi(t)$ = deterministic time modulating function

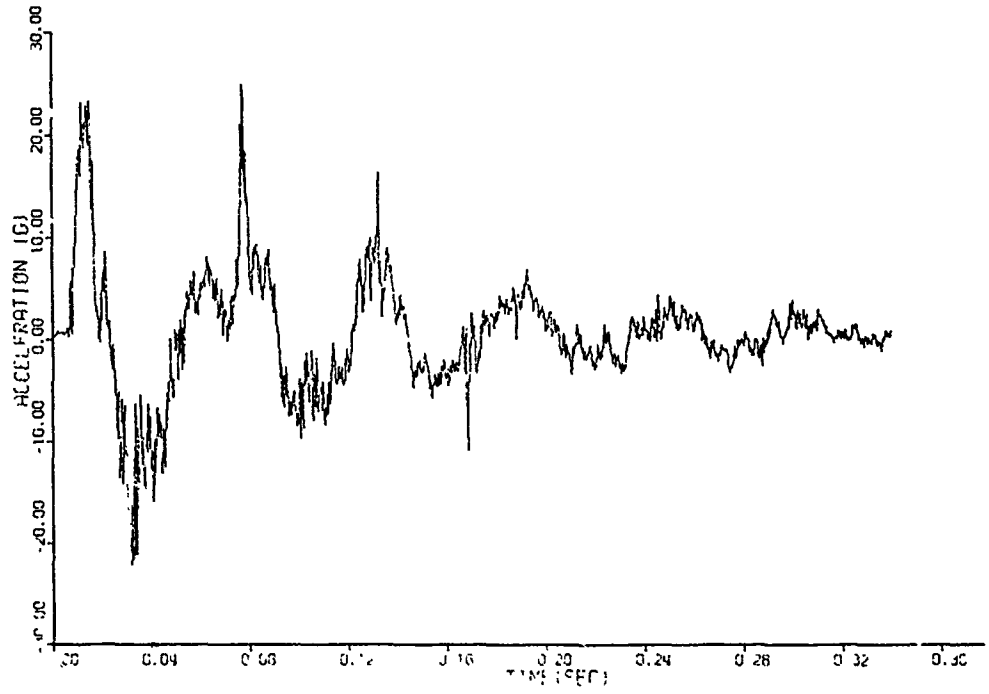

Figure 1. Ship Shock Time History

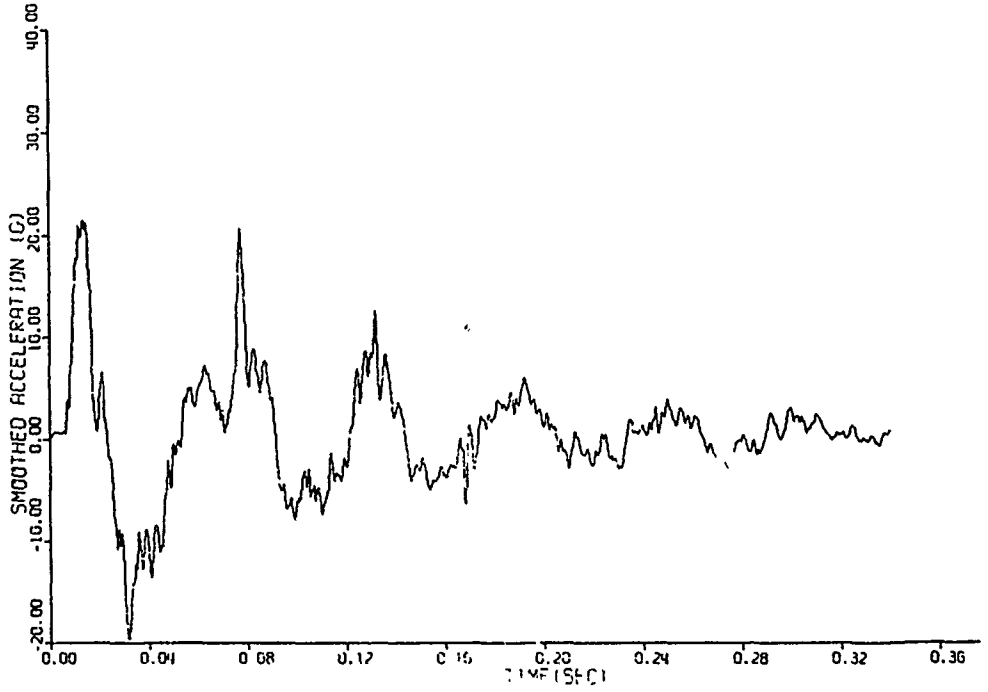

Figure 2. Ship Shock Time History - 3 Hanning Smoothings

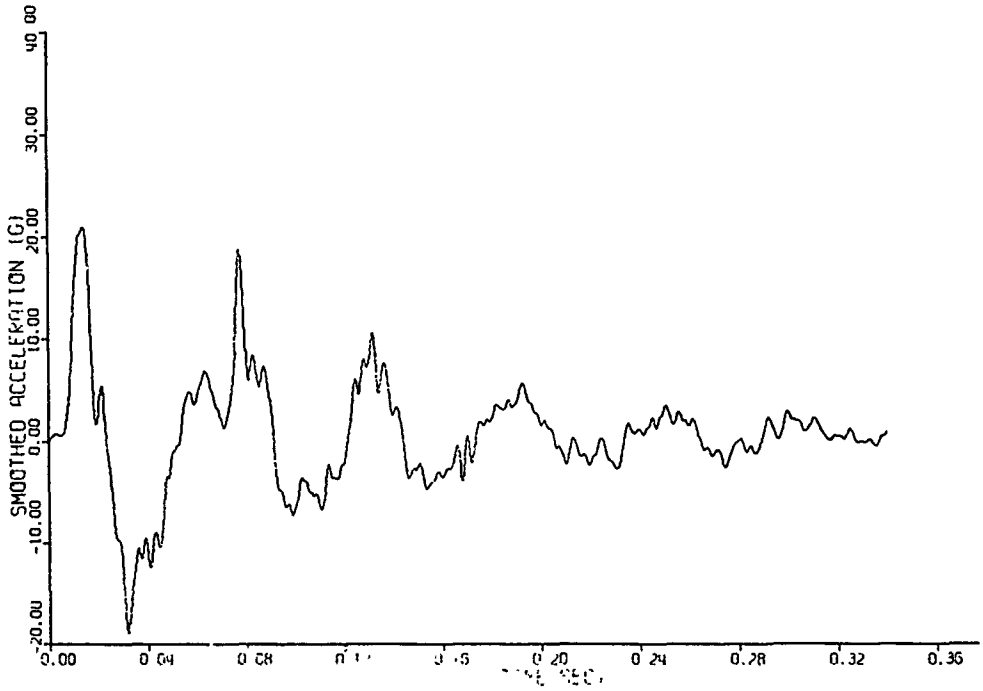

Figure 3. Ship Shock Time History - 21 Hanning Smoothings

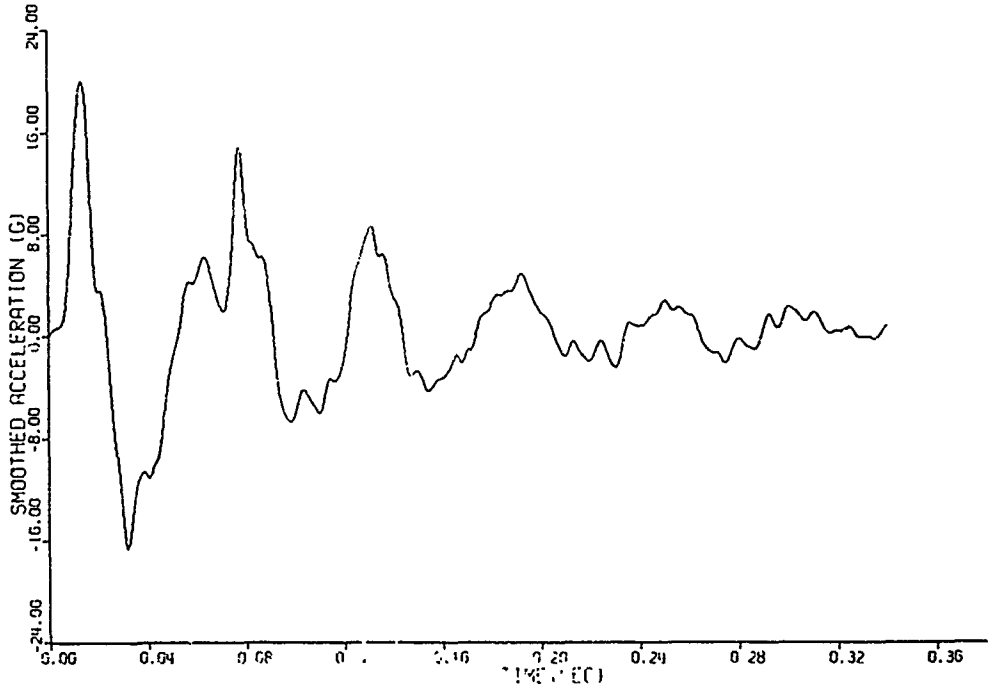

Figure 4. Ship Shock Time History - 101 Hanning Smoothings

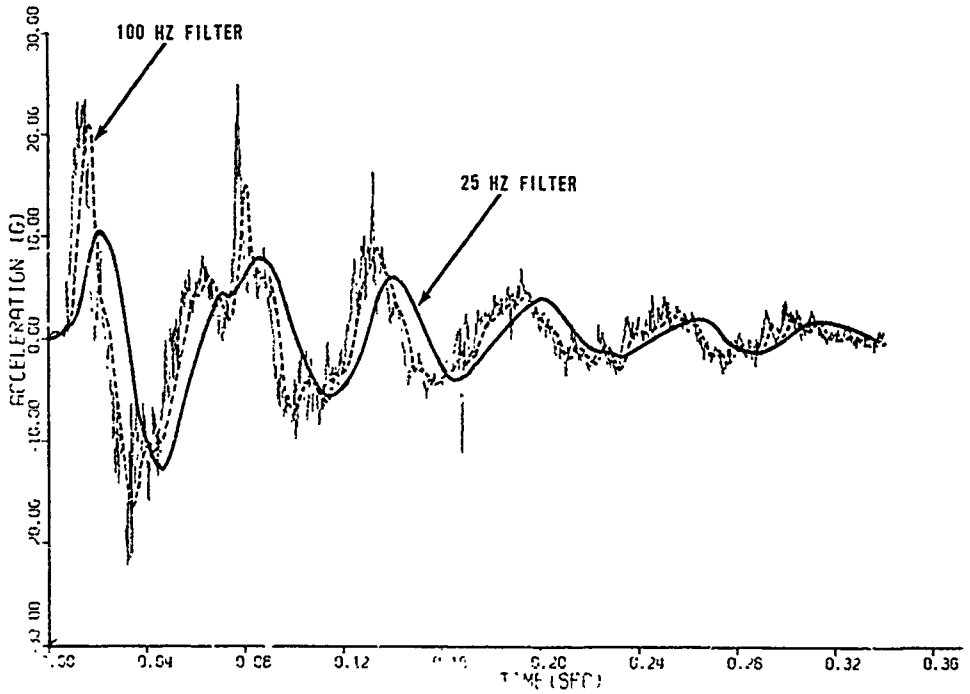

Figure 5. Ship Shock Time History with Filtered Data Imposed

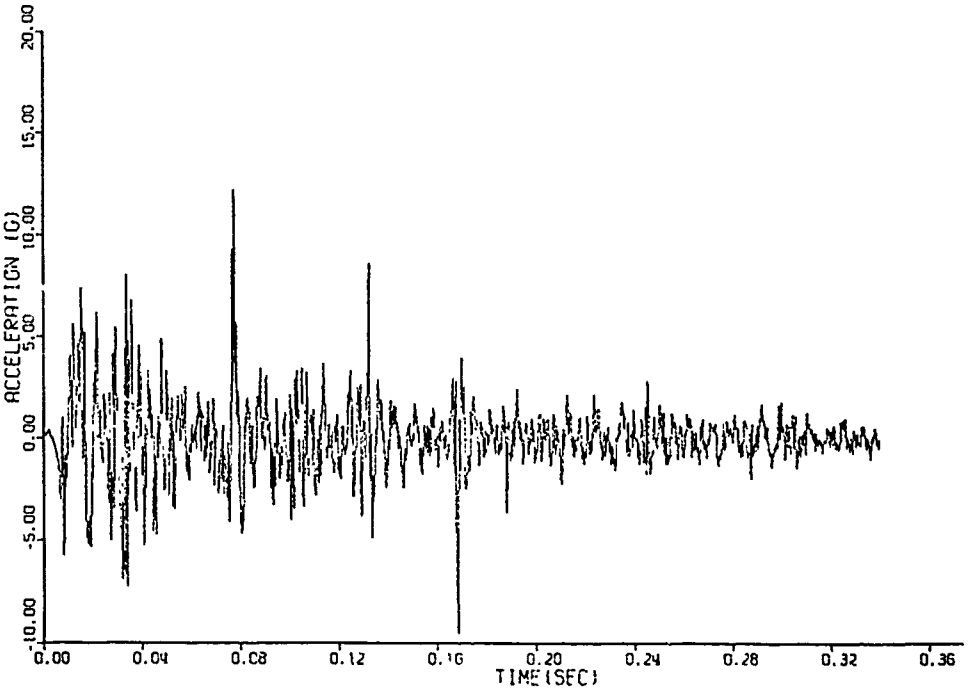

Figure 6. Shock Record minus Mean Value Function

the form of the modulating function is estimated with the aid of the previously discussed Hanning smoothing process. The smoothed root-mea.. square of y(t) can be used to obtain an estimate for $\psi(t)$ The power spectral density function is used to characterize the frequency content of x(t).

The modulating function is estimated using y(t) as defined in Equation (4). The mean-value function shown in Figure 4 is subtracted from the original ship-shock record (see Figure 1) and the resulting time-history is shown in Figure 6.

The root-mean-square (RMS) time-history is related to the record's modulating function [5] and the RMS time-history is obtained when the data are averaged using the equation

$$Y_{RMS}(t_i) = \left\{ \frac{1}{n+1} \left[y^2(t_{i-n/2}) + \ldots + y^2(t_{i-1}) + y^2(t_i) + y^2(t_{i+1}) + \ldots + y^2(t_{i+n/2}) \right] \right\}^{1/2} \quad (6)$$

where

$Y_{RMS}(t_i)$ = root-mean-square response at $t = t_i$

$n+1$ = number of averaging points (odd)

$t_i = i(\Delta t)$

Δt = time increment

The net effect of this averaging process is to smooth out the shock irregularities (peaks) in the record so as to ease interpretation. Figures 7 through 9 show the RMS results using different values for the number of averaging points.

The spikes which appear at the approximate times of 0.08, 0.12, and 0.16 seconds become spread out as the averaging time gets large. Extending the averaging time further leads to a smoother-shaped function resembling a random staircase. From a practical point of view, this might be acceptable, although not intuitively appealing at first glance. The main objection is that if the characteristics of the raw data are to be reproduced, the spikes should be represented as spikes and not spread out. It is possible that the spikes are the result of measurement error; e.g., loose cables, and should be ignored altogether. However, this speculation was not carried further, and an alternative approach was tried in an effort to smooth out the data.

The 21-point RMS record of Figure 8 was Hanning-smoothed 101 times to produce the results shown in Figure 10.

Finally, the decaying exponential also shown in that figure was fit to the data. This function was used in subsequent analyses as the time-modulating function. There is admittedly some ambiguity involved in selecting this function. If a family of similar records were being processed, this function could be defined in precise mathematical terms. When only a single record is being used, there must be some judgment involved.

The power spectral density function is the last of the three characteristic functions needed to define the simulated shock process. The power spectral density function was approximated by the following procedure:

(1) Compute the zero-percent damped pseudo-velocity spectrum for each sample record of the process.

(2) Envelope the peaks of the zero-damped spectra.

(3) Square the envelope function and normalize it to give unit area, i.e., $\sigma^2 = 1$.

The zero-percent damped pseudo-velocity spectrum for each sample was calculated instead of the Fourier modulus because it represents a close upper bound to the Fourier modulus and only an envelope spectrum was sought.

In the present analysis, an autocorrelation function of the form

$$R_x(\tau) = e^{-\alpha|\tau|} \cos p\tau \quad (7)$$

was selected to fit the data. The two parameters α and p define the spread and center frequency of a unimodal power spectral density function

$$S_x(\Omega) = \frac{\alpha}{\pi\left[\alpha^2 + (p-\Omega)^2\right]}\left\{1 - \left[\frac{2p\Omega}{\alpha^2 + (p+\Omega)^2}\right]\right\} \quad (8)$$

By analogy to the frequency response function of a single degree-of-freedom system, the half-power-point bandwidth is approximated by 2α.

Figure 11 shows the enveloped peaks of the zero-damped pseudo-velocity response spectrum for the record. These spectra reflect steps (1) and (2) above. Since the center frequency and bandwidth of Equation (8) can be estimated directly from these envelope functions without squaring and dividing by duration, it is not actually necessary to carry out the third step in this case. If a more general form of PSD were used, step (3) would be carried out and either the resulting PSD would be used directly or an analytic function could be fit by a procedure such as least-squares. Equation (8) was used because the computer program used to evaluate the nonstationary response had this particular function built in.

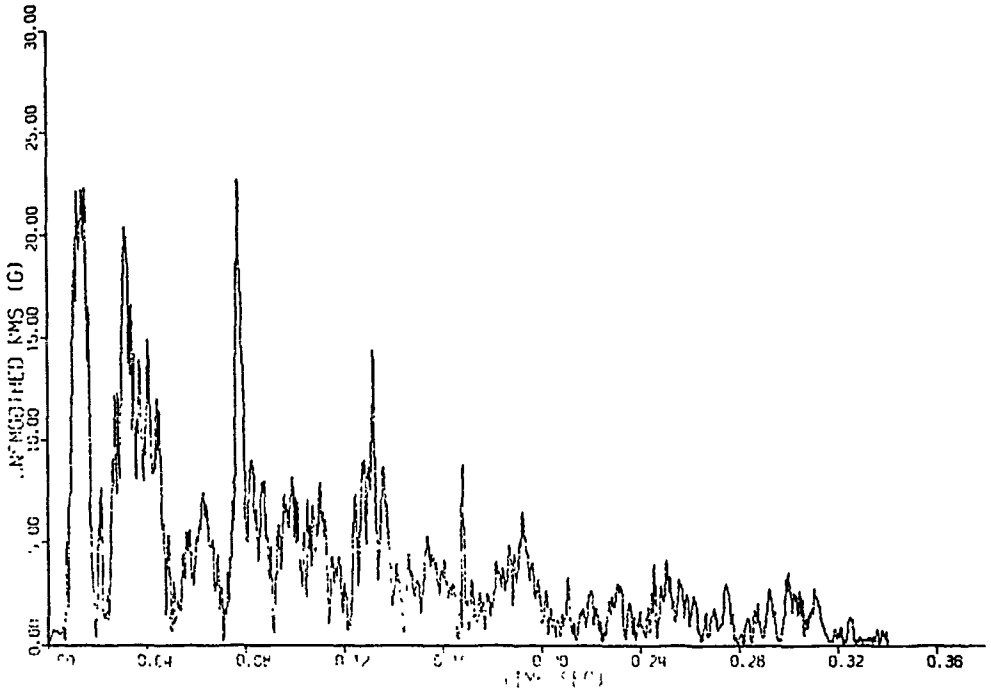

Figure 7. RMS Record - 1 Point Average

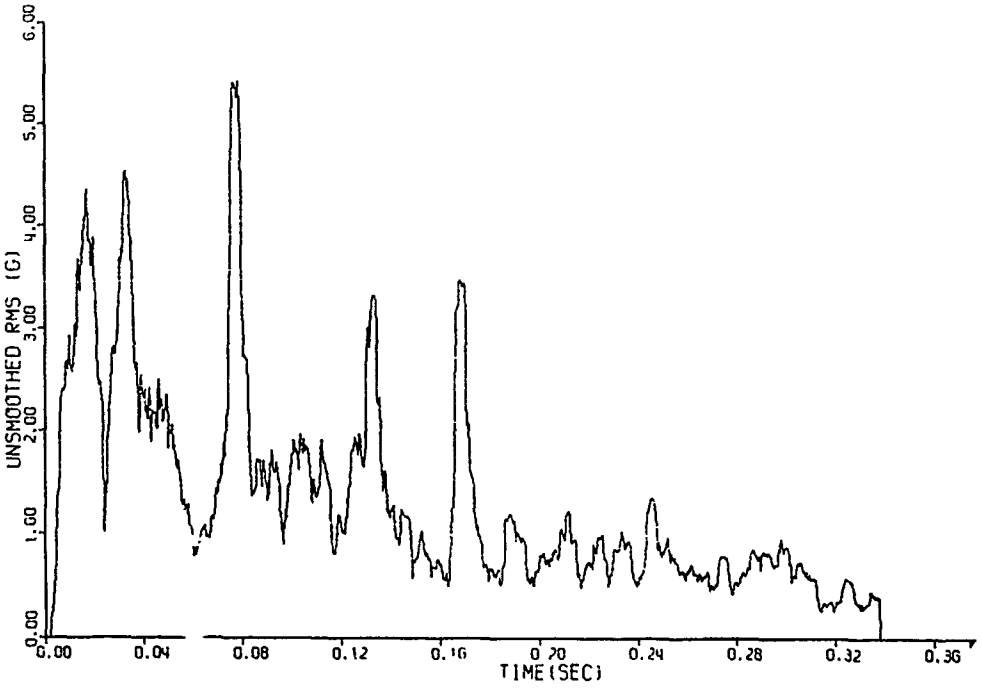

Figure 8. RMS Record - 21 Point Average

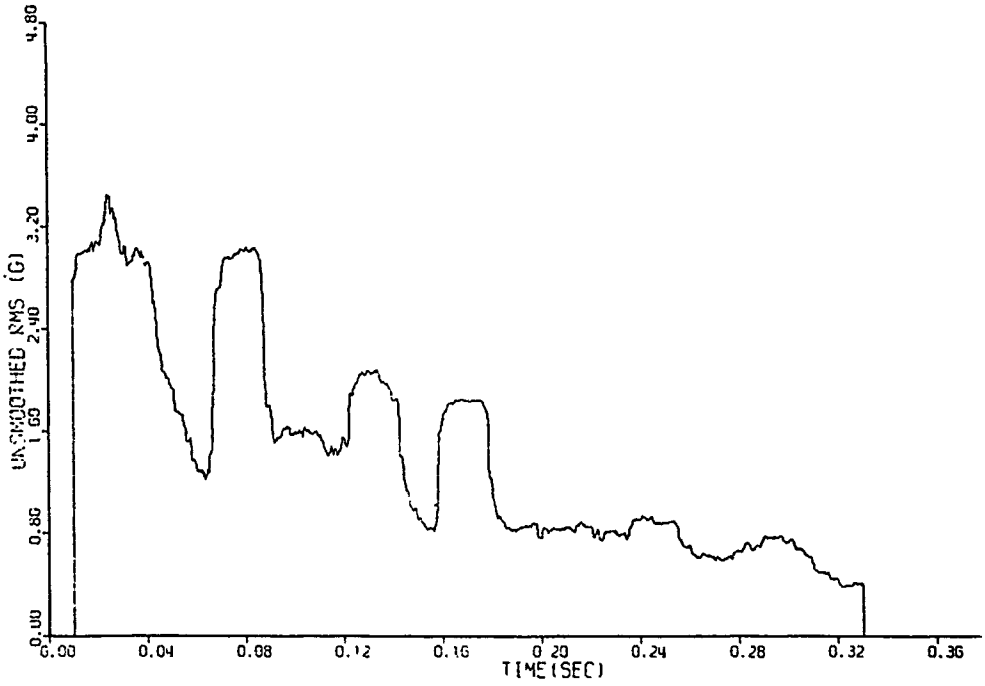

Figure 9. RMS Record - 101 Point Average

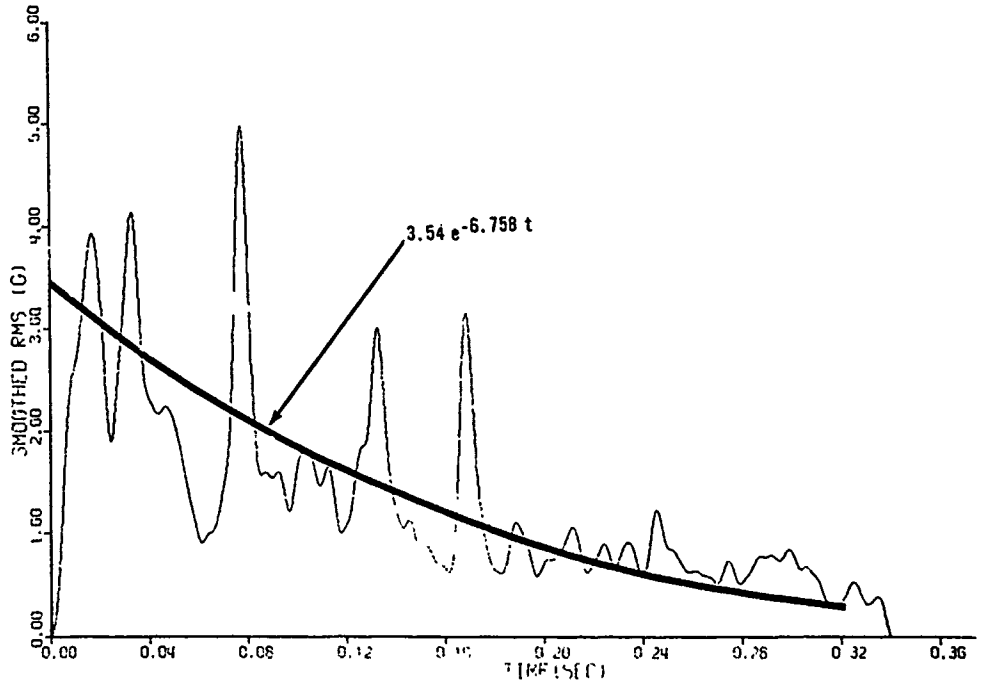

Figure 10. Smoothed RMS Record - 21 Point Average, 101 Hanning Smoothing

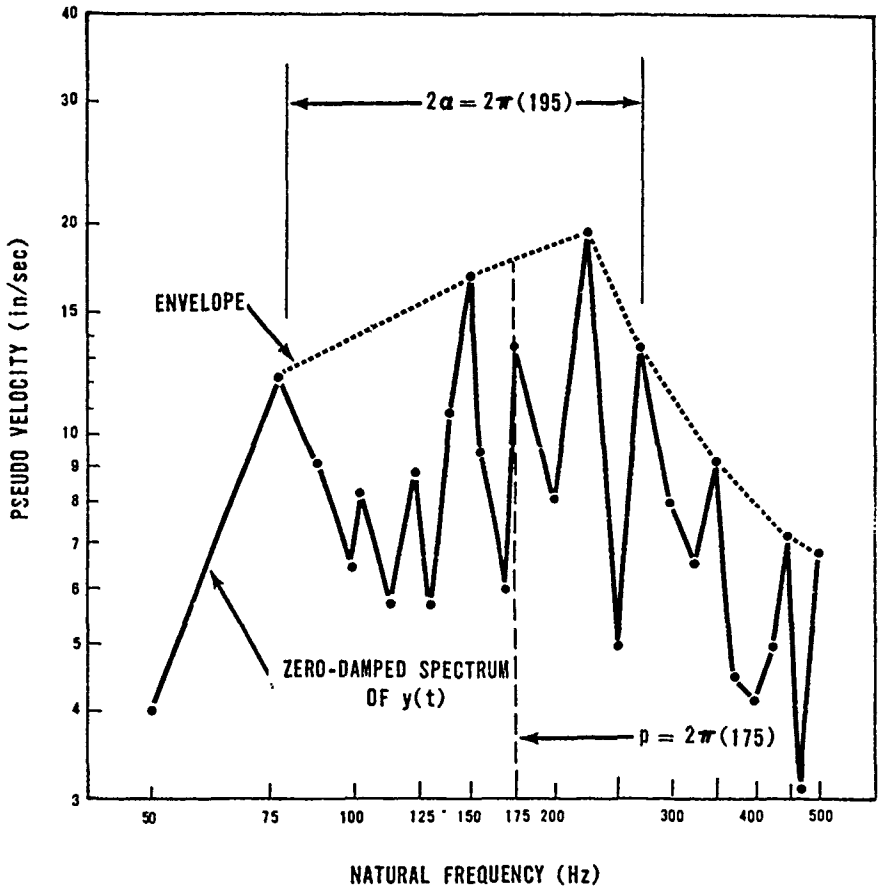

Figure 11. Pseudo-Velocity Spectrum for the Ship Shock Record

SPECTRAL CHARACTERIZATION OF SHIP SHOCK DATA

The response of a single-degree-of-freedom oscillator to base acceleration is an important part of most structural design considerations. If the structure mounted on its support can be modeled as a single-degree-of-freedom system, then the response solution provides an exact analytical-response solution. When the structure must be modeled using more than one degree of freedom, response spectra procedures are applicable.

Shock spectra have been used for many years in vibration analysis. When the base acceleration time-history is considered to be deterministic, the shock spectrum is unique. A probabilistic shock spectrum may be derived when the input is stochastic. The response in this case may be expressed in probabilistic terms or confidence levels.

Probabilistic shock spectra were computed from the simulated shock processes $a(t) = m(t) + \psi(t)x(t)$. For each oscillator natural frequency and damping ratio, a deterministic response to $m(t)$ and a nonstationary RMS response to $\psi(t)x(t)$ were computed. The latter utilized the method of Reference [6]. These response time histories were added for the 1σ, 2σ and 3σ cases, i.e., the mean plus one, two or three standard deviations. The resulting time-histories were scanned for absolute response peaks to establish each point over the frequency spectrum. Figures 12 and 13 show these response levels for the ship shock data under consideration.

The deterministic spectrum should be viewed as resulting from the deterministic response analysis of one sample function. The magnitude of the spectrum at each frequency point is thus a random variable and hence when one analyses a measured shock record for a particular value of oscillator natural frequency, one obtains only one sample point. Figures 12 and 13 compare the probabilistic and deterministic spectra. These figures show that the deterministic spectra exhibit this randomness and correspond to different mean plus standard deviation levels at different values of oscillator natural frequency.

Direct component response points are also indicated in Figures 12 and 13. They represent peak response measurements of equipment components mounted on the deck of the ship, at the predominant frequencies of their oscillation. While these points are rather crudely estimated, they do provide a realistic reference for comparing the probabilistic and deterministic spectra. It should be understood that the shock records associated with "direct component response" were measured somewhere on the component away from its base, whereas the shock records used to compute response spectra were measured at the base of such components.

Probabilistic spectra can be used in design because once a confidence level is set for the design, the corresponding response amplitude follows directly. Based upon a comparative study of the type shown in Figures 12 and 13, one can determine the level of confidence, or probability of exceeding, deterministic response spectra amplitudes.

DESIGN CONSIDERATIONS

The preceding sections demonstrated, using actual ship shock data, a proposed characterization procedure. The procedure has the advantage of being compatible with nonstationary probabilistic-response techniques and also test-simulation techniques. This section takes a critical look at the procedure. It seeks to address important items which should be considered during the development of any standard design specification. Each of the three phases of the characterization (mean-value function, envelope function, and power spectra) are addressed separately.

Basic concerns in the definition of a ship shock mean-value function are its repeatability and its general applicability to many ship positions. With only one ship shock test, repeatability cannot be statistically verified. Other considerations such as "least favorable response" may apply here. In order to obtain a purely statistical statement of reliability many shock tests must be performed. Therefore, engineering experience must be used to verify that the general characteristics of the estimated mean-value function are acceptable. For example, the general rigid-body motions of the ship must be present in the data. If a general design standard is sought for application at many locations throughout the ship, then the mean-value function which must be characterized for design may reflect an average waveform. From a numerical analysis standpoint (i.e., smoothing, low-pass filtering, etc.) amplitude variations are not of major significance because the random component of the data provides a compensating buffer. Stated differently, since the random component is obtained from the original record by subtracting the mean, it represents and includes all amplitude differences.

The envelope function was obtained herein using the root mean square of the shock record [5]. This method of estimation is particularly useful when an analytical form for the modulation function is sought because visual inspection of the RMS record very often provides significant guidance. As an alternative to this approach one can estimate the modulating function from the energy content of the random component of the shock record [5]. This procedure involves integrating the square of the shock record and, therefore, tends to smooth out its shape. However, it is possible to relate the total energy of the shock's random component of motion to the modulating function, and this is a very important consideration. It was shown here that the general shape of the modulating function is stable with smoothing and this is important from

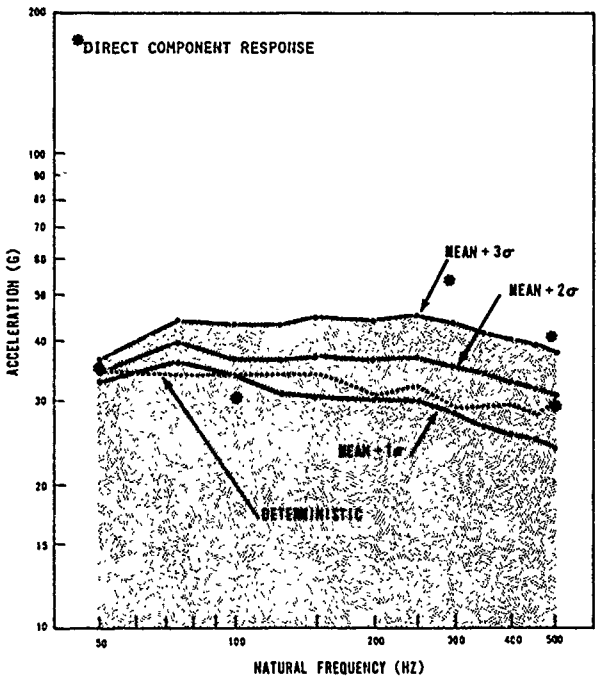

Figure 12. Deterministic and Probabilistic Spectra, 5% Damping

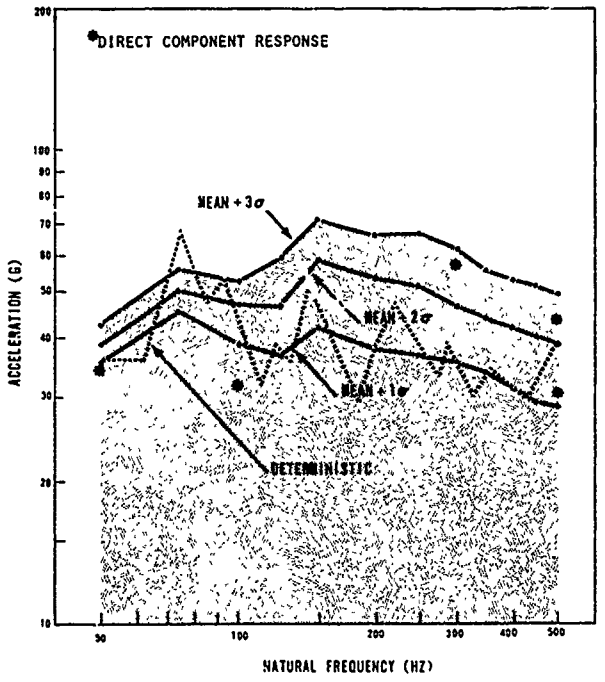

Figure 13. Deterministic and Probabilistic Spectra, 1% Damping

an estimation point of view. In the ship shock record discussed herein the general character of the exponential decay is evident in Figures 7 to 9. In the extension and generalization of the envelope function for ship shock specifications it is possible, and seems important, to relate the modulating function's intensity parameter (i.e., the 3.54 value for the shock under study) to a physically meaningful quantity. The total energy of the shock process is a particularly good way to quantify this parameter.

A final item which must be addressed is the power-spectral-density (PSD) function of the random component of motion. The shape of the PSD must be quantified for shock specification. However, only the shape need be specified since its area is unity. For narrow banded spectra (i.e., bandwidth less than 20% of the center frequency), the spectral shape in the vicinity of the center frequency is most critical. The use of the enveloped zero-percent damped shock spectrum in lieu of the Fourier spectrum may be used when only one shock record is analyzed because it provides an upper bound for the record. Finally, it may happen that the frequency content of the random component of the shock varies with time (i.e., different pulse arrivals with correspondingly unique frequency content). The characterization procedure described herein is sufficiently general to incorporate such a process with only minor modification. In particular, Equation (5) can be expanded to take on the form

$$y(t) = \psi(t)[x_1(t) + x_2(t) + \ldots + x_n(t)] \tag{9}$$

or alternatively the form

$$y(t) = \psi_1(t)x_1(t) + \psi_2(t)x_2(t) + \ldots + \psi_n(t)x_n(t) \tag{10}$$

CONCLUSIONS

A practical method for characterizing shipboard shock, leading to the derivation of consistent design and test criteria, has been demonstrated with actual shock data. The method involves application of modern analytical and experimental techniques. A particular shock environment is first modeled as a nonstationary random process characterized by a zero mean with time-varying intensity, superimposed upon a deterministic time-varying mean. The parameters of this model may be derived from measured shock data even when limited data are available. This representation of the shock process enables probabilistic shock spectra to be computed directly without recourse to Monte Carlo methods. These shock spectra constitute a valid basis for design specification. Simulated shock motions may be generated from the same model and may be input to a shaker system for laboratory testing. The parameters of the simulated shock process provide a basis for test specification.

Since the design spectra and the test environment are both derived from the same idealization of the measured shock process, they are inherently consistent.

In addition to providing a basis for developing consistent design and test criteria, the proposed approach offers other advantages over currently used techniques:

1. The method is very flexible in that a broad range of shock environments can be simulated. Shock motion measured on the superstructure of a ship can be simulated as readily as keel shock.

2. Equipment hardness can be established quantitatively on the basis of probabilistic concepts which are mathematically tractable as well as practical to implement in the test lab. Any number of simulated shock transients can be generated for input to the test article.

3. In addition to enhancing the reliability of test hardware, the generation of a random shock environment for test purposes should minimize problems of shaker control since only statistical parameters of the simulated environment need be controlled, not individual waveforms themselves.

While it is recognized that implementation of these methods would indeed require a significant developmental effort, the potential payoff is great in terms of increased equipment reliability and its ability to withstand anticipated shock environments. The basic tools are available. It is time they were put to use.

ACKNOWLEDGMENT

This work was sponsored by the Naval Weapons Center at China Lake, California, under Contract Numbers N60550-74M-G582 and N60530-75M-278W.

REFERENCES

1. Hasselman, T.K., W.N. Jones, and G.C. Hart, "Characterization of Shipboard Shock for Design and Test," SAE Paper 74080, presented at SAE National Aerospace and Engineering Meeting, San Diego, Calif., October 1-3, 1974.

2. Favour, J.D., J.M. LeBrun, and J.P. Young, "Transient Waveform Control of Electromagnetic Test Equipment." Shock and Vibration Bulletin, Vol. 40, Part 2 (December 1969), pp. 157-171.

3. Drenick, R.F., "Aseismic Design by Way of Critical Excitation," J. Engr. Mech. Div., ASCE, Vol. 99, No. EM4, August 1973.

4. Cornelius, K.T., "The Effects on Weapon Systems of Shock Tests on USS Stoddert (DDG-22)(U)," Department of the Navy, David Taylor Model Basin, Encl. (1) to DTMB ltr. Ser. 0647 of 18 June 1965.

5. Saragoni, G.R., and G.C. Hart, "Simulation of Artificial Earthquakes." Journal of Earthquake Engineering and Structural Dynamics, Vol. 2, 1974.

6. Hasselman, T.K., "Linear Response to Non-stationary Random Excitation," Journal of the Engineering Mechanics Division, ASCE, Vol. 98, No. EM3, Proc. Paper 8961, June 1972, pp. 519-530.

Discussion

Mr. Bolton (Westinghouse Electric Corp.): I was a little surprised by your terminology of random. This is the first time I have heard of a characterization of a multiperiodic or a non periodic system as random. Is that really correct?

Mr. Hart: It depends on where you went to school. I think it is a commonly understood definition in the sense that there are several text books and major universities where that characterization or that particular definition is used. I think the time modulated non station approach is common in that sense.

Mr. Bolton: There are certain disagreements with the terminology. You characterize the higher frequency record as stationary random, does this neglect damping of the higher frequency modes?

Mr. Hart: First of all this is a non stationary process. It is a special class of a non stationary process; but we are talking about characterizing the record and I was not using any particular damping values in characterizing the record. In developing the shock spectrum from that particular record the damping values were selected at 1% a 5% critical damping, but that was only after the record was characterized completely and the response due to a single degree of frequency oscillator was determined. That was the only point where the damping was entered into the system. I might refer you to Bendat's and Piersol's book on random data analysis. I think that might also answer your first question.

Mr. Forkois (Naval Research Laboratory): I gathered from your presentation that the inclusion of the high frequency components which have high acceleration values raises the level of the spectrum but the energy content is significantly smaller than those of the low frequency content; would you care to comment on this?

Mr. Hart: I didn't really calculate the energy content of the mean value function and then the fan the random fluctuation so I can't comment on their relative total energy in each one. The only thing I can say is that there was a significant difference between the response of the oscillator due to just the mean and the response of the oscillator due to the mean plus one standard deviation, so I would be inclined to believe that the energy content from the high frequency part of the record was significant.

Mr. Rzepka (Naval Surface Weapons Center): Has this actually been applied to any test specification for any item yet?

Mr. Hart: I think we would be happy to apply it if you would fund it. The answer to your question is that we would hope that we would apply it; two small contracts have been funded by the Naval Weapons Center and the procedure has been clearly demonstrated to be appropriate in my opinion and it should be applied. Your question whether it will be applied is one that is not always technical.

Mr. Rzepka: If this procedure is applied does it constitute qualification for shipboard shock as the Navy defines qualification for shipboard shock at the present time, like MIL-S-901C?

Mr. Hart: I can't answer that.

Mr. Rzepka: Has anybody presented this to NAVSEC to see whether this would either take the place of MIL-S-901C or if you could qualify your item for MIL-S-901C?

Mr. Hart: I don't know.

PLANE HARMONIC WAVES IN LIQUID OVERLYING A MONOCLINIC, CRYSTALLINE LAYER

SAGADHAR DE
Old Engineering Office (Qrs.), P.O. Santiniketan,
Birbhum, West Bengal (India)

The boundary value problem concerning the propagation of plane harmonic waves in liquid overlying an infinite, monoclinic, crystalline layer of finite depth is solved. Solution of the frequency equation is obtained and the dispersion curves are presented. Some interesting particular cases are derived and new results are given. The results thus obtained in the case of crystalline media are clarified in contrast with an elastic isotropic case or with an orthorhombic material.

INTRODUCTION

The problem of the wave propagation of Rayleigh type in a system consisting of a liquid layer of finite depth overlying a semi-infinite homogeneous isotropic o transversely isotropic elastic medium has been discussed by numerous investigators [b-f]. The author [h-j] recently investigated some problems of the propagation of Love waves in liquid and crystalline media. The author [k] further discussed the problem of the formation of stationary waves in an infinite, monoclinic, crystal plate. In the present problem, the propagation of plane harmonic waves in liquid resting on an infinite, monoclinic, crystalline layer of finite depth is investigated. The layer of water is bounded on one side by the ocean bottom, and on the other side by the surface of water.

The dispersion equation is obtained. Phase velocities of the waves are calculated numerically as functions of wave number and the dispersion curves are presented. The results are compared with those obtained when the solid medium is isotropic or nonisotropic. Some particular cases are discussed and interesting results are presented.

FUNDAMENTAL EQUATIONS

We choose the rectangular coordinate system. Let the liquid has density ρ_1, bulk modulus λ_1, and has depth h.

The equation of motion in the liquid can be expressed in terms of the displacement potential Φ_1 given by [b]

$$\frac{\partial^2 \Phi_1}{\partial x_2^2} + \frac{\partial^2 \Phi_1}{\partial x_3^2} = \frac{1}{v_1^2} \frac{\partial^2 \Phi_1}{\partial t^2} , \qquad (1)$$

where $v_1 = (\lambda_1/\rho_1)^{1/2}$ is the velocity of sound in the liquid. The displacement, u_1, in the liquid is given by

$$u_1 = \Phi_{1x_2} \qquad (2)$$

and the pressure, p, in the liquid is given by

$$p = -\rho_1 \frac{\partial^2 \Phi_1}{\partial t^2} . \qquad (3)$$

Let the waves in the liquid have wave number k and phase velocity v in the x_3-direction. So, the displacement potential can be written in the form

$$\Phi_1 = \Phi_1^{(0)}(x_2) \exp\{ik(x_3 - vt)\} . \qquad (4)$$

Using (1) and (4), we get

$$\Phi_1 = \left[A\cos(\kappa_0 x_2) + B\sin(\kappa_0 x_2)\right] \times \exp\left\{i\kappa(x_3 - vt)\right\}, \tag{5}$$

where A, B are any two constants,

and $$k_0^2 = \kappa^2\left(v^2/v_1^2 - 1\right). \tag{6}$$

Let the liquid layer stands on an infinite, monoclinic, crystalline layer of finite thickness, H. We consider waves with normal in the direction of x_3 and displacement in the direction of x_1. The stress-strain relation of a rotated -Y-cut quartz plate, referred to a rectangular cartesian coordinate system x_1, x_2, x_3 with x_1 a diagonal axis, exhibits monoclinic symmetry [1]. For a monoclinic crystal, we have

$$c_{15} = c_{25} = c_{35} = c_{45} = c_{16} = c_{26} = c_{36} = c_{46} = 0, \tag{7}$$

c_{qr} = elastic constants.

We use an abbreviated notation where a pair of indices which range over the integers 1, 2, 3 is replaced by a single index ranging over the integers 1, 2, 3, 4, 5, 6 according to the scheme given below :

Replace ij =	11	22	33	23 or 32	31 or 13	12 or 21
by q =	1	2	3	4	5	6

Stress equations of motion

$$\begin{aligned} T_{1,1} + T_{6,2} + T_{5,3} &= \rho\ddot{u}_1 \\ T_{6,1} + T_{2,2} + T_{4,3} &= \rho\ddot{u}_2 \\ T_{5,1} + T_{4,2} + T_{3,3} &= \rho\ddot{u}_3 \end{aligned} \tag{8}$$

where, dot denotes partial differentiation with respect to time and a (a = 1, 2, 3) denotes the partial derivative, $\partial/\partial x_a$.

$$T_q = c_{qr}S_r, \quad (q, r = 1, 2, 3, 4, 5, \text{ or } 6) \tag{9}$$

where

$$\begin{aligned} S_1 &= u_{1,1}, \quad S_2 = u_{2,2}, \quad S_3 = u_{3,3}, \\ S_4 &= u_{3,2} + u_{2,3}, \quad S_5 = u_{1,3} + u_{3,1}, \\ S_6 &= u_{2,1} + u_{1,2} \end{aligned} \tag{10}$$

We write simply $u_1 = u$ and $(x_1, x_2, x_3) = (x, y, z)$ respectively. Now, assuming

$$u = U(y)e^{ik(z-vt)}, \quad u_2 = u_3 = 0, \tag{11}$$

we have

$$\begin{aligned} T_1 &= T_2 = T_3 = T_4 = 0, \\ T_5 &= c_{55}\frac{\partial U}{\partial z} + c_{56}\frac{\partial U}{\partial y}, \\ T_6 &= c_{56}\frac{\partial U}{\partial z} + c_{66}\frac{\partial U}{\partial y}. \end{aligned} \tag{12}$$

The only non-vanishing equation of motion will now take the form

$$\frac{d^2U}{dy^2} + \alpha\frac{dU}{dy} + \beta U = 0, \tag{13}$$

where

$$\alpha = \frac{2c_{56}i\kappa}{c_{66}}, \quad \beta = \frac{\kappa^2\left(\rho_2 v^2 - c_{55}\right)}{c_{66}}, \tag{14}$$

ρ_2 is the density of the monoclinic, crystalline layer. The solution of equation (13) is given by

$$U = \exp\left(-\alpha y/2\right)\left[C\cos my + D\sin my\right], \tag{15}$$

where C, D are any two constants, and

$$\begin{aligned} m &= \kappa\left\{\frac{\gamma_{55}}{c_{66}}\left(v^2/v_2^2 - 1\right)\right\}^{1/2}, \\ \gamma_{55} &= c_{55} - c_{56}^2/c_{66}, \\ v_2^2 &= \gamma_{55}/\rho_2 . \end{aligned} \tag{16}$$

BOUNDARY CONDITIONS

The boundary conditions are the vanishing of pressure at the free surface of the liquid and the continuity of stresses and normal displacement at the liquid-crystal interface. Thus for all z and t, we have

$$\begin{aligned} p &= 0 \quad \text{on} \quad y = -h \\ T_6 &= -p \quad \text{on} \quad y = 0 \\ (u)_1 &= (u)_2 \quad \text{on} \quad y = 0 \\ T_6 &= 0 \quad \text{on} \quad y = H . \end{aligned} \tag{17}$$

FREQUENCY EQUATION AND DISPERSION CURVES

Using (5), (9), (15) and (17), we get

$$\tan\left[\kappa h\left(v^2/v_1^2 - 1\right)^{1/2}\right] = -\frac{\left\{\gamma_{55}c_{66}\left(v^2/v_2^2 - 1\right)\left(v^2/v_1^2 - 1\right)\right\}^{1/2}}{c_{11}v^2} \times \tan\left[\frac{\kappa H}{c_{66}}\left\{\gamma_{55}c_{66}\left(v^2/v_2^2 - 1\right)\right\}^{1/2}\right]. \tag{18}$$

This is the frequency equation. The wavelength $2\pi/k$ is a multi-valued function of the phase velocity, v, each value corresponding to a different mode of propagation.

The group velocity can be calculated from the formula

$$U_g = v + \kappa \frac{dv}{d\kappa}$$

$$\text{or, } U_g/v_1 = \varkappa + \gamma \frac{d\varkappa}{d\gamma}, \qquad (19)$$

where

$$\gamma \equiv \kappa h, \quad \varkappa \equiv v/v_1 .$$

We take the dates for sodium thiosulfate crystal (monoclinic, density (ρ_2) = 3.3 gms./c.c.) for the crystalline layer (cf. [a_7]).

$$c_{55} = 11.1, \quad c_{66} = 6.0, \quad c_{56} = 7.4,$$

$$v_2 = 0.7206 \text{ km./sec}$$

If the crystalline layer is replaced by orthorhombic material (say, barytes type, density = 4.50 gms./c.c.), we have

$$c_{55} = 12.0, \quad c_{66} = 27.7, \quad v_2 = 1.833 \text{ km./sec.}$$

For the isotropic material (density = 2.72 gms./c.c.), we take

$$c_{55} = c_{66} = \mu = 31.5, \quad v_2 = 3.4031 \text{ km./sec.}$$

(All the above elastic constants are measured in units of 10^{10} dynes/cm.^{2})

For the liquid layer, we take $v_1 = 1.440$ km./sec. density (ρ_1) = 1.0025 gms./c.c.

The dispersion relation is studied for various values of H/h for the crystalline, orthorhombic and isotropic cases. The nature of the dispersion curve (variation of the phase velocity with the wave number) in each case is shown in Figs. 1, 2 and 3 respectively.

The displacement in the liquid layer is expressed as

$$u_1 = K_0 \{-A \sin K_0 y + B \cos K_0 y\} \exp\{ik(x - vt)\} \qquad (20)$$

and so the amplitude variation is given by

$$A_{n,v} = \left[-\tan\left\{kh\left(v^2/v_1^2 - 1\right)^{1/2}\right\} \sin\left\{k\gamma\left(v^2/v_1^2 - 1\right)^{1/2}\right\} + \cos\left\{k\gamma \times \left(v^2/v_1^2 - 1\right)^{1/2}\right\}\right] . \qquad (21)$$

The amplitude variation of the wave with respect to y in relation with the computed phase velocity, v, (for the first mode) in each case is shown in Fig.4.

LIMITING CASES

(i) As $v \to v_2$, we have

$$kh \to n\pi v_1/\left(v_2^2 - v_1^2\right)^{1/2}, \quad n = 1, 2, 3, \ldots \qquad (22)$$

(ii) As $v \to v_1$, $kh \to n\pi/\left(v^2/v_1^2 - 1\right)^{1/2} \to \infty$. (23)

(iii) As $Kh \to 0$ (the waves have wavelengths large compared with the depth of the liquid layer and thus the effect of the layer is negligible), we have

$$kH\left\{\frac{c_{55}}{c_{66}}\left(v^2/v_2^2 - 1\right)\right\}^{1/2} \to n\pi$$

i.e.,

$$\omega^2 = \frac{c_{66}}{\rho_2}\left(\pi/H\right)^2\left[n^2 + \frac{c_{55}}{c_{66}}\left(\frac{kH}{\pi}\right)^2\right], \qquad (24)$$

$$(n = 0, 1, 2, \ldots).$$

This gives the frequency of the thickness-twist mode of vibration of the crystal layer.

Introducing as a reference frequency the frequency, ω_s, of the lowest x-y thickness-shear mode of a uniform plate of thickness H, i.e.

$$\omega_s = \frac{\pi}{H}\left(c_{66}/\rho_2\right)^{1/2}, \qquad (25)$$

we find for the nondimensional frequencies, Ω_n, of the n th mode of thickness-twist,

$$\Omega_n \equiv \frac{\omega_n}{\omega_s} = \left[n^2 + \frac{c_{55}}{c_{66}}\left(\frac{kH}{\pi}\right)^2\right]^{1/2}. \qquad (26)$$

In Fig.5 the nondimensional frequencies, Ω_n, are plotted as functions of K^2.

(iv) As $Kh \to \infty$ (the wavelength becomes small compared with the depth of the layer), we have

$$\tan\left[\frac{kH}{c_{66}}\left\{c_{55}c_{66}\left(v^2/v_2^2 - 1\right)\right\}^{1/2}\right] = -\frac{\rho_1 v^2}{\left\{c_{55}c_{66}\left(1 - v^2/v_1^2\right)\left(v^2/v_2^2 - 1\right)\right\}^{1/2}} . \qquad (27)$$

This equation is identified as the dispersion equation of Love waves in a crystalline layer. If v be the common wave velocity along the interface, we must have

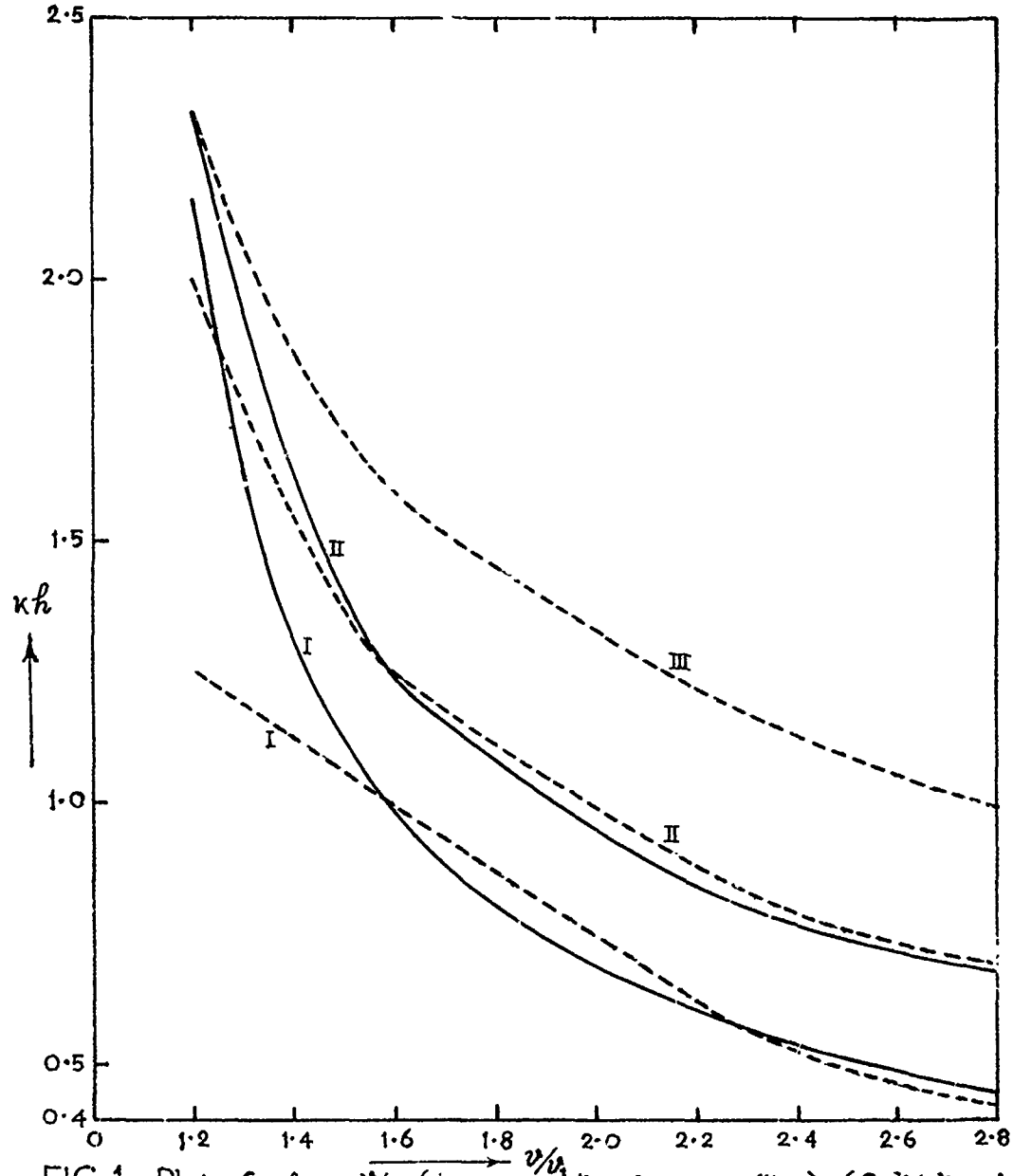

FIG.1. Plot of κh vs. v/v_1 (Lower medium is crystalline). (Solid line is for $H/h = 0.5$, dotted line is for $H/h = 2.0$, I = first mode, II, III etc. = higher modes).

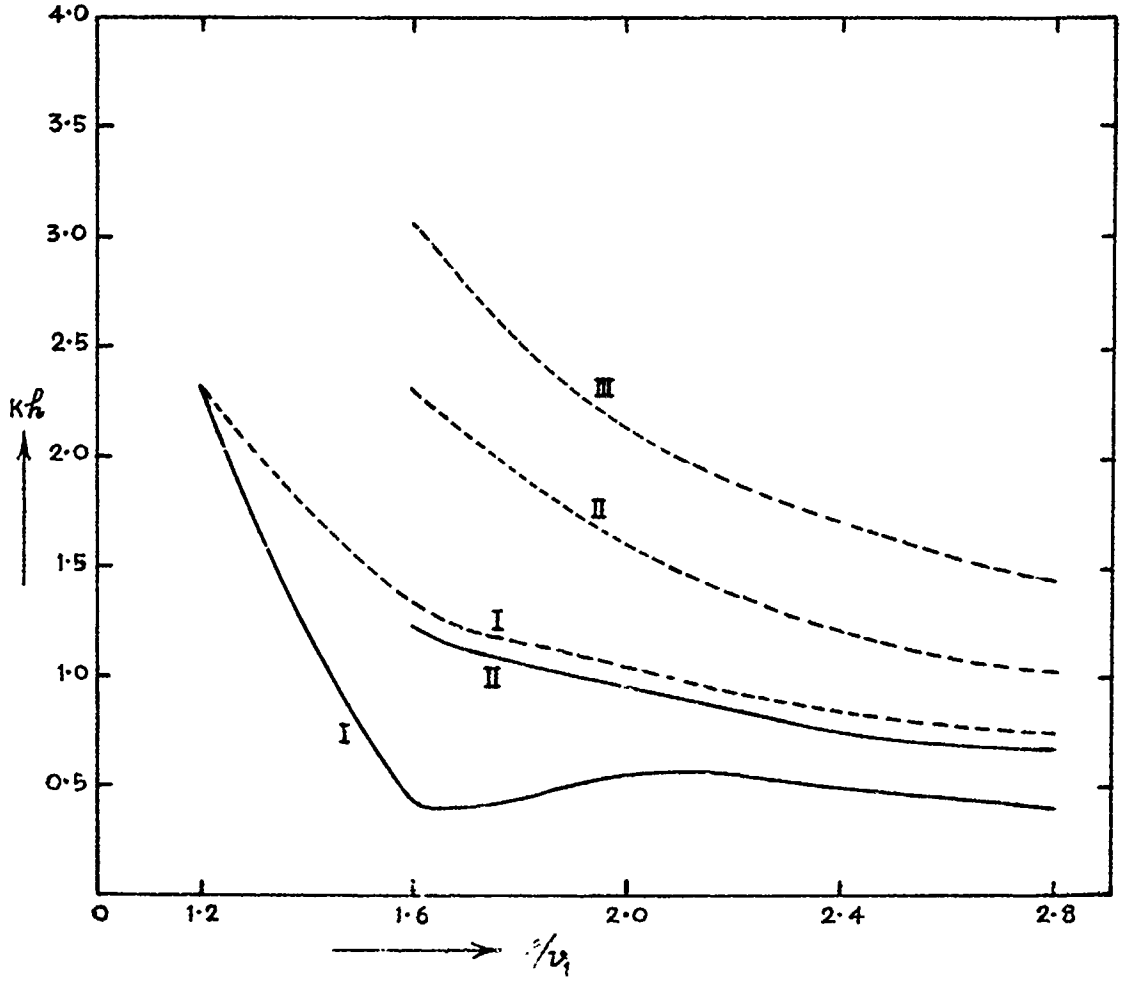

FIG. 2. Plot of Kh vs. v/v_1 (Lower medium is anisotropic).
(Solid line is for $H/h = 0{\cdot}5$, dotted line is for $H/h = 2{\cdot}0$).

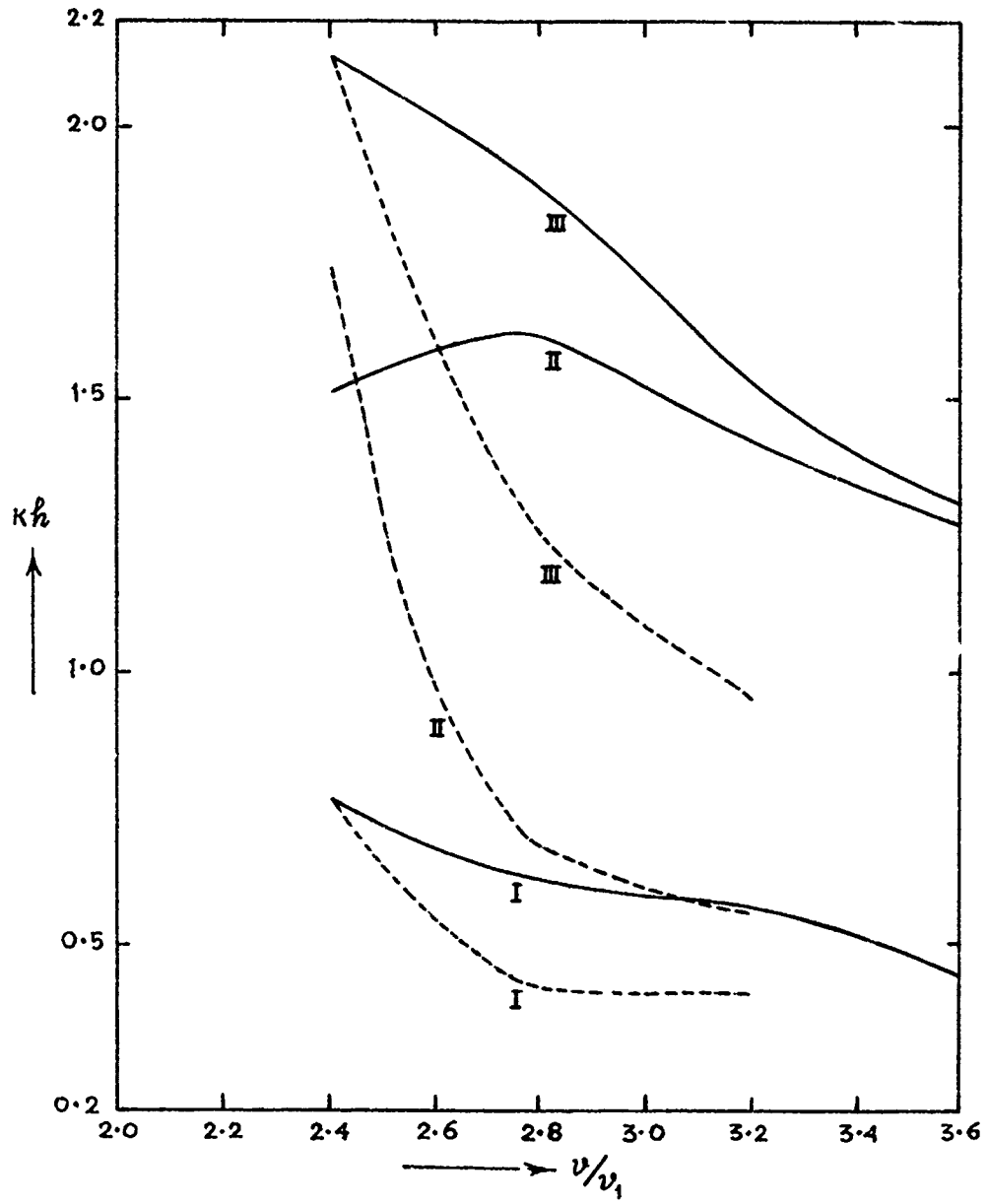

FIG. 3. Plot of Kh vs. v/v_1 (Lower medium is isotropic)
(Solid line is for $H/h = 0{\cdot}5$, dotted line is for $H/h = 0{\cdot}2$).

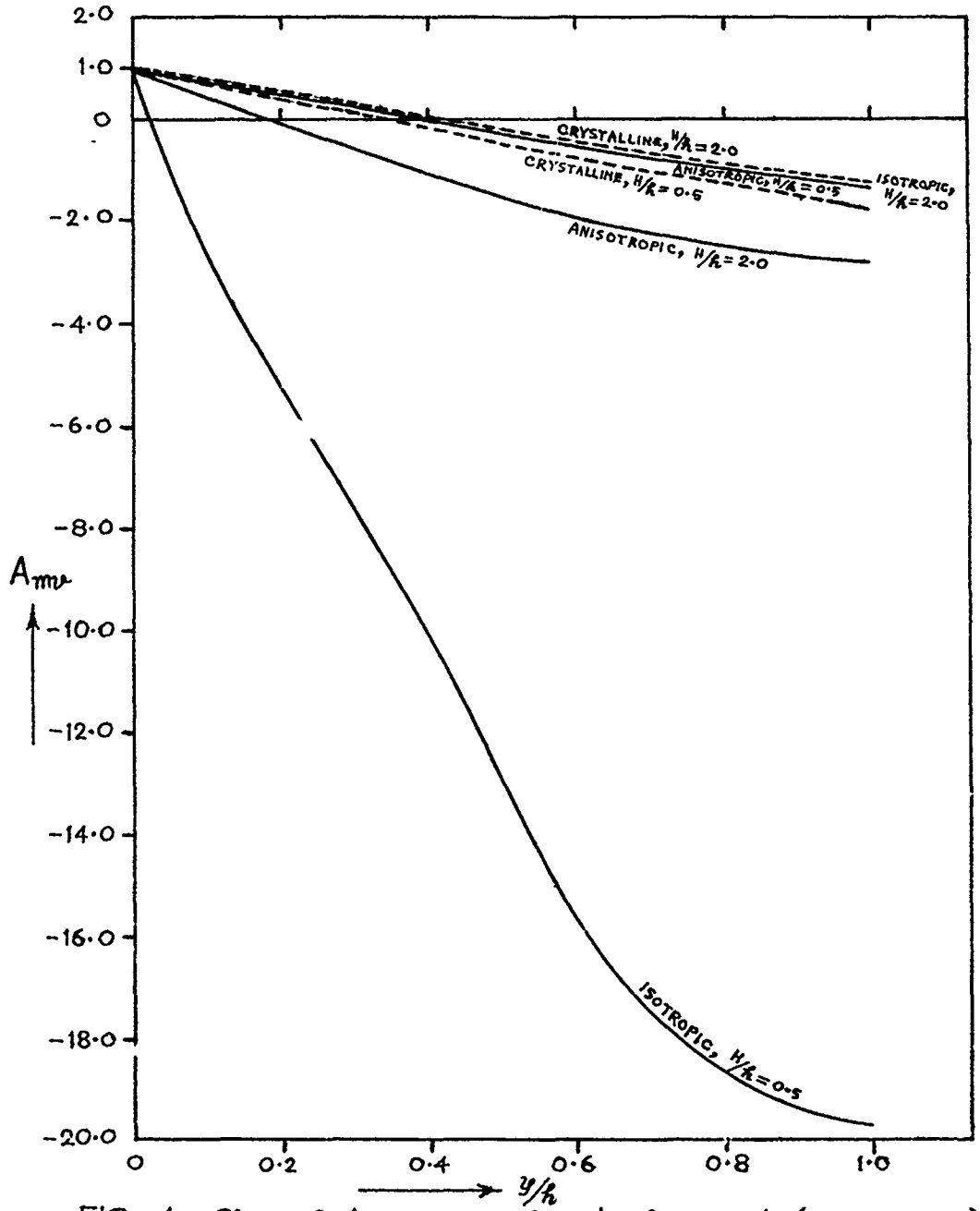

FIG. 4. Plot of A_{mv} vs. y/h for the first mode ($v = 4.0320$).

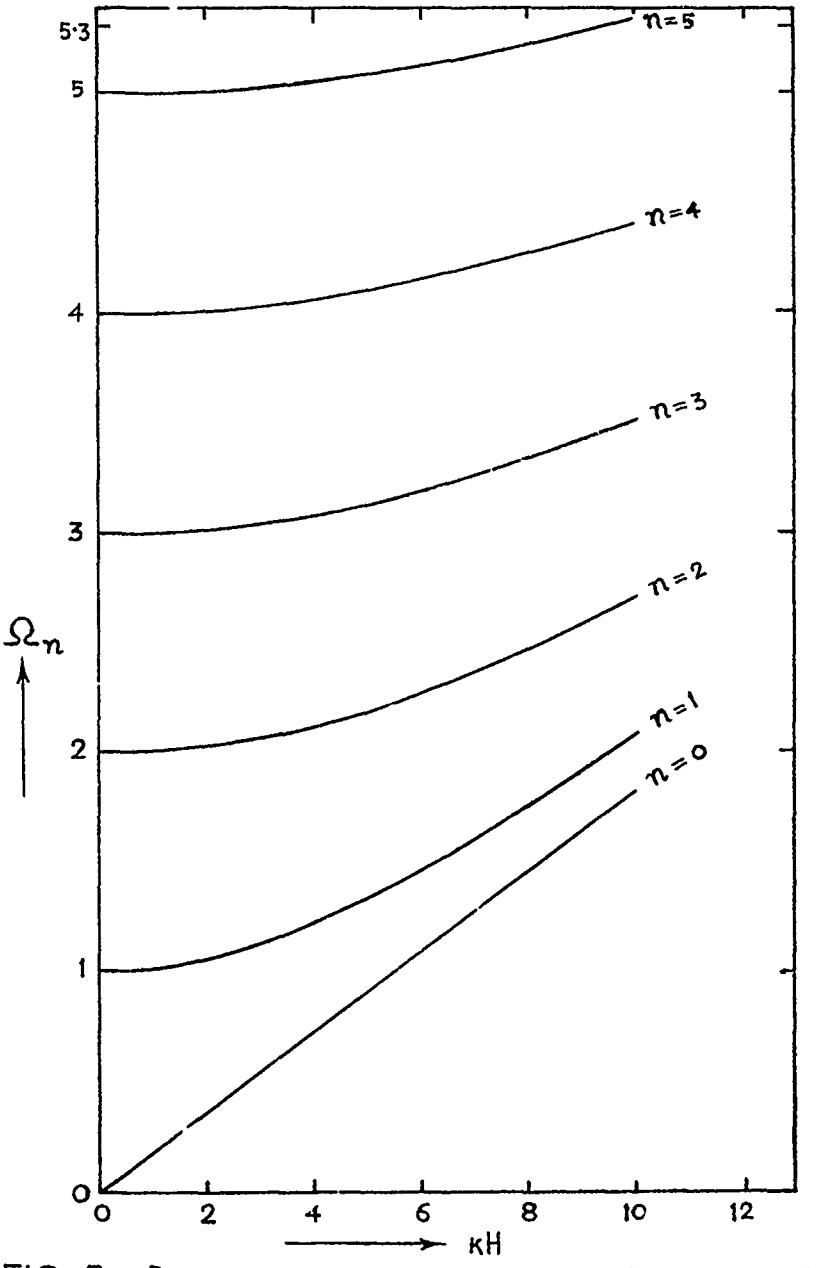

FIG. 5. Dimensionless frequencies as a function of KH.

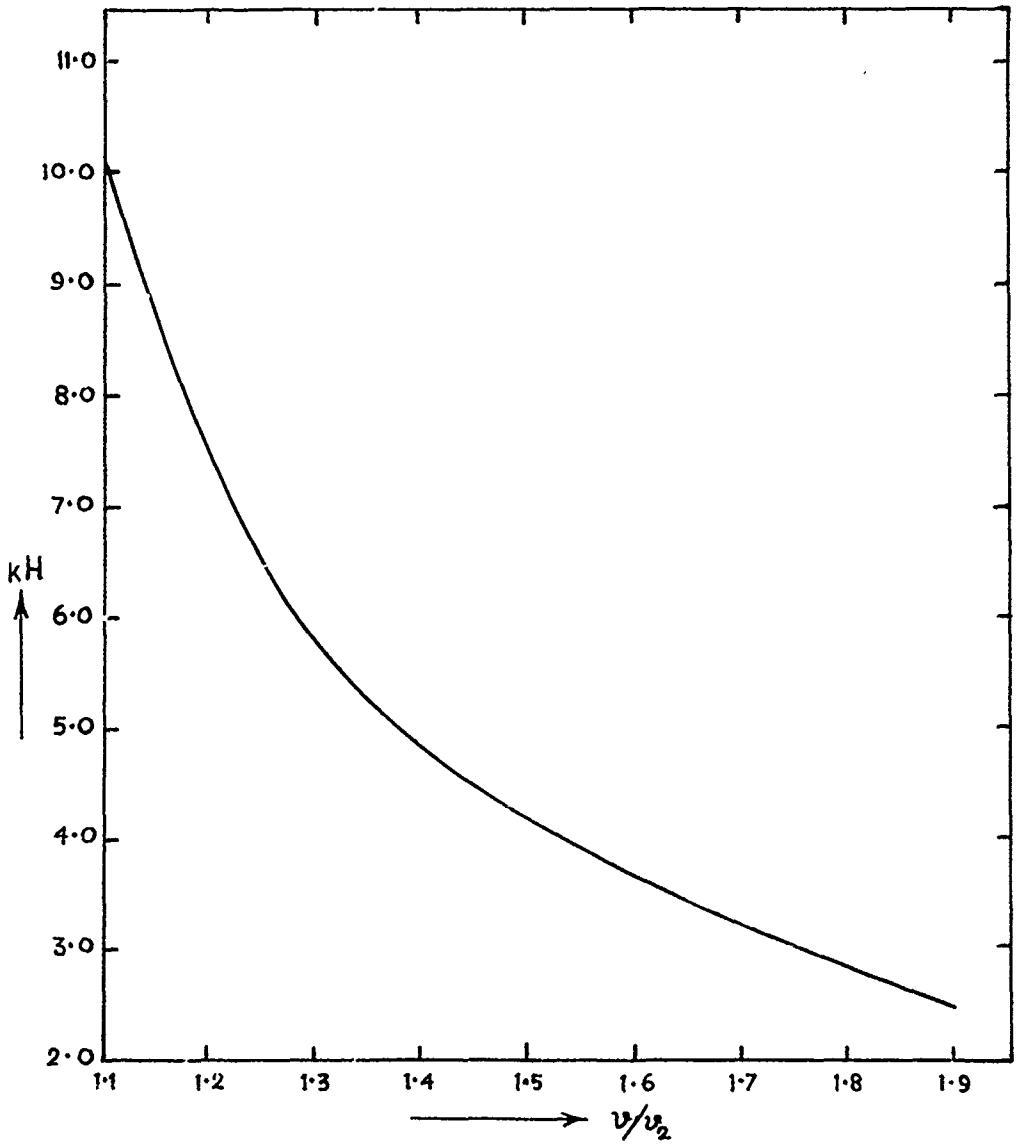

FIG. 6. Plot of kH vs. v/v_2

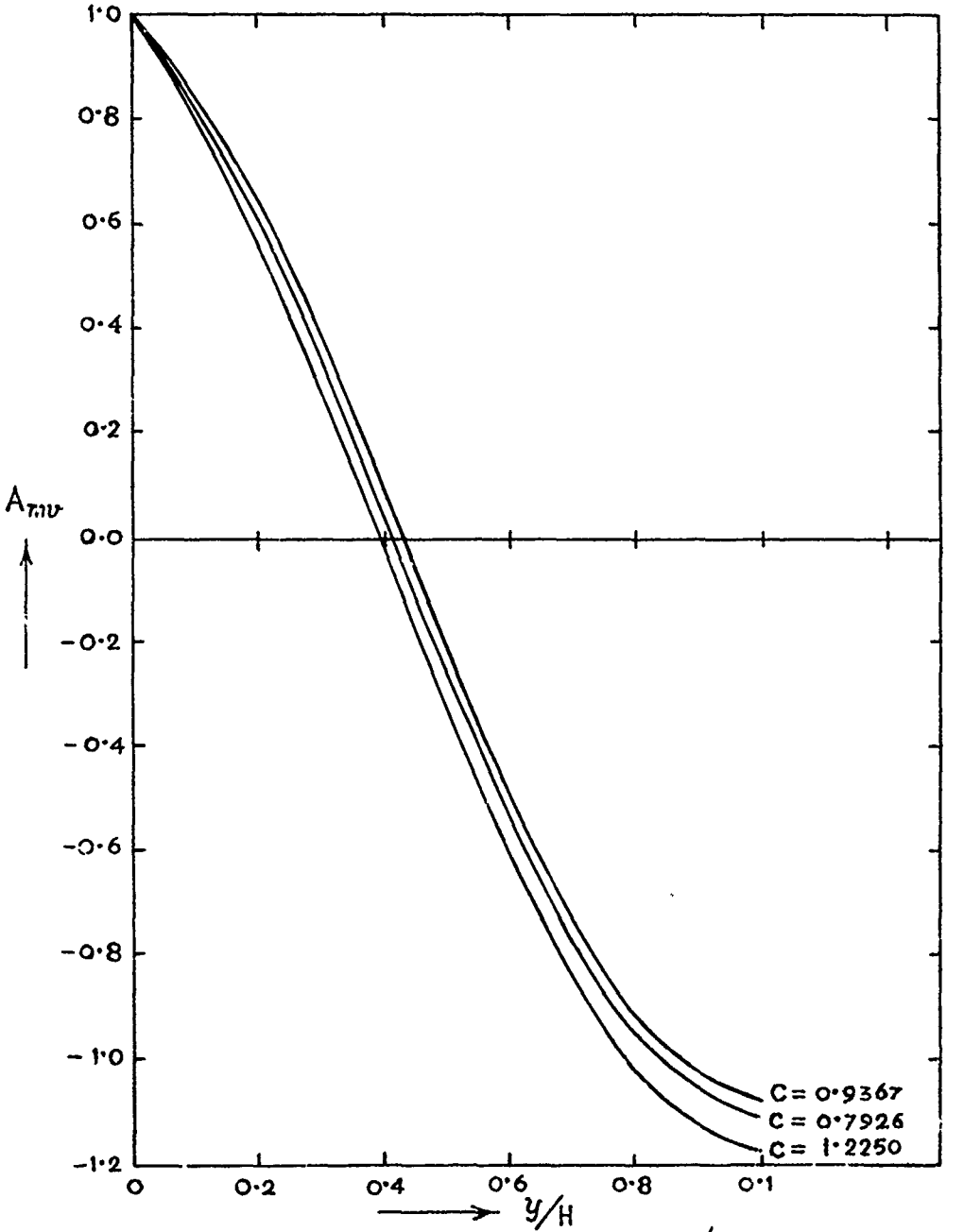

FIG. 7. Plot of A_{mv} vs. y/H.

$$v_2 < v < v_1$$

The amplitude of the waves in the crystalline layer varies as (C cos ny + D sin ny) and so the amplitude variation is expressed as

$$A_{nv} = \cos\left[k\gamma\left\{\frac{\gamma_{55}}{c_{66}}\left(v^2/v_2^2 - 1\right)\right\}^{1/2}\right] + \tan\left[\frac{kH}{c_{66}}\left\{\gamma_{55}c_{66}\left(v^2/v_2^2 - 1\right)\right\}^{1/2}\right] \times \sin\left[k\gamma\left\{\gamma_{55}c_{66}\left(v^2/v_2^2 - 1\right)\right\}^{1/2}\right]. \quad (28)$$

The dispersion relation is shown in Fig.6 and the amplitude variation with respect to y for different values of v is shown in Fig.7. Although the computed values of phase velocity correspond to all greater than $\pi/2$, the Love waves discussed here is seen to be the fundamental mode (cf. [1]).

ACKNOWLEDGMENT

The author is grateful to the C.S.I.R. (New Delhi) for the financial support.

REFERENCES

[a] D.E. Gray (Co-ordinating editor), American Institute of Physics Hand Book, 3rd ed., pp.2-58, 1972. (R.F.S. Hearmon, "The Elastic Constants of Anisotropic Materials -II," Advances in Physics, Vol.5, 323, 1956).

[b] I. Abubakar and J.A. Hudson, "Dispersive Properties of Liquid Overlying an Aeolotropic Half-space," Vol.5, No.5, Part-I, pp.217-223, Part-II, pp.223-229, 1961.

[c] I. Tolstoy, "Dispersive Properties of a Fluid Layer Overlying a Semi-infinite Elastic Solid," Bull. Seismol. Soc. Am., Vol.44, pp.493-512, 1954.

[d] M.A. Biot, "The Interaction of Rayleigh and Stoneley Waves in the Ocean Bottom," Bull. Seismol. Soc. Am., Vol.42, pp.81-93, 1952.

[e] R. Stoneley, "The Transmission of Rayleigh Waves across an Ocean Floor with Two Surface Layers," Part-I : Theoretical, Bull. Seismol. Soc. Am., Vol.47, pp.7-12, 1957.

[f] R. Stoneley, "The Effect of the Ocean on Rayleigh Waves," Mon. Not. R Astro. Soc. Geophys. Suppl., Vol.I, pp.349-56, 1926.

[g] R.D. Mindlin, "Thickness-Twist Vibrations of an Infinite, Monoclinic, Crystal Plate," Int. J. Solids Structures, Vol.1, pp.141-145, 1965

[h] S. De, "On the Propagation of Love Waves in a Liquid Layer," Geophys., (Submitted), 1975.

[i] S. De, "On the Propagation of Love Waves in a Crystalline Medium," Jr. Phys. Earth, Vol.23, No.3, pp. 219-226, 1975.

[j] S. De, "Love Wave Dispersion in Crystalline Media Due to Irregularities in Thickness of the Layer," Geophysical Res.Bull.(In press), 1975.

[k] S. De, "Formation of Stationary Waves in an Infinite Monoclinic, Crystal Plate," Bull.De L'Acad. Polo. Des Sciences, Vol.23, No.1, pp.29-32, 1975.

[l] W.P. Mason, Piezoelectric Crystals and Their Applications to Ultrasonics, D. Van Nostrand Company, New York, 1950.

[m] W.M. Ewing, W.S. Jardetsky and F.Press, Elastic Waves in Layered Media, McGraw-Hill, 1957.

POWER SERIES EXPANSION OF THE DYANMIC STIFFNESS MATRIX INCLUDING ROTARY INERTIA AND SHEAR DEFORMATION

Mario Paz and Lam Dung
University of Louisville
Louisville, Kentucky

The dynamic stiffness matrix for a beam element is derived from the Timoshenko differential equation with the inclusion of rotary inertia and a shear deformation. The terms of this matrix are expanded into a power series as a function of the vibrating frequency. It is shown that the first two terms of the resulting series correspond respectively to the stiffness and mass matrices, which are usually derived in the technical literature from assumed static displacement functions. Higher order terms up to the second order are also obtained explicitly. Also a discussion is presented for establishing the region of convergence of the series expansion.

INTRODUCTION

The dynamic analysis of frame-type structures whose members have distributed mass is usually sought by transforming the continuous structure into an approximate discrete system [1]. The derivation of the required stiffness, mass, and geometric matrices is generally obtained from static displacement functions. The process of discretizing based on the classical Bernoulli-Euler theory of flexural vibration or on the more accurate Timoshenko beam theory results in transcendental trigonometric and hyperbolic functions [2]. Mathematical singularities and the complexity of these functions [3] make the Bernoulli-Euler or Timoshenko beam theory less attractive than the approximate method of discretizing.

It is noteworthy that the stiffness, mass, and geometric matrices derived from static displacement functions have also been obtained through a power series expansion of the general stiffness matrix based on Bernoulli-Euler beam theory [4]. The stiffness and mass matrices are in fact the first-order terms of the resulting series expansion. Second-order terms have also been obtained [4] and higher-order matrices could be obtained simply by extending the series expansion. This mathematical approach delineates the range of convergence of the series. Hence, it provides the analytical basis to ascertain the approximations inherent in the heuristic derivation of the stiffness, mass, and geometric matrices from static displacement functions.

The power series expansion of the dynamic stiffness matrix based on the Bernoulli-Euler beam theory does not account for rotary inertia and shear deformation effects. As an extension of previous work, in the present paper the derivation of the stiffness and mass matrices is obtained by expanding in power series the dynamic stiffness matrix based on the Timoshenko beam theory which includes rotary inertia and shear deformation.

DYNAMIC STIFFNESS MATRIX

The Timoshenko beam equation may be written conveniently in the notation used by Snowdon [5] as

$$\frac{\delta^4 y}{\delta \lambda^4} + (n\alpha)^2(\alpha+\beta)\frac{\delta^2 y}{\delta \lambda^2} + (n\alpha)^2[(n\alpha)^2\alpha\beta - 1]y = 0 \qquad (1)$$

where k' is a shearing constant depending on the shape of the cross-section,

$$n^4 = \frac{\omega^2\rho}{Er^2} \qquad \lambda = \frac{X}{a}$$

$$\alpha = \frac{r^2E}{ka^2G} \qquad L = 2a \qquad (2)$$

$$\beta = \frac{r^2}{a^2} \qquad I = Ar^2$$

The dynamic stiffness matrix based on equation (1) is found by solving this equation and imposing the pertinent boundary conditions [3].

In reference to the coordinates indicated in Fig. (1) the final form of the dynamic stiffness matrix relating end harmonic forces and displacements is given by equation (3)

$$\begin{pmatrix} V_i \\ M_i \\ V_j \\ M_j \end{pmatrix} = \begin{bmatrix} S_{11} & \text{Symmetric} & & \\ S_{21} & S_{22} & & \\ S_{31} & S_{32} & S_{33} & \\ S_{41} & S_{42} & S_{43} & S_{44} \end{bmatrix} \begin{pmatrix} \delta_i \\ \theta_i \\ \delta_j \\ \theta_j \end{pmatrix} \qquad (3)$$

where

$$S_{11} = B\left[\frac{n^4}{\theta\eta}(\eta^2+\theta^2)(\eta cS+\theta sC)\right] \qquad (4)$$

$$S_{21} = Bn^4\left[\left(\frac{\theta^2-\eta^2}{\theta\eta}\right)(1-cC) + 2sS\right] \qquad (5)$$

$$S_{22} = B(\theta^2+\eta^2)(\theta cS-\eta sC) \qquad (6)$$

$$S_{31} = -Bn^4\left(\frac{\theta^2+\eta^2}{\theta\eta}\right)(\eta S+\theta s) \qquad (7)$$

$$S_{32} = B(\theta^2+\eta^2)s\eta(c-C) \qquad (8)$$

$$S_{33} = B\frac{n^4}{\theta\eta}(\theta^2+\eta^2)(\eta cS+\theta sC) \qquad (9)$$

$$S_{41} = B(\theta^2+\eta^2)\theta\eta(c-C) \qquad (10)$$

$$S_{42} = B(\theta^2+\eta^2)(\theta S-\eta s) \qquad (11)$$

$$S_{43} = -Bn^4\left[\left(\frac{\theta^2-\eta^2}{\theta\eta}\right)(1-cC) + 2sS\right] \qquad (12)$$

$$S_{44} = B(\theta^2+\eta^2)(\theta cS-\eta sC) \qquad (13)$$

$$B = \frac{EI}{2\theta\eta(1-cC)+(\eta^2-\theta^2)sS} \qquad (14)$$

and

$$(2\theta a)^2 = (na)^4(\alpha+\beta)+\sqrt{(na)^8(\alpha-\beta)^2+4(na)^4}$$

$$(2\eta a)^2 = -(na)^4(\alpha+\beta)+\sqrt{(na)^8(\alpha-\beta)^2+4(na)^4} \qquad (15)$$

$$s = \sin\theta a\lambda \qquad S = \sinh\eta a\lambda$$

$$c = \cos\theta a\lambda \qquad C = \cosh\eta a\lambda$$

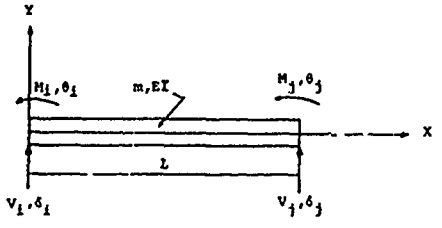

Figure 1: Beam Element with End Forces

POWER SERIES EXPANSION

For the sake of discussion the dynamic stiffness coefficients S_{42}, which is given by equation (11), is expanded in power series. In the derivation, iperations with power series, including addition, subtraction, multiplication, and division are employed. The validity of these operations and convergence of the resulting series is proved in Knopp[6]. The known expansions in power series about the origin of trigonometric and hyperbolic functions as well as the expansion of polynominals raised to a fractional exponent are used and substituted into equation (11) to obtain after considerable algebraic work the series given by equation (16)

$$S_{42} = \frac{EI}{a}\left[1+n^4a^4\left(\frac{2}{35}+\frac{1}{35}(\alpha+\beta)+\ldots\right)\right.$$

$$\left. + n^8a^8\left(\frac{4387}{2,182,950} + \frac{168}{18,900}(\alpha+\beta)+\ldots\right)+\ldots\right] \qquad (16)$$

The substitution of the symbols from equation (2) into equation (16), yields directly the dynamic stiffness coefficient, S_{42} in terms of the geometric and mechanical properties of the beam; namely,

$$S_{42} = \frac{2EI}{L} + \frac{mL^2\omega^2}{140} + \frac{1097m^2L^2\omega^4}{69,854,400EI} + \frac{mL^3\omega^2}{30}\left(\frac{r}{L}\right)^2\left(1+\frac{E}{k'G}\right)$$

$$+ \frac{m^2L^2\omega^4}{3600EI}\left(1+\frac{r}{k'G}\right) + \ldots\ldots \qquad (17)$$

It may be recognized that in equation (17) the first and second terms are respectively, the stiffness and mass coefficients which are obtained from approximate displacement functions. The third term is a higher-order term involving the square of the mass and the last two terms represent the combined effect of rotary inertia and shear deformation. It should be pointed out that the terms of this series, with the exception of the shear factor, have been derived previously in a different formulation by Przemieniecki[7].

The series expansion of all the terms in the dynamic stiffness matrix equation (3) are obtained by the method described in expanding the stiffness coefficient S_{42}. The final series expansion may be written in matrix notation as

$$[S] = [K] - [M_0]\omega^2 - [R_0]\omega^2 - [M_1]\omega^4 - [R_1]\omega^4 \text{ -----} \qquad (18)$$

Where the first two coefficients [K] and $[M_0]$ are, respectively, the stiffness and mass matrices derived from displacement function with exclusion of rotary

inertia and shear deformation, $[M_1]$ a second order mass matrix, and $[R_0]$ and $[R_1]$ the first and second order matrices accounting for rotary inertia and shear deformation effects. These matrices are given explicitly in the Appendix I.

The series expansion in equation (18) is convergent in the complex plane in a circle with center at the origin and radius the closest complex root to the origin of the function

$$f(Z) = 2\theta^2\eta^2(1-cC) + (\theta^2+\eta^2)sS = 0 \qquad (19)$$

where the functions θ, η, s, S, c, and C are defined in equation (15) but now are assumed to be functions of the complex variable Z given in

$$\eta^4 = \frac{Z^2\rho}{Er^2} \qquad (20)$$

APPENDIX I

The power series expansion of the dynamic stiffness matrix based on the Timoshenko beam equation is given by

$$[S] = [K] - [M_0]\omega^2 - [R_0]\omega^2 - [M_1]\omega^4 - [R_1]\omega^4 \text{ -----}$$

where ω is the vibrating frequency and $[K]$, $[M_0]$, $[R_0]$, $[M_1]$ and $[R_1]$ are the following matrices.

The elastic stiffness matrix:

$$[K] = \frac{EI}{L^3}\begin{bmatrix} 12 & & \text{Symmetric} & \\ 6L & 4L^2 & & \\ -12 & -6L & 12 & \\ 6L & 2L^2 & -6L & 4L^2 \end{bmatrix}$$

The first order mass matrix:

$$[M_0] = \frac{mL}{420}\begin{bmatrix} 156 & & \text{Symmetric} & \\ 22L & 4L^2 & & \\ 54 & 13L & 156 & \\ -13L & -3L^2 & -22L & 4L^2 \end{bmatrix}$$

The first order rotary inertia-shear matrix:

$$[R_0] = \frac{mL}{30}\left(\frac{r}{L}\right)^2\left(1+\frac{E}{kG}\right)\begin{bmatrix} 36 & & \text{Symmetric} & \\ 3L & 4L^2 & & \\ -36 & -3L & 36 & \\ 3L & -L^2 & -3L & 4L^2 \end{bmatrix}$$

The second order mass matrix:

$$[M_1] = \frac{m^2L^3}{1000EI}\begin{bmatrix} \frac{59}{161.7} & & & \text{Symmetric} \\ \frac{223L}{2910.6} & \frac{71L^2}{4365.9} & & \\ \frac{1279}{3880.8} & \frac{1681L}{23284.8} & \frac{59}{161.7} & \\ -\frac{1681L}{23284.8} & -\frac{1097L^2}{69854.4} & -\frac{223L}{2910.2} & \frac{71L^2}{4365.9} \end{bmatrix}$$

The second order rotary inertia-shear matrix: $[R_1] = \frac{m^2L^5}{1000EI}\left(\frac{r}{L}\right)^2\left(1+\frac{E}{kG}\right)$

$$\begin{bmatrix} 0.31746 & & \text{Symmetric} & \\ 0.79365L & 0.31746L^2 & & \\ -0.31746 & 0.59524L & 0.31746 & \\ -0.59524L & -0.27778L^2 & -0.79365L & 0.31746L^2 \end{bmatrix}$$

APPENDIX II - NOTATION

a = half length of beam element

A = cross-sectional area

c = cos2θa

C = cosh2ηa

E = modulus of elasticity

G = Shear modulus of elasticity

I = cross-sectional moment of inertia

i,j = designation of the end of beam element

k' = shearing constant

L = length of beam element

m = mass per unit length

M_i, M_j = bending moment at the ends of beam element

$n^4 = \frac{\omega^2\rho}{ER^2}$

r = cross-sectional radius of gyration

s = sin2θa

S = sinh2ηa

S_{ij} = element of the dynamic stiffness matrix

V_i, V_j = shear forces at the ends of beam element

x = coordinate along beam element

Z = complex variable

$\alpha = \frac{Er^2}{k'a^2G}$

$\beta = \frac{r^2}{a^2}$

$\lambda = \frac{x}{a}$

δ_i, δ_j = transverse deflection at the ends of beam element

θ_i, θ_j = angular deflection at the ends of beam element

ω = vibrating frequency

$[K]$ = elastic stiffness matrix

$[M_0]$ = first order mass matrix

$[M_1]$ = second order mass matrix

$[R_0]$ = first order rotary inertia-shear matrix

$[R_1]$ = second order rotary inertia-shear matrix

$[S]$ = dynamic stiffness matrix

REFERENCES

1. Archer, J. S., "Consistent Mass Matrix for Distributed Mass Systems" Journal Structural Division, Pro. ASCE, Vol. 89, 1963.

2. Henshell, R. D. and Warburton, G. B. "Transmission of Vibration in Beams Systems", International Journal for Numerical Methods in Engineering. Vol. 1, pp. 47-66, 1969.

3. Paz, Mario, "Mathematical Observations in Structural Dynamics", Int. Journal Computers and Structures, Vo. 3, pp. 385-396, 1973.

4. Paz, Mario and Dung, Lam, "Power Series Expansion of the General Stiffness Matrix for Beam Elements", Int. Journal for Numerical Methods in Engineering, Vo. 9 No. 2, pp. 449-459, 1975.

5. Snowdon, J. C., Vibration and Shock in Damped Mechanical Systems, John Wiley & Sons Inc., New York, 1968.

6. Knopp, K., Theory and Application of Infinite Series. Blackie, London, 1963.

7. Przemieniecki, J. S. "Quadratic Matrix Equations for Determining Vibration Modes and Frequencies of Continuous Elastic Systems". Proc. Air Force 1st Conference on Matrix Methods in Structural Mechanics, Wright-Patterson Air Force Bas, Ohio Oct. 26-28, 1965.AFFDL TR 66-80,1966.

EFFECT OF PHASE SHIFT ON SHOCK RESPONSE

Charles T. Morrow
Vought Corporation Advanced Technology Center
Dallas, Texas

Whereas the Fourier transform, complete with phase-versus-frequency information, uniquely defines a shock excitation time history and the corresponding response of any mechanical system, the shock spectrum does not. Any phase characteristic, compatible with the magnitude characteristic in the sense that it does not imply a negative time delay, can be assumed. Each choice would lead to a different time history. Concern that shock tests performed at different laboratories to the same shock spectrum requirement may lead to different failures of the same test item has led to various proposals for supplementary constraints on shock testing. At the 45th Shock and Vibration Symposium a suggestion was made that a phase curve with tolerances be provided to supplement the magnitude spectrum and its tolerances.

For the present theoretical investigation, an electromagnetically applied terminal step function of acceleration is selected as a starting point. It is simpler to analyze than a terminal peak sawtooth, but it induces similar responses. A simple all-pass phase-shift network is assumed to be inserted in the electronic system. This permits a theoretical investigation of effect of phase shift on response peaks and on energy absorption by a procedure that could be approximated on a laboratory shaker.

The inserted phase-shift network has negligible influence on the response transient of a simple resonator and negligible influence on the individual response transients of a two-degree-of-freedom system. But it does alter the relative phase of the latter and thereby the timing and magnitude of the first maximum of their combined envelope. The energy absorption in the second resonator is also changed. Without the phase shift network, two transients nearly equal in frequency start out approximately opposite in phase, so that the first maximum of the envelope does not occur until they have experienced part of their decay. The phase-shift network alters the amount of this decay. The influence of relative phase shift on damage potential is greatest when the damping is highest.

It is not clear whether the study of phase effects will lead to a feasible way of controlling more closely the variability of a shock test specified in terms of a shock spectrum or clarify some persisting uncertainties the specification writer must accept. Some future steps toward settling the problem are outlined. If, however, there must be significant uncertainty of effect regardless of the wording of the test specification it is important to recognize this. Otherwise shock tests may be called upon the prove things they are incapable of proving about a test item.

INTRODUCTION

Environmental simulation will never be an exact engineering procedure, but we try to make available the best possible techniques, within reasonable cost and schedule limitations, and to understand the effects.

In spite of much recent discussion and some accumulating new ideas, mechanical shock simulation has been persistent in evading attempts at major improvement in realism or reproducibility or in assessment of these factors. In conjunction with the 44th Shock and Vibration Symposium, the Institute of Environmental Sciences held a special meeting to discuss possible ways of specifying shocks so environmental tests at different laboratories would be comparable. This is indeed a timely fundamental and practical topic.

For simplicity, a specification writer would like to prescribe a test acceleration pulse shape or a test spectrum, but not both. However, at one extreme, two test shocks within typical tolerances of a nominal test pulse in the time domain can have widely different spectra, especially at high frequencies. In principle, confidence in this type of test prescription would be raised by specifying tolerances on the first derivative with respect to time in addition to tolerances on simple deviation of points from the nominal curve. At the other extreme, a spectrum of magnitudes in the frequency domain, even with the most meticulous wording, does not uniquely prescribe excitation or response time history. This is especially a fundamental consideration in the use of shaker-applied synthesized shock. In principle, confidence in the reproducibility of a test specified by a spectrum can be raised by requiring also at least qualitative conformance to a prescribed pulse shape.[1]

A recent paper[2] on the spectral approach offered an alternative of specifying also a nominal phase versus frequency curve, with tolerances especially on the slope with respect to frequency. It identified some of the phase-dependent effects that could occur in coupled systems, including a variation in the energy absorption from the shock, and showed on the assumption of an abrupt shock termination in spite of spurious phase shifts that these effects could be held within bounds for two degree of freedom systems even with resonance frequencies in near coincidence. Three degree of freedom systems with near coincidence of resonance frequencies may be interpreted as such gross bad design that survival of the first environmental test even with poor shock test reproducibility is unlikely. That previous paper was preliminary and did not consider any explicit input. Yet the method of investigation pursued further, theoretically or experimentally, can provide a means of gaining further insight into the effects of shock variabilities on test items.

In the present paper, influences of phase as investigated previously will be made plausible by considering an explicitly defined input. This paper will explore the effect of a simple electrical phase-shift network on response of both a single and a double resonator excited by a pulse in a random vibration test system. Except for the phase-shift network, the system is equalized to produce an acceleration that is an exact duplication of the wave shape of an input voltage. For simple illustrative purposes, it will be assumed that the system has no frequency response or displacement limitations, and no problems of resonant loading of the shaker. Partly to simplify the mathematics as much as possible, and partly to meet the need to focus on particular excitations of special theoretical or practical importance, the original input voltage will be taken to be a unit terminal step function, equal to unity for negative time and equal to zero for positive time. The results will be strongly indicative also of the effect of phase shift on response to an input voltage in the form of a more practical terminal peak sawtooth or approximation to such a pulse.

In practical shock testing, whether by drop tower or shaker, phase shift rates with frequency many times those of the present paper may be encountered. The practical significance of phase shift in general shock testing can be investigated by a series of carefully chosen computer studies. But, unless such studies are also carefully explained, they tend to obscure the phenomena they are intended to clarify. In any event, the existence of a small number of closed-form solutions will be a useful hedge against such risk.

PHASE-SHIFT NETWORK

Figure 1 shows a simple all-pass phase-shift network consisting of an ideal center-tapped transformer, a capacitor, and a resistor. In practical situations, such a network, with a phase inverter circuit instead of a transformer, could be cascaded, with various successive R-C products (time constants) so as to tailor a phase versus frequency characteristic to a prescribed curve. It would proba-

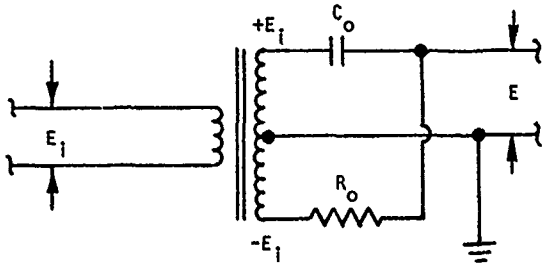

Figure 1. Simple All-Pass Phase Shift Network with Ideal Transformer

bly not be used in practice as a single-stage phase shifter for any simple pulse, because its single-stage output is not a particularly desirable time history, but it does lend itself with relative ease to the mathematical analyses to follow.

If a periodic signal $E_1 e^{j\omega t}$ is applied to the primary of the transformer of Figure 1, the secondary current is $2E_1 e^{j\omega t}/(R_o + 1/j\omega C_o)$. Summation of the secondary voltage and voltage drop in either half of the R-C circuit, on the assumption that any additional electrical load impedance will be much larger than R, yields the simple relationship

$$\frac{E}{E_i} = \frac{j\omega - 1/R_oC_o}{j\omega + 1/R_oC_o} \qquad (1)$$

where E is the complex amplitude of the output signal, measured to electrical ground. Accordingly, extreme high frequency signals are transmitted to the output without modification, through the capacitor, in accordance with the limiting relationship $E/E_i = 1$. Extreme low frequency signals, on the other hand, are transmitted to the output through the resistor but, because of the polarity of the lower secondary winding, are reversed in sign or shifted in phase by 180 degrees, in accordance with the other limiting relationship $E/E_i = -1$. Equation (1) can also be expressed as

$$\frac{E}{E_i} = \frac{\omega^2 + 1/R_o^2C_o^2}{\omega^2 + 1/R_o^2C_o^2} e^{-j\phi} = e^{-j\phi} \qquad (2)$$

where

$$\phi = -2 \tan^{-1}(1/\omega R_oC_o) = -2 \tan^{-1}(f_o/f). \qquad (3)$$

with the magnitude of the signal independent of frequency, but the phase shifting continuously from -180 degrees at near zero frequency to 0 degrees at infinite frequency. In particular, for $\omega = 1/R_oC_o$ radians/sec or $f = 1/2\pi R_oC_o = f_o$ Hz, $\phi = 90$ degrees.

The rate of change of phase angle with angular frequency is

$$\frac{d\phi}{d\omega} = \frac{2/\omega^2 R_o C_o}{(1 + 1/\omega^2 R_o^2 C_o^2)^{1/2}} \qquad (4)$$

Therefore, the rate of change of phase angle lag per ten percent change in frequency is

$$\Delta\phi_{10} = .1f \frac{d\phi}{df} = .1\omega \frac{d\phi}{d\omega} = \frac{.2/\omega R_oC_o}{(1 + 1/\omega^2 R_o^2 C_o^2)^{1/2}}$$

$$= \frac{.2}{(1 + \omega^2 R_o^2 C_o^2)^{1/2}} = \frac{.2}{(1 + \omega^2/\omega_o^2)^{1/2}}$$

$$= \frac{.2}{(1 + f^2/f_o^2)^{1/2}} \qquad (5)$$

The phase shift and phase rate are plotted in Figure 2.

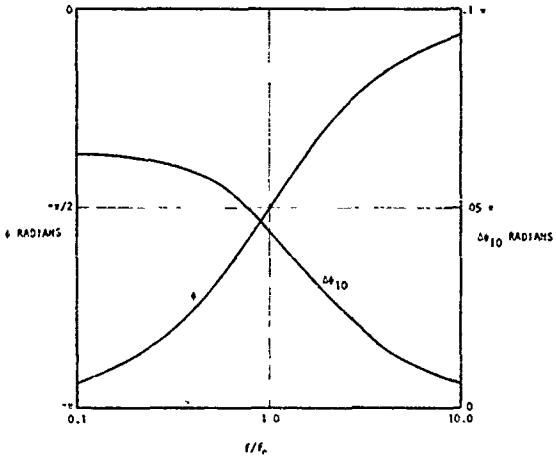

Figure 2. Phase Angle and Phase Rate for All-Pass Phase Shift Network

Generalization of Equation (1) to complex frequency, with the real part indicating transient decay rate at any resonance frequency, yields the transfer function of the phase shift network, which is also the Laplace transform of the response of the network to an impulse function of unit area. In Appendix 1, the output corresponding to this impulse is obtained by the Heaviside expansion theorem, and the output corresponding to an initial unit step function is obtained by integration. It follows that the output corresponding to a terminal unit step function is

$$e = -2e^{-t/R_oC_o}, \qquad (6)$$

for positive time, or, for arbitrary time,

$$e = -1 + 1(t)\ (1 - 2e^{-t/R_oC_o}), \qquad (7)$$

as shown in Figure 3. The symbol 1(t) stands for the Heaviside unit function, zero for negative time. The output time history, of course, is strikingly different in appearance from the input terminal step function, but it has the same Fourier spectral magnitude for every frequency and therefore the same undamped residual shock spectrum.

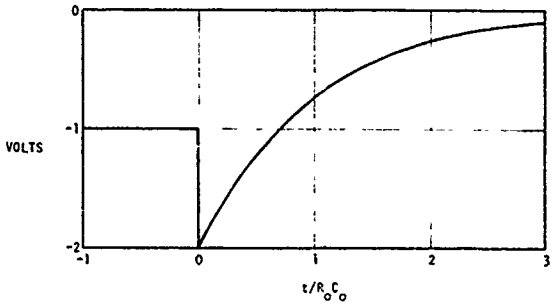

Figure 3. Response of Phase Shift Network to Unit Terminal Step Function

A similar exponential occurs also when the modified terminal step of acceleration is applied to a single or double resonator. For the single resonator, it has the form

$$\frac{2\,(\alpha_1^2 + \omega_1^2)}{(\alpha_1 - 1/R_oC_o)^2 + \omega_1^2}\, e^{-t/R_oC_o}\,, \qquad (8)$$

where α_1 and ω_1 are respectively the decay constant and angular frequency of the resonator, and for the double resonator with no loading of the first resonator by the second,

$$\frac{2(\alpha_1^2+\omega_1^2)(\alpha_2^2+\omega_2^2)\, e^{-t/R_oC_o}}{[(\alpha_1-1/R_oC_o)^2+\omega_1^2][\alpha_2-1/R_oC_o)^2+\omega_2^2]} \qquad (9)$$

However, since the single-stage phase-shift network is unlikely to be used in practical shock testing, our interest here is, for illustrative purposes and clarification of phenomena only, primarily in the effect on the oscillatory transients at the resonance frequencies. From this point on, only these transients will be considered and only for special cases of interest. The general solution for the response of the double resonator to the modified step is formidable. The primary challenge in the preparation of this paper has been to avoid being trapped in tedious derivations that would be distractions from the more important results.

SINGLE RESONATOR RESPONSES

We will compare responses to the unmodified and modified terminal step functions. From Equation (40) of Appendix 2, the oscillatory transient for positive time induced in a simple linear mechanical resonator by a terminal step of acceleration is

$$a_{1s}(t) = e^{-\alpha_1 t}\,[(\alpha_1/\omega_1)\sin\omega_1 t + \cos\omega_1 t], \qquad (10)$$

where

$$\omega_1 = k_1/m_1 \qquad (11)$$

is the angular resonance frequency and

$$\alpha_1 = c_1/2m_1 = \pi f_1/Q_1 = \omega_1/2Q_1 \qquad (12)$$

is the decay constant.

For an assumed lowest $Q_1 = 10$, $\alpha_1/\omega_1 = 1/20$. The sine term is at most 5 percent of the cosine term.

From equation (41) of Appendix 2, the phase shift network multiplies

$$e^{(-\alpha_1 + j\omega_1)t}$$

by

$$\frac{-\alpha_1 - k/R_oC_o + j\omega_1}{-\alpha_1 + 1/R_oC_o + j\omega_1} \qquad (13)$$

and $e^{(-\alpha_1 - j\omega_1)t}$ by a complex conjugate factor. For $Q \geq 10$ or $\alpha_1/\omega_1 \leq 2D$, the primary effect of varying the R_oC_o product or time constant on a transient is to shift its phase. For example, if $R_oC_o = 1/\omega_1$, numerator and denominator of the complex multiplier each contribute approximately a 45 degree shift, or collectively they contribute approximately a 90 degree shift in accordance with

$$\frac{-\omega_1 + j\omega_1}{\omega_1 + j\omega_1} = -\frac{1-j}{1+j} = -\frac{(1-j)^2}{2} = j. \qquad (14)$$

The starting time of the transient is however, unaltered. Equation (10) for oscillatory transient response to a terminal step is converted to

$$a_{ols} = e^{-\alpha_1 t}\,[(\alpha_1/\omega_1)\cos\omega_1 t - \sin\omega_1 t], \qquad (15)$$

approximately.

The difference in peak response, for positive time, is that due to a time difference of 1/4 period in the attainment of the first peak, if the direction of the peak is not considered important. (The input pulse could be reversed if desired).

$$1 - e^{-\alpha_1/4f_1} = 1 - e^{-\pi/4Q_1} = 1 - e^{-\pi/40}$$

$$= 1 - .92 = .08 \qquad (16)$$

or only 8 percent decrease in peak response for the simple resonator for the lowest Q_1 of 10, or assumed worse case.

The difference in energy absorbed by the damper for the two phase lags, is approximately proportional to

$$\int_0^\infty e^{-2\alpha_1 t} (\cos^2 \omega_1 t \cdot \sin^2 \omega_1 t)\, dt$$

$$= \int_0^\infty e^{-2\alpha_1 t} \cos 2\omega_1 t\, dt = \frac{\alpha_1}{\alpha_1^2 + \omega_1^2} \approx \alpha_1/\omega_1^2 \qquad (17)$$

But the energy absorbed, for the original phase, is proportional to

$$\int_0^\infty e^{-2\alpha_1 t} \cos^2 \omega_1 t\, dt$$

$$= \int_0^\infty e^{-2\alpha_1 t} \cdot \frac{1 + \cos 2\omega_1 t}{2}\, dt$$

$$= \frac{1}{4\alpha_1} + \frac{\alpha_1/2}{\alpha_1^2 + \omega_1^2} \approx \frac{1}{4\alpha_1} \qquad (18)$$

This yields a ratio

$$\left(\frac{\alpha_1}{\alpha_1^2+\omega_1^2}\right)(4\alpha_1) = 4\alpha_1^2/\omega_1^2 = 1/Q_1^2 = .01 \qquad (19)$$

or only 1 percent effect of a 90 degree shift for the simple resonator for the assumed minimum Q of 10, or assumed worse case for shock effect variability.

Such amplitude and energy results would not be proportionate to phase angle over any significant range--adding 360 degrees would have no effect. Therefore, large phase shifts with frequency in practical shock testing would not greatly increase these results.

RESPONSE OF A DOUBLE RESONATOR

We will again compare responses to the unmodified and modified terminal step functions, but observe now a potentially large influence of relative phase shift versus frequency. For a double resonator, as shown in Figure 4, there are two oscillatory transients. Output transients at nearly the same frequency, in response to an unmodified step function, are larger than for the single resonator and start out simultaneously at t = 0 but in approximately opposite phase. Consequently, the second mass does not attain its peak response until some time after time zero, or until both transients have experienced part of their exponential decay. Peak response and energy absorption become sensitive to relative phase changes (one resonance frequency versus the other) whereas for the single resonator there could be only absolute phase changes.

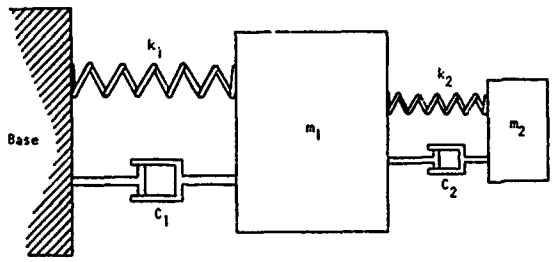

Figure 4. Double Resonator or Two-Degree-of-Freedom System

From Equation (47) of Appendix 3, on the assumption that the second resonator does not load the first, the sum of the oscillatory transients experienced by the second mass, in response to an unmodified terminal step function of acceleration, is given by

$$a_{2s}(t) = \frac{e^{-\alpha_1 t}}{2(\omega_2-\omega_1)} (\alpha_1 \sin \omega_1 t - \omega_1 \cos \omega_1 t)$$

$$- \frac{e^{-\alpha_1 t}}{2(\omega_2-\omega_1)} (\alpha_1 \sin \omega_2 t - \omega_1 \cos \omega_2 t)$$

$$= \frac{e^{-\alpha_1 t}}{\omega_2-\omega_1}[\alpha_1 \sin \tfrac{1}{2}(\omega_1-\omega_2)t \cos \tfrac{1}{2}(\omega_1+\omega_2)t$$

$$+ \omega_1 \sin \tfrac{1}{2}(\omega_1 - \omega_2)t \sin \tfrac{1}{2}(\omega_1 + \omega_2)t]$$

$$= \frac{e^{-\alpha_1 t} \sin \frac{1}{2}(\omega_1-\omega_2)t}{\omega_2-\omega_1}[\alpha_1 \cos\omega_1 t + \omega_1 \sin\omega_1 t)] \qquad (20)$$

for $\alpha_1 = \alpha_2 \ll \omega_1$ and $\omega_1 \approx \omega_2$.

The ratio of the second term to the first term is

$$\alpha_1/\omega_1 = 1/2Q_1 \leqslant 20 \qquad (21)$$

for minimum $Q_2 \simeq Q_1 = 10$.

The time function to the left of the bracket is a time-varying envelope, with both exponential and trigonometric factors. The latter, involving a half difference frequency, has zero initial value and reaches its first maximum when cos 1/2 $(\omega_1 - \omega_2)t = 0$, after much of the exponential decay has taken place. The maximum of the combined factors occurs only a little earlier. This type of phenomenon was discussed at length in the earlier paper on phase effects, except that the two transients were merely postulated, with arbitrary

phases, without being derived from any explicitly described excitation. Whether a moderate relative phase shift increases the peak acceleration of m_2 and the energy absorbed in c_2 by making the peak of the envelope occur earlier, or decreases both by making the peak of the envelope occur later, depends on the sign of the shift and therefore on which resonance frequency is greater.

Examination of Equation (47) in Appendix 3 shows the effect of the phase shift network on the terms involving $e^{(-\alpha_1+j\omega_1)t}$ and $e^{(-\alpha_1+j\omega_2)t}$ to be represented by the factors

$$(-\alpha_1 + j\omega_1 - 1/R_oC_o) / (-\alpha_1 + j\omega_1 + 1/R_oC_o) \quad (22)$$

and

$$(-\alpha_1 + j\omega_2 - 1/R_oC_o) / (-\alpha_1 + j\omega_2 + 1/R_oC_o), \quad (23)$$

respectively. For $Q_2 \approx Q_1 \leq 10$, it follows that $\alpha_1/\omega_1 = 1/2Q_1 \leq 20$, so that the two complex multipliers have little effect on magnitudes of individual transients — the effect of primary interest is a relative phase shift. The two multipliers differ in form from Equation (1) only by the inclusion of α_1, which can be neglected without further analysis when $1/R_oC_o$ is of the order of ω_1 and ω_2 larger. At the other extreme, for large R_oC_o, Expression (21) yields an absolute phase angle

$$\phi_1 = \tan^{-1}\frac{\alpha_1 + 1/R_oC_o}{\omega_1} + \tan^{-1}\frac{-\alpha_1 + 1/R_oC_o}{\omega_1}$$

$$\approx \frac{\alpha_1+1/R_oC_o}{\omega_1} + \frac{-\alpha_1+1/R_oC_o}{\omega_1} = \frac{2}{\omega_1 R_oC_o}, \quad (24)$$

still in close agreement with Equation (3). Accordingly, the primary new effect of the phase shift network on the oscillatory transients for small frequency differences, is a relative phase shift with frequency in accordance with Equation (5). This is plotted in Figure 2, along with the approximate absolute phase shift of each from Equation (3).

If phase shifts ϕ_1 and ϕ_2 are incorporated in the approximate trigonometric functions of the initial formula of Equation (20), the final formula for oscillatory transient response to the modified terminal step function is found to be

$$a_{2os}(t) \approx \frac{e^{-\alpha_1 t}\sin\frac{1}{2}[(\omega_1-\omega_2)t-\Delta\phi]}{\omega_2-\omega_1}$$

$$[\alpha_1\cos(\omega_1 t - \frac{\phi_1+\phi_2}{2} + \omega_1\sin(\omega_1 t - \frac{\phi_1+\phi_2}{2})] \quad (25)$$

where $\Delta\phi = \phi_1 - \phi_2$. The important effect is in the envelope.

Much as in the previous paper[2] on phase sensitivity, the time of the maximum of the combined exponential and trigonometric envelope is found by setting

$$\frac{d}{dt}\left[e^{-\alpha_1 t}\sin\frac{(\omega_1 - \omega_2)t - \Delta\phi}{2}\right]$$

$$= -\alpha_1 e^{-\alpha_1 t}\sin\frac{(\omega_1 - \omega_2)t - \Delta\phi}{2}$$

$$+ \frac{\omega_1 - \omega_2}{2} e^{-\alpha_1 t}\cos\frac{(\omega_1 - \omega_2)t - \Delta\phi}{2} = 0, \quad (26)$$

which yields

$$t = \frac{2\tan^{-1}\frac{\omega_1-\omega_2}{2\alpha_1} + \Delta\phi}{\omega_1 - \omega_2}$$

$$= \frac{2\tan^{-1}[Q_1(\omega_1 - \omega_2)/\omega_1] + \Delta\phi}{\omega_1 - \omega_2}$$

$$= \frac{\tan^{-1}[Q_1(f_1 - f_2)/f_1] + \Delta\phi}{\pi(f_1 - f_2)}, \quad (27)$$

with the phase difference measured in radians. For negligible damping and frequency difference the time of the first envelope maximum occurs when

$$t = \frac{2\tan^{-1}\infty}{\omega_1 - \omega_2} = \frac{\pi}{\omega_1 - \omega_2} \quad \text{or}$$

$$\sin\frac{1}{2}(\omega_1 - \omega_2)t = \pi/2, \quad \text{as it should.}$$

But Equation (27) is merely a step on the way to estimating the sensitivity to phase shift. It follows that

$$\frac{dt}{d\Delta\phi} = \frac{1}{\omega_1 - \omega_2} \quad (28)$$

or, for small $\Delta\phi$,

$$\Delta t = \Delta\phi/(\omega_1 - \omega_2), \quad (29)$$

during which the decay is

$$e^{-\alpha_1\Delta t} = e^{-\alpha_1\Delta\phi/(\omega_1 - \omega_2)}$$

$$= e^{-\omega_1\Delta\phi/2Q_1(\omega_1 - \omega_2)}$$

$$= e^{-f_1\Delta\phi/2Q_1(f_1 - f_2)}, \quad (30)$$

as in the previous paper on phase sensitivity[2]. In short, the effect on the envelope peak response is determined entirely by the phase shift per fractional bandwidth between the two frequencies, divided by their Q. If the phase shift is approximately proportional to fractional bandwidth, it is sufficient to set $(f_1 - f_2)/f_1 = .1$ and obtain $\Delta\phi_{10}$, the shift per 10 percent change in bandwidth from Figure 2. If, further, $Q_1 = 10$ as a minimum value, the maximum percentage effect on peak envelope is given by

$$100e^{-\alpha_1 \Delta t} = 100e^{-\Delta\phi_{10}/2} \qquad (31)$$

This is plotted versus $f/f_o = 2\pi f R_o C_c$ in Figure 5 with the aid of Equation (5) or Figure 2. The frequency f is taken to be approximately equal to f_1 or f_2. However, Equations (3) and (31) remain applicable when phase shift occurs for other reasons than the network chosen for the present study.

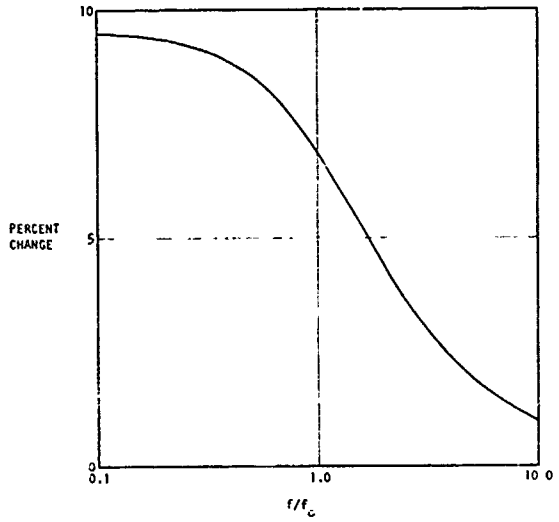

Figure 5. Percent Change in Peak Envelope versus f/f_o

An upper limit to the sensitivity of the energy absorbed in c_2 to the relative phase shift can be obtained from Figure 3 of the previous paper[2]. That plot was computed on the assumption of a worst case such that the transients observed in the relative motion of the second mass with respect to the first were equal. The assumption holds here to ten percent or so for the situations of most interest.

In practical testing, much larger effects of relative phase shift on peak response and energy absorption are possible because spurious phase shift with frequency, from phase errors in equalization for example, can be more rapid than the phase shift of the all-pass network considered here.

DISCUSSION

The foregoing analyses illustrate the point of the previous paper[2], that a change in phase versus frequency characteristic, even without altering the undamped residual shock spectrum or the magnitude of the Fourier transform, can alter the combined damaging effect of transients in a multiple degree of freedom system. One interesting development is that the timing of initiation of the two response transients is unaffected. Evidently any relative time delay at the two frequencies is expressed in the sum of the transients plus transmitted excitation.

If we seriously intended to use the chosen phase-shift network as a single-stage network for altering phase in a practical test, we would have to go further and combine the transients with the altered excitation as transmitted through the resonator. We will have to do that for whatever we actually use.

This paper does not by itself settle whether it is feasible to supplement a nominal magnitude spectrum and tolerances by a nominal phase characteristic and tolerances so as to make the damaging effect of a specified shock on an invariant test item reproducible. However, it is possible now to indicate some additional steps that would provide more adequate insight into this problem.

The first step is to decide on some standard magnitude and phase spectra (or corresponding practical excitation time histories) that are of sufficient interest to warrant further investigation.

One nominee, closely allied to the excitation studied in this paper, is a phase and magnitude spectrum for a step function or terminal peak sawtooth of acceleration altered by high and low frequency cutoffs of a random vibration shaker facility. The "sawtooth" voltage input can be a step function terminating a ramp or square law curve. The latter will have a magnitude spectrum closer to that of the step function alone, or in other words a flatter spectrum at high frequencies, because it involves no initial discontinuity of slope.

A second, closely allied, nominee is a practical terminal peak sawtooth test as applied in a drop tower with a lead pellet or other suitable decelerating mechanism. The characteristic rounding of the peak is equivalent to a high frequency cutoff.

A third nominee, utilizing, like the first, the technique of shock synthesis on a shaker, is a step or terminal peak sawtooth as altered by high and low frequency cutoffs and by the phase characteristic of a commercial third octave or other constant fractional octave filter set whose outputs are recombined. Single section filters crossing over at the 3dB point would not alter the time history. However,

commercial filters are multiple section and cross over in such a way as to produce 360 degrees shift between adjacent center frequencies, and hence a time delay inversely proportional to frequency for fractional octave filters.

The complex transients exemplified by pyrotechnic shock in an aerospace structure may have phase characteristics that are too complicated to be a useful addition to routine data reduction, and not very useful. However, once the test time histories and nominal magnitude and phase characteristics, as above, have been selected, a second step is to compare the test responses of a two-degree-of-freedom system to its responses to one or more exponentially decaying transients. This will provide further indications of realism of simulation. Except perhaps for effects of high and low frequency cutoffs, most of this can be accomplished by theoretical analysis.

A third step is to explore the effect on the two-degree-of-freedom system of possible variations in high and low frequency cutoff characteristics as an aid to estimating how far beyond the cutoffs it may be feasible and useful to apply tolerances to a phase characteristic.

A fourth step is to explore the effect on the two degree of freedom system of fixture resonance and resonant interactions with the test item. In the drop tower technique, no electrical equalization is possible, for either magnitude or phase. It is worth noting, in passing, that the first application of the shock spectrum to a specification requirement avoided the problem of feasible magnitude tolerances by specifying a minimum spectrum.[1] In the technique of shock synthesis on a shaker, magnitude equalizers are always a standard part of the test setup. However, the bandpass filters commonly used today for convenience of equalization in random vibration testing will not compensate as well as the earlier peak-and-notch filters for phase errors in shock testing.

Much of the investigation outlined would be too cumbersome for theoretical analysis alone. However, the shock spectrum computer, with suitable internal modifications or with suitable variations of technique, is an ideal experimental tool. Three modes of operation are potentially useful.

1. Use a response time history from one computer as the input to another computer, or

2. Record the first response on tape or in a memory and use it as an input to the same computer, or

3. Operating in real time, use the response time history of one channel of the shock spectrum computer as the input to the other channels of the same computer.

4. Use as the input to the initial shock spectrum computer a step, impulse or terminal peak sawtooth voltage, modified by any circuits, such as high or low-frequency filters, whose phase shift effects may be of interest. This should include a peak-notch filter (simulating resonant interaction of test item and shaker armature) magnitude equalized by a constant bandwidth or fractional-octave filter set.

5. Use the final computer in the conventional manner to obtain peak response, or extract the absolute and relative instantaneous response, square the latter and integrate with respect to time to obtain a measure of energy absorbed in the second resonator.

In short, to demonstrate feasibility of controlling the variability of effect of a shock test by specifying phase as well as magnitude spectra, with tolerances on both, or by any other modification to specification language, it will be necessary to explore phase effects in plausible test situations, starting from additional basic inputs of sufficient interest. For such investigation, shock spectrum computers can be so used as to simulate two-degree-of-freedom systems, thereby saving much effort in tedious theoretical analysis.

CONCLUSION

At the very least, the phase characteristic of a test shock provides an avenue for further investigation of effects of the test on multiple degree of freedom systems. Whether it will provide a means for close control of the reproducibility of effects of shock tests, or merely disclose the extent of some uncertainties we may have to learn to live with, remains to be seen. In any event, it is desirable that we improve our knowledge of the limitations of our test techniques, as well as of their best use, as a protection when requirements placed on us are motivated by unrealistic expectations.

In the meantime, the author is taking no strong generalized position for or against existing or emerging environmental specification or shock test practices, such as specification of a particular machine, pulse or spectrum, or such as shock synthesis according to a spectrum. The question is not what is the perfect way to simulate shock — there is none and will be none. There are in fact limitations other than those discussed here[3]. The sensitivity to considerations, such as phase shift, that are not controlled by a simple spectrum, can become greater when more than

two degrees of freedom are likely to be involved in a test item failure mode[4]. The question is, rather, which practice is best for a particular purpose, what refinements may be desirable, and what uncertainties of effect may remain.

REFERENCES

1. C. T. Morrow, "Shock Spectra, Residual, Initial and Maxima as Criteria of Shock Severity", Shock and Vibration Bulletin 45, Part 5, June 1975, pp 191-205.

2. C. T. Morrow, "Energy Absorption and Phase Effects in Shock Excited Coupled Systems", Shock and Vibration Bulletin 45, Part 5, June 1975, pp 19-26.

3. C. M. Harris and C. E. Crede, Shock and Vibration Handbook, 2nd ed. McGraw-Hill, 1976, especially chapters 21 and 24.

4. NASA CR #91356, "Final Report for the Study of Mechanical Shock Spectra for Spacecraft Applications," prepared by TRW Systems for GSFC under Contract NAS 5-10166, April 1967.

APPENDIX 1

TIME HISTORY OF A MODIFIED STEP FUNCTION

For this derivation and others to follow, there are some mathemtical subtleties that should be considered at this time. For mathematical simplicity, it is preferable to start with a terminal step function rather than a pulse, like a terminal peak sawtooth, which is a sum of two elementary functions initiated sequentially. Yet, a terminal step, zero for positive time, has no useful Laplace transform. Therefore, it is expedient to derive time histories initiated by an initial step and subtract them from whatever responses are produced by a constant acceleration, or in terms of an electrical network for processing the excitation signal, a constant voltage. Secondly the Laplace transform of each time history to be derived will contain a factor s in the denominator where s is a variable complex frequency. In more detail, the transform of an initial step is 1/s. The transform of the response of any electrical network or mechanical system or combination is 1/s times the appropriate transfer function, which, in this paper, will not contain s as a compensating factor in the numerator. Division of a transform by s is equivalent to an integration of the inverse transform with respect to time. In the derivations to follow, the time history corresponding to the transfer function above (i.e. the response to a delta function) will be obtained from the Heaviside expansion theorem and then integrated once with respect to time. The constant of integration, if of sufficient interest to evaluate, will be addusted in conformance with engineering insight into what the response should be immediately after time zero. Finally, the subtraction from the response to unit input will take place to yield the response to the terminal step. When the integration constant is of insufficient interest to evaluate, the practical effect of this subtraction is merely to reverse the sign of the more important terms.

The constant of integration could also be obtained from either of two limiting relationships. If L(s) is the transform of a(t),

$$\lim_{s\to\infty} sL(s) = \lim_{t\to 0} a(t) \qquad (32)$$

and

$$\lim_{s\to 0} sL(s) = \lim_{t\to\infty} a(t) \; . \qquad (33)$$

Alternately, the appropriate form of the Heaviside expansion theorem could be applied directly to yield the response to a step function.

The initial and simplest problem is to derive the time history of the step function modified by the phase shift network. Generalization of Equation (1) to utilize the complex frequency s, with

$$s_o = -1/R_oC_o \; , \qquad (34)$$

yields the transfer function

$$\frac{L_{oi}(s)}{1} = \frac{s + s_o}{s - s_o} \; , \qquad (35)$$

where the denominator on the left is the transform of an impulse function of unit area. The time history corresponding to Equation (35) is obtained by the Heaviside expansion theorem as

$$a_{oi} = 2\, s_o e^{s_o t} \; , \qquad (36)$$

for a positive time.

Integration yields

$$a_o = -1 + 2\, e^{s_o t} \; , \qquad (37)$$

for positive time, with the integration constant chosen so that $a_o = +1$ immediately after time zero. A steady unit voltage at the input yields -1 at the output of the phase shift circuit. Subtraction of Equation (36) from this yields Equation (6) and (7).

APPENDIX 2

RESPONSE OF A SIMPLE RESONATOR

The transfer function of a simple viscously damped mechanical resonator, expressed as the ratio to the Laplace transform of a unit-area impulse function, is

$$\frac{L_{1i}}{1} = \frac{\alpha_1^2 + \omega_1^2}{(s + \alpha_1)^2 + \omega_1^2}$$

$$= \frac{\alpha_1^2 + \omega_1^2}{(s + \alpha_1 - j\omega_1)(s + \alpha_1 + j\omega_1)} . \quad (38)$$

Accordingly, the response to the impulse of acceleration is obtained by the Heaviside expansion theorem as

$$a_{1i}(t) = \frac{\alpha_1^2 + \omega_1^2}{j2\omega_1} e^{(-\alpha_1 + j\omega_1)t} + \frac{\alpha_1^2 + \omega_1^2}{-j2\omega_1} e^{(-\alpha_1 - j\omega_1)t} \quad (39)$$

for positive time.

Integration yields as the response to an initial unit step function of acceleration

$$a_{1s}(t) = 1 + \frac{-\alpha_1 - j\omega_1}{j2\omega_1} e^{(-\alpha_1 + j\omega_1)t} + \frac{-\alpha_1 + j\omega_1}{-j2\omega_1} e^{(-\alpha_1 - j\omega_1)t} \quad (40)$$

for positive time, if the constant of integration is chosen to make the response zero immediately after time zero.

The response of the resonator to a unit positive acceleration constant over all time is a unit positive acceleration. Subtraction of Equation (40) from this and conversion from exponential to partially trigonometric functions of time yields Equation (10) for the response to a terminal step.

The transfer function of the simple resonator and the phase shift network, expressed as the ratio to the Laplace transform of a unit-area impulse function, is

$$L_{oli} = \frac{(s + s_o)(\alpha_1^2 + \omega_1^2)}{(s - s_o)(s + \alpha_1 - j\omega_1)(s + \alpha_1 + j\omega_1)} . \quad (41)$$

The transfer function of the simple resonator and the phase shift network, expressed as the ratio to the Laplace transform of a unit-area impulse function, is

$$\frac{L_{ol}}{1} = \frac{(s + s_o)(\alpha_1^2 + \omega_1^2)}{(s - s_o)(s + \alpha_1 - j\omega_1)(s + \alpha_1 + j\omega_1)} . \quad (42)$$

Accordingly, the overall response to a unit-area impulse function of voltage applied to the input of the phase shift network is obtained, by the Heaviside expansion theorem and some supplementary algebra, as

$$a_{oli} = \frac{2s_o(\alpha_1^2 + \omega_1^2)}{(\alpha_1 + s_o)^2 + \omega_1^2} e^{s_o t} + \frac{(-\alpha_1 + j\omega_1 + s_o)(\alpha_1^2 + \omega_1^2)}{j(-\alpha_1 + j\omega_1 - s_o)\,2\omega_1} e^{(-\alpha_1 + j\omega_1)t} + \frac{(-\alpha_1 - j\omega_1 + s_o)(\alpha_1^2 + \omega_1^2)}{-j(-\alpha - j\omega_1 - s_o)2\omega_1} e^{(-\alpha_1 - j\omega_1)t} \quad (43)$$

By integration, the response to a step function of acceleration, with the integration constant neglected, becomes

$$a_{ols} = \frac{2(\alpha_1^2 + \omega_1^2)}{(\alpha_1 + s_o)^2 + \omega_1^2} e^{s_o t} + \frac{(-\alpha_1 + j\omega_1 + s_o)(-\alpha_1 - j\omega_1)}{j(-\alpha_1 + j\omega_1 - s_o)2\omega_1} e^{(-\alpha_1 + j\omega_1)t} + \frac{(-\alpha_1 - j\omega_1 + s_o)(-\alpha_1 + j\omega_1)}{-j(-\alpha_1 + j\omega_1 - s_o)2\omega_1} e^{(-\alpha_1 - j\omega_1)t} \quad (44)$$

Sorting of reals and imaginaries, so as to yield solutions in trigonometric form, for the purposes of this paper is done only for particular cases of interest.

APPENDIX 3

RESPONSE OF A DOUBLE RESONATOR

The transfer function of a viscously damped double resonator, with no loading of the first resonator by the second, expressed as the ratio to the Laplace transform of a unit-area impulse, is given by

$$\frac{L_{2i}}{1} = \frac{(\alpha_1^2 + \omega_1^2)(\alpha_2^2 + \omega_2^2)}{[(s + \alpha_1)^2 + \omega_1^2][(s + \alpha_2)^2 + \omega_2^2]} = \frac{(\alpha_1^2+\omega_1^2)(\alpha_2^2+\omega_2^2)}{(s+\alpha_1-j\omega_1)(s+\alpha_1+j\omega_1)(s+\alpha_2-j\omega_2)(s+\alpha_2+j\omega_2)} \quad (45)$$

Accordingly, the response to the unit-area impulse of acceleration is obtained by the Heaviside expansion theorem as

$$a_{2i}(t) = \frac{(\alpha_1^2+\omega_1^2)(\alpha_2^2+\omega_2^2)\, e^{(-\alpha_1+j\omega_1)t}}{j2\omega_1[(-\alpha_1+\alpha_2)+j(\omega_1-\omega_2)][(-\alpha_1+\alpha_2)+j(\omega+\omega_2)]}$$

$$+\frac{(\alpha_1^2+\omega_1^2)(\alpha_2^2+\omega_2^2)}{-j2\omega_1[(-\alpha_1+\alpha_2)-j(\omega_1-\omega_2)][(-\alpha_1+\alpha_2)-j(\omega_1+\omega_2)]}e^{(-\alpha_1-j\omega_1)t}$$

$$+\frac{(\alpha_1^2+\omega_1^2)(\alpha_2^2+\omega_2^2)}{j2\omega_2[(-\alpha_1+\alpha_1)+j(\omega_2-\omega_1)][(-\alpha_2+\alpha_1)+j(\omega_2+\omega_1)]}e^{(-\alpha_2+j\omega_2)t}$$

$$+\frac{(\alpha_1^2+\omega_1^2)(\alpha_2^2+\omega_2^2)}{-j2\omega_2[(-\alpha_2+\alpha_1)-j(\omega_2-\omega_1)][(-\alpha_2+\alpha_1)-j(\omega_2+\omega_1)]}e^{(-\alpha_2-j\omega_2)t} \quad (46)$$

Integration yields, for the response for the unit step function of acceleration, with the integration constant neglected,

$$a_{2s}(t)$$

$$=\frac{(\alpha_1-j\omega_1)(\alpha_2^2+\omega_2^2)}{j2\omega_1[(-\alpha_1+\alpha_2)+j(\omega_1-\omega_2)][-\alpha_1+\alpha_2)+j(\omega_1+\omega_2)]}e^{(-\alpha_1+j\omega_1)t}$$

$$+\frac{(\alpha_1+j\omega_1)(\alpha_2^2+\omega_1^2)}{-j2\omega_1[(-\alpha_1+\alpha_2)+j(\omega_1-\omega_2][-\alpha_1+\alpha_2)-j(\omega_1+\omega_2)]}e^{(-\alpha_1-j\omega_1)t}$$

$$+\frac{(\alpha_1^2+\omega_1^2)(\alpha_2-j\omega_2)}{j2\omega_2[(-\alpha_2+\alpha_1)+j(\omega_2-\omega_1)][(-\alpha_2+\alpha_1)+j(\omega_2+\omega_1)]}e^{(-\alpha_2+j\omega_2)t}$$

$$+\frac{(\alpha_1^2+\omega_1^2)(\alpha_2+j\omega_2)}{-j2\omega_2[(-\alpha_2+\alpha_1)+j(\omega_2-\omega_1)][(-\alpha_2+\alpha_1)-j(\omega_2+\omega_1)]}e^{(-\alpha_2-j\omega_2)t}$$

$$\simeq\frac{-\alpha_1-j\omega_1}{-j4(\omega_1-\omega_2)}e^{(-\alpha_1+j\omega_1)t}+\frac{-\alpha_1+j\omega_1}{j4(\omega_1-\omega_2)}e^{(-\alpha_1-j\omega_1)t}$$

$$+\frac{-\alpha_1-j\omega_1}{-j4(\omega_2-\omega_1)}e^{(-\alpha_1+j\omega_1)t}+\frac{-\alpha_1+j\omega_1}{j4(\omega_2-\omega_1)}e^{(-\alpha_1-j\omega_2)t} \quad (47)$$

if $\alpha_1 \simeq \alpha_2 \ll \omega_1$ and $\omega_1 \simeq \omega_2$.

The transfer function of the double resonator and the phase shift network, expressed as the ratio to the Laplace transform of a unit-area impulse function is

$$\frac{L_{o2i}}{1}=\frac{(s+s_o)(\alpha_1^2+\omega_1^2)(\alpha_2^2+\omega_2^2)}{(s-s_o)(s+\alpha_1-j\omega_1)(s+\alpha_2 j\omega_1)(s+\alpha_2-j\omega_2)} \quad (48)$$

Accordingly, by reference to the effect of the phase shift network on single resonator response, as in Equation (43), the sum of the ω_1 and ω_2 transients is

$$a_{02s}\simeq\frac{(-\alpha_1+j\omega_1+s_o)(-\alpha_1-j\omega_1)}{-j4(\omega_1-\omega_2)(-\alpha_1+j\omega_1-s_o)}e^{(-\alpha_1+j\omega_1)t}$$

$$+\frac{(-\alpha_1-j\omega_1+s_o)(-\alpha_1+j\omega_1)}{j4(\omega_1-\omega_2)(-\alpha_1-j\omega_1-s_o}e^{(-\alpha_1-j\omega_1)t}$$

$$+\frac{(-\alpha_1+j\omega_2+s_o)(-\alpha_1-j\omega_1)}{-j4(\omega_2-\omega_1)(-\alpha_1+j\omega_2-s_o)}e^{(-\alpha_1+j\omega_2)t}$$

$$+\frac{(-\alpha_1-j\omega_2+s_o)(-\alpha_1+j\omega_1)}{j4(\omega_2-\omega_1)(-\alpha_1-j\omega_2-s_o)}e^{(-\alpha_1-j\omega_2)t} \quad (49)$$

As with the single resonator, sorting of reals and imaginaries, so as to express the results in trigonometric form, is for the purposes of this paper, done only for particular cases of interest.

FLUID-STRUCTURE TOPICS

DETERMINATION OF DYNAMIC LOADS FROM MISSILE MODEL WIND TUNNEL DATA

Phyllis G. Bolds and David K. Barrett
Air Force Flight Dynamics Laboratory
Wright-Patterson AFB, Ohio

The Air Force Flight Dynamics Laboratory has measured, recorded, and reduced acoustic and vibration data to describe the dynamic pressure environment on the leeward surface of a missile model. The test was conducted in the 16T Wind Tunnel at Arnold Engineering Center, Tullahoma, Tennessee. The data recorded at Pitch Angle 2/9Π and Π/2 rad have been selected to illustrate their vortex shedding pattern and their effect upon the natural and dynamic response frequencies of the model to a prototype missile. From the analysis of the data presented in this study, pressure coefficients greater than 632.45 Pa occur at 2/9Π and Π/2 rad pitch angle, and peaks in the frequency analysis at 2/9Π rad occur in the natural frequency range of the full scale missile.

INTRODUCTION

The Air Force Flight Dynamics Laboratory (AFFDL), at the request of the Air Force Space and Missile Systems Organization (SAMSO), has obtained unsteady pressure data on a model of a proposed long range attack missile. The missile is required to fly at high angles of attack during the initial portion of the trajectory. During this portion of the flight, if Von Karman vortices are shed, there will be side loadings which could cause undesirable dynamic response of the missile structure. Two missile model bodies and six different nose configurations were tested at free-stream Mach numbers ranging from 0.3 to 1.3 and Reynolds numbers ranging from 1.84 X 10^6 to 18.4 X 10^6. Unsteady pressure measurements were made on the leeward side of the missile for angles of pitch ranging from -Π/36 to Π rad.

The objective of this paper is to discuss the flight conditions that produce significant (>150 dB, or 632.45 Pa, Reference 1) unsteady pressure on the surface of the missile. At the very low angles of pitch (<Π/9 rad) generally a symmetrically disposed pair of vortices will be produced. By increasing the angle of pitch through a Π/9 to Π/4 rad range, an asymmetric (Von Karman) vortex pattern is produced An asymmetric vortex occurs when at any instant of time the difference between the free-stream pressure and the pressure occurring on the surface of the missile is positive for one side and negative for the opposite side of the missile with correlation occurring along the missile length. When the frequency of an asymmetric vortex pattern corresponds to any of the missile's free-free modes, then resonance of the missile in bending could occur. The amplitude of this bending will depend on the magnitude and frequency of the pressure and its distribution over the surface of the missile. Finally, as α approaches Π/2 rad, the distinct vortices may be replaced by a random pattern for Reynolds numbers greater than 10^5, Reference 2. The frequencies of the dynamic pressure fluctuations will be scaled to what should occur on the full scale missile by means of the Strouhal number.

MEASUREMENT AND ANALYSIS

Test Facility. This test was conducted at Arnold Engineering Development Center (AEDC), Tennessee, in the 4.88 meter transonic wind tunnel (16T). Tunnel 16T is a closed

circuit continuous flow wind tunnel capable of operating at Mach numbers from 0.2 to 1.60. It operates in a stagnation pressure range from approximately 5.746 kPa to 191.521 kPa and a stagnation temperature range of 26°C to 71°C depending on Mach number. The specific humidity of the air is controlled by removing tunnel air and supplying conditioned makeup air from an atmospheric drier. A more extensive description of the tunnel facility and its operating characteristics is contained in Reference 3.

Model Description. The 19.30 cm diameter cylindrical model was tested with two basic body lengths, B-1 and B-2, and with various combinations of four ogive and two triconic nose configurations. The two body lengths B-1 and B-2 represent an 11.57 percent scale model and an 8.57 percent scale model of the missile respectively. A diagram of the missile model and its various nose configurations is shown in Figure 1.

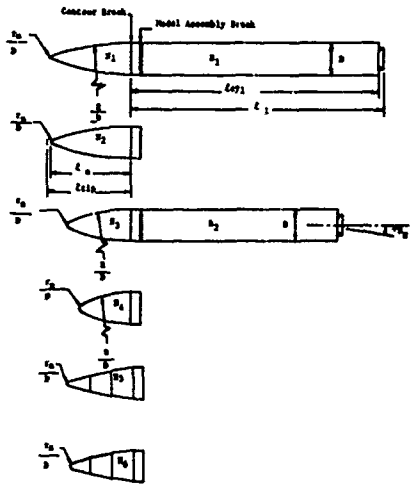

Figure 1 Model Configuration

Four rows of microphones were placed along the model length in order to measure the dynamic pressures on the leeward model surface. Two different mounting systems were used to achieve the objective of the test. The first was a standard sting mount connected to a high pitch mechanism capable of pitching the model to pitch angles up to Π/4 rad. The second mounting configuration utilized a strut mount out the side of the model connected to an adjustable knuckle enabling pitch angles greater than Π/4 rad to be obtained (Figure 2).

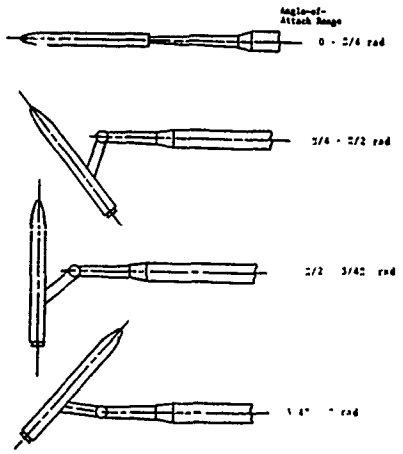

Figure 2 Model Support Arrangements

Data Acquisition. Thirty-two piezoelectric microphones were placed on the leeward side of the model to measure the unsteady pressures (see Figure 3). The outputs of these microphones were directed through approximately 60 meters of shielded cable to a set of Intech line-driver amplifiers. The outputs of these amplifiers were then fed through 450 meter long landlines into the AFFDL mobile data acquisition van. Inside the van, the signals were conditioned by Ithaco auto-ranging amplifiers and recorded on three 14-channel FM tape recorders. A tape speed of 19.05 cm/sec was used yielding a 2.5 kHz cut-off frequency. IRIG "B" time code and voice annotation were also recorded to provide correlation capability between tunnel data and the recorded unsteady pressure data (see Figure 4). A thirdy second record was made at each condition to allow for time needed for the statistical analysis of the data, Table I.

Model and support system resonances were determined by attaching four piezoelectric crystal accelerometers to the model and recording a series of impacts delivered to the model in various directions. Location of the accelerometers can be seen in Figure 5.

TABLE I Tunnel Conditions

M	RE	N2B1								N3B1	N4B1	N3B2										N4B2	N5B2	N6B1
		0	45		90		135			0	0	45		(+)	90		(-)	135		(-)	45	0	0
		P	P	J	P	J	P	J		P	P	P	J	D	P	J	D	P	J	D	P	P	P
0.3	6.6													*									
0.4	1.6		*																				
	3.3	*.	*							*.	*.												*
	6.6	*.	*	*	*	*	*	*		*.	*.			*									
0.6	1.6	*.	*							*.													*
	3.3	*.	*	*						*.	*.						*	*	*			*	
	9.8	*.	*	*						*.	*.												*
	6.4	*.	*	*								*	*	*			*						
	13.4	*.	*		*	*				*.	*.												
0.7	16.4									*.													
0.8	1.6	*.								*.													
	3.3	*.								*.	*.												*
	9.8	*								*.	*.												
	16.4	*								*.	*.	*	*	*				*	*	*	*	*	*
0.9	15.7	*.								*.	*.	*											*
1.0	15.1	*.								*.	*.	*											*
1.1	14.4	*.								*.	*.												
1.2	13.8											*											*
1.3	13.1	*.								*.	*.												*

.Crit P - Pressure J - Jet On D - Jet On Deflected RE = RE/m x 10^{-6} M= MACH

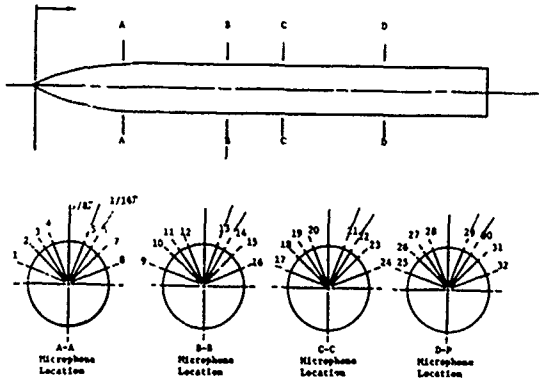

Figure 3 Microphone Location - N2B1

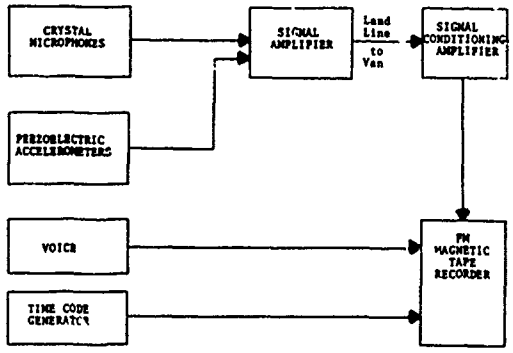

Figure 4 Data Acquisition System

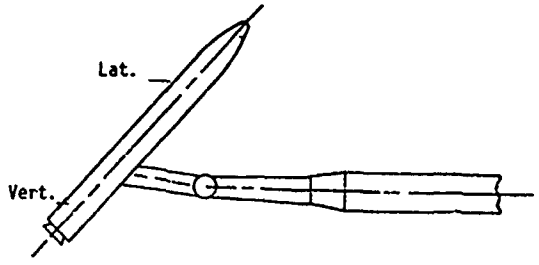

Figure 5 Accelerometer Locations

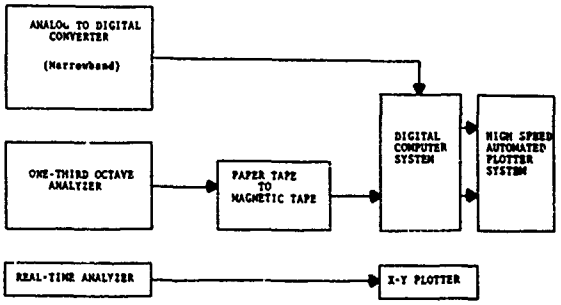

Figure 6 Data Analysis System

Data Analysis. Analog tapes recorded during the wind tunnel test were analyzed in the AFFDL Vibration and Aeroelastic Laboratory located at WPAFB, Ohio. Figure 6 shows a block diagram of the analysis system used on the data. Using the results of a "quick look" one-third octave analysis performed on the data, two tunnel conditions were selected for comprehensive narrow band (0.9 Hz) analysis. Analysis of the vibration data was performed using a "real-time" spectrum analyzer in the transient capture mode.

Data Presentation. The data in this paper in Figures 7, 8, and 11 through 30 was obtained during the following conditions:

TABLE II Selected Tunnel Conditions

Nose Configuration	N2B1
Mach	0.6
Velocity	206.3 meters/sec
Reynolds Number	18.4 X 10^6/meter

The RMS pressure coefficients $(C_p)_{RMS}$ were computed thusly:

$$(C_p)_{RMS} \equiv \left(\frac{P}{q_\infty}\right)_{RMS} \qquad (1)$$

where p is the measured unsteady pressure and $q_\infty = 1/2\ \rho V^2$. The RMS pressure coefficients were plotted versus θ, the transducer location in degrees from the zero degree location (see Figures 7 and 8) to show the overall amplitude variations both longitudinally and radially. Power spectral density (PSD), PHI value, was calculated from the measured data using a reduced frequency to ultimately yield the frequencies of concern associated with the non-dimensional vortex shedding frequency (Strouhal number) expected on the full scale prototype.

$$PHI = \frac{|C_{pi}|^2}{\frac{\Delta\omega D}{V}} \qquad (2)$$

where $\Delta\omega$ is the frequency in radians ($2\pi\Delta f_i$) and Δf_i is the broad (constant percentage of $.23f_i$) bandwidth for the ith band under consideration, D is the diameter of the missile model, and V is the free-stream velocity. PHI is plotted versus $\omega D/V$. The value of PHI is useful in determining potential coupling of the unsteady air loads with natural modes of the missile (see Figures 11-12). Cross correlation functions were computed from the narrow band analysis of selected data (Table II) both longitudinally and radially to determine if the vortex shedding was symmetric, asymmetric, or random in nature (see Figures 18-34).

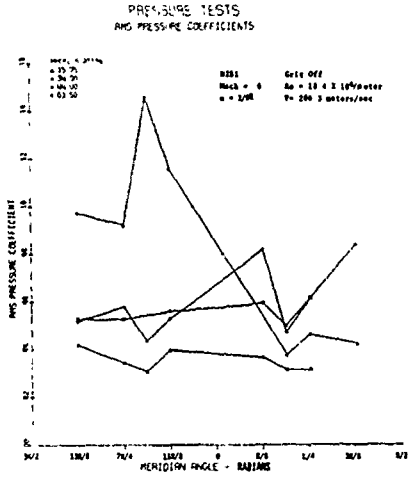

Figure 7 RMS Pressure Coefficient, at $\alpha = 2/9\pi$

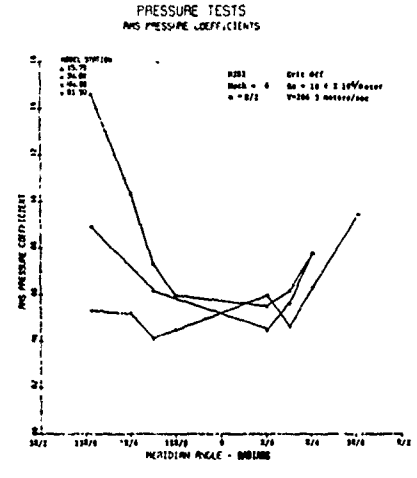

Figure 8 RMS Pressure Coefficient, at $\alpha = \pi/2$

DISCUSSION OF RESULTS

Figures 7 and 8 indicate that for the RMS pressure coefficients calculated from Equation 1 for the selected tunnel condition, Table II, there are values greater than 150 dB or which indicate a significant overall unsteady pressure. A PSD analysis of these data was then obtained by Equation 2. The natural frequencies of the model and support system occur at 7.2, 13, and 16.2 Hz as shown in Figures 9 and 10 and correspond to reduced frequencies 0.044, 0.076, and 0.095 Hz. These data were used to test the validity of the unsteady pressure response. Figures 11 and 12 show the PSD analysis versus the reduced frequency for the excessive measurement at $\alpha = 2/9\Pi$ and $\alpha = \Pi/2$ rad, respectively. The peaks in the power spectrum at reduced frequencies for each microphone, <0.118 Hz, correspond to the natural frequencies of the missile model and support system. The peaks in the power spectrum occurring above the reduced frequency of 0.118 Hz correspond to vortex shedding frequency range at the specified microphone location.

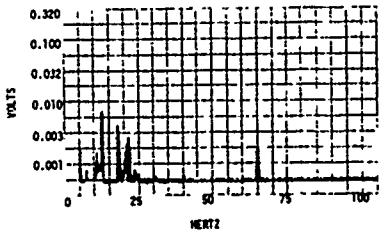

Figure 9 Lateral Frequency Analysis of Model

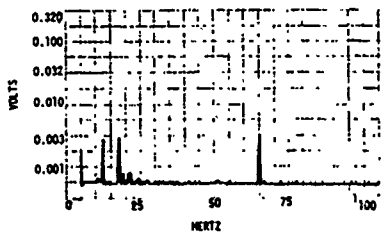

Figure 10 Vertical Frequency Analysis of Model

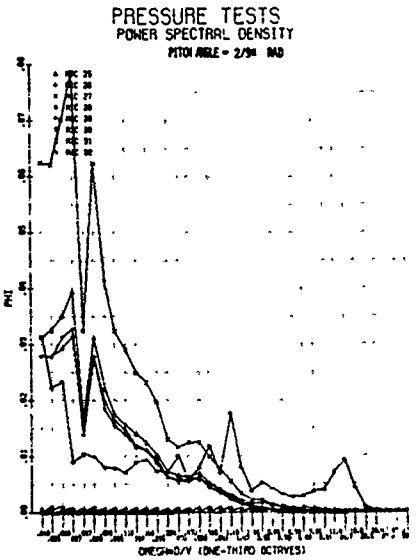

Figure 11 The Related Frequencies of the Full Scale Missile at Station D, $\alpha = 2/9\Pi$

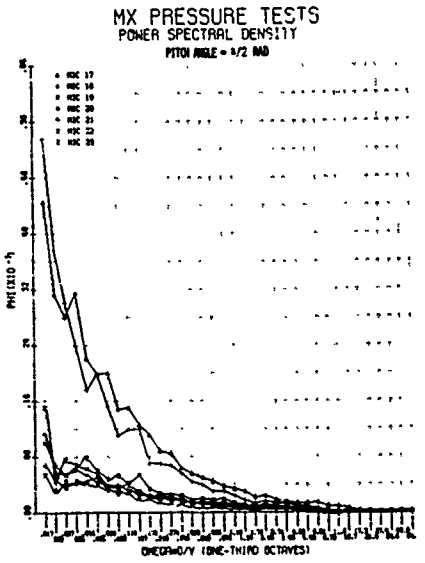

Figure 12 The Related Frequencies of the Full Scale Missile at Station C, $\alpha = \Pi/2$

Figures 13 through 21 show the cross-correlation of the microphones measured during $\alpha = 2/9\Pi$ rad condition. The radial cross-correlations were computed using Microphone 1 as the reference and correlated it with Microphones 2 through 7. Figures 13 through 15 show a very high correlation with Microphone 1 at values near 150 dB in the positive direction. Figures 16 through 18 show the correlation of Microphone 1 to Microphones 5, 6, and 7 which are located on the opposite side of the missile to be highly correlated approaching 150 dB in the negative direction. The results of the radial cross-correlation analysis show side loading at microphone Station A for $\alpha = 2/9\Pi$ rad are approaching the significant level.

Figures 19 through 21 show the longitudinal cross-correlation using Microphone 1 of ring A as the reference to the corresponding microphone at the same radial locations on microphone rings B, C, and D. Microphone 1 is positively correlated with Microphones 9 and 17 at values near 150 dB, but negatively correlated with Microphone 25 at a value greater than 150 dB. The overall frequency and time domain analyses show that at $2/9\Pi$ rad pitch angle an asymmetric vortex pattern occurs.

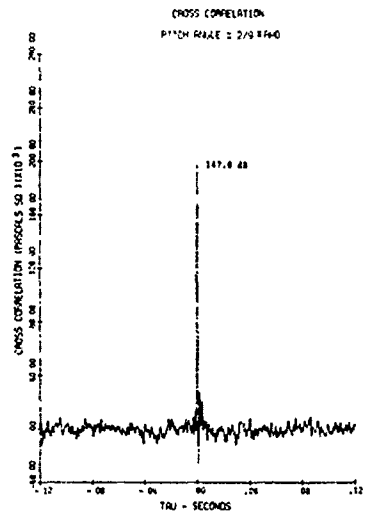

Figure 14 Cross Correlation Analysis of Microphones 1 and 3

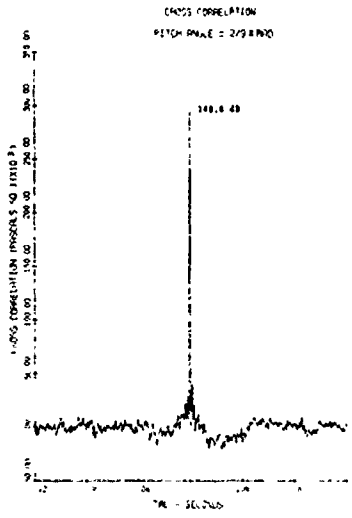

Figure 13 Cross Correlation Analysis of Microphones 1 and 2

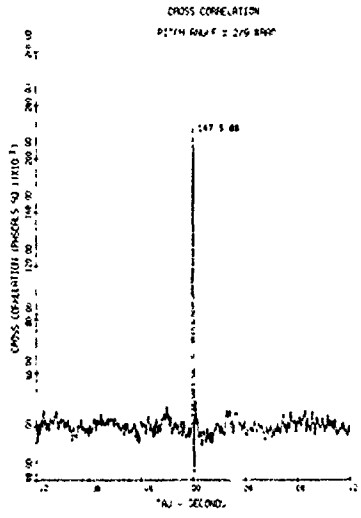

Figure 15 Cross Correlation Analysis of Microphones 1 and 4

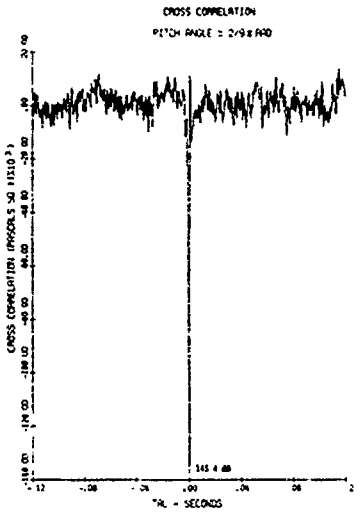

Figure 16 Cross Correlation Analysis of Microphones 1 and 5

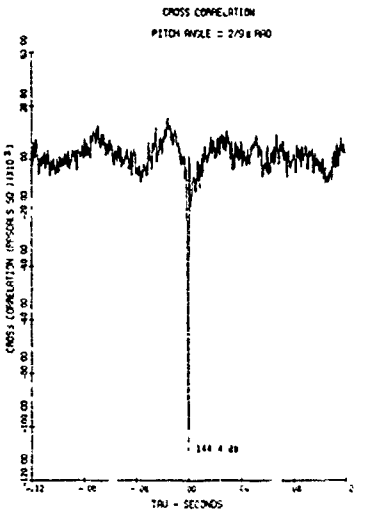

Figure 18 Cross Correlation Analysis of Microphones 1 and 7

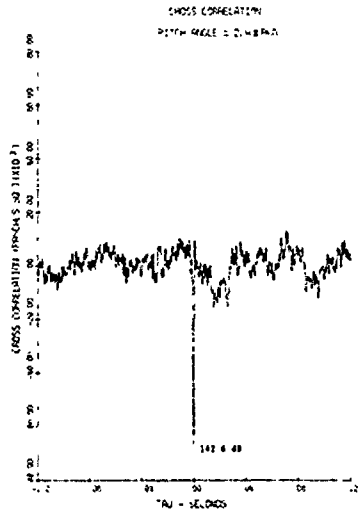

Figure 17 Cross Correlation Analysis of Microphones 1 and 6

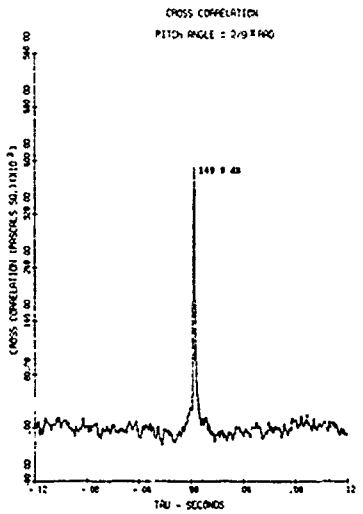

Figure 19 Cross Correlation Analysis of Microphones 1 and 9

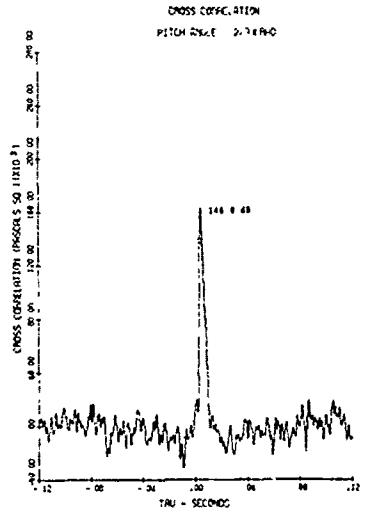

Figure 20 Cross Correlation Analysis of Microphones 1 and 17

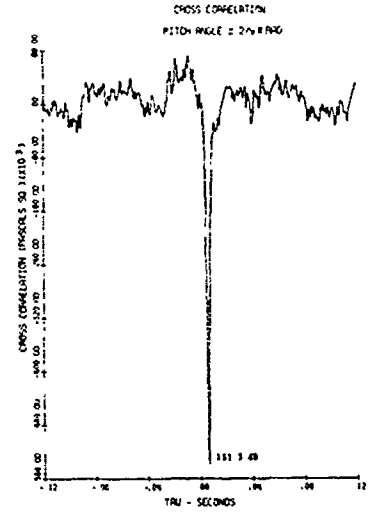

Figure 21 Cross Correlation Analysis of Microphones 1 and 25

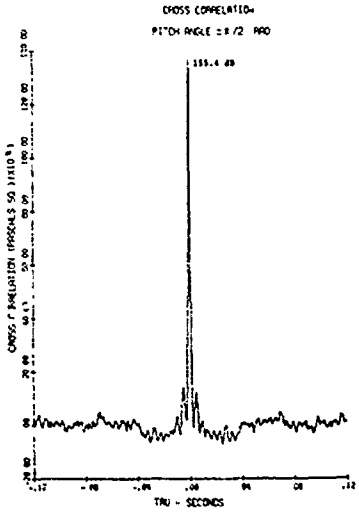

Figure 22 Cross Correlation Analysis of Microphones 9 and 10

Figures 22 through 30 show the cross-correlation analysis for the $\Pi/2$ rad angle of attack condition. Microphone 9 is the reference microphone selected for cross-correlation analysis of the $\alpha = \Pi/2$ rad condition. Figures 22 through 28 show the radial correlation of Microphone 9 to Microphones 10, 11, 12, 13, 14, 15, and 16. Microphones 10, 11, and 12 show a positive but at a significant level that decreases directly as the distance. Microphones 13, 14, 15, and 16, located on the opposite side of the missile, show correlation to Microphone 9 in the positive and negative direction at values near the significant level. Figures 29 and 30 show the longitudinal correlations at the $\Pi/2$ rad pitch angle condition. Microphones 18 and 25 show values approaching the significant level in the positive and negative correlation to Microphone 9 but the correlation occurs at many tau values. Consequently the $\alpha = \Pi/2$ rad condition produces a random vortex shedding pattern.

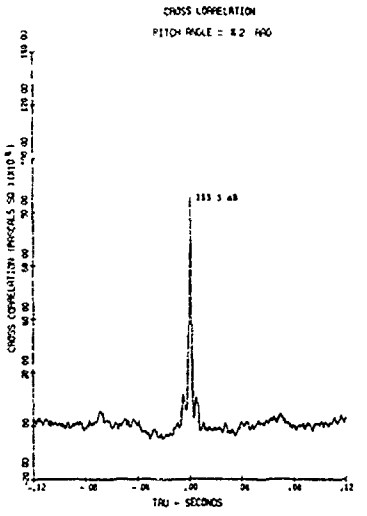

Figure 23 Cross Correlation Analysis of Microphones 9 and 11

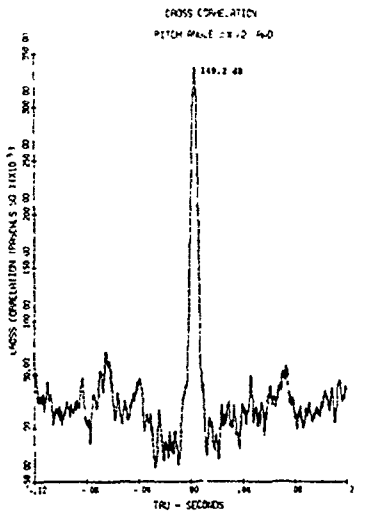

Figure 24 Cross Correlation Analysis of Microphones 9 and 12

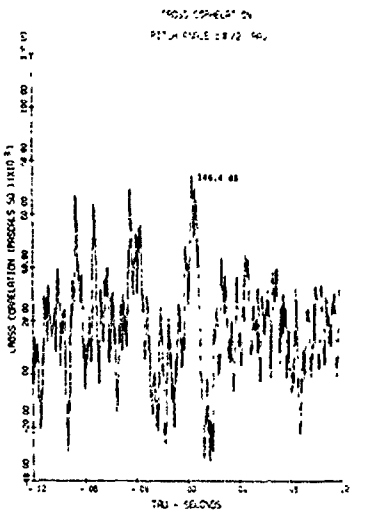

Figure 25 Cross Correlation Analysis of Microphones 9 and 13

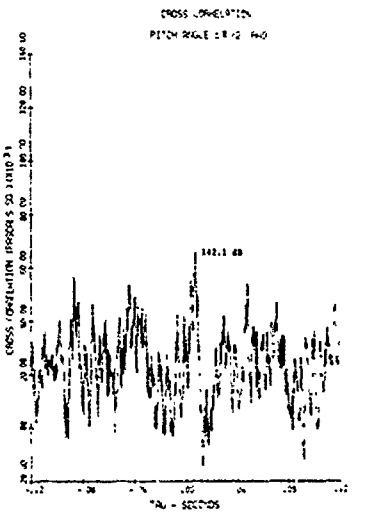

Figure 26 Cross Correlation Analysis of Microphones 9 and 14

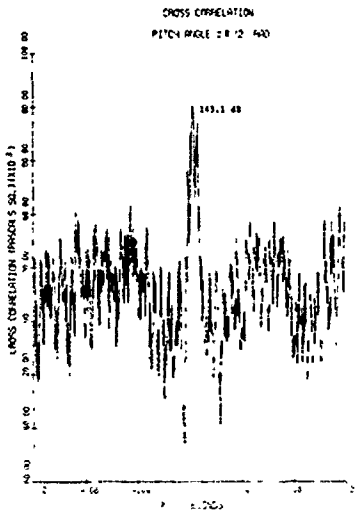

Figure 27 Cross Correlation Analysis of Microphones 9 and 15

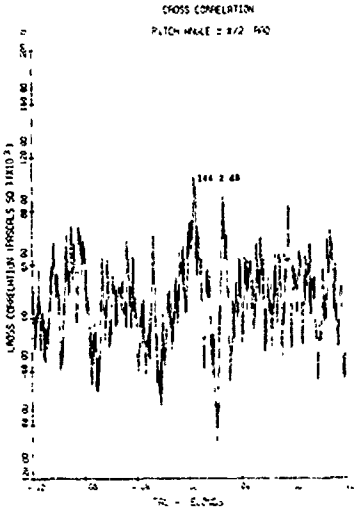

Figure 29 Cross Correlation Analysis of Microphones 9 and 18

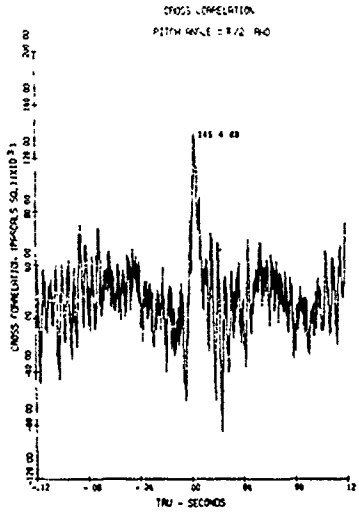

Figure 28 Cross Correlation Analysis of Microphones 9 and 16

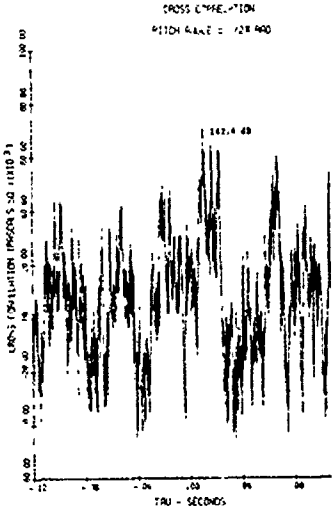

Figure 30 Cross Correlation Analysis of Microphones 9 and 25

CONCLUSIONS

From the analysis of the data presented in this study, the following conclusions are reached:

1. Pressure coefficients greater than 150 dB or 632.45 Pa occur at $2/9\pi$ rad and $\pi/2$ rad pitch angle tunnel conditions at specific locations.

2. Peaks in the frequency analysis at $\alpha = 2/9\pi$ rad occur in the natural frequency range of the full scale missile.

3. Asymmetric vortex shedding patterns occur around $2/9\pi$ rad pitch angle at Mach 0.6.

4. A random vortex shedding pattern occurs around $\pi/2$ rad pitch angle at Mach 0.6.

REFERENCES

1. Rogers, O. R. and Cook, R. F., "Environmental Aspects of Sonic Fatigue," WADC TN 57-68, Feb 1957.

2. Clark, W. H., Peoples, J. R., and Briggs, M. M., "Occurrence and Inhibition of Large Yawing Moments during High-Incidence Flight of Slender Missile Configurations," Journal of Space and Rockets, Vol. 10, No. 8, August 1973, pp. 510-519.

3. Test Facilities Handbook (Tenth Edition). "Propulsion Wind Tunnel Facility, Vol. 4," Arnold Engineering Development Center, May 1974.

ACKNOWLEDGEMENT

The authors would like to thank the Dynamics Technology Applications Branch for their assistance in the measurement and analysis of these unsteady pressure data, Mr. Robert Cook and Mr. Donald Shereda all of AFFDL, and Mr. Warren Koerner (TRW).

Discussion

Mr. Van Ert (Aerospace Corporation): A 180 degree angle attack sounds kind of ferocious, did you investigate that over a broad Mach number range or was that over a restricted Mach number range?

Ms. Bolds: No that was over a broad Mach number range from .3 to 1.3. It seems kind of ridiculous that it would be flying backward but that possibility hasn't been dismissed.

Mr. Smith (Bell Aerospace): I wonder if it is thought to be a problem that you may get vortices correlating at frequencies that are close to the structural modal frequencies of a missile? Isn't it possible, as we find with telegraph wire and twigs in the wind and so on, that the vortex frequencies themselves would be determined by the structural modal frequencies, and that they would lock into the structural modal frequencies, and you would get an automatic signing? That is the modal frequencies themselves may determine the vortex shedding frequencies and you might have a natural resonance.

Ms. Bolds: It is quite possible; we didn't look at them in very narrow correlation, we did however do some coherence function analyses and they did correlate with them.

Mr. Smith: I think when you hear a telephone wire singing in the wind it isn't because the vortex shedding frequency happens to coincide with the frequency of the wire, it is because the vortices shed in sympathy with the frequency of the wire. That is the frequency of the wire determines the vortex frequency and I wonder, if you had a flexible modal that represented the modal frequencies to some scale, whether you might not find that the vortex shedding frequencies would lock in on these modal frequencies.

Ms. Bolds: That is quite possible but since we had a rigid model of this missile it didn't.

Mr. Galef (TRW Systems): I question whether it is true that the frequency of the vortex shedding can be affected by the telegraph wire motion; I believe that the wire motion tends to lock in the correlation along the length, so that we do have correlation along the length of the multimode telegraph wire. This is exactly the same thing that we are concerned about for the missile program that Ms. Bolds is talking about and we are trying to get a handle on this.

FEASIBILITY STUDY OF AN ACOUSTIC ENCLOSURE FOR SHUTTLE PAYLOADS *

M. Ferrante and C. V. Stahle
General Electric Space Division
Philadelphia, Pennsylvania

and

F. J. On
NASA Goddard Space Flight Center
Greenbelt, Maryland

This paper presents the analysis, design and experimental evaluation of a viscoelastic laminated acoustic enclosure that will shield sensitive instruments from the high low-frequency acoustic environment of the Space Shuttle payload bay. It provides a cost effective method of reducing payload developmental costs by circumventing this more severe dynamic environment.

A cylindrical enclosure configuration with two face sheets joined by a viscoelastic shear layer was analyzed to determine the optimum wall construction. The wall construction was optimized for a 0.914 meters (three foot) diameter considering a 500 Hz minimum resonant frequency as a design goal. The analysis considered aluminum, magnesium and graphite epoxy materials for the face sheets. The results indicate that surface densities on the order of 1.22 to 2.44 KG/m^2 (0.25 to 0.5 lbs/ft^2) can be obtained using thin face sheets with a core made of strips of viscoelastic epoxy 6.35 millimeters (1/4 inch) wide on 127 millimeter (5 inch) centers. Although the design was optimized for a 0.914 meter (3 foot) diameter, the results incidate that larger diameter enclosures are also feasible.

The experimental evaluation of the acoustic enclosure was performed in the NASA-Goddard Space Flight Center reverberant chamber and showed excellent agreement with predicted noise reductions. Two configurations were tested: one with the fiberglass liner and one without the fiberglass liner. Average reductions in the overall acoustic level of 20 dB and 12 dB were obtained with and without the fiberglass liner. In the low frequency range, attenuations were on the order of 20 to 30 dB. At high frequencies, attenuations were increased from approximately 25 dB to over 40 dB by the fiberglass liner. Minimum attenuations of 17 and 7 dB occurred in the 200 to 500 Hertz range with and without the fiberglass liner, respectively.

* This work was performed for NASA-Goddard Space Flight Center

INTRODUCTION

The general arrangement of the Shuttle places the payload close to the rocket engine exhaust which results in a more severe acoustic environment than that of current launch vehicles. A design goal for Shuttle has been to limit the acoustic environment within the payload bay to 145 dB. However, current estimates of the attenuation provided by the Shuttle structure indicate that the levels are more likely to be on the order of 150 dB as shown in Fig. 1, [1,2,3,4]. The Shuttle structure must provide more attenuation than obtained with smaller diameter launch vehicle shrouds as indicated in the figure. On the other hand, continuing efforts to minimize the structural weight of the Orbiter has resulted in numerous design changes not yet factored into acoustic predictions. One of the most recent changes was to use lightweight graphite composite honeycomb doors. This weight reduction will probably reduce the acoustic attenuation provided by the Orbiter structure as will the effects of vents and door seals which have not yet been included. To further complicate the predictions, the results of recent acoustic model tests at NASA-MSFC have indicated that the noise levels in the low frequency range shown in Fig. 1 should be increased. The current indications are that the low frequency acoustic environment within the Shuttle payload bay will be higher than the 145 dB Shuttle design goal and will be considerably more severe than that of current launch vehicles, particularly in the low frequency range.

The random vibration of the experiments resulting from the acoustic environment will be much higher than that of current spacecrafts. The random vibration levels of spacecraft components predicted for Shuttle by ESRO and by extrapolating NASA-GSFC spacecraft data are compared with current spacecraft random vibration requirements in Fig. 2. Although these predictions do not include the most recent acoustic model test results or the graphite composite honeycomb Shuttle door effects, the vibration levels underline the damaging effects of the high acoustic environment. It is not only the acoustic pressure effects on thin films that must be considered but it is also the high random vibration levels of the

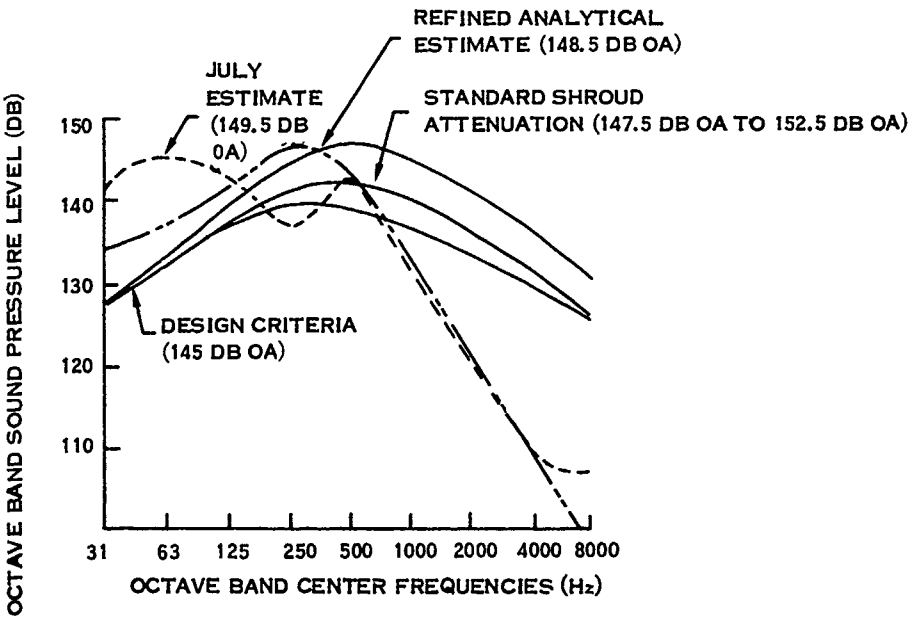

Fig. 1. Internal payload bay acoustic spectra

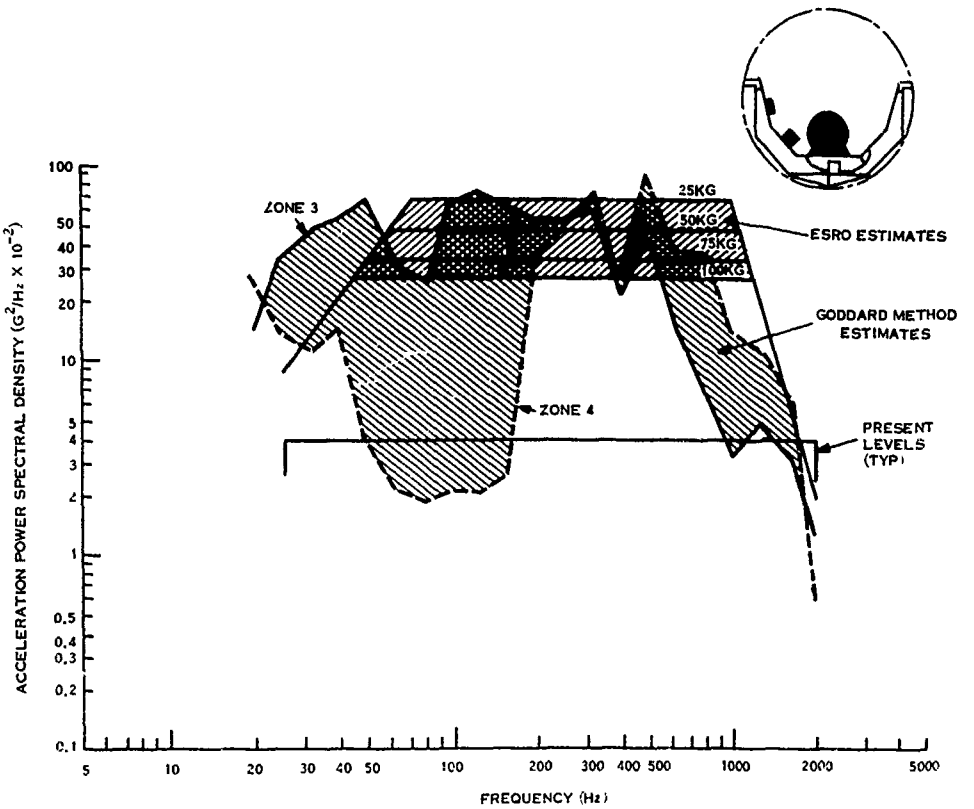

Fig. 2. Random vibration spectra of payload components mounted to spacelab pallets

experiments that can cause failures within electronic packages that are important.

The objective of this study was to investigate small acoustic enclosures as a cost effective method of reducing payload development costs. The high low frequency acoustic environment will result in a more severe dynamic environment than that of current launch vehicles. Consequently, it is anticipated that many new problems in experiment development will arise and that the use of existing experiment components and instruments will require qualification for the Shuttle environment. One method of circumventing the more severe dynamic environment is to provide protective enclosures for sensitive portions of the experiments. If this can be accomplished effectively, generic experiment components can be used with a high degree of confidence in subsequent orbital operation and development costs will be substantially reduced. For this approach to be effective, a lightweight protective enclosure design must be used. This paper describes a preliminary design and experimental evaluation of a lightweight acoustic enclosure. A 0.914 meter (three foot) size was selected for this study.

ACOUSTIC ENCLOSURE DESIGN CONSIDERATIONS

Several major factors involved in the design of an acoustic enclosure for Shuttle payloads must be considered. These include the basic characteristics of acoustic-barriers, damping properties of viscoelastic epoxy materials, geometric configuration and wall construction. Three fre-

quency regions are of primary interest in the design of an acoustic enclosure as shown in Fig. 3. In the lowest region, the acoustic reduction (transmission loss) is controlled by the stiffness and damping characteristics of the enclosure. In the second region, the mass of the enclosure is the controlling factor. At very high frequencies, the attenuation is controlled by wave coincidence. The first of these three regions is of primary interest in this application.

In the low frequency range, large acoustic attenuation can be provided if the enclosure is very stiff and contains a large amount of damping. The frequency range where enclosure stiffness is the controlling factor depends on the lowest resonant frequency of the structure. The acoustic attenuation in this frequency range is limited to estimates of the attenuation at very low frequencies, [4, 5, 6]. For flat panels of the type used in architectural acoustics, this range is of little interest in that the enclosure resonant frequencies are very low. However, this is not necessarily the case for aerospace structures. For semi-monocoque cylindrical aerospace structures, resonant frequencies can be above 100 Hertz. As these resonances occur, the effectiveness of the enclosure varies widely depending on the damping in the structure as indicated in the figure. If a lightweight enclosure for low frequency acoustic attenuation is desired, the objective becomes that of providing an enclosure with a high resonant frequency and, to extend the frequency range of effectiveness, high damping. A design goal of 500 Hertz was selected for the fundamental resonant frequency.

In the high frequency range, acoustic absorption can be used to obtain a high noise reduction. Acoustic liners have relatively high absorption coefficients in this frequency range but are relatively ineffective in the low frequency range.

A preliminary indication of the amount of acoustic attenuation required can be obtained by comparing the prediction of Frank On [3] with the current acoustic require-

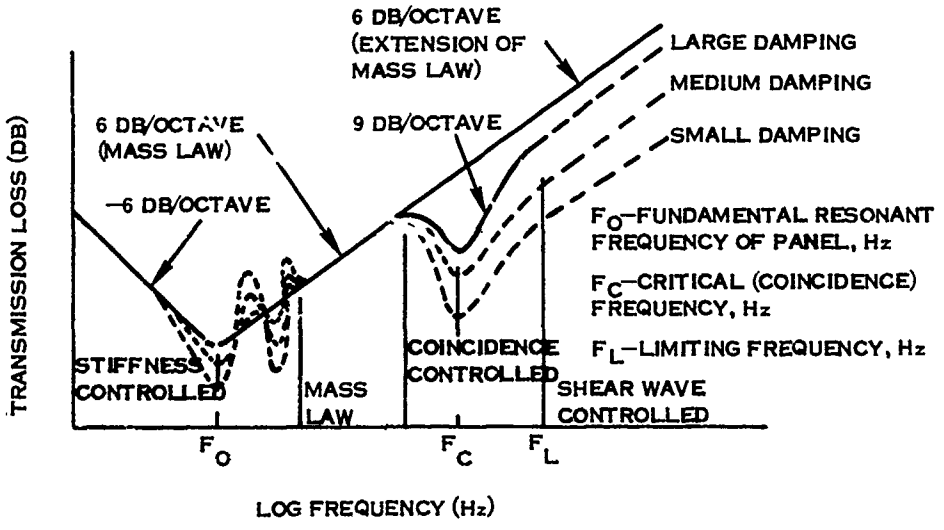

Fig. 3. General form of transmission loss characteristics of single flat wall panels

ments for the Delta launch vehicle, Fig. 4. This comparison indicates that a reduction on the order of 15 to 7 dB is required in the frequency range from 100 to 500 Hertz. This provides an order of magnitude indication of the reduction required although balloon launch experiments being considered for Shuttle missions have no significant dynamic environments to consider. For these types of equipments, an additional 5 to 10 dB reduction is desirable.

The General Electric Space Division has been actively pursuing the development and application of high damping viscoelastic epoxy materials (SMRD) for the control of spacecraft vibration. Initial applications of damping materials were for the control of electronic part vibration in Landsat 1 packages, [7]. Subsequently, a number of IR&D programs and studies have been used to develop and apply damping materials, [8, 9, 10, 11]. A wide variety of viscoelastic epoxy compounds having loss factors on the order of 1.5 to 2.0 and a range of stiffness values have been developed. These epoxy compounds are castable, have low outgassing characteristics, and a low density compared to otner high damping materials.

For the acoustic enclosure, SMRD provides the capability of providing the required stiffness and extending the frequency range of high acoustic attenuation by providing high damping. A viscoelastic shear layer used between two aluminum sheets behaves in much the same manner as a honeycomb configuration. The stiffness of the sandwich is governed by the face sheet thickness with the shear continuity provided by the viscoelastic material. The added advantage over a honeycomb configuration is the high damping. The shear layer is an effective damping mechanism. This high damping prevents the acoustic enclosure from becoming a "window" at its resonant frequencies. As a result, a high acoustic reduction can be obtained above the lowest resonant frequency of the enclosure. This provides an additional opportunity to reduce the surface density of the enclosure by making it more flexible than an equivalent honeycomb configuration.

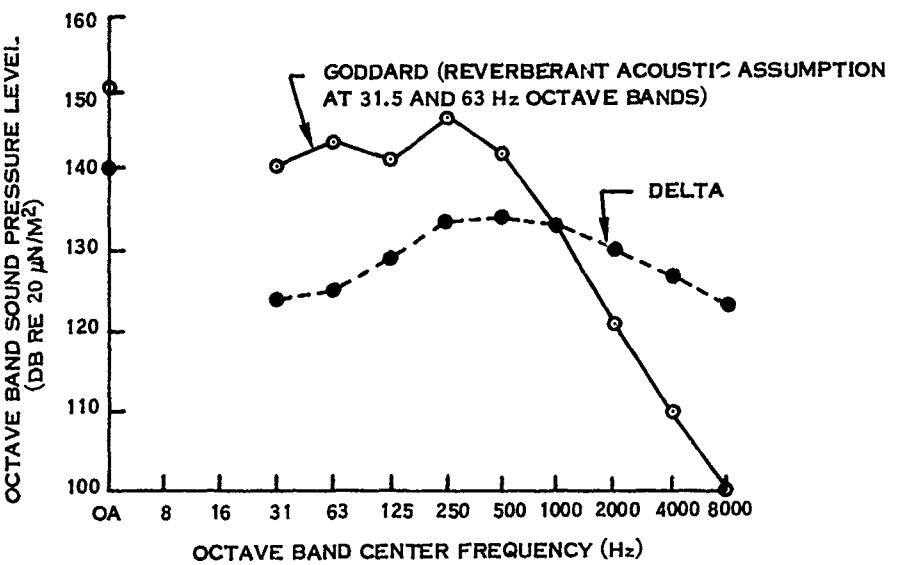

Fig. 4. Comparison of Shuttle Cargo Bay lift-off acoustic levels (Ref. 3) with Delta internal levels

A cylindrical configuration was selected to maximize the stiffness of the enclosure so that it provides stiffness controlled attenuation of the acoustic environment that is compatible with the Shuttle application. A cylindrical configuration provides a fundamental resonant frequency that is an order of magnitude higher than a flat panel configuration.

A series of 36 cylinder configurations were analyzed initially to determine an optimum viscoelastic laminated configuration. All configurations were 0.914 meters (three feet) in diameter and 0.914 meters (three feet) long. These configurations considered variations in the aluminum skin thickness from 0.406 to 2.29 millimeters (0.016 to 0.090 inches) with SMRD strips connecting the skins of variable width and thickness. A summary of the best configurations is shown in Table 1. It was found that a series of 6.35 millimeters (quarter inch) wide strips, forming ring and longitudinal shear attachments between the skins, was the most effective. The table summarizes the estimated minimum cylinder frequencies for 6.35 millimeters (1/4 inch) wide shear strips placed on 127 millimeters (5 inch) centers which was found to be optimum. As indicated by the table, the thin skins with the deep shear layers of viscoelastic material provide both optimum stiffness and damping. Of the configurations shown in Table 1, the 0.406 millimeters (16 mil) aluminum skins connected by a 12.7 millimeters (1/2 inch) thick viscoelastic shear layer satisfies the design goal of 500 Hertz minimum resonant frequency with a composite loss factor of 0.65 and a surface density of 3.222 KG/m^2 (0.66 lb/ft^2). The variation in the resonant frequencies of the cylinder with the height of the SMRD strips is shown in Fig. 5 for the 6.35 millimeters (1/4 inch) wide strips with the 0.406 millimeters (16 mil) aluminum skins. The composite loss factor and resonant frequencies of the viscoelastic laminated construction is calculated by an experimentally verified computer program.

Additional analysis was performed to determine if a lower surface density could be achieved with 0.254 millimeters (0.010 inches) face sheets of various materials, Table 2. The materials considered were aluminum, graphite composite and magnesium. As indicated in the table, lower surface densities can be obtained with either the magnesium or graphite composite. For

TABLE 1
Summary of Analytical Results for 6.35 mm
(1/4") Wide SMRD Strips on 127 mm (5") Centers

Skin Thickness		Core Thickness		f_{min}	Loss	Surface Density	
(mm)	(In)	(mm)	(In)	(Hz)	Factor	KG/m^2	Lbs/ft^2
0.406	0.016	6.35	0.25	350.	0.52	2.734	0.56
0.406	0.016	12.7	0.50	550.	0.65	3.222	0.66
0.406	0.016	25.4	1.0	875.	0.81	4.101	0.84
0.762	0.03	6.35	0.25	250.	0.67	4.687	0.96
0.762	0.03	12.7	0.50	440.	0.77	5.175	1.06
0.762	0.03	25.4	1.0	610.	0.87	6.054	1.24
1.524	0.06	6.35	0.25	245.	0.72	8.886	1.82
1.524	0.06	12.70	0.50	315.	0.83	9.277	1.90
1.524	0.06	25.4	1.0	440.	0.90	10.523	2.1

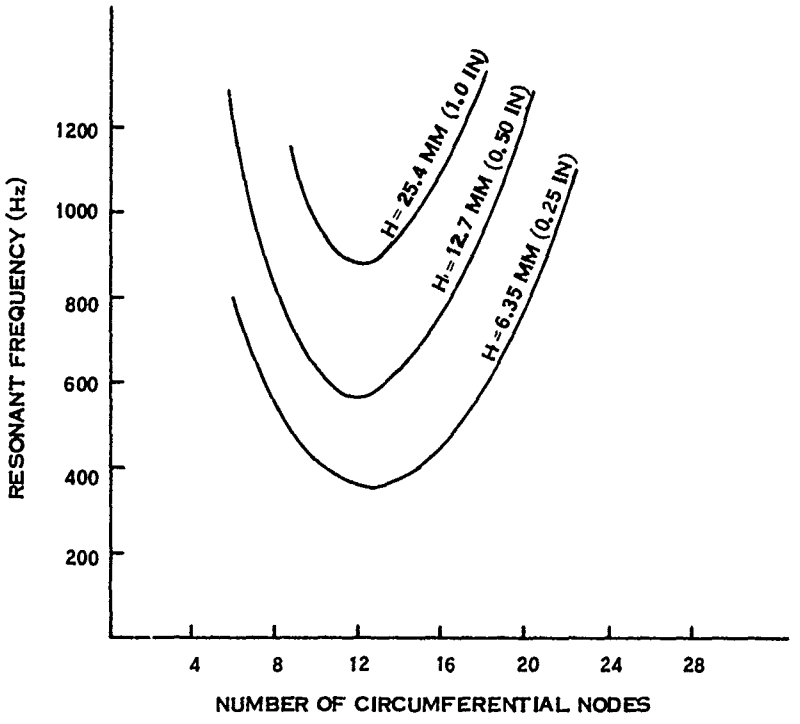

Fig. 5. Resonant frequencies of cylindrical barrier using 6.35 mm (1/4") wide SMRD 100F90 strips on 127 mm (5") centers, 0.406 mm (16 mil) fact sheets

TABLE 2
Summary of Results for 6.35 mm (1/4") Wide
SMRD Strips on 127 mm (5") Centers With Various Skin Materials

Skin Material	Skin Thickness		Core Thickness		f_{min} Cylinder (Hz)	Loss Factor	Surface Density	
	(mm)	(In)	(mm)	(In)			KG/m^2	Lbs/ft^2
2-D Graphite	0.254	0.01	6.35	0.25	519	0.41	1.250	0.256
	0.254	0.01	12.7	0.50	831	0.54	1.733	0.355
	0.254	0.01	25.4	1.0	1205	0.74	2.646	0.542
Magnesium Alloy	0.254	0.01	6.35	0.25	407	0.29	1.401	0.287
	0.254	0.01	12.7	0.50	668	0.40	1.860	0.381
	0.254	0.01	25.4	1.0	1044	0.55	2.773	0.568
Aluminum Alloy	0.254	0.01	6.35	0.25	375	0.40	1.865	0.382
	0.254	0.01	12.7	0.50	584	0.50	2.324	0.476
	0.254	0.01	25.4	1.0	960	0.68	3.237	0.663

the 0.914 meters (three foot) cylinder using a minimum frequency requirement of 500 Hertz, the graphite composite with a 6.35 millimeters (1/4 inch) high SMRD strips provides a surface density of 1.25 KG/m^2 (0.256 lbs/ft^2) and is the lightest configuration. Magnesium with 12.7 millimeters (1/2 inch) high SMRD strips also appears attractive and has a surface density of 1.860 KG/m^2 (0.381 lbs/ft^2) compared to 2.324 KG/m^2 (0.476 lbs/ft^2) for a comparable aluminum configuration. The results indicate that the shear modulus of the SMRD is ideally suited to the thinner face sheets and is capable of maintaining shear continuity. For the thicker skins, the SMRD is not as effective and results in lower resonant frequencies. The analysis indicates the feasibility of providing similar designs for larger diameter enclosures using magnesium or graphite composite. The feasibility of these very thin face sheets needs to be studied further considering the possible effects of acoustic fatigue.

A fiberglass liner having a 25.4 millimeters (one inch) thickness was selected to prevent reverberation within the cylinder and enhance the high frequency noise reduction characteristics.

TEST ENCLOSURE CONSTRUCTION

In order to provide the test enclosure within the tight schedule constraints of the program, some deviations from the optimum design were required. This included the use of thicker face sheets than the optimum configuration. The objective was to provide a test enclosure and corresponding analysis that is sufficiently rigid to enable theorectical and experimental comparisons to be made for the low frequency range of interest. The test results can then be projected to lighter weight flight configured enclosurers.

The test enclosure consists of a cylinder using two 0.508 millimeters (0.020 inches) aluminum sheets joined by a SMRD viscoelastic epoxy shear layer of 6.35 millimeters (1/4 inch) strips 12.7 millimeters (1/2 inch) high, and two conical shaped bulkheads. The cylinder is attached at both ends to stiff angle rings to provide lateral stiffness and attachment provisions for the bulkhead. Each bulkhead consist of a 3.17 millimeters (1/8 inch) flat aluminum plate and a 1.59 millimeters (1/16 inch) conical shaped sheet joined by viscoelastic epoxy wedges. The conical shape was chosen to provide higher stiffness than a flat configuration. The viscoelastic shear strips on the cylinder are 127 millimeters (five inches) on centers in the longitudinal and circumferential direction, while for the bulkheads wedge shaped pieces of viscoelastic epoxy were placed circumferentially at every 15° to give approximately 25 percent coverage. Figs. 6 and 7 show the cylinder wall construction and the bulkhead construction. A removable 25.4 millimeters (1 inch) thick fiberglass liner was also provided to prevent reverberation within the enclosure. The complete assembled enclosure is shown in Fig. 8.

The cylinder surface density for this test configuration is 3.71 KG/m^2 (0.76 lbs/ft^2). The bulkhead surface density is considerably higher since added stiffness was needed for this configuration. Weight of the bulkheads for flight type enclosures can be equal to the cylinder if a deeper cone or a spherical shape is used. Analysis of this configuration indicates a cylinder minimum resonant frequency of approximately 500 Hz and a loss factor of 0.66.

NOISE REDUCTION ANALYTICAL PREDICTIONS

Analytical predictions of the enclosure noise reduction were made using the general theory for single flat wall panels. The frequency characteristics of sound transmission loss (TL) for a single panel wall can be divided into several regions as indicated in Fig. 3 and discussed in Ref. 3. Below the natural frequency, sound transmission is

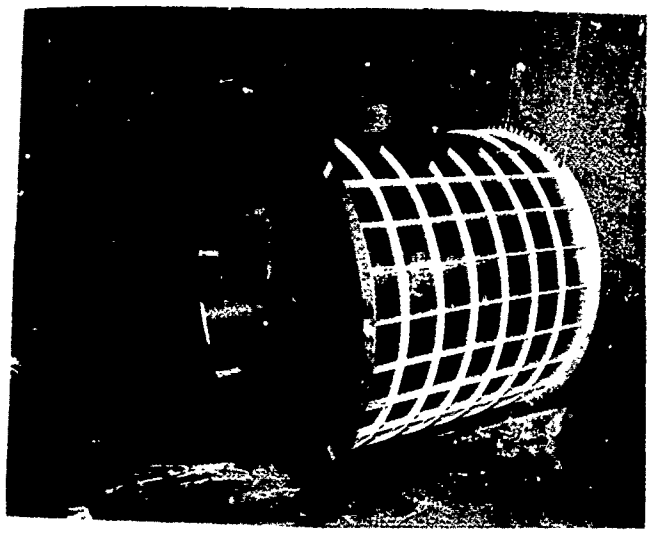

Fig. 6. Acoustic enclosure cylinder, viscoelastic epoxy damping material layout

Fig. 7. Acoustic bulkhead, viscoelastic epoxy damping material layout

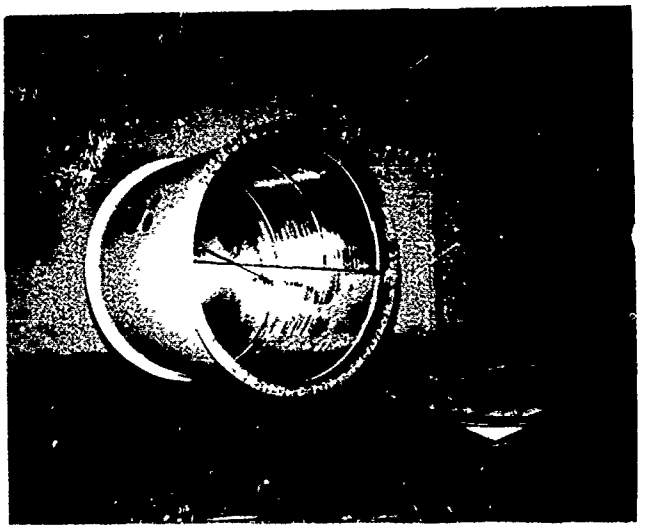

Fig. 8. Acoustic enclosure, one bulkhead removed with the fiberglass liner

controlled by panel stiffness, TL decreases with frequency at -6 dB per octave. At the panel fundamental natural frequency, f_o, TL reaches the minimum value determined by damping. When the resonance effects become negligible at frequencies 3 f_o to 4 f_o, TL is governed by the mass law which increases with frequency at + 6 dB per octave. At higher frequencies, the coincidence effect occurring at the critical frequency, f_c, causes a considerable drop of TL. At the critical frequency, the bending waves of the panel move at the same speed as a glancing acoustic wave in the adjacent air. This effect is defined as the "coincidence effect" and causes a drop in TL determined by the loss factor of the panel. At frequencies greater than f_c, the TL increases with frequency at 9 dB per octave until the panel wave motion changes from a bending wave to predominantly a shearing wave at a frequency denoted by the limiting frequency f_L. At frequencies greater than f_L, the TL is governed predominantly by shear wave effects on the panel and increases at 6 dB per octave with frequency. The prediction of noise reduction NR(f) for the enclosure assumes a reverberant sound field in the mid and high frequency range and was calculated using the following expression:

$$NR(f) = TL(f) - 10 \text{ Log} \left[0.25 + \frac{S_w}{R(f)}\right], \text{ dB} \quad (1)$$

where TL (f) = Transmission Loss =

$$10 \text{ Log } \frac{\Sigma S_i}{\Sigma \tau_i S_i} ; i = 1, 2 \quad (2)$$

S_w = Common area connecting the the source and receiver (Total area of cylinder and bulkhead)

$R(f) = \frac{S \alpha (f)}{1 - \alpha (f)}$, Acoustic enclosure constant with total interior surface areas S and sound absorption coefficient α (f)

S_1, S_2 = Surface area of cylinder and bulkhead respectively

τ_1, τ_2 = Transmission coefficient of the cylinder and bulkhead respectively = 10^{-} (TLi/10)

The transmission loss TL_1 of the cylinder and TL_2 of the bulkhead were calculated using transmission loss expressions for

single flat wall panels. The transmission loss at 500 Hertz and above was determined using the mass law. For the low frequency range noise reduction was estimated using the stiffness controlled law, a 6 dB slope below 500 Hz. The critical frequency of the acoustic cover was calculated to be much greater than 10,000 Hz, therefore, transmission loss laws within the coincidence controlled region were not applied.

Margins were included in the calculations as indicated by the shaded areas of Figs. 9 and 10. For the low frequency, the impedance relations [4] were used. Using these relations a noise reduction of 39 dB was calculated. The reference also reports that these relations over-estimate noise reduction by as much as 15 dB compared to experimental results. Therefore, a margin of + 3 dB and - 15 dB from 39 dB was used at the 31.5 Hz 1/3 octave band. At 500 Hz the noise reduction was calculated using expressions for single flat panels and a + 3 dB and - 6 dB margin was used to account for the uncertainty at resonance. Above 500 Hz a minimum of $\pm$ 3 dB margin was used. These margins were connected by straight lines.

EXPERIMENTAL INVESTIGATION

An experimental investigation of the test enclosure was performed at the NASA Goddard Space Flight Center Acoustic Facility. The principal objective of the investigation was to determine the noise reduction provided by the enclosure and to correlate the measured noise reduction with analytical predictions.

The instrumented enclosure was suspended freely in the acoustic chamber, Fig. 11. The enclosure was instrumented with nine accelerometers, eight microphones to measure internal sound pressure levels and four microphones to measure external sound pressure levels. The approximate locations of the microphones and accelerometers is also shown in Fig. 11. The internal microphones are supported on bungee cords which attach to eight eye bolts mounted to the angle rings. The four external microphones are suspended from cables which attach to the ceiling of the chamber. The test program consisted of various runs of the acoustic chamber with the acoustic spectrum shaped to that of the shuttle payload accommodations manual, [13], and an overall level of 150 dB. Additional runs were also made with the spectrum shape of Ref. 3 and an overall level of 154 dB. The enclosure was evaluated both with and without the fiberglass liner.

TEST RESULTS

Test results from the acoustic data are presented in terms of noise reduction using the following expression

$$NR = SPL\,(f)_{ext} - SPL\,(f)_{int} \qquad (3)$$

where $SPL(f)_{ext}$ is the external 1/3 octave sound pressure level spatial average of the four external microphones and $SPL(f)_{int}$ is the internal sound pressure level of each microphone or the spatial average of the eight internal microphones.

The measured noise reduction is compared with the analytical predictions in Figs. 9 and 10. Fig. 9 shows the results for the enclosure without the acoustic liner and Fig. 10 shows the results with the acoustic liner. The noise reduction based on the spatial average of the internal microphones sound pressure level measurement and based on the individual microphone measurements are included in the figures.

DISCUSSION OF TEST RESULTS AND CORRELATION TO PREDICTED VALUES

The noise reduction results compare quite well with the predictions and repre-

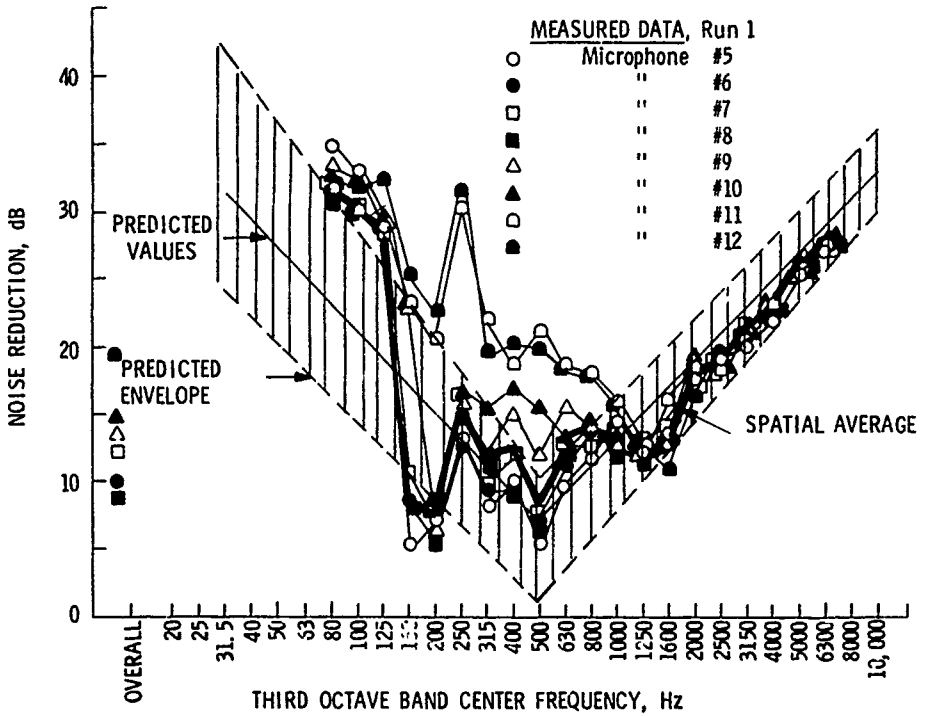

Fig. 9. Acoustic enclosure, measured noise reduction comparison to predicted values; without acoustic fiberglass liner (OA external SPL = 150.5 dB)

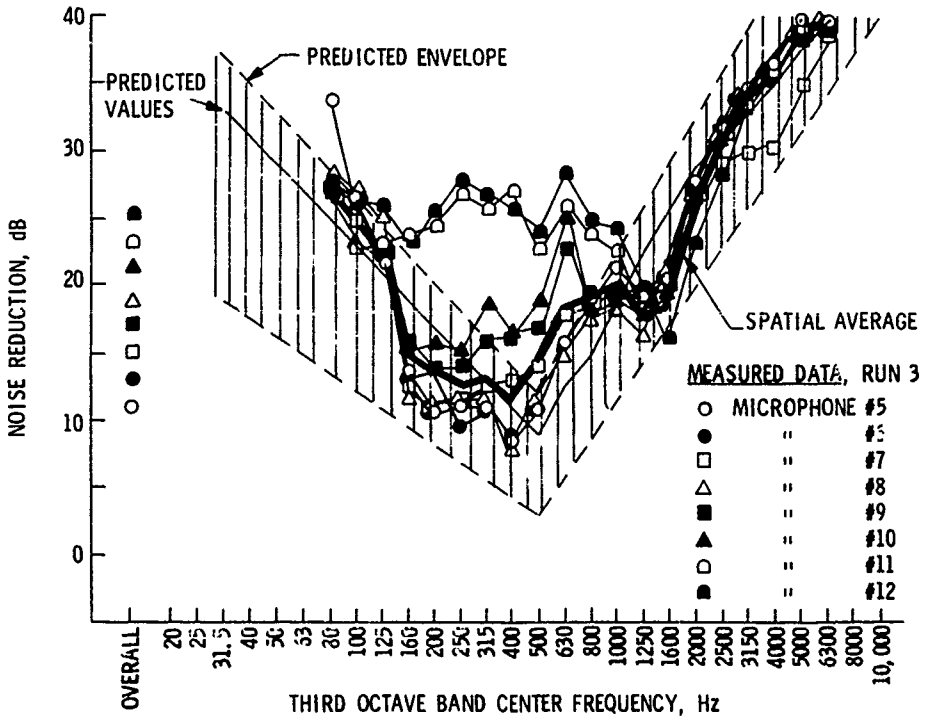

Fig. 10. Acoustic cover, measured noise reduction comparison to predicted values; with acoustic liner (OA external SPL = 150 dB)

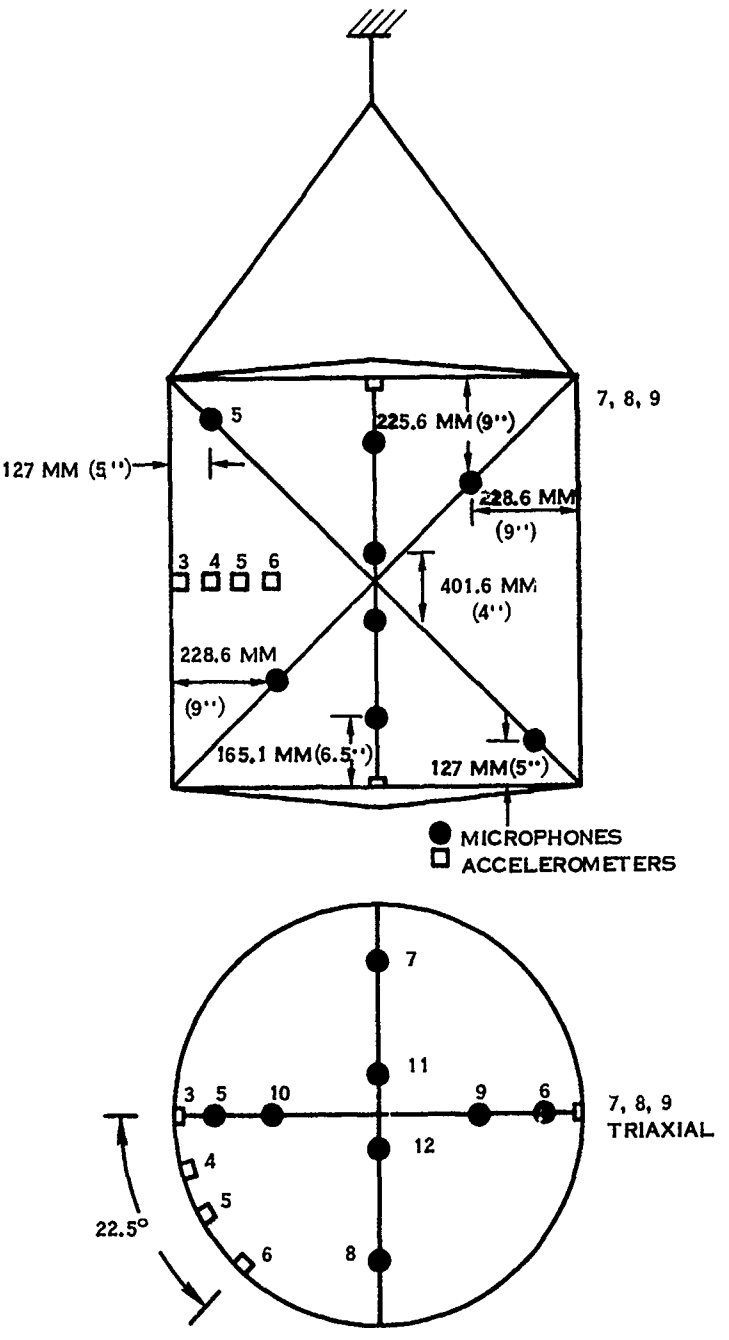

Fig 11. Acoustic enclosure configuration within acoustic chamber and approximate locations of microphones and accelerometers

sent an order of magnitude reduction in the overall acoustic pressures with even larger reductions in the frequency range below 160 Hz and at frequencies greater than 600 Hz. The configuration with no acoustic liner shows overall noise reduction of 9.5 to 19.5 dB (spatial average of 12 dB) with as much as 30 to 35 dB below 125 Hz. The lowest noise reduction for this configuration is 5 dB (spatial average 7.5 dB) at 160

Hz and 500 Hz. The 500 Hz frequency is the estimated fundamental frequency of the enclosure cylindrical section. The configuration with the acoustic liner shows an overall noise reduction of 18 to 29 dB (spatial average of 20 dB) with as much as 30 to 40 dB below 125 Hz and for frequencies greater than 2000 Hz. The lowest noise reduction for this configuration is 13 dB at 400 Hz (spatial average of 17 dB). The high noise reduction levels in the low frequency range are of greater significance since the space shuttle acoustic environment is quite severe in this frequency range and many payload experiments are considered more susceptible to the high environment in this frequency range.

The spatial average noise reduction in the mid-frequency range is not theoretically rigorous but provides a good basis for comparison. In the mid-frequency range, large variations in the measured internal acoustic levels are apparent with variations at some frequencies as high as 20 dB with the lower level measured at the center of the cylinder. The calculation of the spatial average noise reduction is based on a reverberant noise field both inside and outside the enclosure. Although the external noise field is reverberant, the internal noise field is not reverberant as indicated by the large variation in microphones measurements. At very low frequencies, the variation ceases to be large so that errors introduced by the spatial average are less significant. The spatial average provides a convenient method of comparison but the individual measurements should be considered in interpreting the results in the mid-frequency range.

The noise reduction levels below 80 Hz are considered to be invalid because of instrumentation limitations and the lack of a reverberant acoustic field within the test chamber. Typical external levels fall off sharply below 63 Hz with indicated levels on the order of 25 dB below the overall. Similarly, the internal microphone measurements fall off sharply below 160 Hz with typical values of 100 Hz more than 30 dB down from the overall. These levels tax the dynamic range of the instrumentation particularly when a tape recorder is used for off-line data analysis. In addition, the external acoustic field ceases to be reverberant below approximately 80 Hz. The spatial variation of the spectra has been reported by Cyphers, Munson and On [12] to be less than 3 dB for third-octave bands with center frequencies greater than 80 Hz. Accordingly the external acoustic environment is a reverberant-diffuse acoustic field with a spatial distribution in spectra levels better than 3 dB. Any variation in the internal acoustic characteristics which lie outside a 3 dB amplitude tolerance band would not be attributed to spatial variations in the external acoustic spectra. Below 80 Hertz there is a non-reverberant-diffuse region of the external acoustic field which would be accomplished by spatial variations greater than 3 dB.

The cut-off frequency below which the enclosure internal acoustic field is no longer predominantly reverberant-diffuse is shown in Fig. 12. For the empty enclosure the cut-off frequency occurs at about 500 Hz, and for the 50 percent and 75 percent payload volumes this frequency occurs respectively at 630 and 800 Hz. The assessment of the cut-off frequency is based on an accepted criteria that the third octave band modal density is greater than 7 modes and that the modal overlap is greater than 1/3. The modal overlap characteristics is shown in Fig. 13. The dashed portion of Fig. 13 represents the region below the cut-off frequency for each occupied payload volumes. This information is required in determining the type of acoustic principles which one must use to compute noise reduction characteristics. It should be noted that a solid payload of wood surface and volume of surface area ratio of 0.122 meters (0.4 feet) has been assumed.

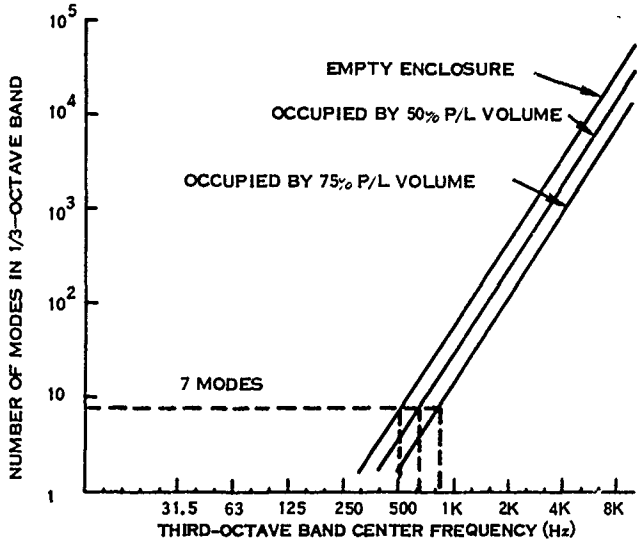

Fig. 12. Third-octave band acoustic mode density

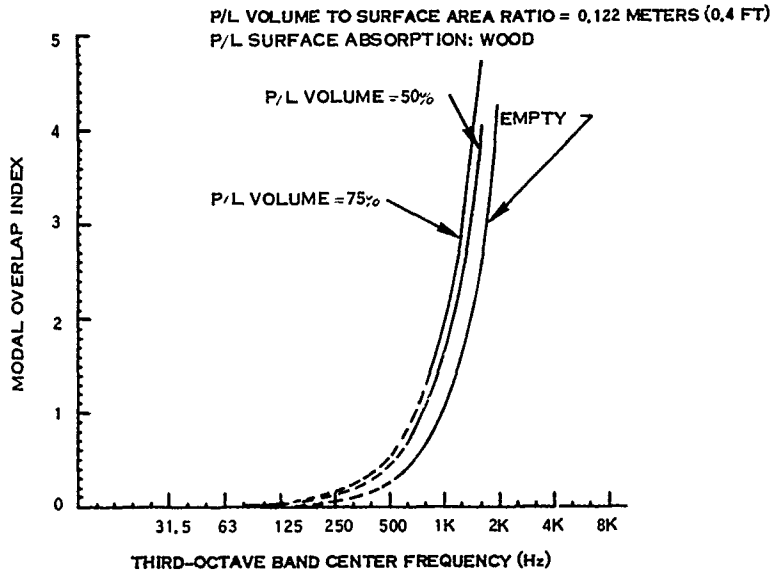

Fig. 13. Acoustic modal overlap

The spatial variation in standard deviations of dB for the empty case is computed from test data and is presented in Fig. 14 (with and without an acoustic liner). From the large spatial variations below the cut-off frequency it is evident that the interior acoustic field below this frequency is not reverberant-diffuse. In particular, the spatial variations peak in the frequency region where the occurrence of the lowest acoustic radial or circumferential, and axial modes of the container are suspected (~ 160-200 Hz). The effect of these modes causes the dip or decrease in noise reduction in this region.

Fig. 15 presents the spatial averaged noise reduction characteristic for the empty

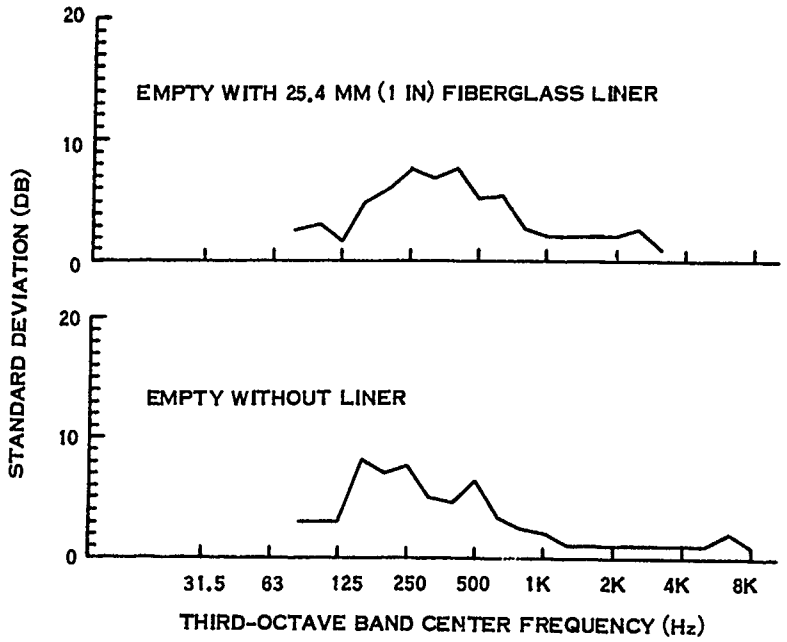

Fig. 14. Spatial variation of empty internal SPL

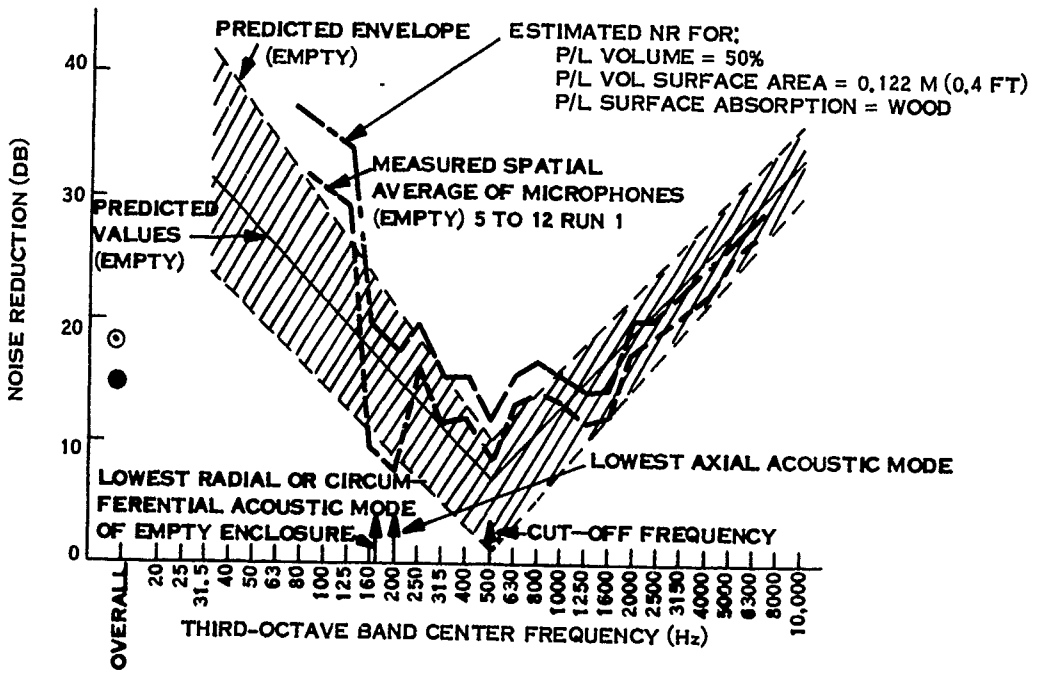

Fig. 15. Acoustic cover, measured spatial average noise reduction, comparison to predicted values, (OA external SPL = 150.5 dB)

enclosure and for the enclosure occupied by an irregular shaped payload of solid wood which is about 50 percent of the full enclosure volume and has a payload volume to surface area ratio of 0.122 meters (0.4 ft). For the 50 percent payload volume case, the predicted noise reduction results are based on modification of the measured results for the empty test case. The modification in the frequency range above the cutoff frequency is based on architectural acoustical principles in computing the change in reverberation cavity constants due to the occupied payload. Below the cutoff frequency the modification is quasi-qualitative in nature. When occupied by a payload, the nonexistence of the first radial and axial modes results in an increase in noise reduction for the occupied condition. It is anticipated that larger noise reductions than those measured for the empty enclosure will occur when packages are placed within the enclosure.

Although the original intent of the vibration measurements was to determine the fundamental resonant frequency of the enclosure, the results were inconclusive. The vibration measurements had peaks in the acceleration power spectral densities (PSD) at 280 and 420 Hz. The lowest of these frequencies corresponds to the approximate acoustic frequency of the enclosure and, as indicated by the individual microphone measurements, large variations in the internal noise field exist throughout the range from 280 to 1000 Hz. Because the enclosure response reflects both acoustic and structural resonances, the data do not provide a clear indication of the structural resonant frequencies.

The vibration levels of the enclosure were high with the lowest levels occurring on the ring structure. On the cylindrical portion of the enclosure the vibration levels varied from approximately 25 g RMS to 90 g RMS without the liner and were reduced to 20 g RMS to 70 g RMS with the fiberglass liner. The bulkheads showed slightly lower levels. The triaxial accelerometer mounted to the ring had levels of approximately 6 to 11 g RMS without the liner and 5 to 8 g RMS with the liner.

CONCLUSIONS

Based on the results of this feasibility study, the following conclusions are made:

1. Light weight acoustic enclosures can be used effectively to protect small experiments or portions of experiments from the Shuttle Payload Bay acoustic environment.
2. The test enclosure provided an order of magnitude reduction in the acoustic levels. This is three times greater than that of current launch vehicle shrouds yet the test enclosure had only half the surface density.
3. The measured spatial average noise reduction is stiffness controlled while at high frequencies it is mass law controlled. The minimum attenuation occurs at approximately 500 Hz, the estimated resonant frequency of the cylindrical portion of the enclosure.
4. There is a large scatter in the internal acoustic levels with measurements near the center being as much as 20 dB lower than measurements near the walls.
5. There was no apparent damage to the test enclosure after approximately 1/2 hour of exposure to acoustic levels from 146 to 154 dB.
6. An internal sound absorbing liner should be provided within the enclosure to provide increased

attenuation by preventing reverberation.

7. Acoustic enclosures with surface densities on the order of 1.22 to 2.44 KG/m^2 (0.25 to 0.50 lbs/ft^2) are feasible. This is less than one third the surface density of current launch vehicle shrouds.

8. Preliminary results from the optimization of the wall construction for a 0.914 meter (three foot) diameter indicate that larger enclosures are feasible.

9. High vibration levels occur on the surface of the enclosure but the vibration levels at structural mounting points for packages are much lower.

10. It is estimated that the enclosure noise reduction will increase when packages are placed within the enclosure.

REFERENCES

1. Stahle, C.V. and Gongloff, H. R., "Final Report, Astronomy Sortie Vibration, Acoustics and Shock, Program Planning, Phase 1," GE Document No. 74SD4246, September 27, 1974.

2. Stahle, C.V., Gongloff, H.R. and Bangs, W.F., "Cost Effective Dynamic Design and Test Requirements for Shuttle Payloads," Presented at 22nd Annual Institute of Environmental Sciences Meeting, Anaheim, California, April 1975.

3. On, F.J., "Shuttle Orbiter Payload Bay Internal Acoustics During Lift-Off," NASA-GSFC Memorandum Report 741-29, January 1975.

4. Cockburn, J.A., "Evaluation of Acoustic Testing Techniques for Spacecraft Systems," Wyle Labs Report 7-17, June 1971.

5. Sutherland, L.C., Editor, "Sonic and Vibration Environments for Ground Facilities - A Design Manual," Wyle Labs Report 68-2, 1968.

6. Lyon, R.H., et al., "Low Frequency Noise Reduction of Spacecraft Structures," NASA CR-589, September 1966.

7. Stahle, C.V. and Tweedie, Dr. A. T., "A Layered Viscoelastic Epoxy Rigid Foam Material for Vibration Control," Shock and Vibration Bulletin No. 42, P4, January 1972.

8. Stahle, C.V., Tweedie, A.T. and Gresko, T.M., "Viscoleastic Epoxy Shear Damping Characteristics," Shock and Vibration Bulletin No. 43, P4, June 1973.

9. Stahle, C.V. and McCandliss, W.H., "Controlling Vibration of Viking Lander Electronic Packages," 44th Shock and Vibration Symposium, December 1973.

10. Stahle, C.V. and Tweedie, A.T., "Broad Temperature Range Epoxy Damping Material Development," GE TIS No. 73SD222, April 1973.

11. Sardella, G., Stahle, C.V. and Tweedie, A.T., "Damping Material Application Development," GE TIS No. 73SD238, December 1973.

12. Cyphers, H.D., Munson, A.N. and On, F.J., "Comparative Evaluation of Predicted and Measured Performance of a 68-Cubic Meter Truncated Reverberant Noise Chamber" NASA Technical Note, NASA TND-7755, January 1975.

13. "Space Shuttle System Payload Accommodations, Level II Program Definition and Requirements," JSC 07700, Vol-

ume XIV, Revision C, Lyndon B. Johnson Space Center, July 3, 1974.

ACKNOWLEDGEMENT

This work was supported by the National Aeronautics and Space Administration, Goddard Space Flight Center, under Contract No. NAS 5-24021 Mod. 74.

The authors gratefully acknowledge the assistance provided by R. Kinsley of NASA-GSFC who was responsible for the performance of the experimental portion of this project and J. O'Brien who was the technical monitor.

Discussion

Mr. Van Ert (The Aerospace Corporation): Did you examine the effect of filling the internal space with any volume of any sort?

Mr. Ferrante: No, we did not. Analytically, we did, we include a block of wood approximately 50% volume and the paper shows that the noise reduction increases.

Mr. Van Ert: Does the noise reduction increase or diminish?

Mr. Ferrante: This is for analytical predictions. We did not make any measurements.

Mr. Van Ert: In a typical shroud we have seen some very small noise reductions when the internal space is very nearly filled in some areas and I wonder if that effect will tend to be seen in this kind of set up?

Mr. Ferrante: That is something that should definitely be investigated.

Mr. Van Ert: What about the inherent strength of this sort of structure? Is it sufficiently strong to withstand 150 to 155 db levels inside the Orbiter?

Mr. Ferrante: Yes, the levels that we are talking about vary from 146 to 154 db overall and the 146db shape is the typical 7700 document shape and the 154 db shape is the prediction from the Goddard Space Flight Center. The testing duration was approximately 30 minutes if you include all of the tests that we did, and there were no failures that we know of.

Mr. Van Ert: You mentioned that Goddard Space Flight Center had generated a prediction that was 150 db and yet it looked as if the octave band values were almost that high, did you mean 150 db or is it in excess of 150 db?

Mr. Ferrante: I think it is around 150 db now and that data agrees quite well with Rockwell's predictions.

Mr. Van Ert: I thought that maybe the overall was higher.

Voice: The payload will act as filter to the noise from outside to the inside so obviously the noise environment from outside as provided by Rockwell or NASA would be different from the noise environment inside. Have you studies the effect of a different noise environment?

Mr. Ferrante: Yes, the environment external to the cover can vary from 146 to 154 db overall and the attenuations in each case were in the same order of magnitude as I have shown.

Voice: Have you studied the effectiveness of the shield to a different power spectra density?

Mr. Ferrante: We considered two spectrum shapes, one was 145 db overall as described by the NASA 7700 document, and the other was 150 db overall and the levels were different at each octave band or third octave band. We have used different spectrum shapes and we have observed the same type of attenuations.

Dr. Smith (Bell Aerospace Company): What acoustical mode can you get on a three foot long cylinder at about 180 Hz?

Mr. Ferrante: You get two modes; one is an axial mode or a breathing mode, the other is a radial type of mode. The frequency is a function of the length of the cylinder and the radius of the cylinder, and we calculated 180 Hz and 210 Hz.

Mr. Knauer (Hughes Aircraft): Do you know if Frank On's or the Rockwell calculations of that predicted bay environment were for an open bay or were they for a bay filled with different volumes of space vehicles?

Mr. Ferrante: I believe that the 150 db is for an empty bay but I know that the Goddard Space Flight Center is presently investigating the testing in the case where the bay is filled. I think the original estimate of 140 db is for an empty bay.

Mr. Vedrenne (Centre National de'Etudes Spatiales): Do you have a model to predict the noise environment during the launch of space shuttle and can this technique be used for the structures of fairings for launch vehicles?

Mr. Ferrante No, but this has been done by the Goddard Space Flight Center, Rockwell International, the LBJ Space Flight Center. To answer your second question, I think larger covers might be feasible but it would take a lot of investigation because we only have one data point. We would have to extrapolate to a larger cover.

EXPERIMENTAL DETERMINATION OF ROCKET MOTOR STRUCTURAI RESPONSE TO INTERNAL ACOUSTIC EXCITATION

F. R. Jensen and L. R. West
Hercules Incorporated
Bacchus Works
Magna, Utah

Acoustic pressure oscillations in the combustion cavity of a solid propellant rocket motor can impose excessive dynamic loads on structural components and attached motor hardware. The problem of combustion instability has concerned the industry in recent years because of these structural effects. Hercules is currently engaged in a Motor Component Vibration study program to develop analytical techniques for the prediction of motor component response to acoustic pressure oscillations. The program is sponsored by the Air Force Rocket Propulsion Laboratory at Edwards Air Force Base, California.

One experimental task was included in the RPL Component Vibration Program to provide data for evaluation of the analytical techniques. The objective of the task was to measure the response of a motor to an acoustic loading that would simulate an unstable acoustic pressure oscillation. This paper describes the testing setup and the testing procedures used to obtain the motor structural response. The test results are also presented and discussed.

The acoustic excitation was provided by a cone-type loudspeaker placed in the centerbore of the motor. An oscillator was attached to the loudspeaker through an audio amplifier. Frequency sweeps were conducted by varying the oscillator frequency in the range from 0 to 1000 Hz. A microphone was placed in the combustion cavity to monitor pressure oscillation amplitudes. The microphone was mounted on a shaft that could be moved along the motor centerline to map the accustic modes. An accelerometer was used on the motor structure and components to map structural mode shapes.

The motor was pressurized to 344.7 kPa (50 psi) so that the dome of the case would be forced out away from the propellant grain. Nitrogen gas was used to pressurize the motor for most of the testing; however, some studies were made with helium gas to change the frequency at which various acoustic modes occurred. Since structural natural frequencies remain constant, variation of the acoustic natural frequencies simplified the problem of separating structural resonance from acoustic resonance in test data.

Two types of tests were conducted: (1) Frequency response, and (2) mode mapping. The frequency response tests were conducted by recording the accelerometer output on an X-Y plotter while the frequency was varied slowly over a certain frequency range. The accelerometer was then moved to another point and the frequency response test repeated. By examining results from the frequency response tests, major resonance frequencies were selected for mode shape mapping. The mode shape mapping was conducted by turning the oscillator to a particular frequency and then moving the accelerometer from one structural point to another to map the mode of response. The accelerometer signal amplitude and phase were recorded at each point.

Results from this experimental project are presented by way of frequency response plots and mode shape plots. The acoustic cavity resonances compare well with those determined previously by test and by analysis. No data were available for evaluation of the structural response results.

INTRODUCTION

The use of experimental data for the evaluation of new or different analytical techniques is nearly always desirable. The experiment discussed was intended to provide "clean" data (compared to hot firing data), for evaluation of analytical models. The objective of the experimental work described in the report was to measure the structural response of a solid rocket motor to a known loading distribution. The objective was achieved by measuring the response of an inert rocket motor to acoustic excitation provided by a loudspeaker in the motor combustion cavity. Pressure mode shapes were mapped by using a movable microphone.

Solid rocket motor acoustic pressure oscillations that occur during motor operation cause structural vibrations that can be measured and recorded by using accelerometers. However, analysis of typical accelerometer data indicates that the structure is probably responding to several different loads during motor operation time. Determination of the portion of the measured response which is due to acoustic pressure oscillations and that portion which is due to other forcing functions is sometimes difficult. Another factor which must be considered in interpretation of motor static firing or flight data is the large motor-to-motor variability of the data.

Use of experimental data from this program had the following advantages over accelerometer data from static firings for evaluation of finite element models:

(1) The measured response of the motor structure represents response to a single well-defined forcing function, whereas static firing data contain response information for several ill-defined forcing functions.

(2) Since the testing was conducted under carefully controlled laboratory conditions, variability in the data for repeated test sequences was small, whereas the variability in accelerometer data from motor firing tests is large.

(3) Measurement and mapping of the acoustic mode shapes resulted in good definition of the loading distributions, whereas motor static firing tests typically have only one pressure measurement made at one location.

(4) Use of double-backed adhesive tape and a movable accelerometer made possible the mapping of structural response mode shapes in considerable detail. Because data channels are limited in number, only four to six accelerometers are normally recorded during a routine static firing. Even specially instrumented motors generally have only one to two dozen accelerometer measurements.

Results from the testing program were intended to complement static firing data, rather than replace it, for use in evaluation of analysis results. Filtering and other data reduction techniques are used to obtain meaningful comparisons between analytical results and static firing data.

The discussion of this program would not be complete without a listing of some of the shortcomings of the selected testing approach:

(1) The applied loads and corresponding responses are of very small magnitude compared with those that occur during motor operation. Therefore, nonlinearities are not accounted for by this test procedure.

(2) Dynamic properties of the inert propellant (HDLK) were not the same as those for the live propellant (FKM).

(3) Boundary conditions used for the acoustics testing do not exactly match those of the static firing or flight test conditions.

In spite of these shortcomings, the testing program produced useful motor response data.

The work described in this report was performed and reported under Contract F04611-73-C-0025 with the Air Force Rocket Propulsion Laboratory at Edwards Air Force Base, California. The test setup, procedure, results, and conclusions are discussed in the remainder of the paper.

TEST SETUP

An inert solid propellant rocket motor with hydraulic power unit, gas generator, flight electronics unit, and two nozzle actuators attached was used as the test vehicle. Trial testing was performed with the motor in both the horizontal and vertical attitudes. Results from the vertical attitude tests appeared to be more realistic. With the motor in the horizontal attitude, the propellant grain slumped into contact with both unbonded domes and affected the dome responses by the grain contact. Since the motor is statically fired in a vertical nozzle-up position, that attitude was used for the majority of the testing. The motor was pressurized to 344.7 kPa (50 psi) to obtain a separation between the grain and the domes to simulate conditions during motor operation. Even when the motor was pressurized, the forward dome and grain were probably still making contact because the gravity load on the grain causes it to slump downward. Most of the acceleration measurements, therefore, were made

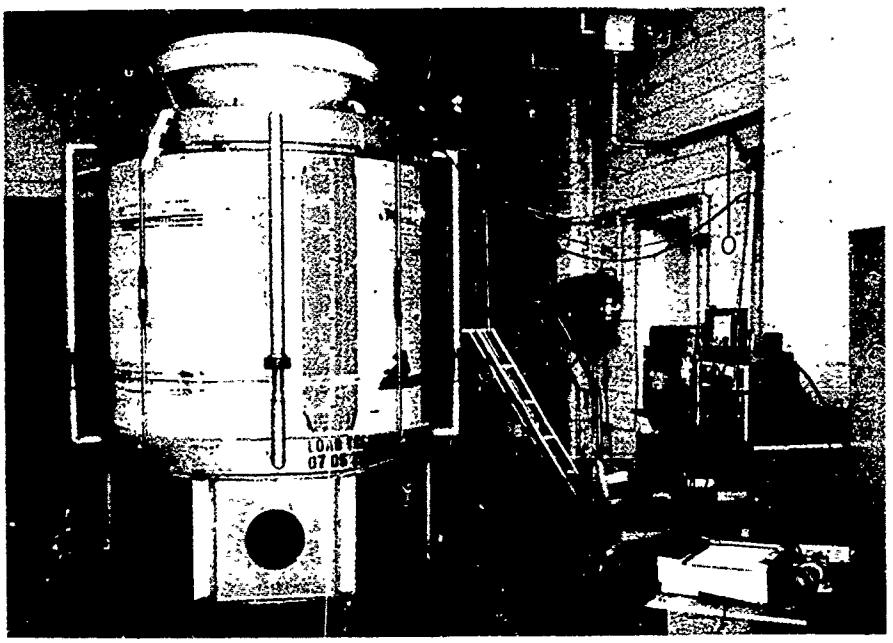

Figure 1. Test Setup with Motor in Vertical Position

on the aft end of the motor. A photograph of the testing setup is shown in Figure 1, above.

A block diagram showing the instrumentation used to record pressure and acceleration responses is shown in Figure 2. Using the setup shown, the frequency of a particular resonance was determined accurately with the frequency meter. The phase meter was used to measure between the reference accelerometer output and the movable accelerometer output (or the microphone output). A digital voltmeter was used to measure movable accelerometer output at a particular frequency. For frequency sweeps, the movable accelerometer output was plotted as a function of frequency on the X-Y plotter.

An 8-inch, cone-type loudspeaker was placed in the slotted region of the combustion cavity to provide the source of acoustic excitation. The approximate location of the loudspeaker is indicated in the sketch in Figure 3. A special nozzle closure for containing the 344.7 kPa (50 psi) chamber pressure was designed, constructed, and installed in the chamber. Nitrogen gas from standard pressurized cylinders was used to pressurize the motor to 344.7 kPa (50 psi); the pressure gage and regulator supplied with the commericial nitrogen tank were used to control motor chamber pressure.

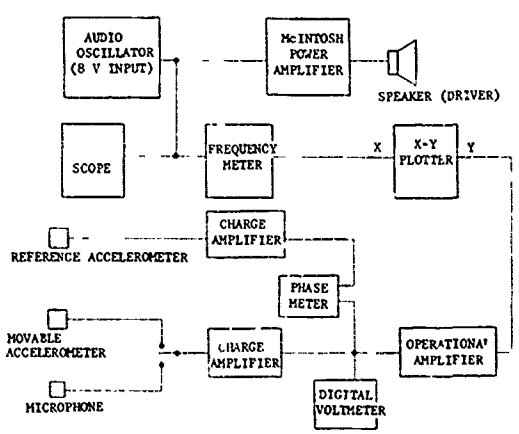

Figure 2. Electrical System for Acoustic Testing

TEST PROCEDURE

Two basic test procedures are described here, one procedure for frequency response testing and one procedure for mode shape mapping. The

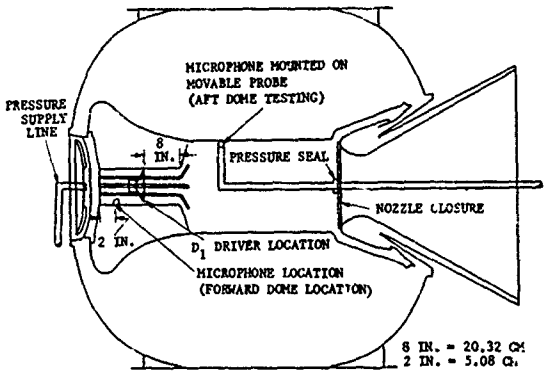

Figure 3. Driver and Microphone Locations

frequency response testing was performed first so that results could be used as a guide in choosing frequencies for mode shape mapping.

The frequency response testing was performed for a limited number of points selected on the domes and on the components. The movable accelerometer was mounted at a selected location by using double-backed adhesive tape. The power amplifier supplying the speaker was adjusted for an eight volt output. The audio oscillator dials were then slowly turned to sweep the frequency from 50 to 1000 Hz while the accelerometer output was plotted as a function of frequency on the X-Y recorder. The resulting plot of acceleration amplitude versus frequency was examined to determine apparent resonant frequencies. Peaks may occur in the plot either due to acoustic cavity resonance or due to structural resonance. Frequencies of major peaks were selected for mode shape mapping.

Double-backed adhesive tape provided a satisfactory accelerometer mounting system that provided easy and quick installation and removal of the movable accelerometer. Data from checkout tests performed to determine the adequacy of the double-backed tape are discussed in the paragraph entitled "Results."

To map a mode shape, the audio oscillator was set to the selected frequency and the power amplifier output (speaker input) was adjusted to eight volts. Generally, the audio oscillator was fine-tuned to maximize the oscilloscope signal as the oscillator frequency control was adjusted. The reference accelerometer was installed at a specified location. The movable accelerometer was moved from location to location until each point in the area being mapped was covered. For each point at which the movable accelerometer was stopped, the accelerometer output was read on the digical voltmeter and recorded on a data sheet. The phase angle between the response from the reference accelerometer and the response from the movable accelerometer was noted on the phase meter and recorded on the data sheet. Results from a mode shape mapping were thus obtained in the form of a table showing acceleration amplitude and phase at a set of mapping points.

Frequency response testing and acoustic mode mapping were carried out for the combustion cavity by using the microphone in place of the movable accelerometer in the procedures described above. For the aft dome testing, the microphone was mounted on a probe so that acoustic modes could be mapped in the cylindrical section between the speaker and the nozzle closure. Mapping locations for the cavity are defined in Figure 4.

Accelerometer locations for mapping the aft dome are shown in Figure 5. For various reasons, all locations shown were not used. Accelerometer locations for mapping the component responses are shown in Figure 6 and nozzle accelerometer locations are shown in Figure 7.

RESULTS

Frequency Response Testing

Frequency response data were obtained for several points on the aft end of the motor. A separate graph was obtained from the X-Y plotter for each point, showing acceleration response as a function of frequency. The frequency response recorded at point 300 (refer to Figure 5) is shown in Figure 8. The responses at points 585, 594, and 662 are shown in Figures 9, 10, and 11, respectively. The frequencies read from the frequency meter have been marked near some of the major peaks.

Frequency response plots were also obtained for various microphone locations. The frequency response for the microphone at position number 1 (Figure 4) is shown in Figure 12.

Mode Shape Mapping

By reviewing the frequency response plots, several significant frequencies were selected for mode shape mapping. The mode shapes mapped are not natural modes of the structure, but rather are the modes of response to a forcing function. To illustrate the use of the recorded data, consider two different measurements labeled y_1 and y_2.

At point one, the amplitude, $y_1(t)$, may be expressed as a function of time as

$$y_1(t) = Y_1 \cos(\omega t + \Phi_1) \qquad (1)$$

At point two, the amplitude would then be

$$y_2(t) = Y_2 \cos(\omega t + \Phi_2) \qquad (2)$$

The terms, Φ_1 and Φ_2 are the phase angles measured relative to some arbitrary reference, and Y_1 and

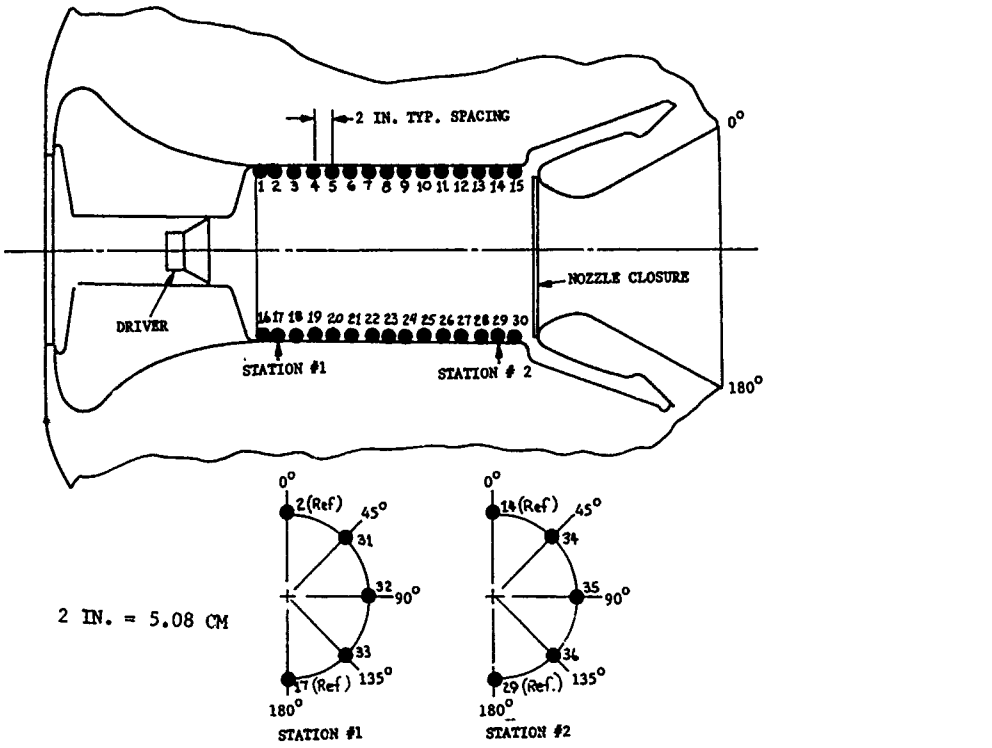

Figure 4. Microphone Locations for Mapping Acoustic Modes

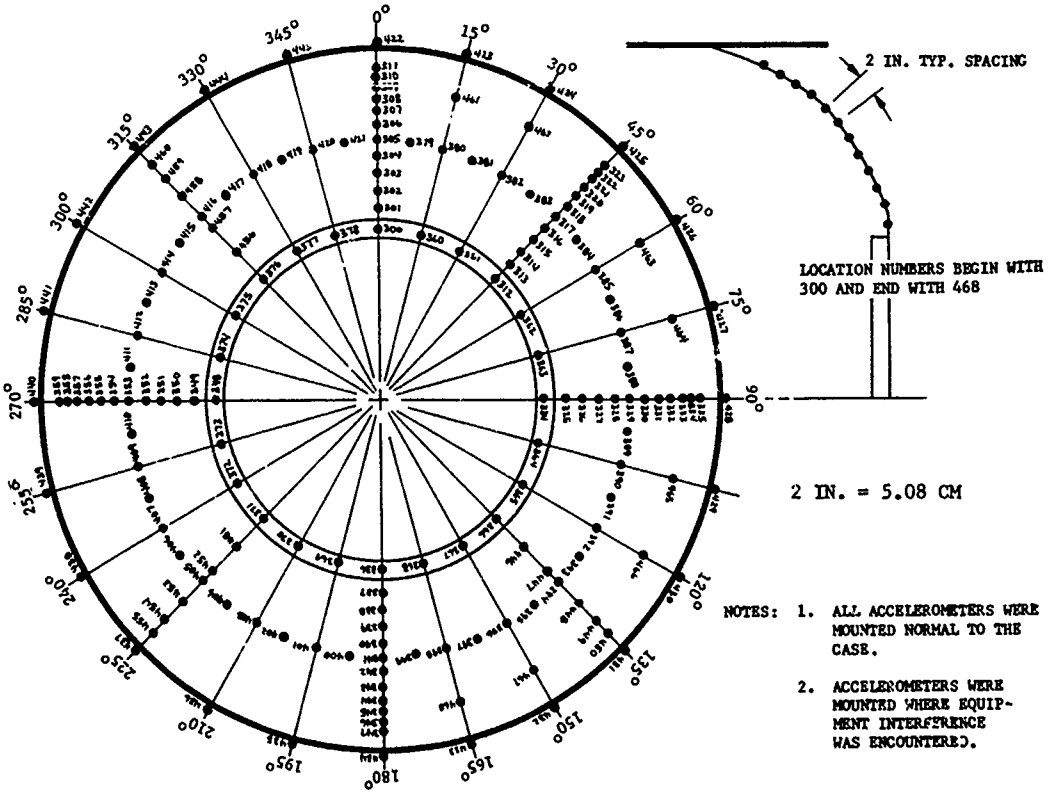

Figure 5. Accelerometer Locations for the Aft Dome

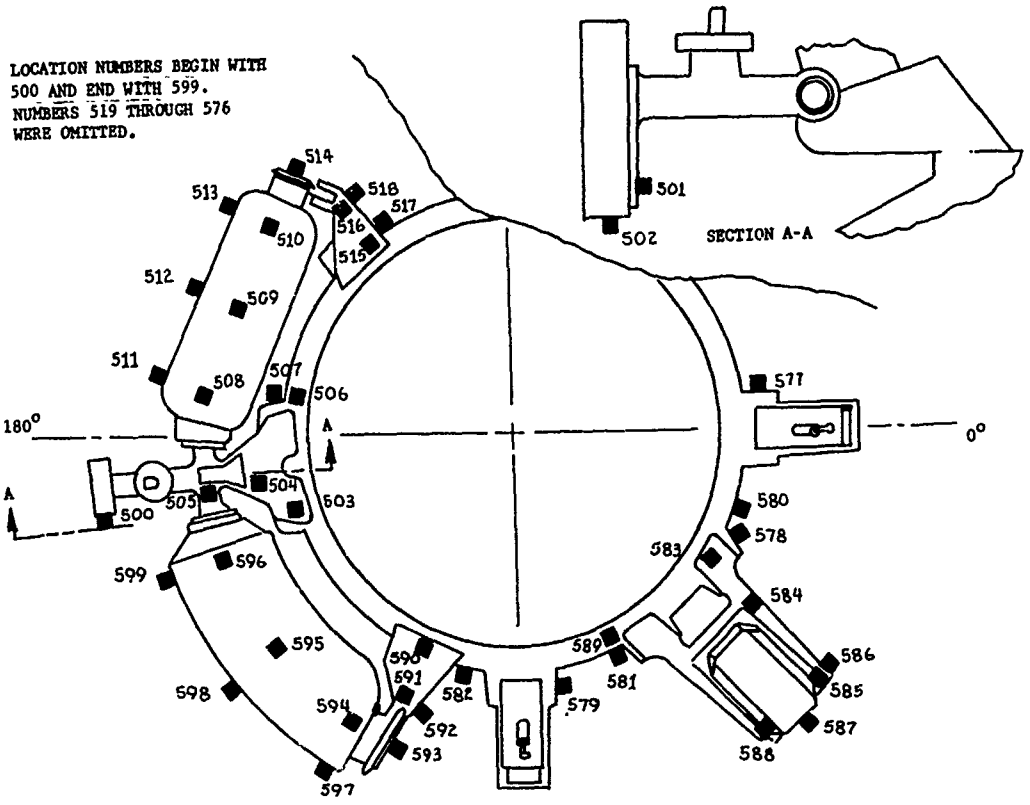

Figure 6. Component Accelerometer Locations

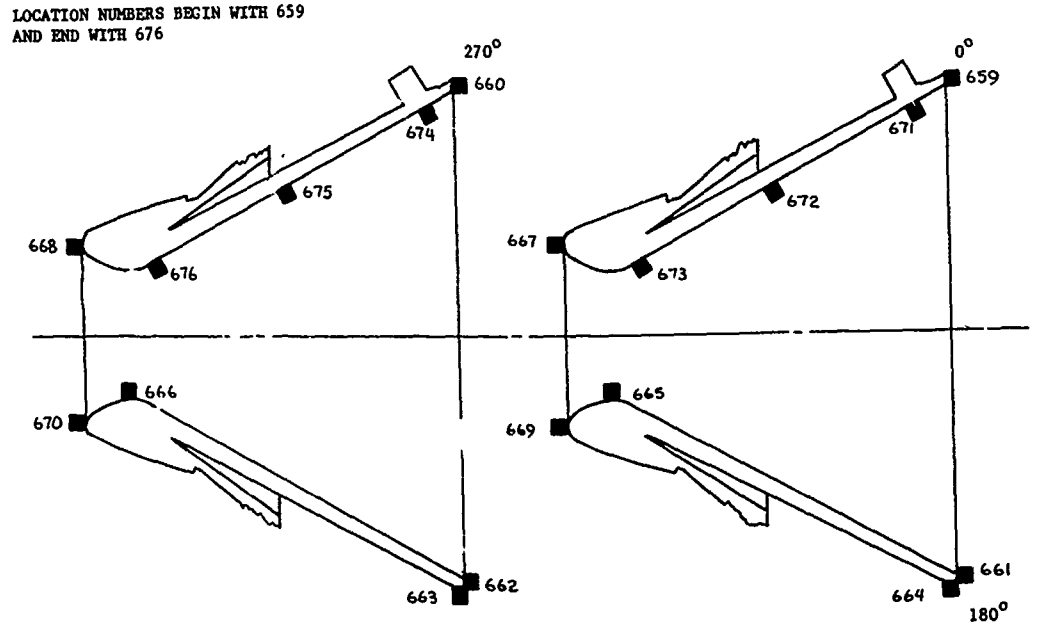

Figure 7. Nozzle Accelerometer Locations

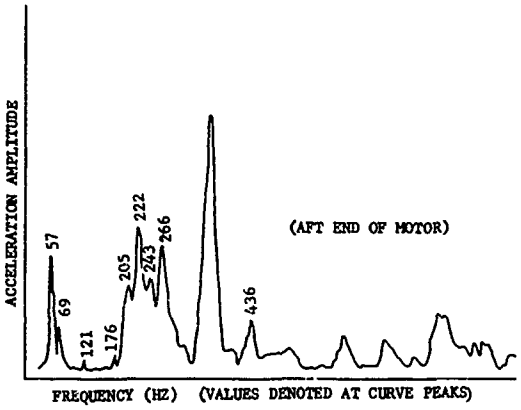

Figure 8. Frequency Response at Point 300

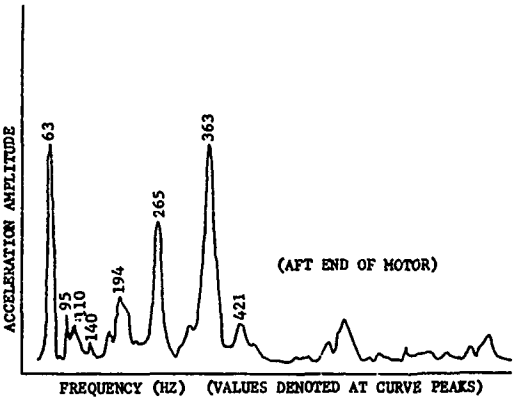

Figure 10. Frequency Response at Point 594

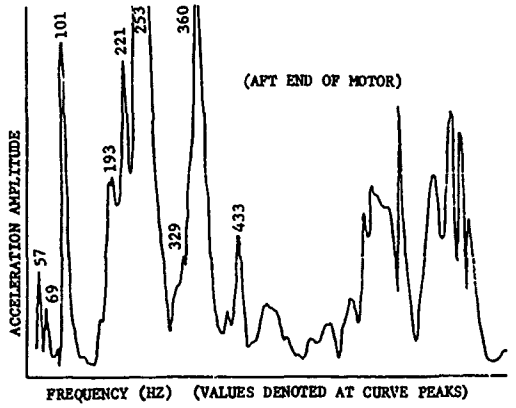

Figure 9. Frequency Response at Point 585

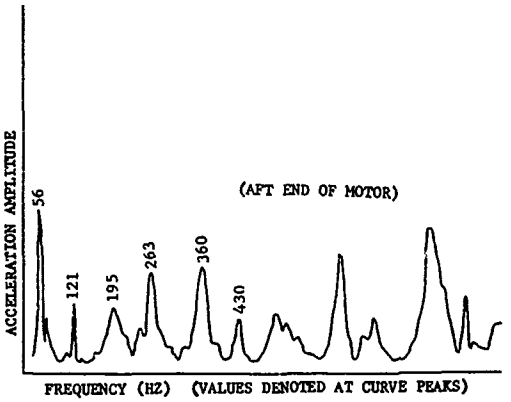

Figure 11. Frequency Response at Point 662

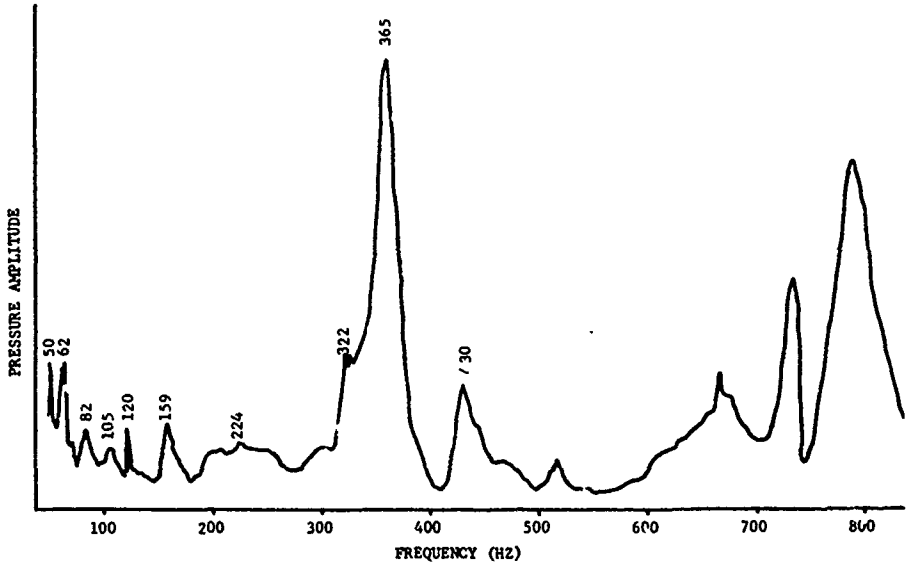

Figure 12. Combustion Cavity Pressure Frequency Response with the Microphone at Position No. 1

Y_2 are the corresponding maximum (single amplitude) response magnitudes at points one and two. During the mapping process, maximum amplitudes Y_i and phase angles Φ_i are obtained. To study the mode shape of the response oscillations, a particular response of interest is usually maximized; a time, t_o, is commonly chosen so that $y_i(t) = Y_i$ for an i of interest. Thus, a time, t_o, so that $\omega t_o + \Phi_1 = 0^o$, would maximize $y_1(t)$ and the mode shape at t_o would be

$$\begin{Bmatrix} y_1(t_o) \\ y_2(t_o) \end{Bmatrix} = \begin{Bmatrix} Y_1 \\ Y_2 \cos(-\Phi_1 + \Phi_2) \end{Bmatrix} \quad (3)$$

As with the frequency response testing, the volume of data collected by mapping mode shapes is too great to include in this paper. An example of the data collected is shown in Table I. Mode shape plots of the aft dome, made from the mode mapping data, are shown in Figures 13 and 14. An acoustic mode shape mapped along the motor centerline is shown in Figure 15.

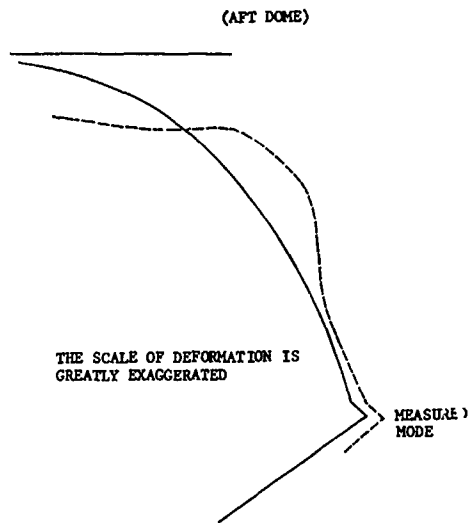

Figure 13. Mode Shape Comparisons for 0^o Section at 365 Hz

Evaluation of Accelerometer Mounting

Checkout tests were made to verify that double-backed adhesive tape could be successfully used to mount the accelerometers. Frequency response tests were conducted by using the following three mounting systems: (1) Accelerometer cemented to the case (usual method), (2) accelerometer mounted on two layers of double-backed adhesive tape, and (3) accelerometer mounted on double-backed adhesive tape over masking tape. The separate responses, as shown in Figure 16 were very

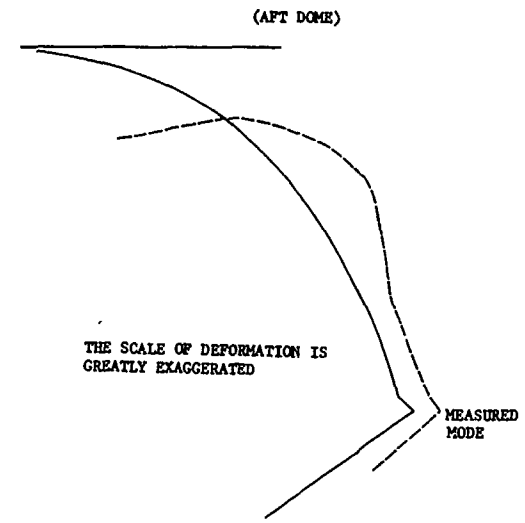

Figure 14. Mode Shape Comparison for 0^o Section at 265 Hz

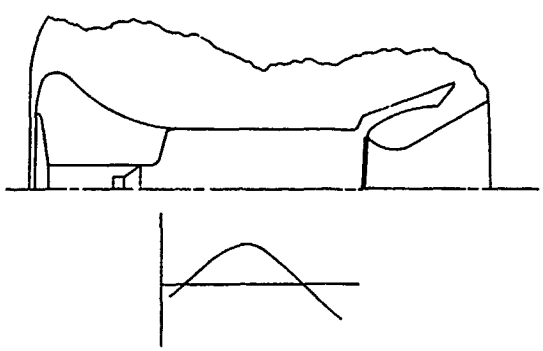

Figure 15. Pressure Mode Shape for 364 Hz Cavity Frequency

similar. For the very low g-levels encountered in these tests, double-backed adhesive tape apparently does provide satisfactory results. The accelerometer on the double-backed tape was removed and replaced several times and another frequency response test was conducted; results were still satisfactory.

Changing Frequencies of Acoustic Modes

The frequency response plots presented up to this point exhibit peaks at various particular frequencies. The peaks occur at resonant frequencies for the total system. Some of the peaks may occur mainly because of structural resonance while others are probably due mostly to acoustic cavity resonance. To identify structural resonant frequencies, gases other than nitrogen (helium and a helium and nitrogen mixture) were used to pressurize the chamber.

TABLE I

EXAMPLE OF DATA COLLECTED DURING MODE SHAPE MAPPING EXPERIMENTS

Motor Pressure	344.7 kPa (50 psi)	Motor Pressure	344.7 kPa (50 psi)
Reference Accel Loc	300	Reference Accel Loc	300
Voltage to Speaker	8 Volts	Voltage to Speaker	8 Volts
Frequency	262 Hz	Frequency	363 Hz

Location No.	Amplitude	Phase	Location No.	Amplitude	Phase
300	0.316	0°	300	0.605	+ 1°
301	0.332	+ 18°	301	0.569	+ 40°
302	0.369	+ 34°	302	0.859	+ 71°
303	0.472	+ 48°	303	1.535	+ 78°
304	0.741	+ 50°	304	2.465	+ 74°
305	0.994	+ 48°	305	2.974	+ 63°
306	1.077	+ 46°	306	2.573	+ 45°
307	0.869	+ 42°	307	1.672	+ 8°
308	0.494	+ 36°	308	1.825	- 54°
309	0.157	- 30°	309	2.446	- 85°
310	0.510	-120°	310	2.441	-108°
311	0.881	-132°	311	1.691	-132°
312	0.390	+ 16°	312	0.635	+ 6°
317	0.270	+ 12°	317	2.084	+ 85°
318	0.452	+ 6°	318	1.90	+ 72°
319	0.599	+ 9°	319	1.256	+ 46°
320	0.530	+ 21°	320	0.928	+ 20°
321	0.408	- 40°	321	1.3[illegible]	- 68°
322	0.258	-122°	322	1.[illegible]	
323	0.467	-169°	323	0.844	
324	0.315	- 20°	324	0.317	
325	0.327	- 30°	325	0.312	
326	0.289	- 38°	326	0.641	[illegible]°
327	0.252	- 29°	327	1.10	+133°
328	0.231	- 31°	328	1.425	+124°
329	0.252	- 31°	329	1.304	+ 97°
330	0.391	- 74°	330	1.148	+ 41°
331	0.435	- 72°	331	1.563	+ 16°

The different gases have different speeds of sound, which results in different frequencies of oscillation for a given acoustic mode.

At the beginning of this testing, the goal was to obtain two sets of frequency response data for a selected group of accelerometer locations, with the only differences in the data being the gas used to pressurize the chamber. With this goal in mind, frequency response plots were obtained for several different points while nitrogen gas was used to pressurize the chamber. During the testing, various testing system failures were experienced. The digital frequency counter was repaired, an accelerometer cable was replaced, and the speaker/driver was replaced. To cancel out the effects of changes in the testing system, the tests using nitrogen were repeated at three locations (points 304, 585, and 594). Results from these tests are given in Figures 17, 18, and 19.

Immediately following completion of the above test, where three frequency response plots were obtained using nitrogen, a gas mixture was created and three corresponding frequency plots were obtained for comparison. The gas mixture was obtained by bleeding off the nitrogen gas until a chamber pressure of 172.35 kPa (25 psi) was measured. The chamber was then repressurized to 344.7 kPa (50 psi) by using helium gas. The frequency response plots obtained with the nitrogen/helium mixture are shown in Figures 20, 21, and 22.

A final series of frequency response tests was run by using only helium gas to pressurize the motor to 344.7 kPa (50 psi). Data from the helium tests are presented in Figures 23, 24, and 25.

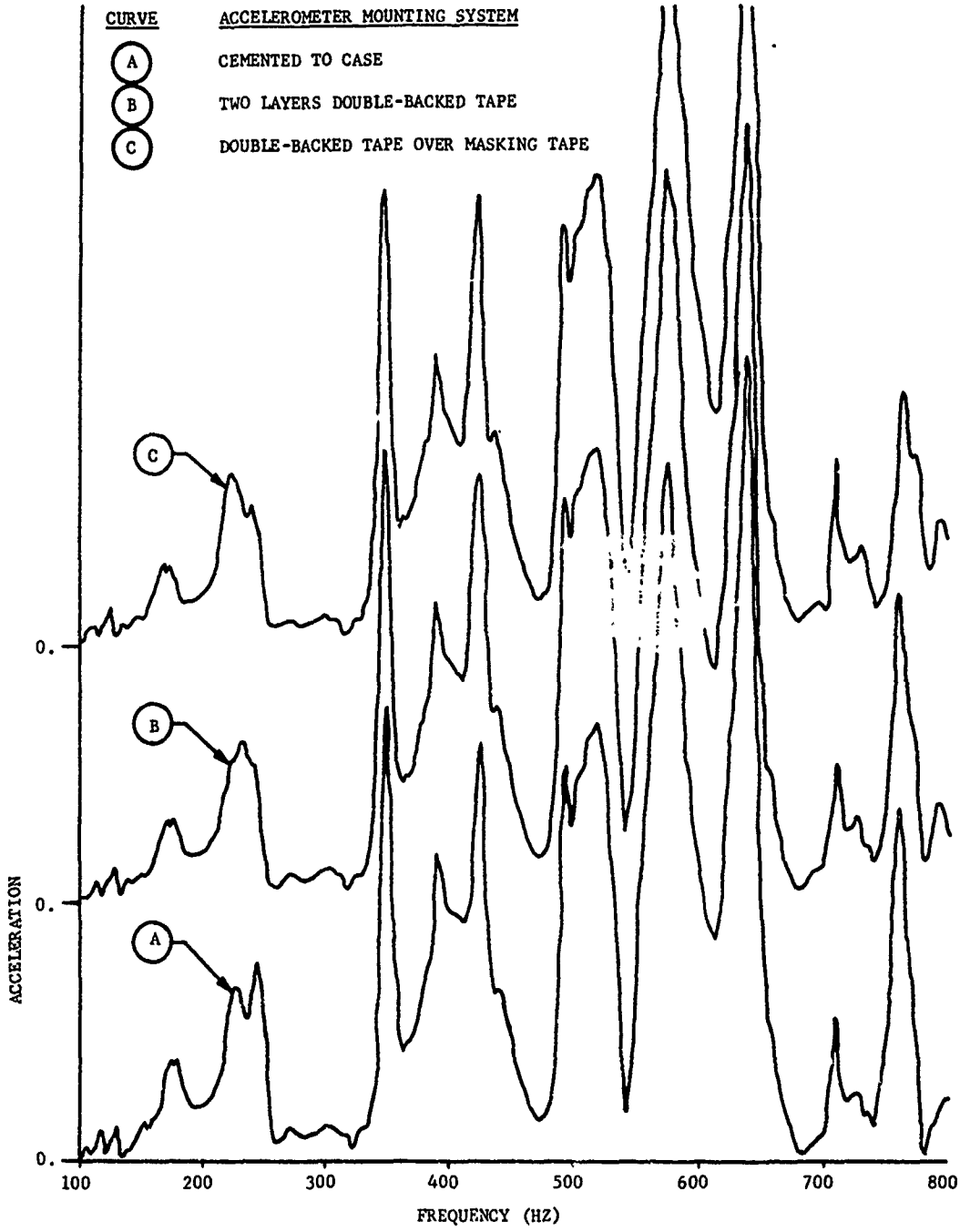

Figure 16. Comparison of Frequency Response for Three Different Accelerometer Mounting Systems

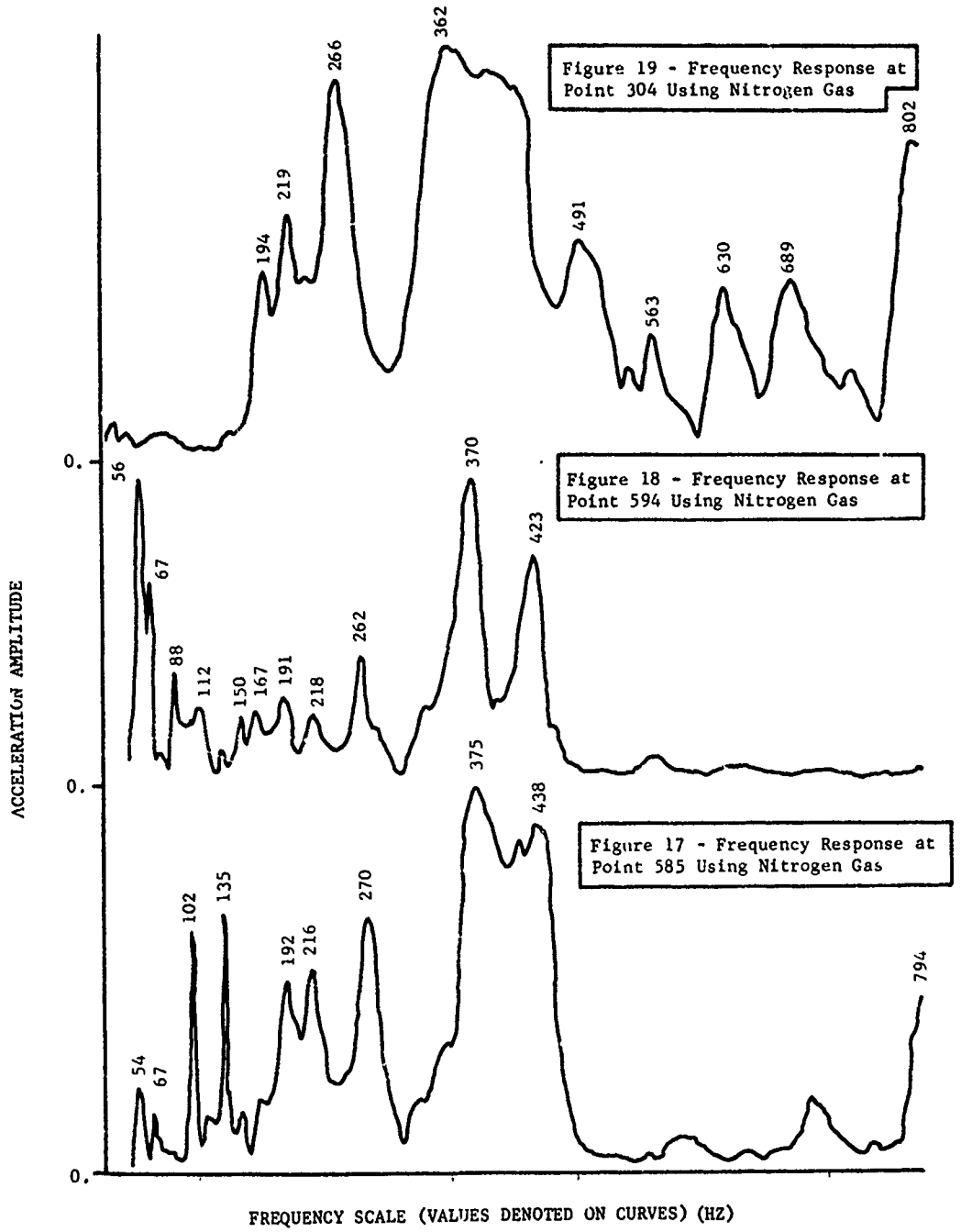
Figure 19 - Frequency Response at Point 304 Using Nitrogen Gas
Figure 18 - Frequency Response at Point 594 Using Nitrogen Gas
Figure 17 - Frequency Response at Point 585 Using Nitrogen Gas
ACCELERATION AMPLITUDE
0.
0.
0.
56
67
88
112
150
167
191
218
262
370
423
54
67
102
135
192
216
270
375
438
794
194
219
266
362
491
563
630
689
802
FREQUENCY SCALE (VALUES DENOTED ON CURVES) (HZ)

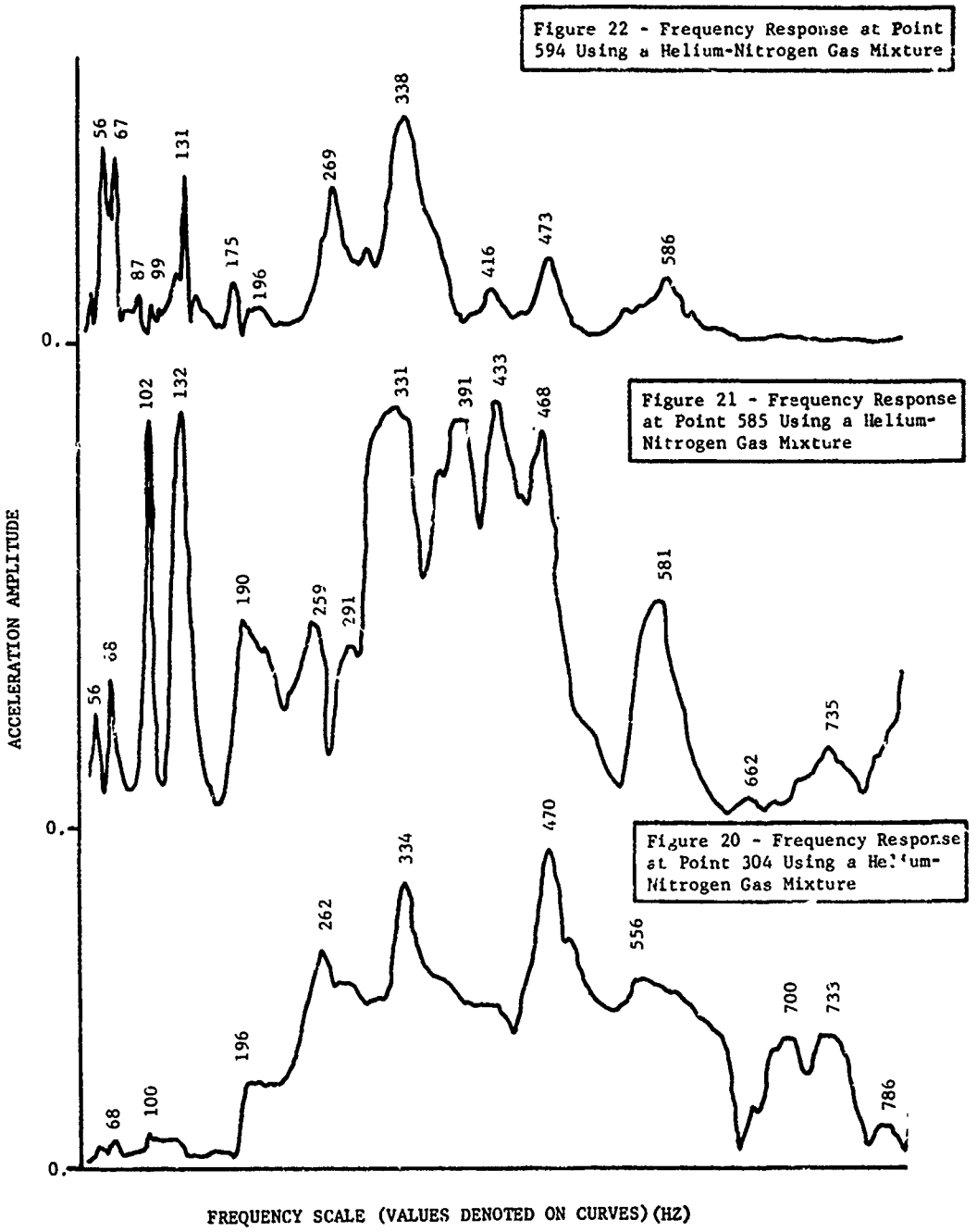
Figure 22 - Frequency Response at Point 594 Using a Helium-Nitrogen Gas Mixture
Figure 21 - Frequency Response at Point 585 Using a Helium-Nitrogen Gas Mixture
Figure 20 - Frequency Response at Point 304 Using a Helium-Nitrogen Gas Mixture
ACCELERATION AMPLITUDE
0.
0.
0.
56
67
131
87
99
175
196
269
338
416
473
586
56
68
102
132
190
259
291
331
391
433
468
581
662
735
68
100
196
262
334
470
556
700
733
786
FREQUENCY SCALE (VALUES DENOTED ON CURVES) (HZ)

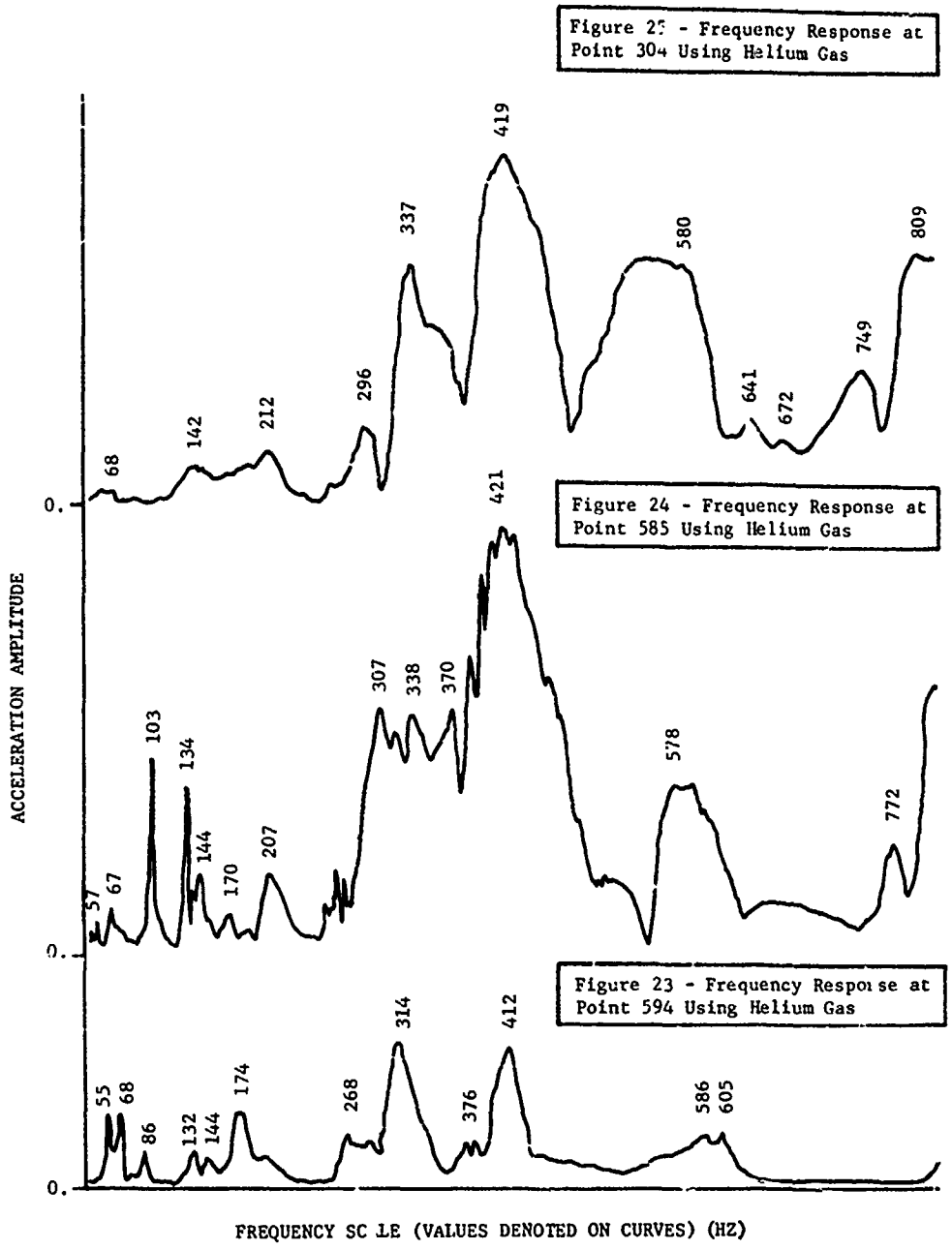
Figure 23 - Frequency Response at Point 304 Using Helium Gas
Figure 24 - Frequency Response at Point 585 Using Helium Gas
Figure 23 - Frequency Response at Point 594 Using Helium Gas
ACCELERATION AMPLITUDE
0.
0.
0.
68
142
212
296
337
419
580
641
672
749
809
57
67
103
134
144
170
207
307
338
370
421
578
772
55
68
86
132
144
174
268
314
376
412
586
605
FREQUENCY SCALE (VALUES DENOTED ON CURVES) (HZ)

DISCUSSION

A major peak on most of the frequency response plots occurred at approximately 365 Hz. Figure 12 shows that the microphone, when located at position 1, had a maximum response at 365 Hz. The high microphone response indicated the presence of an acoustic mode. The acoustic mode shape shown in Figure 15 verified that the cavity oscillates in the fourth longitudinal mode at 365 Hz. The limited axial travel of the microphone resulted in the partial mode shape shown in Figure 15. However, when the measured partial shape was compared with full-length acoustic testing results and acoustic analysis results, the presence of the fourth longitudinal mode was verified.

Additional acoustic mode shape plotting was conducted at some of the smaller peaks on the frequency response curves. When a natural acoustic mode is not being excited, a plot of the acoustic response mode shows an irregular low amplitude pressure distribution. When a natural acoustic mode is excited, the pressure response is of greater magnitude and a plot of the response mode shows a definite and smooth pattern. The third longitudinal mode was determined to occur at approximately 265 Hz.

The response mode shapes shown in Figures 13 and 14 represent structural response to a measured and well-defined loading distribution; therefore, the objective of this experimental work has been achieved. It should be noted that absolute pressure or acceleration amplitudes were not required. The normalized loading distribution (acoustic mode shape) and frequency are sufficient to determine a normalized structural response mode.

The nitrogen gas used to pressurize the chamber for most of the testing was replaced with helium gas to change acoustic mode frequencies. The ratio of the speed of sound in helium to that of nitrogen is about 2.88. Therefore, the major acoustic mode that occurs at 362 Hz, as shown in Figure 19, could be expected to shift to 1042 Hz when helium was used. Since all frequency sweeps were terminated at approximately 1000 Hz, the shift to 1042 Hz could not be verified. The 263-Hz acoustic mode that occurs in Figures 17, 18, and 19 at frequencies of 270, 262, and 266 Hz, respectively, would be expected to shift to frequencies of 778, 755, and 766 Hz, respectively. Figures 24 and 25 show corresponding peaks at 772 and 749 Hz, but Figure 23 does not have any peak in the 770 Hz vicinity.

There appears to be a structural mode, possibly a dome mode, at either or both 55 Hz and 68 Hz. Figures 17 through 25 show a response at about 68 Hz without regard to gas mixture. All but Figure 25 also show a response at about 55 Hz without regard to gas mixture. Measured responses near 60 Hz are always under suspicion because of the correspondence with the electrical power supply frequency. Since response peaks occurred at about 102 Hz and 134 Hz in Figures 17, 21, and 24, a component resonance at position 585 apparently occurs at these frequencies. Similar comparisons can be made at other frequencies.

CONCLUSIONS

Since modes that represent the response of the structure to well-defined acoustic loads were measured, the objectives of the testing program were achieved. The measured modes were found to provide a realistic characterization of the motor structure. Results have been used to show that the test procedure described is a reasonable and practical way to obtain structural response of solid rocket motors to load distributions that are created by unstable acoustic oscillations. The structural response obtained during the program was used to evaluate finite element models and analysis results.

The use of different gases to pressurize the motor to change the frequency of acoustic modes was also shown to be a useful technique. In future tests, a gas mixture could be created to provide an acoustic resonance that would excite a particular known structural resonance of interest.

Discussion

Mr. Mustain (Rockwell International): You say it is an organ pipe but you have propellant in there that changes the modes as it burns; are you treating that as a closed-open pipe or an open-open pipe, or how do you treat that? I checked some chamber pressures on some motors and tried to get an answer that correlated and my results weren't too good.

Mr. Jensen: That is true it is somewhat of a problem and I think there is a shock wave near the throat and our acoustics people who do these analyses have kind of a feel for where they ought to put the cut off point around the throat of the nozzle; you can change the frequency that occurs in the cavity by changing the boundary conditions or changing the length of the cavity to consider whether you go way down the nozzle or whether you put the boundary condition right at the throat. It turns out that the best place to put it to get a good comparison with the firing results is right near the throat area. So we treat it as a shock wave near the throat and that essentially a closed-closed cavity.

Mr. Mustain: What are the acoustic velocities for the regular propellants? Does 3,000 ft/sec sound reasonable?

Mr. Jensen: I think that is in the ballpark. I was going to say maybe 5,000 ft/sec. but I think it is in that range between 3000 and 5000 ft/sec.

Mr. Mustain: Did you run your test with speakers in an empty chamber?

Mr. Jensen: No, the motor had inert propellant in it.

Mr. Mustain: It had propellant in it but you were able to move your microphones. Did you ever test that same type of chamber with an actual firing, and compare your chamber pressures against yous speaker test results?

Mr. Jensen: We have looked at accelerometer data and we have analyzed it and tried to identify through different kinds of analyses what frequencies were present. Our tests were run with a cold gas so the thire longitudinal mode with a hot gas test would occur at a different frequency than with a cold gas test. We used a conversion factor to convert the hot gas test results to cold test results and when we did that we felt that we got correlation. I think that in the "hot motor" the third longitudinal mode occurred at 770 Hz where as in the"cold motor" it occurred at 265 Hz.

VISCOELASTIC DAMPING SYSTEM USE AS A REMEDY FOR POGO EFFECT ON THE DIAMANT SATELLITE LAUNCH VEHICLE

M. POIZAT, P. VIALATOUX
Société METRAVIB - 24bis Chemin des Mouilles
69130 ECULLY - FRANCE

and

P. COCHERY, M. VEDRENNE
CENTRE NATIONAL D'ETUDES SPATIALES
Tour Lorraine - Boulevard de France
91000 EVRY - FRANCE

After a description of the POGO effect experienced on the French launch vehicles DIAMANT B, this paper deals with the technique of vibration damping by a viscoelastic coating and the approach which led to its implementation.

In the second part, the results obtained on samples and mock-up are presented together with improvements brought by this technique to the launch vehicles DIAMANT B P4 n° 1 and 2.

INTRODUCTION

The purpose of the present paper is to demonstrate how the POGO phenomenon can be eliminated, or substantially reduced, by the provision of additional damping in a specific zone of the launch vehicle structure.

After a brief description of POGO effect and its consequences on launch vehicles DIAMANT B n° 1 to 5, we give details of the logic behind and the work involved in evaluation of the viscoelastic damping procedure, leading to application of the latter on launch vehicle DIAMANT B P4.

The results obtained in flight subsequent to this processing, are compared with those obtained with previous firings, and future perspectives for the use of this procedure on launch vehicles are reviewed.

The theoretical and experimental work covered by the present paper was carried out conjointly by METRAVIB and the CENTRE NATIONAL D'ETUDES SPATIALES.

DESCRIPTION OF POGO EFFECT

The DIAMANT B satellite launch vehicle, and the DIAMANT B P4 derived from same, are three-stage launch vehicles :

- The first stage (L 17), identical for both types, is driven by a Valois engine, using the thrust of two hypergolic liquids, N_2O_4 and UDMH (Plates 1 and 2).
- The two upper stages are solid fuel (powder) driven.

DMB.

Plate 1

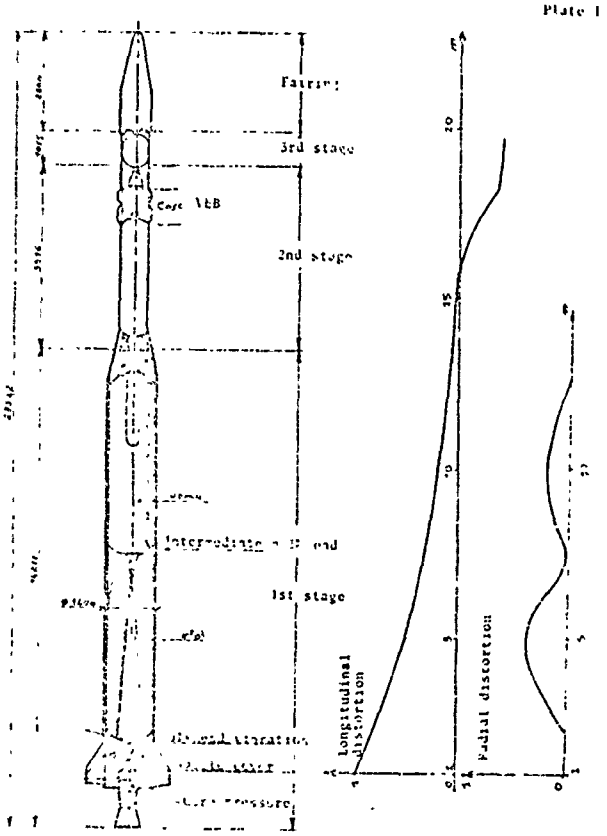

DIAMANT B P 4

Plate 2

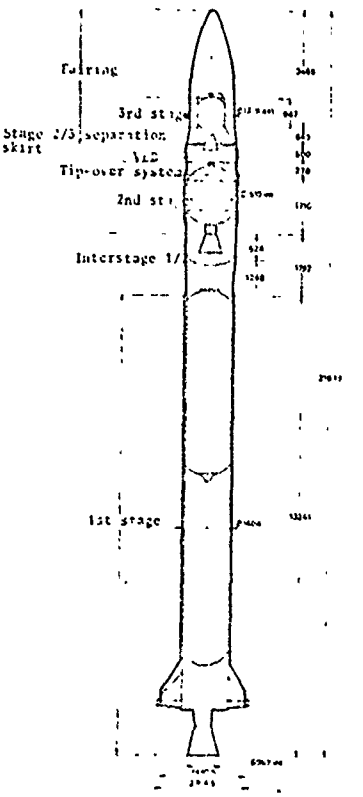

During flight, the liquid powered stages are subjected to numerous vibratory phenomena, the most troublesome and restrictive of which for the mission is the POGO effect. This effect is characterized by the appearance of low frequency longitudinal vibrations in the structure, associated with fluctuations in pressure in supply pipes and engine core.

The DIAMANT B launch vehicle has not escaped this phenomenon, and during the first five flight firings, for the first 30 or 40 seconds of combustion of stage L 17, this effect was observed with frequently substantial structural acceleration, reaching maximum levels of 20 to 30 g at certain points, with a frequency of about 45 Hz.

The consequences of this phenomenon can extend to the destruction of the launch vehicle or satellite.

To obtain a better understanding of the phenomenon and find a remedy for same, a measurement plan was adapted to the problem, this being used to discover the vibratory levels of the structure, and pressure variations on the main points of the launch vehicle.

In the following table, we show a comparison of the main values for the five firings of DIAMANT B. From the vibration values, the distortion curve for the launch vehicle can be established, this curve plotting longitudinal and transverse vibration amplitude against vehicle height, the latter with respect to a reference point, this being the nozzle cover (point of engine/structure attachment).

VIBRATION LEVELS

MEASUREMENT	LAUNCH VEHICLE				
	DMB 1	DMB 2	DMB 3	DMB 4	DMB 5
Core pressure (bar)	± 3	± 1.65	± 3.5	± 2.8	± 0.3
N_2O_4 tank bulkhead pressure (bar)		± 0.25	± 0.9	± 1.05	
UDMH pressure on injection (bar)			± 2.45	± 2.55	
Nozzle cover vibration (g)		± 4.75	± 11	± 13	± 6
N_2O_4 tank bulkhead vibration (g)	± 11.5	± 7	± 20.5	± 17.5	± 1.5
Intermediate bulkhead vibration (g)		± 1.5	± 10	± 8.5	± 0.3
VEB vibration (g)		± 0.8	± 6.5	± 4.5	± 0.1

This curve shows us that it is the rear part of stage L 17 which is subject to the highest level of radial distortion.

Distortion data obtained for DIAMANT B is shown in Plate 1.

In parallel to these experimental measurements, a complete theoretical model of the POGO loop was developed :

- The launch vehicle structure is represented by its modal characteristics, these being modal frequencies, modal shapes, and generalized damping and mass values.
- The hydraulic systems are represented by a transfer function, connecting pressure and flow on the tank bulkheads, to core pressure inside the engine.
- The engine is represented by a transfer function, connecting core pressure to the excitation stress applied to the structure.

This constitutes a loop which can become unstable under certain conditions.

Status variable $\Phi(t)$, which characterizes the evolution of core pressure, flow values, and the modal characteristics of the structure, is represented by :

$$\Phi(t) = \Phi_0 e^{\zeta \omega t} e^{i \omega t}$$

where :

$$\Phi(t) = \begin{Bmatrix} P \\ \dot{m}_N \\ \dot{m}_O \\ q_i(t) \end{Bmatrix}$$

with P : Core pressure

$\dot{m}_N$, $\dot{m}_O$: Flow values

$q_i(t)$: Structure i^{th} modal coordinate

ω : Pulsation of the phenomenon
ζ : Divergence of the phenomenon
$\zeta = 0$: Limit of loop stability
$\zeta > 0$: Loop unstable
$\zeta < 0$: Loop stable

On first approximation, we can consider the structure as non-dissipative at the loop stage, and we can introduce generalized damping of the structure, ζ_s, for a given mode, on divergence term ζ.

Under these conditions, we define critical damping ζ_c, as being connected to ζ and ζ_s by :

$$\zeta = \zeta_c - \zeta_s$$

It is then just as if divergence of the POGO phenomenon was due to the result of the two terms, the first, ζ_c, characterizing the complete loop, and the other, ζ_s, characterizing structure damping. We should therefore have term ζ_s as high as possible, although the corresponding value is generally about 1 % on launch vehicle structures.

In the case of the DIAMANT launch vehicle, respective values are as follows at start of flight :

$$\zeta_s \simeq 1\%$$

$$\zeta_c \simeq 1\%$$

$$\zeta \simeq 0{,}1\%$$

A slight variation in term ζ_s or ζ_c is enough to reobtain stability, due to the low divergence value.

To ensure or improve stability, the conventional technique consists in changing the transfer functions of the hydraulic pipes, modifying their capacitance and self-inductance values by the introduction of an accumulator or the injection of gas. This reduces ζ_c .

Unfortunately, with DIAMANT B, the reduction of ζ_c on one structural mode resulted in an increase of ζ_c for neighbouring modes.

Nevertheless, it was possible to adjust this term for structure/hydraulic system interaction, by slight modification of the modal characteristics of the structure on the thrust frame (stiffening of rear frame on DIAMANT B 5).

The results obtained were highly conclusive, but the POGO phenomenon remained at low level (see Plate 4 : Comparison of curves for vibration levels measured on the N_2O_4 tank bulkhead, for five firings).

To eliminate this phenomenon completely in this context, the only answer is an increase in term ζ_s.

The recent technique of damping the structure by means of a viscoelastic coating might make it possible to advance in this direction, without modification of the frozen configuration of the launch vehicle.

EVALUATION OF STRUCTURAL DAMPING OBTAINED BY THE INTRODUCTION OF LOCAL DAMPING PROCESSING

We give below the main guide lines used to obtain an estimate of the damping effect introduced by local covering.

A programme for calculating the longitudinal modal shapes of the launch vehicle, which takes account of the presence of the liquids, makes it possible to obtain, after separation of the problem into a number, n, of degrees of freedom (see figure, Plate 5), the mass and stiffness matrices, modal shapes and frequencies of the system, which is assumed non-dissipative.

We then introduce a damping matrix which is proportional to that of the stiffness for the structural sub-assembly treated with the coating, to make allowance for the fact that the composite obtained has a YOUNG modulus with the form :

$$E = E^*(1 + j\eta)$$

η : Structural damping of the composite (see following chapter).

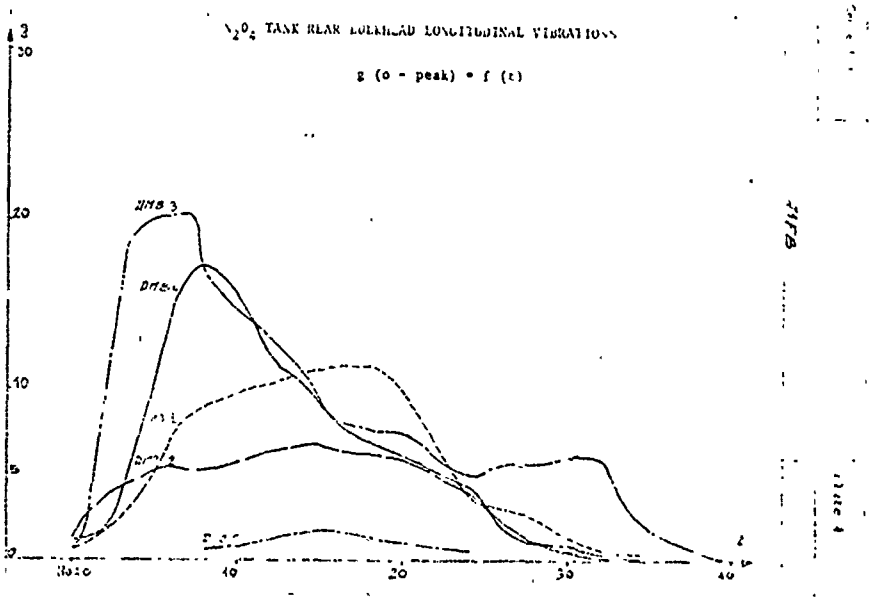

Plate 5

DIAGRAMMATIC REPRESENTATION

OF STAGE L 17 USING 14 ELEMENTS

After passing through the space of the complex modes, and separation of the real and imaginary parts, we obtain a system of linear equations of the order 2n, which make it possible to obtain, for various excitation frequency values, modal coordinates and structural displacements under the effet of a force applied to the thrust frame.

The generalized damping factor (ratio of damping to critical damping) is finally obtained by measurement of bandwidth at 3 dB for response at one point on the structure.

The method was first applied for studying sensitivity of modal damping at the point of treatment, and according to the importance of same.

For example, for fixed structural damping of 10 % on one of the elements, resultant modal damping is given in the table below and clearly shows, in accordance with the configuration of the deflection curve, that it is the rear part, subject to maximum radial movement, which allows introduction of maximum damping for a given supplementary mass value.

Element treated	Modal damping
4	1.5 %
5	2.9 %
9	3.5 %
10	6.2 %

PRINCIPLE OF VISCOELASTIC DAMPING

a/ - GENERAL

The conventional law of elasticity (Hooke) relating to the behaviour of materials, $\sigma = E\varepsilon$, characterizing the proportionality between stress and strain is to be taken in its general form :

$$\sigma = A_0 \varepsilon + A_1 \frac{d\varepsilon}{dt} + A_2 \frac{d^2\varepsilon}{dt^2} + \cdots$$

which we can write as follows for a given frequency :

$$\bar{\sigma} = E_{(\omega)} \left[1 + j\eta(\omega) \right] \bar{\varepsilon}$$

where

$$\bar{\sigma} = E^*_{(\omega)} \bar{\varepsilon}$$

The law of behaviour of E must be used with a complex elasticity modulus. If we express the damping properties of a material by the phase φ existing between stress and strain we can express the elasticity modulus by a complex number : $E^* = E(1 + j\eta)$, with $\eta = \operatorname{tg} \varphi$ representing the coefficient of structural damping, namely the capacity of the structure to reduce part of the vibratory energy of the system.

The response of a damped structure to a given excitation is considerably affected by the damping value, as shown in Figure 1 (Plate 6), which gives the Q factor for a first order system, representing one structure mode which is sufficiently decoupled from the others. Figure 2 (Plate 6) shows the first mode shape of a beam at a given level of excitation, for various structural damping values.

Plate 6

RESPONSE OF A DAMPED STRUCTURE

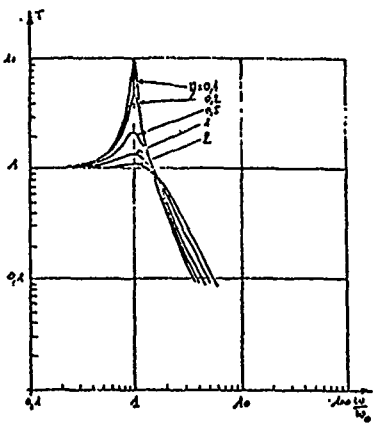

Overload on a 1st order system, with hysteretic damping

$\eta = 0,2$
$0,4$
$0,3$
1
2

Fig. 1

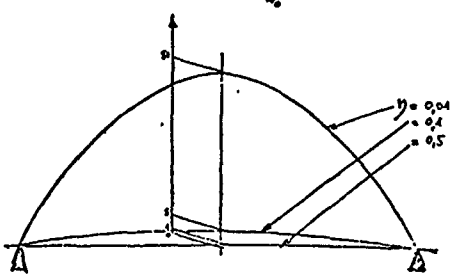

1st mode distortion amplitude on a beam, at η = 0,01 - 0,1 - 0,5

Fig. 2

Among the various solutions which can be used to increase structural damping, the viscoelastic coating technique certainly shows the best results.

Pratical research relating to materials suitable for increasing structural damping has shown that it appears impossible to obtain, simultaneously, a high elasticity modulus and marked damping.

It should be remembered that structural damping for a bar in standard materials is about 10^{-4} to 10^{-3}, while damping can attain 10^{-2} or a few 10^{-2} (as is the case with launch vehicle structures) for assembled structures. Metal alloys which are known for their damping properties, reach an internal damping factor of about 0.01 or 0.03 (possibly 0.1 under high stress) in the most favourable cases, and are extremely costly. On the other hand, we find viscoelastic materials which present, under certain conditions, a damping factor in excess of 2, but with an elasticity modulus under 10^9 N/m2, and which are therefore unsuitable as such for mechanical construction. The technique of viscoelastic coating therefore makes it possible to associate the good mechanical strength of materials with a high modulus, with the damping capacity of viscoelastic materials.

The composite structures thus obtained which we refer to as simple coating in a case where a layer of viscoelastic material is associated with a layer of elastic material, and stressed coating in a case where an elastic layer or stress plate is added to the above, making it possible to obtain structural damping factors of $0.01 < \eta < 1$

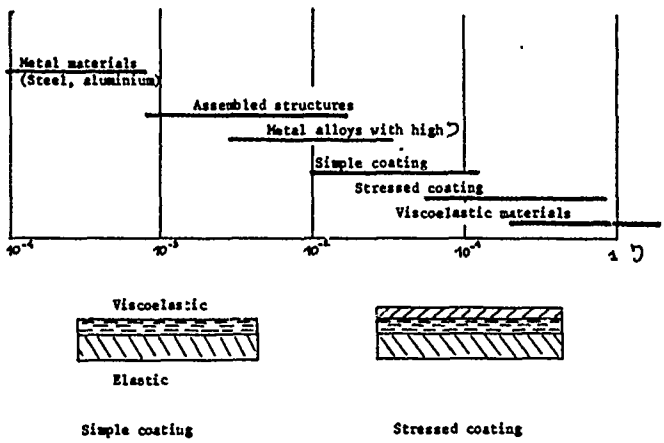

As for the viscoelastic material itself, performance of the composite depends on frequency and temperature.

The damping characteristics of viscoelastic materials, $E^* = E'(1 + j\beta)$, pass through a maximum in the area of transition from the rubbery state to the vitreous state. This area generally covers a fairly limited temperature interval for a given frequency, thus making viscoelastic materials extremely sensitive to temperature. The effect of frequency is of the same kind, but considerably less marked.

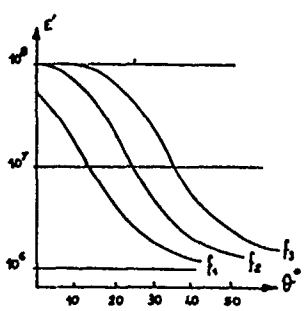

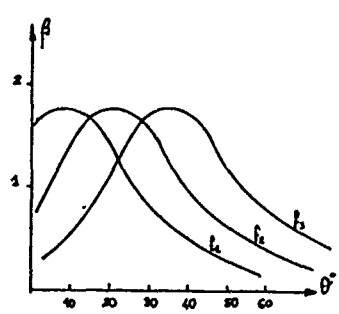

Correlatively, composite structures are sensitive to the same parameters, and calculation models can be used to forecast the conjugated effect of variation in elasticity modulus and damping.

b/ - PERFORMANCE COMPARISON BETWEEN SINGLE AND STRESSED COATING

Without going into the details of the calculation, nor of the technological methods used, the essential characteristics of single and stressed coatings, making same suitable for separate applications, should be noted.

The dynamic performance of the single coating, where the viscoelastic layer is subject to tensile and compressive stresses, varies with :

- The ratio of the modulae for the viscoelastic and elastic materials, E_V/E_1
- The ratio of the corresponding layer thicknesses, e_V/e_1
- And naturally, the intrinsic damping factor (β) of the viscoelastic material (Figure 1 below).

In consequence, this technique, which is better adapted to thin structures (2), calls for viscoelastic materials with a high elasticity modulus. Under these conditions, it is then possible to obtain composite damping factors (η) which are very marked (for example : 0.1 - 0.2).

The stressed viscoelastic coating makes it possible to improve performance by increasing the energy dissipated in the viscoelastic layer, which is then subject to shear stress (Figure 2 below). Performance is linked to a greater number of parameters, regulated by a beam calculation model which is already very complex (3) (4). In this case, we show

that it is possible to attain a high composite damping factor, for example $0.1 < \eta < 1$, provided geometric dimensioning of the layers is optimized, and provided we select characteristics which are appropriate for the viscoelastic product ($10^6 < E' < 10^9$), implying specific calculation for each case.

It is possible to improve composite damping by multiplying the number of alternate layers (elastic and viscoelastic), in which case the ratio of composite damping η to intrinsic damping β comes close to 1, indicating that for each application, a compromise must be found between desired performance, technological complexity, and increase in mass, not forgetting the participation of each layer in the rigidity of the whole as also in static dimensioning.

Single coating Stressed coating

Figure 2

The example shown in Plate 7, illustrates the effect of damping by stressed viscoelastic coating, and its dependence on temperature, on the response curve for a simple parallelepipedic beam, excited in the middle.

EVALUATION OF THE PROCESS WITH A VIEW TO APPLICATION TO SPACE VEHICLE STRUCTURES

The principle of increase in damping of the structure having been selected to compensate start of flight POGO effect on the DIAMANT B P4 launch vehicle, a preliminary experiment was run on a steel disc measuring 1 400 mm in diameter and 2.5 mm thick, representing an idealized model of a tank bulkhead.

The objectives set for this experiment were the search for maximum damping, using the stressed viscoelastic coating technique, whilst restricting the thickness of the counter-plate to 0.5mm (mass increase of about 20 %), and examination of technological conditions for application : attachment and subdivision of the stress plates.

After primary dynamic calculations, the disc was ballasted with two annular weights, as shown in Plate 8, so as to appropriate a mode to two nodal circles at 40 to 50 Hz. Without going into the details of all results obtained, Plate 8 shows the axial deflection of the disc under central harmonic excitation on the modal shape under study. Excitation force was held at constant level.

Experiment curve 1 relates to the basic disc without coating. This curve correlates closely with initial calculations.

Curve 2 relates to the disc with stressed coating damping : 0.2 mm of type VP 71 viscoelastic material, with steel plate 0.5 mm thick (VP 71 is a Hoechst product).

Deflections are attenuated by 7.5 and 17.5 dB respectively, for a mass increase of 6 kg on the 56 kg of the initial structure (10.7 %). The damping factor measured is then $\eta = 0.15$.

This performance, allowing for the initial stresses, appeared sufficiently interesting to justify examination of the technological problems, with a view to subsequent application to space vehicle structures.

Thus experiments on the damped disc enabled us to check that subdivision of the counter-plate into sectors has no effect on the composite damping factor. Furthermore, if we reduce the surface treated by deleting certain sectors symmetrically, experience confirms theoretical analysis, showing that composite damping is proportional to the surface treated for the symmetric mode concerned.

NOTE : ATTACHMENT OF COUNTER-PLATES

The stress plates are only attached to the basic structure via the viscoelastic layer, and the adhesion of the latter to adjacent layers (the viscoelastic material is either self-adhesive or glued on). According to the nature of these materials, we may look for a better behaviour of the counter plate, this involving supplementary links between the elastic layers (welding, rivetting, etc...). Experiments have shown that these links are possible from the technological point of view, without any great effect on performance. Naturally, the nature of materials used and the thickness of same will condition the solution to be adopted. For example, on the test disc, spot welding was used to connect base plate and counter-plate, welds being spaced at approximately 150 mm intervals. In this case, the damping factor moved from 0.15 to 0.10.

Plate 7

INLUENCE OF TEMPERATURE ON DAMPING

Mechanical impedance

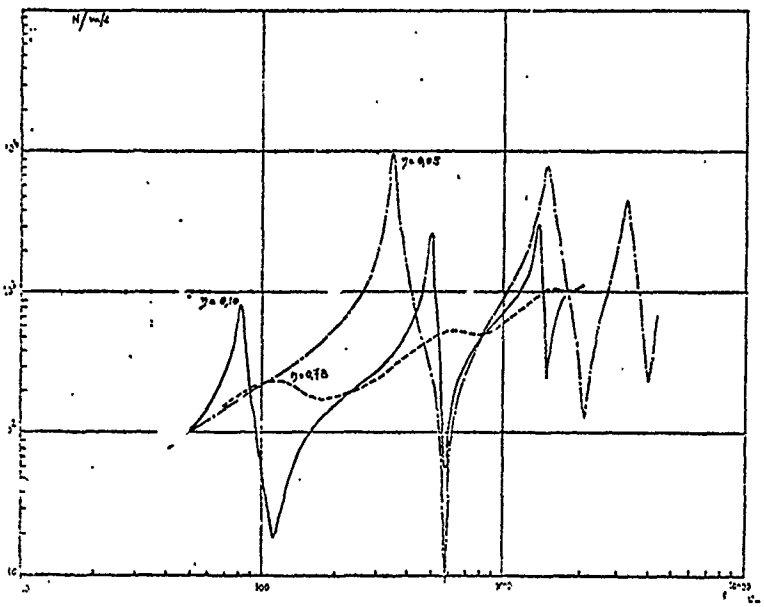

Optimized sandwich beam, at + 25° C and 100 Hz

Response of same beam at 3 temperature levels:

EVALUATION OF DAMPING ON STEEL DISK

Plate 8

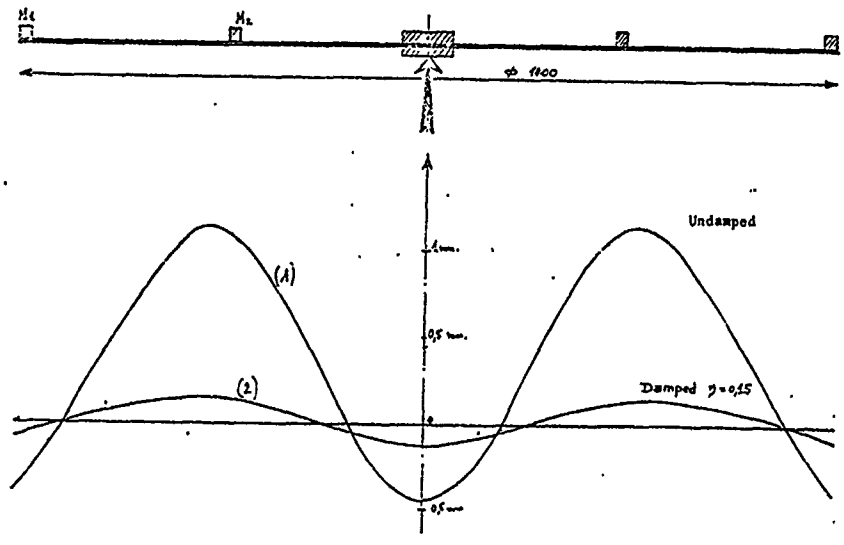

Axial distortion of the disk

Conclusions

Evaluation of the process having demonstrated a good correlation between calculations and experience, making it possible to attain interesting performance levels without difficulty, and involving no major technological difficulties from an operating point of view, it was then decided to consider the case of a mock-up structure such as a tank full of liquid.

APPLICATION OF THE DAMPING TECHNIQUE TO A DMB P4 FIRST STAGE TANK MOCK-UP, FOR THE PURPOSE OF REDUCING START OF FLIGHT POGO EFFECT

The purpose of this application was to reproduce a POGO type mode on a tank mock-up, then correlating the results of calculations and actual experiments so as to be able to extrapolate the comparison to the actual tank, for which only calculations can be made.

To be sufficiently representative, the mock-up must have a first longitudinal mode at a frequency of less than 100 Hz.

Situation of the problem

The principal phases of the study are as follows :

a/ Definition by calculation of the dimensions for a tank mock-up full of water, with a weight on the upper part, such that the first longitudinal mode has a frequency of less than 100 Hz.

b/ Definition of test conditions for isolating the first longitudinal mode, and measuring corresponding characteristics (skin + liquid).

c/ Definition of optimum damping, acting on this mode (characteristics of coating, geographical distribution on the tank), and evaluation of its effect.

d/ Correlation of calculations and experience following studies on the mock-up, the calculation models should make it possible to extrapolate and forecast the damping which could be obtained on the actual tank.

Definition of the tank mock-up by calculation

The various calculations on the tank mock-up were carried out using programmes giving the longitudinal deflection of tanks filled with liquid (ARCHER and RUBIN method).

Composition of the tank mock-up

The tank mock-up comprised a cylinder in AG5 aluminium alloy, 1 mm thick (diameter 880 mm - height 1 480 mm). This cylinder was fabricated by the roll weld method, the weld joint running along one generator. The bottom of the tank comprised a hemi-sphere welded onto the cylinder (Plate 12).

Identification of the vibration mode sought

Principle of experimental procedure.

The essential characteristics of the tank mode excited under POGO effect is the axisymmetrical behaviour of the structure, coupled to the fluid, producing in the latter a pressure field which is also axisymmetrical. Now in the case of harmonic excitation at variable frequency, a number of modes appear (Plate 9), and in particular, circumferential wave effect modes (festoon modes, $\eta\theta$ cosine modes).

For a clearer study of the POGO mode with which we are concerned, it is necessary to isolate same from all the others. For this, a number of possibilities can be considered :

- For example, we can isolate the POGO mode analytically, starting with the initial development of the transfer function under driving point harmonic excitation, then ascending to the modal characteristics, these being sought by means of an identification technique. Refer (5) (6) (7) (8).

- We can also act on the structure itself : either by pressurizing the tank (these are actual flight conditions), thus pushing the circumferential modes to higher frequencies, or by harnessing the tank cylinder axisymmetrically, using strong stiffener bands.

The latter solution is the one adopted, by reason of its advantages of safety, ease of operation, and efficiency.

Obviously this modification will change the inherent characteristics of the longitudinal mode, but the objective at which we are aiming is to avoid changing its behaviour characteristics (axisymmetrical behaviour, coupling with the fluid). This structural modification makes it possible to preserve the revolution symmetry of the tank, so as to

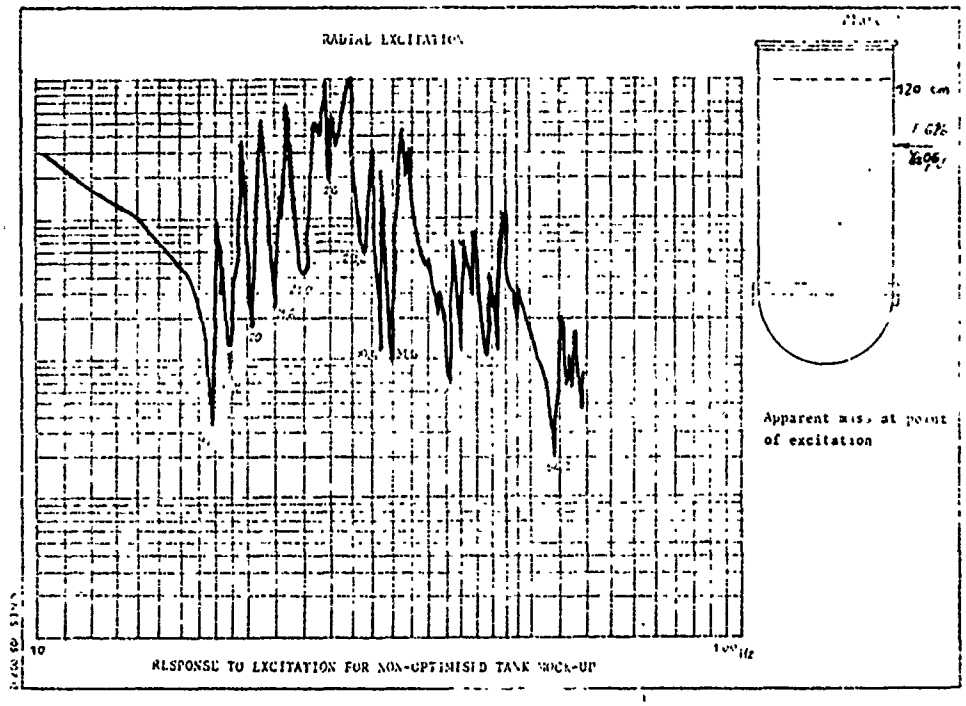

RESPONSE TO EXCITATION FOR NON-OPTIMISED TANK MOCK-UP

favour the appearance of axisymmetrical modes and to minimize the development of all circumferential modes (cos (nθ) modes with n > 1). The axisymmetrical mode sought after is in fact a circumferential mode with n = 0.

L.D. PINSON and C.G. BROWN (9) have shown, confirming experimentally, that the curve giving the frequency of a circumferential vibration mode (festoons) according to order n of this mode, is a curve passing through a minimum corresponding to an order n which is non-zero. This minimum depends on tank geometry, liquid level, and also internal pressure.

This curve was traced experimentally (Plate 10) in the case of the tank mock-up. The various deflection show the coupling existing between the different circumferential modes (Plate 11). In fact at 20 Hz coupling n = 4 and n = 6 is visible. At 23.8 Hz we have n = 3 with n = 8, and at 30.4 Hz, n = 2 with n = 9. We can therefore deduce from the curve shown in Plate 12 that mode n = 0 is coupled with a mode n = 11, 12 or 13.

The harnessing was therefore introduced to minimize the effect of these festoon modes, and to eliminate their coupling with mode n = 0.

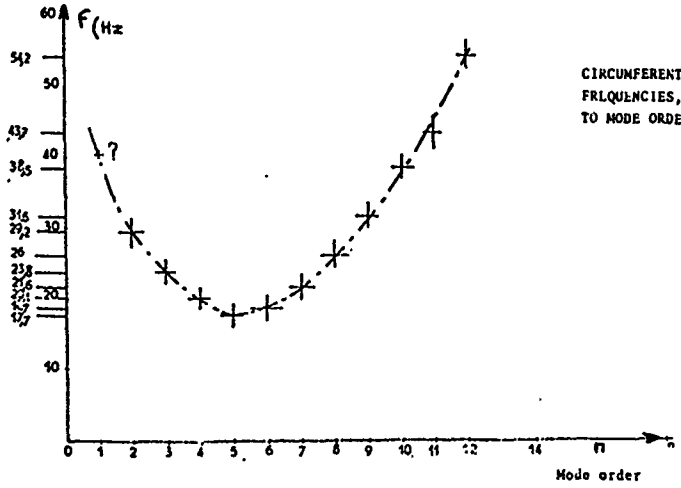

CIRCUMFERENTIAL MODE FRLQUENCIES, ACCORDING TO MODE ORDER

Plate 10

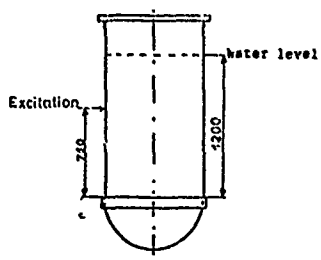

Plate 11

RADIAL DISTORTION AT DIMENSION + 70 CM

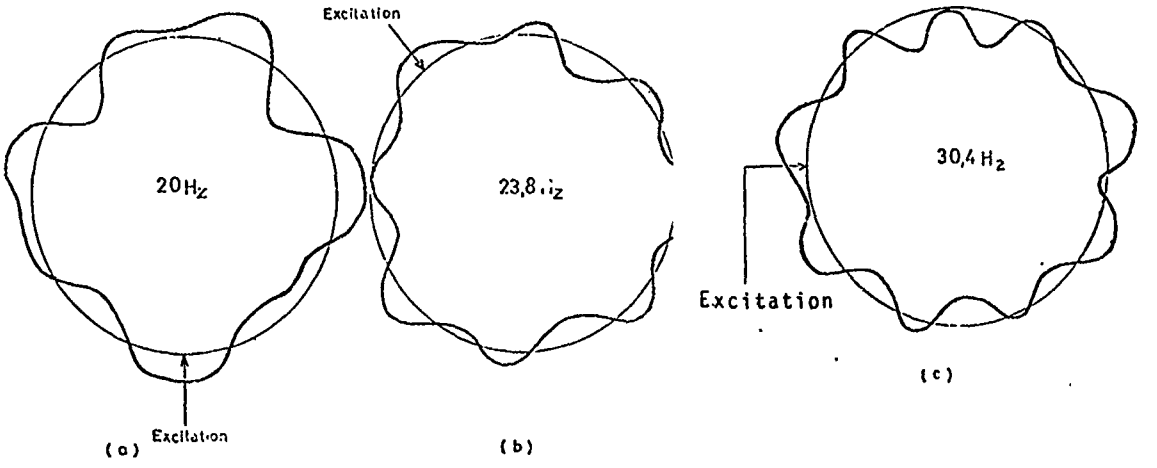

Plate 12

CONFIGURATION OF TANK MOCK-UP

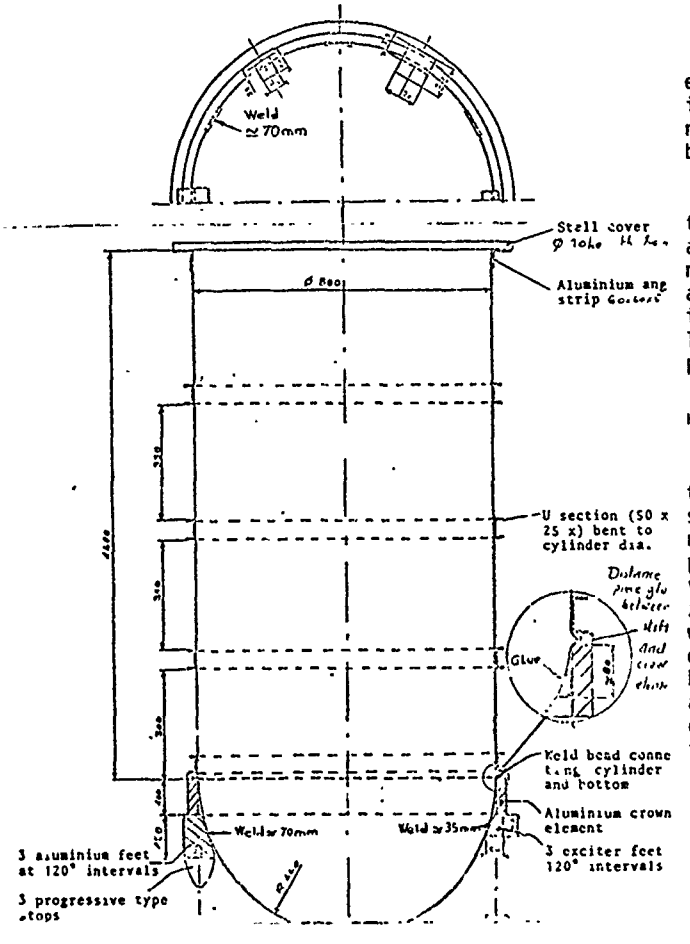

Operation

a/ - Choice of longitudinal excitation

To favour appropriation of excitation effect to the mode, it is essential to provide longitudinal (axial) excitation, translation being as axisymmetrical as possible.

After a period of development, the form of excitation selected was achieved by means of three synchronized electro-dynamic exciters, applied to a thick crown element integral with the bottom of the lower tank cylinder (Plate 12 and photo below).

b/ - Elimination of festoon modes

After a number of preliminary tests, it was found that radial stiffening of the cylinder at a number of levels (Plate 12) made it possible to obtain a longitudinal vibration mode in the frequency zone scanned (20 to 100 Hz), for which there is high participation on the part of the liquid, with a high degree of clarity (Plates 13 and 14). When isolated, this mode can then be characterized accurately.

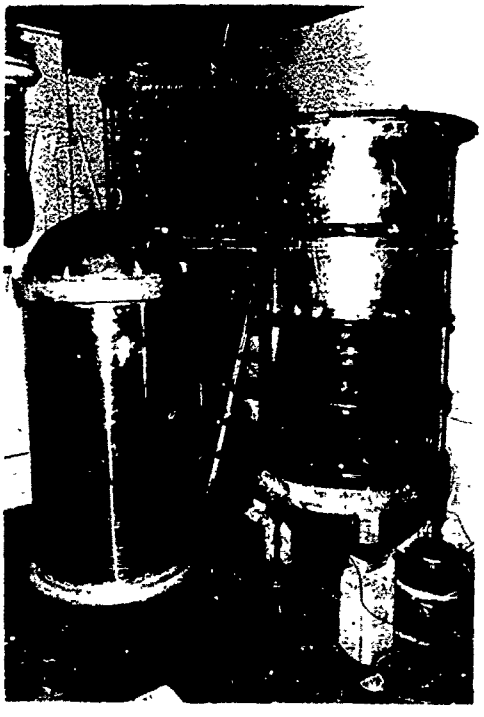

Plate 13

VIBRATORY EXCITATION

3 pots at 120° intervals $E_1 = E_2 = E_3$ = 0.1b
- 1 cover, 130 kg
- 3 radial stiffeners, glued
- 1 lower crown element, glued

water level = + 120 cm

Trace of $\frac{1}{1/3}$ longitudinal, at bottom of cylinder

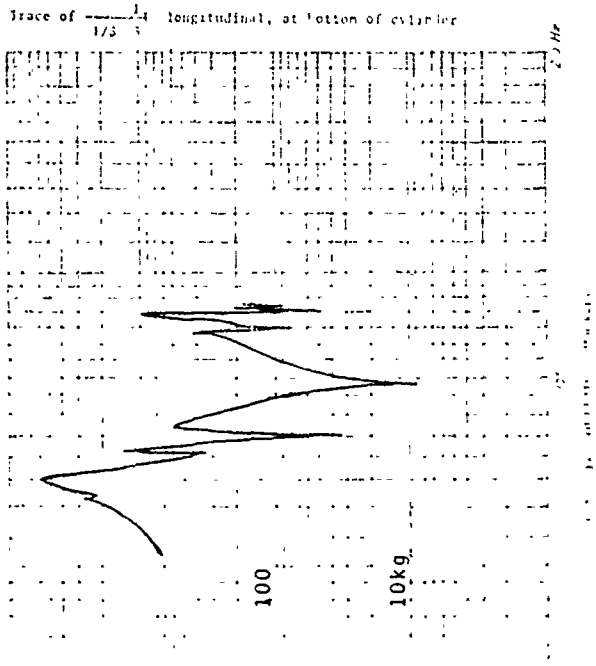

Plate 14

COUPLING OF LIQUID WITH STRUCTURE FOR POGO TYPE MODE PRESSURE

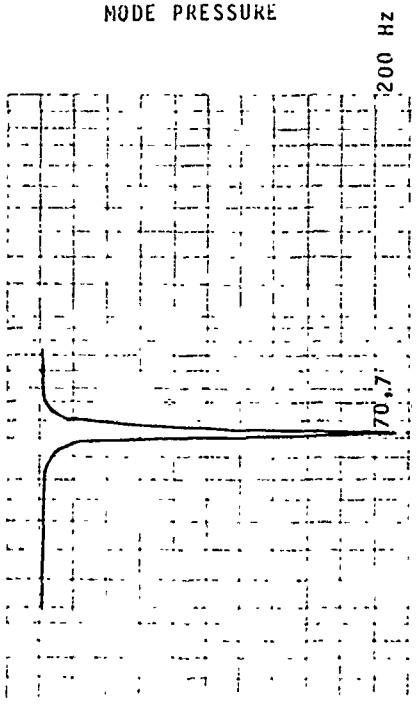

Characteristics of the mode

By reason of the very low coupling with neighbouring modes, response for the stiffened structure is very close to its modal shape. It can be obtained by exploring the displacement field on the tank, and compared with the modal calculation. Systematic readings of tank deflection and the pressure field in the liquid were taken, this information being given on Plates 15 and 16. Exploration of dynamic pressures on a number of different verticals indicates that the complete volume of water is coupled with structural deflection. Forecast deflection values for the tank, obtained by calculation, are shown on the same figure (Plate 16). Good concordance is obtained with experimental results, insofar as we are interested in global phenomena obtained on the tank : distension between the stiffeners, radial nodes on the latter, deployment of the complete bottom.

Frequency deviation between calculation and test is explained by the high degree of sensitivity of the mode to any perturbation of radial stiffness, but the configuration shown here provides the best compromise between frequency and modal shape, with respect to experimental results.

Deflection and pressure field are axisymmetrical, but are sensitive to imperfections in the structure (discontinuity due to the presence of the weld bead).

As the POGO mode was shown up clearly on the non-damped tank, it was possible to undertake a comparison with a damped tank.

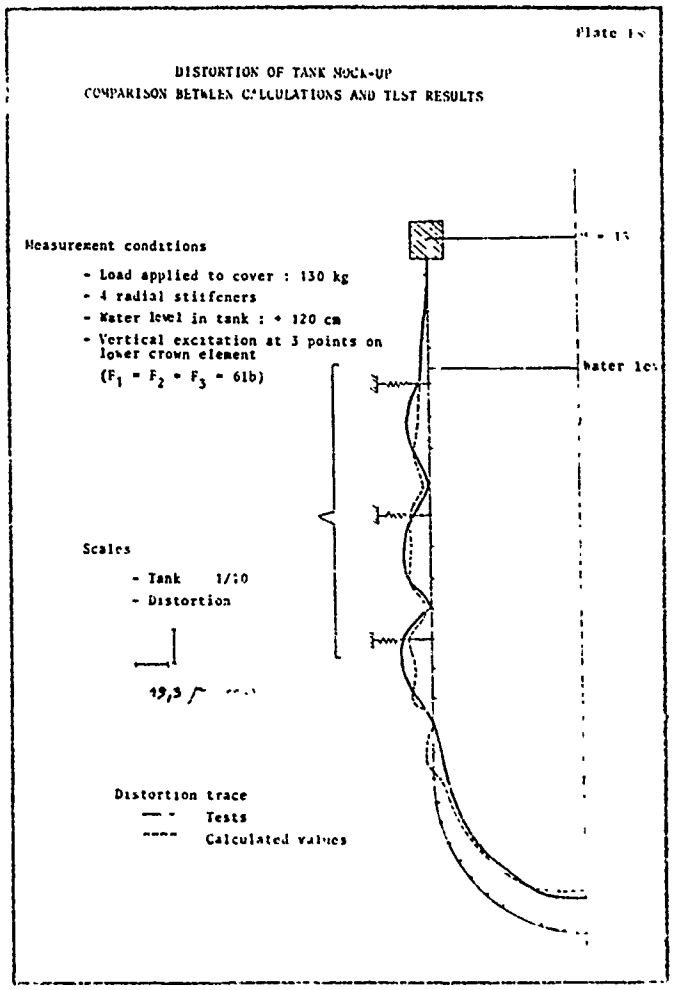

Plate 16

DISTRIBUTION OF DYNAMIC PRESSURES IN LIQUID AT POGO

TYPE MODE FREQUENCY

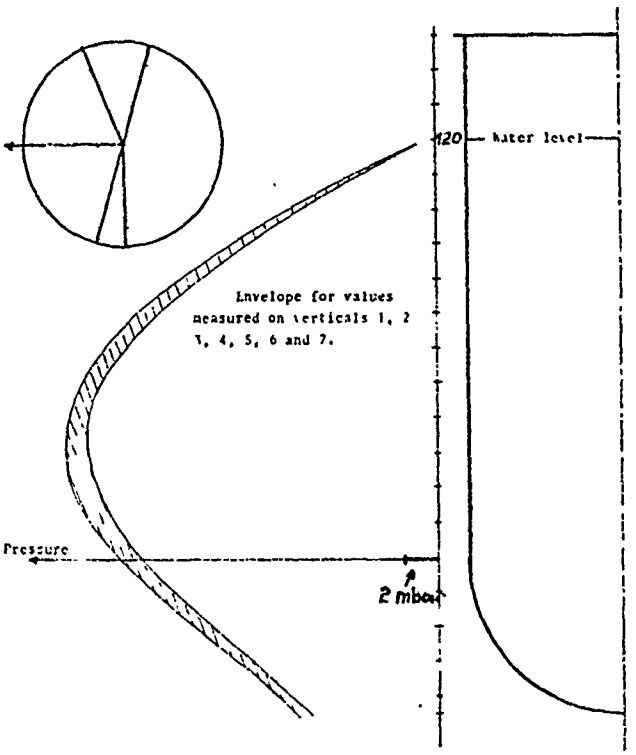

Definition of damping configuration

In paragraph 3, we showed by calculation that partial damping of the tank structure in the aeras where radial deflection is high, was sufficient to obtain valid damping, $3s$, of the assembly.

The area which we are interested in treating is the rear part of the N_2O_4 tank cylinder. The same principle was therefore adopted on the mock-up.

Two damping techniques were used :

- Simple coating with Lord M Manufacturing type L D 400 materials, thickness 1.6 mm
- Stressed coating, using Hoechst VP 71 material, thickness 0.5 mm. Counter plate in aluminium, thickness 1 mm.

Experimental results

For the two damping configurations, deflection and pressure amplitude were read in the same way, and using the same procedure as indicated in the previous paragraph, and these values were compared with results obtained on the non-damped mock-up.

The following results were obtained (same excitation force) :

Result \ Tank	Non-damped	Damped using sandwich technique	Damped using simple coating technique
Relative increase in mass	0%	0.8%	0.5%
Damping factor	$\sim$ 1%	$\sim$ 5%	$\sim$ 4%
Ratio of radial/ longitudinal displacement	0.75%	0.50%	0.56%
Maximum dynamic pressure in fluid at mode frequency	22 mbar rms	3.8 mbar rms	4.9 mbar rms

$$rms = \frac{Peak}{\sqrt{2}}$$

Plate 17 and 18 give comparative results for deflections and pressures in the liquid.

We note :

- That the damping provided gives a reduction in pressure in the fluid by a factor of 6.
- That the damping technique using stressed coating is difficult to apply, by reason of the curvature of the cylinder walls, and this can lead to imperfections in execution. In consequence, the result to be obtained by the stressed coating technique is more difficult to forecast since it depends too much on application.

This is one of the reasons why the simple coating technique was selected for the DMB P4 tank. The results which can be obtained with this technique are sufficiently interesting with an acceptable mass increase.

COMPARISON OF RADIAL DISTORTION Plate 17

- Non-damped tank
- Damped tank

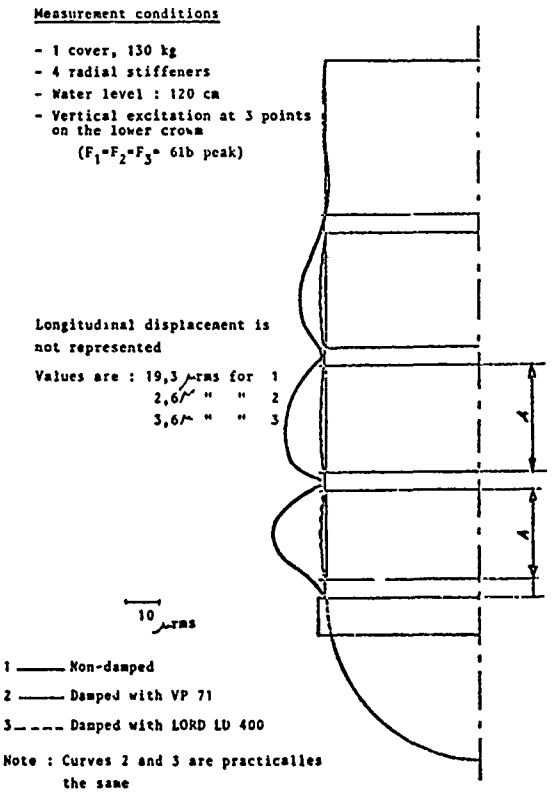

Plate 18

COMPARISON OF DYNAMIC PRESSURE IN LIQUID BETWEEN :

- Non-dampod tank ————————
- Tank damped with LD 400 (ep : 1,6mm) —·—·—·—
- Tank damped with thickness VP 71 (ep : 0,5mm + aluminium plate thickness 1 mm) — — — —

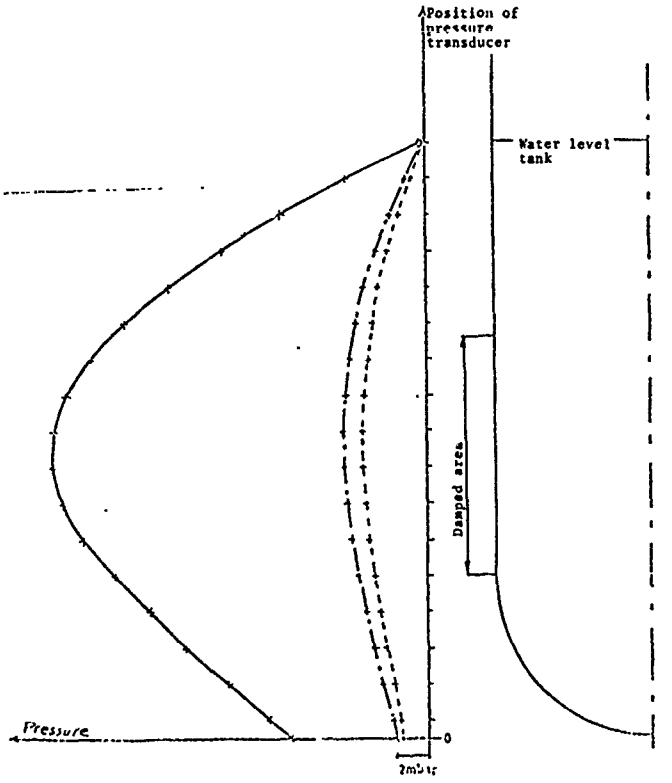

TRANSPOSITION TO THE ACTUAL CASE OF DIAMANT B P4

We have seen that in the current state of DIAMANT B P4 launch vehicle design, the start of flight POGO phenomenon presents low ζ divergence. Only a few thousandths of additional damping are required to eliminate start of flight POGO.

The method of calculation discussed in section 3 makes it possible to provide generalized damping of the longitudinal POGO mode, using structural damping introduced on a tank element.

We set the objective of introducing 1 % additional damping, this value presenting no problems with respect to divergence, and seemingly sufficiently easy to obtain, allowing for applicational, mass and temperature constraints. The results of calculation for the tank, with damping applied to the lower half of the N_2O_4 tank, are shown in the table below.

Damping applied to element 10	Increase in modal damping
0	0
0.012	0.007
0.025	0.014
0.05	0.027
0.10	0.052
0.15	0.082

This calculation shows that it is sufficient to provide damping of about 0.0015 on element 10 to meet the objectives set.

Estimation of damping at element level

Calculations are not made on a complete representation of the damped structure, since this would necessitate the creation of a model of the tank skin and its viscoelastic coating, and this problem has so far only been properly solved for simple structures of the beam or plate type.

We assimilated the skin and coating assembly to a composite, having equivalent mass, rigidity, and damping characteristics. Damping characteristics were estimated from test results and calculations for sandwich beams having the same conformation as the structure under study.

If calculation of the tank mock-up and complete launch vehicle are relatively easy for this reason, estimation of the damping provided at composite level is the difficult point of this method.

We must consider the manner in which the composite acts on the actual structure : traction, compression, and bending, and carry out tests on a test beam selecting test conditions (excitation, length, and temperature) which reproduce the characteristics of stresses applied to the mock-up and launch vehicle in flight.

In fact if we consider a composite beam corresponding either to the treatment applied to the tank mock-up (1 mm of AG3 + 1.6 mm of LD 400 material), or to the processing provided on the actual tank (2.3 mm of steel + 3 mm of LD 400), damping values are as follows :

Nature of composite beam	Traction, compression η_t	Bending (at 80 Hz) η_B
1 mm AG3 + 1.6 mm LD 400	0.024	0.07 to 0.15 Average = 0.11
2.6 mm steel + 3 mm LD 400	0.006	0.085 to 0.125 Average = 0.105

As already stated, allowance must be made for both bending and traction/compression. We have assumed equal distribution of each load, this giving a damping factor equivalent to the arithmetical average $\frac{\eta_t + \eta_B}{2}$

Configuration	Nature of beam	η of element
Mock-up	1 mm AG3 + 1.6 mm LD 400	0.065
L 17 tank	2.6 mm steel + 3 mm LD 400	0.055

Forecast values for the actual tank

With the result data shown in the above table, we have all elements necessary for estimating the damping applied to stage L 17 if the lower part of the tank is treated to a height of 2.75 m with a layer of type LD 400 material 3 mm thick (additional mass 60 kg). Given the model selected, it is prudent to apply an inaccuracy factor of 2 when interpreting the result.

a/ Comparison of calculations and experience for the tank mock-up

Damping applied to element	Increase in modal damping		Calculation/experience correction factor
	Calculated	Measured	
0.065	0.035	0.020	1.75

b/ Forecast of performance of actual tank, extrapolating with the same correction factor

Damping applied to element	Calculated increase in modal damping	Correction factor	Likely increase in modal damping
0.055	0.030	1.75	0.017

This forecast result, divided by an inaccuracy factor of 2 ($\frac{1}{2}$ = 0.008) provides a sufficient degree of safety with respect to the desired objectives, to justify application to the actual tank.

Results obtained in flight on launch vehicles DIAMANT B P4 n° 1 and 2

Local damping treatment was carried out in accordance with the definitions given in the preceding pages.

The launchings took place on 6th February 1975 and 17th May 1975 from the KOUROU base, on which occasion it was possible to check the accuracy of forecast values under actual operating conditions.

Start of flight POGO had disappeared and the additional damping was adequate to reduce the divergence term below zero and thus ensure stability of the loop.

CONCLUSION

The increase in structural damping obtained by localized viscoelastic coating of certain sub-assemblies produced satisfying results, in a case where other remedies would have made it necessary to reconsider design of the DIAMANT B P4 satellite launch vehicle.

Start of flight POGO effect was completely eliminated, and the purpose of the present article has been to provide details of the various steps, both theoretical and experimental, which contributed to this result.

The same procedure was also applied with success when DIAMANT B P4 n°02 was fired, being used to obtain substantial reduction in end of flight POGO effect, this having appeared, as forecast, during the flight of DIAMANT B P4 n° 01.

As with all other possible remedies, this does not eliminate the need for close knowledge of the POGO loop, particulary in terms of structural behaviour. Furthermore, the effectiveness of the procedure must be considered with respect to its sensitivity to operating parameters such as temperature and frequency, and in the light of the mass increase which it represents. However, and in contrast to systems such as the use of accumulators or the injection of gas, this procedure can be applied very late in the development plan, or even during manufacture of liquid powered launch vehicles.

BIBLIOGRAPHY

1 - J. MARTINAT

Amortissement des structures par revêtement viscoélastique avec plaque de contrainte mécanique, matériaux, électricité

Janvier 1972 - N° 265

2 - H. OBERST u. K. FRANKENFELD

Uber die Dämpfung der Biegeschwingungen dünner Bleche durch festhaftende Beläge

ACUSTICA 2, AB 181 - 1952

3 - J.E. RUZICKA, T.F. DERBY, W. SCHUBERT, J.S. PEPI

Damping of structural composites with viscoelastic shear damping mechanisms

NASA CR 742

4 - D.J. MEAD, S. MARKUS

Cos-factors and resonant frequencies of elastic damped sandwich-beams

J.S.V. - 1970 - 12 (1) - 99 - 112

5 - D.R. GAUKROGER, C.W. SKINGLE, K.H. HEROW

Numerical analysis of vector response laws

J.S.V. - 1973 - 29 (3) - 341.353

6 - W.G. FLANELLY et al. (Kamon Aerospa- Corp.)

Research on structural dynamic testing by impedance methods

7 - KLOSTERMAN

On the experimental determination and use of modal representations of dynamic characteristics

Ph. D. THESIS - University Cincinnati - 1971

8 - D. BONNECASE, M. POIZAT (Sté METRAVIB)

Analyse modale des structures par excitation ponctuelle en regime sinusoïdal entretenu

9 - L.D. PINSON, C.G. BROWN

A finite element method for non axisymmetric vibrations of pressurized shells of revolution, partially filled with liquid

AIAA Paper N° 73 399

10 - Documentation concerning CNES - METRAVIB research contracts (Programmes - Study reports).

Discussion

Mr. Lepor (Naval Undersea Center): What was the thickness of your structure?

Mr. Vedrenne: Two millimeters.

Mr. Lepor: Did you try damping tapes that we developed for aircraft damping consisting of a viscoelastic layer of 7 mills and aluminum foil thickness on the order of eleven mills? Did you use damping tapes which consist of aluminum foil and adhesive that wrapped around your structure? We found it to be very effective in aircraft structure damping, did you try that on your vehicle?

Mr. Vedrenne: The techniques used are certainly different from the aircraft techniques, the "POGO" effect is a low frequency phenomena and there is no problem of noise or flutter. It is used to increase the damping of the loop of the "POGO" effect assisted by the structure, the hydraulic system, and the thrust.

Mr. Lepor: So you say that several layers of the aluminum foil combination may not do the job? The reason I bring this up is we are very weight conscious in aircraft and we have found that damping tapes of this nature can be much more effective than just mass as exhibited by damping compounds.

Mr. Vedrenne: On the first stage the increase of mass is not very important. It is one or two percent of the satellite mass in the second or third stages it is very difficult to apply this technique.

Mr. Lepor: At what point did you go through the "max" Q? How many seconds after launch were you in the "max" Q?

Mr. Vedrenne: The maximum pressure occurs about 50 seconds or the first minute after launch.

Mr. Lepor: So your "POGO" effect occurred right after dynamic stress?

Mr. Smith (Bell Aerospace Company): It is my impression that a lot of effort on "POGO" in the "States" went into damping the fluid motions, such as supression of slosh. Did you not think that this was a worthwhile attack?

Mr. Vedrenne: The sloshing motion in the fluid is not important for the "POGO" effect. The sloshing is important for the bending modes, for the possibility of the launch recall. The frequency of the sloshing modes are very far removed from the frequency of the longitudinal modes because this launch vehicle is small; for big launch vehicles, for example, an Atals, a Titan, or an Ariel, the problem is not the same.

Mr. Mustain (Rockwell Space Division): I assume this is a pressure fed type engine and hypogolic fuels are being used. Do you have any turbopumps.

Mr. Vedrenne: Hypogolic fuel was used.

Mr. Mustain: Do you have any experience with the other type of engines where they have pumps feeding it such as liquid oxygen, hydrogen as we used in our programs? Did you have any "POGO" experience there?

Mr. Vedrenne: We have not had any experience with very low temperature cryogenic fuels. Have you?

Mr. Mustain: Yes, we have had lots of experience with them.

Mr. Vedrenne: Have you had any experience with "POGO" effects?

Mr. Mustain: Yes. Did you ever try devices other than damping such as accumulators and trying to change the frequencies and the lines?

Mr. Vedrenne: The philosophy for interrupting the loop is to put an accumulator in the hydraulic system, but for this launch vehicle it was very difficult to apply this technique because we had one stable mode for several unstable modes since the accumulator makes the other modes unstable. Certainly the "POGO" effect on the DIAMANT B is not classical "POGO" effect; it is not in accordance with the frequency of the structural modes and the frequency of the hydraulic lines. There is only a possibility of coupling with the hydraulic system but it is not at the same frequency.

Mr. Coleman(Naval Undersea Center): I notice that when we talk about rockets, which are devices or structures that are vertical, we are concerned with "POGO" effects. For those of us who are concerned with similar shaped structures that go underwater we call them accordian effects, so we talk about accordian modes. The difference in concern is that instead of the energy flow through the loop within the fluid within the structure we talk about coupling of energy outside through the fluid and the infinite extent of the liquid. In your studies of "POGO"effects have you also looked at some of the accordian effects and are there any ways to take advantage of the many many hours and expenditure of effort in the accordian mode problems.

Mr. Leondis (General Dynamics/Convair): What is the weight per unit surface area of the damping application?

Mr. Vedrenne: The mass is around 60 kilograms.

Mr. Leondis: Is that for the entire vehicle?

Mr. Vedrenne: For the half of one.

Mr. Leondis: Was the application of the damping material limited to the outside of the tank?

Mr. Vedrenne: Yes.

Mr. Leondis: In one of the slides I thought I saw a metallic outer surface.

Mr. Vedrenne: In the slide, you saw the thermal protection before the launching.

Mr. Leondis: Is that jettisoned?

Mr. Vedrenne: This technique seems very good for Diamant B.

Mr. Leondis: The question was what is the application? In the slide there appears to be a metallic surface on the outside of the tank.

Mr. Vedrenne: No, this is the thermal protection before the launching, with closed cell material to conserve the temperature of the propellant at 17 degrees, but after the launch this protection is jettisoned.

Mr. Leondis: At what time during flight does it fall off?

Mr. Vedrenne: We used the same first stage in the old DIAMANT B program and the "POGO" effect is suppressed during the first 60 seconds after launch, but it appears from 60 to 120 seconds after launch. We used the same suppression technique; we applied a viscoelastic layer on the interstage because the shape of the longitudinal mode was such that the displacement was zero at this emplacement and this technique increased the modal damping; the "POGO" effect is suppressed at the end of flight for the same reason as at the beginning of flight.

VIBRATION AND STABILITY OF FLUID-CONVEYING PIPES

Hsuan-Chi Lin and Shoei-Sheng Chen
Argonne National Laboratory
Argonne, Illinois 60439

The dynamics of a fluid-conveying pipe, clamped at the upstream end and elastically supported at the downstream end, are studied and applied to the special case of an LMFBR* steam generator tube. First, the governing equations of the mathematical model are presented in a universal dimensionless form. The stability/instability boundaries of the system are then discussed. Finally, an approximate solution based on the modal expansion technique is presented for transient response; several numerical examples are presented to illustrate the method of analysis. It is shown that the pipe may lose its stability by buckling, flutter, or both, depending on the magnitudes of the displacement as well as rotational spring constants at the end. In general, the critical flow velocity is very high; hence, system components such as steam generator tubes are unlikely to lose stability in practical flow velocity ranges. However, the response in subcritical flow velocity ranges is also important; the method presented can accurately predict the response of a system to an excitation with an arbitrary initial condition and time-dependent boundary condition. The method can also be applied to other nonconservative systems.

I. INTRODUCTION

Lateral vibration of tubes containing or surrounded by flowing fluid has received considerable attention in recent years. The state of the art on this subject can be found in [1]. The dynamic behavior of tubes subjected to transverse loading is of importance in system components such as oil pipelines, heat exchangers, etc. In particular, the failure of a tube in an LMFBR superheater or evaporator will result in a sodium/water reaction and generate a large pressure pulse. To analyze the effects of this pressure on the structural integrity of the heat transport system, it is necessary to evaluate the dynamic response of components inside the steam generators and, in particular, the dynamic response of the ruptured tube. At the same time, an estimation of the natural frequencies and stability limit of a system is necessary in designing a highly sophisticated component. In this report, the dynamics of a fluid-conveying pipe, clamped at the upstream end and elastically supported at the downstream end, are studied and applied to the special case of an LMFBR steam generator tube. First, the governing equations of the mathematical model are presented in a universal dimensionless form. The stability/instability boundaries of the system are then discussed. Finally, an approximate solution based on the modal expansion technique is presented for transient response; several numerical examples are presented to illustrate the method of analysis.

*Liquid Metal Cooled Fast Breeder Reactor

II. STATEMENT OF THE PROBLEM

Consider a uniform tube of length ℓ, flexural rigidity EI, and mass per unit length m. The tube is clamped at one end and supported by a rotational spring and a displacement spring with spring constants k_t and k_d, respectively, at the other end as shown in Fig. 1. The tube is conveying fluid of mass per unit length M

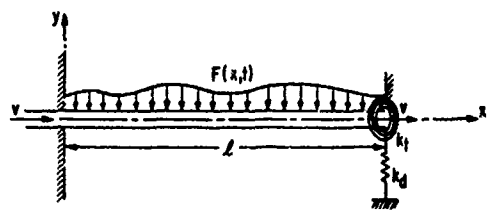

Fig. 1. Schematic of a tube conveying fluid.

at a constant flow velocity v and is subjected to the loading F(x,t). The equation of small transverse motion can be found in [2]:

$$EI\frac{\partial^4 y}{\partial x^4}+Mv^2\frac{\partial^2 y}{\partial x^2}+2Mv\frac{\partial^2 y}{\partial x\partial t}+c\frac{\partial y}{\partial t}+(M+m)\frac{\partial^2 y}{\partial t^2}=F(x,t)\quad,\tag{1}$$

where y is transverse displacement, x is the axial coordinate, t is time, and c is the damping coefficient of the tube. Assume the clamped end is subjected to a time-dependent motion. The boundary conditions are as follows:

$$y=y_o g(bt) \text{ and } \frac{\partial y}{\partial x}=0 \text{ at } x=0\ ;$$
and
$$k_t\frac{\partial y}{\partial x}+EI\frac{\partial^2 y}{\partial x^2}=0;\ k_d y-EI\frac{\partial^3 y}{\partial x^3}=0 \text{ at } x=\ell.\tag{2}$$

where y_o and b are constants. The initial conditions are

$$y(x;0)=u_o(x),\text{ and }\frac{\partial y(x,0)}{\partial t}=v_o(x).\tag{3}$$

For convenience, the following dimensionless quantities are used:

$$Y=\frac{y}{\ell},\ \tau=\left(\frac{EI}{m+M}\right)^{1/2}\frac{t}{\ell^2},\ \zeta=[EI(m+M)]^{-1/2}c\ell^2,$$
$$\xi=\frac{x}{\ell}\ ,\ u=\left(\frac{M}{EI}\right)^{1/2}v\ell,\ \eta=\frac{y_o}{\ell},\tag{4}$$
$$\bar{\alpha}=\frac{k_d\ell^3}{EI},\ \beta=\left(\frac{M}{m+M}\right)^{1/2},\ \delta=\left(\frac{EI}{m+M}\right)^{-1/2}b\ell^2,$$
$$\bar{\beta}=\frac{k_t\ell}{EI},\text{ and }f=\frac{F\ell^3}{EI}\ .$$

Substituting Eqs. (4) into Eqs. (1)-(3) gives

$$\frac{\partial^4 Y}{\partial\xi^4}+u^2\frac{\partial^2 Y}{\partial\xi^2}+2\beta u\frac{\partial^2 Y}{\partial\xi\partial\tau}+\zeta\frac{\partial Y}{\partial\tau}+\frac{\partial^2 Y}{\partial\tau^2}=f(\xi,\tau),\tag{5}$$

$$Y=\eta g(\delta\tau)\text{ and }\frac{\partial Y}{\partial\xi}=0\text{ at }\xi=0,\tag{6}$$

$$\bar{\alpha}Y-\frac{\partial^3 Y}{\partial\xi^3}=0;\ \bar{\beta}\frac{\partial Y}{\partial\xi}+\frac{\partial^2 Y}{\partial\xi^2}=0\ \text{ at }\xi=1,$$

and

$$Y(\xi,0)=U_o(\xi);\ \frac{\partial Y(\xi,0)}{\partial\tau}=V_o(\xi).\tag{7}$$

Eqs. (5), (6), and (7) are the complete mathematical statement of the problem.

Note that this is a nonconservative system because of the energy flux associated with the flowing fluid. In addition, there is a time-dependent boundary condition. The problem cannot be analyzed using conventional methods. Before proceeding to solve the transient response problem, the stability and instability boundary in terms of the system parameters will be investigated.

III. STABILITY ANALYSIS

Let

$$Y(\xi,\tau)=\phi(\xi)e^{i\Omega\tau},\tag{8}$$

where $i=\sqrt{-1}$ and Ω is the dimensionless frequency of oscillation. Substituting Eq. (8) into Eq. (5) and neglecting the damping and forcing function terms gives

$$\frac{d^4\phi}{d\xi^4}+u^2\frac{d^2\phi}{d\xi^2}+i2\beta u\Omega\frac{d\phi}{d\xi}-\Omega^2\phi=0.\tag{9}$$

The solution of Eq. (9) is

$$\phi=\sum_{n=1}^{4}D_n e^{ir_n\xi},\tag{10}$$

where r_n is the solution of the following equation:

$$r_n^4-u^2r_n^2-2\beta u\Omega r_n-\Omega^2=0.\tag{11}$$

Substituting Eq. (10) into (6) for the fixed and supported end boundary conditions ($g(\tau)=0$) yields four homogeneous equations with four unknowns D_n:

$$\sum_{n=1}^{4}D_n=0;\ \sum_{n=1}^{4}r_nD_n=0;\ \sum_{n=1}^{4}(\bar{\alpha}+ir_n^3)e^{ir_n}D_n=0;$$
and
$$\sum_{n=1}^{4}(i\bar{\beta}-r_n)r_n e^{ir_n}D_n=0.\tag{12}$$

A nontrivial solution of these equations exists if and only if the determinant of the coefficients of D_n (n=1.2,3,4) vanishes. Thus the characteristic equation is

$$\begin{vmatrix}1 & 1 & 1 & 1\\ r_1 & r_2 & r_3 & r_4\\ j_1 & j_2 & j_3 & j_4\\ jj_1 & jj_2 & jj_3 & jj_4\end{vmatrix}=0,\tag{13}$$

where $j_n=(\bar{\alpha}+ir_n^3)e^{ir_n}$, $jj_n=(i\bar{\beta}-r_n)r_n e^{ir_n}$, n=1, 2,3,4.

For a given system, the parameters $\bar{\alpha}$, $\bar{\beta}$, and β are known. Then for each u, a series of Ω_n can be found. Note that Eq. (13) is complex. Beginning from u=0, the complex frequency can be solved as a function of u. From the loci of the complex frequency, the dynamic behavior of the system can be determined: (1) when Ω is real, the system performs undamped oscillations; (2) wher Ω is complex having a positive imaginary part, the system performs damped oscillations; and (3) when Ω is complex having a negative imaginary part, the system becomes unstable by buckling or flutter. Figs. 2 and 3 show the complex frequencies of the four lowest modes for two cases. (The numbers in the figures indicate the values of u.) The computational procedures used here are the same as Ref. [3].

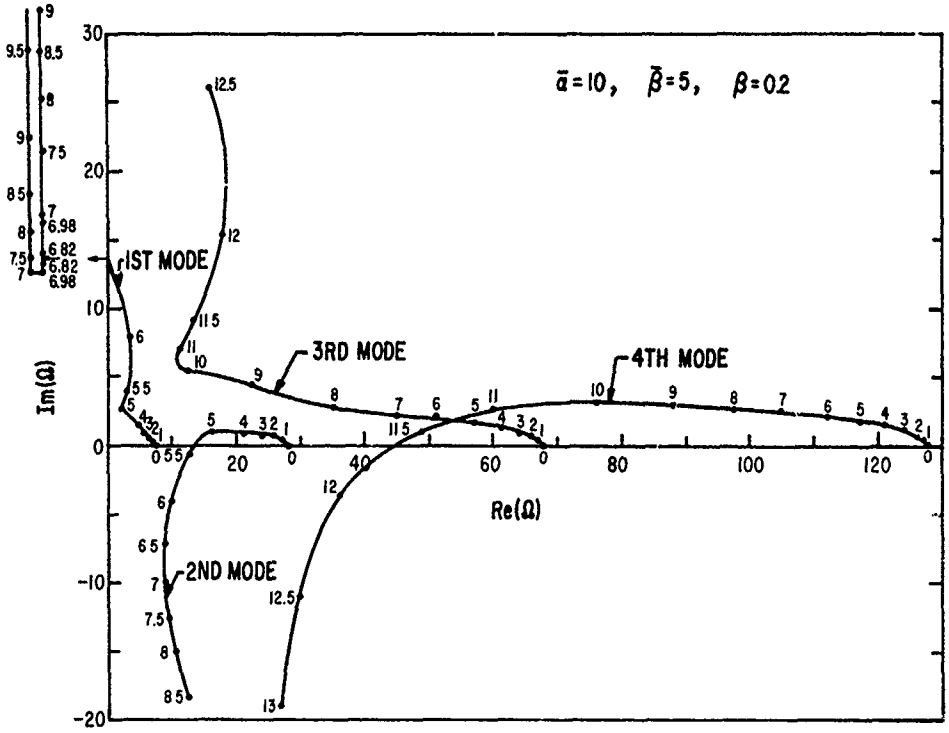

Fig. 2. Dimensionless complex frequency of the four lowest modes of the system as a function of dimensionless flow velocity. ($\bar{\alpha}$ = 10, $\bar{\beta}$ = 5, β = 0.2, and the numbers in the figure indicate flow velocity u)

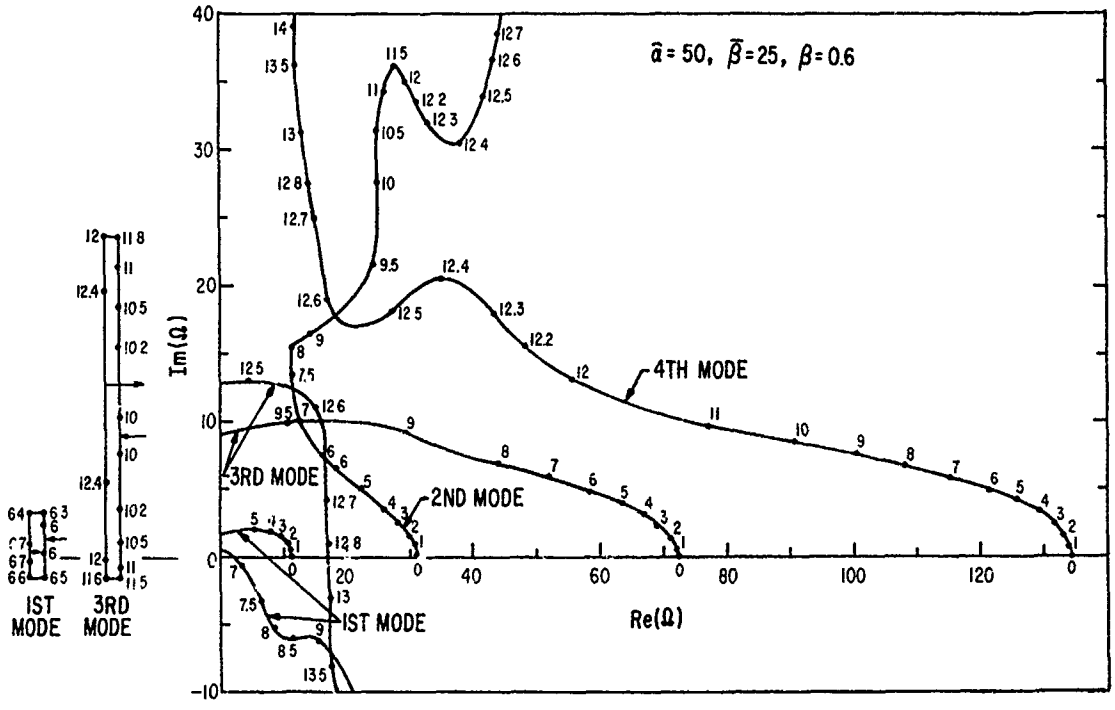

Fig. 3. Dimensionless complex frequency of the four lowest modes of the system as a function of dimensionless flow velocity. ($\bar{\alpha}$ = 50, $\bar{\beta}$ = 25, β = 0.6, and the numbers in the figure indicate flow velocity u)

In the case of $\bar{\alpha} = 10$, $\bar{\beta} = 5$, and $\beta = 0.2$ (Fig. 2), for increasing u, the locus of the first mode bifurcates on the Im(Ω)-axis. (The loci on the Im(Ω)-axis are shown in the diagram at the left in Figs. 2 and 3; in this range of flow velocity, the real part of Ω is zero.) Since it does not cross the origin, buckling-type instability does not occur in this mode.* The second mode locus crosses to the lower half of the complex plane at $u \approx 5.4$, therefore the system will have flutter-type instability in its second mode. For the ranges of flow velocity presented here, the third mode is always stable; while the fourth mode locus indicates that a flutter-type instability occurs at $u \approx 11.6$ which is higher than that associated with the second mode instability. In comparison with results in Ref. [3] for the same system parameters without the rotational spring, it is seen that the rotational spring destabilizes the system as far as the flutter-type instability is concerned. ($u \approx 6.27$ and 13.5 were found in Ref. [3] for the corresponding second and fourth mode flutter instability.)

Next consider the case of $\bar{\alpha} = 50$, $\bar{\beta} = 25$, and $\beta = 0.6$ (Fig. 3). One branch of the first mode locus crosses the origin at $u \approx 6.1$, which is the threshold for buckling-type instability. With increasing flow velocity, the negative branch of the first mode locus crosses the origin again at $u \approx 6.71$; thus the system regains stability. With increasing flow-velocity, the system stability is lost again due to flutter type at $u \approx 6.9$. For the ranges of flow-velocity considered, the second and fourth modes are always stable. The locus of the third mode is similar to that of the first mode: the system loses stability by buckling at $u \approx 10.8$, regains stability at $u \approx 12$, and becomes unstable by flutter at $u \approx 12.85$.

The complex frequencies shown in Figs. 2 and 3 illustrate the existence of two types of instabilities. For practical purposes, the ranges of flow-velocity over which the system is stable are of interest. The critical flow velocity at which the tube loses stability is designated by u, and the corresponding frequency by Ω. The limits of stable and unstable regions for buckling and flutter instabilities in terms of system parameters will be determined.

A. Flutter

The critical flow velocity for flutter-type instability is obtained directly from Eqs. (11) and (13) by setting $\mathrm{Im}(\Omega) = 0$. The computational procedures involve a systematic search for sets of u and $\mathrm{Re}(\Omega)$ satisfying frequency equation (13). The stability criterion here is that the motion of the system is bounded; i.e., the system frequency with a positive imaginary part is considered as stable. Numerical examples of critical flow velocity and the corresponding critical frequency for a flutter-type instability are presented in Figs. 4 and 5 as a function of system parameter β for various values of $\bar{\alpha}$ and $\bar{\beta}$. The

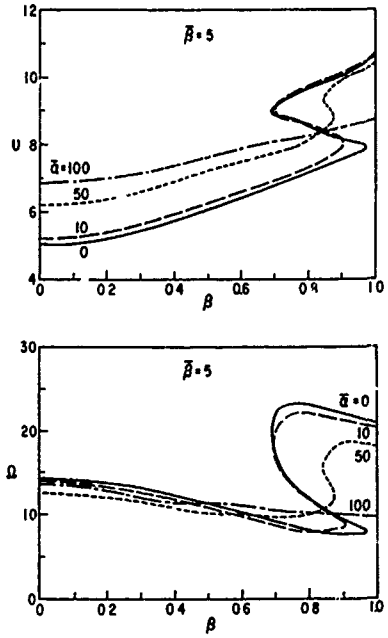

Fig. 4. Dimensionless critical flow velocity and frequency as a function of parameter β.

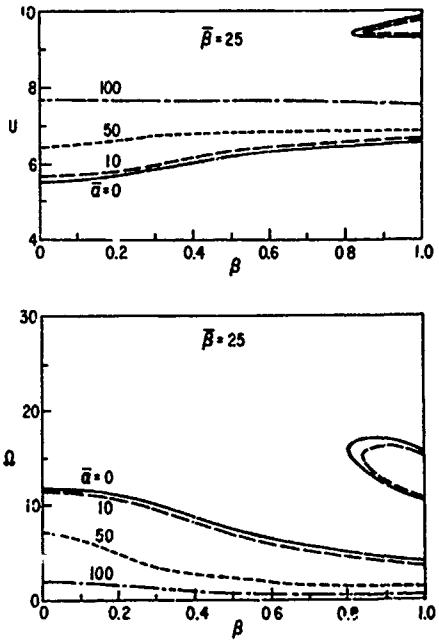

Fig. 5. Dimensionless critical flow velocity and frequency as a function of parameter β.

*See Eq. (8), the threshold of a buckling-type instability corresponds to $\Omega = 0$.

system is stable below the curves and unstable otherwise. Note that the results presented here are the lowest mode of flutter-type instability. The S-shape of some branches that occurs at higher values of β is due to the fact that the locus of complex frequency for that specific mode crosses the real axis several times. For example, for increasing u the locus crosses the Re(Ω)-axis, which corresponds to the lowest critical flow velocity. With increasing u, the locus may cross the Re(Ω)-axis again from the negative to positive side and thus the system regains stability. With further increase in u, the locus may pass the Re(Ω)-axis toward the negative side, and the system loses its stability again. Thus in Fig. 4, for $\beta = 0.8$ and $\bar{\alpha} = 10$, $u \approx 7.2$ is the lowest critical flow velocity, the system is stable for $7.2 < u < 9.7$, but becomes unstable for $u > 9.7$. For the small values of β, large values of $\bar{\alpha}$ have a stabilizing effect. However, for β close to 1.0, depending on system parameters, increasing $\bar{\alpha}$ may destabilize the system. This is because the load is nonconservative and, hence, an increasing elastic constraint does not always tend to make the system less susceptible to instability. As far as engineering applications are concerned, the most important design criteria is to find the lowest critical flow velocity and its corresponding frequency; beyond those critical values, the model may not be valid unless there is a physical mechanism for the system to bypass the lowest critical velocity.

B. Buckling

To obtain the condition for divergent motion, let $\Omega = 0$ in Eq. (9). Then the solution of $\phi(\xi)$ becomes

$$\phi(\xi) = c_1 \sin u\xi + c_2 \cos u\xi + c_3 \xi + c_4 \quad . \quad (14)$$

Substituting Eq. (14) into Eqs. (6) and equating the determinant of the coefficient matrix of the resulting homogeneous equations to zero yields

$$u^4 + 2\bar{\alpha}\bar{\beta} + (\bar{\alpha}+\bar{\beta}u^2-\bar{\alpha}\bar{\beta})u \sin u - (2\bar{\alpha}\bar{\beta}+\bar{\alpha}u^2)\cos u = 0. \quad (15)$$

Note that Eq. (15) is independent of β; thus the Coriolis acceleration (which is associated with β) does not affect buckling instability. For a given value of $\bar{\alpha}$ and $\bar{\beta}$, Eq. (15) gives a series of u; those u are the limits of the buckling-instability region.

The lowest critical flow velocities for both flutter-type and buckling-type instabilities of the system are presented in Figs. 6 and 7. Fig. 6 shows the instability maps in the $u^2 - \bar{\alpha}$ plane for $\beta = 0$ and three different values of β. In Fig. 6(a), a buckling-type instability will not occur for $\bar{\alpha} < \alpha_2$. At $\bar{\alpha} = \alpha_1$, the critical flow velocities for the first flutter instability and second buckling instability coincide. For $\alpha_2 < \bar{\alpha} < \alpha_1$, there are multiple stable and unstable ranges of flow velocity. For $\bar{\alpha} > \alpha_1$, the system may lose stability by buckling and flutter, but the lowest critical flow velocity is associated with buckling. In Fig. 6(b), no buckling instability exists for $\alpha_3 < \bar{\alpha} < \alpha_2$, multiple stable and unstable regions exist for $\bar{\alpha} < \alpha_3$ and $\alpha_2 < \bar{\alpha} < \alpha_1$, and for $\bar{\alpha} > \alpha_1$, the lowest critical flow velocity is attributed to buckling. Fig. 6(c) has the same implication except that at $\bar{\alpha} = \alpha_1$ and α_4, the flutter-type instability are in coincidence with the values of buckling type. We have not extended the investigation beyond α_4 for flutter-type instability because the system is unlikely to survive to that region after the two lowest buckling loads. Based on the results presented in Fig. 6 and others, Fig. 7 is the stability map in the $\bar{\alpha} - \bar{\beta}$ plane. The numbers in the figure indicate the square of the lowest critical flow velocity; solid lines are for buckling-type and dashed lines are for flutter-type. The region bounded by the two dotted lines does not have buckling-type instabilities, therefore only flutter-type instability exists there. Outside the region bounded by the dotted lines, the lowest critical flow velocity of flutter-type is always higher than those of buckling-type, thus only buckling-type critical flow velocities are shown there. Note that on the left side of the flutter region, for a given $\bar{\beta}$, increasing $\bar{\alpha}$ tends to increase the buckling flow velocity; while on the right side, increasing $\bar{\alpha}$ tends to reduce the critical flow velocity. On the other hand, for a given $\bar{\alpha}$, increasing $\bar{\beta}$ tends to destabilize the system on the left side and stabilize the system on the right side of the flutter region. For large values of $\bar{\alpha}$ or $\bar{\beta}$, the lowest critical flow velocities are associated with buckling.

IV. DYNAMIC RESPONSE (FORCED VIBRATION)

An elastic system subjected to nonconservative forces has been studied extensively by many investigators in recent years: a literature survey concerning this subject can be found in Ref. [4]. To find the dynamic response of an elastic system subjected to both conservative and nonconservative forces and time-dependent boundary conditions is a very complicated problem. The method of analysis here is based on the separation of the original problem into two kinds of problems as proposed by Mindlin and Goodman [5] for conservative systems, and on the properties of the linear differential operators intrinsic to the equations of motion and boundary conditions. The problem is first separated into a series of "quasi-static" problems where the inhomogeneous boundary terms are retained, while the inertia term is neglected, and a dynamic problem with homogeneous boundary conditions. The quasi-static problems can be solved by conventional methods. Then the dynamic problem is solved by an eigenfunction expansion that accounts for

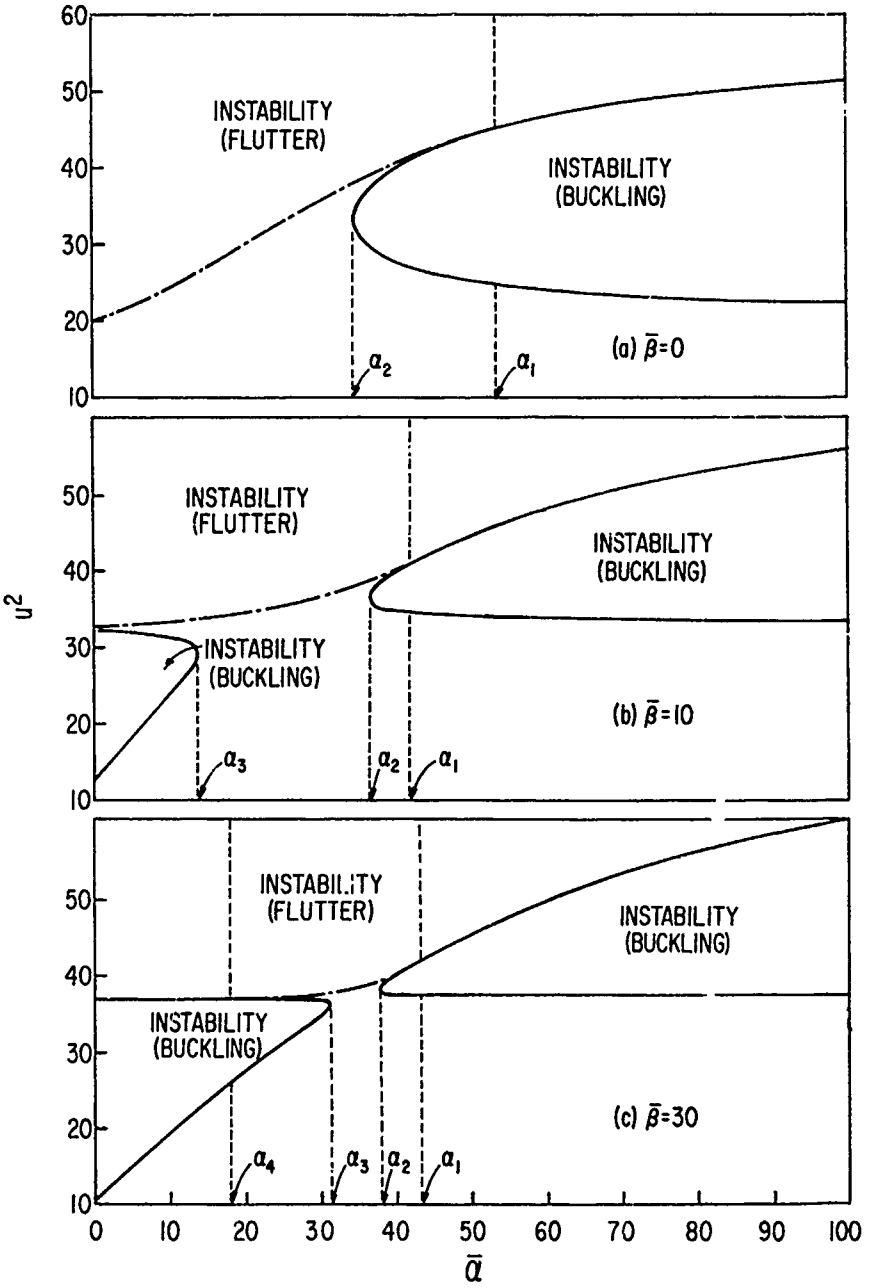

Fig. 6. Stability maps in $\bar{\alpha} - u^2$ plane.

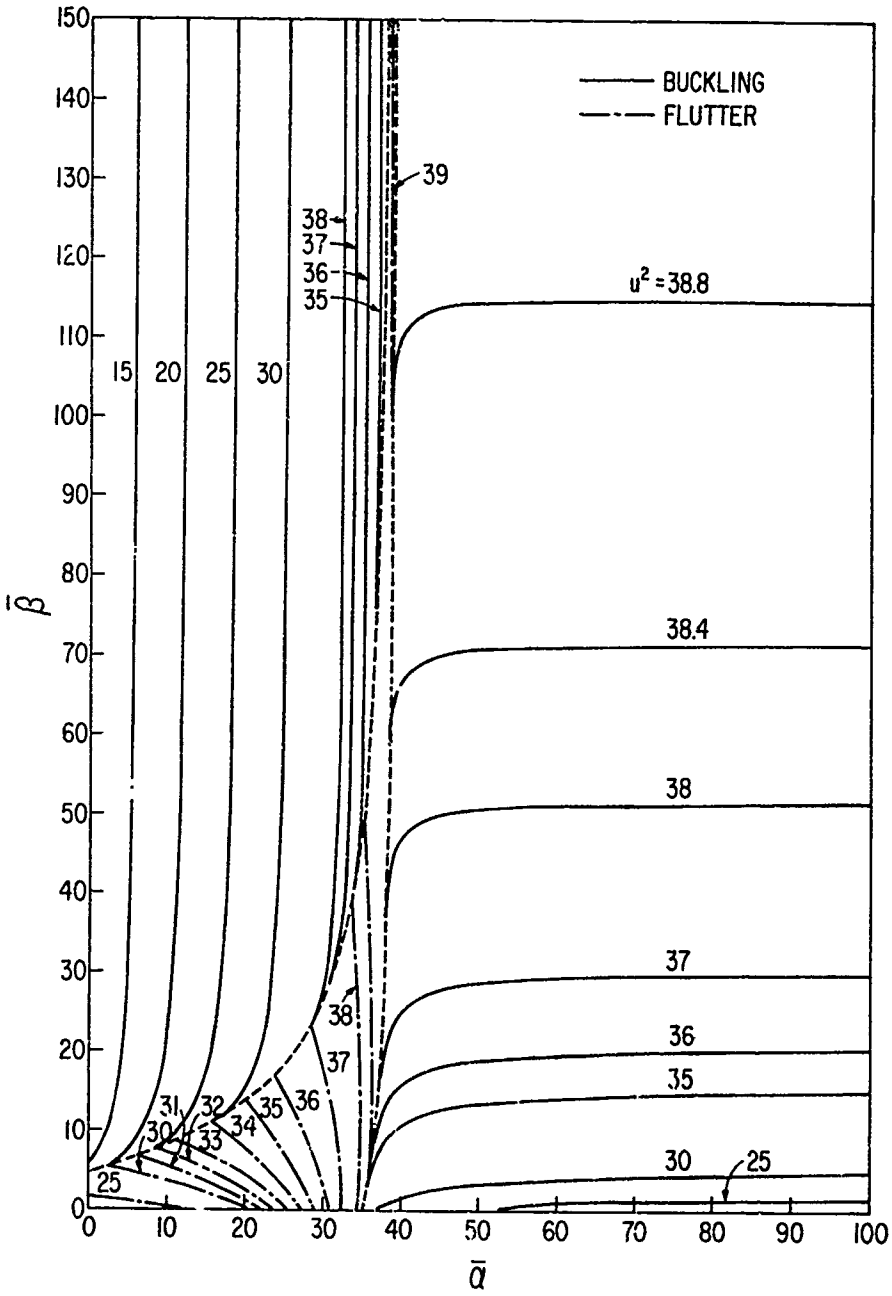

Fig. 7. Stability maps in $\bar{\alpha} - \bar{\beta}$ plane.

initial conditions, the inertia term and damping effect.

A. Method of Analysis

For convenience, Eq. (5) is written as

$$\frac{\partial^2 Y}{\partial \tau^2} + D\frac{\partial Y}{\partial \tau} + LY = f(\xi,\tau), \tag{16}$$

where D and L are spatial linear differential operators over the region R' of the elastic system (which is bounded by the surface S), and represented respectively by

$$D = 2\beta u\frac{\partial}{\partial \xi} + \zeta, \tag{17}$$

$$L = \frac{\partial^4}{\partial \xi^4} + u^2\frac{\partial^2}{\partial \xi^2}. \tag{18}$$

On the surface S, the boundary conditions are specified as

$$BY(\xi,\tau) = G(\xi,\tau), \tag{19}$$

where B is a linear spatial differential operator on S and $G(\xi,\tau)$ is a column vector which can be expressed as

$$G(\xi,\tau) = \sum_{i=1}^{r} h_i(\tau)G_i(\xi), \tag{20}$$

where r may be finite or infinite.

The objective is to determine the displacement field $Y(\xi,\tau)$ which satisfies equations of motion (16) throughout the region R', boundary conditions (19) on S, and initial conditions (7). The general solution for the displacement field $Y(\xi,\tau)$ can be expressed in the following form

$$Y(\xi,\tau) = \sum_{i=1}^{r} h_i(\tau)V_i(\xi) + W(\xi,\tau), \tag{21}$$

where $V_i(\xi)$ and $W(\xi,\tau)$ are column vectors to be determined. Substitution of Eq. (21) into (16) and (19) gives

$$\frac{\partial^2 W}{\partial \tau^2} + D\frac{\partial W}{\partial \tau} + LW + \sum_{i=1}^{r} h_i(\tau)LV_i(\xi) = f(\xi,\tau) - \sum_{i=1}^{r}\left[\frac{dh_i(\tau)}{d\tau}DV_i(\xi) + \frac{d^2h_i(\tau)}{d\tau^2}V_i(\xi)\right], \tag{22}$$

and

$$BW + \sum_{i=1}^{r} h_i(\tau)BV_i(\xi) = \sum_{i=1}^{r} h_i(\tau)G_i(\xi). \tag{23}$$

From Eqs. (22) and (23), it is seen that the solution is given by Eq. (21) provided that

$$\left.\begin{aligned} LV_i(\xi) &= 0 \quad \text{in } R', \\ BV_i(\xi) &= G_i(\xi) \quad \text{on } S, \end{aligned}\right\} \; i = 1,2,\ldots,r \tag{24, 25}$$

and

$$\frac{\partial^2 W}{\partial \tau^2} + D\frac{\partial W}{\partial \tau} + LW = f - \sum_{i=1}^{r}\left[\frac{dh_i}{d\tau}DV_i + \frac{d^2h_i}{d\tau^2}V_i\right] \quad \text{in } R', \tag{26}$$

$$BW = 0 \quad \text{on } S. \tag{27}$$

The system of Eqs. (24) and (25) define a series of "quasi-static" problems, while Eqs. (26) and (27) define a "dynamic" problem. The initial conditions for the dynamic problem are obtained by substituting Eq. (21) into (7) which gives

$$W(\xi,0) = U_o(\xi) - \sum_{i=1}^{r} h_i(0)V_i(\xi), \tag{28}$$

and

$$\frac{\partial W(\xi,0)}{\partial \tau} = V_o(\xi) - \sum_{i=1}^{r}\frac{dh_i(0)}{d\tau}V_i(\xi). \tag{29}$$

In order to illustrate the method, consider a time-dependent boundary condition at the clamped end as follows

$$Y = \eta e^{i\delta\tau} \quad \text{at } \xi = 0. \tag{30}$$

For such a time-dependent boundary condition, r = 1. Thus the quasi-static problem becomes

$$LV = 0, \quad \text{where } L = \frac{d^4}{d\xi^4} + u^2\frac{d^2}{d\xi^2}. \tag{31}$$

The boundary conditions are

$$V = \eta \quad \text{and} \quad \frac{dV}{d\xi} = 0 \quad \text{at } \xi = 0,$$

and

$$\bar{\alpha}V - \frac{d^3V}{d\xi^3} = 0; \quad \bar{\beta}\frac{dV}{d\xi} + \frac{d^2V}{d\xi^2} = 0 \quad \text{at } \xi = 1. \tag{32}$$

The general solution of Eq. (31) is

$$V(\xi) = a_1 + a_2\xi + a_3\sin u\xi + a_4\cos u\xi. \tag{33}$$

Using Eqs. (32), Eq. (33) becomes

$$V(\xi) = \eta - \bar{\alpha}\eta\left\{\frac{\sigma_1(-u\xi+\sin u\xi)+\sigma_2(-1+\cos u\xi)}{\sigma_3}\right\}$$

$$\text{for } u \neq 0, \tag{34}$$

where

$$\sigma_1 = \bar{\beta}\sin u + u\cos u$$

$$\sigma_2 = (-1+\cos u)\bar{\beta} - u\sin u$$

$$\sigma_3 = u^4 + 2\bar{\alpha}\bar{\beta} + (\bar{\alpha}+\bar{\beta}u^2-\bar{\alpha}\bar{\beta})u\sin u - (2\bar{\alpha}\bar{\beta}+\bar{\alpha}u^2)\cos u \qquad (34)$$

and (Contd.)

$$V(\eta) = \eta - \bar{\alpha}\eta \quad \frac{2(\bar{\beta}+1)\xi^3 - 3(\bar{\beta}+2)\xi^2}{4\bar{\alpha}+12\bar{\beta}+\bar{\alpha}\bar{\beta}+12} \quad \text{for } u = 0.$$

The dynamic problem reduces to

$$\frac{\partial^2 W}{\partial \tau^2} + D\frac{\partial W}{\partial \tau} + LW = \chi, \qquad (35)$$

with boundary conditions

$$W = 0; \ \frac{\partial W}{\partial \xi} = 0 \quad \text{at } \xi = 0,$$

and (36)

$$\bar{\alpha}W - \frac{\partial^3 W}{\partial \xi^3} = 0; \ \bar{\beta}\frac{\partial W}{\partial \xi} + \frac{\partial^2 W}{\partial \xi^2} = 0 \quad \text{at } \xi = 1,$$

and initial conditions

$$W(\xi,0) = U_o(\xi) - V(\xi),$$

and (37)

$$\frac{\partial W(\xi,0)}{\partial \tau} = V_o(\xi) - i\delta V(\xi),$$

where

$$\chi = f(\xi,\tau) - \delta e^{i\delta\tau}\{(i\zeta-\delta)\eta + [i2\beta u^2(-1+\cos u\xi) + (i\zeta-\delta)(-u\xi+\sin u\xi)]a_3 + [-i2\beta u^2\sin u\xi + (i\zeta-\delta)(-1+\cos u\xi)]a_4,$$

$$a_3 = -\frac{\sigma_1\bar{\alpha}\eta}{\sigma_3} \qquad (38)$$

$$a_4 = -\frac{\sigma_2\bar{\alpha}\eta}{\sigma_3}$$

An approximate solution will be presented for the dynamic problem. Let

$$W(\xi,\tau) = \sum_{n=1}^{\infty} q_n(\tau)\phi_n(\xi) \qquad (39)$$

where $\phi_n(\xi)$ is the orthonormal modal function of the tube in air, and is obtained from the following eigenvalue problem:

$$L_1\phi = \lambda^4\phi, \quad L_1 = \frac{d^4}{d\xi^4},$$

$$\phi = 0; \ \frac{d\phi}{d\xi} = 0 \quad \text{at } \xi = 0, \qquad (40)$$

and

$$\bar{\alpha}\phi - \frac{d^3\phi}{d\xi^3} = 0; \ \bar{\beta}\frac{d\phi}{d\xi} + \frac{d^2\phi}{d\xi^2} = 0 \quad \text{at } \xi = 1.$$

The solution for ϕ is

$$\phi(\xi) = c_1\sin\lambda\xi + c_2\cos\lambda\xi + c_3\sinh\lambda\xi + c_4\cosh\lambda\xi. \qquad (41)$$

Substituting Eq. (41) into the above given boundary conditions (40) gives

$$\begin{bmatrix} 0 & 1 & 0 & 1 \\ \lambda & 0 & \lambda & 0 \\ \bar{\alpha}\sin\lambda+\lambda^3\cos\lambda & \bar{\alpha}\cos\lambda-\lambda^3\sin\lambda & \bar{\alpha}\sinh\lambda-\lambda^3\cosh\lambda & \bar{\alpha}\cosh\lambda-\lambda^3\sinh\lambda \\ \lambda(\bar{\beta}\cos\lambda-\lambda\sin\lambda) & -\lambda(\bar{\beta}\sin\lambda+\lambda\cos\lambda) & \lambda(\bar{\beta}\cosh\lambda+\lambda\sinh\lambda) & \lambda(\bar{\beta}\sinh\lambda+\lambda\cosh\lambda) \end{bmatrix} \begin{bmatrix} c_1 \\ c_2 \\ c_3 \\ c_4 \end{bmatrix} = \begin{bmatrix} 0 \\ 0 \\ 0 \\ 0 \end{bmatrix}. \qquad (42)$$

Setting the coefficient matrix in Eq. (42) equal to zero gives the characteristic equation for this eigenvalue problem:

$$\Delta(\bar{\alpha},\bar{\beta},\lambda) = 0. \qquad (43)$$

Once the eigenvalues are obtained, the coefficient c_n $(n = 1,2,3)$ can be found in terms of c_4, thus Eq. (41) becomes

$$\phi(\xi) = \left[\left(\frac{-\bar{\alpha}\cos\lambda+\lambda^3\sin\lambda+\bar{\alpha}\cosh\lambda-\lambda^3\sinh\lambda}{\bar{\alpha}\sin\lambda+\lambda^3\cos\lambda-\bar{\alpha}\sinh\lambda+\lambda^3\cosh\lambda}\right)\times (-\sin\lambda\xi+\sinh\lambda\xi) + (-\cos\lambda\xi+\cosh\lambda\xi)\right]c_4, \qquad (44)$$

and the magnitude of c_4 is determined such that

$$\int_0^1 \phi_n^2(\xi) = 1. \qquad (45)$$

Substituting Eq. (39) into (35), multiplying the resulting equation by ϕ_m and then integrating with respect to ξ from 0 to 1 yield

$$\ddot{q}_n + 2\beta u \sum_m a_{nm}\dot{q}_m + \zeta\dot{q}_n + u^2 \sum_m b_{nm}q_m + \lambda_n^4 q_n = H_n, \tag{46}$$

where

$$\begin{aligned} a_{nm} &= \left\langle \frac{d\phi_m}{d\xi}, \phi_n \right\rangle, \\ b_{nm} &= \left\langle \frac{d^2\phi_m}{d\xi^2}, \phi_n \right\rangle, \\ H_n &= \langle \chi, \phi_n \rangle, \\ q_n(0) &= \langle (U_o - V), \phi_n \rangle, \\ \frac{dq_n(0)}{d\tau} &= \langle (V_o - i\delta V), \phi_n \rangle, \end{aligned} \tag{47}$$

and $\langle\ \rangle$ denotes the inner product; i.e., $\langle \phi_m, \phi_n \rangle = \int_0^1 \phi_m \phi_n d\xi$. Eqs. (46) comprise a system of linear ordinary differential equations which are coupled through the coefficients a_{nm} and b_{nm}. Eqs. (46) may be written in matrix form:

$$\{\ddot{q}\} + [C]\{\dot{q}\} + [K]\{q\} = \{H\}, \tag{48}$$

where

$$\begin{aligned} c_{nm} &= 2\beta u\, a_{nm} + \zeta\delta_{nm}, \\ k_{nm} &= u^2 b_{nm} + \lambda_n^4 \delta_{nm}. \end{aligned} \tag{49}$$

Eq. (48) may also be written as follows:

$$\begin{bmatrix} -K & 0 \\ 0 & I \end{bmatrix} \begin{Bmatrix} q \\ \ddot{q} \end{Bmatrix} + \begin{bmatrix} 0 & K \\ K & C \end{bmatrix} \begin{Bmatrix} q \\ \dot{q} \end{Bmatrix} = \begin{Bmatrix} 0 \\ H \end{Bmatrix}. \tag{50}$$

Let

$$[A] = \begin{bmatrix} -K & 0 \\ 0 & I \end{bmatrix}, \quad [B] = \begin{bmatrix} 0 & K \\ K & C \end{bmatrix}, \quad \text{and} \quad \{X\} = \begin{Bmatrix} 0 \\ H \end{Bmatrix}, \tag{51}$$

Eq. (50) is simplified to

$$[A] \begin{Bmatrix} \dot{q} \\ \ddot{q} \end{Bmatrix} + [B] \begin{Bmatrix} q \\ \dot{q} \end{Bmatrix} = \{X\}. \tag{52}$$

The damped free vibration modes are obtained by solving the equation

$$[\Gamma][A][Q] = -[B][Q], \tag{53}$$

where $[\Gamma]$ is a 2n x 2n diagonal matrix formed from the eigenvalue $i\Omega$, and $[Q]$ is a 2n x 2n modal matrix. Note that both $[A]$ and $[B]$ are, in general, asymmetric matrices. Consider the adjoint system of Eq. (52),

$$[\Gamma][A]^T[R] = -[B]^T[R], \tag{54}$$

where $[R]$ is the modal matrix of the adjoint system. It is well known that if γ_n is an eigenvalue of Eq. (53), it is also an eigenvalue of its adjoint equation (54). Furthermore, the sets of eigenfunctions $[Q]$ and $[R]$ are biorthogonal; i.e.,

$$[R]^T[A][Q] = [I], \tag{55}$$

Premultiplying Eq. (54) by $[Q]^T$ and taking its transpose gives the following relation:

$$[\Gamma] = -[R]^T[B][Q]. \tag{56}$$

Let

$$\begin{Bmatrix} q \\ \dot{q} \end{Bmatrix} = [Q]\{P\}, \tag{57}$$

Substituting into Eq. (52), and then premultiplying the resulting equation by $[R]^T$ gives

$$\{\dot{P}\} - [\Gamma]\{P\} = [R]^T\{X\}. \tag{58}$$

Eqs. (58) represent a set of uncoupled first order ordinary differential equations. The general solutions of Eqs. (58) are as follows:

$$p_n = p_{an}e^{\gamma_n\tau} + p_{bn}e^{i\delta\tau}, \tag{59}$$

where the coefficients p_{an} and p_{bn} can be determined from the initial condition and prescribed forcing function. For example, if the forcing function in Eq. (38) is represented by

$$f(\xi,\tau) = f_1(\xi)e^{i\delta\tau}, \tag{60}$$

then the right hand side of Eq. (58) can be written as $g_n e^{i\delta\tau}$; consequently,

$$p_{bn} = \frac{g_n}{i\delta - \gamma_n}, \tag{61}$$

and

$$p_{an} = p_n(0) - p_{bn}, \tag{62}$$

where $p_n(0)$ is obtained from Eq. (57) for the given initial data. The solution of the dynamic part is given by

$$W(\xi,\tau) = \sum_{n=1}^{\infty} \sum_{j=1}^{\infty} \lambda_{nj} P_j(\tau)\phi_n(\xi). \tag{63}$$

Finally, the complete solution of dynamic response for the time-dependent boundary condition is given by Eq. (21) which is the sum of the "quasi-static" and "dynamic" solutions.

B. Numerical Examples

Several numerical examples to demonstrate the dynamic behavior of tubes conveying fluid have been carried out by means of the method presented in the previous section. Consider a tube with the following system parameters: $\bar{\alpha} = 10$, $\bar{\beta} = 5$, $\beta = 0.2$, $\zeta = 0.01$, and $\eta = 0$ (i.e., fixed end boundary condition). Suppose the tube is subjected to an external loading which is of the form

$$f(\xi,\tau) = \sin\pi\xi\cos\delta\tau. \tag{64}$$

Fig. 8 shows the lowest four fundamental mode shapes for the given system parameters. For $\delta = \pi$ and $u = 3$ (which is less than the critical flow velocity), the displacement history at the spring-supported end ($\xi = 1$) is shown in Fig. 9. Fig. 10 shows the corresponding displacement along the tube at selected times (approximately one cycle). These figures show that most of the dynamic response at this flow velocity are the first mode. Figs. 11 and 12 are the results for the flow velocity $u = 5.6$ which is slightly higher than the critical flow velocity of flutter-type instability. Note that the definition of instability here is interpreted as unbounded motion. From the displacement history at $\xi = 1$ for $u = 5.6$, it is seen that the amplitude is exponentially increasing. The displacement profiles presented in Fig. 12 are dominated by the second mode response. As the flow velocity increases from subcritical to overcritical, the major response contribution changes from the first to the second modes. This is in agreement with the results of Fig. 2 which predicts the lowest flutter flow velocity is associated with the second mode. Fig. 12 also indicates the presence of a traveling wave which propagates along the tube. This phenomena arises from the contribution of the Coriolis force and, hence, the system does not possess classical normal modes.

Note that the results presented in the "stability analysis" section are based on the exact solution for the complex frequency while the present dynamic response is the approximate solution by the modal expansion method. The numerical results for both techniques are in good agreement as far as the first few natural frequencies are concerned. Therefore the instability maps presented in the previous section may also be constructed by using this approximate solution.

For a stable system, the steady-state response is given by the second term in Eq. (59). Fig. 13 shows the steady-state response for the first mode under the external excitation given in Eq. (64). The abscissa is the frequency ratio of external excitation (δ) to the lowest natural frequency (Ω_1). The ordinate represent the normalized amplitude $|p_b|$ with amplitudes at zero frequency ratio to be one. As the flow velocity increases, the maximum normalized amplitude decreases. The decrease of the normalized amplitude is due to energy dissipation and is a damping effect associated with fluid flow.

Next consider the tube with an initial displacement produced by a concentrated load acting at the right end, then released at $\tau = 0$ without any other excitation. The initial displacement in this case can be obtained from the equation of equilibrium:

$$\frac{d^4Y}{d\xi^4} + u^2\frac{d^2Y}{d\xi^2} = 0; \tag{65}$$

and the boundary conditions:

$$Y = 0;\ Y' = 0 \quad \text{at } \xi = 0,$$

and (66)

$$\bar{\alpha}Y - Y''' = s \quad \text{and} \quad \bar{\beta}Y' + Y'' = 0 \quad \text{at } \xi = 1.$$

Here s is the magnitude of the concentrated force. The initial displacement is thus obtained as follows:

$$U_o(\xi) = s\left\{\frac{\sigma_1(\sin u\xi - u\xi) + \sigma_2(\cos u\xi - 1)}{\sigma_3}\right\}$$

for $u \neq 0$, (67)

and

$$U_o(\xi) = \frac{s\xi^2[\xi - 2(\bar{\beta}+1)\xi + 3(\bar{\beta}+2)]}{4\bar{\alpha}+12\bar{\beta}+\bar{\alpha}\bar{\beta}+12} \quad \text{for } u = 0.$$

With the above initial disturbance, the dynamic responses at $\xi = 1$ for $u = 0,1,2,3$ are shown in Fig. 14. It is seen that the larger the flow velocity, the more the tube deflects at the beginning; when the tube deflects, there is a tendency to deviate further away from its equilibrium position due to the centrifugal force acting on the tube arising from the fluid flow. This figure also reveals some damping characteristics for varying flow velocity. The response for $u = 0$ attains its steady-state motion shortly after release from its initial disturbance. As flow velocity increases, the amplitudes begin to attenuate. For $u = 3$, the response almost dies out after several cycles. As mentioned before, due to the nonconservativeness of the system, the dissipative energy increases when the flow velocity increases as a result of the energy effluence at the right-hand support.

To show the influence of the flow velocity and other system parameters on the damping characteristics, consider a one-mode

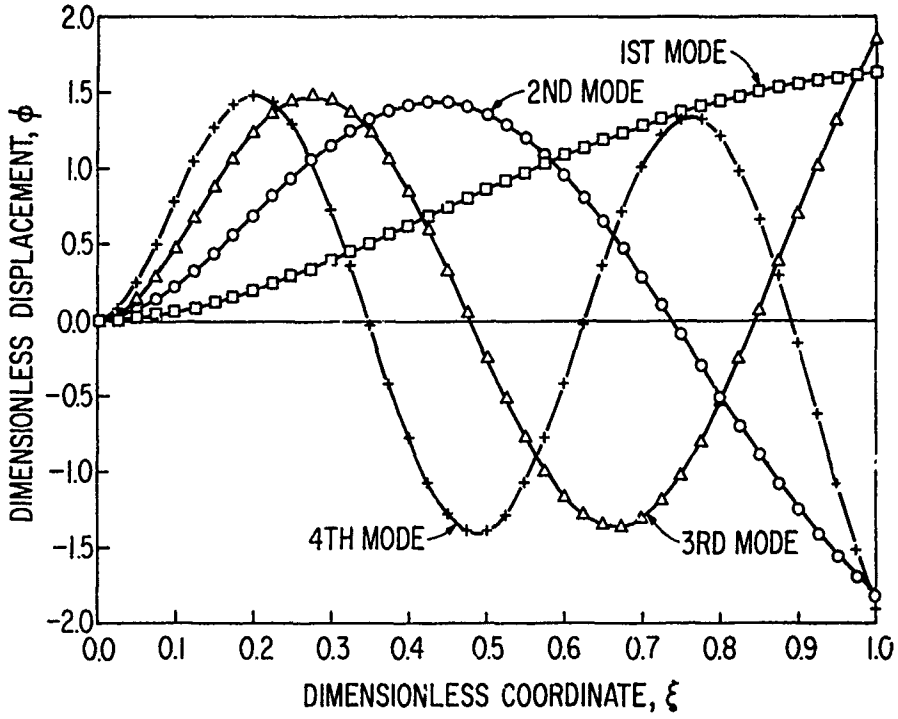

Fig. 8. Mode shapes of lowest four modes for $\bar{\alpha} = 10$ and $\bar{\beta} = 5$.

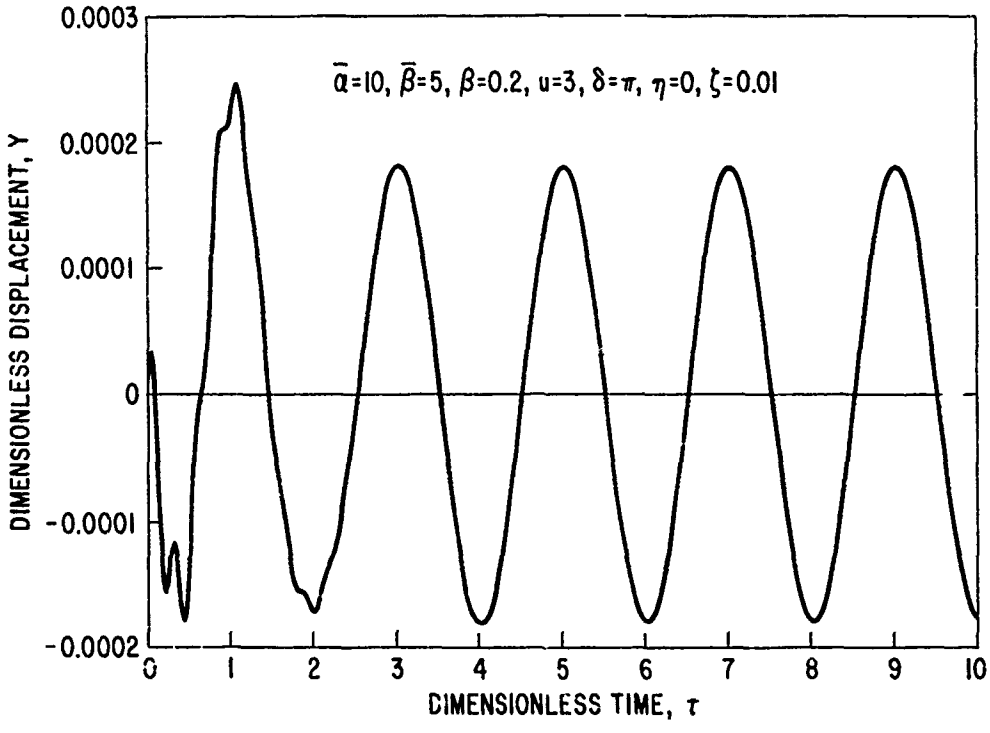

Fig. 9. Displacement history at $\xi = 1$. ($u = 3$, $\bar{\alpha} = 10$, $\bar{\beta} = 5$, $\beta = 0.2$, $\delta = \pi$, $\zeta = 0.01$, $\eta = 0$)

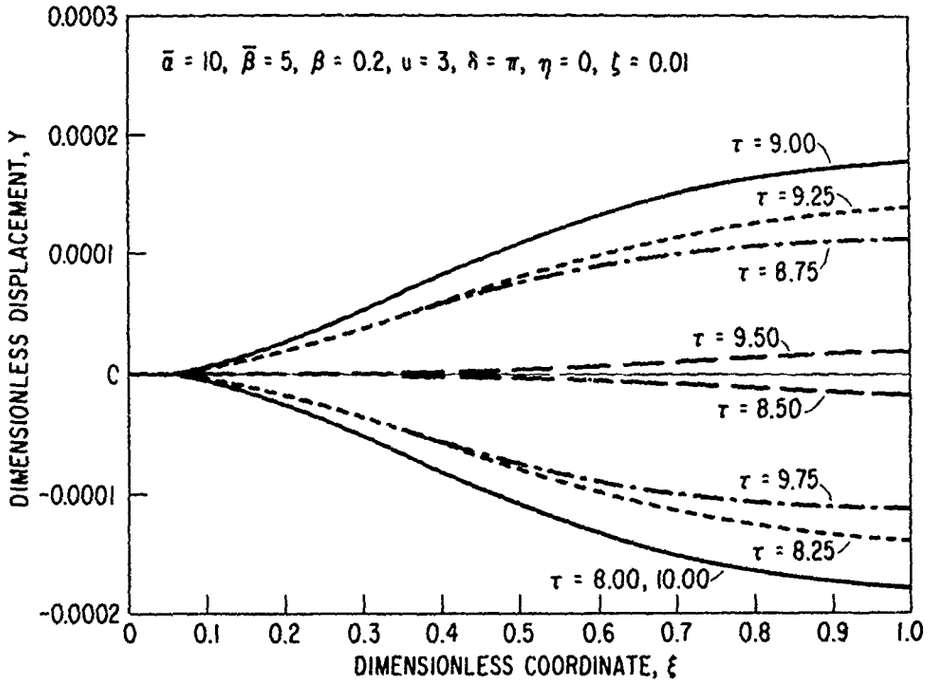

Fig. 10. Displacement profile along the tube at selected times. (u = 3, $\bar{\alpha}$ = 10, $\bar{\beta}$ = 5, β = 0.2, $\delta = \pi$, ζ = 0.01, η = 0)

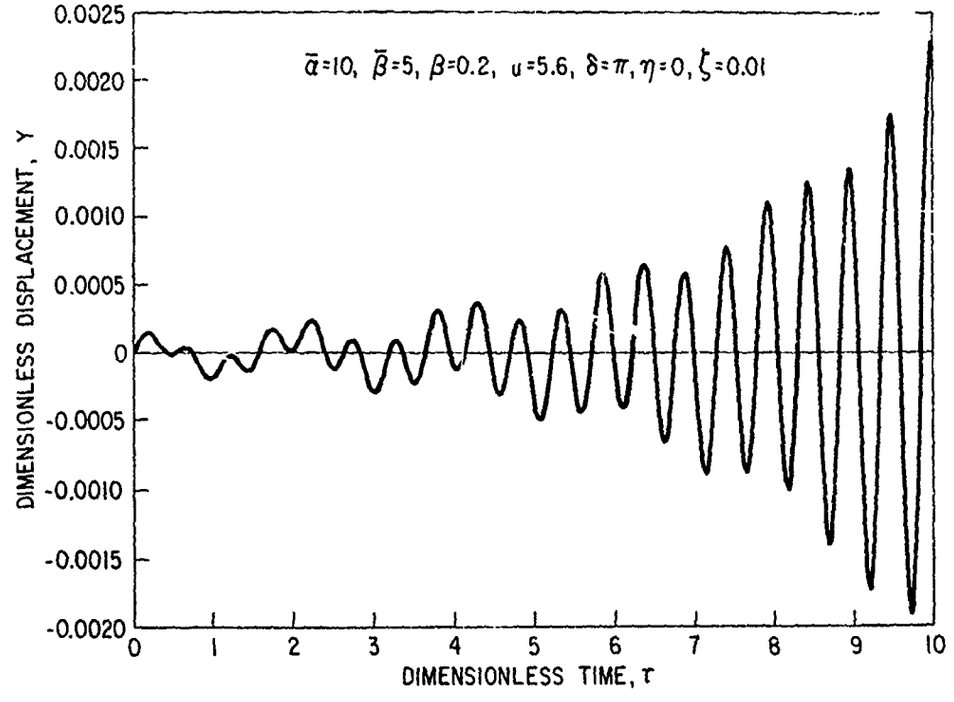

Fig. 11. Displacement history at ξ = 1. (u = 5.6, $\bar{\alpha}$ = 10, $\bar{\beta}$ = 5, β = 0.2, $\delta = \pi$, ζ = 0.01, η = 0)

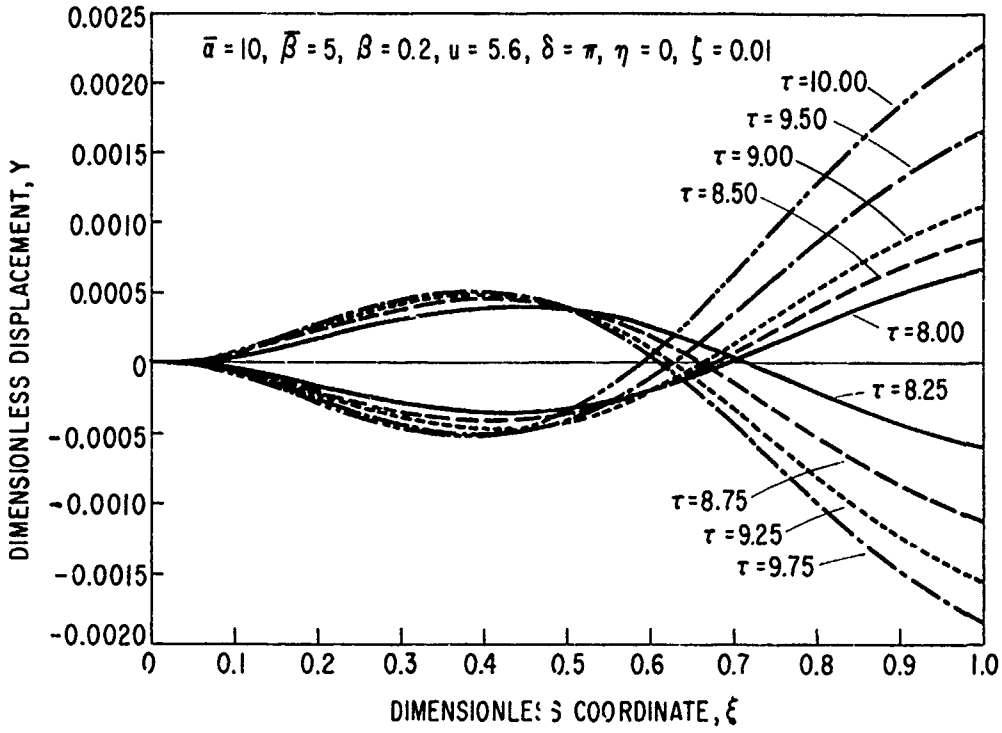

Fig. 12. Displacement profile along the tube at selected times. (u = 5.6, $\bar{\alpha}$ = 10, $\bar{\beta}$ = 5, β = 0.2, δ = π, ζ = 0.01, η = 0)

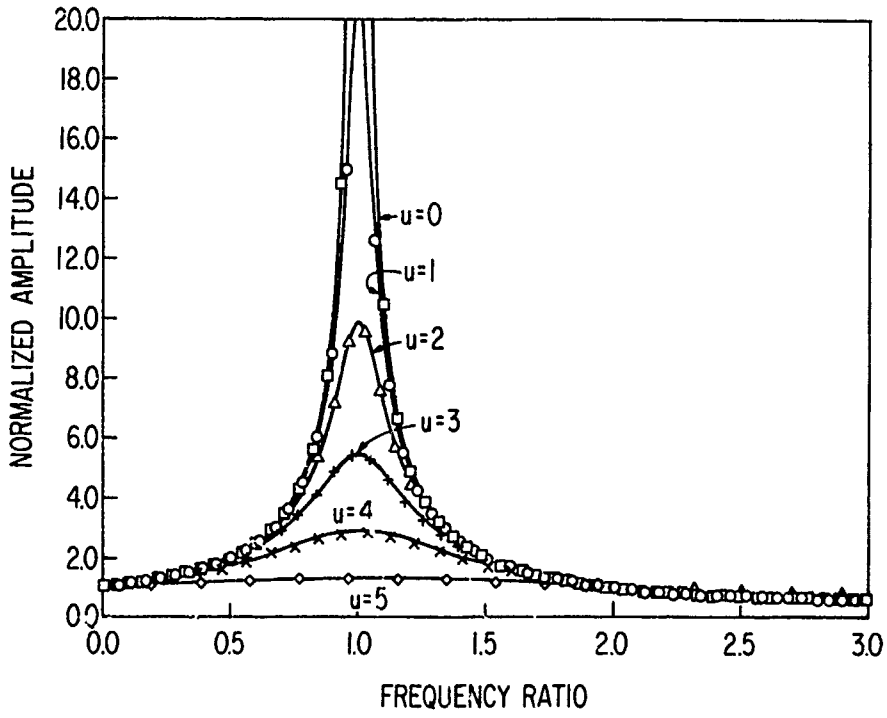

Fig. 13. Steady-state response of first mode. ($\bar{\alpha}$ = 10, $\bar{\beta}$ = 5, β = 0.2, ζ = 0.0_)

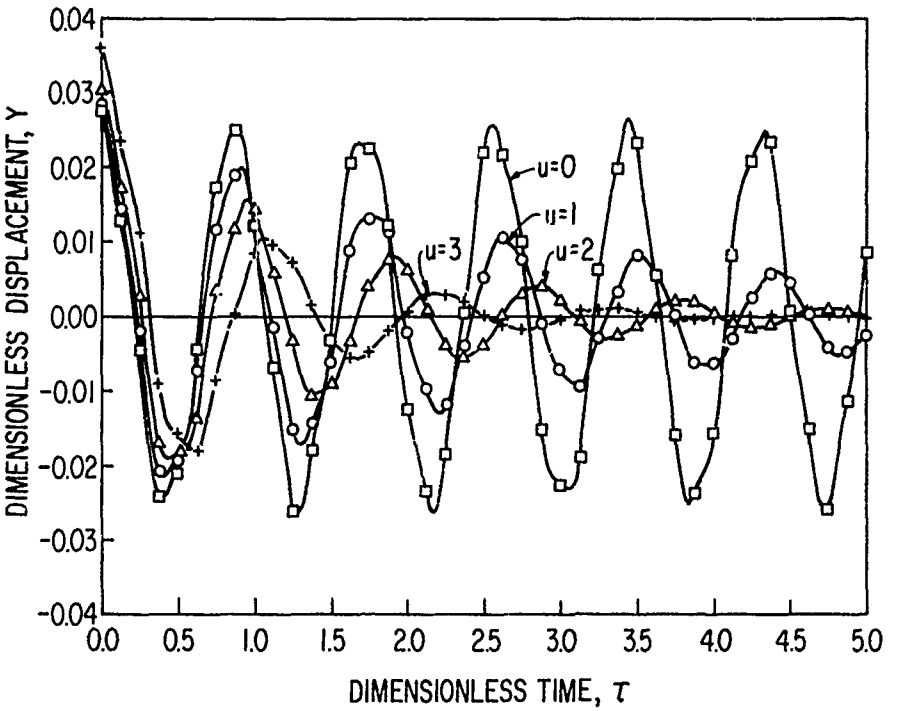

Fig. 14. Displacement history at $\xi = 1$. ($\bar{\alpha} = 10$, $\bar{\beta} = 5$, $\beta = 0.2$, $\zeta = 0.01$)

approximation. From Eq. (48), the equation of motion representing the first mode is

$$\ddot{q} + 2z\Omega\dot{q} + \Omega^2 q = 0, \tag{68}$$

where z is the damping factor. Let $q = e^{\gamma\tau}$, and substitute into Eq. (68) giving

$$\gamma^2 + 2z\Omega\gamma + \Omega^2 = 0. \tag{69}$$

The solution of Eq. (69) is

$$\gamma = -z\Omega \pm i\sqrt{1-z^2}\,\Omega. \tag{70}$$

Introduce a new variable a,

$$a = -\frac{\mathrm{Re}(\gamma)}{\mathrm{Im}(\gamma)} = \frac{z}{\sqrt{1-z^2}}. \tag{71}$$

The damping factor z is

$$z = \sqrt{\frac{a^2}{1+a^2}}, \quad 0 \le z \le 1. \tag{72}$$

Numerical results have been carried out for three sets of system parameters and are presented in Table 1. It is seen that the damping factor shown in the table for the first mode is higher than the second mode. However, the variation of damping factor is not necessarily monotonic with changes in system parameters or flow velocity. For example, the case of $\bar{\alpha} = 10$ and $\bar{\beta} = 5$ has a higher damping factor than the other cases for $u = 5$. From Eqs. (71) and (72), it is seen that damping characteristics can be predicted from the loci of complex frequency shown in the stability study. Therefore, it is important to have stability analysis before looking into the dynamic response of the system.

V. APPLICATION

To have a physical understanding of the dimensionless quantities presented in the previous sections, consider a typical segment of tube in CRBRP* steam generators resulting from "guillotine" type failure. The general geometry and material specification of the segment are shown in Fig. 15. Numerical calculations of the dimensionless system parameters are also shown in the figure. The lowest critical flow velocity for flutter-type instability can roughly be estimated from Figs. 4 and 5; the exact value can be calculated from Eq. (13). The lowest $\bar{u}$ is approximately equal to 4. This is based on the assumption that the tube is resting on the right baffle plate so that the boundary condition is similar to that assumed in the previous sections. It is seen that for the flow velocity equal to 45.72 m/s, the corresponding dimensionless flow

*Clinch River Breeder Reactor Project

Table 1. Damping Characteristics

System Parameter	Flow Velocity	Damping Factor	
		1st Mode	2nd Mode
$\bar{\alpha} = 0$	0	0.00273	0.00045
$\bar{\beta} = 0$	1	0.12985	0.02280
$\beta = 0.2$	2	0.24564	0.04508
$\zeta = 0.01$	3	0.34199	0.06442
	4	0.43606	0.05985
	5	0.67722	0.14945
$\bar{\alpha} = 10$	0	0.00113	0.00034
$\bar{\beta} = 5$	1	0.04658	0.01566
$\beta = 0.2$	2	0.10189	0.03182
$\zeta = 0.01$	3	0.18495	0.04925
	4	0.35496	0.06729
	5	0.78836	0.07121
$\bar{\alpha} = 50$	0	0.00062	0.00028
$\bar{\beta} = 25$	1	0.02047	0.01204
$\beta = 0.2$	2	0.04172	0.02516
$\zeta = 0.01$	3	0.06614	0.04134
	4	0.09944	0.06417
	5	0.18367	0.10199

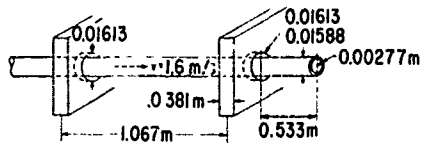

$E = 2.068 \times 10^5$ MPa

$I = \frac{\pi}{4}\left(r_0^4 - r_i^4\right) = 0.2547 \times 10^{-12}$ m^4

$EI = 528.79$ N-m^2

$\rho_{steel} = 7.833 \times 10^3$ kg/m^3

$\rho_{water} = 1 \times 10^3$ kg/m^3

$m = \rho_{steel} \times A_{steel} = 0.04876$ kg/m

$M = \rho_{water} \times A_{water} = 0.198$ kg/m

$\beta = \left(\frac{M}{m + M}\right)^{1/2} = 0.896$

$u = \left(\frac{M}{EI}\right)^{1/2} V\ell = 0.0165$ (for $\ell = 0.533$ m)

$\bar{\alpha} = 0$

$\bar{\beta} = 0$

Fig. 15. Schematic configuration of CRBRP steam tube.

velocity is u = 0.0165 which is far below the critical flow velocity $\bar{u}$. If the tube has a contact at the left baffle plate only, then u = 0.0495 (for ℓ = 1.6 m). Therefore, as long as the mass flow rate remains at this level, instability will not occur in this configuration.

VI. CONCLUDING REMARKS

In this report, a complete analysis is presented for the dynamics of a fluid-conveying pipe, clamped at the upstream end, and elastically supported at the downstream end by both displacement and rotational springs. It is shown that the pipe may lose its stability by buckling, flutter, or both depending on the magnitudes of the displacement as well as rotational spring constants at the end; the stability-instability boundaries are constructed in terms of the system parameters. In sub-critical flow velocity ranges, a method is presented to study the response to an arbitrary excitation; the proposed method is sufficient to predict accurately the dynamic response of the system with an arbitrary initial condition and time-dependent boundary conditions. The method can also be applied to other nonconservative systems.

The onset of instability in engineering system could be catastrophic. Therefore, the most important consideration from a practical point of view is to avoid the onset of instability. As long as the system parameters are known, stability can be checked using the results obtained in the paper. Fortunately, in most practical system designs, the critical flow velocity is high, except in the cases where tubes are very long or tube flexural rigidity is small. Therefore, for practical applications, the responses to excitations in the sub-critical ranges of flow velocity are much more important.

REFERENCES

1. Chen, S. S., "Parallel-Flow-Induced Vibrations and Instability of Cylindrical Structures," Shock and Vibration Digest 6(10), 2-12 (1974).

2. Gregory, R. W., and Paidoussis, M. P., "Unstable Oscillation of Tubular Cantilevers Conveying Fluid, I. Theory, II. Experiment," Proceedings of the Royal Society of London 293(A), 512-542 (1966).

3. Chen, S. S., "Flow-Induced Instability of An Elastic Tube," ASME Paper No. 71-Vibr-39.

4. Herrmann, G., "Stability of Equilibrium of Elastic Systems Subjected to Nonconservative Forces," Appl. Mech. Rev. 20(2), 103-108 (1967).

5. Mindlin, R. D., and Goodman, L. E., "Beam Vibrations with Time-Dependent Boundary Conditions," J. Appl. Mech. 17, 377-380 (1950).

Discussion

Mr. Kuo (Rockwell International): I think you used a linear system and in a linear system how can you tell if the instability is buckling or flutter when you have the two boundary coefficients joined together? The frequency is aero, and beyond "U criticals" you can't tell anything except that the system is unstable.

Mr. Chen: Yes, you can only use linear theory to predict the lowest critical flow velocity and this is what I have presented.

Mr. Kuo: If you consider a nonlinear system and if you have a forced excitation into a system than it may affect the flutter stability boundary. Have you looked into this problem?

Mr. Chen: We have not, but you are quite correct. The external excitation definitely will affect the critical flow velocity or even with a larger displacement the other terms will become more important.

Voice: A critical part of your analysis depends upon your mass ratio, how do you get about including fluid structure interaction between the fluid and the structure which is a function of the frequency and the mode number under consideration; since you are presenting results in that domain it doesn't seem adequate to simply take the mass per unit length of the fluid, or of the structure, and simply add them together; one would have to take the modes into consideration. How and why is that left out? That is what is normally done in other types of analysis, for example in the structural acoustic interation of plates or cylinders.

Mr. Chen: In this case we considered a very long tube therefore the mass effect is independent of the mode shape. In the acoustic case if you use compressible fluid theory then the added mass will depend on the frequency; of course you would get a more exact answer where you use compressible fluid theory but the compressibility effect are very small, say within 1 or 2 percent, so we neglect them.

Voice: What is your fluid, water or air?

Mr. Chen: Water.

Voice: Water is compressible and heavy. How can you neglect it?

Mr. Chen: That is correct, but you have to consider compressibility relative to something.

Voice: It should add a substantial amount of mass relative to the structural mass in each mode or at least in significant modes.

Mr. Chen: Yes, we have accounted for the added mass.

Mr. Smith, (Bell Aerospace Co.): I think the effect of the fluid is really being split into two parts; one is the added mass of the fluid as a result of the fact that it moves with the tube.

Voice: How is the added mass being represented?

Mr. Smith: As a mass per unit length.

Voice: That is a constant.

Mr. Smith: But then there are additional terms because the fluid in any part of the tube is changing from instant to instant due to its velocity. I think if you really wanted to get down to the fine grain stuff and actually satisfy boundary conditions on the inside of the tube you could show that the approximation is justified. We are not going to do it this afternoon, but I think that is true.

Mr. Chen: If you are interested in further details you can find them in papers either by Paidoussis or Mendenbrook.

Mr. Smith: The theory presumably assumes that the tube moves in a plane but the experiment doesn't constrain it to move in a plane. Were there any significant differences on this account?

Mr. Chen: I think that depends on how perfect the tube is; if you have initial imperfections that are very large in two planes then you will have large orbital motion, but if the tube is straight then you can design your system in such a way that the tube will have nearly uniaxial motion.

EXPERIMENTAL LIQUID/POSITIVE EXPULSION BLADDER DYNAMICS

Martin Wohltmann
Staff Engineer
Martin Marietta Aerospace
Orlando, Florida 32805

An experimental program was conducted at Martin Marietta Aerospace, Orlando, Florida to 1) investigate fuel slosh effects on the stability and control of the Advanced Strategic Air Launched Missile (ASALM), and 2) evaluate the performance of two candidate positive fuel expulsion bladder devices.

Since the test was only recently completed, evaluation of the bladder concepts, through means of stability analyses, has yet to be accomplished. However, sufficient data has been gathered, reduced, and analyzed to assess the relative performance between the two bladder concepts. Slosh frequencies, damping ratios, slosh forces, and moments have been measured. Fatigue testing was conducted to evaluate bladder wear and tear. Tank roll tests were performed to determine if twisting of the bladders inside the tank occurred. Liquid expulsion during maximum sloshing was evaluated. Finally, slosh parameters for a bladderless tank were obtained.

INTRODUCTION

Due to general mission requirements, the ASALM executes thrusting climbs, constant altitude/velocity trajectories, thrusting or non-thrusting vertical dives, and bank-to-turn maneuvers. As a result, the acceleration field direction seen by the bladder-encased liquid fuel varies over a significant range. "Coffee cup" slosh effects include the usual lateral type; in addition, longitudinal slosh is induced by ramjet thrust variations causing pitch and yaw plane perturbations. To define these conditions, slosh testing was conducted with the tank mounted horizontally and then vertically, and excited both laterally and longitudinally.

Two candidate positive expulsion devices (called bladders) were slosh tested. One candidate, called the tension bladder, was made of a nitrile elastomer material (manufactured by Bell Aerospace Corporation of Buffalo, New York)*. This bladder had the capability of stretching as well as flexing. As liquid was introduced, the tension bladder expanded in a balloon-like manner to fill out the tank volume. This cylindrically shaped bladder initially had a diameter of 6.5 inches (16.51 cm), and in the empty condition its material was 0.10 inch (0.254 cm) thick. About 4 psi (27.58 KPa) pressure was required to fill the bladder which was strained 200 percent in the fully fueled condition.

The second candidate was made of a nitrile/nylon composite material. This composite bladder had the capability of flexing but not stretching. The central core of the material was nitrile rubber, and the two outer cores were nylon impregnated with nitrile rubber. This bladder was constructed to fill out the tank volume, going around or over any protuberances into the tank. Total thickness of the material was 0.032 inch (0.081 cm). Before the filling operation took place, the bladder was evacuated of all air, resulting in the formation of numerous wrinkles and folds. As filling proceeded, the weight of the liquid and the friction between the bladder and the tank wall prevented the wrinkles on the bottom of the bladder from smoothing out. As a result, the bladder was not stretched to its maximum capability in the full condition, and voids occurred between the tank wall and the bladder. Jiggling or tank reorientation to remove wrinkles during the fill operation was not possible since the tank was part of a complete missile.

APPARATUS AND INSTRUMENTATION

Test Facility

The experimental test facility, similar to the facility described in Reference 1, is shown in Figures 1 through 4. The full scale ASALM fuel tank was mounted on a test bed that was suspended from a frame through four load cells, three vertically oriented and one horizontally oriented. The frame, suspended from overhead crossbeams, was free to oscillate in one direction in the horizontal plane. A hydraulic piston and cylinder provided the driving force. The excitation amplitude could be varied from 0 to 2.0 inches (0 → 5.08 cm) double amplitude.

* Tension Mode Bladder Patent 3,883,046.

A sinusoidal excitation waveform was used for this test, and the excitation frequency was varied from 0.5 to 5.0 Hz. The electric and hydraulic control circuits for the driving mechanism were designed so that the oscillatory motion of the frame, the test bed, and the tank could be "quick-stopped" to zero velocity during any given cycle of oscillation to enable measuring only the residual forces resulting from the liquid sloshing. A micro switch, located between the shaker frame and the rigid ground support, closed at peak shaker frame displacement, triggering an electronic circuit that cut off the alternating driving signal and replaced it with a dc voltage applied directly to the hydraulic servovalve.

All load cells were of the strain gage type, having sensitivities of 50 millivolts per pound (4.45N) of force. Force measurements as low as 2 pounds (8.896N) were measured during testing.

Using the three vertical load cells made it possible to discriminate between two modes (termed "clean" and "dirty"). This terminology, in describing load cell data, indicates when a single mode has been excited (clean mode), or when more than one mode has been excited (dirty mode). For example, with the tank mounted horizontally and the input excitation direction parallel to the tank longitudinal axis, pure longitudinal slosh motion should result in load cell response data (at the tank end where the two vertical load cells are located) that are in phase with each other. In addition, these data should be 180 degrees out of phase with the data recorded by the angle vertical load cell located at the other end of the tank. When the tension bladder was shaken in the manner described above at a particularly high input displacement amplitude (at the natural frequency), the readings of all three vertical load cells were in phase, indicating that a vertical mode had been excited in addition to the longitudinal mode. The vertical motion was strong enough to obliterate the longitudinal slosh motion data. With sufficient reduction in input displacement amplitude, the longitudinal slosh motion data became predominant. In another instance, with the tank mounted in a vertical orientation, and with the tank excitation in the horizontal plane and perpendicular to the line joining the dual vertical load cells, and at a sufficiently high input displacement amplitude, lateral slosh motion was induced resulting in out of phase readings on the dual load cells. Again, with sufficient reduction in input displacement amplitude, the cross coupling effect disappeared.

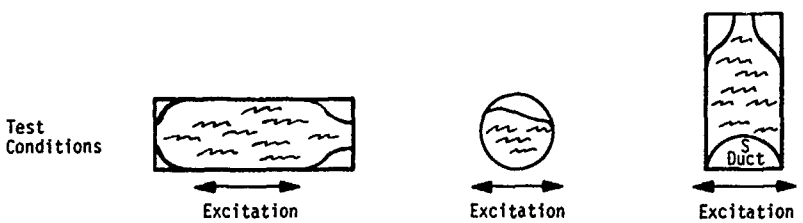

1. Rigid Ground Support
2. Zonic Hydraulic Shaker (Includes LVDT)
3. Shaker Frame, 4-Inch (10.16 cm) Welded Aluminum Channels
4. Vertical Load Cell Support Frame, 4-Inch (10.16 cm) Welded Aluminum Channels
5. Support Bracing, 1.5-Inch (3.81 cm) Welded Aluminum Tubing
6. Pendulum Support Arms, Pin-Jointed 2-Inch (5.08 cm) Square Steel Tubing
7. Load Cell Support Welded Aluminum Plates
8. Test Bed, 4-Inch (10.16 cm) Welded Aluminum Channels
9. Tank Support Frame, 3-Inch (7.62 cm) Welded Aluminum Channels Topped by a Bolted-on 3/8-Inch (0.953 cm) Aluminum Plate
10. Aluminum Fuel Tank Bulkheads and Saddles
11. 0.5-Inch (1.27 cm) Thick, 18-Inch (45.72 cm) Dia 45-Inch (114.3 cm) Long Plexiglass Tank
12. Elastomeric Bladder
13. Load Cell
14. Load Cell
15. Load Cell
16. Load Cell
17. Steel Strap Cross Bracing
18. Quick-Stop Micro Switch
19. Accelerometers

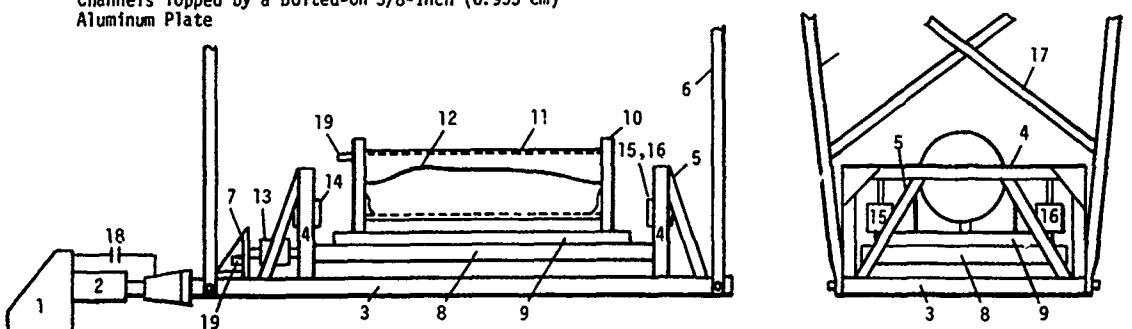

Total Weight of Suspended Structure (No Liquid) 483 lb (218.9 Kg)
(Add 82 lb (37.2 Kg) for Vertical Tank Orientation Fixturing)

Figure 1. Test Setup Schematic

Figure 2. Test Facility

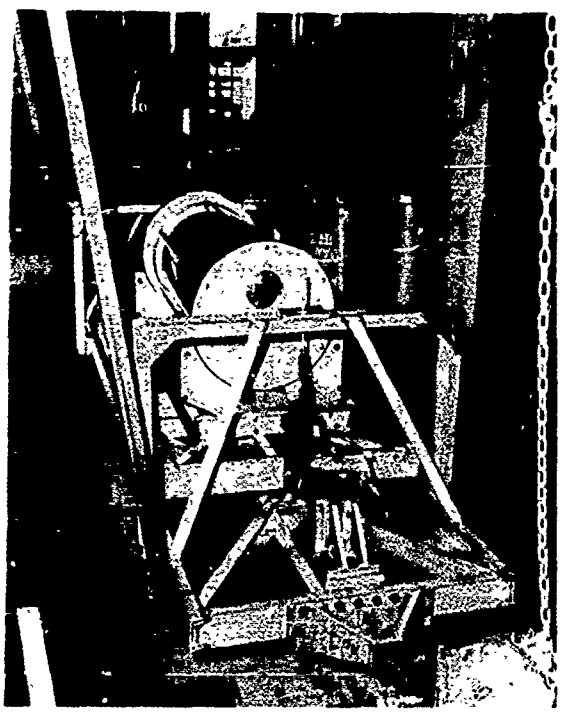

Figure 3. Experimental Test Facility (End View)

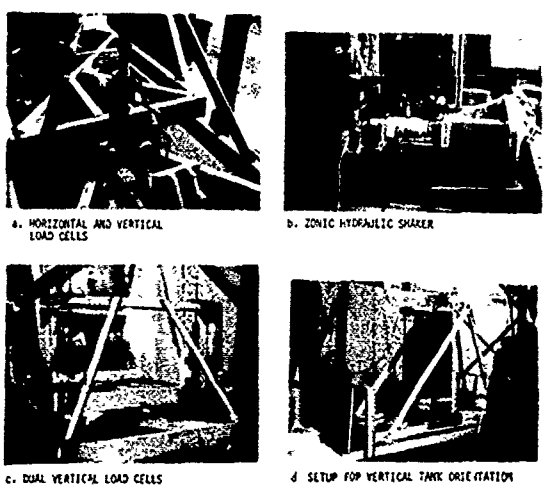

Figure 4. Experimental Test Facility Equipment

Test Units (Tank, Liquid, and Bladders)

A full scale model of the ASALM fuel tank was fabricated from clear acrylic plastic. Figure 5 illustrates the tank and its installation. Dimensions of the tank are approximately 18 inches (45.72 cm) in diameter, 45 inches (114.3 cm) in length, and 0.5 inch (1.27 cm) thick. In flight, the fuel tank is pressurized for fuel expulsion purposes. During the testing, the tank was not pressurized. The effect of pressurization on slosh is minimal since the density of the ullage gas under pressure is insignificant compared to the density of the bladder and its contained fluid; thus, inertial effects of the ullage gas are minimal. Both bladders were effectively pressurized to 14.7 psi (101.4 KPa), since the bladders were evacuated prior to filling with liquid.

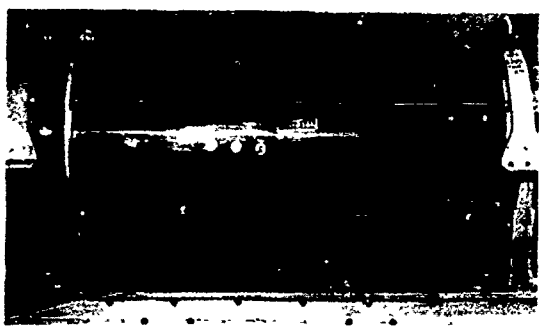

Figure 5. Acrylic Plastic Tank Installation (Composite Bladder Displaced in Natural Slosh Mode)

The contained fluid used in the bladders was distilled water. Viscosity at room temperature of the ASALM ramjet fuel is 30 centipoises (0.03 Pa-s), while water viscosity is 1 centipoise (0.001 Pa-s). When it is recognized that castor oil viscosity is 500 centipoises (0.5 Pa-s), water appears to be a reasonable substitute for ramjet fuel.

Figure 6 shows photographs of the tension and composite bladders. The collector tube (a coiled spring) is shown mounted between end plates in Figure 6a. Although not shown, a similar device is used in the composite bladder.

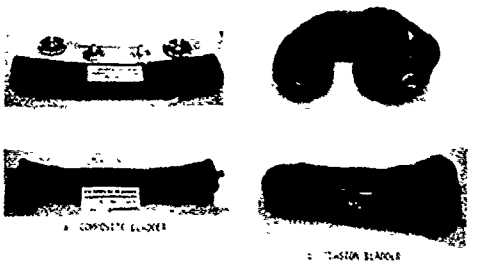

Figure 6. Expulsion Bladders Prior to Installation

Test Conditions

The testing was limited to three tank orientation/tank excitation directions. These three conditions, illustrated in Figure 1, are described as follows.

1 Longitudinal slosh condition - Longitudinal tank axis parallel to the horizontal, excitation direction in a horizontal plane parallel to the tank longitudinal axis.

2 Lateral slosh condition - Longitudinal tank axis parallel to the horizontal, excitation direction in a horizontal plane perpendicular to the longitudinal tank axis.

3 Vertical slosh condition - Tank vertically oriented, longitudinal axis perpendicular to the horizontal, and excitation direction in a horizontal plane perpendicular to the longitudinal tank axis.

At a later time, testing is to be expanded to include other tank orientation/excitation directions. Figures 7 through 11 illustrate the various conditions tested to date.

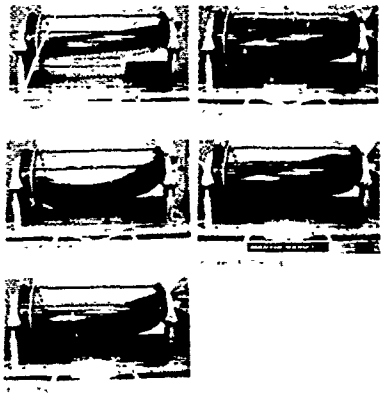

Figure 7. Tension Mode Bladder-Horizontal Orientation

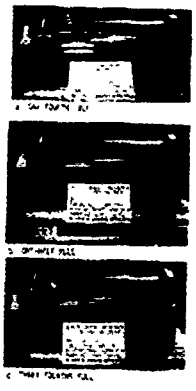

Figure 8. Composite Bladder-Tank Horizontal Orientation, Longitudinal Excitation

Figure 9. Tension Mode and Composite Bladders-Horizontal Orientation and Lateral Excitation

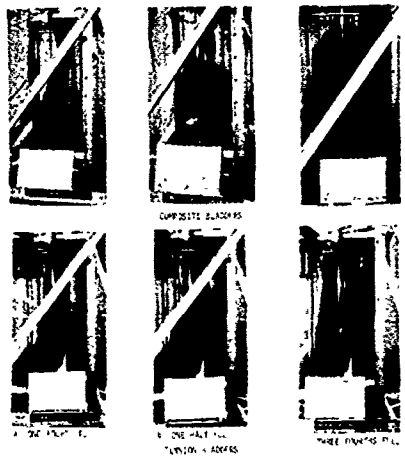

Figure 10. Tension and Composite Bladders-Vertical Orientation

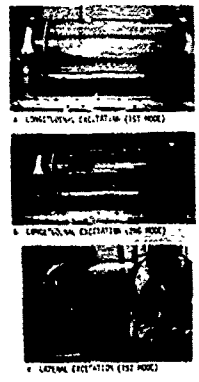

Figure 11. One-Half Full Bladderless Tank-Horizontal Orientation

PROCEDURE AND DATA REDUCTION

The tank was oscillated sinusoidally incrementally over a frequency range of 0.5 to 5.0 Hz. After steady state conditions had been attained, the tank was quick-stopped. The peak slosh force measured during this sweep identified a natural sloshing frequency. Amplitudes of excitation were kept as low as possible consistent with attaining good measurable data. Amplitudes were subsequently increased to determine linearity of response.

The following information was recorded on a direct write recorder for each of the runs:

1. Horizontal slosh force
2. Three vertical slosh forces
3. Acceleration of the tank
4. Acceleration of the shaker frame
5. Linear displacement of the shaker frame
6. Timing signal.

Frequencies were calculated by using the first several slosh force peaks occurring after the quick-stop. Damping ratios were calculated by measuring the slosh force amplitudes at two separate points in the response following the quick-stop. The logarithmic decrement was calculated as follows:

$$\delta = \frac{1}{N} \ln \frac{X_0}{X_N},$$

where X_0 is the amplitude of the slosh force at the Oth peak and X_N is the amplitude at the Nth peak. N is the number of peaks. Viscous damping ratios were calculated by dividing the logarithmic decrement (δ) by 2π:

$$\zeta = \frac{\delta}{2\pi}$$

EXPERIMENTAL DATA

Fundamental Frequency

Figures 12 through 14 present natural slosh frequencies for three fill levels (1/4, 1/2, 3/4) and three tank orientation/excitation directions. At the 1/4 fill level, no measurable response was obtained for the composite bladder, and the bladderless tank was not tested due to the existence of a capillary screen expulsion device located in the tank bottom. This screen did not affect slosh at the 1/2 and 3/4 fill level. Examination of all three figures shows that slosh frequencies are increased by the addition of bladders into the tank. The tension bladder produced significantly higher frequencies than the composite bladder (2.0 to 4.0 Hz for the tension bladder and 0.67 to 2.0 Hz for the composite bladder). Why the tension bladder exhibits constant frequency with fill level for the horizontal tank orientation and shows a severe dropoff in frequency with decreasing fill level (for vertical tank orientation) is as yet unexplained. Second modes (appearing in a bladderless tank) do not exist with bladders, at least up to 5.0 Hz, the maximum frequency tested.

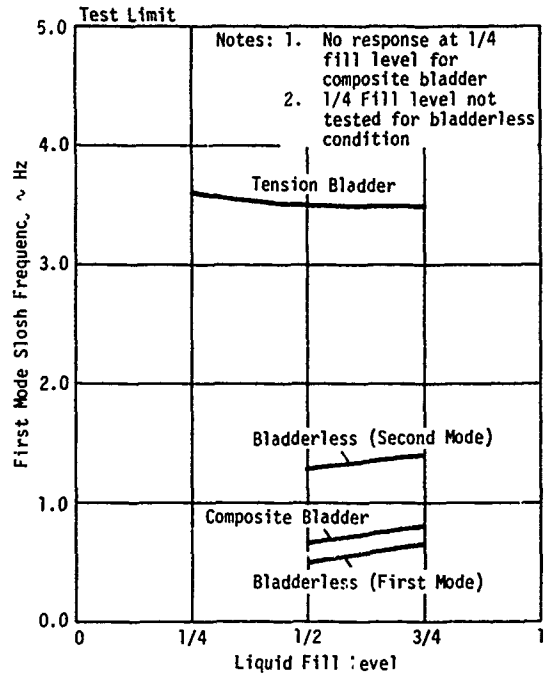

Figure 12. First Mode Slosh Frequencies for Horizontal Tank Orientation, Longitudinal Excitation

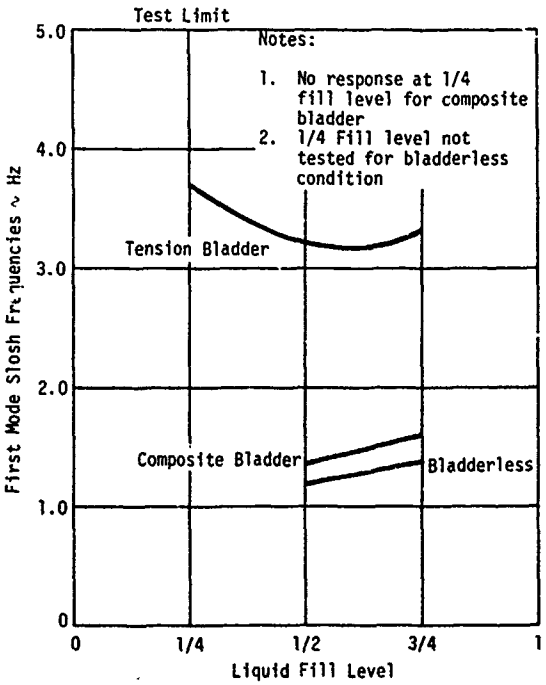

Figure 13. First Mode Slosh Frequencies for Horizontal Tank Orientation, Lateral Excitation

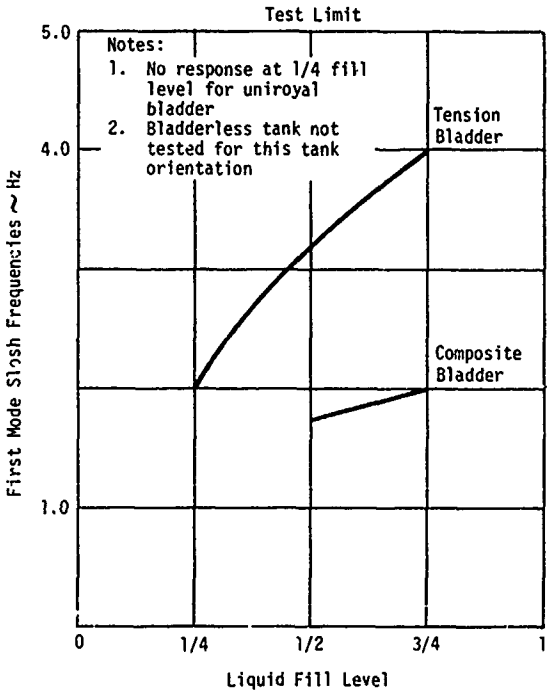

Figure 14. First Mode Slosh Frequencies for Vertical Tank Orientation, Pitch Plane Excitation

Damping

Figures 15 through 17 present viscous damping ratios for three fill levels and three tank orientation/excitation directions. Bladders provide at least four times as much damping in the first mode than a bladderless tank. Maximum damping in the first mode for a bladderless tank was 1 percent. Bladder damping ranged from a minimum of 4 percent up to 12.8 percent (a desirable characteristic from a stability standpoint). No general conclusion as to relative damping merit between the tension and composite bladders could be made from the data. A word of explanation is in order as to the difference in performance of the two bladders. In the horizontal tank orientation, the composite bladder at any tank fill level always exhibits a flat surface at the ullage air interface. Everywhere else the bladder is against the tank surface. On the other hand, the tension bladder (being balloon-like) exposes more surface to the ullage air, and is less in contact with the tank wall. During sloshing, the tension bladder undergoes more bladder/tank wall interaction than the composite bladder. Perhaps this difference in performance disallows clear conclusions.

Table I summarizes the data presented in Figures 12 through 17.

TABLE I

ASALM Fuel Tank Liquid Slosh Frequencies and Damping Ratios

Tank Orientation	Excitation Direction	Liquid Fill Level	Bladderless Tank		Composite Bladder		Tension Bladder	
			Natural Slosh Frequency (Hz)	Viscous Damping Ratio	Natural Slosh Frequency (Hz)	Viscous Damping Ratio	Natural Slosh Frequency (Hz)	Viscous Damping Ratio
Horizontal	Longitudinal	3/4	0.66* 1.41**	0.022* 0.009**	0.80	0.048	3.50	0.100
		1/2	0.50* 1.30**	0.031* 0.010**	0.67	0.056	3.50	0.110
		1/4	Not Tested	-	No Response	-	3.60	0.123
	Lateral	3/4	1.36	0.005	1.60	0.100	3.30	0.042
		1/2	1.18	0.011	1.35	0.062	3.20	0.061
		1/4	Not Tested	-	No Response	-	3.70	0.128
Vertical	Pitch Plane	3/4	Not Tested	-	2.00	0.100	4.00	0.100
		1/2	Not Tested	-	1.74	0.059	3.20	0.065
		1/4	Not Tested	-	No Response	-	2.00	0.088

* First Mode
** Second Mode

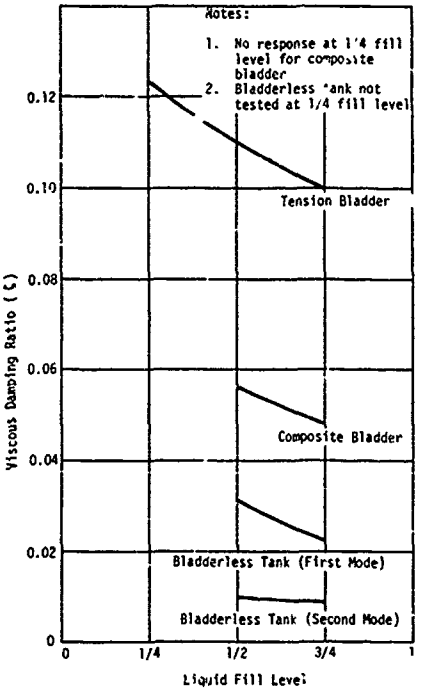

Figure 15. First Mode Slosh Viscous Damping Ratios for Horizontal Tank Orientation, Longitudinal Excitation

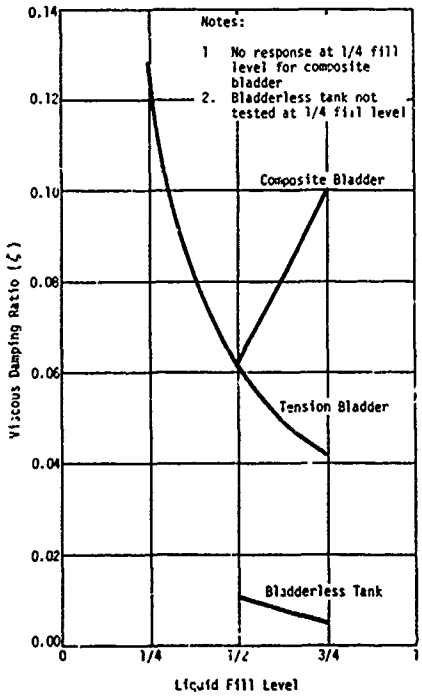

Figure 16. First Mode Slosh Viscous Damping Ratios for Horizontal Tank Orientation, Lateral Excitation

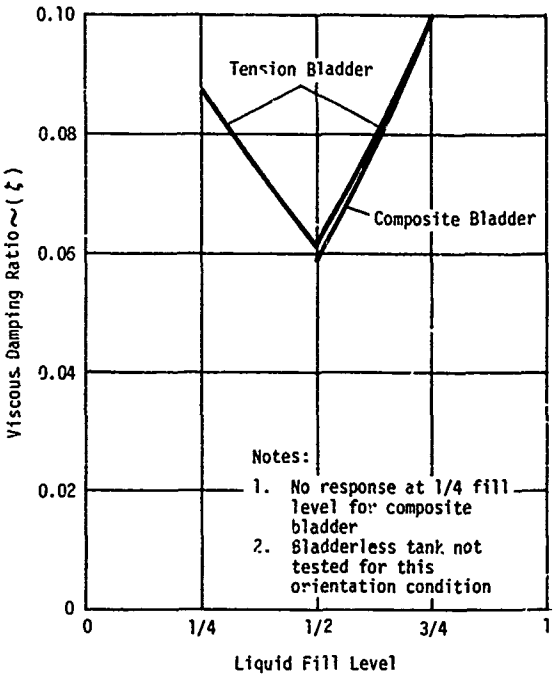

Figure 17. First Mode Slosh Viscous Damping Ratios for Vertical Tank Orientation, Pitch Plane Excitation

Slosh Frequency Response

Figures 18 and 19 present frequency response data as measured by the horizontal slosh force for two test conditions. Force and moment data taken from off-resonance conditions similar to those represented here will be used to generate parameters for a dynamically equivalent spring-mass model. It may be noted that for very small input displacements (0.05 inch) (0.127 cm), the tension bladder produces about the same slosh forces as the composite bladder and the bladderless tank, both of which have much larger input displacements (0.5 and 1.8 inch, respectively) (1.27 and 4.57 cm).

Effect of Input Amplitude on Slosh Force Response

Figures 20 and 21 show the effect of input amplitude displacement on peak slosh force response for the tension bladder and the bladderless tank configurations. Amplitude variations were not made during composite bladder testing. In computing slosh masses for a spring-mass model to be used in stability analyses, the slosh force and input amplitude displacement enter into the calculation (Reference 1). Due to the nonlinearities exhibited in Figures 20 and 21, it is essential to make this calculation with numbers generated from small input displacement data. Tables II and III tabulate the data given in these two figures. Table IV includes data from the composite bladder test conducted at single amplitudes for individual test conditions.

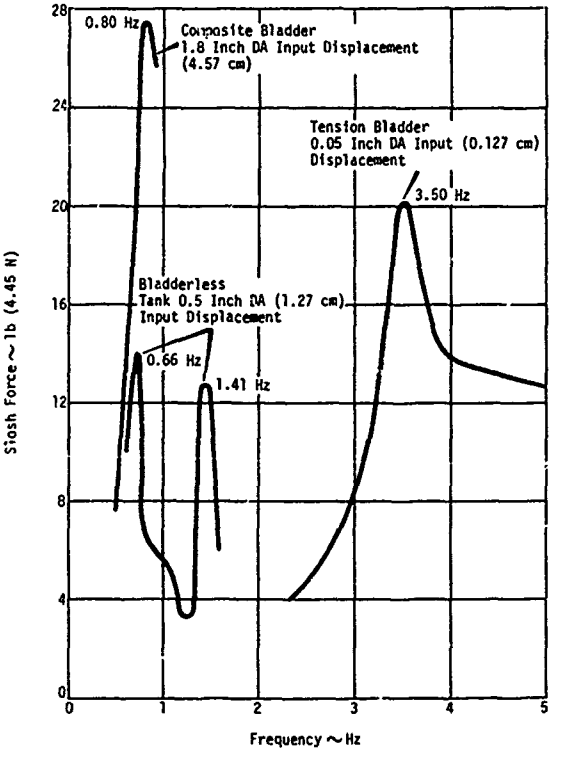

Figure 18. Slosh Force Response for 3/4 Full Longitudinal Excitation Condition

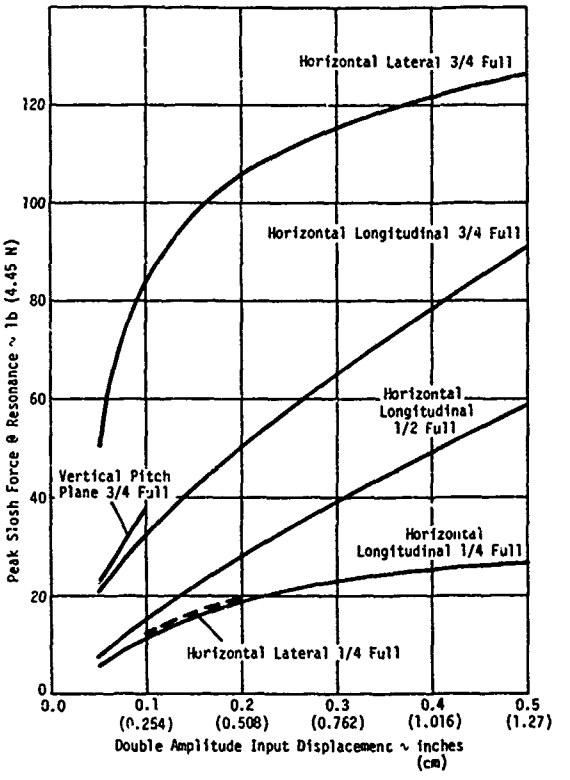

Figure 20. Peak Resonant Forces versus Input Displacement Amplitude for the Tension Bladder Configuration

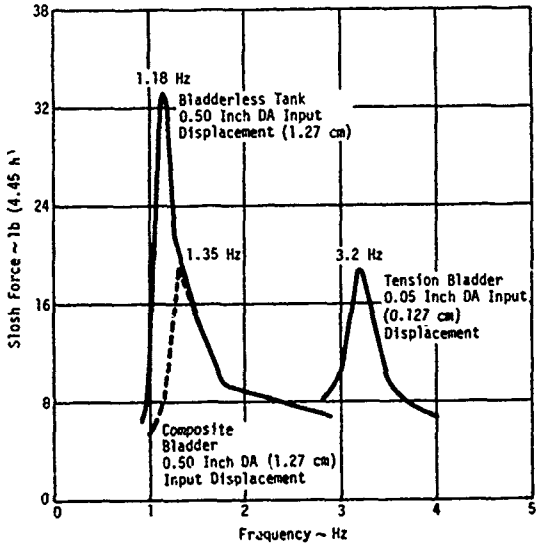

Figure 19. Slosh Force Response for 1/2 Full Lateral Excitation Condition

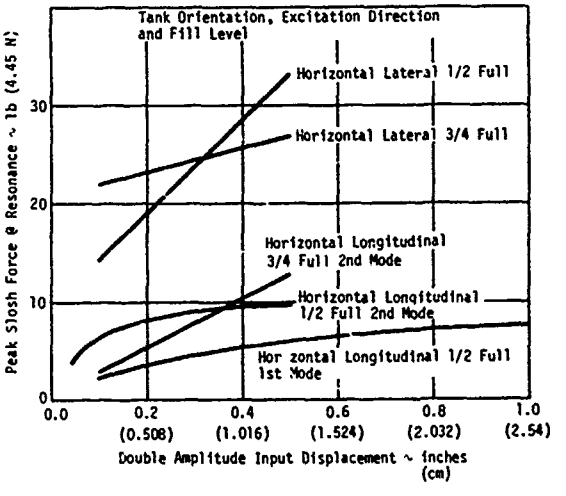

Figure 21. Peak Resonant Forces versus Input Displacement Amplitude for the Bladderless Tank Configuration

TABLE II

Peak Resonant Slosh Forces for the Tension Bladder Configuration

Tank Orientation	Excitation Direction	Fill Level	Resonant Frequency (Hz)	Input Displacement (inch DA)(cm)	Peak Slosh Force (lb)(N)
Horizontal	Longitudinal	3/4	[illegible]	0.05 (0.127)	20.7 (92.1)
				0.10 (0.254)	32.7 (145.5)
				0.50 (1.27)	91.1 (405.2)
		1/2	[illegible]	0.05 (0.127)	6.7 (29.8)
				0.10 (0.254)	14.7 (65.4)
				0.50 (1.27)	58.7 (261.1)
		1/4	3.6	0.05 (0.127)	4.7 (20.9)
				0.10 (0.254)	11.3 (50.3)
				0.5 (1.27)	26.7 (118.8)
	Lateral	3/4	3.3	0.05 (0.127)	49.0 (218.0)
				0.10 (0.254)	83.3 (370.5)
				0.20 (0.508)	126.5 (562.7)
		1/2	3.2	0.05 (0.127)	18.7 (83.2)
		1/4	3.7	0.10 (0.254)	11.3 (50.3)
				0.20 (0.508)	19.3 (85.9)
	Pitch Plane	1/4	4.0	0.05 (0.127)	22.0 (97.9)
				0.10 (0.254)	37 (166.4)
		[illegible]	3.2	0.10 (0.254)	20.0 (89.0)
		[illegible]	[illegible]	0.20 [illegible]08)	9.3 (41.4)

TABLE III

Peak Resonant Slosh Forces for the Bladderless Tank Configuration

Tank Orientation	Excitation Direction	Fill Level	Resonant Frequency (Hz)	Input Displacement (inch DA)(cm)	Peak Slosh Force (lb)(N)
Horizontal	Longitudinal	3/4	0.66 1st Mode	0.5 (1.27)	14.0 (62.3)
			1.41 2nd Mode	0.1 (0.254)	2.7 (12.0)
				0.5 (1.27)	12.7 (56.5)
		1/2	0.50 1st Mode	0.1 (0.254)	2.0 (8.9)
				0.5 (1.27)	6.0 (26.7)
				1.0 (2.54)	7.3 (32.5)
			1.30 2nd Mode	0.05 (0.127)	4.0 (17.8)
				0.10 (0.254)	6.0 (26.7)
				0.5 (1.27)	9.7 (43.1)
	Lateral	3/4	1.36	0.1 (0.254)	22.3 (99.2)
				0.5 (1.27)	26.7 (118.8)
		1/2	1.18	0.1 (0.254)	14.0 (62.3)
				0.5 (1.27)	33.3 (148.1)

TABLE IV

Peak Resonant Slosh Forces for the Composite Bladder Tank Configuration

Tank Orientation	Excitation Direction	Fill Level	Resonant Frequency (Hz)	Input Displacement (inch DA)(cm)	Peak Slosh Force (lb)(N)
Horizontal	Longitudinal	3/4	0.80	1.8 (4.572)	[illegible].5 (122.3)
		1/2	0.67	1.8 (4.572)	21.5 (95.6)
		1/4	No Measurable Response		
	Lateral	3/4	1.60	0.5 (1.27)	20.0 (89.0)
		1/2	1.35	0.5 (1.27)	18.7 (83.2)
		1/4	No Measurable Response		
Vertical	Pitch Plane	3/4	2.0	0.5 (1.27)	8.0 (35.6)
		1/2	1.74	0.5 (1.27)	14.7 (65.4)
		1/4	No Measurable Response		

Data Time Histories

Figures 22 through 24 present time histories of the measured data for typical runs of the tension bladder, composite bladder, and bladderless tank configurations. The higher frequency recorded on the traces prior to quick-stop is a structural frequency which damps out quickly (less than one cycle) after the quick-stop. The remaining high frequency data resulted from mechanical transmittance of noise through the lab floor into the shaker and then into the shaker frame. When the lab air conditioner broke down, the data became clean. Hand filtering of the data was applied to ferret out the slosh forces. Figures 23 and 24 show the result of this hand filtering on data obtained from the composite bladder test and the bladderless tank test.

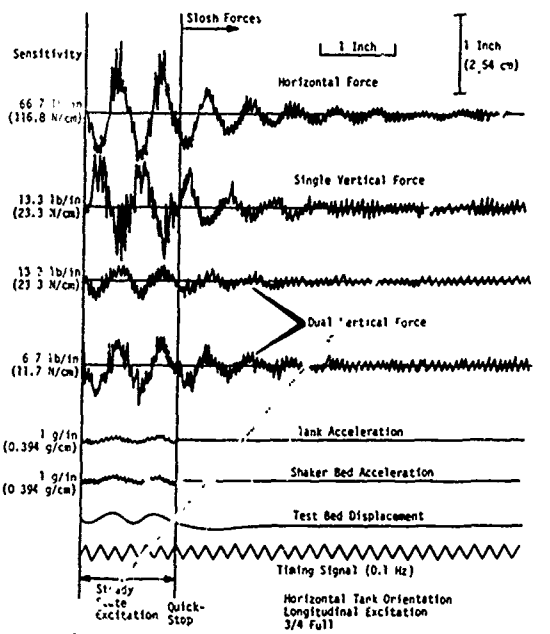

Figure 22. Slosh Response Tension Bladder at 3.5 Hz Resonant Frequency 0.05-Inch DA Input Displacement (0.127 cm)

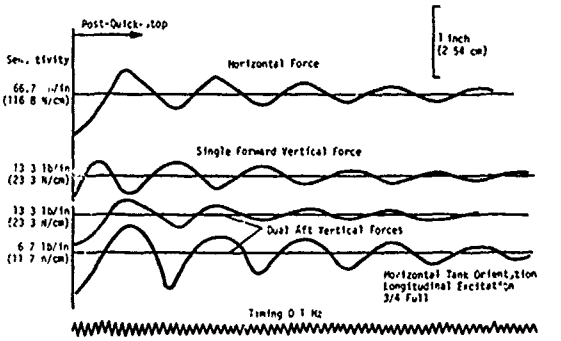

Figure 23. Slosh Response Composite Bladder at 0.8 Hz Resonant Frequency 1.8 Inch DA Input Displacement (4.57 cm)

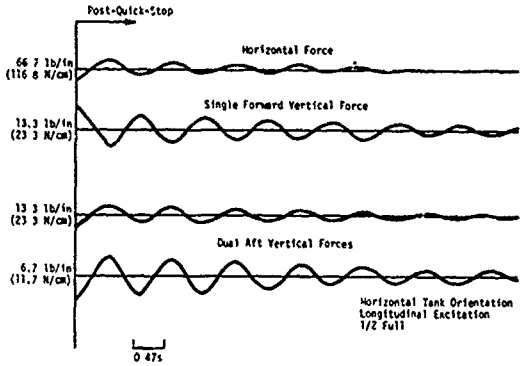

Figure 24. Slosh Response Bladderless Tank at 0.5 Hz Resonant Frequency 1.0 Inch DA Input Displacement (2.54 cm)

Fatigue Tests

Both the tension and composite bladders were cycled 10,000 times at a frequency and amplitude that induced severe bladder motion. Figure 25 (a and b) illustrates the fill level conditions under which the fatigue test was conducted. The composite bladder was at a fill condition (full) that simulates conditions existing during ASALM ground transportation and aircraft carry. At nominal temperatures there is a small ullage volume in the ASALM tank. The top of the bladder is approximately 2 inches (5.08 cm) below the top of the tank. At an excitation frequency of 1.5 Hz in the longitudinal direction (tank horizontal), severe impacting of the bladder on the tank top occurred during the fatigue test. With the tension bladder at the same fill condition as the composite bladder, about 80 percent of the bladder was in contact with the top of the tank and not much bladder action resulted during cycling. Thus the fill level was reduced to 3/4 and excitation was begun at 3.2 Hz (a resonant condit[illegible].

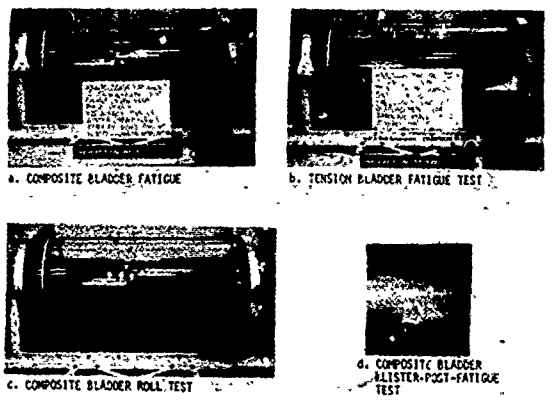

Figure 25. Fatigue and Roll Test Configurations

At the completion of the fatigue tests, neither bladder exhibited any tears or leaks. However, the composite bladder had developed numerous blisters on the surface. Post-test examination of this bladder revealed blisters on the internal surface of the bladder at the same locations as the external blisters. The blisters were not mushy when squeezed, and it can be concluded they were filled with water. Manufacturer representatives stated this was not a normal occurrence and could be attributed to manufacturing and/or material defects.

Roll Test

To determine if rolling of an ASALM missile during maneuvered flight or rotation of a missile mounted on a B-1 aircraft spindle from a top position to a bottom eject position would cause twisting of the bladder within the tank, a roll test was conducted for both the composite and tension bladder configurations. Reference points were noted on the bladders and tank, and the tank was then hand rolled on the test bed saddles through 360 degrees. At the completion of the tests, visual observation of the reference points indicated that both bladders had rotated essentially as a rigid body with the tank. Comparison of Figure 25c with 25a shows the results for the composite bladder. Lack of a visual marker on the tension bladder that was capable of being photographed prevented the taking of data.

Limited Liquid Expulsion During Slosh

Water was expelled from a fully loaded tension bladder to an empty condition while resonant longitudinal slosh was occurring (tank in horizontal orientation). No ill effects were observed on expulsion during slosh.

SUMMARY OF RESULTS

The results of the experiments showed that compared to a bladderless tank, use of either bladder raised the first mode slosh frequency.

In the frequency range investigated (0 to 5 Hz), second mode slosh did not exist with the use of either bladder, whereas second mode slosh frequencies did appear when the tank was bladderless.

For all tank orientations and excitation directions, the first mode slosh frequencies obtained with the composite bladder ranged from 0.66 to 2.0 Hz. With the tension bladder configuration, these frequencies ranged from 2.0 to 4.0 Hz.

First mode viscous slosh damping ratios for the bladderless tank configuration did not exceed 1 percent. Damping ratios obtained with both bladders ranged from 4 to 12.8 percent,

the particular value depending on tank orientation and excitation direction. These high damping ratios are desirable from a flight stability and control aspect. For the horizontal tank orientation and with longitudinal excitation, the tension bladder damping was twice as high as the composite bladder damping at all fill levels. For the vertical tank orientation, both bladders produced the same amount of damping.

At the 1/4 full level the composite bladder did not produce any measurable slosh characteristics whereas the tension bladder did.

For the conditions tested, the sloshing of the tension bladder produced slosh forces 5 to 10 times as high as the bladderless tank slosh forces. No direct comparison of the above forces with forces produced by composite bladder sloshing can be made. However, composite bladder slosh forces were very moderate for very large input displacement amplitudes.

Both bladders successfully passed a 10,000 cycle fatigue test. Bladder motion was severe in both cases. Roll tests showed that both bladders rotated as a rigid body with the tank rather than differentially slipping.

REFERENCES

1. Irving E. Sumner, Andrew J. Stofan, and Daniel J. Shramo, "Experimental Sloshing Characteristics and a Mechanical Analogy of Liquid Sloshing in a Scale-Model Centaur Liquid Oxygen Tank," NASA TM X-999, August 1964

2. Andrew J. Stofan and Irving E. Sumner, "Experimental Investigation of the Slosh-Damping Effectiveness of Positive-Expulsion Bags and Diaphragms in Spherical Tanks," NASA TND-1712, January 31, 1963

3. H. Norman Abramson (Editor), "The Dynamic Behavior of Liquids in Moving Containers," NASA SP-106, 1966

4. David R. Lukens, Alfred F. Schmitt, George T. Broucek, "Approximate Transfer Functions for Flexible-Booster-and-Autopilot Analysis," WADD TR-61-93, April 1961

5. Andrew J. Stofan and Albert J. Pavli, "Experimental Damping of Liquid Oscillations in a Spherical Tank by Positive-Expulsion Bags and Diaphragms," NASA TND-1311, July 1962